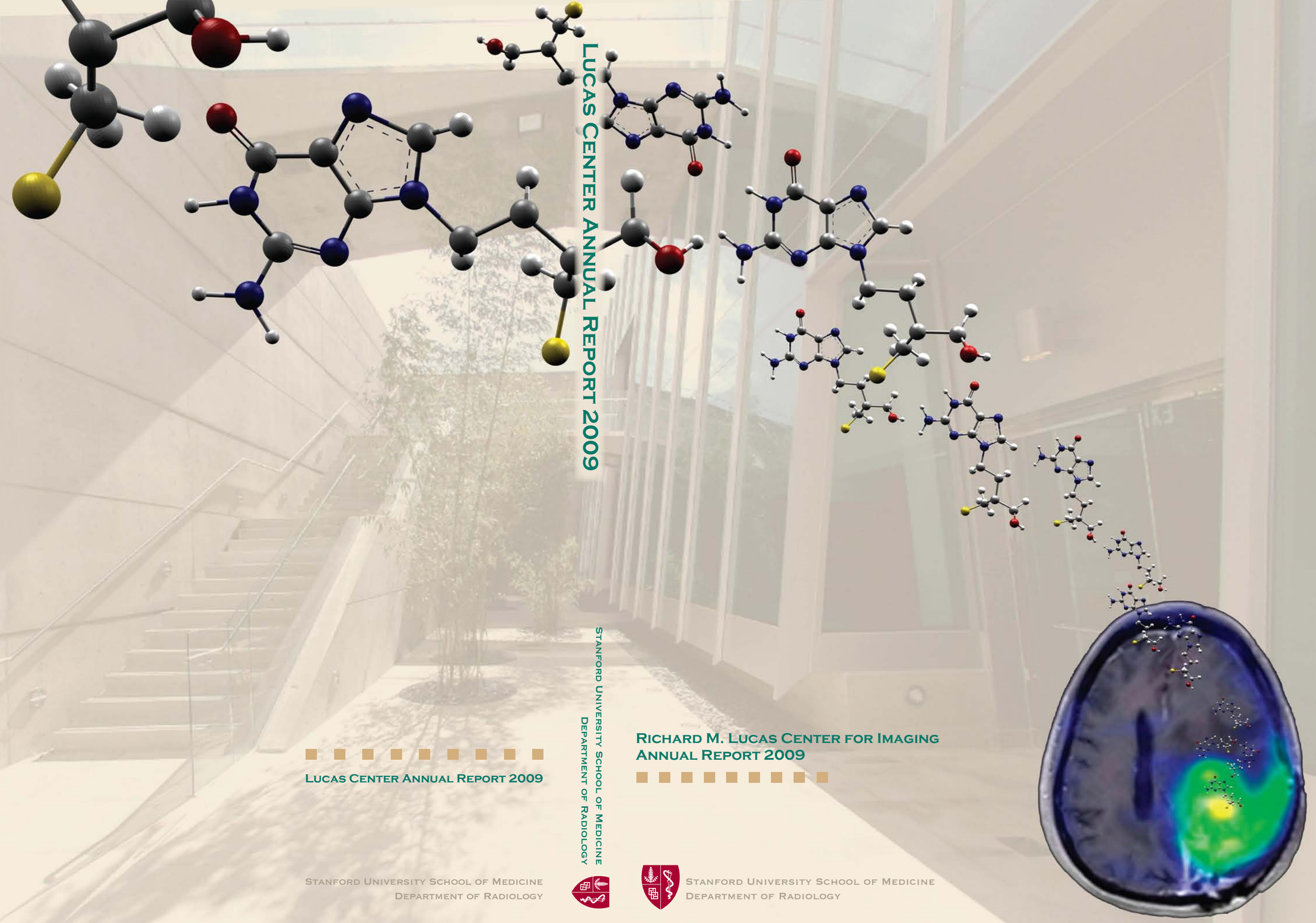

Lucas Center Annual Report 2009

Stanford University School of Medicine
Department of Radiology

Lucas Center Annual Report 2009

Stanford University School of Medicine
Department of Radiology

Richard M. Lucas Center for Imaging
Annual Report 2009

Stanford University School of Medicine
Department of Radiology

Contents

Building Bridges Through Imaging 1

Gold Medal Announcement 3

Lucas Center Overviews 7

Research Overview 8
Radiological Sciences Laboratory and Center for Advanced MR Technology (RSL & CAMRT) 10
Molecular Imaging Program at Stanford (MIPS) 11
Information Science in Imaging at Stanford (ISIS) 12
Centers of Excellence 14
New Initiatives 15
Advanced New Initiatives 16

Research Faculty and Personnel 21

Radiology Research Personnel, Students, and Visitors 22
New Faculty & Research Personnel 24
Faculty & Staff Awards 26

Education and Training 29

Trainee Awards 30
Postgraduate Education 32
- Continuing Medical Education 32
- NIH-supported Training Programs 32
- Advanced Techniques for Cancer Imaging and Detection (T32) 32
- Stanford Molecular Imaging Scholars (R25) 34
- In Vivo Cellular and Molecular Imaging (P50) 35

Lucas Center MR Systems Training and Support 35

Research Group Updates 37

Advanced X-Ray and CT Techniques 38
- Inverse Geometry CT and Conventional CT (Pelc) 38
- X-Ray Guidance of Interventional Procedures (Fahrig) 38

Image Analysis, Bioinformatics, Computational Modeling 39
- Mathematical and Computational Modeling of Cancer (Plevritis) 39
- Radiology Informatics in Translational Medicine (Rubin) 39
- Imaging Bioinformatics (Paik) 40
- Image Display and Analysis (Napel) 40

Magnetic Resonance Research 41
- Interventional and Open MRI (Butts Pauly) 41
- Body MR Imaging (Hargreaves) 42
- High Field MR (Rutt) 42
- Functional Microvascular Neuroimaging (Bammer/Moseley) 43
- Functional Imaging and Technology Development (Glover) 44
- Magnetic In Vivo Spectroscopy and Multinuclear Imaging (Spielman) 44

Molecular Imaging 45
- Cellular and Molecular Imaging Lab (Rao) 45
- Molecular Imaging Instrumentation Lab (Levin) 45
- Cardiovascular Molecular Imaging Lab (Wu) 46
- Clinical Molecular Imaging Research (Quon) 46
- Molecular Imaging of Musculoskeletal Illnesses (Biswal) 47
- Translational Molecular Imaging Lab (Willmann) 47
- Multimodality Molecular Imaging Lab (Gambhir) 48
- Cancer Molecular Imaging Chemistry Lab (Cheng) 48
- Molecular Imaging Probe Lab (Chen) 49

Facilities 51

Outpatient Imaging Center 52
3D Medical Imaging Lab 53
Study Model Management 54
Small Animal Imaging Center (SCi3) 54
Lucas Center MR Systems 1.5T, 3T, and 7T Whole Body Magnets 55
Cyclotron Suite Update 56

Abstracts 59

Advanced X-Ray and CT Techniques 60
Image Analysis, Bioinformatics, Computational Modeling 69
Magnetic Resonance Research 83
Molecular Imaging 134

Publications and Presentations 155

Peer-Reviewed Presentations at Scientific Meetings 156
Other Scientific Meeting Presentations 163
Published Papers 171
Books & Book Chapters 185
Papers Submitted or in Press 186

Funded Research Projects 193

NIH Supported Research 194
Stanford Supported Research 196
Professional Society and Foundation Supported Research 197
Other Government Supported Research 198
Industry Supported Research 199
Projects Made Possible In Part by Industry Seed Funding 200

Collaborators 201

Cover Image:

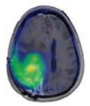

The cover image is of an MRI and PET fusion brain scan with ^{18}F-radiolabelled 9-[4-fluoro-3-(hydroxymethyl)butyl] guanine (^{18}F–FHBG) to detect autologous cytolytic CD8^{+} T cells (CTLs) that express HSV1 tk. For complete details, see the following publication:
Noninvasive detection of therapeutic cytolytic T cells with 18F-FHBG PET in a patient with glioma. Yaghoubi SS, Jensen MC, Satyamurthy N, Budhiraja S, Paik D, Czernin J, Gambhir SS; Medscape. Nat Clin Pract Oncol. 2009 Jan;6(1):53-8. Epub 2008 Nov 18.

2009 Lucas Report Team:

Editor/Production: Susan Kopiwoda
Design: Amy Morris
Photography: Mark Riesenberger
Archiving: John Ralston
Printing: Lahlouh, Inc.

Building Bridges

Through Imaging

A little more than twenty years ago, my family and I packed up and moved from Ann Arbor, Michigan, to Stanford to begin our new lives in California. The centerpiece of my recruitment was the commitment from Stanford University that a new center for biomedical imaging would be constructed to serve as the Medical School's epicenter for imaging. Today, the Richard M. Lucas Center for Imaging is the tangible expression of that commitment. The Lucas Center is much more than a set of buildings with associated labs and equipment. It represents a place where talented individuals choose to spend their lives chasing their dreams to advance imaging and improve the understanding of health and disease.

I am delighted that the atmosphere of the Lucas Center is permeated with collegiality and support, which make our work so enjoyable as we produce serious science that is both inventive and creative. Our physics- and engineering-based research has proceeded at a breakneck pace for the past two decades, approaching the speed of Moore's law. The rate of innovation in other areas such as genomics and nanotechnology is even faster. By establishing connections with these fields and developing an outstanding program in molecular imaging, our opportunities are boundless. As highlighted in this Annual Report, the results from our investigations have already graced the pages and covers of major scientific journals.

We are very hopeful that the platform technologies comprising imaging will serve to unravel the complexities of biology and medicine. To accomplish this goal, we have taken a major step to strengthen our high-field MRI programs this year through the recruitment of Brian Rutt, PhD. He has been a pioneer in pushing the boundaries of conventional MR systems to image single cells. He also intends to explore high-field magnetic resonance to depict the plaques in Alzheimer's disease and to improve our understanding of the developing and aging brain. Led by Sam Gambhir, MD, PhD, we are also just beginning to embark on a major program in the early detection of cancer using imaging and blood-based testing. Much of this work will occur on the edge of campus in a building on California Avenue that we opened just a few months ago, after outgrowing our space in Lucas I and the Lucas expansion (Lucas II). Perhaps one day we can move these programs back on campus into "Lucas III."

Over twenty years ago, as I considered relocating to Stanford University, I envisioned a very bright future for a department with a mandate to improve human health through advancing imaging. I could never have imagined the growth that is chronicled in the Annual Report. I want to thank the Lucas family, our faculty and staff, as well as our supporters throughout the world for making this possible.

Gary M. Glazer, MD
Emma Pfeiffer Merner Professor in the Medical Sciences
Professor and Chairman
Department of Radiology
Stanford University School of Medicine

Gold Medal Announcement

Congratulations, Dr. Glazer!

Glazer wins Radiology's Highest Honor

The Radiological Society of North America has conferred its highest honor, the Gold Medal, on Gary M. Glazer, MD, Emma Pfeiffer Merner Professor in the Medical Sciences.

Since 1919, the RSNA Gold Medal has been given each year to an individual who has rendered exemplary service to the science of radiology and who has received unanimous approval by the RSNA board of directors. Other Stanford winners include Malcolm Bagshaw, MD, in 1999 and Herbert Abrams, MD, in 1995.

Dr. Glazer is chair of the Department of Radiology. Under his leadership, Stanford's programs in radiology and imaging have grown to become epicenters for innovation and education in many different areas, including MRI, CT, and the developing field of molecular imaging. Through his ability to envision and generate advances in the field, he helped establish the Medical School's Richard M. Lucas Center for Imaging, which serves as an international resource bringing together physicists, engineers, chemists, molecular biologists, and physicians to create novel breakthroughs in medical imaging.

Dr. Glazer has also contributed to the field of radiology through his research in tissue characterization using imaging-based techniques. Prior to becoming chair at Stanford in 1989, he was professor of radiology at the University of Michigan, where his work on the staging of neoplasms using CT and MRI received international recognition. In the 1980s, his research regarding the staging of lung cancer was widely adopted into routine clinical practice.

Most recently, Dr. Glazer has concentrated his research efforts on using image-guided tumor insonification to amplify tumor biomarker signals in the blood and to identify the biomarker release site. In addition to early cancer detection, he is dedicated to patient-centered radiology and has developed an outpatient imaging facility designed to enhance the interaction between radiologists and patients.

Dr. Glazer will receive the Gold Medal in December during the 2009 RSNA annual meeting in Chicago.

RSNA® 2009
Quality Counts

Lucas Center Overviews

Research Overview

Norbert Pelc, ScD, Associate Chair for Research
Susan Kopiwoda, MS, MPH, Director, Strategic Research Development

We have been able to elevate the research activity of the Department of Radiology each year, and 2009 was anything but an exception. Through the American Recovery and Reinvestment Act of 2009 (ARRA, also known as stimulus funding), the President and Congress made more than $8B dollars available for research funding. The goal is to stimulate the economy, fuel new research, build infrastructure, and provide or preserve jobs in the academic and industrial sectors. The Stanford Department of Radiology, with a determination to secure research dollars and jobs, submitted 47 proposals ($40.2M) and identified jobs for approximately 70 individuals. Although only a fraction of the funds have been allocated thus far, we have already been notified that the Radiology Department will receive ARRA funding for 4 new projects and 5 supplements to existing projects for a total of $2.8M in FY09 and FY10. See pages 194–195 for the list of funded ARRA projects.

Proposed Research

The combined impact from ARRA initiatives, existing programs seeking renewed funding, and new submissions, especially from new faculty, has spawned an extraordinary number of proposals.

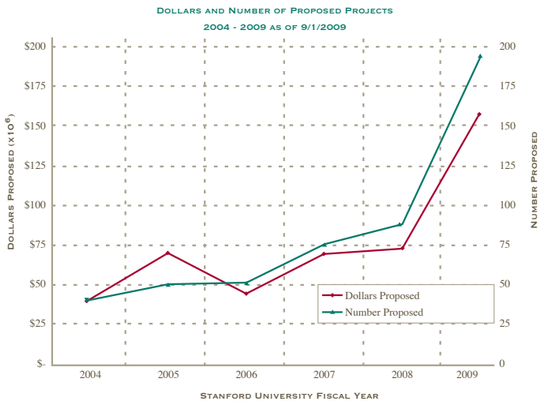

Our average increase in proposals from year to year has been ~20%. This year we experienced an increase of 75% in proposals. Figure 1 shows proposals submitted and dollars requested during FY 2009. The hope, of course, is that many of these proposals result in new research dollars but even for those projects that do not receive funding on the first attempt, the resulting collaborations and commitment to new projects often produce exciting new research opportunities.

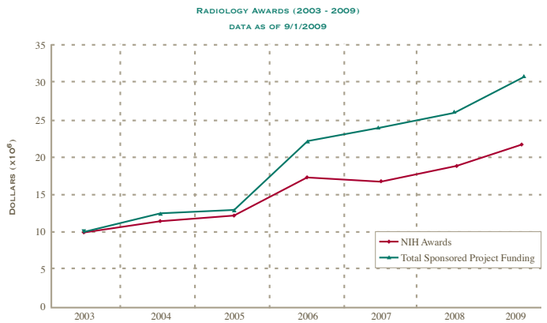

Figure 2: Total sponsored project funding for the Department of Radiology reaches $31M with NIH awards at a new high with 51 active projects that generated $22M in research funding in 2009.

Projects Awarded

Without a doubt, our heroic efforts to submit grants for every deadline is bringing new and substantial benefit to our research program. 2009 brought good news for a significant number of programs: 15 new or continuing projects funded by NIH, and 24 supported by industry, foundations, professional societies, and other government funding sources such as the Department of Defense, State of California, and the Veterans Administration. Figure 2 summarizes our total funding, and shows an increase of >100% between 2003 and 2009, and an increase of 20% for all awards and 21% for NIH awards from 2008 to 2009. Given the increase in the number of proposals submitted this year, we are hopeful the positive funding trend will continue for 2010 but are sobered by the expected drop in the success rate of NIH proposals.

Personnel

Generally, each new research faculty hired results in an increase in staffing by 2-5 individuals as they establish their labs and acquire funding to support their research. Last year we hired four new research faculty, so we anticipate growth in personnel to continue at least through the next two years as the ISIS program grows, the Canary Center fills up, and the High Field MR program expands. Figure 3 shows Radiology research personnel from 2000 to 2009. Over the past nine years, we averaged a growth rate of 17.7%. Our increase this year was 16.6%. At this rate, by 2014 (5 years) we will be well over 500 research personnel. Since we are already frugal with space, even with a slower rate we will need an expansion in research facilities to accommodate growth.

Space

In June, 2009, The Canary Center at Stanford opened its doors at 1201 California Avenue, Palo Alto. This off-campus research site houses the new Center of Excellence for Cancer Early Detection led by Dr. Sam Gambhir and supported by the Canary Foundation. Please see page 16 for additional details about the Canary Center goals and progress in the past several months. The new location is quickly becoming populated with scientists focusing primarily on in vivo and in vitro diagnostics, however, our high field MR imaging coil lab is also housed at this site. Co-location of this MR facility with molecular imaging resources will allow these two disciplines to begin to develop joint projects that utilize extraordinary attributes from each. The concept of merging magnetic resonance imaging with molecular imaging is not new but how to harness magnetic resonance for molecular imaging still evolves. By co-locating a high field MR development lab in the Canary Center, we feel that relationships between the two groups may lead to exciting new research directions.

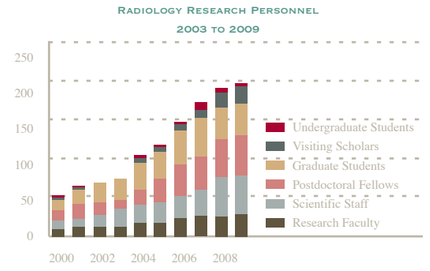

Figure 3: tracks Radiology research personnel and shows an average growth rate of about 16-18% per year.

Although this year has been extremely productive, we continue to have concerns about the state of NIH funding. We are particularly concerned about the likelihood of a tight funding climate that may surface in two years time when most all stimulus funds will have been allocated and spent. Although stimulus funds from Washington have been welcome and our Department has done well in securing~$3M from this program, applying for these funds, reviewing grants and administering the programs have challenged the entire community.. Most programs that have been or soon will be funded will be short lived (two years or less), require substantial achievement, and mountains of paperwork tracking expenditures, accountability, and jobs created (or preserved). We are working with diligence to make sure that our growth persists, even after the bolus of stimulus funds is gone.

We are pleased to present the Lucas Family Foundation and the Board of Trustees with the 2009 Lucas Annual Report. In the next few pages, you will read about our NIH-supported Centers of Excellence (page 14), emerging new initiatives (page 15), and the three Stanford Radiology sections that make up our research effort: 1) Information Sciences in Imaging @ Stanford (ISIS), co-led by Sandy Napel, PhD and Sylvia Plevritis, PhD; 2) the Radiological Sciences Lab (RSL), led by Gary Glover, PhD; and 3) the Molecular Imaging Program at Stanford (MIPS), led by Sam Sanjiv Gambhir, MD, PhD. You will also find a complete listing of all of our sponsored projects on pages 194–200.

It is with continued support of the Lucas Family Foundation and the Canary Foundation that we are able to maintain leadership in research, train the next generation of imaging clinicians and scientists, and, above all, deliver the most advanced diagnostic and therapeutic techniques to benefit our patients and patients worldwide.

RSL Overview

Lucas Center, Radiological Sciences Laboratory and The Center for Advanced MR Technology (CAMRT)
Gary H. Glover, PhD
Director, Radiological Sciences Laboratory

The Lucas Center has been home to the Radiological Sciences Laboratory (RSL), a section of the Radiology Department, since the building's dedication in 1992. In conjunction with the Electrical Engineering Department, the Lucas Center has hosted the Center for Advanced MR Technology, an NIH-funded National Research Resource since 1995. The Center also houses a cyclotron and radiochemistry labs as well as other wet labs for the Molecular Imaging Program led by Dr. Sanjiv Gambhir. The Center's state of the art imaging facilities support research of the RSL and others in the Radiology department as well as hundreds of on-campus and extramural researchers as a core facility. The Center has always been, and remains an exciting and lively nexus for fundamental imaging research. See page 201 for a list of our collaborators.

The Radiological Sciences Laboratory

The RSL comprises 9 faculty, approximately 35 graduate and postdoctoral students, approximately 30 scientific staff and 7 administrative assistants, as well as the Lucas Center/RSL Administrative Services Director, Donna Cronister.

Brian Rutt joined the lab from Robarts Institute and arrived early in 2009. Brian is internationally known for his expertise in many areas of MRI physics and engineering, and has been busy forging collaborations in high field MRI, staffing his lab, and developing a new MRI hardware laboratory. This facility will be housed in the California Ave. building dedicated early this summer and will make possible the development of innovative gradient, shim, and RF coils.

RSL faculty serve in a wide variety of advisory roles to government and foundation agencies such as the NIH and in policy-making positions for international scientific societies such as the ISMRM and RSNA. Many of our faculty, scientific staff, and students have garnered prestigious awards for their exceptional research achievements.

National Center for Advanced MR Technology at Stanford (CAMRT)

The CAMRT has entered its fifteenth year of operation as a National Research Resource, sponsored by a grant from the NIH's National Center for Research Resources with Dr. Glover as PI. Outstanding progress has been made in all six of the core technology development areas that include reconstruction methods (Dwight Nishimura, EE Department, core director), imaging of brain activation (Gary Glover), diffusion and perfusion weighted imaging methods (Mike Moseley), imaging of cardiovascular structure and function (Brian Hargreaves), spectroscopic imaging development (Dan Spielman) and interventional MRI technique development (Kim Butts). Much of this exciting research is chronicled in the scientific reports that follow.

This year saw much activity with writing the proposal application for renewal of the P41 grant. With advice from our National Advisory Board, we proposed to restructure the technical activities into 5 cores that include Reconstruction methods, Hardware, Body imaging, Neuroimaging and Spectroscopy. The new structure reflects both continued need for most of the technology development as well as new opportunities for hardware development. The application was submitted in late May and will be reviewed in early October by an NIH site visit study section.

Lucas Center Facilities Initiatives

The new GE 750 3T magnet installed last year as a prototype has been upgraded early this year (2009) to production hardware, and is in full operation. The system has proven remarkably stable and robust and is in full use. We have added substantial infrastructure for research imaging experiments, most recently including a newly installed custom eyetracker. We continue to have weekly calls with GE engineering as part of our on-going research agreement for this system.

With stimulus money provided to the NIH by the American Recovery and Reinvestment Act, the NCRR issued an RFA for applications to renovate core research facilities. The Department was successful in achieving University permission to submit a grant (only 2 are allowed per institution) and is formulating plans to refurbish the Lucas Imaging Center. The 1.5T and 3T #1 magnets in Lucas are nearing end-of-life and need to be replaced in order to remain at the state of the art, and the proposal seeks to obtain up to $6M for siting the 2 new magnets as well as new gradient and electronics hardware for the 7T. We also plan to create new research staff space by taking advantage of smaller equipment footprints of modern instrumentation. The proposal is being written by Dr. Glover on behalf of the SOM's Dean Pizzo and is due in September 2009.

Kim Butts Pauly:

- Named Fellow of the ISMRM, continues service on Board of Trustees
- Promoted to Full Professor
- Jing Chen: graduated with PhD, now Associate Professor at the Institute of Biophysics in Beijing
- Sonal Josan: graduated with PhD, now postdoc at SRI
- Serena Wong: graduated with PhD, now scientist at Palo Alto Research Center

Gary Glover:

- Member, NIH NIBIB National Scientific Advisory Council
- ISMRM 2009 Outstanding Educator Award (one of 35 given)
- Jason Hsu graduated postdoc, now Assistant Prof. U. of Miami
- Chardonnay Vance, graduated PhD Biochemistry, entering Wake Forest Medical School, Fall, 2009
- Christine Law, graduated PhD EE, postdoc choice of 5 institutions not finalized.

Norbert Pelc:

- Scientific Advisory Board: Munich Center for Advanced Photonics
- AAPM Science Council
- Chair, NIH SBIB P(04) Study Section
- Sam Mazin, JP and Danyele Garnier Fellow, Stanford Summer Institute for Entrepreneurship
- Sam Mazin, Finalist, Kaufmann Fellowship
- Adam Wang, Finalist, Best Student Paper, 2009 SPIE Medical Imaging Conference

Rebecca Fahrig:

- 2009 Breathe California Columbo Award, directed research award in the area of early detection of lung cancer
- Grants awarded-
  - NIH R01 HL087917 C-arm CT for Guidance of Cardiac Interventions
  - R21 HL098683-01 Ultrafast Tomosynthesis for Guidance of Transbronchial Needle Biopsy
  - Arun Ganguly, NIH K99-R00 "Transition to Independence" career development grant

Michael Moseley:

- Editorial Boards: Journal of Magnetic Resonance Imaging (JMRI), Cerebrovascular Diseases (CD), Journal of Cerebral Blood Flow and Metabolism (JCBFM), International Journal of Stroke (IJS)
- Advisory Boards: Scientific Board of Advisors (Chair): University of Hawaii SNRP "New Clinical Specialized Neuroscience Research Program at the University of Hawaii" 1U54 NS056883
- Grant Reviews:
  - NIH study section member Acute Neural Injury/ Epilepsy (ANIE)
  - Four NIH ad hoc study sections, 3 as chair
  - Wellcome Trust
  - Department of Defense (DoD), San Francisco VA Medical Center
  - Review of DoD grants for the SFVAMC.
  - ISMRM "Pilot" General Grant Review Committee
  - Japan NIH (JST)- "ERATO",
- German Research Foundation
- New Grants Funded:
  - NIH 2 R01 NS 047607, Microvascular Measures of Perfusion in Stroke Recanalization
  - NIH RO1 (Zaharchuk, G), Quantifying Collateral Perfusion in Cerebrovascular Disease

MIPS Overview

Molecular Imaging Program at Stanford
Sanjiv S. Gambhir, MD, PhD
Director, Molecular Imaging Program at Stanford

The Molecular Imaging Program at Stanford (MIPS) (http://mips.stanford.edu) continues to experience significant growth. Many faculty within the Department of Radiology and from other Departments continue to help build the program. The faculty received several new grants from the NIH as well as from other agencies over the last year. We are now in the fifth year of the NCI-funded In vivo Cellular Molecular Imaging Center (ICMIC) P50 grant and in the fourth year of the NCI Center for Cancer Nanotechnology Excellence (CCNE) U54 grant. We are also in the fourth year of the NIH R25T training grant, Stanford Molecular Imaging Scholars (SMIS), to train the next generation of cancer molecular imaging post-doctoral scholars. A new NIH post-doctoral training grant (T32) for cardiovascular molecular imaging has just recruited its first year entering class. In addition, all labs continue to grow with many new students, post-doctoral fellows, and outstanding research staff joining the program.

Funding received last year from the Canary Foundation to develop a new center for early cancer detection is helping build bridges with many investigators on campus. Significantly increased funding from the Canary Foundation is expected with continued growth of the program. New off-campus space on California Avenue has recently opened for the effort in early cancer detection including facilities for blood/tissue based detection of disease. We are convinced that more investments are needed in the earlier detection of all disease, including cancer. The ability to detect disease earlier will allow much better potential for cure. This center will work on novel in vitro diagnostics (e.g., using patient blood samples) as well as new imaging strategies with high sensitivity to detect very low burden disease. It is hoped that in the next 3-5 years Stanford can become a world-leader in the important field of early cancer detection.

We continue to have several seminar series on campus to help educate scientists about molecular imaging. The molecular imaging seminar series (http://mips.stanford.edu/public/mi_seminar.adp) is now in its fifth year and has a large collection of videos available online of speakers from the last few years. This year we also initiated students presenting from different MIPS labs. The Nanobiotechnology seminar series (http://mips.stanford.edu/public/nanobiotech_seminar.adp), which focuses on new applications of nanotechnology to cancer, continues to draw attendance for faculty from all over campus. Several speakers from around the country have already presented in the series and all lectures are available on-line.

There are now 18 MIPS faculty who are full members of the program with many more associate members from all over campus. Many of the full members are from the Department of Radiology. The number of graduate students, MSTP students, post-doctoral fellows, research scientists, technicians, and administrative staff continues to grow and is currently approximately 150. We expect a significant growth over the next 2-3 years with the new center on early cancer detection and occupancy of the space on California Avenue.

Construction of a new Molecular Imaging/ Nuclear Medicine clinic is just beginning and is now expected to finish in late 2010. This new facility will consolidate all of the PET-CT and SPECT equipment with new radiochemistry facilities to be added. Newer cardiac and optical imaging equipment is also expected to be placed into this new clinic. We have also designed the clinic so that large animal imaging can be performed there. Research trials that combine state-of-art imaging with in vitro diagnostics (e.g., blood proteomics) should also be possible in this new facility.

We also continue to grow our industrial partnerships with key leaders in the molecular imaging community. Several projects to develop new imaging agents/strategies are underway with General Electric Global Research, General Electric Healthcare, as well as Bayer-Schering. A new relationship with Schering-Plough has just started. It is likely that additional industrial partners will enter into collaborative research relationships over the next several years. These will be key to help translate discoveries at Stanford to the patient bedside. Several faculty are also involved in new startup-company efforts with intellectual property from their laboratories at Stanford. These include new efforts in diagnostics, small animal imaging, and clinical imaging.

ISIS Overview

Information Sciences in Imaging at Stanford

Sandy Napel, PhD and Sylvia Plevritis, PhD
Co- Directors

Fig. 4:Bottom row: David Paik, Sylvia Plevritis, Sandy Napel, Daniel Rubin; 2nd row: Yongjun Ma, Jiajing Xu, Florian Schmitzberger; 3rd row; Konstantinos Sebekos, Jessica Faruque, Debra Frank; 4th row: Andrew Gentles, Peng Qiu, Maggie Bos, Frezghi Habte; 5th row: Aravindakshan Babu, Cesar, Santhosh Kasavajjala, Bao Do. Not shown: Hayit Greenspan, Jingyu Cui, Danny Korenblum, Ankit Gupta, Ray Lin, Nick Hughes, Emily Tsai.

ISIS ("Information Sciences in Imaging @ Stanford) was established last year and aims to gain new knowledge from imaging examinations by integrating and analyzing them with related clinical and molecular data. ISIS aims to achieve this goal by exploring the full spectrum of information-intensive activities in imaging (e.g., image management, storage, retrieval, processing, analysis, understanding, visualization, navigation, interpretation, reporting, and communications) and in non-imaging domains (e.g., pathology, molecular and genetic markers, family history, prior medical reports, and clinical outcomes). Critical to the ISIS mission is the development of a core capability to collect annotated imaging, clinical and molecular data, and to integrate them by creating databases and novel computational models that identify relationships among these data. Through these efforts, we believe that ISIS will improve the diagnostic and treatment planning value of images in uses such as diagnostic decision support, determination of best therapeutic options while minimizing the need for biopsy, and evaluation of response to therapy.

ISIS relies on is evolving database that is populated with annotated image data, as well as whatever additional information is available about the patients whose images are included. Examples of these additional data are clinical (e.g., gender, age, smoking history, results of laboratory tests, co-morbid conditions, response to treatment options), and molecular (as obtained from non-invasive means, and/or through tissue samples). Given such a database, one can imagine searching (or "mining") it for instances of cases that are similar in one or more ways to a particular patient currently being assessed. Examples of the questions that can be addressed are, "given the image features and clinical data for the current patient, What is the distribution of diagnostic possibilities and the probability of each?", "What is the likelihood that this patient has a certain molecular subtype and therefore might be a good responder to a certain drug?", or "What are other diagnostic tests that have been applied to similar patients that have narrowed down the diagnosis?" The magic of ISIS happens through novel computational algorithms that mine the information in the database to answer these and other questions.

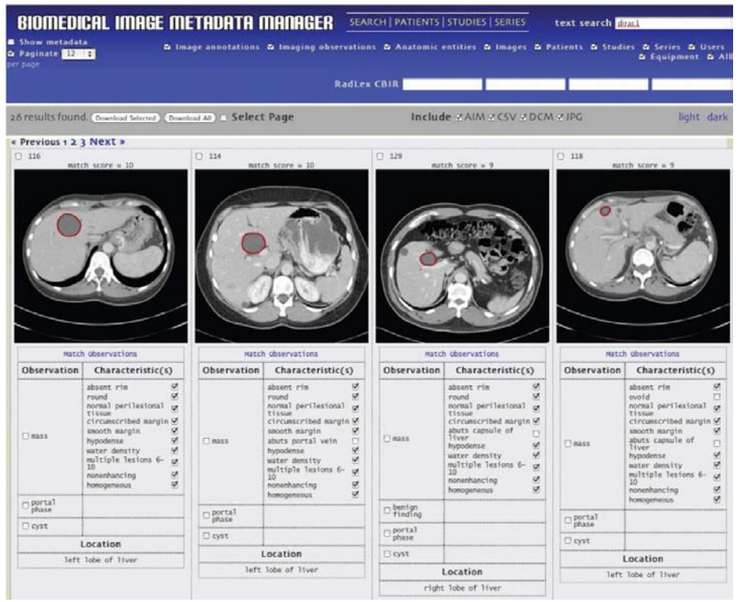

Fig. 1: Biomedical Image Data Manager (BIMM) collects and allows examination of relationships between annotated images. Using the leftmost image as a "query image," BIMM returned images in order of the percentage of semantic characteristics matched to those of the query image. Future enhancements will allow retrieval based on computationally-derived features and clinical data, and may contain additional information such as the molecular profile of lesions that were biopsied or resected

Specific anticipated results of the ISIS effort are: (1) an evidenced-based diagnostic decision support system, whereby patient-specific image, clinical and, if available, molecular data, can be compared to the database to suggest the most likely diagnoses, prognoses, and most relevant treatments, (2) biological discovery, i.e., synthesis and potential testing of hypotheses regarding the underlying biology in the development, progression and hopeful eradication of specific diseases, and (3) the translation of these developments into clinical practice using computers and image storage systems that are ubiquitous in healthcare enterprises today.

For ISIS to achieve its goals requires efforts on several fronts: (1) data collection and database building for specific imaging and disease scenarios, (2) software development for extracting features from images, (3) bioinformatics software development/application for data mining. This year we have made progress on all of these fronts.

We have explored the collection of data from several sources. Within Stanford we have developed collaborations with liver and thoracic surgeons and are presently exploring the availability of image and genomic data for retrospective analysis, as well as the potential to move forward to collect these data prospectively from new patients. Recognizing that large sources of these types of data may come from outside of Stanford, we have begun discussions with colleagues at the University of Michigan (lung and liver), Northwestern University (lung), University of British Columbia (lung), and Keio University in Japan (liver). We have also begun to build a retrospectively collected database of annotated images of liver lesions (>100 so far…) and have used this for developing our software tools and for generating preliminary results for several grant submissions.

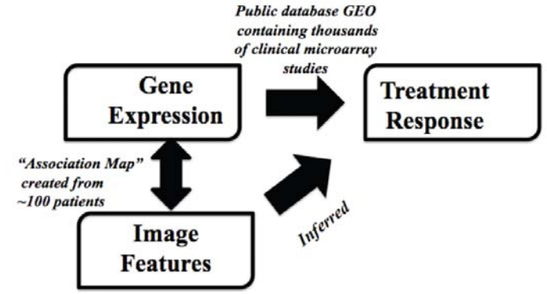

Fig 3: Imaging-genomics ISIS pipeline demonstrating how image features can be used to guide molecularly targeted therapeutics creating a map between imaging and genomic features and exploiting existing relationships between genomic features and treatment response.

We have made great progress in developing software tools for extracting image features. iPAD was developed to simplify the collection of semantic data from interpreting radiologists and is a great success both within our own program as well as its initial distribution to other institutions. BIMM is our prototype database and semantic feature mining software, and already allows the retrieval of similar images based on semantic annotations (Fig. 1). We have also developed several computational tools for automatic annotation of image features, including edge sharpness and internal texture, and are currently working on a boundary shape feature. Figure 2 shows an example of retrieval of similar images to query images based on computationally-derived features using a database of 30 liver lesions.

We have conceptualized a novel bioinformatics pipeline that may enable us to predict the likelihood of a patient's response to a molecularly targeted drug directly from imaging data. The basic idea is to capitalize on the vast amount of genomic data that already exist in the public domain in databases such as the Gene Expression Omnibus (GEO). As of 7/9/09, GEO contains over 12,000 microarray studies, of which 4,620 are related to treatment response, of which 1667 are clinical and 2953 are preclinical. There is no equivalent imaging database that relates image features to treatment response due to lack of standards in image acquisition and interpretation, and high cost. One way to circumvent this problem is to create an "association map" between image features and gene expression patterns from studies of 100 or so patients (Figure 3). By using the public domain data to then relate gene expression patterns to treatment response, we can generate a hypothesis on the relationship of imaging features to treatment response. The hypothesis would need to be validated in a clinical trial. We are in the process of testing this new bioinformatics pipeline on preliminary data.

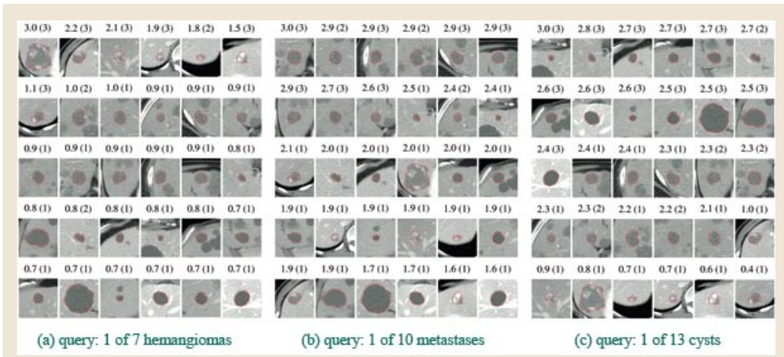

Fig. 2: Three examples of retrieval of similar images to a query image based on computer-generated features, from a database of 30 images of liver lesions. Query image is in upper left of each panel of 30 images, within which rankings go from highest on upper left to lowest on lower right. Numbers above each image, x (y), show x = algorithm's similarity score and y = similarity from a human-generated similarity reference standard, both on a scale of 1 to 3 with 3 best. Perfect retrieval would have all (3)s appearing before all (2)s appearing before all (1)s.

ISIS core faculty include Sandy Napel, Professor of Radiology and co-Director of the Radiology 3D Laboratory, Sylvia K. Plevritis, Associate Professor of Radiology, David S. Paik, Assistant Professor of Radiology, and Daniel L. Rubin, Assistant Professor of Radiology. ISIS also includes affiliate members; our first is Professor Robert J. Herfkens whose expertise will bridge ISIS to clinical imaging and information systems. We are also accumulating an array of very highly talented students and post-doctoral affiliates (Figure 4).

Centers of Excellence

The Stanford Department of Radiology is one of only two academic radiology departments in the United States with four NIH funded Centers of Excellence under the leadership of a single department (the MGH Department of Radiology also has this distinction). Our four Centers have contributed significant advances to improved health care, diagnosis, treatment, and monitoring for patients worldwide. In addition to technological, biochemical, and biological innovation in the imaging sciences, we have formally trained more than 500 individuals (including residents, fellows, postdocs, and graduate students) since our first center, the CAMRT, was established in 1995.

All four of our Centers of Excellence are currently in the process of competing for continued funding. Dr. Gary Glover submitted a competing renewal for the Center for Advanced Magnetic Resonance Technology in May of this year. This past June, Dr. Sylvia Plevritis submitted a competing renewal for the Center for Computational Modeling of Cancer Biology, which is currently a planning center competing for funding as a full Center. Dr. Sam Gambhir is preparing competing renewals for both the In Vivo Cellular and Molecular Imaging Center and the Center for Cancer Nanotechnology Excellence-Focused on Therapy Response. These two applications are due mid and late October this year.

The following text gives a short synopsis of each of these programs.

The National Center for Advanced Magnetic Resonance Technology at Stanford (CAMRT)

The CAMRT is now in its fifteenth year of operation as a National Research Resource, directed by Gary Glover, PhD, and funded by a grant from the NIH's National Center for Research Resources. This Resource has six core technology development areas that include reconstruction methods (Dwight Nishimura and John Pauly, EE Department, core directors), imaging of brain activation (Gary Glover, core director and PI), diffusion and perfusion weighted imaging methods (Mike Moseley, core director), imaging of cardiovascular structure and function (Brian Hargreaves, core director), spectroscopic imaging development (Dan Spielman, core director) and interventional MRI technique development (Kim Butts Pauly, core director). In addition to development of technology projects, the CAMRT provides support for collaborations and service use of the facilities, with users in the Radiology department as well as more than 75 faculty and more than 200 other users from at least 14 departments (http://rsl.stanford.edu/research/camrt.html).

The In Vivo Cellular and Molecular Imaging Center at Stanford (ICMIC)

The ICMIC, directed by Sam Gambhir, MD, PhD, brings together more than 50 faculty across the Stanford campus from 21 different departments, including the Department of Radiology. As only one of eight in vivo cellular and molecular imaging centers (ICMIC) in the country, the ICMIC studies disease by connecting preclinical models with clinical management through advances in multimodality molecular imaging. This molecular imaging program benefits from the highly regarded infrastructure provided by the CAMRT and RSL in the Richard M. Lucas Center for Imaging (http://mips.stanford.edu/public/grants/icmic/).

The Center for Cancer Nanotechnology Excellence-Focused on Therapy Response (CCNE-TR)

Stanford Radiology is one of eight institutions in the nation supported by NIH to develop a major nanotechnology center: the Center for Cancer Nanotechnology Excellence Focused on Therapy Response (CCNE-TR). This center, established in 2006 and led by Sam Gambhir, MD, PhD, includes scientists from Stanford and from five other sites across the country. The goal of this center is to use nanotechnology for the benefit of cancer patient management. The CCNE greatly expands our collaborative efforts, and we now work with an additional 35 faculty in more than 20 departments here at Stanford and across the country (http://mips.stanford.edu/public/grants/ccne/). Please see page 17 for more details of the CCNE program (http://mips.stanford.edu/public/grants/ccne/).

Center for Computational Modeling of Cancer Biology, an Integrative Cancer Biology Program (ICBP)

The Center for Computational Modeling of Cancer Biology, led by Sylvia Plevritis, PhD, consists of 9 academic faculty across 8 departments bridging the Schools of Medicine and Engineering. It is one of nine academic centers nation-wide, funded by the NIH/NCI Integrative Cancer Biology Program initiative, which promotes the analysis of cancer as a complex biological system. The goal for the Stanford Center is to develop and apply the computational tools that identify molecular networks implicated in cancer progression, and thereby aid in the discovery of early detection markers and therapeutic targets (http://icbp.stanford.edu/).

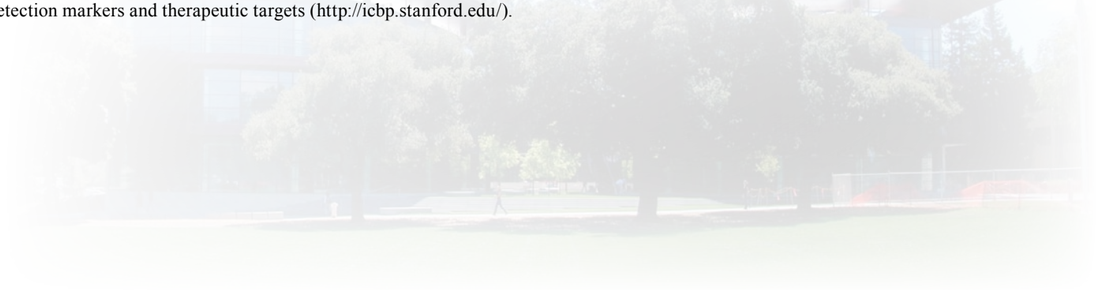

New Initiatives

The Aging Brain and Cognitive Disorders

The Center for the Aging Brain and Cognitive Disorders is a new collaboration among the Radiology, Neurology, Psychiatry, and Psychology Departments at Stanford. Dr. Brian Rutt, who has recently joined the Radiology Department and the Lucas Center faculty, will, in collaboration with Dr. Scott Atlas, lead the development of core MRI technologies and applications underlying this effort. This new collaboration is supported by generous funding from the Richard M. Lucas Foundation, which forms a multidisciplinary center-of-excellence that will focus on the aging brain, Alzheimer's disease, dementias, neurodegenerative disease, psychiatric disorders, and screening for preclinical cognitive decline. We will investigate and develop new diagnostic tools and therapies to care for patients with cognitive disorders. MR neuroimaging, especially at high field (7T), will play a large role in the development of this initiative.

Center for Biomedical Imaging at Stanford (CBIS)

The strategic Center for Biomedical Imaging at Stanford (CBIS), sponsored by Dean Pizzo and the School of Medicine, provides educational and networking opportunities in biomedical imaging, emphasizes applied biomedical imaging, and identifies imaging resources to enable the development of innovative imaging methods. In July 2009, the Center was pleased to award seed funding to seven academic scientists from a number of schools and departments across the Stanford campus. Closely following the seed funding recipients, the Center held its first Annual Symposium, August 21, 2009, at the Hewlett Teaching Center. See page 18 and the Center website for more details about the seed funding recipients and the successful First Annual Symposium (http://cbis.stanford.edu/).

Canary Center for Cancer Early Detection at Stanford

The Canary Center for Cancer Early Detection at Stanford is supported by an alliance between the Canary Foundation and the Stanford Department of Radiology and located in a new off-campus facility of more than 10,000 square feet. The Canary Center open house and ribbon-cutting ceremony took place June 10, 2009 at the 1501 California Avenue location. The mission of the Canary Center, which occupies ~30,000 square feet of the building, is to house and foster research programs leading to the development of blood and imaging tests for early cancer detection. Led by Sam Gambhir, MD, PhD, the Center will develop simple blood and imaging tests to predict the likelihood of disease; detect the presence of disease; plan and monitor therapy; and predict and monitor the progression and recurrence of disease. The Center's efforts will catalyze the work of early disease detection and intervention by creating synergies within the Department of Radiology, across campus, and outside of Stanford. See page 16 for additional details of the Canary Center at Stanford.

Information Sciences in Imaging at Stanford (ISIS)

The vision of ISIS, co-directed by Sandy Napel PhD and Sylvia Plevritis PhD, is to vastly increase the information derived from imaging data by discovering relationships amongst imaging features, molecular markers, pathological and laboratory reports, and patient outcomes. At the heart of the ISIS discovery process is a new database of annotated images and new software mining tools for finding new associations between imaging and non-imaging data. The new knowledge derived from ISIS will lead to higher levels of decision support in disease management, encompassing detection, diagnosis, treatment and surveillance, as well as reveal new underlying biological meaning of imaging features. See pages 12-13 for details.

High Field Magnetic Resonance Program

This initiative, led by Brian Rutt, PhD, has made significant progress this year. Dr. Rutt has spent his first few months developing collaborations, gaining a full understanding of available resources, and identifying ways in which High Field MR can strategically bridge not only the different sections within Radiology but also with other groups across the Stanford campus. Since Dr. Rutt's arrival in early 2009, he has begun to establish a research group, submitted two NIH grants (RC1 and S10) and one Alzheimers Association grant as PI, and is a collaborator on five additional NIH grants as well as two industry grants. Dr. Rutt is also establishing a new MRI instrumentation/technology development lab at the Canary Center on California Avenue, for which an Open House and Ribbon Cutting ceremony was held in June, 2009. The High Field MR Initiative will also drive our Aging Brain Initiative; we anticipate that these two initiatives will mature at a similar rate of success.

Advanced New Initiatives

The Canary Center for Cancer Early Detection at Stanford

Sanjiv Sam Gambhir, MD, PhD, Director
Bonnie King, PhD, Deput.y Director

The Canary Center for Cancer Early Detection at Stanford officially opened in June, 2009, with a ribbon cutting ceremony and open house on the front lawn of the newly-leased facility located at 1501 California Avenue. President Hennesey and Dean Pizzo along with the head of the cancer center (Dr. Beverly Mitchell) were there to help open the center. The mission of the Canary Center, which occupies ~30,000 square feet of the building, is to house and foster research programs leading to the development of blood and imaging tests for early cancer detection. The center represents a novel alliance between the Canary Foundation, the Department of Radiology, the Cancer Center, and the School of Medicine. Additional alliances with the Schools of Engineering and Humanities & Sciences are also planned.

Canary Center Open House, June 11, 2009: It's official! Stanford President John Hennessey, Radiology Chairman Gary Glazer, Canary Foundation CEO Don Listwin, Canary Center Director Sam Gambhir, Medical School Dean Phil Pizzo, and Cancer Center Director Bev Mitchell cutting the ribbon.

The Canary Center mission is based on the striking association between early cancer diagnosis and improved survival rates. The chances of survival are far greater when cancer is detected in the earliest stages, while still localized to the organ of origin and amenable to treatment. To optimize the detection of cancer at this stage, the center is taking a sequential approach to 1) identify blood biomarkers that can be detected by simple blood screening tests, and 2) develop molecular imaging tests to confirm and localize early lesions. The extraordinary technical challenges associated with this dual strategy include the refinement of molecular imaging agents to specifically detect pre-invasive malignant tumors the size of a lentil (< 5-10 mm). They also include the development of proteomic approaches that can reliably detect minute (ng/ml) quantities of cancer-specific proteins released into the bloodstream by these small tumors. Cost-effective solutions are expected by applying a relatively cheap blood test followed by a more expensive imaging study, although in some cases the blood test and the imaging test will be performed concurrently. Having both approaches will also likely lead to a greater overall accuracy.

Canary Center for Cancer Early Detection at Stanford

To accomplish these goals, the center was specifically designed to house state-of-the-art core facilities and collaborative research programs in molecular imaging, proteomics, chemistry, and bioinformatics. The proteomics facility houses cutting-edge mass spectrometry platforms dedicated to the discovery and validation of blood protein biomarkers. The chemistry core will enable the specific design and refinement of molecular imaging agents for early detection, which will undergo preclinical testing using in vivo and ex vivo model systems, including patient blood and tissue samples. These collaborative research efforts will be unified through coordinated bioinformatics platforms to track specimens, and facilitate the exchange and analysis of data. Canary Center research programs will actively interface with other facilities and programs on campus, including MIPS and CCNE-TR in order to leverage the latest developments in molecular imaging and nanotechnology into the early detection effort. Collectively, these initiatives have extensive links to the Cancer Center at Stanford, forming a direct pipeline for the translation of early cancer detection into clinical trials and practice.

A specific example of a novel molecular imaging strategy that is expected to help the goal of early cancer detection is ultrasound with targeted microbubbles. These gas filled microbubbles can be chemically coupled to targeting ligands that allow the bubbles to bind to tumor vasculature. This will allow molecular imaging using a conventional anatomical imaging strategy (ultrasound). This is expected to allow detection of tumors in the 3-5 mm range. A clinical trial using the targeted microbubbles for ovarian cancer detection are planned. A specific example of a novel strategy being pursued for blood biomarker detection is based on magnetonanoarrays being developed as part of the Stanford CCNE-TR. This novel technology is allowing the detection of many different biomarkers at levels that are 10-100 fold better than the most sensitive ELISA tests currently available. Many exciting new developments for early cancer detection are on the horizon and will be pioneered by this center.

Building up the center over the past year kept us busy designing and implementing building renovations, recruiting core personnel to fill the positions of Deputy Director, Proteomics Core Facility Director, Administrative Associate, and Grants Specialist, getting squared away with regulatory permits, populating our cores and labs with an initial round of scientific equipment, and initiating our first studies. As we head into the upcoming year, our goals include recruiting several new faculty members in the areas of in vitro and in vivo diagnostics, hiring a Chemistry Core Director, and setting the wheels in motion to attract federal funding (http://canarycenter.stanford.edu).

The Center for Cancer Nanotechnology Excellence-Focused on Therapy Response

Sanjiv Sam Gambhir, MD, PhD, Director
Bonnie King, PhD, Deput.y Director
Demir Akin, DVM, PhD, Deputy Director

Nanotechnology has the potential to impact cancer patient management profoundly in the coming years due to its capacity to provide enormous sensitivity, throughput, and flexibility. At CCNE-TR, we believe that nanoscience applied to cancer research is critical to the future of eliminating cancer and are convinced that nanotechnology will make a significant impact on cancer diagnosis and management in potentially revolutionary ways. Ex vivo diagnostics used in conjunction with in vivo diagnostics can markedly impact future cancer patient management by providing a synergy that neither strategy alone can offer. Nanotechnology can significantly advance both ex vivo diagnostics through proteomic nanosensors and in vivo diagnostics through nanoparticles for molecular imaging. Yet, there is still much work to be done because clinical tools have not been developed that can help oncologists reliably to predict which patient will respond to a specific anti-cancer therapy regimen and to monitor patient response while undergoing a given therapy. Without these tools, many patients must endure multiple therapies until a successful therapeutic regime can be identified. If methods could be developed that would allow accurate prediction and assessment of a given individual's response to therapy, then, marked improvements in cancer management would likely occur. Our goal at CCNE-TR is to address this unmet urgent need by developing and validating clinical translational nanotechnology platforms so that we will eventually be able to predict which patients will likely respond to a specific anti-cancer therapy and to monitor their response to therapy. Our vision is that eventually patients will have their tumors biopsied and blood samples drawn for protein profiling by ex vivo nanosensors to predict their response to a given therapy. In addition, they will also be imaged by a ring scanner with molecular imaging probes of different types to predict their response. Post-treatment and potentially during treatment, patient response will be evaluated by blood analysis, usually without another biopsy and molecular imaging to ensure the accurate differentiation of responders from non-responders. To achieve this clinical potential, we are currently developing nanosensors for ex vivo protein analysis and nanoparticles for in vivo molecular imaging, thereby combining the advantages of both major strategies, and also testing and validating these in small animal models. Our unique nanoplatforms, such as magneto-nanosensors, carbon nanotube sensors, and Raman nanosensors, are allowing us the investigation of proteins from tissue and blood from pre- and post-treatment cancer patients to predict which patients will most likely respond or are responding to specific anti-cancer therapies. Our newly developed nanoparticles also have the potential to benefit intraoperative staging and to aid in the early diagnosis of cancer. Furthermore, these discoveries are leading to new methods of testing drug efficacy in small animal cancer models, thereby accelerating the process of bringing improved drugs to the clinic.

At CCNE-TR, we are highly optimistic that our research will help bring nanotechnology into the routine arsenal of cancer biologists and oncologists for improved cancer patient management.

Advanced New Initiatives

The Center for Biomedical Imaging at Stanford

Norbert Pelc, ScD, Co-Director
Hans Ringertz, MD, PhD, Co-Director
Susan Kopiwoda, MS, MPH, Program Manager

The Center for Biomedical Imaging at Stanford (CBIS), supported by the Dean's office in the School of Medicine and co-led by Drs. Hans Ringertz and Norbert Pelc, aims to provide educational and networking opportunities for all groups on campus that use or have an interest in biomedical imaging applications. The educational and networking goals of CBIS include increasing knowledge in biomedical imaging; improving access to imaging resources; and facilitating translational research in accordance with the SOM Translating Discoveries plan. During 2009, the CBIS followed its primary goals of educating and facilitating research by awarding seed grant funding and holding its first Annual Symposium.

This year we had 36 applications representing a wide array of imaging approaches, modalities, and scales with applications from schools and departments across the Stanford campus. On August 7, 2009, the CBIS Advisory Board was pleased to announce the awards from this first round of seed funding. The following projects were selected for their innovative, interdisciplinary, and translational potential. CBIS leadership plans a second round of funding spring/summer, 2010.

Name	Department	Title of Project
Kim Butts Pauly, PhD	Radiology	MR-guided Neuromodulation with Focused Ultrasound
Jennifer Cochran, PhD	Bioengineering	Novel Small Molecule-peptide Conjugates for Imaging Carbonic Anhydrase IX Expression in Living Subjects
William Moerner, PhD	Chemistry	Red for STED: Advanced Optical Microscope Development for Superresolution Imaging of Biological Structures
Andrew Olson, PhD	Stanford Institute for Neuro-Innovation & Translational Neurosciences (SINTN)	Neuroscience Microscopy Service 3D Image Analysis Resource
Yuzuru Takashima, PhD	EE	Development of High Throughput and High Resolution NSOM Probe
Philip Yang, MD	Medicine	Molecular MRI for Differentiation, Imaging, and Selection of Cardiac Progenitor Cells
Guy Ziv, PhD	Biochemistry	Studying Actin-based Motility in 3D Using Light-field Microscopy

The first CBIS Annual Symposium, held on August 31st. was largely organized by a group of trainees. We hope that the CBIS Symposium will grow to be a major student-led event on campus, providing a forum for an exchange of ideas across the spectrum of biomedical imaging. For this year's symposium, the organizing committee with help from Susan Kopiwoda and the Advisory Board recruited dozens of abstract submissions from Stanford trainees and built a program including oral and poster presentations. Dean Philip Pizzo, MD, graciously opened the program by describing the School of Medicine's Translating Discoveries Program, which encompasses CBIS (http://cbis.stanford.edu/about/td/index.html). Keynote speaker for the symposium, Jeff Lichtman, MD, Professor of Molecular and Cellular Biology from Harvard University, spoke about his interests in "Connectomics" and the study of synaptic rearrangement and efficacy in muscle tissue. Invited Stanford faculty speakers included Helen Blau, PhD (Stem Cell Imaging in Regenerative Medicine); Chris Contag, PhD (Miniaturized Microscopes); and Sandy Napel, PhD (Content-based Retrieval for Radiological Decision Support). Along with the faculty talks, there were six additional presentations given by postdoctoral scholars and graduate students and a very lively poster presentation session.

During the daylong symposium, Advisory Board members and Dr. Jeff Lichtman scored and selected the best talk among the six postdoc/graduate student presentations and the best poster among the 22 posters submitted. The following two individuals were selected as first prize winners in each category

1st Place award for Best Talk presented by a postdoc or graduate student:
Jonathan Liu, PhD, Department of Pediatrics

"Molecular Image-guided Brain Tumor Resection with Miniature Optical-sectioning Microscopy"

1st Place award for Best Poster presented by a postdoc or graduate student:
Lena Kaye, BS, Department of Radiology (RSL)

"Tissue Displacement Mapping with MR-ARFI"

Please visit the CBIS website for more information about CBIS and Translating Discoveries (http://med.stanford.edu/cbis/). Plans have already begun for the 2010 seed funding program and the Second Annual CBIS Symposium. Look for announcements for both programs beginning in early 2010. We hope to hold the second annual CBIS Symposium during May, 2010.

Research Faculty and Personnel

Radiology Research Faculty, Staff, and Students

Faculty & Staff

Faculty

Roland Bammer, PhD
Sandip Biswal, MD
Kim Butts Pauly, PhD
Xiaoyuan Chen, PhD
Zhen Cheng, PhD
Rebecca Fahrig, PhD
Sanjiv Sam Gambhir, MD, PhD
Gary M. Glazer, MD
Gary H. Glover, PhD
Samira Guccione, PhD
Brian Hargreaves, PhD
Robert J. Herfkens, MD
Craig Levin, PhD
Michael E. Moseley, PhD
Sandy Napel, PhD
David Paik, PhD
Norbert J. Pelc, ScD
Sylvia K. Plevritis, PhD
Andy Quon, MD
Paulmurugan Ramasamy, PhD
Jianghong Rao, PhD
Daniel Rubin, MD
Brian Rutt, PhD
Daniel M. Spielman, PhD
Juergen Willmann, MD
Joseph Wu, MD, PhD
Greg Zaharchuk, MD, PhD

Administrative & Support Staff

Karen Aguilar
Mary Bobel, MA, MBA
Maggie Bos
Michelle Christierson
Bonita Crabbe
Donna Cronister
Lin Davis
Debra Frank
Elizabeth Gill
Sofia Gonzales, MS
Sondra Horn
Mandeep Kaur, BA
Susan Kopiwoda, MS, MPH
Marlys Lesene
John Mendoza
Amy Morris, BA
Teresa Newton, BA
Donna Nierberger, RN
Kala Raman, MS
John Reuling
Patricia Riley
Lanzie Rivera
Billie Robles, BS
Julie Ruiz, PhD
David Russel
Monique Schareck, MHA
Susan Singh
Susie Spielman
Jean Stevens
Lakeesha Winston
Wei Xiong

Scientific Staff

Demir Akin, DVM, PhD
Marcus Alley, PhD
Priti Balchandani, PhD
Sanjiv Bhandari, MS
Wendy Baumgardner, RVT, LATg
Rhona Berganos, BS
Sunil Bodapati
Thomas Brosnan, PhD
Carmel Chan, PhD
Edwin Chang, PhD
Danye Cheng
Frederick Chin, PhD
Garry Chinn, PhD
David Dick, PhD
Aloma D'Souza, PhD
Aihua Fu, PhD
Arundhuti Ganguly, PhD
Andrew Gentles, PhD
Gayatri Gowrishankar, PhD
Frezghi Habte, PhD
Pam Hertz, RVT
Samantha Holdsworth, PhD
Fangjun Jia
William Johnsen, RT (CVI)
Richard Kimura, PhD
Bonnie King, PhD
Keshni Kumar, CRT
Andrew Lamb
Jelena Levi, PhD
Amelie Lutz, MD
Dirk Mayer, PhD
Sam Mazin, PhD
George Mendoza
Mohammed Namavari, PhD
Arutselvan Natarajan, PhD, DVM
Linda Novello, RT (MRI)
Rafael O'Halloran, PhD
Laura Pierce, MPA, RT (CT)
Laura Pisani, PhD
Sam Quezada, MBA
Kala Raman, MS
Paulmurgan Ramasamy, PhD
Robert Reeves, MA
Viola Rieke, PhD
Sandra Rodriguez, RT (R)(MR)
Jarrett Rosenberg, PhD
Ataya Sathirachinda
Anne Marie Sawyer, BS, RT (R)(MR)
Greig Scott, PhD
Stefan Skare, PhD
Marc Sofilos, RT
Mark Stolowitz, PhD
Matus Straka, PhD
Murugesan Subbarayan, PhD
Martin Tall. MS
Robert Teed
Shannon Walters, (CT)
Sen Wang, PhD
Nancy Ware, RT (CT)
Ron Watkins
Shahriar Yaghoubi, PhD
Xinrui Yan, PhD
Sung-Won Yoon, PhD

Our group photo represents approximately half of the 211 Radiology research personnel found in various locations on the medical school campus.

Trainees

Post Doctoral Fellows

Priti Balchandani, PhD
Deepak Behera, PhD
Kai Chen, PhD
Constantin Dragos, PhD
Ben Cosgrove, PhD
Moses Darpolor, PhD
Nirupama Deshpande, PhD
Anca Dragulescu-Andrasi, PhD
Kira Foygel, PhD
Hewei Gao, PhD
Sarah Geneser, PhD
Zhumur Ghosh, PhD
Will Grissom, PhD
Meng Gu, PhD
Benjamin Hackel, PhD
Aileen Hoehne, Phd
Sharon Hori, PhD
Shijun Hu, PhD
Mei Huang, PhD
Nicholas Hughes, PhD
Michelle James, PhD
Jesse Jokerst, PhD
Sonal Josan, PhD
Brian Kim, MD
Sri-Rajasekhar Kothapali, PhD
Feng Lan, PhD
Joo Hyun Lee, PhD
Zongjin Li, PhD
Zhe Liu, PhD
Zheng Miao, PhD
Hua Fan-Minogue, PhD
Kazim Narsinh, PhD
Gang Niu, PhD
Natesh Parashurama, MD, PhD
Kyeongsoon Park, PhD
Peng Qiu, PhD
Hao Peng, PhD
Jennifer Prescher, PhD
MaryBeth Pysz, PhD
Rebecca Rakow-Penner, PhD
Gang Ren, PhD, MD
Hongjun Ren, PhD
Ying Ren, PhD
John Ronald, PhD
Laura Sasportas, PhD
Bin Shen, PhD
Bryan Smith, PhD
Virginia Spanoudaki, PhD
Ning Sun, PhD
Kyung Sung, PhD
Moriah Thomason, PhD
Alessia Tognolini, MD
Stephanie van de Ven, MD
Arne Vandenbroucke, PhD
Hui Wang, PhD
Pauline Worters, PhD
Yun Wu, PhD
Zuyong Xia, PhD
Yung Xing, PhD
Tao Xu, PhD
Grace Tye, MD
Cristina Zavaleta, Ph.D.
Keren Ziv, PhD

Graduate Students

Murat Aksoy, MS
Jongduk Baek, MS
Catie Chang, MS
Jingyu Cui, MS
Adam de la Zerda, MSc
Jessica Faruque, MS
Erin Girard-Hughes, MS
Kristin Granlund, MS
Alex Grant
Yi Gu, MS
Ankit Gupta
Misung Han, MS
Andrew Holbrook, MS
Scott Hsish
Caroline Jordan, MS
Elena Kaye, MS
Hojin Kim
Kranthi Kode, BS
Danny Korenblum
Frances Lau, MS
Christine Law, MS
Andrew Lee, BS
Prasheel Lillaney, MS
Ray Lin, MS
Peter Olcott, MS
Jeremy Pearl, BS
Guillem Pratx, MS
Julia Rasooly, BS
Paul Reynolds, MS
Jesse Rodriguez
Debashis Sahoo, MS
Heiko Schmiedeskamp, MS
Florian Schmitzberger
Harpeet Singh
Jared Starman, MS
Ernesto Staroswiecki. MS
Emily Tsai, BS
Adam Wang, MS
Kitch Wilson, MD
Jiajing Xu
David Yerushalmi, MS
Jinjian Zhai
Jian Zheng, MS

Visitors

Visiting Researchers & Scholars

Cheol-Hee Ahn, PhD
Byeong-Cheol Ben Ahn, MD, PhD
Colin Carpenter
Ya-Fang Chang, PhD
Hadassa Degani, PhD
Sjoerd Elias, MD, PhD
Andreas Fieselmann
Hayit Greenspan
Joachim Hornegger, PhD
Sun Kim, PhD
Daniel Kopenigg, PhD
Yongjun Ma
Tarik Massoud, PhD
Christine Niebler
Carsten Nielsen, MSc
Catherine Planey
Emilio Sacristan
Konstantinos Sebekos
Monica Sigovan
Ron Summer, PhD
Avnesh Thakor, PhD
Zhengming Xiong, MD, PhD
Zianzhong Zhang, PhD
Kurt Zinn, PhD

Welcome New Research Faculty

Ramasamy Paulmurugan, PhD

Assistant Professor of Radiology
Molecular Imaging Program at Stanford (MIPS)

Ramasamy Paulmurugan, PhD, Assistant Professor of Radiology in the Molecular Imaging Program at Stanford (MIPS), trained in molecular imaging at UCLA and joined the MIPS program in 2003 as research scientist. The reporter protein-fragment assisted complementation strategy developed by Dr. Paulmurugan has made it possible to image protein-protein interactions, the heart of signal transductions, and important therapeutic targets in cells at different pathological conditions, for the first time in living animals. His research mainly focuses on the use of complementation strategies for studying the biology of breast cancer including tamoxifen resistance in estrogen receptor (ER) positive breast cancer, tissue specific action of ER in response to different ER-ligands and the collaborative role of ER-sub types (a/b) in regulating the ER-pathway. He will also focus on developing high affinity ER-ligands for the early diagnosis of ER-positive breast cancers.

Welcome Senior Scientists

Amelie Lutz, MD

Clinical Instructor/Research Scientist in Radiology
Molecular Imaging Program at Stanford (MIPS)

Amelie M. Lutz, MD, PD, Clinical Instructor and Research Scientist, Department of Radiology recently joined our department following a research fellowship in molecular imaging. After completing medical school and internship in Internal Medicine/Endocrinology at the Albert-Ludwigs-University in Freiburg, Germany, Dr. Lutz did her residency in Diagnostic Radiology at the University Hospital in Zurich, Switzerland and a fellowship in Body Imaging/Musculoskeletal Imaging at the Kantonal Hospital in Frauenfeld, Switzerland. In 2008 she received the venia legendi (member of the academic faculty, PD) in Diagnostic Radiology at the University of Zurich. Her research interests include the development of novel diagnostic strategies for early detection of cancer, especially of ovarian cancer. She is currently working on preclinical and translational studies including multimodality strategies using blood biomarker tests and imaging for ovarian cancer early detection as well as the development of novel PET probes for cancer staging.

Arutselvan Natarajan, PhD

Instructor of Radiology
Molecular Imaging Program at Stanford (MIPS)

Arutselvan Natarajan, PhD, recently joined the Molecular Imaging Program at Stanford (MIPS) as an Instructor in the Department of Radiology. Dr. Natarajan completed his PhD in biological/industrial chemistry at the Alagappa University Karaikudi, India. After completion of his PhD he became a Research Associate in a CSIR lab, in India. Subsequently, he joined the University of California Davis as an advanced postdoctoral fellow in the Radiodiagnosis and Therapy section in the School of Medicine. In 2005, he was promoted to Assistant Research Professor in UC Davis Medical Center. At UC Davis, his research focus was the development of GMP grade radiopharmaceutical doses for the NCI sponsored clinical trials for human cancer patients, using antibody, antibody fragments, small molecules, peptides, and selective high affinity ligands for multi modality cancer imaging and therapy. His current research focus at Stanford is the development of antibody based imaging agents, clinical translational science for human patient studies, and early diagnosis of cancer using protein biomarkers, miRNA, and nanotechnology.

Welcome Senior Scientists

Mark Stolowitz, PhD

Science and Engineering Associate
Director of the Proteomics Core Facility
Canary Center for Cancer Early Detection

Mark L. Stolowitz, PhD, is the Director of the Proteomics Core Facility in the Canary Center for Cancer Early Detection at Stanford. A seasoned technical professional with over 25 years experience involving conceptualization and development of life sciences research tools, his efforts are recently focused on the development of an immunoaffinity mass spectrometry platform for biomarker verification. This technology will be exploited by the Canary Center at Stanford to develop a high throughput biomarker verification platform. A prolific innovator, Dr. Stolowitz has been issued 43 United States Patents related to bioconjugation, SPR biosensors, protein biochips, protein and nucleic acid immobilization, protein chromatography, and protein sequencing.

Welcome Scientific Staff

Sanjiv Bhandari, MS - Programmer and Web Page Designer for Radiological Sciences Lab, Lucas Center, Radiology

Edwin Chang, PhD - Research Associate, Molecular Imaging Program at Stanford

Samantha Holdsworth, PhD - Research Associate, Radiological Sciences Lab, Lucas Center, Radiology

Richard Kimura, PhD - Research Associate, Molecular Imaging Program at Stanford

Jelena Levi, PhD - Research Associate, Molecular Imaging Program at Stanford

George Montoya - Research Assistant, Molecular Imaging Program at Stanford

Rafael O'Halloran, PhD - Research Associate, Molecular Imaging Program at Stanford

New Administrative Support Staff

Patricia Riley joined the Department in May of 2009 and works with Zhen Cheng, PhD and Fred Chin, PhD. Pat's office is located in the Lucas Center Expansion building.

Jean Stevens joined the Radiology Department in March, 2009 and has been involved in the start up of the Canary Center for Cancer Early Detection at Stanford. Her office is located at the California Avenue site.

Faculty and Staff Awards

Recipient	Award
Marcus Alley, PhD; Garry Gold, MD; Robert Herfkens, MD; Michael Lustig, PhD; John Pauly, PhD; Shreyas Vasanawala, MD, PhD	SCBT/MR 2009 Lauterbur Award for research project “Faster Pediatric MRI with Compressed Sensing.”
Scott Atlas, MD	2008 Homecoming Comeback Guest, University of Illinois
Roland Bammer, PhD	Fellow, Freiburg Institute of Advanced Studies (FRIAS), University of Feiburg, Germany. Fellowship, German Science Foundation.
Neal Bangerter, PhD; Garry Gold, MD; Brian Hargreaves, PhD; Seungbum Koo, PhD; Ernesto Staroswiecki, PhD; Ronald Watkins.	SCBT/MR Cum Laude Award for project "Early Detection of Osteoarthritis in Patients with ACL Injury Using Sodium MRI."
Kim Butts Pauly, PhD	Named Fellow of the ISMRM, 2009.
Kim Butts Pauly, PhD	Promoted to Full Professor, 2009.
Rebecca Fahrig, PhD	2009 Breathe California Columbo Award for her tomosynthesis work in early detection of lung cancer.
Sanjiv Sam Gambhir, MD, PhD	Elected as member of the Institute of Medicine of the National Academies.
Gary Glover, PhD	ISMRM 2009 Outstanding Educator Award (one of 35 given internationally)
Gary Glover, PhD	Member, NIH NIBIB National Scientific Advisory Council
Gary Glazer, MD	RSNA 2009 Gold Medal Award - The Society’s highest honor given for Dr. Glazer’s exemplary service to the science of radiology.
Brian Hargreaves, PhD	SCBT/MR Cum Laude Award, Society of Computed Body Tomography and Magnetic Resonance. In vivo sodium MRI at 3.0T of patients with previous ACL injury
Andrei Iagaru, MD	SNM Alavi-Mandell Award for paper "90Y-Ibritumomab Therapy in Refractory Non-Hodgkin's Lymphoma: Observations from 111In-Ibritumomab Pretreatment Imaging."
Andrei Iagaru, MD, PhD; Erik Mittra, MD, PhD; Michael Goris, MD, PhD	2009 Society of Nuclear Medicine Image of the Year Award
Debra Ikeda, MD	Honorary Membership, Royal College of Radiology Breast Group, King's College Hospital, London
William Kuo, MD	Featured Manuscript - American College of Radiology (ACR)/Reuters National Press Release.
William Kuo, MD	Society of Interventional Radiology (SIR) Leadership Academy
Craig Levin, MD; Angela Foudray, PhD ; Frezghi Habte, PhD	"Impact of high energy resolution detectors on the performance of a PET system dedicated to breast cancer imaging." One of top 10 papers published in Physica Medica.
John MacKenzie, MD	Board Certification (CAQ) in Pediatric Radiology, November 2008.
Sam Mazin, PhD	Kauffman Entrepreneur Postdoctoral Fellowship
Sam Mazin, PhD	JP and Danyele Garnier Fellow, Stanford Summer Institute for Entrepreneurship
Michael Moseley, PhD	Member of NIH Study Section (ANIE), 4 ad hoc Study Sections and grant reviewer for many other organizations including DoD, SFVAMC, ISMRM, Japan NIH, German Research Fd.
Michael Moseley, PhD	Lifetime member of the Society of Magnetic Resonance Technologists (SMRT)
Norbert Pelc, PhD	Chair, NIH SBIB P(04) Study Section and AAPM Science Council
Norbert Pelc, PhD	Scientific Advisory Board: Munich Center for Advanced Photonics

NOTE: Please see pages 198-204 for Funded Research Awards (Sponsored Projects) and pages 30 and 31 for Trainee Awards.

Recipient	Award
Daniel Rubin, MD, MS	RSNA Cum Laude Award, exhibit "'Saying It in Pictures': Annotation and Image Markup in Radiology."
Daniel Rubin, MD, MS; Flanders; Kim; Kahn; Siddiqui	Ontology-Assisted Analysis of Web Queries to Determine the Knowledge Radiologists Seek. Top Paper Selected at the SIIM Annual Meeting.
Geoffrey Rubin, MD	2008 "Minnie" as the "Most Effective Radiology Educator"
Brian Rutt, PhD.	Election to Fellow of the American Institute for Medical and Biological Engineering (AIMBE)
Juergen Willmann, MD	Walter Friedrich Award for outstanding research in the field of radiology, German Society of Radiology, Berlin
Juergen Willmann, MD	2008 RSNA Research Award in the category of "Molecular Imaging;" 2009 Phillip H. Meyers, MD, Research Award.
Juergen Willmann, MD	2008 Editor's Recognition Award with Distinction given by the Journal Radiology
Joseph Wu, MD, PhD	2009 Douglas P. Zipes Distinguished Young Scientist Award from the American College of Cariology (ACCR)
Joseph Wu, MD, PhD	Parmley Prize, outstanding paper awarded by the Journal American College of Cardiology

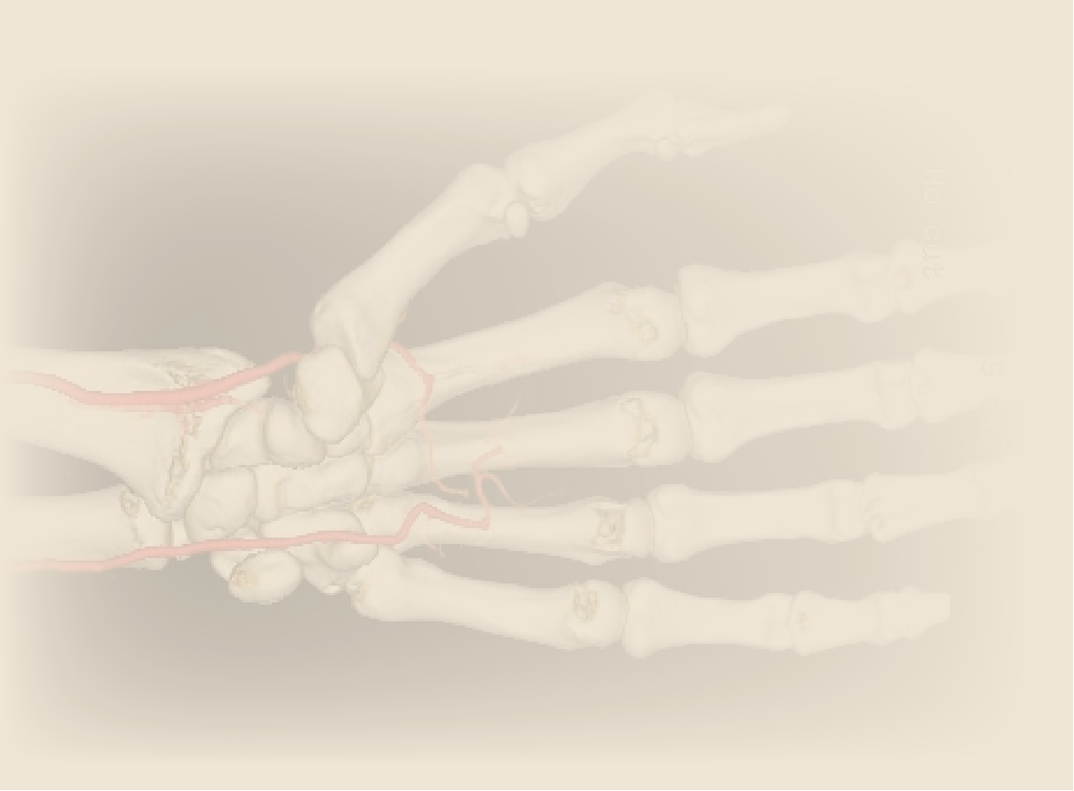

NOTE: Please see pages 198-204 for Funded Research Awards (Sponsored Projects) and pages 30 and 31 for Trainee Awards.

Education and Training

Trainee Awards

Recipient	Award
Qizhen Cao, PhD	SNM Travel Award to attend the 56th Society of Nuclear Medicine's Annual Meeting in Toronto, Canada
Jing Chen, PhD	Graduated with PhD, now Associate Professor, Institute of Biophysics, Beijing, China
Adam de la Zerda, PhD	World Molecular Imaging Congress, Young Investigator Award Travel Award.
Adam de la Zerda, PhD	Bio-X Travel Award
Adam de la Zerda, PhD	Society of Photographic Instrumentation Engineers (SPIE) Best Poster Award for "Enhanced Sensitivity Photoacoustic Imaging Agents."
Yi Gu, MS; Frances Lau, MS; Guillem Pratx, MS; Paul Reynolds, MS; Arne Vandenbrouke, PhD.	Institute of Electrical and Electronics Engineers, Inc. Medical Imaging Conference Medical Imaging Conference (IEEE MIC) Trainee Grants to attend conference in Dresden, Germany.
Jason Hsu, PhD	Graduated wiith PhD, now Assistant Professor Professor at the University of Miami.
Sonal Josan, PhD	Graduated with PdD and currently a postdoc at SRI
Shin Kamaya, BSE	RSNA Award, scientific paper "Manganese-Enhanced MRI (MEMRI) Functionally Highlights Injured Peripheral Nerves in Neuropathic Pain," completed under the mentorship of Dr. Sandip Biswal.
Sri-Rajasekhar (Raj) Kothapalli, PhD	Hamalainen Pelican Postdoctoral Fellowship, Sir Peter and Lady Michael Foundation
Christine Law, PhD	Graduated with PhD in Electrical Engineering, postdoc choice of 5 institutions not final as of 9/1/09.
Andrew Lee, BS	HHMI Fellowship in developing novel methods of reprogramming induced pluripotent stem (iPS) cells.
Cristoph Lee, MD	American Medical Association (AMA) Foundation's 2009 Leadership Award
Cristoph Lee, MD	Robert Wood Johnson Foundation Clinical Scholar, 2010-2012
Hen-Tzu Jill Lin, PhD	World Molecular Imaging Congress Travel Award, Montreal, Canada by Helena Anna Henzl Gabor Young Women in Science Fund
Yueyi Irene Liu, PhD	RSNA Trainee Research Prize for project, "Bayesian Approach to Decision Support for Evaluating Thyroid Nodules Based on Multi-Variate Features."
Zheng Miao, PhD	SNM First Prize, Basic Science Award for abstract "A Protein Scaffold Based Molecule for EGFR PET Imaging."
Kazin Narsinh, MD	2009 Howard Hughes Medical Institute (HHMI) Research Fellowship.
Gang Niu, PhD	Society of Nuclear Medicine Travel Award
Peter Olcott, MS	SNM Research and Education 2008 Predoctoral Molecular Imaging Scholar Program award for proposal "Optically coupled pulse width modulation PET detectors for combined whole body clinical PET/MR systems."
Natesh Parashurama, MD, PhD	International Society for Cellular Therapy Young Investigator Award, Presentation "Stably Expressed Multimodality Fusion Reporter Genes For Tracking Mesenchymal Stem Cell Status in Hearts of Living Subjects."
Natesh Parashurama, MD, PhD	2009-2010 Stanford University, School of Medicine Dean's Fellowship for proposal, "Quantitative, Multimodality Molecular Imaging of Spatiotemporally Regulated Cardiac Stem Cell Functions In Vivo."
Jeremy Pearl, BS	Howard Hughes Medical Institute (HHMI) Second-Year Fellowship

NOTE: Please see pages 198-204 for Funded Research Awards (Sponsored Projects) and pages 26 and 27 for Faculty & Research Staff Awards

Trainee Awards

Recipient	Award
Guillem Pratx, MS	"Bayesian reconstruction of photon interaction sequences for high-resolution PET detectors." Featured Article in Journal, Institute of Physics
Guillem Pratx, MS	2008 IEEE Medical Imaging Conference, Dresden, Germany top student paper award for "Fast, Accurate and Shift-Varying Line Projections for Iterative Reconstruction using the GPU."
John Ronald, PhD	Canadian Institutes of Health Research (CIHR) Fellowship
Laura Sasportas, PhD	Society of Nuclear Medicine (SNM) Student Fellowship Award
Anne Marie Sawyer, BS, RT(R)(MR)	Food and Drug Administration (FDA), Member, Circulatory System Devices Panel, Medical Devices Advisory Committee.
Min-Kyung So, PhD	World Molecular Imaging Congress 2008, Young Investigator Award
Virginia Spanoudaki, PhD	Postdoctoral Fellowship for work in new concepts to advance time-of-flight positron emission tomography awarded by the AXA Research Fund
Avnesh Thakor, MA, MB Bchir, PhD.	International Union Against Cancer (UICC) and American Cancer Society International Fellowship for Beginning Investigators.
Chardonnay Vance, PhD	Graduated with PhD in Biochemistry; entering Wake Forest Univ Medical School, September 2009.
Adam Wang, MS	2009 Society of Photo-Optical Instrumentation Engineers (SPIE) Medical Imaging Conference Finalist, Michael B. Merickel Student Paper Award
Serena Wong, PhD	Graduated with PhD, currently a scientist at Palo Alto Research Center
Joong-Ho (Johann) Won, PhD, MS	Bio-X Travel Award for presentation "Towards a Single Uncluttered View of the Abdominal Aortic Vessel Tree from CTA or MRA: Method and Preliminary Results," RSNA Annual Meeting, 2008
Jim Xie, PhD	Society of Nuclear Medicine (SNM) Travel Award
Keren Ziv, PhD	Life Sciences Research Foundation Fellowship (LSRF) Postdoctoral Fellowship

NOTE: Please see pages 198-204 for Funded Research Awards (Sponsored Projects) and pages 26 and 27 for Faculty & Research Staff Awards

Postgraduate Education

Continuing Medical Education Program

Susie Spielman

Director, Strategic Initiatives and Program Management

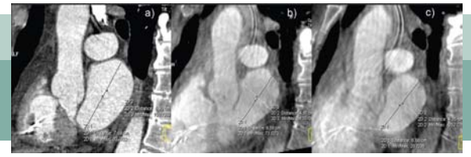

Over the past 19 years, Stanford University, Department of Radiology has constructed a world class CME program targeted to practicing physicians, academic scientists, radiologic technologists, industry-based engineers, and scientists. Stanford Radiology is distinguished by an international reputation for excellence and innovation in postgraduate medical education. The Department was motivated to create such a program to fulfill its educational mission and disseminate radiological advances. Further, the benefits of such an effort include an increase in reputation for the Department overall and for the individual faculty, as well as an opportunity to foster relationships globally with academic institutions and societies.

In FY 2009, Stanford Radiology presented 14 courses to over 3,000 registrants. These included our traditional CME programs such as our Breast MRI, PET/CT, and Diagnostic Imaging Updates along with specialty courses for interventional fellows, small animal imaging scientists, and collaborations with partners in Asia and Europe. Our MDCT program returned to San Francisco this year (after a one year stint in Las Vegas) and continues to serve as the premier meeting for global CT education.

In FY 2010 we are scaling back our traditional conferences and working to build our programs with greater international focus. The economy as well as policy changes have contributed to this shift in direction. We have always had an international reach to our programs, however, now we hope to heighten these efforts with on campus training courses specifically for this audience. There are eight CME meetings planned for the upcoming year and several (non-cme) new educational efforts are underway. We have just completed our second joint conference in China. This program included 300 radiologists from throughout the region and was developed in partnership with the Chinese Society of Radiology (CSR). We have an agreement signed with the CSR to continue this symposium annually. Additionally, we are now planning for two one-week advanced training programs on campus for physicians from China and Europe. These programs will be modeled after our highly successful course for the Japanese Society of Radiological Technology, which just completed its fourth summer and will be returning in 2010. We are proud of the partnerships we have formed with many distinguished organizations and institutions. These efforts enable us to provide education to radiology communities around the world and establish important linkages with imaging scientists in leading Chinese, Japanese, and European universities. For a list of upcoming CME courses, please visit our website: http://radiologycme.stanford.edu

NIH/NCI T32 CA09695

NCI Training Program – Advanced Techniques for Cancer Imaging and Detection - T32

PI – Gary M. Glazer, MD

Program Manager – Lanzie Rivera

The Department of Radiology at Stanford University offers qualified individuals a unique research opportunity through our Advanced Techniques for Cancer Imaging and Detection Program, which began its 17th year of training on February 1, 2009. The goal of our program is to provide MD and PhD research fellows training in cancer-related imaging research. Fellows have the opportunity to work with our world-renowned faculty who are committed to sharing their knowledge and mentoring the future leaders in radiology. Our program allows basic scientists in medical imaging (PhD) and clinical scientists (MD post-residency) to collaborate in an unparalleled environment that combines medical imaging sciences, clinical sciences, a strong cancer focus, and an institutional commitment to training academic radiologists and basic scientists in imaging science.

A specific aim of our training program is to position our trainees for a career in academic radiology. To date, we have graduated 28 trainees from our program. Our trainees continue to be extremely productive. We often collaborate with them in their new positions both locally and throughout the country. We are grateful to the National Institutes of Health for its recognition of the strength and success of our training program

Current trainees are Rachel Bitton, PhD, Moses Darpolor, PhD, Dragos Constantin, PhD and Grace Tye, MD. Their research interests are shown in the table below.

Rachel Bitton, PhD, joined the Radiological Sciences Lab as an NCI fellow March, 2008. Her research interests include photoacoustic imaging of micro-vasculature using high frequency ultrasonic transducers, MR temperature guidance for interventional high intensity focused ultrasound therapy (HIFU), and targeted contrast agents for photoacoustic imaging and therapy.

Moses Darpolor, PhD, joined the RSL group as an NCI fellow June, 2008. He is interested in applying multi-parametric MR and multimodality imaging in oncology. His previous and ongoing projects include DSC-MRI in conjunction with micro-CT imaging of vascular function and morphology of brain tumor with antiangiogenic treatment; 1H decoupled 31P CSI of tumor bioenergetics to detect early response of subsequent CPT11 and flavopiridol treatment; and hyperpolarized 13C imaging to detect early tumor response to radiation therapy. .

Dragos Constantin, PhD, joined RSL as an NCI fellow in 2008. His research interests involve theoretical and experimental investigation of the magnetic resonance imaging integration with a medical linear accelerator to provide real-time image guidance to target temporally changing tumor anatomy, particularly for cancers in the thorax and abdomen.

Grace Tye, MD, very recently joined the RSL group in July, 2009. She is in the process of finalizing her research plans for her two years of research training

T32 Program Graduates

NCI Fellow	Completed Training	Current Position	Current Institution	Primary Mentor
John Strang, MD	1995	Assistant Professor	University of Rochester, Rochester, NY	Herfkens
Susan Lemieux, PhD	1996	Assistant Professor	Diagnostic Imaging Western Virginia Univ., Morgantown, WV	Glover
Ian Chen, MD	1996	Radiologist	Southwest Washington Medical Center, Vancouver, WA	Li
Yi-Fen Yen, PhD	1997	Research Scientist	GE Advanced Health Care	Glover
Garry Gold, MD	1997	Associate Professor	Radiology, Stanford University, Stanford, CA	Macovski
Bruce Daniel, MD	1997	Associate Professor	Radiology, Stanford University, Stanford, CA	Herfkens
Roger Shifrin, MD	1998	Assistant Professor	University of Florida, FL	Pelc & Herfkens
Esther Yuh, PhD	1998	Clinical Fellow	Radiology (Neuroradiology), UCSF, CA	Li & Napel
Steven Heiss, MD	1999	Radiologist	Radiology Imaging Associates, Denver, CO	Li
Martin Blum, MD	2000	Researcher	PET/Nuclear Medicine, Palo Alto VA, CA	Jeffrey
Curtis Coulam, MD	2001	Radiologist	Gem State Radiology Group, Boise, ID	Sommer
Lawrence Chow, MD	2002	Assistant Professor	University of Oregon, Eugene, OR	Sommer
Yishan Yang, PhD	2002	Research Associate	Radiology, Stanford University, Stanford, CA	Bednarski
Samira Guccione, PhD	2002	Assistant Professor	Radiology, Stanford University, Stanford, CA	Bednarski
Charles Liu, MD	2003	Radiologist	La Jolla Radiology, La Jolla, CA	Herfkens & Sommer
Susan Hobbs, MD, PhD	2003	Radiologist	CT Section Chief, Kaiser Permanente, Walnut Creek, CA	Bednarski
Karl Vigen, PhD	2003	Research Scientist	University of Wisconsin-Madison, Madison, WI	Butts Pauly
Laura Pisani, PhD	2004	Postdoctoral Fellow	Radiology, Stanford University, Stanford, CA	Glover
John Levin, MD	2004	Radiologist	St. Luke's Medical Center & Clinic, Minneapolis, MN	Herfkens & Sommer
Daniel Margolis, MD	2005	Assistant Professor	Dept. of Radiology, UCLA, Los Angeles, CA	Jeffrey
Daniel Ennis, PhD	2006	Postdoctoral Fellow	University of Washington, Seattle, WA	Pelc
Michael McDonald, PhD	2007	Research Scientist	NIH, Washington, DC	Guccione
Anthony Faranesh, PhD	2007	Research Scientist	NIH, Washington, DC	Pelc & Hargreaves
Lewis Shin, MD	2007	Assistant Professor	Radiology, Stanford University, Stanford, CA	Herfkens
Jinha Park, MD, PhD	2008	Assistant Professor	University of Southern California, Los Angeles, CA	Gambhir
Byard Edwards, MD, PhD	2008	Scientific Researcher	Vanderbilt University	Jeffrey
Cristina Zavaleta, PhD	2008	Scientific Researcher	MIPS, Radiology, Stanford University, Stanford, CA	Gambhir
Stephanie Bailey, PhD	2009	Scientific Researcher	Comprehensive San Diego State University/UCSD Cancer Center Partnership	Plevritis

NIH/NCI R25 CA118681

Stanford Molecular Imaging Scholars – SMIS R25

PI – Sam Gambhir, MD, PhD

Program Manager – Sofia Gonzales, MS

The Stanford Molecular Imaging Scholars (SMIS) program is a diverse training program bringing together more than 13 departments, predominantly from the Stanford Schools of Medicine and Engineering. Oncologic molecular imaging is a rapidly growing area within molecular imaging, which combines the disciplines of chemistry, cell/molecular biology, molecular pharmacology, bioengineering, imaging sciences, and clinical medicine to advance cancer research, diagnosis, and management. The goals of SMIS are to train postdoctoral fellows by providing mentorship through a diverse group of over 40 basic science and clinical faculty mentors representing eight program areas; by incorporating formal courses in molecular imaging, molecular pharmacology, cancer biology, cancer immunology, virology, and gene therapy; and by including a clinical component such as hematology/oncology rounds. To date, we have recruited 13 postdoctoral fellows. Our first year of training began in September 2006. Three new fellows were recently selected to join the program, due to start later this year.

The following list summarizes SMIS trainees and where they are currently. NIH/NCI R25 CA118681 supports the R25 program.

R25 Program Trainees

SMIS Fellow	Training Period	Current Position	Institution	Primary Mentor
Richard Kimura, PhD	2006-2009	Postdoctoral Fellow	Stanford University	Jennifer Cochran, PhD
Jennifer Prescher, PhD	2006-2009	Postdoctoral Fellow	Stanford University (MIPS)	Christopher Contag, PhD
Bryan Smith, PhD	2006-2009	Postdoctoral Fellow	Stanford University (MIPS)	Sam Gambhir, MD, PhD
Hua Fan-Minogue, MD, PhD	2007-2010	Postdoctoral Fellow	Stanford University (MIPS)	Sam Gambhir, MD, PhD
Benjamin Cosgrove, PhD	2008-2011	Postdoctoral Fellow	Stanford University	Helen Blau, PhD
Henry Haeberle, PhD	2008-2011	Postdoctoral Fellow	Stanford University (MIPS)	Christopher Contag, PhD
Sharon Hori, PhD	2008-2011	Postdoctoral Fellow	Stanford University	Sam Gambhir, MD, PhD
Marybeth Pysz, PhD	2008-2011	Postdoctoral Fellow	Stanford University	Juergen Willmann, MD, PhD
Nicholas Conley, PhD	2009-2011	Postdoctoral Fellow	Stanford University	TBD
Eric Gonzalez, PhD	2009-2011	Postdoctoral Fellow	Stanford University	Craig Levin, PhD
Jesse Jokerst, PhD	2009-2011	Postdoctoral Fellow	Stanford University	TBD

R25 Program Graduates

Keith Hartman, PhD	2008-2009	Consultant	Boston Consulting Group, Washington , DC	Sam Gambhir, MD, PhD
Jill Lin, PhD	2006-2009	Consultant	Beghou Consulting, Emeryville, CA	Sam Gambhir, MD, PhD

SMIS Trainee Research Interests

Richard Kimura, PhD, is a member of Dr. Jennifer Cochran's lab in the Department of Bioengineering. He uses yeast surface display to evolve peptides to bind targets involved in cancer. He has developed several novel probes to detect and image angiogenesis and cancer cell surface markers.

Jennifer Prescher, PhD, joined Dr. Christopher Contag's lab in 2006. Her research is focused on elucidating the molecular mechanisms of T cell homing and infiltration into tumor tissue. She is also interested in developing new tools to visualize the migration patterns of multiple immune cell types in vivo using bioluminescence imaging.

Bryan Smith, PhD, joined Dr. Sanjiv Sam Gambhir's lab in 2006. His research interests involve monitoring and understanding the microscale behavior of various targeted and untargeted nanoparticles in real time in the tumors and vasculature of small living animals using intravital microscopy. This work is performed to accelerate the progression of nanoparticles into humans and to generate the data needed to optimize nanoparticle formulations to best target, image, and treat cancer.

Hua Fan-Minogue, MD, PhD, started her research in Dr. Sanjiv Sam Gambhir's lab in 2007. Her research focuses on developing optical imaging sensors for protein-protein interactions in vivo. This work provides a new way to monitor cell signaling in abnormal or tumor cells and drug development for cancer therapy. She is also interested in stem cell imaging and early cancer detection using a variety of imaging modalities.

Benjamin Cosgrove, PhD, is interested in developing novel molecular imaging technologies to investigate stem cell signaling phenotype relationships. These molecular imaging technologies will be employed to generate multivariate dynamic stem cell signaling response data collected under a wide variety of microenvironmental stimuli, including tethered and soluble growth factors in a multi-well three-dimensional hydrogel system, which will then be used to identify key intracellular signaling activities that govern specific stem cell differentation programs. This work will be conducted under the joint supervision of Drs. Sam Gambhir and Helen Blau.

Henry Haeberle, PhD, joined Dr. Christopher Contag's in September 2008. He is interested in developing molecular markers to better detect tumor margins in the central nervous system and in developing fluorescent markers for the brain tumors medulloblastoma and glial blastoma.

Sharon Hori, PhD, began her appointment in September, 2008. Her research interests include: 1) data-driven mechanistic biomodeling in relation to cancer and other diseases; 2) math modeling, parameter estimation and identifiability methods; 3) developing imaging probes and optimizing delivery to molecular targets via an integrative imaging/experimental and kinetic modeling approach. She is working with Drs. Plevritis and Gambhir.

Marybeth Pysz, PhD, joined Dr. Juergen Willmann's lab in October, 2008. She is interested in multi-modality imaging of pancreatic cancer and identifying new molecular targets for early detection using molecular ultrasound and/or PET-CT imaging.

NIH/NCI P50CA114747

In Vivo Cellular and Molecular Imaging - ICMIC P50

PI – Sam Gambhir, MD, PhD

Program Manager – Billie Robles, BS

The vision of the In Vivo Cellular and Molecular Imaging Center at Stanford (ICMIC@Stanford) is to bring together researchers from various disciplines to form synergistic teams that will make significant advances in the use of multimodality molecular imaging strategies for better linking pre-clinical models of cancer with the clinical management of cancer. The career development component of this P50 is designed to be as flexible as possible to attract highly qualified candidates with the passion and ability to make an impact on cancer research that will benefit patient care in terms of diagnosis, therapy, and monitoring. This overarching theme will guide the process of candidate selection and lead to successfully trained individuals who will be capable of leading their own independent research teams in the field of molecular imaging cancer research. As we enter the fifth year of the ICMIC@Stanford, we have three trainees in the program. Selected candidates attend various educational activities in the Molecular Imaging Program at Stanford (MIPS) and work to bridge activities between a minimum of two laboratories. The candidates invited to join the ICMIC@Stanford Program are expected to be well trained in basic science or in imaging science and to have the energy and drive to influence the growing field of molecular imaging cancer research. NIH/NCI P50CA114747 supports the P50 program.

P50 Program Trainees

ICMIC Fellow	Completed Training	Current Position	Current Institution	Primary Mentor
Sheen-Woo Lee, PhD	2005	Musculoskeletal Imaging Fellow	Asian Medical Center, Seoul, Korea	Sandip Biswal, MD
Frank Cochran, PhD	2008	Post Doctoral Fellow	Bioengineering, Stanford University	Jennifer Cochran, PhD
Erhan Yenilmez, PhD	2007	Post Doctoral Scholar	Materials Science & Engineering, Stanford University	Nicholas Melosh, PhD
Mike Helms, PhD	2008	Post Doctoral Fellow	Pediatrics, Stanford University	Christopher Contag, PhD
Mike Benoit, PhD	2009	Post Doctoral Fellow	Microbiology & Immunology	A.C. Matin, PhD
Priti Balchandani, PhD	2009	Post Doctoral Fellow	Radiology (RSL)	Dan Spielman, PhD

Lucas Center MR Systems Training and Support

1.5T, 3T (2), and 7T Whole Body Magnets

Anne Marie Sawyer, BS, RT (R)(MR)
Sandra Rodriguez, RT (R)(MR)

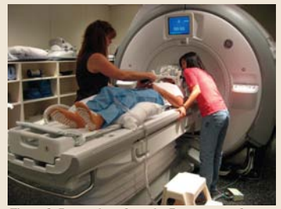

Figure 3. Researchers from the Department of Pediatrics (Principal Investigator Heidi Feldman, MD) prepare a young scan subject for a research functional brain (fMRI) examination at the 3T2 at the Lucas Center.

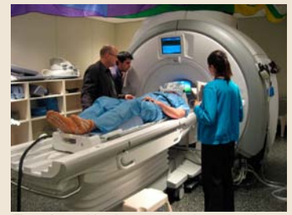

Figure 2. A subject is seen undergoing preparation to be scanned at the 3T2 by Sean Mackey, MD, PhD, and members of his laboratory from the Department of Anesthesiology conducting research in chronic pain.

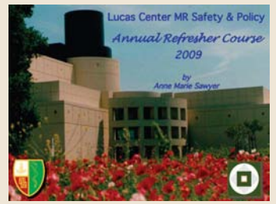

Figure 1. The Lucas Center annual refresher course for MR safety, screening, polices, and procedures is now conducted online via an instructional tutorial. This annual training is required for all researchers using the magnets at the Lucas Center including faculty, staff, and students from all departments.

Safety Training and System Operation Instruction 2008 - 2009

Safety training and system instruction have been provided to 174 new researchers conducting experimental MR studies at the Lucas Center over the last twelve months. Initial magnet safety training and the annual refresher course is required for all researchers assisting or conducting studies on any of the magnet systems at the Lucas Center. The annual magnet safety refresher course has recently been developed as an on-line tutorial and will provide instruction to 253 researchers during August (Figure 1). This ensures that all users and assistants are qualified to operate the MR systems and satisfies Lucas Center and University requirements for safety. System and safety support is provided to the researchers 7 days a week, 24 hours a day to ensure that research endeavors are successful, generate valuable data, and, above all, are safe for the researchers, the human subjects and the MR system and its components (Figures 2 and 3). Magnet safety is an on-going concern as the MR environment can be a potentially lethal setting without continuing education and persevering support.

The research environment generates many new yet prototype designs in RF imaging coils, imaging accessories, monitoring and response devices such as button boxes, eye trackers, and electroencephalogram (EEG) recorders, and sensory devices (Figures 2 and 3). Evaluation of these new devices is on-going to ensure that neither the image data, the safety of the human subject, nor the integrity of the MR system is compromised by the presence of these devices in the magnet room, in the bore of the magnet, or in the presence of an RF coil.

Research Group Updates

Research Group Updates

Advanced X-Ray and CT Techniques

Inverse Geometry CT and Conventional CT

Norbert Pelc, ScD

left to right: Linus Ong (standing), Jongduk Baek, Scott Hsieh, Adam Wang, Norbert Pelc, Arun Ganguly, Sam Mazin

Our research efforts concentrate on the development of technology and applications of computed tomography (CT). The long-term aim of his work is to push the limits of CT performance and to aid in the development of new applications. Intrinsic in this aim is the need to understand the basic limitations in current systems and, when physically possible, to develop solutions to effectively address them. Aside from scientific progress, we recognize this year Jongduk Baek, who completed his oral defense for a PhD in Electrical Engineering, Linus Ong, who completed his MS in Bioengineering, and Sam Mazin, who was awarded a Kauffman Entrepreneur Postdoctoral Fellowship.

One large current project is to develop a system that can image an arbitrarily thick section of anatomy (e.g. an entire organ) in a single fast rotation while producing uncompromised image quality and outstanding dose efficiency. The specific approach we are pursuing employs an inverse geometry (therefore the term IGCT), with one critical aspect being a distributed x-ray source whose length is comparable to the thickness of the section being imaged. The approach presents many opportunities, and we have already demonstrated excellent spatial resolution and complete freedom from cone beam artifacts, which can plague conventional systems when trying to image a thick region in a single scan. With funding from NIH and significant additional support from GE, we are collaborating with GE Global Research Center to build a gantry-based prototype (Pelc abstract, p61). We expect to begin collecting data with this system later this year, which will initiate a period of intensive algorithm refinement and image quality testing.

The distributed source provides the IGCT system with the possibility to carefully control not just the overall intensity but also the distribution of x-rays incident on the patient, a concept called “virtual bowtie”. This opens the possibility of engineering this distribution so that the radiation dose necessary for a given image quality is minimized to the patient (Hsieh abstract, p62).

We are also working on a number of problems relevant to all CT configurations. Continuing our work on energy selective CT, we showed that weighted sums of the data from energy discriminating photon counting detectors can extract all the information in the full spectrum into very few “sufficient statistics” (Wang abstract, p61). We also continued our work on noise power spectra (NPS) and their eventual use for system evaluation. We derived analytical expressions for the 3D NPS of cone beam systems (Baek abstract, p63) and began our development of tools for experimental measurements (Ong abstract, p62).

X-Ray Guidance of Interventional Procedures

Rebecca Fahrig, PhD

Clockwise from left: Erin Girard-Hughes, Prasheel Lillaney, Hewei Gao, Jared Starman, Sungwon Yoon, Arun Ganguly, Dragos Constantin, and Dr. Rebecca Fahrig. (not pictured: Alessia Tognolini, Marlys LeSene.)

Our group conducts research with the broad goal of improving the x-ray guidance of minimally invasive procedures, and we are expanding this definition to include guidance of radiation therapy. The Axiom Lab (C-arm CT system) is used for in vivo investigations and the Advanced X-Ray Imaging Lab is used for hardware and software development (table-top digital x-ray imaging, cone beam CT, and X-ray/MR system development).

Basic investigations into image quality improvement continue, including optimization of our modulator-based scatter correction (Gao abstract, p65) and continuing work on lag characterization and reduction in amorphous silicon flat-panel detectors (Starman abstract, p67). Dr. Arun Ganguly, Research Associate, has been awarded an NIH K-99 Young Investigator award to develop and characterize a new, high-speed, high-resolution detector for application to brain perfusion imaging in collaboration with RTR Inc. (Ganguly abstract, p64).

We continue to develop new imaging protocols using ECG-gated C-arm CT, and have now completed a study that demonstrates the ability to visualize radiofrequency lesions in myocardium for the first time (Girard-Hughes, p 65). Using similar multi-sweep acquisition protocols on the C-arm system but without ECG gating, we are developing protocols to provide quantitative measures of brain perfusion during interventions in the cath-angio suite. This technology could be used to provide a ‘1-stop shop’ for stroke assessment and interventional therapy (Ganguly and Fieselman, p68).

Our design of an MR-compatible rotating anode x-ray tube has progressed. We have built a prototype motor that uses an external field (e.g. generated by the static field of the MR system) to generate torque. Modeling to predict behavior of our motor with realistic design parameters is underway (Lillaney abstract, p68). The focus of our new program in therapy guidance is an extension of this approach to x-ray/MR system integration, working with colleagues in Radiation Oncology to provide MR guidance during radiation therapy treatment. First steps include identification of appropriate geometries for Linac/MR systems, and finite-element modeling of each component of the Linac in the presence of external magnetic fields (Constantin abstract, p 64).

Image Analysis, Bioinformatics, Computational Modeling

Computational Cancer Research Lab (CCRL)

Sylvia K. Plevritis, PhD

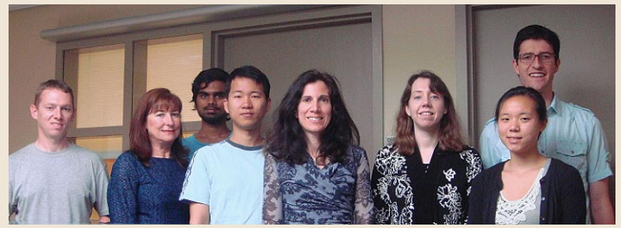

Andrew Gentles, Maggie Bos, Aravind Babu, Peng Qiu, Sylvia Plevritis, Allison Kurian, Emily Tsai, Nick Hughes.
Missing: Ray Lin, Santhosh Kasavajjala.
Group Members who have left during the past year – Bronislava Sigal, PhD; Stephanie Bailey, PhD

The Computational Cancer Research Lab (CCRL) embraces a “systems biology approach” to the study of cancer biology and cancer outcomes. We aim to provide new insights into cancer progression, detection and treatment by integrating genomic, proteomic, pathological, imaging, and patient outcomes data using novel computational methods. We develop multi-scale models of the natural history of cancer that describe the stochastic behavior of tumor growth and metastatic spread. At the patient and population level, we apply these models to address important health policy questions, such as: how does screening mammography and MRI impact breast cancer mortality; what are the expected survival outcomes for individuals at high risk for breast cancer who choose varying combinations of screening and prophylactic interventions; and how would CT screening for lung cancer impact lung cancer mortality rates.

At the molecular level, we analyze cancer progression by developing and applying computational models to understand how the “molecular circuits” of cancer cells are fundamentally different than those of normal cells. One of our major research goals is to analyze global gene and protein expression data to understand the transformation of lymphoma from low grade to high grade disease. By doing so, we identify molecular targets that may eradicate low grade disease before it progresses. In CCRL, computational scientists work side-by-side with biological experimentalists and clinical researchers to ensure the biological and clinical relevance and translation of our work. We believe that computational models contribute to a comprehensive, multi-scale understanding of cancer progression and identify new approaches to help save lives.

Radiology Informatics in Translational Medicine

Daniel L. Rubin, MD

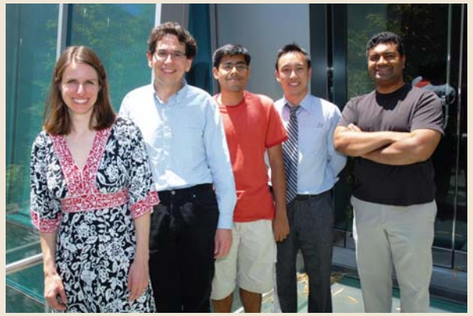

Left to right: Mia Levy, Daniel Rubin, Ankit Gupta, Bao Do, Cesar Rodriguez; Missing: Irene Liu

Our research group uses computational methods to leverage the information in radiology images to enable biomedical discovery and to guide physicians in personalized care. Just as biology has been revolutionized by online genetic data, our goal is to advance radiology by making the content in images computable and to electronically correlate images with other clinical data such as pathology and molecular data. Our work develops and translates basic biomedical informatics methods to improve radiology practice and decision making in several areas: tools to efficiently and thoroughly capture the semantic terms radiologists use to describe lesions; standardized terminologies to enable radiologists to describe lesions comprehensively and consistently; image processing methods to characterize the shape of lesions; content-based image retrieval with structured image information to enable radiologists to find similar images; methods to enable physicians to quantitatively and reproducibly assess tumor burden in images and to more effectively monitor treatment response in cancer treatment; natural language techniques to enable uniform indexing, searching, and retrieval of radiology information resources such as radiology reports; and decision support applications that relate radiology findings to diagnoses to improve diagnostic accuracy.

We collaborate with a variety of investigators at Stanford both in Radiology (including Sandy Napel, Chris Beaulieu, Brooke Jeffrey, Terry Desser, and Aya Kamaya) and Oncology (including Sandra Horning and George Fisher) as well as with investigators outside Stanford. We are engaged in scientific collaborations with the National Center for Biomedical Ontology, and we participate in a national working group that is developing imaging informatics infrastructure for the cancer Biomedical Informatics Grid program at National Cancer Institute. Our ultimate goal is to bridge the divide between radiological knowledge and practice--for all radiological knowledge and research data to be structured, accessed, and processed by computers so that we can create and deploy decision support applications in image workstations to improve radiologist clinical effectiveness.

Image Analysis, Bioinformatics, Computational Modeling

Paik Lab Research Group: Imaging Bioinformatics

David Paik, PhD

The Imaging Bioinformatics Lab, led by Dr. Paik, is primarily interested in how biological information is extracted from both anatomic and molecular imaging, how it is represented, how it is modeled, and how it is disseminated with an outlook toward combining imaging-derived information with other sources of biological and clinical information. We are particularly interested in applying computational techniques toward a better understanding of cancer. While most computational models and analyses focus on a single source or modality of data, it is becoming increasingly clear that models must integrate across a wide variety of data types as well as spatial and temporal scales. Our focus is on developing these types of models.

Beginning with information extraction, we have projects in detecting and characterizing lung tumors from chest CT images in collaboration with Drs. Rubin, Napel, and Roos, as well as projects in extracting quantitative measurements from an array of different molecular imaging modalities. In the area of modeling, we have an ongoing collaboration with Dean Felsher's laboratory in mathematically modeling oncogene addiction through quantitative imaging. This has led to new areas of investigation including using rate kinetics equations of the apoptosis caspase cascade in order to better predict the effect on overall tumor growth kinetics. Another new line of investigation in collaboration with Stefanie Jeffrey's lab is in linking gene expression from circulating tumor cells to imaging characteristics. At the knowledge and dissemination level, we have several related projects in nanoparticle agent knowledge bases in collaboration with the CCNE-TR, National Center for Biomedical Ontology and Dr. Nathan Baker of Washington University in St. Louis.

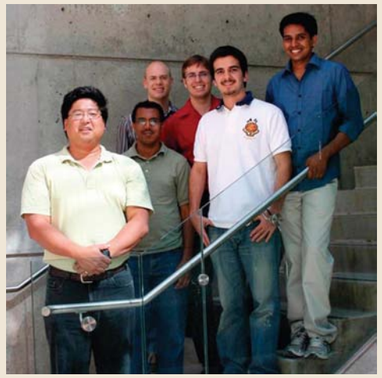

left to right: David Paik, Frezghi Habte, Jesse Rodriguez, Florian Schmitzberger, Konstantinos Sebekos, Kranthi Kode

Our long-term goal is to enable and simplify the problem of information extraction and information flow from medical/molecular imaging to be on par with that of genomic and proteomic profiling technologies so that these very different types of information may be treated as siblings computationally. Our philosophy is that for an integrative approach to imaging and non-imaging information to come to fruition, a major pre-requisite is to be able to maximally extract and represent information from imaging, with emphasis on the specificity of molecular imaging.

Radiology 3D Visualization and Analysis Laboratory

Sandy Napel, PhD; Christopher F. Beaulieu, MD, PhD; Dominik Fleischmann, MD; Justus Roos, MD; Geoffrey D. Rubin, PhD

Our group addresses the field of medical image analysis, focusing on volumetric visualization, structure segmentation, quantitative analysis, and computer-aided detection of lesions. In addition, we are making great strides in the development of imaging analysis and informatics techniques (see ISIS Overview, page 12-13) to render radiological images amenable to biological discovery and decision support. We see the future of radiology as benefiting from the continuously increasing "computations/dollar" in computing technology, as we continue to refine and evaluate these techniques and apply them and their derivatives to new areas.

left to right: Hayit Greenspan (Visiting Professor), Florian Schmitzberger, Danny Korenblum, Jessica Faruque, Daniel Rubin, Christopher F. Beaulieu, Jingyu Cui, Martin Tall, Cesar Rodriguez, Yongjun Ma, Grace Tye, Jiajing Xu, Sandy Napel, David Paik Missing: Dominik Fleischmann, Justus Roos, Geoffrey D. Rubin, Ankit Gupta , Group Members who have left –Gennadiy Chuyeshov, Markus Kukuk, Tejas Rakshe, Ushah Kiran Kommi Reddi, Anthony Sherbondy, David Tran, Johann Won

Advances here have impact in many technical and clinical areas. Examples are: automated visualization and quantitation of vascular image data, virtual colonoscopy, intra-procedural registration of 2D fluoroscopic images of instruments with 3D volume data, automated computation of peak flow velocity using a novel ultrasound transducer, for reproducible determinations of carotid stenosis, automatic generation of curved-planar images through blood vessels, determination of likely neuronal connections of the visual tracts in the brain. Our group is highly collaborative, working with many radiology department investigators (including Chris Beaulieu, Dominik Fleischmann, Rusty Hoffmann, Brooke Jeffrey, Justus Roos, Geoff Rubin) as well as many other Stanford faculty (including Pierre Khuri-Yakub, electrical engineering). This year we have focused on automated feature extraction from liver CT images, visualization of occluded blood vessels, distributed evaluation of CAD of lung nodule data, evaluation methods for CAD in the absence of ground truth, and gaze tracking for improving interpretations. Based on our work this past year, 9 new manuscripts have been accepted for publication, 4 are under review, 7 presentations were given at international meetings, and 4 grant proposals, all related to our ISIS initiative, were submitted to the NIH.

Magnetic Resonance Research

Interventional and Open MRI

Kim Butts Pauly, PhD

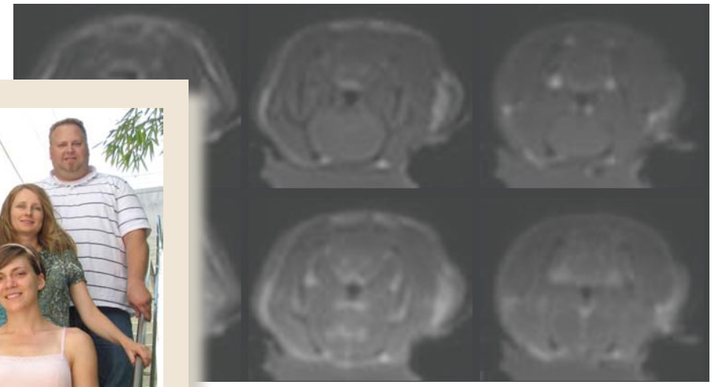

left to right, front row: Ron Watkins, Katie Planey. second row: Rachel Bitton, Kelly Townsend. third row: Kim Butts Pauly, Hyo-seon Yoon, Lena Kaye. last row: Andrew Holbrook, Will Grissom, Viola Rieke, Randy King.

Our group has continued a collaborative project to develop a system for MR-guided focused ultrasound (FUS) ablation of liver tumors. Andrew Holbrook developed real-time thermometry and demonstrated image quality of moving thermal lesions equivalent to that of stationary lesions. In collaboration with Pierre Khuri-Yakub, Serena Wong developed therapeutic capacitive micromachined ultrasonics transducers. Together with Ron Watkins, she demonstrated on MR images their ability to heat a gel phantom. She graduated and is now at the Palo Alto Research Center. Her work will be carried on by Hyo-Seon Yoon. Will Grissom joined the group and quickly developed an improved RF pulse and an improved reconstruction method for referenceless MR thermometry. For visualizing the focal spot without a temperature rise, Jing Chen developed an MR-acoustic radiation force method based on line scan imaging. She graduated and is now at the Institute of Biophysics in Beijing. Randy King has demonstrated the use of MR-guided thermometry in FUS ablation of hepatocellular carcinoma in a small animal model. Katie Planey visited for the summer and helped out with the real-time interface. Sonal Josan demonstrated artifacts on MR-thermometry when echo planar imaging and/or spiral imaging are used for the acquisition. She has graduated and is now working at the Stanford Research Institute in Menlo Park.

We continued our collaborative project with Graham Sommer and Chris Diederich from UCSF on MR-guided high intensity ultrasound ablation in the prostate with transurethral ultrasound applicators. Andrew Holbrook redesigned the MR thermometry interface in RTHawk on the 3T system. Temperature within regions of interest can now be transfered to the ultrasound control system in real-time. Chris Diederich's team uses these values to control and improve treatment.

Viola Rieke and Randy King investigated the feasibility of cardiac FUS ablation in collaboration with Mike McConnell. They demonstrated that enough sound can penetrate beyond the rib cage to make thermal lesions. Rachel Bitton is carrying on the work done by Viola Rieke and visiting scientist AnneMarie Schmitz, where focused ultrasound lesions circumscribe the tumor to provide a visible and palpable lump at surgery.

In MR-guided FUS in the brain, Lena Kaye took over the MR-ARFI project and is developing a version based on spin echo imaging for improved SNR and image quality. Kelly Townsend and Randy King have begun initial investigations into FUS blood brain barrier opening.

Our MR-guided cryoablation work in collaboration with Bruce Daniel is picking up steam at 3T. Lena Kaye demonstrated that PRF shift in frozen tissue changes rapidly as the tissue freezes, then appears to follow a similar curve to the PRF shift in warm tissue. In a collaborative project with Emmanuelle Canet-Soulas, Monica Sigovan visited from Lyon, France to investigate the use of ultrashort TE MRI to image SPIO labeled stem cells

We have also continued a collaboration with Amit Sawant and Paul Keall on the topic of MR-guided radiotherapy. Amit Sawant is investigating imaging methods for real-time visualization of lung lesions

Magnetic Resonance Research

Body MR Imaging

Brian A. Hargreaves, PhD

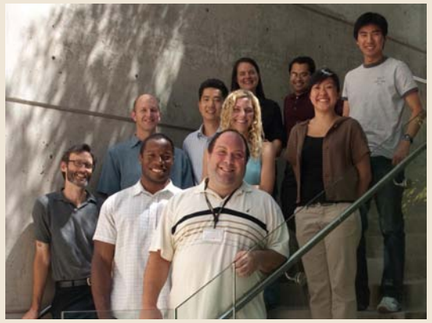

Back Row: Kristin Granlund, Shreyas Vasanawala, Ho Jin Kim. Middle Row: Brian Hargreaves, Kyung Sung, Caroline Jordan, Pauline Worters. Front Row: Marcus Alley, Anderson Nnewihe, Ernesto Staroswiecki. Missing: Misung Han. Group Members who have left – Wenmiao Lu

The body MR imaging group addresses applications of MRI to clinical body imaging. Our research includes abdominal imaging, musculoskeletal imaging, breast imaging and cardiovascular imaging, collaborating with numerous clinical faculty, engineering faculty and General Electric Healthcare. More information is at http://bmr.group.stanford.edu.

Wenmiao Lu completed his PhD, in 2008 and is now Assistant Professor in Singapore. Misung Han continues work on advanced parallel imaging for bilateral breast MRI, as well as studying methods to suppress flow artifacts. Ernesto Staroswiecki, together with Dr Garry Gold has been studying early osteoarthritis using sodium MRI. Kristin Granlund is working on robust fat/water separation for rapid breast MRI at 3T, as well as on non-contrast methods to assess perfusion. Anderson Nnewihe has built several new coils for sodium MRI, and is now concentrating on a high-density phased array coil for both rapid and high-resolution breast MRI on the new GE MRI scanners. Caroline Jordan is validating models that show the susceptibility-induced off-resonance in particularly difficult extremities areas such as the ankle and breast. Ho Jin Kim has been working with us, studying new quantitative fat/water separation methods. Two postdoctoral students, Kyung Sung and Pauline Worters have joined our group. Kyung is working on compressed sensing and dynamic contrast-enhanced imaging while Pauline is focused on non-contrast-enhanced vascular imaging. Marcus Alley continues to support a wide array of advanced clinical techniques for breast imaging, for dynamic contrast-enhanced MRI, for musculoskeletal MRI and many more. Brian Hargreaves continues to work on methods for MRI of orthopedic implants, which are now being used at Stanford Hospital.

The body MR group continue to collaborate with numerous radiologists including Bruce Daniel, Bob Herfkens, Garry Gold, and Shreyas Vasanawala, as well as researchers in radiation oncology, mechanical engineering, and electrical engineering.

Awards – (Both Shreyas Vasanawala first author) Lauterbur Award – SCBT/MR, Caffey Award, Society of Pediatric Radiology

Funding sources – National Institutes of Health, GlaxoSmithKlein, California Breast Cancer Research Program, GE Healthcare

High Field MR Group

Brian Rutt, PhD

Left to Right: Lin Davis, Ron Watkins, Brian Rutt, Michael Zieneh, Mohammad Khalighi, Jason Su

The long-term objective of the High Field MR Group is to develop a next-generation 7 Tesla whole-body magnetic resonance imaging (MRI) facility at Stanford, to serve as a platform for cutting-edge imaging research and development, as well as for radiological and neuroscience research. The scientific scope of the projects that will use this new facility will span the range from fundamental biology to patient-based clinical imaging research. The group approach will be interdisciplinary, bringing together researchers from the specialties of physics, engineering, bioengineering, biology, physiology, radiology, neurology, psychiatry, and psychology. The 7T MR facility will act as a catalyst and common platform for these broad groups to create, refine, implement, validate, and utilize the most advanced forms of magnetic resonance imaging. Major patient-based imaging research applications of the next-generation 7T MRI platform will include studies of brain development, psychopathology, drug dependence, alcohol-induced brain damage, and its functional consequences, neurodegenerative processes, brain injury, musculoskeletal disorders, and therapeutic interventions associated with some or all of the above.

Major technology development directions that will be enabled by this next-generation 7T MRI platform include MR spectroscopic imaging (MRSI) of the proton (1H) nucleus as well as non-proton nuclei, in both brain and musculoskeletal systems, advanced perfusion and diffusion tensor imaging in brain, and importantly, parallel transmit technology for mitigating B1 inhomogeneities that limit the use of high magnetic field MRI in any organ system. The initial goals of the high field MR group are to develop software and hardware methods to allow 7T MRI to have a much greater impact on clinical research than possible before, as well as to extend the capabilities of high field MRI to unprecedented levels of spatial resolution, metabolite and iron sensitivity, and tissue characterization. Major users are expected to come from interdisciplinary laboratories directed by international leaders in imaging research. Projects and research foci have already been established in the following areas: high field and high sensitivity MRI methodology development, developmental disorders and clinical neuroscience, DTI methodology development, musculoskeletal and breast MRI methodology development, parallel transmit and RF pulse technology development, psychiatric disorders and neuroimaging, MR spectroscopic imaging methodology development, psychiatric disorders and clinical neuroscience, cognitive neuroscience and neuroimaging and neurovascular imaging.

Magnetic Resonance Research

Functional "Microvascular" Neuroimaging

Roland Bammer, PhD, and Michael Moseley, PhD

From left to Right: Samantha Holdsworth, Heiko Schmiedeskamp, Roland Bammer, Matus Straka, Eun Soo Choi, Murat Aksoy, Lanzie Rivera, Stefan Skare, Daniel Kopeinigg, Didem Aksoy, Michael Moseley.

State-of-the-art advances in magnetic resonance imaging (MRI) continue to improve adult and pediatric neuroimaging. Using functional MRI methods developed here at Lucas, we now routinely map and measure brain tissue water diffusion rates and direction, the perfusion of blood, and the brain's response to many functional activation tasks (such as vascular responses to mild reversible stresses) in a large number of diseases.

Over the past year, we continued to make significant progress in developing functional imaging technologies in several key areas. These included high-definition "HD" diffusion and perfusion techniques for the imaging of acute stroke and for the imaging of white matter structure and integrity. We are now funded to use the new 7 tesla MRI whole-body scanner to improve higher-resolution tools of high-field and high-speed MRI, focusing on disease processes in "brain attacks" (cerebral stroke) in both adults and in children using diffusion MRI (DWI), tissue perfusion mapping (PWI), as well as the new field of mapping the brain connectivity, DTI. By responding to the needs of our collaborators and colleagues here at Stanford and worldwide, we have found that diffusion and perfusion techniques have significantly advanced far beyond the experimental arena into everyday, routine clinical applications in a wide variety of fields where they are being actively and effectively used in numerous self-initiated and collaborative studies. The state-of-the-art in stroke MR imaging worldwide uses one of the sequences pioneered and developed here at Lucas.

Major strides have been made to improve research acquisition and reconstruction methods to our hospital systems with optimal performance to facilitate clinical studies. Moreover, considerable improvements in image quality have been achieved for DTI at 3T. In the next year, we are eager to move these methods from our scanners to those worldwide. With two clinical 3T MRIs now housed at Lucas and six being installed in our out-patient facilities, we will further advance our MR imaging tools and sharpen our focus on the critical clinical issues in the coming year with new experimental and clinical MR methods to predict eventual brain injury; to detect diffuse abnormalities in the brain occult to conventional imaging; to further map how the brain and spine are "wired"; to understand the complex physiological stresses and changes that the brain experiences during ischemia and other pathologic processes; and to extend these tools to better evaluate evolving therapies.

In addition to stroke, our team is intensely intersted in reducing image blur and artifacts by developing real-time motion correction of MRI scans with a special focus on children. This prospective approach is a major paradigm change and will help to reduce the sedation needed during the imaging of children.

Over the last few years, a critical mass of highly qualified and remarkably creative researchers who are well sought-after in their field came together at the Lucas Center. With success in funding, this number is growing. Their unique expertise and industriousness have allowed them to design highly innovative methods that significantly strengthened the quality of both diffusion-weighted and perfusion-weighted MRI.

Roland Bammer is an established faculty member at the Lucas Center where he is being promoted to Associate Professor of Radiology and is the key imaging faculty for Pediatric Radiology. He has created several significant collaborations with the Departments of Neurology and Pediatrics and has pioneered the active pediatric DTI program on the Lucile Packard Children's Hospital MRI scanner. Roland is an expert in parallel imaging with a special focus on applying this method to diffusion and perfusion imaging. He was a visiting professor at Bosporus University, Istanbul, Turkey, and he is also a university docent at the University of Graz, Austria. Roland has five funded peer- reviewed grants from the NIH. He directs multi-center trials, and has been named as "key personnel" on ten others. During the last year, Roland served as reviewer on several NIH study sections and is a full member on the editorial board of Magnetic Resonance in Medicine. Mike Moseley is a past president and Gold Medal winner of the International Society of Magnetic Resonance in Medicine (ISMRM) and was last year elected as a Lifetime Member of the Society of Magnetic Resonance Technologists (SMRT). Mike is a leading expert and pioneer of stroke imaging. He also sits on many NIH study sections and journal editorial boards.

The neuroimaging team remains involved in white matter tensor "fiber-tracking" neuroimaging projects as well as building collaborative programs. Samantha Holdsworth, from New Zealand, is working as a Research Associate on high-resolution diffusion and susceptibility-weighted sequences. Heiko Schmiedeskamp, a graduate student from the ETH in Zurich, is a visiting researcher developing several promising new multi-echo sequences for functional neuroimaging. Heiko was admitted to the Stanford Bioengineering PhD Program and will complete his PhD here at Stanford. Matus Straka, a postdoctoral scholar from the Vienna General Hospital (Austria) and the Computer Graphics Department of the University of Vienna, is focused on parallel computing issues for image reconstruction and quantitative parameter mapping for cerebral blood flow in clinical patients. Eun Soo Choi is a Masters graduate student from the Department of Electrical Engineering here at Stanford and will continue as a PhD candidate. Murat Aksoy is a fifth-year graduate student working with Roland on the exciting applications in fiber tractography and on motion correction projects. Stefan Skare is a Research Associate and Visiting Faculty Scholar from Sweden focused on multi-shot MR sequences for high-resolution diffusion in the presence of patient motion. Daniel Kopeinigg is a visiting researcher who works with Roland, Marcus Alley, and Dominik Fleischmann on contrast-enhanced angiography with a special focus on improving contrast injection profiles to achieve desired enhancement profiles in the arterial system. He will continue to work with us as a PhD candidate graduate student. Didem Aksoy is a Staff Scientist at the Stanford Stroke Center and at the Lucas Center. Thomas Brosnan is the Lucas Center Computational Manager who directs and coordinates the research and clinical computing and post-processing efforts in the Department of Radiology and the Lucas Center. Jian Zhang is a fifth-year graduate student actively involved in 3D volume spiral imaging for diffusion applications. He will direct GE research at the National Institutes of Health next year. Chunlei Liu received a highly-regarded K99/R00 award from the NIH on high-field 7Tesla applications of DWI. As his R00 award takes effect this year, Chunlei is now faculty in the Department of Radiology at Duke University.

Magnetic Resonance Research

Functional Imaging

Gary Glover, PhD

Glover Lab (L-R): Enmanuel Perez (summer student), Justin Brown, Neil Chatterjee, Christine Law, Catie Chang, Sean Mackey, Allyson Rosen, Paul Mazaika, Gary Glover

The functional MRI group continues to develop and optimize methods for the acquisition of functional imaging data. Projects include the development of alternative fMRI contrast methods, real-time biofeedback for training brains and reduction of physiological noise in fMRI signals. In addition, we continue to play an active role in the NCRR-funded FIRST BIRN schizophrenia test bed project, with Gary Glover as the chair of the calibration working group.

The group has seen several students graduate this year, including postdoc Jason Hsu, moving to a faculty position at the University of Florida; Chardonnay Vance, who moved to University of Minnesota for postdoctoral studies but is soon off to Wake Forest University. Not satisfied with just one doctorate, she is entering Med School this fall. Moriah Thomason is still a postdoc, but has relocated to Los Angeles because her husband (former RSL grad student Chris Caires) took a position there. Moriah is expecting her second child in August. Finally, Christine Law is concluding her doctoral studies and will be leaving soon. She has an embarrassing number of postdoctoral offers to chose from. We are always sad to see our 'kids' leave, but delighted at their opportunities for the next phase of their scientific careers.

The following are a few of the highlights of scientific progress; see abstracts for further details.

Graduate student Christine Law has had several papers accepted this year, concluding her dissertation work on spiral imaging with sparse sampling. She is finalizing a new endeavor this year using compressed sensing for timeseries analysis with concomitant deconvolution of the hemodynamic response function.

Jung Jiin (Jason) Hsu concluded the development of rapid methods of T1-based oximetry measurement for the CSF, working in conjunction with Greg Zaharchuk; a paper was published on this novel work.

Chardonnay Vance has concluded her study of placental insufficiency using T1 relaxation times to characterize the stage of disease. Her results indicate that a simple scan procedure may be diagnostic and useful in treatment decisions.

Graduate/MD student Rebecca Rakow-Penner has spent most of this year in clinical rotations, but is anxious to get back to developing functional methods to characterize breast cancer using Blood Oxygen Dependent contrast this fall.

Postdoc Moriah Thomason Caires has published her seminal work on development of working memory in children and also found that brain perfusion differs in subjects with different genetic composition.

Grad student Catie Chang has been remarkably productive, with 4 papers this year continuing to explore the dynamics of brain connectivity. In this exploration, she first had to develop methods of removing confounding noise and continues to study these effects. She has discovered that the brain's resting state networks are highly variable in their inter-region activity, and is developing new methods of investigation of this unexpected phenomenon.

Magnetic Resonance Research

Magnetic In Vivo Spectroscopy and Multinuclear Imaging

Daniel Spielman, PhD

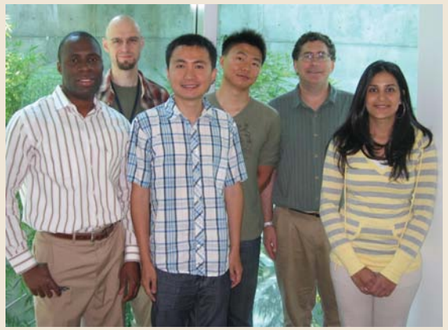

left to right: Moses Darpolor, Dirk Mayer, Calvin Lew, Meng Gu, Dan Spielman, Priti Balchandani.

The major thrust of our research during the past year was focused along three distinct lines. Research on the technical development of ultra-high field (7T) proton spectroscopy of the brain continues from last year with an added emphasis on the design and evaluation of novel RF excitation pulses for addressing the magnetic field inhomogeneities encountered at 7T. A highlight of this year's work is the development of a novel RF pulse design approach using the Shinnar-Le Roux algorithm to design adiabatic pulses. Under an ongoing program in the development of volumetric 1H MRSI at 1.5 T and 3.0 T, funded through an NIBIB Bioengineering Partnership grant (EB000822), we have successfully implemented a volumetric echo-planar spectroscopic imaging sequence and developed associated conversion software so that the data can be processed using a general purpose MRSI software package, MIDAS. Finally, our efforts in the area of hyperpolarized 13C MRS and MRSI continues to move forward at a rapid pace. Hyperpolarized 13C is an exciting new technology capable of directly probing key metabolic pathways by providing several orders of magnitude of increased signal than previously available. Over the past year we have successfully developed several fast MRSI protocols (temporal resolution = 120 ms/) and associated metabolic modeling tools, and are currently applying these techniques to the study of a number of pathologies including liver metabolic disorders, hepatocellular carcinoma, alcoholism, and pediatric arthritis. This work is now funded under NIH grant EB009070 entitled "Dynamic Metabolic Imaging of Hyperpolarized Substrates".

Molecular Imaging

Cellular and Molecular Imaging Lab

Jianghong Rao, PhD

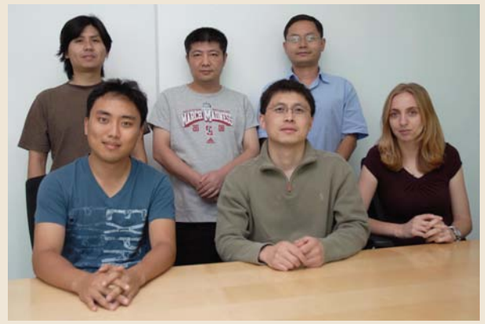

Sitting from left to right: Jungjoon Lee, JR, Anca Dragulescu-Andrasi, Standing from left to right: Zuyong Xia, Hongjun Ren, Gaolin Liang

The general research interest in the Rao lab is to develop novel molecular probes and imaging strategies for in vivo imaging by combining chemical synthesis and macromolecular engineering with imaging technology. Current projects are broadly defined in three areas: 1) imaging enzyme activity in vivo. As a unique class of protein molecules, enzymes catalyze biochemical transformations and are widely implicated in biological processes and diseases. We are developing "smart" activatable probes for imaging and detection of beta-lactamase activity from Mycobacterium tuberculosis (TB) in vivo to study TB biology and to evaluate the efficacy of therapeutics in preclinical animal models. The second class of enzyme target we are interested in is proteases, many of which display aberrant activity in diseases such as cancers and arthritis. We are employing both small molecular weight probes and nanoparticles-based nanosensors to in vitro detection and in vivo imaging of the activity of proteases such as matrix metalloproteinase-2 (MMP-2) and furin in cancer cells. 2) A second major area of interest is developing general strategies to label proteins and RNAs in living cells for in vivo imaging. Our approach is to design small organic dye molecules that are not fluorescent initially but that become fluorescent after binding to a receptor or tag fused to either a protein or RNA molecule of interest. We are combining rational design and library selection methods, such as SELEX and phage display, to discover such novel molecular tags for super high resolution single-molecule imaging in living cells. 3) The third research focus is to develop novel sensing and imaging technologies. We mimicked the naturally occurring bioluminescence resonance energy transfer (BRET) system in the sea pansy, Renilla reniformis, and developed a QD-BRET technology widely applicable for in vitro biosensing and in vivo imaging.

Molecular Imaging Instrumentation Laboratory (MIIL)

Craig Levin, PhD

Bottom row, left to right: Frances Lau, Jenny Kwan, Craig Levin, Monica Omid-Zohoor, Virginia Spanoudaki; Middle row, left to right: Arne Vandenbrouke, Yi Gu, Jinjian Zhai, Hao Peng, Garry Chinn, Naran Bayanbat, Joohyun Lee, Michael Liu; Top row, left to right: Kanguk Kim, Peter Olcott, Peter Bullen, Guillem Pratx, Paul Reynolds, Alex Grant, Tom McLaughlin;

Our research interests are to advance instrumentation and algorithms for the non-invasive imaging of basic cellular and molecular signatures associated with disease. These new "cameras" image photon emissions from molecular probes designed to target specific molecular processes associated with disease in cells located deep within the tissues of living subjects. The technical goals of the instrumentation projects are to advance the photon detection efficiency and spatial, spectral, and temporal resolutions. The algorithmic goals are to understand the physical system comprising the subject tissues, photon transport, and camera, and to realize the best available reconstructed image quality and quantitative accuracy. The work involves the design, development, and testing of novel position sensitive photon sensors and systems; low-noise readout electronics; data acquisition electronics; computer modeling; computer graphics; tomographic image reconstruction algorithms; signal/image processing algorithms; and data/image analysis.

Key goals of our research are to incorporate these innovations into practical imaging devices and introduce new in vivo imaging tools to advance studies of molecular mechanisms and aid discovery of novel treatments of disease in the clinic as well as in preclinical research. If successful, these novel systems will substantially enhance the visualization and quantification of subtle molecular signatures associated with disease with the hope that molecular imaging can play a role in earlier disease management. The research is supported by grants from the National Cancer Institute, National Institute of Biomedical Imaging and Bioengineering, and GE Medical Systems. Trainee fellowships are supported by Stanford's Bio-X Program and School of Medicine Dean's Fellowship Program, the Society of Nuclear Medicine, and the AXA Research Fund.

Molecular Imaging

Cardiovascular Stem Cell and Gene Therapy Imaging

Joseph Wu, MD, PhD

Ischemic heart disease is the number one cause of morbidity and mortality in the United States. The repeated ischemic insults can lead to congestive heart failure, which is the leading cause of hospital admissions for people aged 65 years and over. In the next decade, cardiovascular diseases will likely be targeted at the basic cellular and molecular levels. The Cardiovascular Gene & Cell Therapy lab (http://mips.stanford.edu/research/lab?lab%5fid=2883) combines expertise in molecular and cell biology, cardiovascular physiology, and molecular imaging. We work on the biological mechanisms of adult stem cells, embryonic stem cells, and induced pluripotent stem cells. We use a combination of gene profiling, tissue engineering, physiological testing, and molecular imaging technologies to better understand stem cell biology in vitro and in vivo. For adult stem cells, we are interested in monitoring stem cell survival, proliferation, and differentiation. For ESC, we are currently studying their tumorigenicity, immunogenicity, and differentiation. For iPSC, we are working on novel derivation techniques. We also work on development of novel vectors and therapeutic genes for cardiovascular gene therapy applications. The eventual goal is to establish molecular imaging as a platform for translational research in cellular and gene therapies for ischemic heart disease in the 21st century.

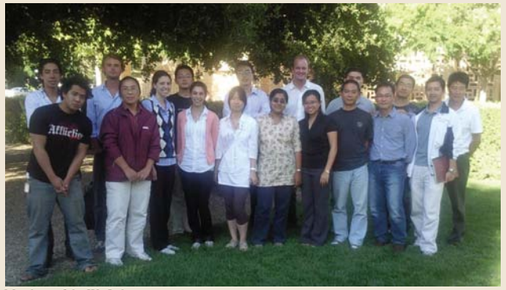

Members of the Wu Lab.

Clinical Molecular Imaging Research

Andrew Quon, MD

Our group is focused on applying emerging molecular imaging techniques into clinical practice. Current projects include:

•Evaluation of the radiotracer NaF for orthopedic disease

•A comparison of FDG PET/CT and DCE MRI for monitoring targeted therapy

•Pilot study of the novel radiotracer 18F-5FU to assess modulation 5FU receptors by bevacizumab

•3D volume rendered PET/CT to aid laparoscopic gastrectomies

•Development of computer aided diagnosis tools for PET/CT

News & Updates

Awards: Maurice Zissen was awarded the MedScholars Scholarship

Andrei Iagaru was awarded 2009 Image of the Year at the Society of Nuclear Medicine Annual Meeting

Notable articles that have been published in the past year:

Quon A, Chang ST, Chin F, Kamaya A, Dick DW, Loo BW, Jr., Gambhir SS and Koong AC. “Initial evaluation of 18F-fluorothymidine (FLT) PET/CT scanning for primary pancreatic cancer.” Eur J Nucl Med Mol Imaging 2008 35(3): 527-31.

Iagaru A, Mittra E, Yaghoubi SS, Dick DW, Quon A, Goris ML, Gambhir SS. Novel Strategy for a Cocktail 18F-Fluoride and 18F-FDG PET/CT Scan for Evaluation of Malignancy: Results of the Pilot-Phase Study. J Nucl Med 2009; 50 (4):501-5.

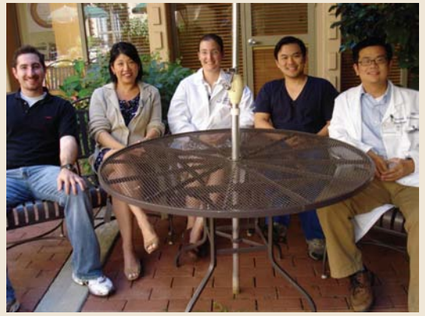

left to right: Maurice Zissen, Lindee Burton, Meike Schipper, Kristen Hirabayashi, Andrew Quon, Frank Lin. Andrei Iagaru (not pictured)

Molecular Imaging

Multimodality Molecular Imaging Lab

Sanjiv Sam Gambhir, MD, PhD

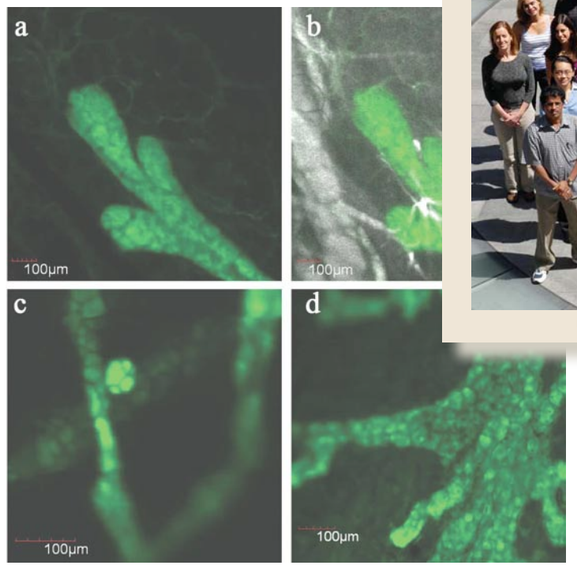

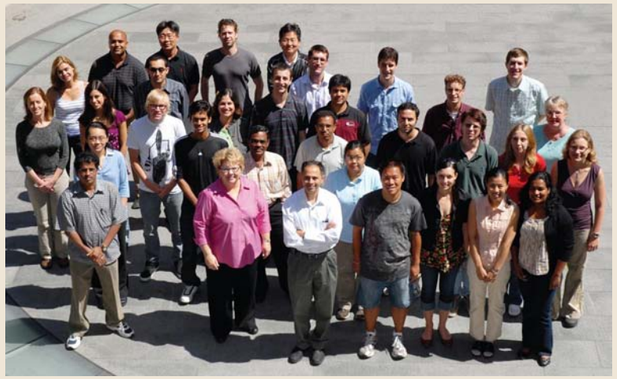

Multimodality Molecular Imaging Lab

We are developing imaging assays to monitor fundamental cellular events in living subjects. We are actively investigating technologies such as micro-positron emission tomography (micro-PET); bioluminescence optical imaging with a charge coupled-device (CCD) camera; fluorescence optical imaging; micro-computerized axial tomography (microCAT); photoacoustics; and Raman spectroscopy in small animal models. Our goals are to marry fundamental advances in molecular/cell biology with those in biomedical imaging to advance the field of molecular imaging. We have a particular focus on cancer biology. We have developed several reporter genes/reporter probes compatible with all of the above imaging modalities. These reporter genes are being used in cell trafficking models, gene therapy models, as well as in transgenic models for studying cancer biology. Assays to interrogate cells for mRNA levels, cell surface antigens, protein-protein interactions, protein phosphorylation, and intramolecular folding are also under active development. We are also extending many of these approaches for human clinical applications. New patient trials for PET imaging of T-cell trafficking in patients are being performed with our reporter gene strategies. Over this last year we have also developed mathematical models that allow one to understand minimal tumor burdens that are likely to be detectable based on blood protein levels. These models are now being linked to experiments with new nanosensors to detect low levels of tumor blood proteins and novel molecular imaging strategies for earlier cancer detection.

Molecular Imaging

Translational Molecular Imaging Lab

Jürgen K. Willmann, MD

In the United States, cancer continues to be the leading cause of death in patients between 25 and 64 years of age, and the second leading cause of death in patients both above 65 years and between 1 and 14 years. Since prognosis and survival of patients with cancer highly depend on the tumor stage at the time of diagnosis, early cancer detection shows great promise in prolonging survival and improving quality of life in cancer patients. Therefore, novel imaging strategies that allow detection of cancer at early, still curable stages are highly desirable. Furthermore, with the advent of novel therapeutic options for cancer patients, there is an increasing demand for non-invasive imaging biomarkers to identify those patients early on who will benefit most from a given treatment or to terminate or modify treatment for those patients not responding to a certain treatment.

In my laboratory we focus on the development and clinical translation of novel molecular and functional imaging biomarkers with special focus on imaging abdominal and pelvic cancer including pancreatic, liver, renal, ovarian, and prostate cancer. We further advance clinically available radiological imaging modalities such as ultrasound, magnetic resonance imaging (MRI), and positron emission tomography (PET) as promising imaging tools for early detection and treatment monitoring of abdominal and pelvic cancer. Our mission is to integrate novel molecular and functional imaging strategies into clinical protocols for improved patient care in the near future.

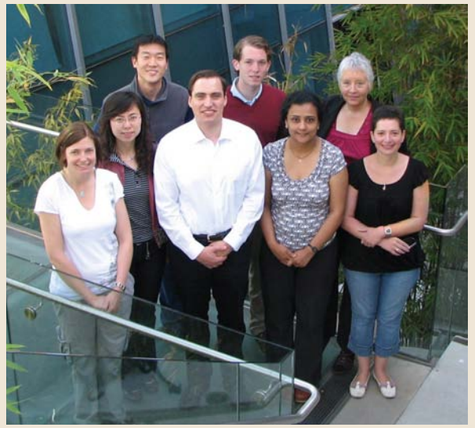

Front row (from left to right): Marybeth Pysz, PhD; Ying Ren, MD; Juergen K. Willmann, MD; Nirupama Deshpande, PhD; Kira Foygel, PhD. Back row (from left to right): David Wang, MD; Cedric Panje, medical student; Alice Gardner.

Cancer Molecular Imaging Chemistry Lab (CMICL)

Zhen Cheng, PhD

Our group is interested in developing novel multimodality imaging agents and techniques for non-invasive detection of cancer and its metastasis at the earliest stage, so that cancer can be cured or transformed into a chronic, manageable disease. We have aimed to identify novel cancer biomarkers with significant clinical relevance, explore new chemistry and platforms for imaging probe preparation, and develop new cancer imaging strategies for clinical translation. To accomplish these goals, a multidisciplinary team composed of members with expertise in organic chemistry, radiochemistry, biochemistry, molecular an cell biology, radiological science, medicine and molecular imaging have been built up over the past one and half year.

Currently, we are actively studying several important problems in the molecular imaging field. First, we are investigating a variety of new platform molecules (peptides, proteins, nanoparticles) as universal strategies for cancer imaging; Second, we are establishing new methodologies for site-specific labeling these platform molecules for multimodality imaging; Third, by applying the knowledge obtained from the above research, we are optimizing the agents for imaging of melanoma MC1R, ovarian cancer integrin and breast cancer HER2 and EGFR expression, and we hope to quickly move two molecular probes into clinic PET imaging in near future.

Our research is currently supported by the Department of Radiology, GE Global Research Center, and grants from the California Breast Cancer Research Program, Society of Nuclear Medicine, and ICMIC at Stanford.

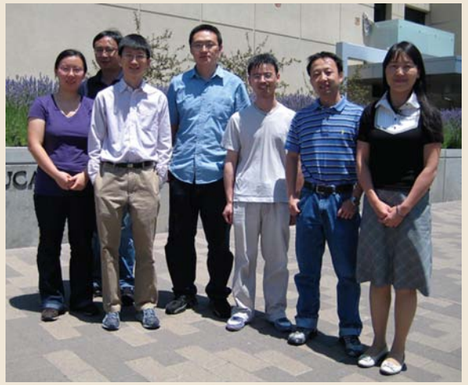

(l-r), Lei Jiang, Song Wu, Zhen Cheng, Hongguang Liu, Zhen Miao, Gang Ren, Yihong Wang. Missing: Edwin Chang

Molecular Imaging

Molecular Imaging Probe Laboratory (MIPL)

Xiaoyuan (Shawn) Chen, PhD

Shawn Chen's group is interested in developing and validating novel molecular imaging probes (nanoparticles, antibodies, proteins, peptides and small organic molecules) for the visualization and quantification of molecular targets that are aberrantly expressed during tumor growth, angiogenesis and metastasis. We are trying to combine both anatomical and molecular imaging techniques to pinpoint molecular and functional information related to tumor growth and dissemination, and monitor specific molecular therapeutic efficacy. We are currently working closely with two important angiogenesis targets: integrin alpha(v)beta(3) and vascular endothelial growth factor receptor subtype-2 (VEGFR-2). Integrins expressed on endothelial cells modulate cell migration and survival during angiogenesis. Integrins expressed on carcinoma cells potentiate metastasis by facilitating invasion and movement across blood vessels. In several malignancies, tumor expression of integrin alpha(v) beta(3) correlates well with tumor progression. VEGF is a key regulator of tumor angiogenesis and is the most potent endothelial cell mitogen. Binding of VEGF to its receptor on the endothelial cell membrane stimulates the VEGF signaling pathway. VEGFR-2 (KDR/Flk-1) is the primary VEGF receptor on endothelial cells. Specific projects include nanoplatform-based molecular imaging, multimodality imaging of angiogenesis and metastasis, as well as targeted delivery of gene, chemo, and radiotherapeutics.

Our research efforts are currently supported by NIH and DOD. The eIND application of one of the novel integrin specific PET tracers 18F-FPPRGD2 has gained FDA approval and first-in-human studies are being conducted. The iron oxide nanoparticle work done by Dr. Ha-Young Lee was chosen as one of the best basic science papers published in J Nucl Med in 2008. Dr. Seulki Lee's review article on dual-modality probes was selected as cover feature in Molecular Imaging journal. The collaborative effort between Dai and Chen labs on carbon nanotube based nanotherapeutics was cover featured in Cancer Research. Collaborative research on ultrasmall iron oxide nanoparticles with Brown University received various media coverage. The paper published in Nano Lett on quantum dots was identified as the highest cited paper in the research area of "imaging tumor vasculature". Drs. Qizhen Cao, Gang Niu and Jin Xie received travel award for attending the 56th SNM annual conference. Dr. Seulki Lee also received travel award for 2009 World Molecular Imaging Congress (WMIC). Overall, we are proud to say that 2009 has been very busy and productive.

Dr. Chen moved to NIH at beginning of August to become the Chief, Laboratory of Molecular Imaging and Nanomedicine at the National Institute of Biomedical Imaging and Bioengineering (NIBIB). His new lab will house over 20 staff members, research fellows, postdocs, and visiting students. Dr. Chen will be missed but we will collaborate with him and hope to continue to develop many new projects with frequent opportunity to interact with him and his new NIH colleagues.

Front row (l-r): Gang Niu, Shuanglong (Scott) Liu, Kai Chen, Euesoon Jang, Yingding (Bryan) Xu, Edwin Chang, Jin Xie; back row (l-r): Jinhao Gao, Jiandong Wang, Qizhen Cao, Yongjun Yan, Xiaoyuan (Shawn) Chen, Seulki Lee, Xin Lin, Xilin Sun, Lihong Bu, Jing Huang

Facilities

Outpatient Imaging

Volney Van Dalsem, MD —Director

Susie Speilman — Director, Strategic Initiatives and Program Management

Growth in Outpatient Imaging

Stanford has experienced a doubling of its imaging capacity with the addition of two new outpatient imaging centers over the last 18 months. Through their leading-edge equipment, these centers will ensure Stanford remains at the forefront of clinical and research innovations, while offering additional imaging capacity in close proximity to Stanford Hospital, and an expansion of our services to the surrounding community.

Stanford Medicine Imaging Center (SMIC), Palo Alto

In February of 2009, Stanford Medicine Outpatient Center (SMOC) opened in Redwood City, and is home to an advanced imaging center along with specialized services previously located in the Stanford University Medical Center. Orthopaedic Surgery, Sports Medicine, Pain Management, and Sleep Medicine have now all been moved to the 360,000 square foot facility in Redwood City, of which more than 16,000 square feet are devoted to imaging. A new Digestive Health Center is scheduled to be added in 2010. The imaging center at SMOC has two of the most advanced 3T MRIs as well as one state-of-the-art CT scanner and will eventually expand to include a total of three MRIs and three CTs. Studies are focused on musculoskeletal and abdominal exams to accommodate the center's clinics.

The Stanford Medicine Imaging Center (SMIC), Palo Alto, celebrated its first anniversary in June 2009 and has achieved great success in its delivery of a new paradigm in imaging services. SMIC was created to deliver an entirely new approach to medical imaging, offering patients access to the most advanced diagnostic imaging capabilities available, provided in a refined, "healing" environment similar to that of a private practice. The 10,000-square foot space serves as a combined clinical and research center and features the latest CT and MRI equipment, as well as the subspecialty imaging expertise of Stanford radiologists. The rapid advance of imaging technology (typically in 18–24 month cycles) requires frequent upgrading of equipment. With the goal of keeping technology current in our outpatient facilities, we have already replaced one 3T MRI scanner and one CT scanner within the first year of the Center's opening; upgrades to the remaining MRI and CT scanners will be completed in the fall of 2009.

While most imaging centers are designed to separate the patient from the professionals, we have created a center in which the physical layout promotes interaction between the patient, radiologist, and technologist, under the premise that more communication results in better patient care. The design and exceptional service standards create a warm, private, and caring environment. We further included amenities such as individual rooms to enhance patient privacy, an on-site concierge, as well as a Stanford Health Library kiosk and patient education center. We have begun to use the Center as a test site to study patients' preferences for the delivery of imaging results and the impact of the technology and facility in their care. We will soon begin delivering results to patients immediately after their exams as part of a study we have recently initiated with the Department of Oncology.

Stanford Medicine Outpatient Center (SMOC), Redwood City

The Center's commitment to staying ahead of the imaging technology curve makes the facility uniquely suited to a wide array of research activities, speeding the translation of research advances into clinical practice. Along with the innovations of our 200 Lucas Center researchers and scientists, the research performed in our Center will be translated directly to patient care. Our scientists are working every day to create software enhancements that can markedly improve imaging studies, and many of the new MR methods developed by Stanford are not available on commercial scanners. However, we are able to implement these advances at SMIC and our other sites so that patients can immediately benefit from our research in many clinical areas including breast cancer detection, stroke, and musculoskeletal imaging. Future advances and the availability of on-site blood testing capabilities will also draw healthy patients to the Center for early diagnosis and treatment. The blood testing laboratory at SMIC will be an important tool for our new Center of Excellence in Early Cancer Detection as we work to combine data from blood and imaging tests to predict the likelihood of disease.

Stanford 3D medical imaging laboratory

Geoffrey Rubin, MD

Sandy Napel, PhD

Laura Pierce, MPA, RT (CT), Lab Manager

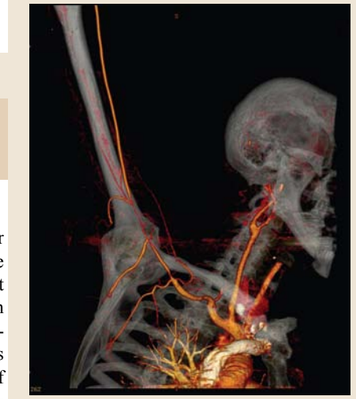

The Stanford 3D medical imaging laboratory is guided by the mission of developing and applying innovative techniques for efficient analysis and display of medical imaging data through interdisciplinary collaboration. Since 1996, our clinical goal has been to deliver 3D imaging advances as rapidly as possible for the swift and accurate diagnosis and treatment of disease; our educational goal is to disseminate knowledge and duplicate our 3D services at other institutions. To facilitate the bridge between innovation and other clinical use of technology, we also continue to serve as an imaging core lab for medical device developers.

Progress

Clinical: Over the past year, the 3D laboratory has continued its operations simultaneously in the Lucas Center as well as the James H. Clark Center, a building dedicated to interdisciplinary science. With the addition of the Stanford Medical Imaging centers in Palo Alto and Redwood City, our average monthly 3D volume has increased to approximately 915 examinations, and we have processed over 67,000 examinations overall since our inception. The majority of our referrals continue to come from vascular surgery, cardiothoracic surgery, gastroenterology, cardiology, urology, reconstructive surgery, orthopedics, and neurosurgery. Laura Pierce, 3D Lab Manager, describes the significant increase in 3D technology in all types of CT employment settings from 1993 through 2007 in a recent article entitled Trends in 3-D CT Postprocessing.

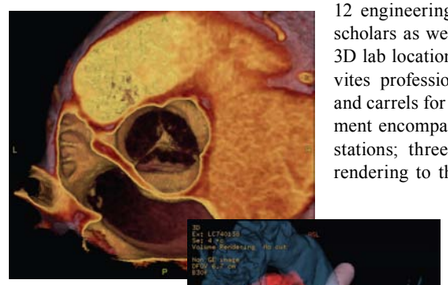

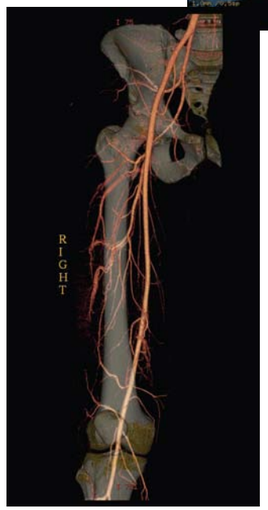

Education: This year the 3D lab has been attended by international visiting scholars from Japan, as well as Stanford Radiology fellows, residents, and medical students who acquire skills in 3D interpretation as part of their medical training. Stanford researchers from engineering and medical departments have also been trained in acquiring 3D images and data for research projects, including video microscopy, electron microscopy, and multimodality small animal imagers. The 3D lab has hosted visiting radiologists and technologists from other medical centers through our 3D clinical fellowship program.

Infrastructure

3D imaging specialists include: Laura Pierce, 3D lab manager; senior 3D technologists Marc Sofilos and Linda Novello; 3D technologists Keshni Kumar; William Johnsen, Nancy Ware and Shannon Walters. Our technologists offer not only expertise in 3D imaging, but also experience in CT and MRI scanning techniques as well. Support staff includes administrative assistants Lakeesha Winston and Debra Frank, and database administrator, Kala Raman. The research arm of the lab retains an annual average of 12 engineering graduate students and postdoctoral scholars as well as 2 clinical MD researchers. Both 3D lab locations include a central area table that invites professional collaboration and student desks and carrels for independent research. The lab equipment encompasses a total of 13 advanced 3D workstations; three servers, which provide remote 3D rendering to the Stanford medical community; and two research and development servers for image and data storage. Two remote PACS workstations allow access to all Stanford medical imaging and reporting.

We continue our excellent relationships with corporate developers of 3D workstations (e.g., GE Healthcare, TeraRecon, and Vital Images) who site their hardware and software in the 3D lab in anticipation of our feedback. These relationships ensure that we maintain the most advanced multi-dimensional analytical technologies available. To expedite workflow, future clinical applications include migration of all 3D software applications to centrally located vendor-supplied servers, for immediately sharing post-processed patient data throughout our enterprise.

Conclusion

The 3D Medical Imaging Lab continues to function as an international leader in clinical care, teaching, and research in medical imaging analysis. The confluence of talented, medical and engineering expertise as well as the most up-to-date equipment has been a consistent source of innovative developments in diagnostic and treatment planning approaches.

References: Pierce LP, Rosenberg J, Neustel S. Trends in 3-D CT Postprocessing. Radiologic Technology, Sept/Oct 2009, Vol 81, No1.

Study Model Management

Wendy Baumgardner, RVT, LATg

Pam Hertz, RVT

Research studies involving animal models at The Richard M. Lucas Center enhance both overall healthcare and diagnostic imaging. In our continuing efforts to provide support to the Radiology investigators, we are entrusted with the responsibility of overseeing all animal model protocols within our Department and all other Stanford departments conducting research at our center and satellite facilities. Two experienced California registered veterinary nurses (RVTs) attend all animal model studies where diligent care is taken during all procedures. Animals are treated with great respect, compassion, and professional care. Deviation from the protocols is not permitted. All personnel working with animals under approved Institutional Animal Care and Use Committee (IACUC) protocols have attended "required" seminars from the University's Department of Comparative Medicine. Specifically tailored, one-on-one training is available for more advanced techniques. In addition, we ensure compliance to all government and university regulations and policies. We realize that living subjects are needed to advance our knowledge, and commit to the proper respect for life in this quest. Work at the center develops and improves new invasive and non-invasive procedures that use magnetic resonance imaging, x-ray fluoroscopy, focused ultrasound, and computed x-ray tomography to guide them. Research studies currently involve the study of infarct modeling, radiofrequency cardiac ablation, stroke, liver and prostate cancers, neuroimaging of the brain, and stent/graft implantation. Research is enhanced by the ability to keep pace with the latest application of medical equipment and continuing education through conferences and seminars. The techniques currently being explored at the center all contribute to more efficient and effective medical treatment for illness and disease in both humans (adults and children) and animals. We look to the future with hope that through quality biomedical research the necessity for animal use will decrease with the increased use of computerized models or other non-living systems. With this in mind, we realize the privilege we are granted and strive for continued excellence in all research taking place within the Richard M. Lucas Center and the Department of Radiology.

Veterinary Technicians, Pam and Wendy in the CT Axiom Lab

Small Animal Imaging Center – SCi3

Tim Doyle, PhD -Head, Small Animal Imaging Facility, MIPS

2009 is the sixth year the small animal imaging facility has been in the basement of the Clark Center, and the fourth year of being a full University core facility, with grant support from the Department of Radiology (ICMIC P50), the Stanford Cancer Center, and the Digestive Disease Core. Oversight of the core has moved this year from the Department of Pediatrics to the School of Medicine. The Small Animal Imaging Workshop that we had hosted the past few Novembers will be discontinued for the foreseeable future, in compliance with the Stanford Industry Interactions Policy. The core continues to be one of the premier small animal imaging facilities in the USA.

Dr. Tim Doyle, Scientific Director of the facility, provides regular training on the IVIS Imaging Systems (both bioluminescence and fluorescence imaging), MicroCT scanners, MicroSPECT scanners, and the Vevo Ultrasound. The facility has benefitted from the loan of two additional ultrasound systems through collaborations between Dr. Juergen Willmann, Assistant Professor in Radiology, with Siemens and Visualsonics. Dr. Doyle also shows users how to use the Visual Sonics (Mauna Kea) Cellvizio microscope, cryomicrotome and cryomacrotome systems.

Dr. Laura Pisani, MRI Physicist for the facility, manages the 7T MRI system, provides regular training sessions and individual assistance for any users on this system, helping many groups here at Stanford to expand their pre-clinical research to utilize MRI. Connections continue to grow between this imaging facility, and the two large MRI development groups on campus (the Lucas Center and Electrical Engineering). Ron Watkins, Radiology Senior Research Associate, contributes his well-honed skill and experience in radiofrequency (RF) coil building. Core facility MRI users have also benefited this year from the arrival of Dr. Brian Rutt, Professor in Radiology, who has brought not only his single-cell MR imaging expertise, but also customized RF coils which he has made available to any MR imagers in the facility. Dr. Pisani also provides training on the use of radionuclides in the imaging facility, as well as training on the MicroPET systems. Finally, Dr Pisani provides training on the ART Optix and CRI Maestro fluorescence imaging systems.

Dr. Frezghi Habte provides image quantification expertise to all users of the imaging facility. He runs regular classes focusing on different commercial software applications such as Amira, Microview, ASI Pro and AMIDE; free image analysis software such as ImageJ and Osirix; and in-house software applications such as RT Image (written by Ted Graves, Assistant Professor in Radiation Oncology). Dr. Habte also provides assistance with specific image quantification challenges as required.

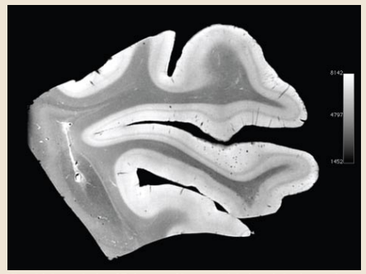

Ultra-high resolution 3D image of human Alzheimer's brain specimen acquired using 7T MRI, showing section of visual cortex. Voxel size is 100 micron, isotrope 3D resolution. At this resolution and field strength, individual amyloid-beta plaques can be detected.

Lucas Center MR Systems

Anne Marie Sawyer, BS, RT (R)(MR)
Sandra Rodriguez, RT (R)(MR)

The 1.5 Tesla (Figures 1 and 3) and 3.0 Tesla #1 G.E. Healthcare MR systems are currently operating at 14.0 systems revision; the 7.0 Tesla (Figure 2) at 12.0; and the 3.0 Tesla #2 "750" (Figure 4) installed April 2008 at 20.0 software. The systems operate at a maximum slew rate of 150 Tesla per meter per second and maximum gradient amplitudes of 50 milliTesla per meter (1.5T and 3T2) and 40 milliTesla per meter (3T1 and 7T). The hardware currently allows the use of 8-channel phased array coils at 1.5T; 16 channels at 3.0T and 7.0T; and 32 channels at 3.0T #2.

Figure 1. Marcus Alley, PhD, research associate (right), assists Chris Elkins, PhD, a researcher from Mechanical Engineering (left) with a mechanical flow phantom at the 1.5T whole body magnet. Images are generated that resolve spatially in 3 directions plus time resulting in a "4D"scan.

Figure 2. At the 7.0T whole body magnet, research engineer Ron Watkins (middle) demonstrates a prototype radiofrequency (RF) coil to faculty Brian Rutt, PhD (left) and research associate Arundhuti Ganguly, PhD (right) being used for research studies.

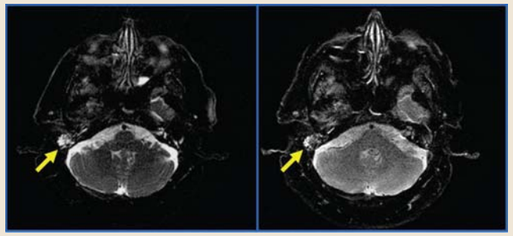

Figure 3. Example of a research study being conducted at 1.5T: High Resolution Structural and Quantitative MRI in Cholesteatoma (see arrows). This collaboration is between Samantha Holdsworth, PhD (Lucas Center, Radiology), Nancy Fischbein, MD (Radiology) and Nikolas Blevins, MD (Otolaryngology). Research sequence "rs-epi" (right) displays increased spatial resolution and reduced echo time versus that of a product propeller sequence (left).

Daily support in MR system operation and screening and safety is provided to all researchers including faculty, post-doctoral fellows, graduate students, and visiting scholars in the Lucas Center and Department of Radiology; researchers from other University departments such as Psychology, Psychiatry, Neurology, Neurosurgery, and Nephrology; and service center users from outside of the University.

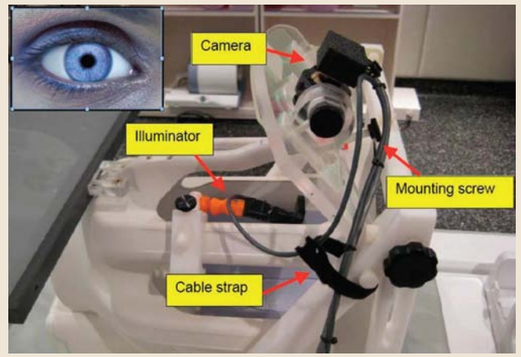

Figure 4. A new eye tracker was designed and constructed (www.magconcept.com/MRI) for use with the 8-channel receive-only phased array head coil during functional brain imaging at the 3T2 MRI. Knowing where the eye gaze is focused or what the pupil diameter is reveals behavior important to understanding brain results for many studies.

Cyclotron Suite Update

Frederick Chin, PhD

David Dick, PhD

The Radiochemistry Facility (RF) continues to develop and offer radiotracers for early detection and therapeutic monitoring of disease in both preclinical and clinical imaging settings. In the past year our radiochemistry personnel (faculty, staff, and postdocs) has nearly doubled in number to thirty. Our facility recently recruited Dr. Bin Shen (Postdoctoral Research Scientist) and George Montoya (Production Technician) to help us with our increasing radiochemistry efforts. Newly installed instruments include a GE TRACERlab FX-FN, two gas chromatographs with autosamplers and two additional high performance liquid chromatographs. The facility has expanded to include the Boswell Laboratory A064 for performing clinical-grade radiopharmaceutical labeling of peptides with long-lived radioisotopes (i.e. Cu-64), complementing the existing long-lived radiochemistry lab (Lucas P138) dedicated for providing tracers for pre-clinical investigations. Planned expansion of the RF will continue as part of the new Nuclear Medicine Department in 2010. Additional equipment including lead-shielded hot cells, automated radiosynthesis modules, microfluidic system, and other ancillary analytical instruments will be acquired for our growing radiochemistry program.

From Left to Right: Bin Shen (Postdoctoral Radiochemist), Aileen Hoehne (Postdoctoral Radiochemist), Frederick Chin, George Montoya (Production Technician), Andrew Lamb (Production Technician), David Dick, and Rhona Berganos (Staff Radiochemist). Missing from picture: Murugesan Subbarayan (Staff Radiochemist)

Our staff continues to provide routine clinical tracers for use at the Stanford Hospital. Fluorine-18 labeled fluorodeoxyglucose (FDG) is still produced daily. Nitrogen-13 ammonia (myocardial perfusion assessment) and Fluorine-18 sodium fluoride (bone imaging) are also synthesized for the clinic as needed.

GE TRACERlab radiosynthesis modules are the workhorses in the lab and perform the syntheses of our ^{18}F and ^{11}C-labeled radiotracers for collaborative researchers at Stanford and pharma. These modules have enabled us to perform new radiochemistries, providing [^{18}F]EF-5 (imaging tumor hypoxia) and [^{18}F]FPPRGD2 (imaging tumor angiogenesis) for human studies. Additional PET radiotracers that study the mechanisms and treatment of cancer as well as neurological disorders will soon become available to meet the increasing needs for performing preclinical ([^{11}C]Raclopride, [^{18}F]Saxitoxin, [^{11}C]DPA-713, [^{18}F]PBR-28) and clinical ([^{64}Cu]Rituximab, [^{18}F]SPA-RQ) research studies with PET.

The following table summarizes an updated list of radiolabeled compounds that are made in the research radiochemistry lab, excluding research compounds protected under confidentiality agreements (Bolded tracers = preclinical and clinical use; * = began clinical studies in 2008-2009; † = ready for future clinical studies).

Radiolabeled Compounds

Tracer	Use	Application
[^{11}C]NMSP	Imaging dopamine-2 receptors (D2R)	Monitoring D2R-related neurological disorders (i.e. Parkinson's Disease)
[^{11}C]Raclopride	Imaging dopamine-2 receptors (D2R)	Monitoring D2R-related neurological disorders (i.e. Parkinson's Disease)
[^{11}C]PIB*	Imaging αβ amyloid in brain	Monitoring progression of Alzheimer disease in brain
[^{18}F]fluoroalkyne	Labeling agent used with "Click Chemistry"	Novel method for radiolabeling peptides
[^{18}F]Fluoro-BG-137	Imaging δ-opioid receptor	Imaging the process of chronic pain
[^{18}F] FAZA	Hypoxia imaging agent	Evaluating clinical-relevant hypoxia-directed cancer therapies
[^{18}F]MISO	Hypoxia imaging agent	Evaluating clinical-relevant hypoxia-directed cancer therapies
[^{18}F]EF-5†	Hypoxia imaging agent	Evaluating clinical-relevant hypoxia-directed cancer therapies
[^{18}F]Fluorouracil*	Tumor imaging agent	Evaluating clinical-relevant cancer therapies
[^{18}F]fluorobenzaldehyde	Prosthetic labeling group	1) Radiolabeling peptides for potential clinical use 2) Radiolabeled affibody for imaging of NER2neu
[^{18}F]fluorobenzoic acid	Prosthetic labeling group	Radiolabeling peptides for potential clinical use
[^{18}F]Fluoropropionic Acid	Prosthetic labeling group	Radiolabeling peptides for potential clinical use
[^{18}F]SFB	Prosthetic labeling group	Radiolabeling peptides for clinical use
[^{18}F]FDF	Imaging fructose metabolism and pentose pathway	Imaging fructose metabolism and the pentose pathway
[^{18}F]FEAU	Imaging substrates expressing mutant HSV1-sr39tk	1) Monitoring gene therapies targeting cancer 2) Monitoring cell therapies
[^{18}F]FHBG	Imaging agent for tumors expressing HSV1-tk	Monitoring various cancer therapies
[^{18}F]FLT	Imaging agent for tumor cell proliferation	Monitoring various cancer therapies
[^{18}F]FPRGD2	$\alpha_v\beta_3$ integrin imaging agent	Imaging tumor integrin expression
[^{18}F]FPPRGD2*	$\alpha_v\beta_3$ integrin imaging agent	Imaging tumor integrin expression
Other ^{18}F-RGD peptides	$\alpha_v\beta_3$ integrin imaging agent	Imaging tumor integrin expression

Abstracts

Advanced X-Ray and Computed Tomography (CT) Techniques

Abstracts in this section describe research that is conducted using sophisticated x-ray and Computed Tomography (CT) techniques to improve image quality, decrease the amount of radiation exposure, or reduce the amount of time required to complete an exam. The overall goal of these projects is to improve our ability to detect and monitor disease using these x-ray based methods.

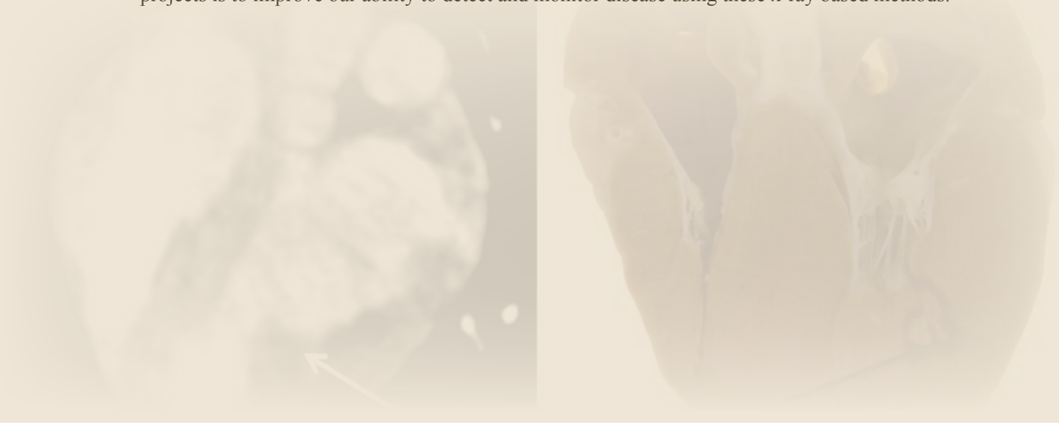

Metal artifact reduction algorithm for X-ray CT using a three-pass approach

S.R. Mazin[1] and N.J. Pelc[1,2]
Depts of [1]Radiology and [2]Bioengineering, Stanford University, CA

Metal objects, such as dental work, joint implants, etc., cause significant artifacts in CT images, sometimes degrading the image quality even in distant anatomic regions. Iterative reconstruction has been proposed as a method to reduce the problems but the processing time is excessive and the results are mixed. We are investigating a three-pass reconstruction approach for metal artifact reduction in x-ray CT. The algorithm consists of: 1) Initial reconstruction from the original sinogram data; 2) Simple thresholding to identify high-density regions (e.g. metal) that can cause artifacts; 3) Delineation of corresponding regions in the original sinogram that are replaced using linear interpolation; 4) Second reconstruction after the interpolation; 5) All pixels in the second image that lie between -500 and +500 HU are replaced with the mean of these pixels; 6) Rays in the sinogram through the metal are estimated a second time through forward projection of the segmented second image; 7) Third and final reconstruction. One additional aspect of the algorithm is that to avoid the need for forward projection across the entire native field-of-view (FOV) during step 6 above, a double-wedge filter is applied in the 2DFT space of the sinogram so that objects outside of the reconstruction FOV are filtered out of the original sinogram. If k and ρ are the view-angle and fan-angle frequency variables, respectively, the double-wedge filter consists of setting to zero all frequencies in the 2DFT of the sinogram for which $|k/(k+\rho)|>R/L$, where R is the reconstruction FOV and L is the source-to-isocenter distance.

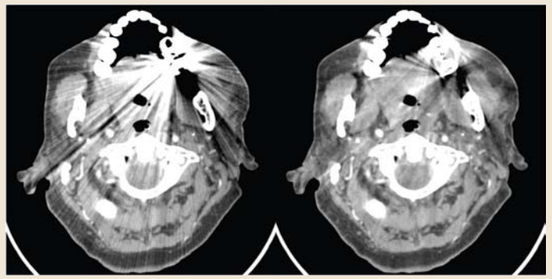

(Left) Original reconstruction with artifacts arising from dental fillings. (Right) Image after proposed metal artifact reduction algorithm.

The algorithm substantially reduces streak and blooming artifacts that are present in the original reconstruction for three scans with dental fillings, and performs better than linear interpolation across missing regions in the sinogram. The double-wedge filter is effective in removing contributions to the sinogram from objects outside of the reconstruction FOV. The algorithm is also computationally practical.

References/Funding Source

GE Healthcare

Optimal Energy Weights for Dual Energy X-Ray Imaging

A.S. Wang[1,2] and N.J. Pelc[1,2,3]
Depts of [1]Electrical Engineering, [2]Radiology, [3]Bioengineering

In traditional x-ray imaging systems, detectors employ an energy integrating technique. The detector's response to a photon is proportional to its energy, and the measurement provided by the detector is the sum of its responses to all incident photons.

Energy selective or spectral imaging (e.g., dual energy imaging) allows improved characterization of the object being studied. Typically, the scanned object is decomposed into the amount of two material basis functions with linear attenuation coefficients $\mu_1(E)$ and $\mu_2(E)$ that would have the same spectral attenuation as the object. To perform energy selective imaging we need to measure x-ray transmission with at least two x-ray spectra. While this can be accomplished with energy integrating detectors, such systems are not ideal because they fail to take advantage of all of the information available from the photons.

Photon counting detectors are able to detect and count individual photons. Energy discriminating photon counting detectors are in addition able to report the energy of each photon. Typical photon-counting detectors "bin" counts based on the measured photon energy, where each bin represents the number of photons within an energy range. If instead one records the energy of each photon, one could make ideal use of the energy information. Moreover, the detector can form a weighted sum of photon counts, where the weight of each photon depends on its energy. We have found that forming two weighted measurements, using the attenuations $\mu_1(E)$ and $\mu_2(E)$ of the basis materials as the weights, provides a sufficient statistic for dual energy decomposition. These two μ-weighted measurements contain all the information available about dual energy decomposition, as if we knew the number of detected photons at each energy. We showed experimentally that μ-weighted measurements lead to basis material decompositions with lower noise than binning schemes in our wedge contrast phantom.

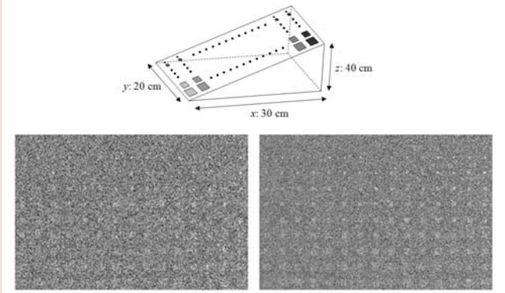

Varying amounts and sizes of our first basis material, calcium, are overlaid on a water wedge (top). The calcium decomposition is shown for a detector with two bins and an optimal threshold (left) and for μ-weights (right). The lower noise and increased conspicuity of the calcium elements when using μ-weights is clear. Because of the large dynamic range of calcium thickness used, the images are shown with a spatially varying grayscale window.

References/Funding Source

A. S. Wang and N. J. Pelc, "Optimal energy thresholds and weights for separating materials using photon counting x-ray detectors with energy discriminating capabilities," Proc. SPIE, vol. 7258, 725821 (2009).
A. S. Wang and N. J. Pelc, "Sufficient statistics for spectral x-ray imaging," in preparation.
GE Healthcare and The Lucas Foundation.

Inverse Geometry CT

N.J. Pelc[1,2,3], J. Baek[1,2], A. Ganguly[1], S. Hsieh1[2], B. DeMan[4]
Depts of [1]Radiology, [2]Electrical Engineering, and [3]Bioengineering, Stanford University, CA; [4]GE Global Research Center, Niskayuna, NY

For several years now, we have been working on Inverse Geometry CT, a new type of CT scanner that employs an array of x-ray sources rather than a single x-ray focal spot. This approach has several potential advantages over conventional CT systems, including the ability to image a thick 3D volume in a single rotation without "cone beam artifacts", higher dose efficiency (i.e., lower radiation dose to the patient for the same image quality), and uniform and high spatial resolution throughout the volume. Under support from NIH and GE Healthcare and through a collaboration between Stanford and GE Global Research Center, we are building a first gantry-mounted system. A very challenging aspect of this project has been the development of the source array, which was done under GE support. The first system will have 8 source spots in a 4x2 configuration. This first module has been built and tested. The x-ray detector consists of modules from a GE HD750 CT system, rearranged into an array of 64x256 cells. These and other components are being integrated into a gantry that will allow rotation as fast a 1 sec. With only one source module we will be limited to a small in-plane FOV but a thick volume. We are seeking additional funding from NIH to expand the source array to 16x2. The goal is to be able to collect CT data under gantry rotation by late 2009, and to perform in-vitro studies to examine the capabilities of this new approach.

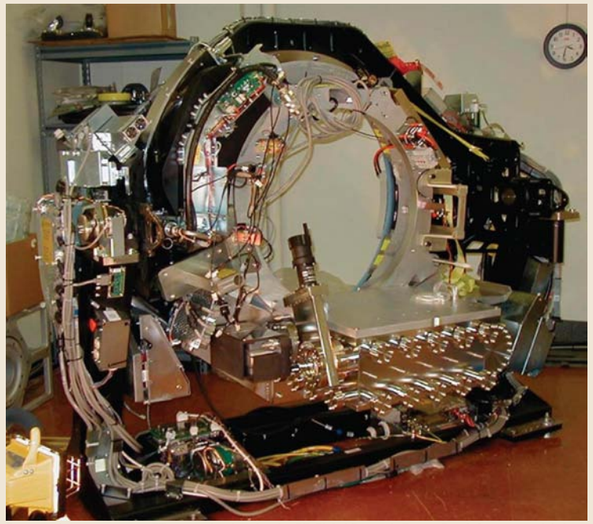

Prototype inverse-geometry CT system developed at the GE Global Research Center. One 4x2 source module has been mounted onto a ring gantry.

References/Funding Source

NIH
GE Healthcare

ANALYSIS OF THE 3D NOISE POWER SPECTRUM OF A CONE BEAM CT SCANNER

Linus Ong[3] and Norbert Pelc[1,2,3]
Depts of [1]Radiology, [2]Electrical Engineering, and [3]Bioengineering, Stanford University, CA

The noise power spectrum (NPS) in CT images can be used to estimate the number of noise equivalent quanta (NEQ) that produced the image. This can be compared with the actual number of photons reaching the detector to arrive at the Detective Quantum Efficiency (DQE), the most fundamental measure of dose efficiency of any x-ray based imaging method. Importantly, it should be possible to measure these quantities at the system level without unusual access to the internal aspects of the system. We wish to investigate this relationship in volumetric CT scanning, and the first step is the measurement of the 3D NPS and the extraction of the NEQ. We first derived an analytical expression for the 3D NPS, especially the dependence on the number of quanta. Next, we generated noise-only images using computer simulation (CATSIM, GE Healthcare), varying several parameters that are expected to affect the 3D NPS. We are now ready to compare the analytical expression to the measured NPS. Further work is needed to find all the factors that scale the computed NPS so that these can be accounted for.

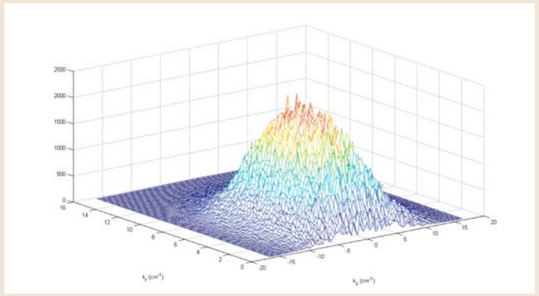

3D NPS as a function of radial spatial frequency and z-spatial frequency

DOSE REDUCTION IN AN INVERSE GEOMETRY CT SYSTEM WITH VIRTUAL BOWTIE

S. Hsieh[1,2] and N.J. Pelc[1,2,3]
Depts of [1]Radiology, [2]Electrical Engineering, and [3]Bioengineering, Stanford University, CA

One of the key advantages of the inverse geometry CT (IGCT) system is the "virtual bowtie," the ability to finely control the intensity distribution of the incident x-ray beams. This allows more power to be used for measurements that otherwise would be noisy while reducing x-ray power away from regions of the sinogram that already have low-noise. In comparison to standard CT bowtie filters, the virtual bowtie promises optimized, customized x-ray control, which could translate into lower radiation dose to the patient while preserving image quality. Maximizing the benefit of the virtual bowtie, then, amounts to solving the optimization problem of minimizing noise for a fixed amount of radiation.

We modeled the CT system by adapting CATSIM (GE Healthcare), and we simulated imaging of standard phantoms. We were able to transform our generic problem into a convex optimization problem, so that the unique, optimal solution may be found. In general, the gains from virtual bowtie will depend on the object being imaged (for example, head versus torso) and the exact specification of the IGCT system. Initial results show the ability to obtain dose reduction using an optimized IGCT virtual bowtie. We plan to continue to apply the virtual bowtie on a variety of different objects, including clinical datasets, in order to quantify the advantages of virtual bowtie over traditional CT systems.

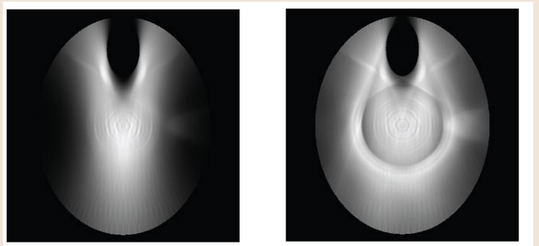

Comparison of the noise distribution on a head phantom before virtual bowtie (left) and after virtual bowtie (right), with constant radiation dose. The images are independently scaled; the image to the left has twice the maximum noise of the right.

REFERENCES/FUNDING SOURCE

NDSEG Fellowship

ANALYTICAL CONSTRUCTION OF 3D NPS FOR A CONE BEAM CT SYSTEM

Jongduk Baek[1], Norbert J. Pelc[1,2,3]
Depts of [1]Radiology, [2]Electrical Engineering, and [3]Bioengineering, Stanford University, CA

The noise power spectrum (NPS) of an imaging system is an important metric, allowing assessment of detection performance and dose efficiency. Measurements of the NPS of cone-beam CT have been described, but less attention has been paid to the analytical derivation of the 3D NPS. It is well known that noise in cone beam CT is non-stationary. When the image is reconstructed by using FDK algorithm, different back-projection and cosine weightings are used for different reconstruction regions. In addition, ray density and cone angle are also spatially dependent. As a result, a cone beam system has non-stationary noise. In order to characterize the noise behavior in a local reconstruction volume, we developed a new method to construct the 3D NPS of a cone beam system. Because cone beam rays passing through a small volume can be approximated as parallel rays, the 3D NPS of a small volume can be constructed by considering all non-stationary effects. The NPS of a large volume was generated by summing 3D NPS of 125 small sub-volumes. It describes the average noise behavior but may not be valid throughout the volume. To validate the derived method, NPS of 3, 6, and 10 cm thick volumes were generated using uniform statistics,and the radial NPS at different kz planes were compared with those of the analytically constructed 3D NPS. The result showed the excellent matching for all cases. With the proposed method, spatially dependent behavior can be analyzed. The non-stationary noise behavior causes a high-frequency roll-off in the large volume NPS, and as the volume size increases, the roll-off frequency decreases because the larger volume has more heterogeneous noise behavior.

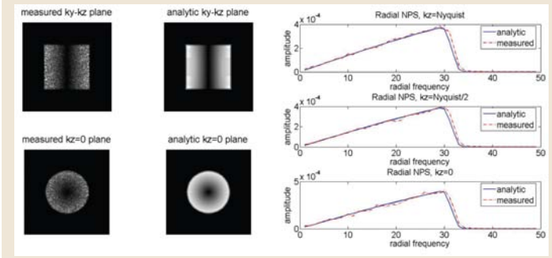

(a) NPS for 3cm volume

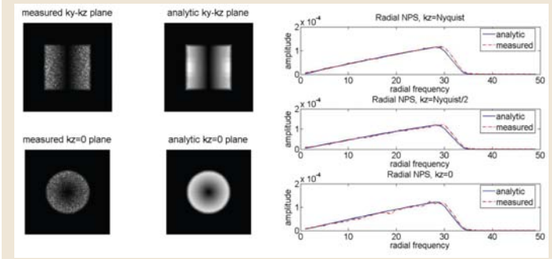

(b) NPS for 6cm volume

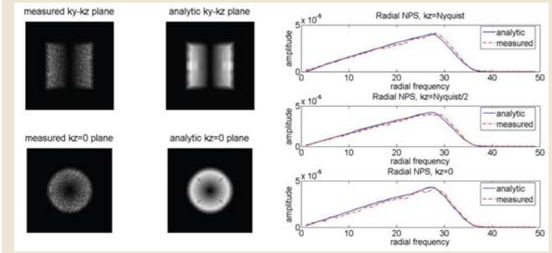

(c) NPS for 10cm volume

REFERENCES/FUNDING SOURCE

GE Health care, Lucas Foundation. NIH grant EB006837

Stanford Electron Linac MRI Apparatus

D. Constantin[1], P. Keall[2] and R. Fahrig[1]
[1]Depts of Radiology and [2]Radiation Oncology, Stanford University, CA

Ideal image guidance in radiation therapy would provide real-time volumetric information of the tumor and surrounding normal tissue during the treatment itself. A compelling approach is to use magnetic resonance imaging (MRI), which provides not only exquisite soft tissue contrast to identify cancerous and healthy regions, but also is a noninvasive imaging technique with no associated radiation dose.

In collaboration with the Department of Radiation Oncology we have started the study and design of a novel prototype integrated MRI-linear accelerator (linac) in which the main magnetic field is aligned with the treatment beam.

We begin by performing computer simulations to quantify the effects of magnetic fields of the entire MeV beam generation process, from the electron gun, through the accelerating structure and treatment head and into patient geometries.

We have modeled a generic Pierce gun to investigate the dependence of current on the external magnetic field. The electron gun was designed to accelerate electrons at 10 KeV, and one can see that even at relatively high values of the magnetic field the electric current does not vanish. The value of the emitted beam current depends on the geometry of the electron gun and the magnitude of the external field. In our case the ratio between the current at 0G and the current at 500G is roughly 64. At high magnetic fields, the electrons follow the magnetic field lines and are thus directed onto the anode rather than through the anode aperture; only those emitted by the central part of the cathode escape the electron gun. The direction of propagation of the electron beam remains unchanged.

Modeling of the other Linac components is underway.

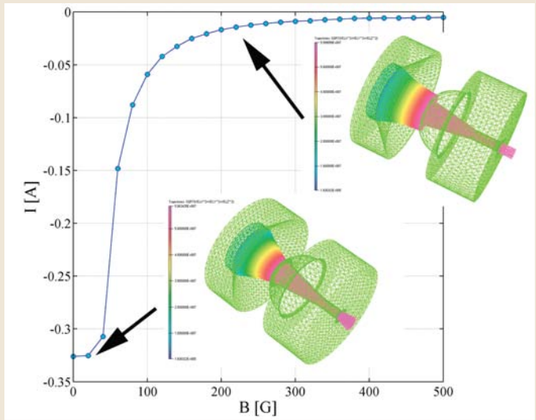

Electron gun current as a function of external magnetic field; two finite element models showing the impact of the external field on the electron trajectories.

Optimal Material Selection of Primary Modulator for Scatter Correction Based On the K-Edge Discontinuity

H. Gao[1], N. R. Bennett[2], L. Zhu[3], and R. Fahrig[1]
[1]Depts of Radiology, Stanford University, CA ; [2]Qualcomm MEMS Technologies, San Jose, CA; [3]Woodruff School of Mechanical Engineering, the Nuclear and Radiological Engineering/Medical Physics Program, Georgia Institute of Technology, Atlanta, GA

A selection of optimal material for the primary modulator is proposed to minimize the effect of beam hardening (BH) in cone-beam CT reconstructions. A measurement-based scatter correction algorithm that uses a checkerboard pattern (primary modulator) of attenuating material placed between the X-ray source and the object has been developed and experimentally verified. In the practical implementation, BH is a limiting factor because the signal modulation depends on the size of the object in the field of view (FOV). The transmission factor, α, for different modulator materials (Be, Al, Cu, Ag, W, Ho, Er and Tm) was calculated for object thicknesses ranging from 0 to 30 cm equivalent water using a simulated spectrum of our tabletop cone-beam CT system at 120 kVp.

We then generated scatter-free projection images of a 30-cm diameter water cylinder, with and without the modulator in place, and reconstructed CT slices after subtraction of the projection images (simulating our correction approach). We also measured the transmission factors of 25 um of Cu, W and Er for different combinations of Al (0-8 mm) and Cu (0-0.3 mm) filtration. The variation of the transmission factor as a function of X-ray energy reaches a local minimum when the K-edge of the modulator material is near the mean energy of the spectrum. For a transmission factor of ~0.9, simulations show that Er provides the least amount of variability as a function of added filtration (max variation<1.8%). The ring artifacts in simulated reconstructions were significantly reduced when using the Er, particularly in the presence of noise. Measured variability of transmission factors were 2.5%, 1.0% and 8.6% for 25 um of Cu, Er and W, respectively.

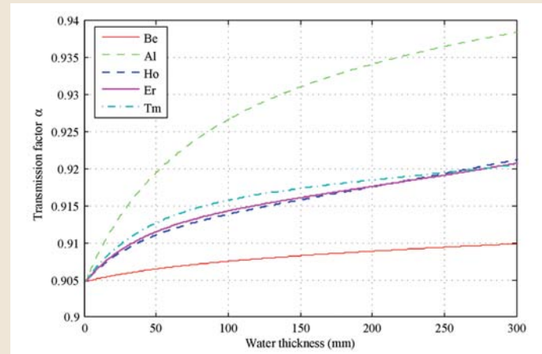

Transmission factor α for different materials with respect to water filtration.

References/Funding Source

NIH R21 EB008186 and the Lucas Foundation

High Performance CMOS Based X-Ray Detector for C-ARM CT Imaging

A. Ganguly[1], and R. Fahrig[1]
[1]Dept of Radiology, Stanford University, CA,

Minimally invasive therapies provide rapid and effective treatments with reduced morbidity, but are critically dependent on the system used for image guidance. One commonly used option is C-arm flat-panel imaging systems, which provide conventional two dimensional (2D) and 3D volumetric imaging for intra-procedural navigation and assessment. The curent flat panel x-ray detectors (FPDs) on C-arm systems impose trade-offs between spatial resolution, field of view (FOV), frame rate, and image noise. A novel detector with a mercuric iodide coated Complimentary Metal Oxide Semiconductor (CMOS) chip has been designed to address these problems. It will provide large FOV imaging with 120 micron pixels at 120 frames/s and only 500e rms noise. Our recently-funded proposal aims to optimize detector design and performance for C-arm CT imaging.

We are working with our collaborator, RTR Inc., to characterize and optimize this new detector technology (see Figure). As a first step, we have started to build a theoretical model of the imaging chain to predict detector performance. The imaging characteristics of small area panels prepared by our collaborator will next be tested on a table-top CT system and compared with these predictions. Any image degradation process will be identified and the detector design will be modified in an iterative process.

The technical innovations of the proposal lie in the ability to use this unique large area high speed detector for extracting maximum 2D, and 3D information for aiding minimally invasive procedures. One of the procedures that will potentially be impacted by this development is endovascular therapy for treatment of stroke.

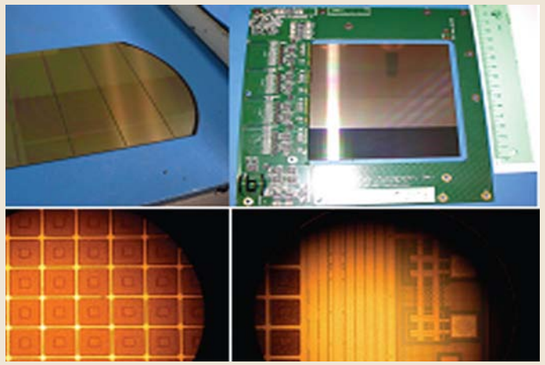

(a)Six inch wafer with three 2.8 x 10.5 cm2 CMOS strips (b) The 3 CMOS strips mounted on an electronic testbed (c) Closeup view of the CMOS pixels with protective gold coating showing pixel pads in the center and (d) pixels on the left and bond pads on the right

References/Funding Source

K99 EB007676-01A2

Visualization of radiofrequency ablation lesions with iodine contrast-enhanced cardiac C-arm CT

E. Girard-Hughes[1], A. Al-Ahmad[2], T. Moore[4], G. Lauritsch[5], J. Boese[5], R. Fahrig[3]
[1]Depts of Bioengineering, [2]Cardiovascular Medicine, and [3]Radiology, Stanford University, CA; [4]Siemens Medical Solutions Incorporation, Malvern, PA; [5]Siemens AG Healthcare Sector, Forchheim, Germany;

Radiofrequency (RF) ablation has become an important strategy in the treatment of many cardiac arrhythmias. The success of the ablation procedure often depends on the extent of the lesion and the creation of lesions at specific anatomic locations and in continuous ablation lines. Currently, three-dimensional (3D) images are often viewed side-by-side or merged with images from an electroanatomical mapping system to delineate cardiac structures and guide ablation procedures. While mapping systems and electrophysiologic techniques give some feedback on the probable extent and location of ablations, it is not possible to non-invasively confirm the creation of scars during the intervention.

The purpose of this study was to evaluate whether contrast-enhanced C-arm CT (3D rotational angiography) can distinguish RF ablation lesions created in the left ventricle. Ablation lesions were created on the endocardial surface of the left ventricle of 6 swine using a 7 F radiofrequency (RF) ablation catheter with a 4 mm electrode. A 6x4s, ECG-gated C-arm CT imaging protocol was used to acquire projection images during iodine contrast injection and every 5 min for up to 30 min, with no additional contrast. Reconstructed images were analyzed offline and the mean and standard deviation of the signal intensity of the ablation lesion, normal myocardium, and blood were measured. Eleven ablation lesions were visualized and the time-attenuation curve of the signal intensity was plotted. Eight lesions (72%) exhibited early hypoenhancement on the first pass image with a mean signal intensity decrease from normal myocardium of -129.2 ±79.0 HU. For images acquired at 10 min after contrast administration, late enhancement was observed in 7 lesions (64%) with a signal intensity increase compared to normal myocardium of 64.8 ±33.6 HU.

This is the first study to demonstrate the potential to visualize RF ablation lesions during a cardiac interventional procedure using ECG-gated C-arm CT imaging.

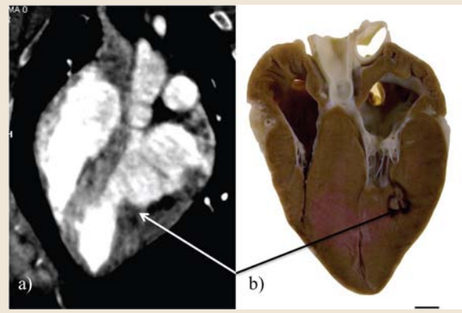

Two lesions visible as perfusion defects in the first-pass image (a) and corresponding lesions on the pathology image (b).

References/Funding Source

Erin Girard-Hughes, Amin Al-Ahmad, Teri Moore, Günter Lauritsch, Jan Boese, Rebecca Fahrig. Visualization and enhancement patterns of radiofrequency ablation lesions with iodine contrast-enhanced cardiac C-arm CT.
Proc. SPIE, Vol. 7262, February 2009.

3D INTRA-PROCEDURAL C-ARM CT IMAGES OF THE LEFT ATRIUM AND PULMONARY VEINS: PRELIMINARY EXPERIENCE WITH ECG-GATING

A.Tognolini[1], R. Fahrig[1], H. Hsia[2], T. Moore[3], J. Rosenberg[1], R. Herfkens[1], A. Al-Ahmad[2]
[1]Dept of Radiology, [2]Cardiac Arrhythmia Service, Stanford University, CA; [2]Siemens AG, Healthcare Sector, Forchheim, Germany

Purpose: Left atrial (LA) ablation has become an important strategy in the treatment of atrial fibrillation (AF). Currently, CT or MR imaging is obtained days or weeks prior to ablation, often during different hemodynamic conditions or a different rhythm. In this study we compare the accuracy of ECG gated C-arm CT (CACT) with non-gated C-arm CT and multidetector CT (MDCT) for LA mapping.

Methods: Gated and non-gated cardiac CACT (AXIOM Artis dTA C-arm system, Siemens AG) and cardiac MDCT images were obtained in 11 subjects. The CACT system was modified to allow acquisition of four bi-directional sweeps during synchronized acquisition of the ECG for retrospective gating; from the previously obtained volumes, a single sweep volume was selected as non-gated comparison. Measurements of LA and PV diameters were obtained on corresponding cut planes after image registration on a dedicated workstation (Syngo-X Workplace,Siemens AG) reducing inter-volume measurement errors due to view selection.

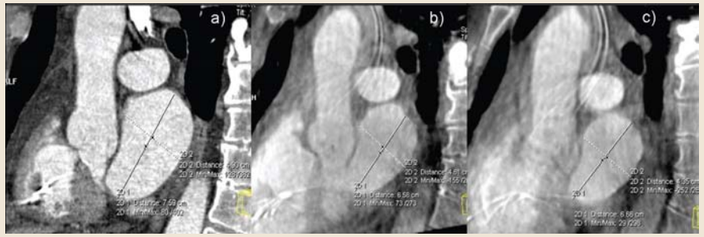

The antero-posterior and craniocaudal diameters of the left atrium obtained on the sagittal plane orthogonal to the major LA axis, were measured on CT, gated, and non-gated CACT (a,b, and c respectively) after image registration.

Results: Overall, gated and non gated CACT measurements were not systematically smaller than MDCT measurements ($p<.546$ and $<.392$, respectively) and showed a coefficient correlation (CC) with MDCT of 0.98. However, a sub-analysis of the individual PVs shows that gating provides significant benefit for inferior PVs, which are most susceptible to pulsation artifact (e.g. right inferior PV, gated vs. nongated, CC: 0.84 vs. 0.57).

Conclusion: CACT has the major advantage of providing the anatomical map at the time of the procedure. Utilization of the ECG-gated protocol improves image quality especially in the region more affected by pulsation artifacts.

REFERENCES/FUNDING SOURCE

Research Grant, Siemens, Healthcare Sector, Forchheim, Germany

ANALYSIS OF ANATOMICAL CLUTTER IN TOMOSYNTHESIS IMAGING OF THE CHEST

S. Yoon[1], J. Gang[2], D. Tward[3], J. Siwersedsen[2,3,4], and R. Fahrig[1]
[1]Dept of Radiology, Stanford University, CA; [2]Inst of Biomaterials and Biomedical Engineering, University of Toronto, Canada; [3]Ontario Cancer Institute, Princess Margaret Hospital, Canada; [4]Dept of Medical Biophysics, University of Toronto, Canada

Tomosynthesis is an imaging technique that is experiencing renewed interest with recent advances in flat-panel digital detectors. Because of the wide range of potential applications, a systematic analysis of 3D tomosynthesis imaging systems would contribute to the understanding and development. We are carrying out a systematic evaluation of thoracic tomosynthetic imaging performance as a function of imaging parameters, such as the number of projections and tomosynthesis orbital extent (TOE).

We evaluate anatomical clutter as a function of TOE using anthropomorphic phantoms and a table-top acquisition system. Tomosynthesis coronal slices were reconstructed using the FDK algorithm for cone-beam geometry from 91 projections uniformly distributed over TOE ranging from 10° to 180°. Anatomical clutter power spectra (PS) are computed and compared.

2D anatomical clutter PS (a) is asymmetric in f_x and f_z. Because of the acquisition geometry, clutter power spectrum along f_x is an order of magnitude larger than the power spectrum along f_z. 1D anatomical clutter PS (b) along f_x and f_z show that the clutter magnitude decreases monotonically as TOE increases. An exception occurs for the anatomical clutter power spectrum along f_z at 180°, where the clutter magnitude increases to values close that of clutter PS along f_x, because 2D tomosynthesis slice PS was computed.

In summary, anatomical clutter PS magnitude of 2D tomosynthesis reconstruction slices decreases as fixed dose is distributed over a larger TOE. In addition, clutter PS whitens as fixed dose is distributed over a larger TOE. Therefore, the combination of the decrease in magnitude and the whitening of the 2D clutter PS results in improvement in detectability as fixed dose is distributed over a larger TOE. Additionally, inspecting a 2D slice for larger TOE (e.g. 120°) implies a decrease in detectability because of the information loss in the depth direction.

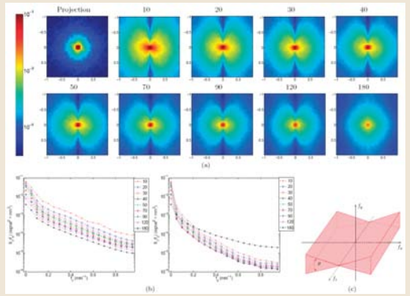

(a) 2D anatomical clutter PS of tomosynthesis reconstructions for 13 different TOE. All images shown in the same window and level, with units of signal2·mm2. Horizontal axis corresponds to f_x and the vertical axis corresponds to f_z. (b) 1D anatomical clutter PS of tomosynthesis reconstructions for 9 different acquisition orbital extents. (c) Sampled double wedge shown in 3D Fourier domain for tomosynthesis acquisition.

REFERENCES/FUNDING SOURCE

S. Yoon, J. G. Gang, D. J. Tward, J. H. Siewerdsen, and R. Fahrig, Analysis of lung nodule detectability and anatomical clutter in tomosynthesis imaging of the chest, Medical Imaging 2009: Physics of Medical Imaging, SPIE, 2009

INVESTIGATION OF PER-REGION BOUND CONSTRAINTS FOR LEVEL SET ITERATIVE RECONSTRUCTION

S. Yoon[1] and R. Fahrig[1]
[1]Dept of Radiology, Stanford University, CA

We have implemented an iterative simultaneous segmentation and reconstruction for tomographic data using the level set method. The algorithm assumes that the reconstruction space is divided into two non-overlapping regions. It iterates between the two processes until convergence: step 1) evolves the zero level set curve, which defines the boundary between the two regions, to segment the reconstruction space; step 2) iteratively estimates the reconstruction pixel values with smoothness constraints for each region.

We applied the algorithm to 21 noisy (simulated) projections from a sub-region of a contrast enhanced CT slice. We compare two algorithms with different reconstruction pixel value constraints: non-constrained(A) and per-region constrained(B). We tested both algorithms with 3 different initial region boundaries and compared the reconstructions.

Algorithm B converges to a consistent reconstruction and is minimally dependent on the initial region boundary (d-f). In contrast, algorithm A is significantly dependent on the initial boundary (a-c), which has also been reported in previous work. Additionally, algorithm B reduced the error (RMSE) by 44% when compared to FBP reconstruction (g) and by 5% when compared to algorithm A with the same initial region boundary.

The proposed algorithm applied to noisy limited view tomography results in accurate reconstruction pixel values as well as superior noise suppression. Such improved reconstruction can be achieved with minimal dependence on the initial region boundary by having separate non-overlapping reconstruction pixel value constraints for each region.

The proposed algorithm is well-suited for reconstructions from noisy limited view tomographic data, which commonly arise as a result of limited temporal resolution and/or is used in an effort to reduce dose.

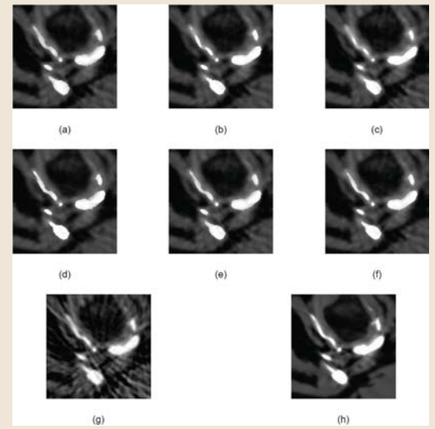

Reconstruction comparison. Top row: Reconstructions using algorithm A. Middle row: Reconstructions using algorithm B. Bottom row: FBP reconstruction (left) and original CT slice (right). Three columns for the top and middle row represent three different initial boundaries for both algorithms.

A NEW METHOD FOR LAG REDUCTION IN FLAT-PANEL X-RAY DETECTORS

J. Starman[1,2], J. Star-Lack[3], and R. Fahrig[1]
Depts of [1]Radiology and [2]Electrical Engineering, Stanford University, CA; [3]Varian Medical Systems, Mountain View, CA

One factor limiting CT reconstruction image quality for a-Si flat panel x-ray detectors is detector lag, caused by charge trapping in the a-Si. In CT reconstructions lag can lead to a range of image artifacts, such as blurring and shading artifacts for non-circular or off-center objects. For a large pelvic phantom scan, artifacts as large as 58HU have been observed.

A software model was constructed to correct for lag artifacts in CT reconstructions. The correction technique fits a multi-exponential model to x-ray lag data. The model attempts to capture and correct for the nonlinear and time variant characteristics of the detector. Specifically, the amount of trapped charge vs incident dose is allowed to vary nonlinearly. The exponential rates of charge uptake and release in the model are also allowed to vary as a function of incident dose. For comparison purposes, a standard correction technique that assumes a linear time invariant (LTI) model of the detector was implemented. Data was collected on an x-ray table top system using a Varian 4030CB flat panel detector. Several phantoms of various sizes and artifact levels were investigated. Reconstruction error and image non-uniformity were investigated in 9 different 10x10mm ROIs in uniform material.

For flat field projection data the current method reduced first frame lag by 49%, as compared to the LTI method which reduced it by 30%. For a large pelvic phantom CT reconstruction, detector lag caused 58 HU in severe shading artifact in one ROI. With an LTI correction the error was 23HU, and was only 4HU using the newly described method. The average error for all ROIs was 38HU with no correction, 20HU with an LTI correction, and 6HU with the new method.

Overall, the described software correction is able to achieve greater image uniformity in the CT reconstructions for selected phantoms.

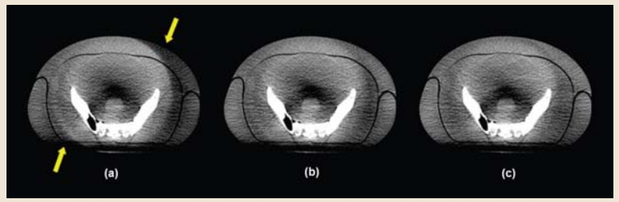

(a) Is a fat pelvic phantom reconstruction with no lag correction and arrows pointing to the lag artifact. Average error across several ROIs was 38HU. The images have not been corrected for scatter or beam hardening. (b) is a reconstruction using a LTI correction with average error of 20HU. (c) is a reconstruction using the described algorithm with average error of 6HU. All images are at 150HU|150HU window and level.

REFERENCES/FUNDING SOURCE

Lucas Foundation

Advanced X-Ray and CT Techniques

Motor Design for an MR-compatible Rotating Anode X-ray Tube

P. Lillaney,[1,2], N.R. Bennet[1], and R. Fahrig[1]
[1]Depts of Radiology, [2]Bioengineering, Stanford University, CA

Typical x-ray tube induction motors do not operate efficiently in the presence of an MR fringe field because the fringe field acts as a brake decreasing the rotation speed of the anode. To overcome this problem we have developed an alternate motor design that uses the fringe field to create rotation. Our design has phase windings embedded directly on the rotor. Applying voltage to a single phase winding creates a magnetic moment that prefers to be parallel with the direction of the fringe field. Continuous torque is generated by switching winding voltages on and off in such a manner that there is always at least one magnetic moment trying to align with the fringe field. This method of torque generation eliminates the need for stator coils that are present in induction motors.

To demonstrate feasibility of our design a proof of concept has been built using a Lucite cylinder as the rotor, magnet wire (AWG 22) for the phase windings, and non-magnetic stainless steel bearings to support the rotor and serve as slip rings for the phase windings. An optical encoder monitors the angular position of the rotor which is used as a feedback control mechanism for the winding voltages. The MR fringe field is simulated by placing the motor in between a Helmholtz coil pair that provides a static magnetic field of approximately 45 mT perpendicular to the axis of rotation of the motor. Rotation speeds of approximately 200 RPM can be achieved with this first iteration when using a 150 watt power supply for the phase windings. By optimizing design parameters with the assistance of a lumped parameter model developed to predict motor behavior, future iterations will achieve rotation speeds comparable to current induction motors.

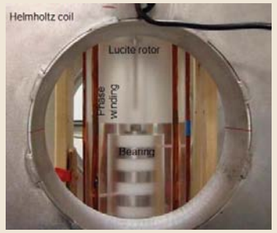

The motor prototype is shown positioned in between the Helmholtz coil pair. The phase windings are fixed in grooves on the surface of the rotor. Each phase winding receives its supply voltage via its respective bearing which are shown towards the bottom of the image. The bearings are insulated from each other by the white Delrin disks. Not shown is the optical encoder which is positioned on top of the rotor.

References/Funding Source

NIHR01 EB 007626

Evaluating the Feasibility of C-arm CT for Brain Perfusion Imaging: An in vitro Study

A. Ganguly[1], A. Fieselmann[2,3,4], J. Boese[4], C. Rohkohl[2,4], J. Hornegger[2] and R. Fahrig[1]
[1]Dept of Radiology, Stanford University, CA, [2]Depts of Computer Science, [3]Graduate School in Advanced Optical Technologies (SAOT), Friedrich-Alexander University Erlangen-Nuremberg, Germany, [4]Siemens AG, Healthcare Sector, Germany.

Conebeam C-arm CT (CBCT) is being used to supplement 2D real-time data with 3D information. Temporal resolution of the 3D volumes is currently limited by the mechanical rotation speed of the C-arm, and is too slow for imaging contrast dynamics in brain perfusion CT (PCT). We present a novel protocol where multiple scans are obtained at different start times with respect to the start of contrast injection. The data is interleaved temporally and interpolated before 3D reconstruction. To evaluate this protocol we designed and built a phantom that generates the range of temporal frequencies relevant for PCT. The highest frequencies are seen in the arterial input function (AIF), which can be modeled as a gamma-variate; Fourier transform analysis showed that 90% of the spectral energy is below 0.06-0.08 Hz. Any signal can be represented by a weighted sum of sinusoids; a sinusoidal contrast phantom was therefore built by partitioning an acrylic cylinder into 25 sections, each of length 1cm and filled with iodinated contrast diluted to provide a half sinusoid over the length of the phantom. The phantom was moved linearly at speeds from 0.5 cm/s to 4 cm/s (temporal frequencies of 0.01 Hz to 0.07 Hz) and imaged using a C-arm system (6x6 sweeps, 4.3 s/sweep, offset -4.6 s to +4.6 s in increments of 1.8 s). Phantom CT numbers in a slice at iso-center were measured and fitted to sinusoids. The fitted sinusoids had frequencies within 3±2% of the actual temporal frequencies of the moving sinusoid phantom. These results show that the offset/interleaved imaging protocol is adequate for PCT imaging with C-arm CT. The impact of scan number reduction on accuracy is currently under investigation.

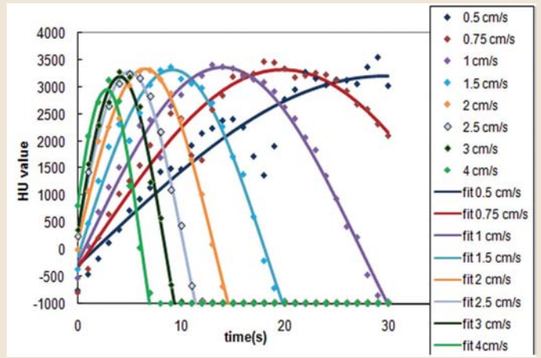

Fit to measured HU values in the reconstructed volume data from sinusoids of various frequencies. The different frequencies (ie. different rates of change in HU as a function of time) were generated by moving a cylindrical phantom at different linear velocities.

Image Analysis, Bioinformatics, Computational Modeling

In this section, you will read about innovations in display and interaction, feature extraction, and computer simulation and modeling techniques. These projects aim to improve the accuracy and efficiency of human interpretation of medical imagery, as well as predict patient prognosis, the molecular subtypes of their disease, and their response to treatment options in a way that is highly personalized for each patient. These efforts share the common goal of developing decision-making tools that assist with patient diagnosis, treatment, and disease monitoring.

A machine learning approach towards automatic circulating tumor cell isolation

Jesse Rodriguez[1], Ashley Powell[2], Stefanie Jeffrey[2], David Paik[1,3]
[1]Depts of [1]Medicine, Biomedical Informatics, [2]Surgical Oncology, and [3]Radiology, Stanford University, CA

It is well-known that epithelial tumors metastasize by shedding cells into the bloodstream. These circulating tumor cells (CTCs) are of epithelial origin and can be easily distinguished from other cells in the blood stream from their surface markers. Studies have shown that the number of circulating tumor cells in patients' blood is correlated with patient survival, but the number alone is not a sufficiently accurate predictor. Current research is aimed at molecular characterization of these cells with the hope of both learning about their biological function and to improve prognostic accuracy.

The Jeffrey lab has recently developed technology to isolate live CTCs using magnetic microbeads, but one of the limiting bottlenecks in the isolation process is the manual identification by microscopy and extraction of cells by micropipette. This makes it difficult to acquire large samples necessary to study CTCs and has thus far the technology's feasibility as a clinical diagnostic tool.

To address this, we have designed an automated machine learning method to identify individual cells in microscopy images against the background of non-specific magnetic microbeads. The overwhelming abundance of non-speciifc microbeads in comparison to an extremely small number of CTCs makes this machine classification particularly challenging. We achieve 90% precision (positive predictive value) and 95% recall (sensitivity) in identifying cells with logistic regression using shape and size-based features of the cells and beads.

This method will improve throughput of isolating CTCs by driving a fully automated robotic system to quickly identify and capture cells and will aid in the development of CTC-based diagnostic and monitoring protocols which will improve our understanding and treatment of metastatic cancer. Ultimately, we aim to correlate gene expression patterns in these CTCs with non-invasive imaging of the primary tumors and metastases.

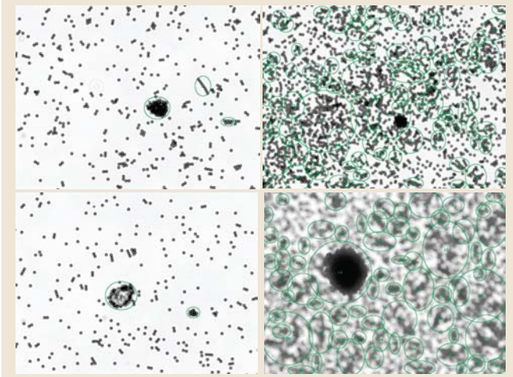

Several examples of candidate detections of circulating tumor cells by light microscopy.

References/Funding Source

Stanford Graduate Fellowship

THIN CLIENT ARCHITECTURE IN SUPPORT OF REMOTE RADIOLOGY LEARNING

F. Schmitzberger[1], J. Roos[1], S. Napel[1], G. Rubin[1], D. Paik[1]
[1]Dept of Radiology, Stanford University, CA

We implemented a system for remote radiology learning, which provides immediate feedback to the learner. Using a thin remote client, expert readers are asked to answer questions about specified radiological findings. These scans are presented as real-time 2D and 3D presentations which allow the user to freely manipulate them using a thin Java client with all 3D rendering performed on the server side. Answers are stored on the server and are used to provide feedback to learners who are presented with the same questions, using the remote client. Learners can practice on real datasets while receiving immediate feedback on their diagnosis and measurements. Novel concepts introduced are (1) the use of server-side rendering in radiology learning, (2) providing immediate and specific feedback to trainees, (3) the ability to provide useful feedback when a definitive gold standard does not exist and (4) a thin, highly compatible client that runs on common, existing hardware which allows to have more people participating in very complex radiological evaluations, even if there are not at the same site.

The learner is presented with an interactive view of a lung nodule and is tasked to answer a number of questions. After completing the questionnaire he is presented with a statistical overview comparing his answer to previously automatically recorded expert answers.

REFERENCES/FUNDING SOURCE

Schmitzberger FF, Roos J, Napel S, Rubin G, Paik DS. "Thin Client Architecture in Support of Remote Radiology Learning." Proceedings of the 24th Annual ACM Symposium on Applied Computing, 842-46, 2009
NIH CA109089

ASSESSING OPERATING CHARACTERISTICS OF CAD ALGORITHMS IN THE ABSENCE OF A GOLD STANDARD

K. Choudhury[1,3], C. Yi[2], S. Napel[3], J. Roos[3], G. Rubin[3], D. Paik[3]
[1]Statistics Dept, University College Cork, Ireland; [2]Samsung Medical Center, Sungkyunkwan University School of Medicine, South Korea; [3]Dept of Radiology, Stanford University, CA

PURPOSE: A 'gold standard' based on independent assessment is typically required for establishing operating characteristics of CAD algorithms. Previous studies of lung nodule CAD have shown significant variation amongst trained radiologists in determining 'true' nodules. We propose a latent class analysis (LCA) based method that does not require an external 'gold standard' to evaluate diagnostic accuracy.

METHOD AND MATERIALS: A binomial model for multiple reader detections is constructed, assuming conditional independence of readings given true nodule status. The true positive fraction (TPF) and false positives per patient (FPP) are estimated by maximum likelihood LCA. Hypothesis of differences in TPF and FPP between detection protocols are tested by resampling based methodology. The methodology is validated on simulated data. LCA was applied to thin section Lung Imaging Database Consortium (LIDC) datasets, comprising 36 thoracic CT scans and free search markings of four radiologists. Four different CAD assisted radiologists also marked the scans.

RESULTS: For LIDC, 1145 nodule candidates were considered. The estimated TPF of free read (55%), was significantly higher (p-value 0.006) than CAD assisted readers' (68%). The estimated CAD assisted TPF using free read as gold standard was 83%. The average FPP of free read (0.95) was not significantly higher (p-value 0.28) than CAD assisted readers' (1.27). With simulated data, LCA estimated TPFs and FPPs are close to true values.

CONCLUSIONS: Whereas a consensus gold standard depends heavily on how many gold standard setting readers must agree, latent class based methodology provides an accurate and consistent means for evaluating diagnostic accuracy.

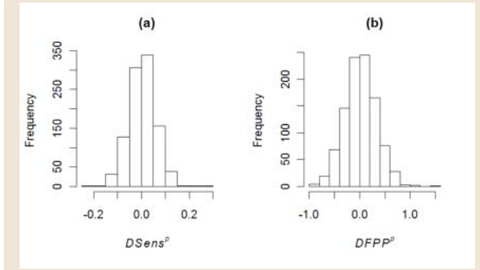

Distribution of test statistics for (a) differences of sensitivity (Δsensp) and (b) differences of average false positives per patient (ΔFPPp) between free read and CAD assisted readings for LIDC dataset. Distributions were calculated under null hypothesis of no difference between reading methods using a randomization test (with 1000 replications).

REFERENCES/FUNDING SOURCE

NIH grant CA109089

QUANTITATIVE UNMIXING OF SPECTRA FOR RAMAN MOLECULAR IMAGING OF LIVING SUBJECTS

K. Kode[2], C. Zavaleta[1], S.S. Gambhir[1], D. Paik[1]
[1]Depts of Radiology, [2]iCME, Stanford University, CA

Purpose: In recent years, surface enhanced Raman spectroscopy has gained interest as a tool for noninvasive molecular imaging of living subjects because of its potential for greater multiplexing as compared to fluorophores. Various strategies have been developed for small-animal optical imaging based on Raman spectrocopy and Raman nanoparticles. However, quantitative unmixing of the Raman spectra poses a significant challenge due to significant autofluorescence in vivo which causes low SNR. We have developed a reliable algorithm to quantitatively unmix the spectra of multiplexed Raman nanoparticles in living subjects.

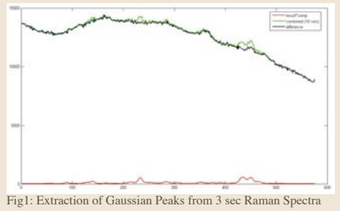

Fig1: Extraction of Gaussian Peaks from 3 sec Raman Spectra

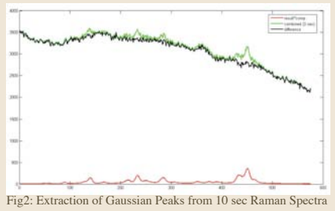

Fig2: Extraction of Gaussian Peaks from 10 sec Raman Spectra

Materials and Methods: Surface-enhanced Raman scattering nanoparticles were used to demonstrate whole-body Raman imaging, nanoparticle pharmacokinetics, multiplexing, and in vivo tumor targeting, using an optical microscope adapted for small-animal Raman imaging. Three female 8-week-old nude mice were used for all Raman spectroscope studies. The unmixing process was carried out on Raman spectra of 4 nanoparticles injected simultaneously 1) using a 'polyfit' background subtraction followed by linear least squares on the Raman spectra followed by 2) our unmixing algorithm that parameterizes individual Raman peaks and uses Levenberg Marquardt optimization, accounting for changes in peak position and width. The results from least squares were used as initial estimate for the optimization process.

Progress: We modeled individual Raman peaks to accurately represent the Raman spectra of nanoparticles and developed an unmixing method that avoids carrying out dubious pre-processing techniques such as blind baseline correction for background subtraction. The signal to noise ratio was estimated to be 0.0010 for the combined spectra. Five Raman peaks having the greatest area under the curve were modeled for each nanoparticle. Percent error in the estimate of concentrations of each nanoparticle for method 1) were 26%, 27%, 45%, 65% and corresponding errors for methods 1+2) were 23%, 16%, 6.7%, 16%.

Discussion: While the narrow peaks of the Raman spectra provide specificity of each nanoparticle's spectrum, their steep slopes can lead to large errors in the presence of very minor spectral shifts or changes in width. Our results demonstrate that accounting for this effect can lead to better and more relaiable performance in quantitative unmixing thereby enabling Raman spectroscopic imaging in living subjects.

REFERENCES/FUNDING SOURCE

NIH U54 CA119367

MATHEMATICAL MODEL OF EFFECT OF DECOY PROTEINS ON EXECUTIONER CASPASE ACTIVATION

[1]K. Sebekos and [1]D. Paik
[1]Dept of Radiology, Stanford University, CA

Apoptosis, programmed cell death, plays a critical role in the development and maintenance of tissue homeostasis in the body. When the balance between cell proliferation and cell death is disturbed adversely, various disease states can occur. If the proliferation route becomes dominant cancer may form, whereas if a cell death exceeds proliferation you may have neurodegenerative diseases. This experiment expands on the work of Fussenegger et al. on a mathematical model of the caspase cascade and observes activation of executioner caspases with respect to decoy protein overexpression.

Instead of focusing on how executioner caspase (cleave essential proteins required by cells) varies with time, we are interested in how the percent of active executioner caspase varies with percent overexpression of decoy proteins. In order to model this we observe that the executioner caspase activation becomes saturated after several hours, thus reaching a constant value. This observation is important in order to link the short timescale dynamics of rate kinetics with the long timescale dynamics of tumor growth and regression. The output of the model was methodically explored in order to take the saturated values of the executioner caspases and plot them against the percent overexpression of decoy proteins (Bcl-2 and ARC). In addition, further modifications were done to observe the effects on active executioner caspase when multiple decoy proteins are overexpressed simultaneously.

It was found that when the IAP (Inhibitors of Apoptosis) where overexpressed 6x, the percent of active executioner caspase dropped to just under 15 percent. A 3-d surface plot was obtained for the decoy protein overexpression, which shows the optimum combinations of decoy proteins needed to inhibit executioner caspases. These findings might lead to less toxic regimen of drugs with stronger additive affects. Furthermore, future work will focus on combining this work into a novel multiscale model that can predict and explain imaging observations of in vivo tumor dynamics as a function of specific molecular interventions.

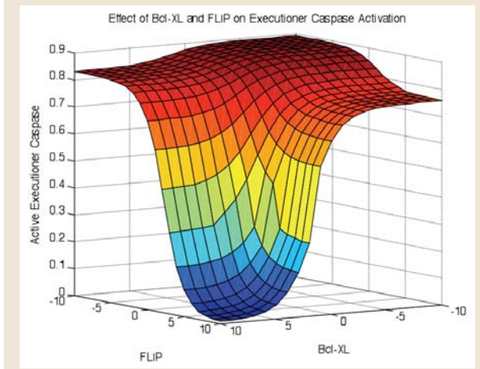

Effect of FLIP (decoy protein) and Bcl-XL (anti-apoptotic protein) on the percentage of active executioner caspase under conditions of both receptor activated and stress induced activation of the caspase cascade. The computational model was run from -10 to +10 log2 orders for both proteins. This demonstrates that both decoy and anti-apoptotic proteins are needed to fully inhibit apoptosis.

PARAMETRIC MODELING OF RAMAN SPECTRA OF NANOPARTICLES FOR QUANTITATIVE UNMIXING

K. Kode[2], C. Shachaf[3], S. Elchuri[3], G. Nolan[3], D. Paik[1]
[1]Depts of Radiology, [2]iCME, [3]Microbiology and Immunology, Stanford University, CA

Purpose: Raman spectroscopy can differentiate the spectral fingerprint of many molecules, resulting in very high multiplexing capabilities. Even with surface enhancement, one of the problems in quantitative unmixing of Raman spectra is related to the presence of a relatively high fluorescence background. Also, changes in experimental conditions can result in subtle widening and shifting of the very narrow Raman peaks, which make quantitative unmixing very difficult. The objective of our study was to apply mathematical techniques on parametric models of the Raman spectra of nanoparticles to unmix the contributions from multiple nanoparticles to allow for simultaneous multiplexed quantitation of nanoparticle concentrations for tumor cell characterization as part of an integrated in vitro diagnostics and in vivo imaging cancer nanotechnology project.

Materials and Methods: A Gaussian is used to model the individual Raman peaks of each COIN (Composite Organic Inorganic Nanoparticle) in solution. Instead of using preprocessing techniques such as baseline separation to remove the broad fluorescent components, Raman peaks were extracted from the spectra.

During modeling, parameters such as the peak height, peak location and full width at half maximum (FWHM) of Raman peaks were extracted from the reference spectra of individual COINs using numerical optimization. These Raman peaks are then subtracted from the combined spectra in different proportions to minimize the Raman nature of the remainder spectrum.

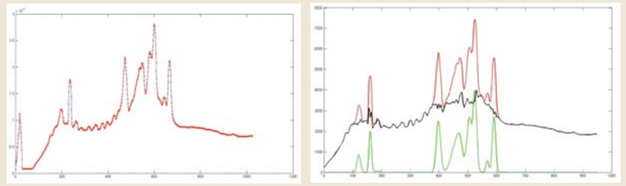

Fig 1: Raman Spectra before preprocessing.
Fig2: Extraction of Gaussian Peaks from Raman Spectra

Progress: We modeled individual Raman peaks to accurately represent the Raman spectra of COINs. We successfully unmixed up to 7 COINS using the algorithm and achieved considerable improvement over the results obtained using direct linear least squares. The errors in estimation of the individual contributions of each nanoparticle using least squares were in the range of 20-70% while the error based on results from our optimization algorithm are in the range of 10-20%.

Discussion: With the accurate Raman peak separation as opposed to blind baseline correction methods, quantitative unmixing of Raman spectra will be much more reliable resulting in huge potential for application of Raman spectroscopy in the analysis of nanoparticles.

REFERENCES/FUNDING SOURCE

NIH U54 CA119367

QUANTITATION ERROR ASSESSMENT FOR SMALL ANIMAL PET

F. Habte[2,5], C.H. Nielsen[2,5], G. Ren[2,5],S. Yaghoubi[2,5], N. Withofs[2,4],T.C. Doyle[3,5,6],L. J. Pisani[2,5], C. Levin[1,2,4,5,6],S.S Gambhir[1,2,4,5,6], D. Paik[1,2,5,6]
Depts of [1]Bioengineering, [2]Radiology, [3]Pediatrics, [4]Division of Nuclear Medicine, [5]Molecular Imaging Program at Stanford (MIPS), and [6]Bio-X Program, Stanford University, CA

In molecular imaging, Positron Emission Tomography (PET) is a powerful imaging instrument due to its capability of quantitative measurement though there are many factors that influence its quantitative accuracy. Some of the common factors include: pre-scan animal preparation, accuracy of scanner calibrations, proper handling of necessary PET error correction mechanisms and the reliability of the entire data analysis procedure. In this study, our goal is to identify the major sources of errors and optimize data analysis procedures to improve the quantitation accuracy. We monitored the accuracy of the calibration parameters on a monthly basis and compared the biodistribution of various organs/tumors using both microPET and a gamma-counter. We also conducted a phantom study with F-18 filled spheres to demonstrate the underestimation of organ activity observed by microPET in various studies for organs expressing high tracer uptake.

The biodistribution comparison showed close agreement (~10% difference) for relatively homogeneous organs/tumors with lower uptake (< 10 uCi/mL) (see Figure Top). A significantly difference (> 30%) is however observed at higher uptake. We further verified the significant underestimation of PET for regions with high tracer uptake using phantom studies (Figure Bottom). In our study, we have applied the vendor recommended attenuation and scatter corrections despite their minimum effect on mouse imaging. The phantom studies indicate that the vendor recommended global deadtime correction has limitations resulting a higher count loss at higher activity concentration (>30 uCi/mL) within the specified regions of interest. A similar phantom study also showed that both detector block effect and inter-detector gap have significant contribution to the quantitation error of PET at higher uptake (Figure not shown). This suggests that additional post-reconstruction corrections may be needed to improve the quantitation accuracy of MicroPET when significant high uptake (> 30 uCi/mL) is expressed within the specified region of interest.

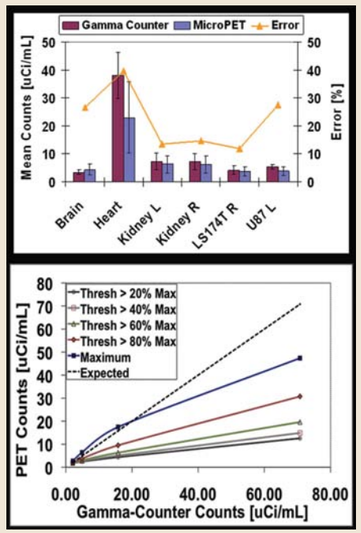

Biodistribution comparison of PET to gamma-counter results (Top), and Phantom study demonstrating the significant under estimation of PET for regions with relatively higher tracer concentration.

REFERENCES/FUNDING SOURCE

Accepted for poster presentation on the upcoming WMIC meeting
This work is supported in part by the ICMIC@Stanford grant (NIH CA114747)

EFFECT OF INTER- AND INTRA- USER VARIABILITY IN QUANTIFICATION OF MOLECULAR IMAGING DATA

F Habte[2,5], S Budhiraja[2], T.C. Doyle[3,5,6,] C. S. Levin[1,2,4,5,6], D. Paik[1,2,4,5,6]
Dept of [1]Bioengineering, [2]Radiology, [3]Pediatrics, [4]Division of Nuclear Medicine, [5]Molecular Imaging Program at Stanford (MIPS), and [6]Bio-X Program, Stanford University, CA

In molecular imaging, absolute image quantitation is generally considered to be critical since it reduces subjectivity and provides important additional information that adds confidence in the data analysis process. Quantitation, however, heavily depends on the region of interest (ROI) analysis method, which normally is performed by manually defining an ROI and querying its statistics. Depending on how the ROI is drawn, the geometry and size of the ROI and the specific software tool used introduce variability and limit the accuracy.

To characterize variability, nine experienced users with no restriction on data analysis tools were selected to read five different data sets three times for each data set. The images were acquired using microPET. In addition, we conducted a survey to study the users' confidence and subjectivity involved in the analysis. Our result indicates that high inter-user variability (s.d. > 30% of the inter-user mean) occurred while the intra-user variability is relatively low (s.d. < 10% of the inter-user mean). We also observed a pattern where each user consistently either under- or over-estimates the mean quantitative value, demonstrating the high degree of subjectivity. There was no direct correlation observed between the inter-user variability and confidence of the users on drawing the specific ROIs. Thus, software tools capable of defining ROIs semi-automatically may be required to improve quantitation accuracy and reduce variability in analysis of molecular imaging data.

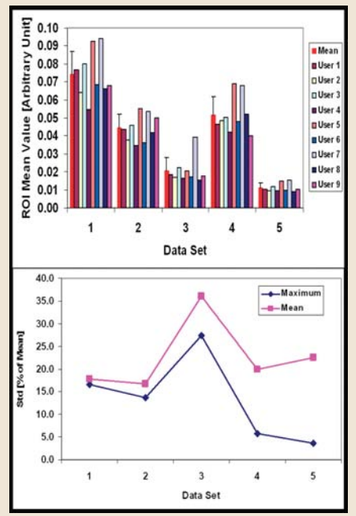

Inter- and Intra- user variability study on five-image data sets acquired using microPET (Top), and the computed percentage of standard deviation with respect to the inter-user mean.

REFERENCES/FUNDING SOURCE

Accepted for poster presentation on the upcoming WMIC meeting
This work is supported in part by the ICMIC@Stanford grant (NIH CA114747)

IMAGING PHYSICIAN ANNOTATION DEVICE (IPAD): INCORPORATING COMPLETENESS FEATURES

C. Rodriguez[1], C. Beaulieu[1], S. Napel[1], D. L. Rubin[1]
[1]Dept of Radiology, Stanford University School Medicine

PURPOSE: We are developing the Imaging Physician Annotation Device (iPAD), a software tool that captures, structures, and transmits human annotations of findings in biomedical images. Our goal this year was to enable iPAD to prompt radiologists to create complete descriptions of lesions.

MATERIALS AND METHODS: iPAD permits radiologists to describe their observations about lesions in a precise and structured manner, and to save their annotations in the Annotation and Image Markup (AIM) format recently developed by the cancer Biomedical Informatics grid (caBIG) effort. iPAD ensures that users completely describe all aspects of lesions via a structured reporting template. Templates are defined using a template editor, which specifies the data entry fields that are specific to a domain, the terms that are valid for each data entry field, and the data entry fields that are required for a complete annotation. We performed a qualitative evaluation by asking a radiologist to use iPAD to annotate 90 CT images of liver lesions.

RESULTS: The iPAD template collected detailed structured information about image findings and anatomy related to the liver lesions, enforcing controlled terminology and prompting the radiologist to report a range of aspects of lesion descriptions. As the radiologist recorded observations, iPAD checked on-the-fly for direct mapping to controlled terminology. If terms were incorrectly typed or did not match a controlled term, the user was notified with text and "text to speech" feedback that the term was invalid. The radiologist found iPAD easy to use, and reported that the tool enabled efficient recording of imaging observations. The required term completion feature of iPAD enabled the radiologist to create a thorough description of each lesion.

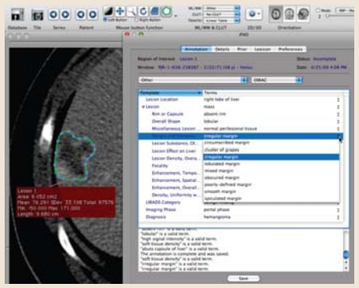

The iPAD tool allows users to create structured annotations that are complete descriptions of lesions seen in images. The user has circumscribed a lesion in an image of the liver (left) and has described the visual features of that lesion in iPAD's reporting template (right). iPAD automatically prompts the user for controlled terms for each type of imaging observation presented in the reporting template.

CONCLUSION: We have added to iPAD a template-based method for recording imaging observations. This enables radiologists to create thorough descriptions of lesions in a semantically interoperable, standardized, caBIG-compatible format.

REFERENCES/FUNDING SOURCE

National Cancer Institute cancer Biomedical Informatics Grid (caBIG) Imaging Workspace and the National Institutes of Health, CA72023

Image Analysis, Bioinformatics, Computational Modeling

Semantic Reasoning with Image Annotations for Tumor Assessment

M. A. Levy[1,2], M. J. O'Connor[2], and D. L. Rubin[1]
[1]Dept of Radiology, [2]Center for Biomedical Informatics Research, Stanford, CA

PURPOSE: Identifying, tracking, and evaluating tumor lesions is a central task in cancer research and clinical practice that could potentially be automated and improved in accuracy. However, information about tumor lesions in imaging studies is not easily accessed by machines for automated reasoning. Our goal is to develop knowledge-based reasoning methods for automated calculation and classification of tumor response from images and a suite of tools for semantic reasoning over image annotations for the particular task of tumor assessment.

METHODS: We used the Annotation and Image Markup (AIM) information model, a project of the cancer Biomedical Informatics Grid, to provide a syntax for encoding the semantic information related to imaging findings, enabling their storage and transfer. In order to apply automated reasoning methods to image information encoded in AIM, we developed a methodology and a suite of tools for transforming AIM image annotations into the Web Ontology Language (OWL), comprising an OWL equivalent of the AIM XML-based information model. We also created an ontology in OWL for reasoning with the resulting image annotations (as OWL instances) for tumor lesion assessment. We created image annotations in AIM obtained from serial CT images in a patient undergoing treatment in a clinical trial. We tested the ability of our system to use these annotations to automatically perform assessments needed to estimate tumor burden.

RESULTS: We successfully transformed the AIM information model into OWL. The AIM image annotations we acquired were processed by our system to perform automated reasoning about the image findings. Our tools successfully executed the following two tasks needed to estimate tumor burden: 1) calculation of the length of each image finding from pixel coordinates, and 2) classification of image findings as measurable and non-measurable using a combination of semantic information about the location and type of finding, and its calculated length.

CONCLUSTION: Our methods enable automated evaluation of tumor response based on the semantic information obtained from cancer lesions in images. These methods could improve the accuracy of cancer response assessment.

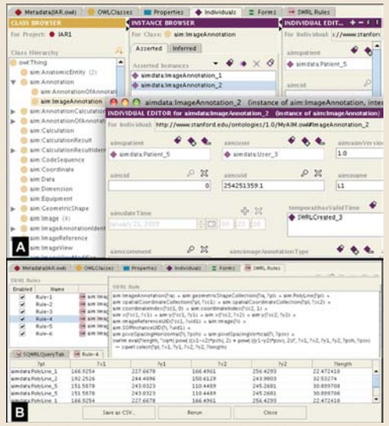

Knowledge-based system for computer reasoning with image annotations. (A) A portion of the AIM ontology in the left hand panel. Two instances of AIM image annotations are shown in the middle panel, and details of the properties of one instance are shown in the window in the lower right. (B) Example query to calculate length of an annotation of a line on an image from (x,y) coordinates and pixel spacing information, with results shown in the last column in the lower panel. This length is subsequently combined with other information in calculating tumor burden by the system.

References/Funding Source

Wu, A., Do, B., Kim, J., Rubin, D. Evaluation of negation and uncertinaty detection and its impact on precision in search. Society for Imaging Informatics in Medicine Meeting. Charlotte, N.C. June 6, 2009.

Evaluation of Negation Detection and its Impact on Precision in Search

A. Wu[2], B. Do[1], J. Kim[2], D. L. Rubin[1]
[1]Dept of Radiology, Stanford University, CA; Dept of Radiology, [2]University of Iowa Hospitals and Clinics, Iowa City, IA

INTRODUCTION: Radiology reports contain information that can be mined, using a search engine, for teaching, research, and quality assurance purposes. Current search engines match a user's search term but do not differentiate between reports containing positive findings from those in which the search term is used in the context of negation. We describe RadReportMiner, a negation-aware semantic search engine, and compare its performance with a generic search engine, Google Desktop.

METHODS: RadReportMiner detects negation by extending NegEx, a rule-based system to detect negation in clinical texts. Rules were added to NegEx to detect negation phrases specific to radiology reports. To test the performance of RadReportMiner , we created a corpus of radiology reports by performing five keyword searches (appendicitis, hydronephrosis, fracture, optic neuritis, pneumonia) on a database of radiology reports. Up to a maximum of 100 reports obtained for each keyword were classified manually by a radiologist as positive or negative (containing the keyword in a positive or negated context). The same reports were then classified by RadReportMiner and Google Desktop, and search performance was compared by calculating recall and precision of retrieving only positive reports.

RESULTS: The five searches returned a total of 464 reports, of which 119 were marked as positive by the radiologist. RadReportMiner achieved a higher precision of 81%, compared with the precision for Google Desktop of 27% ($p < 0.0001$). RadReportMiner had a lower recall of 72% compared with recall of 87% obtained using Google Desktop ($p = 0.006$).

CONCLUSION: Adding negation identification to a word-based radiology report search engine improves the precision of search results over a search engine that does not take the negation context into account. Our approach may be useful to adopt in current report retrieval systems to help radiologists search radiology texts more efficiently.

	RadReportMiner		Google Desktop		p value*
# Results Returned	#		#		
Appendicitis	100		100		
Fracture	100		83		
Hydronephrosis	100		100		
Optic neuritis	64		64		
Pneumonia	100		38		
Total	*464*		*385*		
Precision	#	%	#	%	
Appendicitis	13/20	65%	14/100	14%	**< .0001**
Fracture	16/18	89%	29/83	35%	**< .0001**
Hydronephrosis	21/22	96%	31/100	31%	**< .0001**
Optic neuritis	21/27	78%	21/64	33%	**0.0002**
Pneumonia	15/19	79%	9/38	24%	**0.0001**
*mean (per-term)^*		*81%*		*27%*	**0.042***
*mean (per-document)^*	*86/106*	*81%*	*104/385*	*27%*	**< .0001**
Recall	#	%	#	%	
Appendicitis	13/14	93%	14/14	100%	1
Fracture	16/32	50%	29/32	91%	**0.0008**
Hydronephrosis	21/31	68%	31/31	100%	**0.0008**
Optic neuritis	21/21	100%	21/21	100%	1
Pneumonia	15/21	71%	9/21	43%	0.118
*mean (per-term)^*		*76%*		*87%*	0.273*
*mean (per-document)^*	*86/119*	*72%*	*104/119*	*87%*	**0.0057**

^ per-term means are calculated weighing each search term equally; per-document means are calculated weighing each retrieved report equally
* calculated using Fisher's Exact Test
* calculated using Wilcoxon Signed Ranks Test

Search Performance Comparison between RadReportMiner and Google Desktop. The top third of the table lists the terms searched and the number of results retrieved by each search engine. The middle third shows the precision values associated with each search term and the bottom third shows recall values. The right-most column lists the p-values for differences in precision and recall between the two systems.

References/Funding Source

Wu, A., Do, B., Kim, J., Rubin, D. Evaluation of negation and uncertinaty detection and its impact on precision in search. Society for Imaging Informatics in Medicine Meeting. Charlotte, N.C. June 6, 2009.

A Bayesian Approach to Decision Support for Evaluating Thyroid Nodules Based on Multi-variate Features

Y. Liu[1], A. Kamaya[1], T. S. Desser[1], and D. L. Rubin[1]
[1]Dept of Radiology, Stanford University School Medicine

PURPOSE: To create a Bayesian network that incorporates the multitude of imaging features and patient demographic characteristics to guide radiologists in assessing the likelihood of malignancy in suspicious-appearing thyroid nodules.

METHOD AND MATERIALS: We built a Bayesian classifier to combine multiple indicators of the malignant potential of thyroid nodules, including both imaging and demographic factors. The imaging features and conditional probabilities relating those features to diagnoses were compiled from an extensive literature review. To evaluate our classifier, we randomly selected 21 benign thyroid nodules and 20 malignant nodules from 37 patients who underwent ultrasound-guided biopsy. The final diagnosis in each case was pathologically-established. We compared the performance of our classifier to that of two radiologists specializing in thyroid imaging who independently evaluated each case on a 5-point scale of suspicion for malignancy.

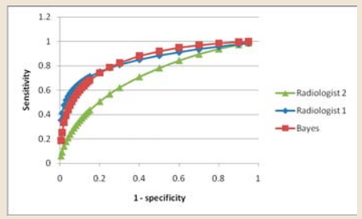

ROC curves for the Bayesian classifier and two expert radiologists in assessing the likelihood of malignancy in suspicious-appearing thyroid nodules.

Performance of the classifier and radiologists was compared using ROC analysis.

RESULTS: Our system had comparable or even slightly better performance to that of the two expert radiologists: area under the ROC curve (Az) for the Bayesian classifier was 0.851 (95% confidence interval (CI): 0.745-0.939), which is similar to or slightly better than those of the expert radiologists (0.846 (CI: 0.678-0.943) for radiologist 1 and 0.719 (CI: 0.543-0.854) for radiologist 2).

CONCLUSION: We created a Bayesian classifier incorporating a range of features to predict whether a thyroid nodule is benign or malignant. Our system may assist radiologists in assessing thyroid nodules by providing an objective basis for making biopsy decisions based on the estimated probability of malignancy

References/Funding Source

Liu YI, Kamaya A, Desser TS, Rubin DL: A Bayesian Approach to Decision Support for Evaluating Thyroid Nodules Based on Multi-variate Features. Scientific Paper, Ninety-fourth annual scientific meeting of the RSNA, Chicago, IL, 2008.

A Natural Language Processor to Detect Uncertainty and Recommendations in Radiology Reports

B. Do[1], A. Wu[2], D. L. Rubin[1]
[1]Dept of Radiology, Stanford University, CA; Dept of Radiology, [2]University of Iowa Hospitals and Clinics, Iowa City, IA

PURPOSE: Our goal is to design and validate a natural language processor (NLP) to detect uncertainty and recommendations in radiology reports.

METHOD: We utilized the Win/Apache/PHP/MySql platform to implement the NLP system. The NLP system processes entire radiology reports. The system first pre-processes input text to eliminate institution-specific statements that do not contain pertinent medical content. The system next identifies terms or phrases indicating uncertainty and recommendations using regular expression rules that specify words or phrases that confer uncertainty about observations and inferential concepts. The system was validated using 1232 sentences contained in 684 reports drawn randomly from reports within a five year period. A radiologist created a gold standard by manually evaluating each sentence, classifying it as an uncertain statement or a recommendation. The NLP system processed these sentences to classify them. Contingency statistics were calculated for detection of uncertainty and recommendations.

RESULTS: The NLP system classified the sentences as follows: 173 (14%), 87 (7.1%), and 972 (79%) as uncertain, recommendation, and declarative, respectively. The sensitivity and specificity for uncertainty detection by the NLP system were 97.1 and 99.6, respectively. The overall accuracy of uncertainty detection was 99.3 %. The sensitivity and specificity for recommendation detection were 92 and 99, respectively. To estimate the frequency of uncertainty in actual reporting practice, 2,828,677 sentences from 900,597 reports between 2005-2009 were evaluated with the NLP system. Uncertain statements and recommendations occurred in 30.9% and 19.2% of reports, respectively. The percentage of reports containing uncertainty were higher when dictated by a resident than when dictated by the same attending radiologist alone ($p < 0.01$, $n = 8$).

UNCERTAINTY CLASSIFICATION		NLP SYSTEM	
		POSITIVE	NEGATIVE
RADIOLOGIST	POSITIVE	168 (TP)	5 (FN)
	NEGATIVE	4 (FP)	1055 (TN)

Confusion matrix for uncertainty detection in NLP system. Precision, recall, specificity, accuracy, and pre-test probability are 97.6, 97.1, 99.6, 99.3, and 14%, respectively.

CONCLUSION: We have developed an NLP system to detect uncertainty and recommendation statements in radiology reports. This system can be useful for comparative analysis of the frequency of uncertain statements and recommendations, and may ultimately be useful to incorporate into reporting systems to improve the clarity of radiologist communication.

References/Funding Source

Bao Do, Andrew Wu, Daniel Rubin, A Natural Language Processor to Detect Uncertainty and Recommendations in Radiology Reports. Radiological Society of North America Meeting. Chicago, Illinois November 2009.

QUANTIFYING MARGIN CHARACTERISTICS OF LESIONS FROM CT IMAGES FOR CONTENT BASED IMAGE RETRIEVAL

A. Gupta[1], S. Napel[2], H. Greenspan[3], C. Beaulieu[2], and D. Rubin[2]
Depts of [1]Computer Science, [2]Radiology, Stanford University School of Medicine, CA; [3]Dept of Biomedical Engineering, Tel Aviv University

Purpose: To develop a method to quantify the sharpness of the margin of liver lesions and to evaluate its performance for retrieval of images with similarly appearing lesions.

Method And Materials: We obtained a set of 30 portal venous phase CT images of the liver containing cysts, metastases, and hemangiomas. Two radiologists reviewed the images in consensus to establish a reference standard of similarity between all pairs of images on a 3-point scale. One radiologist manually circumscribed each lesion, creating a ROI that was dilated to include some normal liver beyond the lesion. We computed a margin sharpness score by measuring filtered intensities along radial lines starting at the center of the ROI to points on its boundary. We then fit a sigmoid function to these values, and averaged its two parameters over all radii to yield a feature vector with 2 elements characterizing the lesion-to-liver intensity and the sharpness of the margin. We defined the similarity between a query image and an image in the database as the inverse of a weighted sum of the absolute difference between the two features.

Results: For each query image, the remaining images in the database were ranked according to their similarity to the query image in descending order. Mean Normalized Discounted Cumulative Gain, (NDCG), a standard information retrieval criterion (best=100%, worst=0%), was then used to compare this ordering with the expected ordering based on the reference standard as a function of K, the number of images retrieved. For K=5, 15, and 30, the NDCGs were 88.20%, 89.68%, and 95.34%, respectively.

Conclusion: We have developed an automatic method to quantify the sharpness of the margin of liver lesions. In these datasets, this image feature accurately distinguished amongst different types of lesions with different margin characteristics, suggesting utility for content-based image retrieval. Evaluation in a larger dataset is warranted.

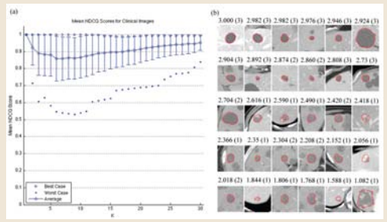

Results from experiments on clinical images. (a) Mean NDCG scores vs. number of images retrieved (error bars represent standard deviation). (b) Retrieval results with the top left image (cyst) as a query image. Query image is in upper left corner of 6 images, within which rankings go from highest on upper middle to lowest on lower right. Numbers above each image, X(y), show X = shape descriptor's similarity score and y= similarity from the reference standard, both on a scale of 1 to 3 with 3 best.

CHARACTERIZING THE SHAPE OF LIVER CT LESIONS FOR CONTENT-BASED IMAGE RETRIEVAL

J. Xu[1], C.F. Beaulieu[2], D.L. Rubin[2], S. Napel[2]
Depts of [1]Electrical Engineering and [2]Radiology, Stanford University

Purpose: To develop an efficient descriptor of the shape of an imaged object for use in content-based retrieval of medical images containing lesions.

Materials and Methods: We used three distinct contour-based shape features: compactness, centroid distance signal, and multi-scale local area integral invariant (LAII). Compactness gives a rough measure of circularity. Centroid distance is calculated by sampling the shape boundary in a polar coordinate system centered at the centroid of the shape. LAII entails the notion of curvature in a scale-space. These features are normalized so as to be invariant to translation, rotation, and scale. We defined the similarity between a query image and an image in the database as the inverse of a weighted sum of the absolute difference between the three features. Weights were trained using machine learning and leave-one-out cross validation methods to avoid training and testing on the same data. We tested this descriptor using a database of 72 portal-venous-phase CT liver images containing lesions classified by radiologists to be either lobular. Ovoid, or round. A similarity reference standard was established by setting pair-wise similarity to 3 if the classifications were identical and 1 if different.

Results: For each of the 72 query images, the remaining 71 images in the database were ranked according to similarity to the query image in descending order. Normalized Discounted Cumulative Gain (NDCG), a standard information retrieval criterion (best=100%, worst=0%), was calculated to compare this ordering with the expected ordering based on the reference standard, as a function of the number of retrieved images, and averaged over all query images. Results were excellent and are given in the Figure along with query examples showing 100% precision.

Conclusions: Our computational shape descriptor is highly correlated with radiologists' annotation and could be used to retrieve images of lesions with similar boundaries, or combined with other features for more general types of similarity queries.

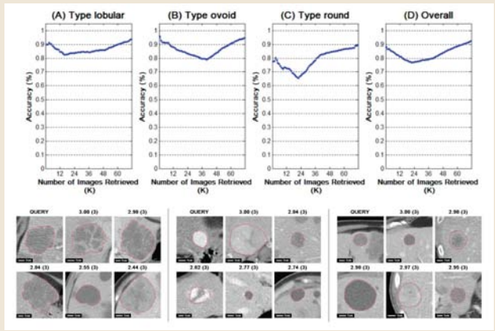

(Top) Mean NDCG plotted vs. K=number of images retrieved for three shape types, with results for K=5, 10, 15 reported in parentheses: (A) 17 images annotated to be lobular (90%, 87%, and 84%). (B) 41 images annotated to be ovoid. (91%, 90%, and 87%). (C) 23 images annotated to be round. (78%, 72%, and 72%). (D) All 72 images. (85%, 82%, and 80%). (Bottom) Example of top 5 retrieved images for 3 queries (left to right: lobular, ovoid, round). Query image is in upper left of each panel of 6 images, within which rankings go from highest on upper middle to lowest on lower right. Numbers above each image, X(y), show X=shape descriptor's similarity score and y=similarity from the reference standard, both on a scale of 1 to 3 with 3 best.

MAPPING EYE MOVEMENTS IN 3D: ANALYZING GAZE PATHS WHEN INTERPRETING VOLUMETRIC CT DATA

M. Tall[1], D. Ly[2], F. Schmitzberger[1], D. Rasooly[1], T-J Kim[1], J. Roos[1], D. Paik[1], S. Napel[1], G.D. Rubin[1]
[1]Stanford University School of Medicine, Stanford CA; [2]Faculty of Medicine, University of Toronto, Canada

Purpose: Previous studies investigating eye movements of radiologist during their image analysis have recorded gaze data on single images containing one or more objects, e.g., nodules in a CT scan. Typically the images are displayed for a fixed duration and the results are illustrated through aggregated visualizations, e.g., fixation plotting, scan paths or heat maps. However, when analyzing search patterns while performing standard interpretation of volumetric chest CT data, paging through a stack of transverse sections warrants three-dimensional analysis of eye movements. To our knowledge this has not been studied.

Materials and Methods: Our solution for recording volumetric gaze data, using a remote corneal reflection system, relies on two-way communication between the eye tracker and our custom DICOM viewer. This enables real-time mapping between on-screen fixations and the 3D DICOM coordinates of the viewed images at a rate of 50 Hz, thereby linking our eye tracker data and the physical space in which the 3D image data were obtained.

Results: Our approach to tracking and visualizing gaze data recordings within the acquired volumetric space utilizes the DICOM coordinate system for rendering graphics in 3D space. It produces several interesting visualizations, such as time-stamped 3D gaze paths, and 3D heat maps revealing direct and foveal dwell time per voxel, all fused with the acquired volume data for simultaneous viewing.

Conclusions: Our approach offers insight into the relationship between recorded gaze data and the volumetric space of the viewed medical images. We are employing it in an investigation of how paging through volumetric lung CT data affects nodule detection though pop-out feature detection in the peripheral visual field. More generally it will facilitate studies across a wide variety of 3D modalities and illuminate specific aspects of volumetric inspection that can be used for training and diagnostic support.

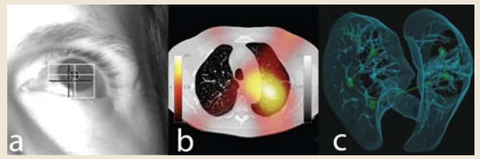

(a). The remote eye tracker sits underneath the monitor and illuminates the eyes with infrared light. Image processing routines identifies the center of the pupil and the two corneal reflections created by the infrared illumination. This creates a vector between the two glints and the center of the pupil which is calibrated against on-screen coordinates (b). Two-dimensional heat-map based on the Gaussian distribution of eye fixations (traditional approach) (c). 3D visualization of a scan path though the entire volumetric space fused with the acquired CT volume data for simultaneous viewing.

CONTENT-BASED IMAGE RETRIEVAL USING TEXTURE FEATURES

J. Cui[1], J. Xu[1], A. Gupta[3], C.F. Beaulieu[2], D.L. Rubin[2], S. Napel[2]
Depts of [1]Electrical Engineering, [2]Radiology, [3]Computer Science, Stanford University, Stanford CA

Purpose: To develop a method to integrate texture based image features of liver lesions for Content-based Image Retrieval.

Materials and Methods: Our dataset consisted of 30 de-identified portal venous phase CT images containing three types of liver lesions: cysts, metastases, and hemangiomas. We extracted several texture features to describe different aspects of the lesions, including Histogram features (e.g., Gabor Transform of Histogram, Peak Position), and Gabor Wavelets features. We defined the similarity between a query image and an image in the database as the inverse of a weighted combination of absolute differences for each feature. We performed a leave-one-out cross-validation to avoid training and testing on the same data. In the training sets, we used a modified Adaptive Boosting algorithm to learn weights that yield optimal ranking of the retrieved results with respect to an independent reference standard, which was set by two radiologists working in consensus to assign the similarity in lesion appearance between all pairs of images on a 3-point scale. The optimal weights were then applied to the test sets and the ranking of the retrieved images was compared to the reference standard.

Results: For each query image, K images (K=1,2,…30) were retrieved from the database and were ranked according to their similarity to the query image in descending order. Normalized Discounted Cumulative Gain (NDCG), a standard Information retrieval criterion (best=100%, worst=0%), was calculated to compare the ordering of the K images with the expected ordering based on the reference standard. For K=5, 10, and 30, the proposed similarity metric achieved average scores of 94.6%, 93.5%, and 97.1%, respectively, over all query images.

Conclusions: The proposed learning-based method integrates multiple texture based image features, gives excellent results, and can be easily extended to a richer feature set and a larger database.

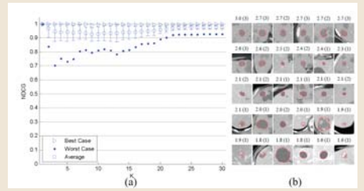

(a): NDCG for combining histogram and Gabor texture features, showing average, best and worst case performance in a set of 30 images containing cysts, metastases, and hemangiomas. (b): Example of retrieval rankings for a query image (cyst). Query image is in upper left of the panel of 30 images, within which rankings go from highest on upper left to lowest on lower right. Numbers above each image, X(y), show X=our method's similarity score and y=similarity from the reference standard, both on a scale of 1 to 3 with 3 best.

Content-based Image Retrieval (CBIR) using Combinations of Features

J. Cui[1], J. Xu[1], A. Gupta[3], C. Beaulieu[2], D.L. Rubin[2], S. Napel[2]
Depts of [1]Electrical Engineering, [2]Radiology, [3]Computer Science, Stanford University, Stanford CA

Purpose: To develop a method to integrate multiple heterogeneous quantitative visual features of liver lesions for CBIR.

Materials and Methods: We selected 30 portal venous phase CT images containing three types of liver lesions: cysts, metastases, and hemangiomas. We extracted several features to describe different aspects of the lesions, including histogram features (e.g., Gabor Transform of Histogram, Peak Position), Gabor Wavelets to represent the texture, and an edge feature measuring sharpness of the lesion boundary. We defined the similarity between a query image and an image in the database as the inverse of a weighted combination of absolute differences for each feature. We performed a leave-one-out cross-validation to avoid training and testing on the same data. In the training sets, we used a modified Adaptive Boosting algorithm to learn optimal weights for ranking of the retrieved results with respect to an independent reference standard, which was set by two radiologists working in consensus to assign the similarity in lesion appearance between all pairs of images on a 3-point scale.

Results: For each query image, K images (K=1,2,…30) were retrieved from the database and were ranked according to their similarity to the query image in descending order. Normalized Discounted Cumulative Gain (NDCG), a standard information retrieval criterion (best=100%, worst=0%), was calculated to compare the ordering of the K images with the expected ordering based on the reference standard. For K=5, 10, and 30, the proposed distance with learned weights achieved average scores of 94.8%, 96.1%, and 98.4%, respectively, while integrating the features using equal weights resulted in scores of 91.7%, 89.0%, and 96.6%, respectively. Using single features alone the average scores ranged from 84.9%-92.5%, 84.6%-92.3%, and 94.6%-97.3%, respectively.

Conclusions: The proposed learning-based method integrates multiple quantitative features, and can be easily extended to a richer feature set and a larger database. In our dataset, it outperformed single features and integrating features with equal weights.

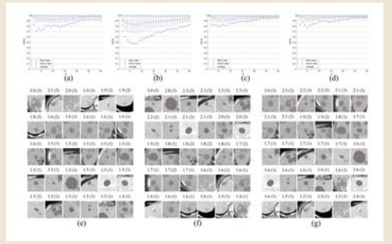

(a)-(d): NDCG for different types of image features, plotted showing average, best and worst case performance in a set of 30 images containing cysts, metastases, and hemangiomas: (a) combined histogram and Gabor features, (b) edge features, (c) semantic features, (d) all features combined. (e)-(g): Examples of retrieval for three queries. Query image is in upper left of each panel of 30 images, within which rankings go from highest on upper left to lowest on lower right. Numbers above each image, X(y), show X=our method's similarity score and y=similarity from the reference standard, both on a scale of 1 to 3 with 3 best.

Biomedical Image Metadata Manager Web-Application

D. Korenblum[1], C.F. Beaulieu[2], S. Napel[2], C. Rodriguez[3], D.L. Rubin[2,3]
Depts of [1]Computational and Mathematical Engineering, [2]Radiology, [3]Biomedical Informatics, Stanford University, CA

Purpose: Advances in radiology increasingly depend on collecting and analyzing features of images that are currently not recorded in way that can be processed by computers. The annotations that radiologists make on images (identifying lesions, delineating their borders, measuring ROIs, and describing the visual features in those ROIs) are currently captured as image graphics that are not directly accessbile for future analyses. Radiologists cannot, e.g., easily process measurements made from images, such as the sum of linear dimensions on serial scans, to evaluate criteria of treatment response. Visual observations made by radiologists are recorded in radiology reports that are disconnected from the images and not easily searched for specific anatomy, findings, and disease. Thus, it is not possible, e.g., to query a PACS to display images showing specific findings. To achieve such functionality, methods are needed to make image metadata accessible for search.

Materials and Methods: Our web-application, Biomedical Image Metadata Manager (BIMM, http://bimm.stanford.edu), makes the key quantitative and qualitative information in images and their associated reports searchable and linked to the images, enabling query and large-scale analysis of image databases. Annotations are uploaded using the Annotation and Image Markup (AIM) standard, part of the National Cancer Institute's cancer Biomedical Informatics Grid (caBIG).

Results: BIMM collects, stores, searches, and analyzes rich AIM metadata, which, in our implementation, is supplied by iPAD, an OsiriX plugin. BIMM finds similar images by analyzing the metadata and ranking images according to the number of matches of annotated terms. The BIMM application enables radiologists and researchers to search for images in flexible ways, by anatomy, findings, or other metadata.

Conclusions: This tool might ultimately improve radiologist interpretion by enabling online decision support, and might facilitate biomedical researchers to access image information as part of their investigations of the biology and the manifestations of disease.

Matching images are ranked in descending order according to match-score. From the "search" page, the user typed a query into the upper-right box, selected four "query" imaging observation characteristics for one of the search results, and clicked "match observations." The resulting match-scores are determined by counting the number of matching characteristics between query and target images

Estimating the Likelihood of Cure from Lung Cancer by CT Screening

R S. Lin[1], B M Sigal[2], and S K Plevritis[2]
[1] Depts of Medicine, Biomedical Informatics and [2]Radiology, Stanford University, CA

Lung cancer is the leading cause of death from cancer in the United States, yet screening for lung cancer is not currently recommended even among current and former smokers. X-ray screening has not been shown to reduce lung cancer mortality, and Computed Tomography (CT) screening is still under investigation. To predict the effect of CT screening on lung cancer cure, we developed a mathematical model of the natural history of lung cancer was developed to estimate the relationship between the size of the primary tumor and the likelihood of cure. The model was applied separately to lung adenocarcinoma, squamous cell carcinoma, large cell carcinoma, and small cell carcinoma, and separately for males and females. Model parameters were estimated using data from the Surveillance, Epidemiology and End Results (SEER) cancer registry. The model reproduces SEER, validates against an external dataset and produces estimates of tumor volume doubling times that are consistent with empirical data. We find that an individual patient who would have been clinically detected in the absence of screening has a 50% probability of cure if their primary tumor were diagnosed and treated by 6 – 8 mm. Fig. 1 shows the predicted lung cancer mortality reduction from CT screening as a function of the screening interval and the detection threshold of CT. Among a population annually screened with a test that can detect tumors 6-8 mm in size, the reduction in lung cancer mortality is 25-30%, provided there was no delay in diagnosis and treatment. The reduction in lung cancer mortality is less than 10% if the mean tumor size at diagnosis and treatment increases to 15mm or greater. Because CT screen detected tumors in the mm-range are often followed for growth to reduce the risk of unnecessary biopsies, the opportunity to cure the patients with deadly disease may be significantly diminished by the time the tumor is diagnosed and treated.

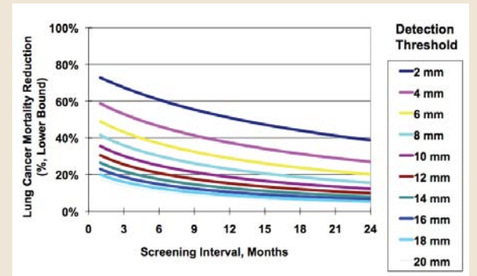

Fig. 1: Lung cancer mortality reduction attributable to CT screening as a function of the screening interval and the detection threshold.

References/Funding Source

NIH R01CA105366, Canary Foundation grant

A Clinical Tool to Guide Cancer Risk-Reduction Decisions in BRCA1/2 Mutation Carriers

S Plevritis[1], A Kurian[2,3], B Sigal[1]
Depts of [1]Radiology, [2]Oncology, and [3]Health, Research and Policy, Stanford University, CA

More than 250,000 women in the United States carry an inherited mutation in the BRCA1 or BRCA2 cancer susceptibility genes, which convey lifetime risks of 45-65% for breast, and 11-39% for ovarian, cancers. Given these greatly elevated risks, management strategies involve earlier, more frequent and more invasive interventions than in the general population. The two disparate alternatives for breast cancer risk-reduction are prophylactic mastectomy or intensive breast screening including magnetic resonance imaging: these approaches yield very different outcomes and side-effects. Clinical decision support tools can provide individualized estimates of patient outcomes, and may yield particular benefit when patient preference dictates the choice between medically acceptable alternatives. We have developed a (preliminary) clinical tool to guide female BRCA1/2 mutation carriers and their physicians in cancer risk-reduction decisions (Fig. 1). Using a web-based interface, women enter their current age and known mutation status, then they can consider a variety of alternative cancer-death risk-reduction strategies and compare the survival outcomes of each strategy side-by-side. For each strategy, women can choose any combination of three interventions: screening, prophylactic oophorectomy (PO), and prophylactic mastectomy (PM); and, they can vary the age at each intervention. The resulting bar charts shown in Fig. 1 illustrate the chances of survival by age 70, and the chances of death from breast cancer, ovarian cancer and other causes. For comparison purposes, outcomes for women at average risk is provided. This work aims to produce a clinical tool that can offer individualized assessments of cancer risk-reduction strategies to women with BRCA1/2 mutations and their physicians, which will have an immediate and direct impact on the clinical care of high-risk women.

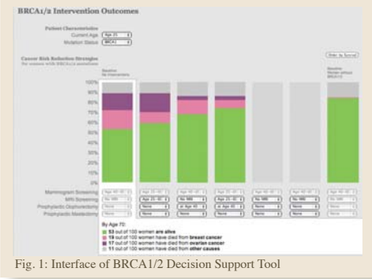

Fig. 1: Interface of BRCA1/2 Decision Support Tool

References/Funding Source

R01CA105366, Stanford Cancer Center Seed Fund

SIGNATURES OF HOST IMMUNE RESPONSE PREDICT TRANSFORMATION AND OUTCOME IN FOLLICULAR LYMPHOMA

A J Gentles[1], A A Alizadeh[2,3], R Levy[2,3], and S K Plevritis[1]
Depts of [1]Radiology, ISIS, [2]Hematology, and [3]Clinical Oncology, Stanford University, CA

Expression signatures of infiltrating immune cells including T-cells [1] have been shown to predict survival in follicular lymphoma (FL), but have not been cross-validated in independent patient cohorts [2,3]. We sought to evaluate the validity of this model in an independent cohort of patients with FL, assessing its relationship to outcomes including histological transformation and death. The immune response (IR) predictor score proposed by Dave et al. [1] was applied to gene expression data from an independent cohort of 88 FL patients [4] with known survival outcomes and history of transformation to diffuse large B-cell lymphoma (DLBCL). Genes (n=66) corresponding to IR1 and IR2 signatures were mapped from Affymetrix microarrays [1] to a custom cDNA array [4] via Entrez Gene ID, and the composite IR score was calculated per the scheme proposed by Dave et al. The IR score was predictive of patient outcome in the 88 patient test set as a continuous variable (p=0.001, HR=2.01, 95% CI 0.50-1.30). Partitioning of patients into high and low risk groups based on the median IR score across the cohort robustly separated survival curves (Figure A). The IR score was significantly higher in FL patients known to undergo transformation to DLBCL (Figure B: mean IR score of -0.6 in non-transforming FL vs. -0.2 in transforming FL; p~10-11, t-test). In conclusion, the IR score of Dave et al. was highly significant as a predictor of survival in the independent patient cohort [4]. Moreover, the score was significantly associated with propensity of FL to transform to DLBCL. To our knowledge, immune cell infiltration has not previously been implicated in transformation.

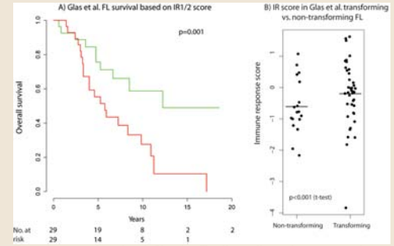

Gene signatures based on infiltrating T-cells predict patient outcome in follicular lymphoma, and propensity to transform to diffuse large B-cell lymphoma.

REFERENCES/FUNDING SOURCE

1. Dave SS et al. (2004) Prediction of survival in follicular lymphoma based on molecular features of tumor-infiltrating immune cells. N Engl J Med 351(21): 2159-2169.
2. Tibshirani R (2005) Immune signatures in follicular lymphoma. N Engl J Med 352: 1496-1497.
3. Chu G Hong WJ, Warnke R, Chu G (2005). Immune Signatures in Follicular Lymphoma (Corres). N Engl J Med. 352: 1496-1497.
4. Glas AM et al. (2005) Gene expression profiling in follicular lymphoma to assess clinical aggressiveness and to guide the choice of treatment. Blood 105(1): 301-307.
NIH 5U56CA112973-03

IDENTIFYING CRITICAL MOLECULAR REGULATORS OF SUBTYPE IN DIFFUSE LARGE B-CELL LYMPHOMA

A J Gentles[1], A A Alizadeh[2,3], R Levy[2,3], and S K Plevritis[1]
Depts of [1]Radiology, ISIS, [2]Hematology and [3]Clinical Oncology, Stanford University, CA.

Diffuse large B-cell lymphoma comprises around 40% of Non Hodgkin's lymphomas. Two major sub-types have been identified, based on putative cell-of-origin, that have significantly different patient survival outcomes. Germinal Center (GCB) DLBCL is associated with better prognosis than Activated B-cell (ABC) subtype. We used a network-based approach to identify critical regulators of the DLBCL subtypes, from high-throughput gene expression data. First, we applied an information theoretic algorithm for reconstructing transcriptional networks of interactions in each of four large publicly available gene expression datasets on DLBCL patients. Mutual information can detect nonlinear relationships that are missed by correlation approaches. In each case, we identified "hub" genes – genes that are highly connected to other genes in the transcriptional network. The set of genes connected to a hub gene were labelled as their putative set of targets.

These target gene sets were then used in a gene set analysis of the original data, with the aim of identifying which target sets were significanly differentially expressed between DLBCL subtypes. The intuition is that if the targets of a particular gene are expressed differently between GCB and ABC DLBCL, then that hub gene is likely to be a critical regulator of the subtype distinction. The complete analysis was carried out in each of the four available expression datasets, to determine which genes arose consistently in independent experiments. Amongst the top genes that we found (Table 1) were targets of LMO2, BCL6, and IRF4. These three genes have previously been identified in the literature as being crucial to distinguishing between ABC and GCB DLBCL. In addition we identified other potential regulators such as KLF12 that have not previously been implicated. Importantly, when we conducted this analysis in four independent datasets on DLBCL, we obtained similar lists of around 10 predicted regulators of the GCB/ABC distinction. Therefore, we identified key regulators in DLBCL subtypes, including new targets for experimental validation.

Hub gene	Score	FDR
TCF4	1.8295	0
IRF4	1.9794	0
BATF	1.9119	0
TGIF1	2.1812	0
SPIB	1.5069	0.03
ETV6	1.4425	0
BCL6	-1.8065	0
LMO2	-2.6217	0
KLF12	-2.3919	0.02
MEF2C	-1.3809	0.05
HDAC1	-2.4342	0

Table 1: Predicted critical regulators of GCB vs ABC subtype in DLBCL

MICROARRAY SAMPLE PROGRESSION ANALYSIS

P Qiu[1], A J Gentles[1], and S K Plevritis[1]
Dept of [1]Radiology, ISIS, Stanford University, CA

Microarray technologies measure the expression levels of thousands of genes simultaneously, from which we may gain insights on the mechanisms of biological processes. We propose a novel computational framework, Sample Progression Analysis (SPA), to identify and analyze progression patterns in microarray samples. Given a set of microarray samples, SPA assumes the samples are sampled from an unknown biological process which can be reflected by the gradual shift in expression of subsets of genes. Under this assumption, each microarray sample represents one unknown point during the progression, and the correct ordering of the microarray samples may lay out the pathway or trajectory of the progression. SPA aims to recover the progression order of the samples and identify the genes that reflect this ordering.

The SPA framework contains three components: (i) clustering gene into modules, (ii) constructing minimum spanning tree (MST), and (iii) statistical comparison between gene modules and trees. The uniqueness of SPA is that comparison between gene modules is performed via MSTs as surrogates. Introducing the MSTs as surrogates makes the comparison more flexible. Modules that fit well with the same trees are not necessarily correlated with each other, which means SPA is able to identify similarities that correlation or regression types of analysis can not. If there exist multiple modules that fit well with multiple trees, these modules are similar because they describe a common progression order of the samples. A common progression order supported by multiple modules is likely to be biologically meaningful.

We have validated SPA's utility in gene expression data of cell cycle and B cell differentiation, where the known progression orders are correctly identified, together with the gene modules that define the progression order (Fig. 1). We have also applied SPA to follicular lymphoma (FL) and diffuse large B-cell lymphoma (DLBCL) samples. Results indicate a progression order from FL to DLBCL. The identified progression order is reflected by increase of proliferation genes, and stem cell genes.

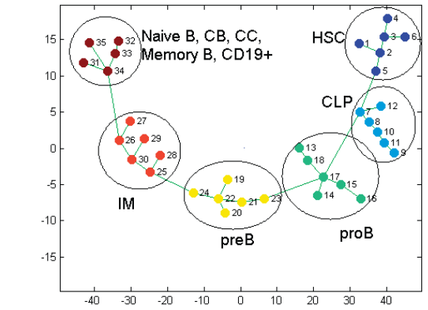

Fig. 1: Identified sample progression order among B cell differentiation microarray sample is found to be consistent with the known B cell differentiation process.

REFERENCES/FUNDING SOURCE

NIH U56 CA112973

A MULTISCALE MODEL OF BREAST TUMOR GROWTH

A Babu[1,2], A Anderson[3], and S Plevritis[1]
Dept of [1]Radiology, [2]Institute of Computational and Mathematical Engineering, Stanford University, CA; [3]Center for Mathematical Oncology, Moffett Cancer Center, FL

Our goal is to simulate breast cancer treatment trials to predict the effects of combination therapies. In this work, we aim to develop a computer model that simulates the effect of chemotherapy alone in breast cancer progression. Toward this aim, we must first develop a multiscale model of breast cancer that bridges cellular level knowledge with patient level outcomes. Our multiscale scale model integrates two previously developed and validated models. The first model is a partial differential equation (PDE) model of the densities of various cell types(normoxia, hypoxia, apoptotic

cells & vasculature) and the chemical factors(nutrient & drugs). The second model is a stochastic model describing the progression of clinical states. The successful integration of these two models

allows us to make inferences at the cellular level from epidemiology data.

The PDE model is of the reaction-diffusion type and models several complex dynamics of tumour development such as cellular diffusion, angiogenesis, metastasis etc at the cellular level. The model is controlled via parameters such as the diffusion and proliferation rates for normoxia

etc. Given a set of parameter values, the PDE system is solved numerically to get the distribution of densities at various instants of time (Fig. 1). These parameter values are used to generate a tumour volume growth curve, which drives the natural history model of clinical stage progression. The natural history model models the relationship between the size of the primary tumour at detection,the disease stage and the survival time of the patient. The model is controlled via parameters such as the growth rate of the primary, the curability threshold, the lethal

metastatic burden etc. Since the growth curve of the primary tumour volume is obtained from the PDE model, the growth rate of the primary is a cellular level(PDE model) parameter(eg proliferation rate of normoxia).

We assume the parameters to be random variables with appropriate distributions. The integrated model is fit to SEER data via a Monte-Carlo based MLE procedure, thus estimating various cellular and tissue level biological parameters. In addition we get detailed insights of the tumour structure in different regimes(curable/not-curable, early stage/advanced stage). In future work, we plan to extend the PDE model by introducing a drug as another chemical factor and studying it's effects on the tumour development.

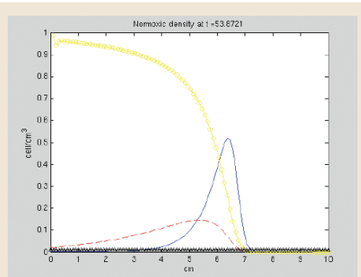

Fig. 1: Cellular composition of a tumor. Normoxic density profile in blue, hypoxic in red, apoptotic in yellow and vasculature in black.

REFERENCES/FUNDING SOURCE

U56 CA112973, U01CA 088248

RELATIVE CONTRIBUTIONS OF SCREENING AND ADJUVANT THERAPY ON BREAST CANCER CURE

R Lin[1,2], and S Plevritis[1]
Dept of [1]Radiology, ISIS; [2]Biomedical Informatics, Stanford University, CA

Our ability to quantify the relative contributions of screening and adjuvant therapy on breast cancer cure is limited by our lack of knowledge about the progression of this disease. We developed a mathematical model of the natural history of breast cancer that estimates the likelihood of cure from breast cancer as a function of primary tumor size. This model allows us to separate the impact of alternative interventions on breast cancer cure. We modeled the natural history of breast cancer using the concept of a "cure threshold." We define the "cure threshold" as the moment that the disease progresses from being curable to not curable, assuming usual care following detection. For patients who are detected at or before the cure threshold, and treated, we assume that they will never die of their disease; but if they are detected after the cure threshold, they die of their disease regardless of treatment, unless they die of other causes first. Our model provides estimates of the primary tumor size at the cure threshold, and the tumor volume doubling time distribution . Also, by comparing the cure threshold to the minimum detectable tumor size of a screening test, we can provide an estimate for the proportion of patients who can be cured by early detection. The model was fit separately to SEER data on patients detected from 1975-79 and separately for 1990-1993.

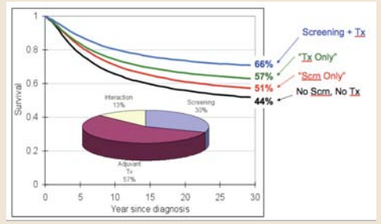

Fig. 1: Effect of Screening ("Scrn") and Adjuvant Therapy ("Tx") on Breast Cancer Survival and Long-term Cure.

By comparing these two calendar years, we estimate that adjuvant treatment shifted the cure threshold from 20 mm to 36 mm, and increased the median time from the moment the tumor is 15mm to none curable from 0.8 years to 2.8 years. Our work also suggests that adjuvant treatment has had a greater impact than screening on reducing breast cancer mortality (57% for adjuvant treatment and 30% for screening), with an interaction effect between adjuvant therapy and screening (of 30%, as shown in Fig.1).

REFERENCES/FUNDING SOURCE

NIH U01 CA088248

Magnetic Resonance Research

This MRI section will explore and highlight new and novel accomplishments made over the last year in the critical areas of MRI instrumentation and applications. These new advances provide improved capabilities to detect pathologies in clinical applications as well as to inform basic science understanding of the human body's physiology, function, and biology.

BODY MR IMAGING

OPTIMAL RANDOM SAMPLING SCHEME FOR COMPRESSED SENSING MRI

K. Sung[1], and B. Hargreaves[1]
[1]Dept of Radiology, Stanford University, CA

Imaging speed of MRI is very important in many applications. The amount of acquired k-space data is one of the key components contributing the speed of MR imaging. However, if one does not fully acquire k-space data to accelerate the speed, the MR image using conventional Fourier reconstruction experiences severe aliasing artifacts.

Compressed sensing (CS) is a technique that allows accurate reconstruction of images from a reduced set of acquired data. Incoherence expresses the idea that objects in the sparse representation domain must be spread out in the measurement domain, just as a spike in the time domain is spread out in the frequency domain, and assures the accurate reconstruction using CS. Random sampling in k-space typically provide the degree of the incoherence, and practical MRI implementations use empirically chosen random sampling patterns. The top row of the figure shows some examples of k-space random sampling patterns. The white dots represent acquired points at certain frequencies in k-space whereas the leftover black space means unacquired data. The conventional MRI typically fills all the black space, and therefore the black space tells how much acceleration is achieved using random sampling (here, only 25% of k-space data was selected). These reduced MR measurements are then recovered by using the nonlinear constrained reconstruction, which simultaneously attempts to achieve a sparse representation that is consistent with the acquired data.

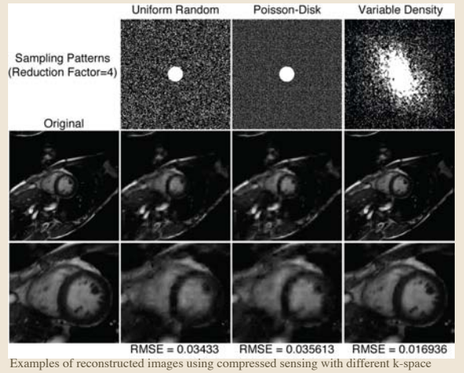

Examples of reconstructed images using compressed sensing with different k-space sampling patterns.

We developed a new sampling design (variable density) to improve the incoherence and compared with other commonly used random sampling (uniform and Poisson-disk random). The density function was determined from the data itself, assuming a low-resolution image for calibration is available. The reconstructed image using the proposed one shows superior performance to the other, and is approximately identical to the original image (RMSE = 0.0169).

REFERENCES/FUNDING SOURCE

This work was supported by NIH EB009055, and GE Healthcare.

Eight Channel Custom Breast Coil for Parallel Imaging in Two Directions

A. Nnewihe[1,2], T. Grafendorfer[3], B. Daniel[1], P. Calderon[3], M. Alley[1], and B. Hargreaves[1]
Depts of [1]Radiology, [2]Bioengineering, Stanford University, CA; [3]General Electric Healthcare

Screening dynamic contrast enhanced (DCE) MRI is recommended by the American Cancer Society for all women with a high risk for breast cancer. Currently, DCE MRI of the breast gives information about lesion morphology, tissue perfusion and enhancement kinetics. However, the lack of specificity as well as the difficulty in diagnosing ductal carcinoma in situ have hampered the adaptation of breast MRI to clinical practice. These issues could potentially be addressed by the acquisition of higher spatial resolution images, while maintaining sufficient temporal resolution through high acceleration factors. A recent study with a small surface coil has shown that high resolution breast MRI can improve sensitivity and specificity of DCIS diagnosis by describing smaller scale features such as ductal and periductal enhancement (Zhu et al., 2007). However, a small surface coil is not suitable for screening exams where volumetric coverage of both breasts is needed. Most industrial breast coils offer volumetric coverage of the breasts, but insufficient signal-to-noise ratio (SNR) and coil geometry severely limit the spatial and temporal resolution.

An 8-channel receive-only array coil is described and tested in vivo for unilateral breast imaging at 3T. The primary purpose of this coil is to provide high SNR and parallel imaging acceleration in two directions. Circular coil elements (65 mm in diameter) were placed on a closed "cup-shaped" platform, and nearest neighbor coils were decoupled through geometric overlap. In normal volunteers and patients, we demonstrated high temporal and spatial resolution scans with 4x net acceleration [2x S/I and 2x L/R]. When compared with a common 8-channel bilateral commercial coil, our custom coil shows 4 - 5 times higher SNR at the center of the breast and higher quality accelerated images (See Figure). Our continued work will include correction for intensity variations, and extending this coil to a full bilateral 16-channel coil.

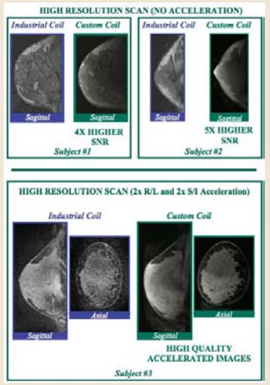

The custom coil shows 4-5 times higher SNR at the center of the breast when compared to a common 8-channel bilateral industrial coil. The custom coil also has higher quality accelerated images in comparison with the industrial coil.

References/Funding Source

Nnewihe A, Grafendorfer T, Daniel B, Calderon P, Alley M, Hargreaves BA. Eight Channel Custom Breast Coil with Parallel Imaging in Two Directions. 17th ISMRM Meeting 2009.
Zhu J, Kurihara Y, Kanemaki Y, Ogata H, Fukuda M, Nakajima Y, Maeda I. Diagnostic accuracy of high-resolution MRI using a microscopy coil for patients with presumed DCIS following mammography screening. Journal of Magnetic Resonance Imaging 2007; 25:96–103.
/NIH Regenerative Medicine Training Grant, California Breast Cancer Research Program IDEA Grant, General Electric Gift Grant

Patient-Specific Models of Susceptibility-Induced B_0 Field Variations in Breast MRI

C. D. Jordan[1,2], B. L. Daniel[1], K. M. Koch[3], H. Yu[4], S. Conolly[5], B. A. Hargreaves[1]
Depts of [1]Radiology, [2]Bioengineering, Stanford University, Stanford, CA; [3]Applied Science Laboratory, GE Healthcare, Waukesha, WI; [4]MR Applied Science Laboratory, GE Healthcare, Menlo Park, CA; [5]Dept of Bioengineering, U. C. Berkeley, CA

MRI images of the breast often have distortion from susceptibility-induced static magnetic field variations, which can cause fat suppression failure at the air-tissue boundary. This work quantitatively modeled these field inhomogeneities based on patient-specific breast shape in three-dimensional image datasets from patient studies. Using a simple dipole-field model to estimate the magnetic susceptibility, the B_0 perturbation was predicted and then compared with the measured field map. These patient-specific estimates of inhomogeneities may provide a model for improved shimming, or estimates for unwrapping frequency shifts in phase-based fat-water separation techniques like IDEAL, or may help correct for off-resonance. Iterative Decomposition of water and fat with Echo symmetry And Least-squares estimation, provides separated water, fat and field-map images by acquiring three images with different phases and echo times. For each dataset, we first generated the tissue susceptibility mask $\boldsymbol{\chi(r)}$, by thresholding using the in-phase image. We created a model-based B_0 field map based on magnetic susceptibility using the equation

$$\Delta B_0(r) = FFT^{-1}\left[B_0\left(\frac{1}{3} - \frac{k_z^2}{|k|^2}\right)FFT[\chi(r)]\right],$$

where $\Delta B_0(r)$ is the distribution of the magnetic field perturbation, B_0 is the static magnetic field, $\boldsymbol{k}$ is the Fourier space coordinate, and $\chi(r)$ is the 3D magnetic susceptibility mask that models the difference between air and tissue [2, 3]. After obtaining $\Delta B_0(r)$ using the above equation, the linear shims used in the original scan were added to the estimated field map and the DC frequency offset was subtracted. The estimated field map was then quantitatively compared with the measured field map, by comparing histograms. Within the tissue, the simulated field map closely modeled the inhomogeneities of the actual field map, as shown by the histograms of the values within the tissue. The empirical model that we developed predicts spatial variations in the magnetic field in the breast based on the shape of the breast.

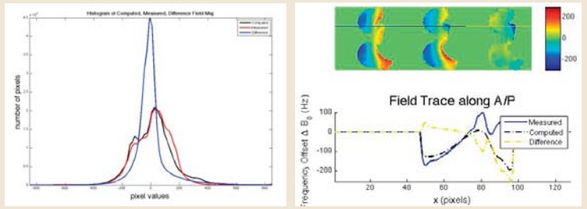

Line Plots along the Measured, Simulated and Difference Images. The estimated field map was then quantitatively compared with the measured field map, by comparing histograms.

References/Funding Source

1.SB Reeder et al, Magn. Reson. Med, 51, 35–45 (2004)
2.JP Marques et al, Concepts in MR B, 25B, 65-78 (2005)
3.KM Koch et al, Phys. Med. Biol, 52, 6381-6402 (2006)
NIH Grant EB009055-01
NIH Grant RR009784
Lucas Foundation
NSF Graduate Research Fellowship Program

Stable Field Map Estimation Using Global & Local Minima

H. Kim[1,2],K. Sung[1], and B.Hargreaves[1]
Depts of [1]Radiology, [2]Electrical Engineering, Stanford University, CA

Stable field map estimation is essential in three point Dixon techniques for accurate water-fat separation. In most of the field map estimation techniques, the field map is the demodulation frequency that minimizes a fitting residue or cost function, defined as. However, there are various challenges to uniform fieldmap estimation since the periodic residual curve has multiple minima during a period. Occasionally, finding the global minimum in cost function may not provide the correct fieldmap. This issue becomes more severe at water or fat dominant areas where the amplitudes of global and local minima are so close that the aliased fieldmap value can easily be selected, leading to an ambiguity in water-fat decomposition. To address this ambiguity, this study suggests a region growing method from a pixel with reliable fieldmap, tracking locations of both global and local minima.

For three echo images from an IDEAL acquisition, it is possible to obtain locations of global and local minima, based on a residual curve. Then, we try to downsample those images, finding two minima just as previously performed. Next step is to search for a location with the true field map for region growing from that pixel. Although the definition of true field map estimation would be obscure, the pixel with a single minimum must be considered to be sufficiently reliable. Empirically, when the ratio of water to fat is from 2:3 to 3:2, including 1:1 with little difference in phase between water and fat, yields a cost function with single minimum. In the case where there are not many pixels with a single minimum, a seed pixel for region growing is captured by previously defined region growing method with IDEAL. In that case, however, to see if a seed pixel has a true field map value, it is necessary to have further steps, such as measuring the variance of locations of global minimum in neighboring pixels, and comparing the ratio of value of global maximum to that of local minimum. Then, the field map of a seed pixel begins to be propagated by computing which one of the two minima is closer to that value. Using bilinear interpolation, resulting field map is enlarged to compare it with both global and local minima from original data set. At each pixel, one of the minima that are closer to resulting field map value is determined as a final field map. Fig.1 illustrates this whole process. With this result, water and fat will be finally decomposed with the least-squares solution.

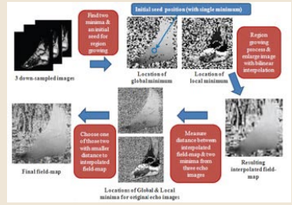

Fig. 1: This shows the procedures of region growing process from a reliable pixel with a single minimum in this case

Fat Suppression with Independent Shims for Bilateral Breast MRI

M. Han[1,2], S. Rodriguez[1], A. M. Sawyer[1], B. L. Daniel[1], C. Cunningham[3], J. M. Pauly[2], and B. A. Hargreaves[1]
Depts of [1]Radiology, [2]Electrical Engineering, Stanford University, CA; [3]Medical Biophysics, University of Toronto, Toronoto, ON, Canada

There exists a significant static magnetic field inhomogeneity for breast MRI related to the shape of the breast and susceptibility difference at air/tissue interfaces [1]. For bilateral breast MRI, large field variation over the two breast volumes makes robust fat suppression more difficult. Conventionally, a constant and linear shim correction is conducted by the scanner to remove field inhomogeneity, but optimal shim values can differ between the two breast volumes. We incorporated independent shims into a dual-band spectral-spatial excitation pulse [2] and compared fat suppression between standard shims and independent shims from ten volunteers at 1.5T.

For practical implementation of independent shims, after obtaining shim values and center frequency for the right and left breasts separately through prescans, an average shim in each axis over the two slabs was set using the shim channels of the scanner and an additional oscillating shim was applied with the gradient waveform as explained in [3]. For acquisition, flyback EPI [4] with the echo train length of four was used with a 20 x 20 cm FOV, 1.6 mm slice thickness with 64 sagittal 3D sections per breast.

Axial reformatted images of inferior breasts from one volunteer (a-d) compare different shim methods by applying (a) the left breast shim values to both breasts, (b) the right breast shim values to both breasts, (c) the average shim values to both breasts, and (d) independent shims.

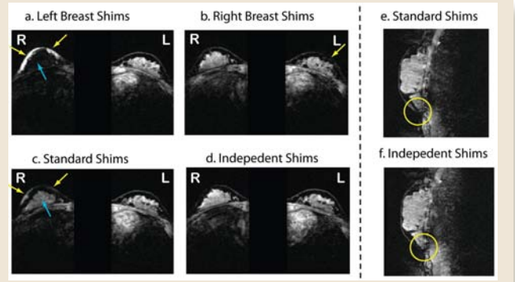

(a-d) Axial reformatted images from the four different shim methods. The regions of failure in fat suppression are shown by arrows (yellow: unsuppressed fat, blue: suppressed water). With independent shims, fat suppression was done robustly over the two breasts. (e-f) Sagittal slices from the standard shims and independent shims.

By using independent shims, fat suppression in each breast is as good as the best case of (a) and (b). In the inferior edge of the breasts, which typically possesses significant field inhomogeneity, independent shims (f) provide more homogenous fat suppression compared to standard shims (e). From our study, seven out of ten subjects show improvement of fat suppression and better delineation of breast tissue by using independent shims.

References/Funding Source

Han M, Rodriguez S, Sawyer AM, Daniel BL, Cunningham C, Pauly JM, Hargreaves BA. Fat Suppression with Independent Shims for Bilateral Breast MRI. Proceedings 17th Scientific Meeting, International Society for Magnetic Resonance in Medicine, Honolulu, 2009, p. 579.
[1] Nimrod Maril, et al., Magn Reson Med, 54(5):1139-1145, 2005.
[2] Pauly JM, et al., Proc., 11th ISMRM, p966, 2003.
[3] Cunningham CH, et al., Proc., 13th ISMRM, p1849, 2005.
[4] Feinberg DA, et al., Magn Reson Med, 13(1):162-169, 1990.
Supported by NIH RR009784, NIH EB009055, and DOD W81XWH-06-1-0358.

TRANSIENT IMAGING IN BALANCED STEADY-STATE FREE PRECESSION WITH INCREASED SIGNAL

P. Worters[1] and B. Hargreaves[1]
[1]Dept of Radiology, Stanford University, CA

Often in balanced steady-state free precession (bSSFP) imaging, there is insufficient time for the magnetization to reach steady-state and acquisition occurs in the transient period. The acquisition block length could be limited by physiological gating or contrast preparation mechanisms. The short acquisition blocks present a beneficial situation in which one can obtain higher signal by modulating the flip angles instead of using a standard sequence of constant amplitude flip angles.

This work presents an algorithm for calculation of variable flip angles in bSSFP acquisition to generate echoes at predefined amplitudes. The main advantage of using variable flip angles is to allow acquisition in the transient stage for images with minimal artifacts and greater signal-to-noise ratio. Any target amplitude, subject to existing magnetization and T1/T2, can be generated but the temporally uniform echo shape is a useful example. The method is referred to as variable-angle uniform signal excitation (VUSE) bSSFP. The exact VUSE flip scheme is dependent on T1, T2, TR and number of echoes. A catalyzation sequence of Kaiser-filtered ramp RF pulses is integrated with VUSE to give minimal oscillations at off-resonance [1]. The VUSE algorithm is iterative but converges quickly in about ten iterations.

Figure 1 demonstrates the VUSE flip angle scheme as calculated by the algorithm, and compares it with the constant flip angle scheme. Both flip angle schemes employ five Kaiser-ramped pulses before acquisition to improve off-resonance behavior (to which bSSFP is highly sensitive, and which can result in artifacts). The signal improvement from VUSE is illustrated in Figure 1B, where the area under the curves during acquisition is higher with VUSE than it is with constant flips.

The VUSE algorithm maximizes the signal for transient bSSFP imaging. The algorithm, however, is not limited to the uniform echo shape and can be used to generate other amplitude profiles (e.g. increasing/decreasing amplitude).

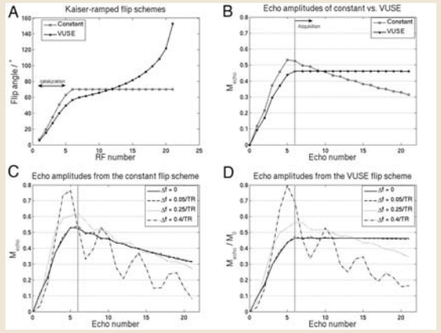

Demonstration of the VUSE method for (A) modulating the flip angles to create (B) temporally uniform echoes in a short bSSFP acquisition. Graphs B, C and D are derived from simulations of the Bloch equation. The area under the curves in (B) during acquisition provides a metric for measuring the possible signal achievable and is higher with VUSE than with constant 70° flips; the area ratio of VUSE to constant flips is 1.13 in this case. (C) and (D) show that the off-resonance (given by Δf) behavior of both schemes are comparable and has minimal oscillations.

REFERENCES/FUNDING SOURCE

[1] P. Le Roux. Simplified model and stabilization of SSFP sequences. J Magn Reson, 163(1): 23-37, 2003.
NIH: 5R01EB009055-02, NIH: 5R01HL075803-05, NIH: 5R01HL039297-22, NIH: 2P41RR009784-1.

IN VIVO SODIUM IMAGING AND RELAXOMETRY OF THE BREAST AT 3T

E. Staroswiecki[1,2], A. Nnewihe[1,3], N. K. Bangerter[4,5], B. L. Daniel[1], B. A. Hargreaves[1]
Depts of [1]Radiology, [2]Electrical Engineering, [3]Bioengineering, Stanford University, CA; [4]Dept of Electrical and Computer Engineering, Brigham Young University, UT; [5]Dept of Radiology, University of Utah, UT

INTRODUCTION: Early detection of breast cancer is crucial for effective treatment and increased survival. Sodium MRI shows potential since it does not require the use of an exogenous contrast agent and neoplasms are known to disrupt some of the sodium regulation mechanisms, so the intra- and extracellular sodium concentrations may change in tumors. In this work, we measured in vivo sodium T1 and T2* of glandular breast tissue with B1-correction at 3T. We show preliminary results showing an increase in the sodium T2* within tumors.

METHODS: A fast sequence using the 3D cones k-space trajectory was developed for sodium imaging on a 3T scanner. This centric trajectory permits short echo times with very high SNR efficiency. The right breast of 7 subjects was scanned using a dual-tuned breast coil. The protocol used consisted of the flip angle measurements, T1 measurements, T2* measurements, and a high-resolution image using the sodium coil. A proton image was also acquired as an anatomical reference.

RESULTS: For the patients with breast tumors the regions identified with lesions appear brighter on the sodium images, with the sodium signal over the lesions being 3 to 5 times brighter than the signal over the healthy tissue. The T2* maps on the regions corresponding to the tumors show typical values of 27ms and higher, and always higher than the healthy tissue. For the healthy volunteers the T2* maps show typical values between 12 and 25ms, while the typical T1 values are between 35 and 50ms.

DISCUSSION: This technique demonstrates measurement of both in vivo sodium T2* and T1 in human breast tissue with good resolution in feasible clinical times. Our preliminary results also show that both the sodium signal intensity and the sodium T2* could be higher in regions with lesions than on healthy glandular tissue.

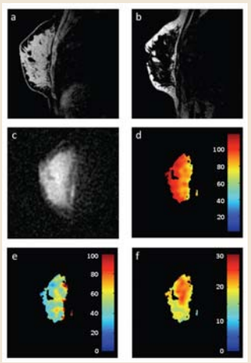

a: IDEAL water image. b: IDEAL fat image. c: High-resolution sodium image. We can see the correspondence between this image and the IDEAL water image, since sodium is more soluble in water than in fat. d: Flip angle map for a prescribed flip angle of 90°. e: T1 map. f: T2* map. The low-resolution maps where only calculated where the signal of the high-resolution sodium image was at least half of the maximum value.

REFERENCES/FUNDING SOURCE

E Staroswiecki, A Nnewihe, NK Bangerter, BL Daniel, and BA Hargreaves, In Vivo Sodium Imaging and Relaxometry of the Breast at 3T, Proc. of the 17th ISMRM Annual Meeting, Honolulu, Hawai'i, 2009, p. 2129.
California Breast Cancer Research Program 13IB-0074, and GlaxoSmithKline

ACCELERATED SLICE ENCODING FOR METAL ARTIFACT CORRECTION

B. Hargreaves[1], W. Chen[2], W. Lu[3], M. Alley[1], G. Gold[1], A. C. S. Brau[2], J. M. Pauly,[4], K. Butts Pauly[1]
[1]Depts of Radiology and [4]Electrical Engineering, Stanford University, CA; [2]General Electric Healthcare, Menlo Park, CA; [3]Dept of Electrical Engineering, Nanyang University, Singapore

With over one million surgeries for hip or knee replacements or spinal fusion performed in the United States alone each year, there is a clear need for non-invasive methods for post-surgical and ongoing evaluation in their recipients. MRI provides excellent soft-tissue contrast for orthopaedic imaging, but the large metal-induced B0 field inhomogeneities cause signal loss, through-slice distortion and in-plane distortion. Recently we have presented a technique to correct these artifacts called slice-encoding for metal artifact correction (SEMAC), Here we demonstrate that SEMAC can include a combination of echo train imaging, parallel imaging and partial Fourier acquisition, to provide useful contrast and reasonable scan times.

The SEMAC technique is a modified spin echo sequence that uses view-angle tilting and slice-direction phase encoding to correct in-plane and through-plane artifacts. Standard spin echo trains and short-tau inversion recovery allow efficient proton-density weighted imaging with optional fat suppression. With a careful implementation, a completely linear reconstruction is possible, which allows simple addition of parallel imaging and partial Fourier imaging. Using SEMAC, we have scanned 11 volunteers and patients with implanted metal devices according to an IRB-approved protocol. These include subjects with spinal fixation hardware and both knee and hip replacements.

Figure 1 shows an example of images in a patient with bilateral hip replacements. The standard spin-echo image shows distortions near the implant that are corrected in the proton-density-weighted, T1-weighted and fat-suppressed SEMAC images. The use of multiple contrast mechanisms allows visualization of fluid posterior to the implant, which was a source of pain for the patient. A coronal view of the standard and SEMAC T1-weighted images shows the dramatic improvement in visualization of the implants when metal artifacts are corrected. We are continuing to study SEMAC in volunteers, while also assessing its use as part of routine patient care at Stanford Hospital.

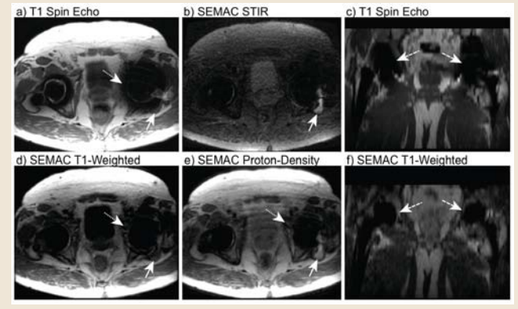

Example of SEMAC images in a patient with bilateral hip replacements and posterior pain on the left hip. Standard axial spin echo image (a) shows signal loss and through-slice distortion near the implant. Axial SEMAC STIR PD (b), T1-weighted (d) and PD-weighted (d) images all show improved signal near the metallic implant (dotted arrows). Fluid posterior to the hip is well seen on the STIR and PD-weighted images (solid arrows). Coronal reformats of the standard (c) and SEMAC PD-weighted spin echo (f) clearly show the improved depiction of the implant with SEMAC (dashed arrows). All SEMAC images took approximately 10 minutes to acquire.

REFERENCES/FUNDING SOURCE

Hargreaves B, Lu W, Chen W, Gold G, Brau A, Pauly J, Butts Pauly K. Accelerated slice-encoding for metal artifact correction. In: Proceedings 17th Scientific Meeting, International Society for Magnetic Resonance in Medicine, Honolulu, 2009. p. 258.
NIH RR009784-11 and NIH EB008190-01

MULTIPLE ACQUISITION FAT-SATURATED BALANCED STEADY STATE FREE PRECESSION IMAGING

M. T. Alley[1], S. S. Vasanawala[1], R. J. Herfkens[1], and B. A. Hargreaves[1]
[1]Dept of Radiology, RSL, Stanford University, CA

While balanced-SSFP (bSSFP) imaging is advantageous in its ability to produce high SNR in short imaging times, its clinical application has been limited due to several well-known shortcomings. The bright signal from fat is typically unwanted, and the short repetition times (TRs) required to avoid banding artifacts lead to limitations in the achievable resolution. This is especially true at higher field strengths where SAR considerations begin to limit the minimum possible TRs. To address these problems we propose the addition of fat suppression to a multiple phase-cycled, 3D bSSFP acquisition to address both issues simultaneously.

Figure 1 shows representative images from a single phase acquisition and the proposed, two phase-cycled technique. Because of the longer TR the single phase acquisition shows the dark banding in the liver that is a typical manifestation of off-resonance effects (yellow arrows). These bands are eliminated using the proposed two-phase cycled approach. In addition, the alpha/2-TR transition to steady state in conjunction with the Kaiser-windowed ramped pulses provides excellent fat suppression throughout the entire image.

We have demonstrated that it is possible to obtain a high quality fat suppressed bSSFP images in reasonable scan times. At higher field strengths the flip angles required for bSSFP imaging often require stretched RF pulses and thus longer TRs in order to avoid SAR limitations. Longer TRs are also needed when high resolution imaging is desired. In the presence of off-resonance effects the resulting signal voids can easily make the resulting images diagnostically unusable. With the proper approach to interrupting and restoring the steady state, phase cycling makes it possible to eliminate these banding artifacts. Although this approach necessitates two acquisitions, parallel imaging techniques make it possible to complete an exam in a reasonable breath-hold.

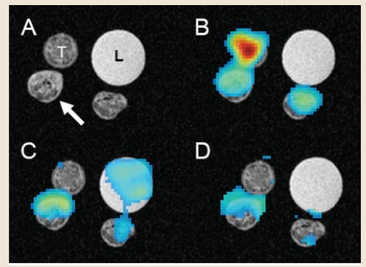

Figure 1: A sample image from a single-cycle fat-suppressed bSSFP acquisition (left) and the same location imaged using the proposed two-cycle technique (right). The multiple phase-cycled approach eliminates the banding artifacts from off-resonance effects (arrows).

REFERENCES/FUNDING SOURCE

M. Alley, S. Vasanawala, R. Herfkens, and B. Hargreaves, Multiple Acquisition Fat-Saturated Balanced Steady State Free Precession Imaging, in Proc., ISMRM, 17th Annual Meeting, Honolulu, page 2768, 2009.
NIH RR009784-11 and NIH EB009055-01

ELIMINATION OF INFLOW ENHANCEMENT BY PARTIAL PRE-SATURATION IN RF SPOILED IMAGING

M. Han[1,2] and B. A. Hargreaves[1]
Depts of [1]Radiology, [2]Electrical Engineering, Stanford University, Stanford, CA

For RF-spoiled gradient echo imaging (ie SPGR, FLASH, T1-FFE), the combination of spoiling gradients and quadratic phase cycling eliminates net transverse magnetization within a voxel to enable pure T_1 contrast [1-3]. Generally, many RF excitations are required to attain steady state magnetization levels. Therefore, when unsaturated spins flow into the imaging volume, inflow enhancement [4] and pulsatile ghost artifacts [5] can result. We hypothesize that partial saturation of an outer slab could provide the desired longitudinal magnetization to avoid inflow artifacts [6]. To test this, we conducted experiments at 1.5T with a flow phantom and volunteers.

Partial saturation of flowing spins is performed by applying RF pulses to an upstream region exterior to the imaging slab. For the imaging slab excitation (32 sections with each 0.3 cm thick) and outer slab partial saturation (16 cm thick slab), the same minimum-phase pulses, 20° flip angle with a quadratic RF phase increment of 117°, were used. To avoid signal from the saturation region, spoilers were added for both before and after image acquisition.

REFERENCES/FUNDING SOURCE

Han M, Hargreaves BA. Elimination of Inflow Enhancement by Partial Pre-Saturation in RF Spoiled Imaging. Proceedings 17th Scientific Meeting, International Society for Magnetic Resonance in Medicine, Honolulu, 2009, p. 2699.
[1] Crawly AP, et al., Magn Reson Med 8:248-260, 1988.
[2] Zur Y, et al., Magn Reson Med 21:251-263, 1991.
[3] Frahm J, et al., J Magn Reson 72:307-314, 1987.
[4] Wehrli FW, et al., VCH Publisher New York, 1988.
[5] Perman WH, et al., J Comput Assist Tomogr 10:473-483, 1986.
[6] Reed FB, et al., Mang Reson Med45:653-661, 2001.
Supported by NIH RR009784 and NIH EB009055.

Images on the left show results from the flow phantom experiment with a tube where water can flow. The mean velocity with flow was set to 10 cm/s. From maximum intensity projection (MIP) coronal reformatted images of the tube, we can see partial saturation almost eliminates inflow enhancement and pulsatile ghost artifacts. The signal intensity profile along the tube is similar to that of stationary spins. Images in the right are results from a neck scan, exhibiting reduction of inflow enhancement in the carotid artery.

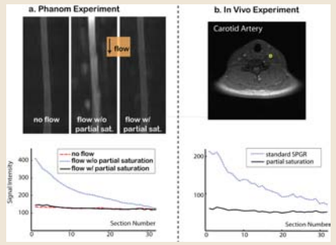

(a) Flow phantom experiment. Maximum intensity projection coronal reformatted images of the tube are shown for stationary water, flowing water without partial saturation and flowing water with partial saturation. Signal intensity changes through the tube are plotted below. (b) In vivo neck experiment. Signal intensity was measured through the carotid artery.

Partial saturation greatly reduces inflow artifacts efficiently by adding only one RF pulse and spoiler gradients to a normal RF-spoiled sequence. More homogeneous signal profiles and T_1 contrast can be achieved. Partial saturation could be useful for perfusion imaging, where accurate T_1 contrast of blood is necessary.

MULTI-CHANNEL RF TRANSMIT TECHNOLOGY DEVELOPMENT

Ron Watkins[1], Brian Rutt[1]
[1]Dept of Radiology, Stanford University, CA

We are developing multi-channel RF transmit systems hardware and methods for improving B1 uniformity for 7 Tesla human MRI imaging. Due to the RF wavelength becoming comparable to human body dimensions at 7T, image quality can be seriously degraded as a result of propagation delays through conductive/dielectric tissue, leading to destructive interference of the transmitted B1 field and serious inhomogeneity. By implementing multiple transmit sources and coil elements, we will create the ability to transmit independently to each coil element. A major application of this new technology will be to improve B1 uniformity. Two specific methods will be investigated. The first is referred to as “B1 shimming”, and is a scalable method which replaces a single large RF power amplifier with an array of smaller amplifiers, permitting independent control of the phase and amplitude of the RF pulse transmitted from each coil element. A second method known as “parallel transmit”, will allow the transmission of multiple RF waveforms simultaneously, one from each coil element, which enables the acceleration of 2D and 3D RF pulses, thereby allowing geometrically tailored excitation volumes.

REFERENCES/FUNDING SOURCE

GE Healthcare

MULTI-COMPONENT T1 AND T2 MAPPING FOR INVESTIGATING BRAIN MYELIN CONTENT

[2]Jason Su, [1]Brian Rutt
Depts of [1]Radiology, [2]Electrical Engineering, Stanford University, CA

Multiple sclerosis is a disease characterized by the demyelination of the spinal cord and brain tissue, especially white matter. Traditionally, quantitative MR imaging has been hampered by unreasonably long scan times. Recent advances have not only allowed for quick and accurate mapping of T1 and T2 relaxation times, but also the characterization of multiple water pools within a voxel using the mcDESPOT technique (multi-component driven equilibrium single pulse observation of T1/T2). Critically, water trapped inside a myelin sheath relaxes more quickly compared to the surrounding extra- and intracellular pools, so it can be discerned using such intra-voxel multi-component relaxometric mapping. The hope is that the progression of MS and other demyelinating diseases can be detected as a variation in the measured characteristics of white matter tissue. The map of the myelin water fraction is of particular interest since it is well estimated by mcDESPOT and should directly show the effects of MS as the loss of myelin releases trapped water into the surrounding pools. Incorporating other information such as diffusion tensor images is another avenue of investigation that may yield crucial insight for diagnosis. We are developing tools in the form of pulse sequences and post-processing software to further this technology and apply it to MS and other neurological disorders.

REFERENCES/FUNDING SOURCE

Canadian Institutes for Health Research

PARALLEL SPECTROSCOPIC IMAGING RECONSTRUCTION WITH ARBITRARY TRAJECTORIES USING K-SPACE SPARSE MATRICES

M. Gu[1], C. Liu[1], and D. Spielman[1]
Dept of [1]Radiology, Stanford University, CA

Parallel imaging reconstruction has been successfully applied to magnetic resonance spectroscopic imaging (MRSI) to reduce scan times. For undersampled k-space data on a Cartesian grid, the reconstruction can be achieved in image domain using a sensitivity encoding (SENSE) algorithm for each spectral data point. Alternative methods for reconstruction with undersampled Cartesian k-space data are the SMASH and GRAPPA algorithms that do the reconstruction in the k-space domain. To reconstruct undersampled MRSI data with arbitrary k-space trajectories, image-domain-based iterative SENSE algorithm has been applied at the cost of long computing times. In this paper, a new k-space domain-based parallel spectroscopic imaging reconstruction with arbitrary k-space trajectories using k-space sparse matrices is applied to MRSI with spiral k-space trajectories. The algorithm achieves MRSI reconstruction with reduced memory requirements and computing times. The results are demonstrated in both phantom and in vivo studies. Spectroscopic images very similar to that reconstructed with fully sampled spiral k-space data are obtained at different reduction factors.

REFERENCES/FUNDING SOURCE

Meng Gu, Chunlei Liu, Daniel M. Spielman “Parallel spectroscopic imaging reconstruction with arbitrary trajectories using k-space sparse matrices”, Magnetic Resonance in Medicine. Volume 61, Issue 2, Date: February 2009, Pages: 267-272
NIH-RR09784, NIH R01 MH080913-01A1, GE Healthcare and The Lucas Foundation.

IN VIVO DETECTION OF NADH REDUCTASE KINETICS WITH HYPERPOLARIZED 1-13C-PYRUVATE MRSI

M. Darpolor[1], D. Mayer[1,2], Y-F Yen[3], C. Contag[4], M. Bachmann[4], and D. Spielman[1]
Depts of [1]Radiology and [4]Pediatrics, Stanford University, CA; [2]SRI International; and [3]GE Healthcare

The goal of this project is to demonstrate the utility of hyperpolarized [1-13C]-pyruvate magnetic resonance spectroscopic imaging (MRSI) as in vivo reporter of enzyme kinetics involved in the biosynthesis pathways of pyruvate. Our long-term goal is to utilize this technique for validating potential therapeutic targets that regulate protein function in vivo with the precision and control conferred by tunable gene technology, and in addition advance our understanding of basic biochemical pathways. We assume that NADH reductase is the key enzyme that regulates (rate limiting step) the NADH to NAD+ reduction. EL4 (C57BL mouse lymphoma) and A20 (BALB/c B cell lymphoma) cells are transfected with cDNA plasmid of NQO1. These cells have been tested and found negative for ectromelia virus (mousepox). The cDNA plasmid of NQO1 expresses the gene for nicotinamide adenine dinucleotide (NADH) quinone oxidoreductase 1 (NQO1). NQO1 is a ubiquitous cytosolic flavoenzyme that catalyzes twoelectron reduction of various quinones, with NADH or NADPH as an electron donor. A flask of 50 million cells in 2.5 ml of RPMI 1640 medium was administered with hyperpolarized [1-13C]-pyruvate followed by data acquisition. A 3.0 Tesla Signa magnet (GE healthcare) and a dynamic nuclear polarizer (Oxford Instruments Hypersense) were utilized. Preliminary results of both EL4 and A20 cell lines showed a production of lactate when hyperpolarized [1-13C}-pyruvate is administered to 50 millions cells in a 2.5 ml medium. The experiments of transfected cells are ongoing.

REFERENCES/FUNDING SOURCE

NIH/NCI T32 CA-09695-19, NIH RR09784

HIGH SPEED VOLUMETRIC MRSI WITH ECHO PLANAR K-SPACE TRAJECTORIES

M. Gu[1] and D. Spielman[1]
Dept of [1]Radiology

Fast proton MR spectroscopic imaging (^{1}H-MRSI) of the human brain with time varying gradient encoding has the advantage of producing metabolite maps within clinically acceptable time. However, lack of standardized imaging, reconstruction and quantification methods hinders comparison of studies conducted on multiple platforms at different sites. To promote a standard volumetric MRSI imaging method, a high speed MRSI sequence with water referencing is needed on GE MR scanners at 3T. A volumetric MRSI sequence with echo-planar k-space readout trajectory and water referencing has been implemented for GE scanners at 3T. The water referencing module uses the gradient echo scheme with a 20 degree excitation pulse and the same readout scheme as the MRSI module. Because the magnitudes of gradient for opposite directions are not equal, k-space trajectory drifts during readout, causing severe artifacts if reconstructed using calculated k-space trajectory. To solve this problem, two reconstruction methods have been implemented. The first one uses measured k-space trajectory from a separate scan. The second method uses self adjusted k-space trajectory to avoid the scan of k-space trajectory measurement. Assuming the k-space trajectory only drifts and doesn't distort, the amount of drifting for each kf point can be calculated from the interval between adjacent times when k-space trajectory passes the origin. This value is then added to the calculated k-space trajectory for reconstruction. Both methods yield spectra with much reduced artifacts and the one uses measured trajectory is slightly better than using self-adjusted k-space trajectory.

REFERENCES/FUNDING SOURCE

NIH-RR09784, NIH R01 MH080913, GE Healthcare and The Lucas Foundation.

SINGLE-SHOT METABOLIC IMAGING OF HYPERPOLARIZED $^{13}C_1$-PYRUVATE USING A HIGH-PERFORMANCE GRADIENT INSERT

D. Mayer[1,2], Y-F. Yen[3], A. Takahashi[3], J. Tropp[3], R.E. Hurd[3], A. Pfefferbaum[2,4], D.M. Spielman[1]
Depts of [1]Radiology and [4]Psychiatry & Behavioral Sciences, Stanford University, CA; [2]Neuroscience Program, SRI International, Menlo Park, CA; [3]GE Healthcare ASL-West, Menlo Park, CA

Hyperpolarization of metabolically active substrates such as $^{13}C_1$-pyruvate permits new approaches to the investiga¬tion of in vivo metabolism using magnetic resonance (MR) spectroscopy and chemical shift imaging (CSI). However, the transient nature of the signal amplification necessitates fast data sampling techniques. Spiral chemical shift imaging simultaneously encodes 1D spectral and 2D spatial information. Therefore, it theoretically permits the acquisition of a complete 2D CSI data set with a single excitation. However, limitations on maximum gradient strength and slew rate often make multiple excitations necessary to achieve a desired spectral bandwidth. This is especially a problem in hyperpolarized ^{13}C imaging as the lower gyromagnetic ratio corresponds to a four-fold decrease in gradient performance when compared to proton CSI. Here we us a high-performance gradient insert (500 mT/m, 1800 mT/m/ms, 160-mm inner diameter) in a clinical MR scanner to achieve single-shot spiral CSI in the rat in vivo after injection of hyperpolarized $^{13}C_1$-pyruvate. The implemented sequence also exploits the sparse spectra and prior knowledge of resonance frequencies to reduce the measurement time by undersampling the data in the spectral domain. The figure shows time-resolved metabolic maps from a 10-mm slice through the kidneys of the substrate pyruvate and the metabolic products lactate and alanine.

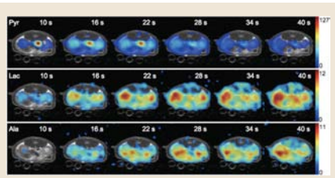

Fig.1: Time-resolved metabolic images from a rat after injection of hyperpolarized pyruvate: the substrate (top) and its metabolic products lactate (middle) and alanine (bottom).

These data demonstrate the feasibility of single-shot dynamic metabolic imaging in vivo of hyperpolarized ^{13}C-labeled metabolites permitting a temporal resolution of 125 ms per slice. The spatially-resolved time courses for each metabolite may be used to estimate tissue and organ specific reaction kinetics and rate constants.

REFERENCES/FUNDING SOURCE

D. Mayer, Y.-F. Yen, A. Takahashi, J. Tropp, R.E. Hurd, A. Pfefferbaum, D.M. Spielman "Single-shot Metabolic Imaging in the Rat In Vivo after Injection of Hyperpolarized 13C1-Pyruvate using a High-Performance Gradient Insert", ENC 2009, 454.
R01 EB009070 "Dynamic Metabolic Imaging of Hyperpolarized Substrates", Dirk Mayer
R37 AA005965, "CNS DEFICITS: INTERACTION OF AGE AND ALCOHOLISM", Adolf Pfefferbaum
U01 AA013521, "INIA: Imaging Core", Adolf Pfefferbaum
P41 RR009784, "Center for advanced MR Technology at Stanford", Gary H. Glover

MEASURING MICHAELIS-MENTEN ENZYME KINETICS USING HYPERPOLARIZED 13C-PYRUVATE

T. Xu[1], D. Mayer[1,2], M. Gu[1], Y. Ye[3], E. Johansson[3], J. Tropp[3], R. Hurd[3], and D. Spielman[1]
Dept of [1]Radiology, Stanford University, CA; [2]SRI International, Menlo Park, CA; [3]GE Healthcare, Menlo Park, CA

The development of hyperpolarized Magnetic Resonance Imaging (MRI) agents presents both unprecedented opportunities as well as new technical challenges. With Signal-to-Noise Ratio (SNR) enhancements on the order of 10,000-fold, Dynamic Nuclear Polarization (DNP) of metabolically active substrates theoretically permits high-resolution in vivo Chemical Shift Imaging (CSI) of both the injected agent and downstream metabolic products [1]. Although hyperpolarized $^{13}C_1$-pyruvate, in particular, has been used to demonstrate metabolic activity in various animal models, robust quantitation remains an important area of investigation. Saturation effects are routinely seen with the doses of hyperpolarized ^{13}C-labeled pyruvate (Pyr) used in published studies, however most metrics proposed to date, including metabolite ratios, time-to-peak of metabolic products, and estimated exchange rates fail to include these saturation effects. Hence, there is a clear need for improved metabolic modeling of the in vivo processes observed using hyperpolarized substrates. In this work, we demonstrate that, following a single bolus injection, the in vivo conversion of pyruvate to its downstream metabolic products of lactate (Lac) and alanine (Ala) is well approximated by Michaelis-Menten kinetics with the resulting estimated apparent Vmax and Km parameters being independent of critical experimental parameters including blood volume and inflow effects, timing and shape of the bolus injection, and pyruvate dose. In particular, in contrast to the commonly used small flip angle excitation approach, we have developed a dynamic MRS acquisition using slice-select 90° flip angle excitations. The technique was evaluated by measuring apparent Michaelis- Menten parameters for Pry-to-Lac and Pyr-to-Ala conversion in the rat kidney. In order to achieve a robust implementation, the original acquisition sequence had to be augmented with an additional lactate-selective saturation pulse to eliminate unwanted confounding signals observed to arise largely from myocardial production of lactate that is subsequently released into the blood stream.

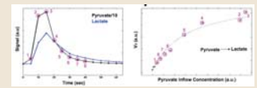

In vivo pyruvate and lactate signals from a rat kidney following a bolus tail vein injection of hyperpolarized 13C-pyruvate (left) and corresponding Michaelis-Menten plot (right).

REFERENCES/FUNDING SOURCE

R01 EB009070 "Dynamic Metabolic Imaging of Hyperpolarized Substrates", Dirk Mayer
R37 AA005965, "CNS Deficits: Interaction of Age and Alcoholism", Adolf Pfefferbaum
U01 AA013521, "INIA: Imaging Core", Adolf Pfefferbaum
P41 RR009784, "Center for advanced MR Technology at Stanford", Gary H. Glover

SIMULTANEOUS QUANTIFICATION OF GLUTAMATE AND GLUTAMINE USING CT-PRESS AT 3T

M. Gu[1], D. Mayer[1,2], D. Spielman[1]
[1]Dept of Radiology, Stanford University, CA; [2]SRI International, Neuroscience Program, Menlo Park, CA

Glutamate and glutamine are two major metabolites in human brain. Accurate quantification of both glutamate and glutamine is essential for understanding brain metabolism and has the potential to reveal mechanisms of various neuronal diseases. Unfortunately, quantification of both glutamate and glutamine using NMR is difficult as their spectra are entirely composed of coupled resonances and overlap with each other. Recently, CT-PRESS with optimized timing has been used to detect glutamate with a collapsed single peak. However, glutamine resonance was not resolved using this technique due to overlap with both glutamate and NAA. In this work, a method that achieves quantification of both glutamate and glutamine was proposed and applied to in-vivo CT-PRESS spectra. In particular, at 3T, using a CT-PRESS sequence optimized for detection of glutamate C4 resonance, resonances of glutamate at 2.3ppm are separated and collapsed to a single peak. Collapsed glutamine resonances, however, overlap with glutamate resonances at 3.7ppm. Using these two peaks in the CT-PRESS spectra, quantification of both glutamate and glutamine is achieved using basis function synthesized using GAMMA simulation with full density matrix. In the simulation, spin-echo FIDs of both glutamate and glutamine are generated with the same timing of the CT-PRESS sequence. These FIDs are then multiplied with exponentials with T2 values reported in the literature to account for the spin-spin relaxation. The FIDs are reconstructed using 2D Fourier Transform and the simulated spectra are calculated by integrating the 2D spectra in magnitude mode along F2 within a ±13-Hz interval around the spectral diagonal. The concentrations of glutamate and glutamine are calculated by equalizing both the 2.3ppm and 3.7ppm peak heights of the simulated and obtained CT-PRESS spectra. This method is applied to in-vivo brain CT-PRESS spectra and the concentrations of glutamate and glutamine estimated are in agreement with that reported in the literature.

REFERENCES/FUNDING SOURCE

NIH-RR09784, NIH R01 MH080913-01A1, GE Healthcare and The Lucas Foundation

B1 AND T1 INSENSITIVE WATER AND LIPID SUPPRESSION USING OPTIMIZED MULTIPLE FREQUENCY-SELECTIVE PREPARATION PULSES FOR WHOLE-BRAIN 1H SPECTROSCOPIC IMAGING AT 3T

M. Gu[1] and D. Spielman[1]
Department of [1]Radiology

A new method for simultaneous suppression of water and lipid resonances using a series of dual-band frequency-selective radiofrequency (RF) pulses with associated dephasing gradients is presented. By optimizing the nutation angles of the individual pulses, the water and lipid suppression is made insensitive to a range of both T_1-relaxation times and B_1 inhomogeneities. The method consists only of preparatory RF pulses and thus can be combined with a wide variety of MRSI schemes including both long and short TE studies. Simulations yield suppression factors, in the presence of ±20% B_1 inhomogeneity, on the order of 100 for lipid peaks with three different T_1s (300 ms, 310 ms, and 360 ms), and water peaks with T_1s ranging from 0.8 s to 4 s. Excellent in vivo study performance is demonstrated using a 3 Tesla volumetric proton spectroscopic imaging (^{1}H-MRSI) sequence for measuring the primary brain metabolites peaks of choline (Cho), creatine (Cr), and N-acetyl aspartate (NAA).

REFERENCES/FUNDING SOURCE

Meng Gu, Daniel M. Spielman "B1 and T1 insensitive water and lipid suppression using optimized multiple frequency-selective preparation pulses for whole-brain 1H spectroscopic imaging at 3T", Magnetic Resonance in Medicine. Volume 61, Issue 2, Date: February 2009, Pages: 462-466
NIH-RR09784, NIH R01 MH080913-01A1, GE Healthcare and The Lucas Foundation.

HYPERPOLARZED ^{13}C-1-PYRUVATE IMAGING OF INFLAMMATORY ARTHRITIS

J. Mackenzie[1], D. Mayer[1,2], Y-F. Yen[3], and D. Spielman[1]
Dept of [1]Radiology, Stanford University; [2]SRI International; [3]GE Healthcare

Few quantitative methods exist to monitor the disease course of adult rheumatoid or juvenile idiopathic arthritis. Anatomic imaging tends to show late and less repairable stages of arthritis where as radioisotope imaging may be non-specific for a particular diagnosis. MRS imaging with hyperpolarized ^{13}C-1-pyruvate may provide an objective and quantitative measure of arthritis, which may be helpful in clinical decision making and treatment planning, since energy metabolism is increased in inflammation and the rate of pyruvate metabolism may be upregulated in arthritic joints. This work examines the feasibility of hyperpolarized ^{13}C-1-pyruvate for detecting and characterizing arthritis. Arthritis was induced in six juvenile Sprague Dawley rats with injection of 0.4 µL/g complete Freund's adjuvant. Arthritic joints were imaged 7 days after induction with ^{13}C MRS on a GE 3 T scanner. 0.5 mL of a 100 mM solution of ^{13}C-1-pyruvate was hyperpolarized by DNP and injected via the tail vein. Single-time point MRS analysis of ^{13}C-1 pyruvate and its metabolites was obtained 20 sec after injection with a FID CSI sequence. Time resolved imaging was obtained with a 1D EPSI sequence during a second hyperpolized ^{13}C-pyruvate injection. Mean signal intensities of pyruvate and lactate were obtained with ROI analysis at the joints and normal and arthritic joints were compared with the T-test. Arthritic joints were erythematous and swollen (mean±SD=0.5±0.2mm greater in thickness), had a histological score of 3/4 for inflammation (compared with 0/4 at the normal joint), and showed T2-weighted changes of inflammation on the anatomic MR images. ^{13}C-1-pyruvate and metabolized ^{13}C-lactate appeared increased at the arthritic joints on the FID CSI images (Figure 1A, B) and tended towards significant difference by ROI analysis of the ratio of metabolite at the joint to total ^{13}C [pyruvate arthritic=0.34 vs. normal=0.28, p< 0.17; lactate arthritic=0.21 vs. normal=0.16, p<0.12].

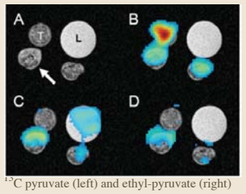

^{13}C pyruvate (left) and ethyl-pyruvate (right) spectroscopic images from a rat brain. Grid displayed at sampled resolution, color overlay images Fourier interpolated.

REFERENCES/FUNDING SOURCE

R01 EB009070 "Dynamic Metabolic Imaging of Hyperpolarized Substrates", Dirk Mayer
P41 RR009784, "Center for advanced MR Technology at Stanford", Gary H. Glover

ALANINE SIGNAL AND T_2 RELAXATION: A POTENTIAL HYPERPOLARIZED ^{13}C METABOLIC MARKER FOR HEPATOCELLULAR CARCINOMA

Y. Yen[1], D. Mayer[2,3], P. Le Roux[4], R. King[2], D. Spielman[2], J. Tropp[1], A. Pfefferbaum[3,5], R. Hurd[1], S. Vasanawala[2]
[1]Global Applied Science Laboratory, GE Healthcare, CA; Depts of [2]Radiology, [5]Psychiatry and Behavioral Sciences, Stanford University, CA; [3]SRI International, Neuroscience Program, Menlo Park, CA; [4]Global Applied Science Laboratory, GE Healthcare, Europe

Elevated lactate signal in malignant tumors has been characterized by proton spectroscopic imaging, as well as by hyperpolarized ^{13}C technique. Recent studies showed increasing ^{13}C-lactate signal correlates with disease progression of prostate tumors in TRAMP model. Another study demonstrated that the TRAMP mice responding to hormone treatment exhibit reduction of ^{13}C-lactate signal, whereas those not responding to treatment continue having high ^{13}C-lactate signal. No differences in alanine signal have been observed previously in any tumor studies. In this work, we investigated potential metabolic markers of hepatocellular carcinoma by using hyperpolarized ^{13}C technique. The signal level and T_2 relaxation time of ^{13}C-labeled metabolites were measured and compared between liver tumors and normal livers in rats. Figure 1 shows that alanine in liver tumors has longer T_2 (mean±std T_2 =1.2 ± 0.1 s) than that in normal livers (T_2 =0.6 ± 0.1 s). All tumors have higher total carbon signal than normal livers (not shown). After normalized to total carbon signal, showed the relative production of alanine in liver tumors is higher than that in normal livers ($p < 3\times10^{-4}$). No significant difference in the relative production of other metabolites between tumors and normal livers. The ratio of alanine in tumors to alanine in normal livers is 2.2 ± 0.6 at the first spin-echo time. After correcting for the respective T_2 decays between the 90° excitation and the first spin-echo (78ms), the alanine signal in tumors is 2.1 ± 0.5 times of the alanine signal in normal livers. Intra-subject variation of alanine signal normalized to total carbon is 15% from the three repeated runs in one control rat and 17% from the repeated runs of a second control rat. This work demonstrates that ^{13}C-alanine may be a new marker for HCC tumors. Its diagnostic values in cancer detection and treatment monitoring are yet to be explored.

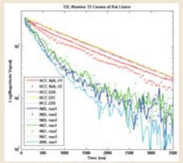
Logarithmic plot of T_2 decay curves of ^{13}C-alanine in liver tumors and normal livers

REFERENCES/FUNDING SOURCE

NIH P41-RR09784, P50-CA114747, and R01-AA005965

MAGNETOTACTIC BACTERIA AS A POTENTIAL MRI CONTRAST AGENT

M. Benoit[1,4], D. Mayer[2,3], Y. Barak[1], I. Chen[2,4,5], W. Hu[6], Z. Cheng[2,5], S. Wang[6], D. Spielman[2,5], S. Gambhir[2,4,5], A Matin[1]
Depts of [1]Microbiology and Immunology, [2]Radiology, [4]Bioengineering, [5]Molecular Imaging Program at Stanford (MIPS), [6]Materials Science and Engineering, Stanford University, CA; [3]SRI International, Neuroscience Program, Menlo Park, CA

Magnetic resonance imaging (MRI) is enhanced by contrast agents such as superparamagnetic iron-oxide (SPIO) particles. The latter resemble magnetite of magnetotactic bacteria. We have shown that Magnetospirillum magneticum AMB-1 ('AMB-1') produces positive MRI contrast when generating ultrasmall (10-40 nm diameter) magnetite particles; positive MRI contrast is superior to negative contrast as it permits clear distinction from image voids. Such bacteria increased T1-weighted MRI contrast 2.2-fold (p=0.013) in vitro and 2.0-fold (p=0.014) when injected in implanted mouse tumors. Intravenously delivered AMB-1 targeted tumors and generated 1.4-fold (p=0.0013) increased positive contrast in them. AMB-1 tumor targeting was confirmed by viable bacterial counts, PET imaging of ^{64}Cu-labeled AMB-1, and staining of tumor sections for bacteria and iron. Magnetotactic bacteria are thus useful in preclinical studies for improving cancer diagnosis and monitoring treatment response.

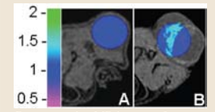

Representative MR images of tumors in mice injected i.v. either with the bacterial growth medium, MSGM (Control, panel A), or with 1×10^9 AMB-1 suspended in MSGM

REFERENCES/FUNDING SOURCE

MIPS-ICMIC Program NIH/NCI P50 (CA114747) and NIGMS F32GM077827 to MB; P41 RR009784; R21 CA140903
M.R. Benoit, D. Mayer, Y. Barak, I.Y. Chen, Z. Cheng, W. Hu, R.J. Wilson, S.X. Wang, D.M. Spielman, S.S. Gambhir, A.C. Matin "Use of Magnetotactic Bacteria for Enhancing MRI Contrast in Tumors", World Molecular Imaging Congress, Nice, France, 2008, 1153.
M.R. Benoit, D. Mayer, Y. Barak, I.Y. Chen, W. Hu, Z. Cheng, S.X. Wang, D.M. Spielman, S.S. Gambhir, A.C. Matin "Visualizing Implanted Tumors in Mice with MRI using Magnetotactic Bacteria", Clinical Cancer Research, in press

K-SPACE TRAJECTORY MAPPING FOR ULTRA-SHORT, SINGLE-SHOT, NON-CARTESIAN IMAGING

F. Wiesinger[1], P. T. Sipilae[1,2], Y-F. Yen[3], D. Mayer[4], E. Fiveland[5], S. A. Greding[1], D. M. Spielman[4], A. Pfefferbaum[4], and R. F. Schulte[1]
[1]Imaging Technologies, GE Global Research, Munich, Germany; [2]Institute for Physics of Electrotechnology, Technical University Munich, Germany; [3]Global Applied Science Laboratory, GE Healthcare, Menlo Park, CA; [4]Dept of Radiology, Stanford University, CA; [5]MRI Laboratory, GE Global Research, Niskayuna, NY

In-vivo MR image encoding speed is physiologically limited by gradient-induced peripheral nerve stimulations. Due to the linear nature of the magnetic gradient field, the acceptable gradient slew rate increases with decreasing subject dimensions. This makes high performance gradient insert coils an attractive choice for performing small-animal MR imaging and microscopy studies in a whole-body, clinical MR scanner. Such enhanced performance also amplifies gradient imperfections due to Eddy currents, coupling effects, mechanical vibrations, etc. On the other hand, the smaller dimensions and higher gradient amplitude often result in only suboptimal gradient calibration results using standard service tools. Recently, magnetic field sensors in the form of small NMR probes have been described as a highly accurate tool for spatiotemporal magnetic field mapping. In this work such magnetic field sensors were used in combination with a high-performance gradient insert coil for ultra-fast, single-shot, high-resolution, non-Cartesian imaging. Uultra-fast, high-resolution, single-shot, non-Cartesian imaging was demonstrated using a high performance gradient insert coil. This was enabled using an NMR-probe based k-space trajectory calibration method. In comparison to alternative kspace trajectory methods, susceptibility-matched, transmit-receive NMR probes provide important advantage like high SNR, and fast single-shot calibration of two gradient axes at once. The method is expected to be particularly valuable for applications, which either perform advanced encoding (single-shot acquisitions, spectral-spatial Non-Cartesian imaging, microscopy, etc.) or are particularly susceptible to gradient imperfections (Diffusion, Phase Contrast, etc.).

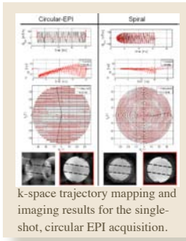

k-space trajectory mapping and imaging results for the single-shot, circular EPI acquisition.

REFERENCES/FUNDING SOURCE

R01 EB009070 "Dynamic Metabolic Imaging of Hyperpolarized Substrates", Dirk Mayer
R37 AA005965, "CNS DEFICITS: INTERACTION OF AGE AND ALCOHOLISM", Adolf Pfefferbaum
U01 AA013521, "INIA: Imaging Core", Adolf Pfefferbaum
P41 RR009784, "Center for advanced MR Technology at Stanford", Gary H. Glover

HYPERPOLARIZED 1-[^{13}C]-ETHYL-PYRUVATE METABOLIC IMAGING IN ANESTHETIZED RAT BRAIN

R.Hurd[1] Y. Yen[1], D. Mayer[2,3], A. Chen[1], D. Wilson[4], S. Kohler[5], R. Bok[4], J. Tropp[1], D. Spielman[3], A. Pfefferbaum[3,6]
[1]Global Applied Science Laboratory, GE Healthcare, CA; Depts of [2]Radiology, [6]Psychiatry and Behavioral Sciences, Stanford University, CA; [3]SRI International, Neuroscience Program, Menlo Park, CA; [4]Dept of Radiology, University of California, San Francisco, CA; [5]Union College, Schenectady, NY

Hyperpolarized 1-[^{13}C]-pyruvate has proven to be an excellent metabolic imaging technology, especially in oncology and cardiology (1,2). Dynamic and tissue level changes in 1-[^{13}C]-pyruvate and its metabolic products, 1-[^{13}C]-lactate, 1-[^{13}C]-alanine and [^{13}C] bicarbonate, have been shown to correlate with metabolic states of interest including disease progression and response to therapy. However, for potential neurological applications, pyruvate transport into brain can be a limiting factor, given the 1-2 minute window of useful hyperpolarized lifetime of 1-[^{13}C]-pyruvate *in vivo*. This is especially true in the case of anesthetized normal rat brain where pyruvate transport has been reported to be 2-3 times slower than in conscious animals. A potential solution is the use of ethyl-pyruvate, a lipophilic analogue of pyruvate that may have faster uptake through the blood-brain-barrier. Like pyruvate, ethyl pyruvate is an anti-inflammatory that has therapeutic potential (6). It has been shown to attenuate kainic acid-induced neuronal cell death in the mouse hippocampus (7) and reduce the impact of stroke (8). In this study, the formulation, polarization and dissolution conditions were developed to obtain a stable hyperpolarized solution of 1-[^{13}C]-ethyl-pyruvate. A maximum tolerated dose was determined for rapid 0.25mL/s injection and ^{13}C spectroscopic imaging was used to compare the uptake of hyperpolarized 1-[^{13}C]-ethyl pyruvate relative to hyperpolarized 1-[^{13}C]- pyruvate into anesthetized rat brain. Hyperpolarized 1-[^{13}C]-ethyl pyruvate metabolic imaging in normal brain is demonstrated in this feasibility study.

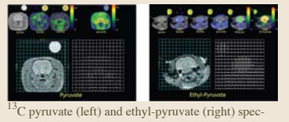

^{13}C pyruvate (left) and ethyl-pyruvate (right) spectroscopic images from a rat brain. Grid displayed at sampled resolution, color overlay images Fourier interpolated.

REFERENCES/FUNDING SOURCE

R01 EB009070 "Dynamic Metabolic Imaging of Hyperpolarized Substrates", Dirk Mayer
R37 AA005965, "CNS DEFICITS: INTERACTION OF AGE AND ALCOHOLISM", Adolf Pfefferbaum
U01 AA013521, "INIA: Imaging Core", Adolf Pfefferbaum
P41 RR009784, "Center for advanced MR Technology at Stanford", Gary H. Glover

Magnetic Resonance Spectroscopy

Vaporized Alcohol Causes Increase in Concentration of Choline-Containing Compounds in the Rat Basal Ganglia

D. Mayer[1,2], N.M. Zahr[2,3], J. Orduna[2], E.V. Sullivan[3], A. Pfefferbaum[2,3]
Depts of [1]Radiology, [3]Psychiatry & Behavioral Sciences, Stanford University, CA; [2]Neuroscience Program, SRI International, Menlo Park, CA

An MRS study using constant time point-resolved spectroscopy (CT-PRESS) of rats reported an increase in the signal from choline-containing compounds (Cho) in the basal ganglia with escalating exposure to vaporized alocohol. This signal change could be explained by either a change in concentration or in transverse relaxation constant (T_2). Here we used the CT-PRESS data to calculate the T_2s and echo-time (TE) corrected signal intensities. The results shown in Fig.1 provide confirmation for the conclusion that the increase in Cho observed with increasing exposure to vaporized alcohol was due to an increase in metabolite concentration rather than a change in T_2. A remaining possible contribution to the change in Cho signal arises from the T_1 of the Cho signal. Increased Cho could be explained by a shortening of T_1, because of the incomplete longitudinal relaxation at the chosen TR of 2 s. Nonetheless, the current analysis provides converging evidence that brain Cho is affected by high doses of alcohol. In other conditions affecting the brain, including multiple sclerosis, HIV infection, and normal aging, elevated Cho has been interpreted as indicative of demyelination, inflammation, or abnormally high glial density.

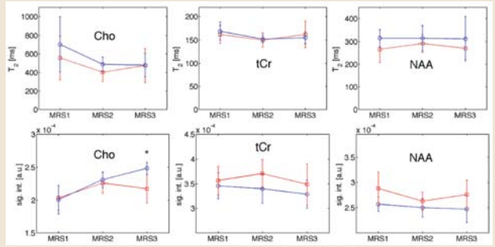

Fig. 1: Mean±STD of metabolite T_2s (top row) and metabolite signal corrected for TE (bottom row) for each of the three MRS acquisitions for the alcohol-exposed (blue circles) and control (red squares) rats.

References/Funding Source

N.M. Zahr, D. Mayer, S. Vinco, J. Orduna, A. Pfefferbaum, E.V. Sullivan "In Vivo MR Spectroscopic Evidence for Alcohol Neurotoxicity in the Rat Without Protracted Withdrawal, Pronounced Thiamine Deficiency, or Severe Liver Damage", Neuropsychopharmacology, 34, 1427-1442, 2009.
D. Mayer, N.M. Zahr, J. Orduna, E.V. Sullivan, A. Pfefferbaum "Evidence that Exposure to Escalating Doses of Vaporized Alcohol Causes Increase in the Concentration of Choline-Containing Compounds in the Basal Ganglia of the Rat", Proc ISMRM, 17th Annual Meeting, Honolulu, 2009, 1079.
R37 AA005965, "CNS DEFICITS: INTERACTION OF AGE AND ALCOHOLISM", Adolf Pfefferbaum
U01 AA013521, "INIA: Imaging Core", Adolf Pfefferbaum

Visualizing Implanted Tumors in Mice with MRI using Magnetotactic Bacteria

M. Benoit[1,4], D. Mayer[2], Y. Barak[1], I. Chen[2,3,4], W. Hu[5], Z. Cheng[2,4], S. Wang[5], D. Spielman[2,4], S. Gambhir[2,3,4], A Matin[1]
Depts of [1]Microbiology and Immunology, [2]Radiology, [3]Bioengineering, [4]Molecular Imaging Program at Stanford (MIPS), [5]Materials Science and Engineering, Stanford University, CA

Magnetotactic bacteria produce magnetite nanoparticles, which locally alter the magnetic field. Researchers have known for more than 60 years that bacteria tend to accumulate within cancerous tumors, suggesting that magnetotactic bacteria might be useful for diagnostic imaging. Recent work has focused on two aspects: 1) studying the effect of bacterial iron-oxide particle size on MRI contrast, and 2) characterizing the ability of magnetotactic bacteria to target tumors and be visualized with MRI. Regarding the first aspect, we showed, using transmission electron microscopy, that iron-oxide particle size can be reduced by altering the bacterial iron source. By reducing particle size, we were able to enhance brightness (i.e., increase the T1-weighted signal) to improve bacterial visualization in mouse tumors. Concerning the second aspect, viable cells were recovered from tumor, liver and spleen of mice injected intravenously with the bacteria. One day post-injection, the number of viable cells recovered was higher in liver and spleen compared to the tumor. This trend reversed by day 3, and by day 6 no viable bacteria were found in liver or spleen; they were found only in tumor. This study showed that while magnetotactic bacteria are cleared from normal tissue, they evade the host immune system in tumorous tissue, providing tumor specificity for MRI detection. An additional study followed the time course of magnetotactic bacteria injected intravenously using MRI. Images showed a 1.22-fold (p=0.003) increased positive contrast in tumors on day 2 and a 1.39-fold increase (p=0.0007) on day 6. Thus, for the first time, it has been shown that magnetotactic bacteria can colonize cancerous tumors in mice and be imaged with MRI. Magnetotactic bacteria therefore provide a new tool for imaging cancer and monitoring treatment response in animals, and future research may lead to their use for improved cancer detection in humans.

References/Funding Source

Benoit, MR, Mayer, D, Barak, Y, Chen, IY, Hu, W, Cheng, Z, Wang, SX, Spielman, DM, Gambhir, SS, and Matin, A. Visualizing implanted tumors in mice with MRI using magnetotactic bacteria. Clinical Cancer Research. 2009. In Press
This research was funded by the ICMIC Program (NIH/NCI P50 CA114747 to SSG) and grants NIH R01 CA125074-01A1 to AM, NIH RR09784 to DMS, and NIH/NIGMS F32GM077827 and NIH T32-AI07328 to MRB.

Interventional & Open MRI

Analysis of focused ultrasound artifact on EPI and Spiral MR Imaging

S. Josan[1], A. Holbrook[1], K. Butts Pauly[1]
Dept of [1]Radiology, Stanford University, CA

MR imaging is often used for monitoring temperature in thermal therapy applications. The purpose of this work was to analyze the appearance of the focused ultrasound (FUS) hotspot on imaging performed with different trajectories. The temperature rise results in a proportional resonance frequency shift, which can produce an off-resonance artifact and can potentially lead to a mis-estimation of the location of the hotspot.

Comparison of the focused ultrasound hotspot appearance and artifact for different MR acquisition trajectories.

The FUS spot was modeled as a Gaussian temperature distribution, with a size of 2 mm full width half max and maximum temperature rise of 15°C at the center. Simulations were performed using 2DFT, EPI and Spiral k-space trajectories. The 2DFT readout bandwidth was 8kHz vs. 125kHz for the others. The image resolution was 1.56x1.56mm2 for all except the EPI single shot scan, which was 2.2x3.2mm2.

The figure compares the magnitude images of the FUS spot for the different trajectories. The phase image from the 2DFT simulation is also shown as an example. The FUS spot appears as a bright spot in the phase image due to the off-resonance. In all images, the frequency encode direction is up/down, and the phase encode direction is left/right. For the 2DFT and EPI trajectories, the artifact on the magnitude image appears as a peak (bright pixels) next to a dip (dark pixels) corresponding to the signal being shifted from off-resonance. For the 2DFT trajectory, the shift appears in the frequency encode direction, while for EPI it is in the phase encode direction due to the low bandwidth. For the spiral trajectory, the signal is blurred out resulting in a ring artifact on the image. The off resonance due to a 15ºC temperature rise results in a significant shift (4.8 mm) in the single shot EPI case. For the other trajectories, the shift was less than 1 mm.

MR-guided focused ultrasound ablation through the ribcage

V. Rieke,[1], R. King[1,2], and K. Butts Pauly[1]
Depts of [1]Radiology, [2]Bioengineering, Stanford University, CA

In recent years, MR-guided focused ultrasound (FUS) ablation has shown promise as a non-invasive alternative for the treatment of various diseases. For FUS applications in the upper abdomen and chest, a major limitation is the restricted acoustic window for FUS delivery, due to the higher acoustic impedance of thoracic bone and cartilage compared to soft tissues. In this study, we investigate if a human size ribcage provides enough acoustic window to ablate tissue in the heart.

Experiments were performed with the InSightec ExAblate 2000 system. A plastic ribcage from a classroom skeleton was placed in a water bath above the transducer. The ribcage was positioned at a slight angle such that the FUS beam path went through the cartilage and ribs next to the sternum. A polyacrylamide gel phantom was placed inside the ribcage at the position of the heart. 25 sonication were performed and monitored with MR thermometry.

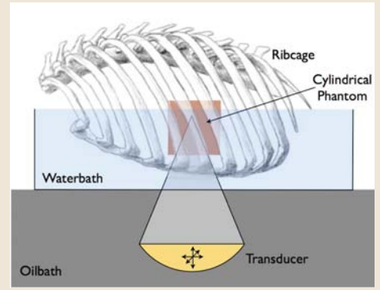

Schematic of the experimental setup (left). The ribcage is positioned at a slight angle. A cylindrical gel phantom is located at the position of the heart.

The results showed that the maximum ablation temperature varied with the amount of rib obstruction. For comparison, no rib obstruction resulted in a temperature of 45°C. Areas with less than approximately 40% rib obstruction reached temperature rises of more than 30°C. A temperature rise of this magnitude would be sufficient to create tissue necrosis in living tissue (final temperature > 55°C). However, temperature elevations as low as 5°C were measured in areas with more than 80% beam path obstruction by the ribs. In addition, surface heating of the ribs was observed, which highlights the need for adaptive mechanisms such as turning off individual transducer elements with beam paths obstructed by ribs.

Our results show that sonications through the ribcage can achieve ablative temperatures with the acoustic windows provided through a human-size rib-cage.

References/Funding Source

V. Rieke, R. King, and K. Butts Pauly,, MR-guided focused ultrasound ablation through the ribcage, ISMRM 2009.
NIH P41 RR009784, NIH R01 CA121163, and the Stanford Cardiovascular Institute Seed Grant.

MR guided Focused Ultrasound Surgery for Localization of Non-Palpable Breast Tumors

R.B. Bitton [1], V. Rieke [1], B.L. Daniel [1], K. Butts Pauly [1]
Dept of [1]Radiology, Stanford University, CA

Breast conservation surgery is crucial to not only the extension of life, but the quality of life of so many patients suffering from breast cancer. Physicians are increasingly confronted with non-palpable breast lesions that are only visible on MRI. Since the tumors are non-palpable, the current method to locate them is pre-operative MRI guided wire placement. However, MR guided wire localization lacks precise accuracy, and has been shown to produce positive tumor margins in 14-57% of patients. The aim of this project is to assess the potential and efficacy of using MR guided Focused Ultrasound (MRgFUS) for pre-operative localization of non-palpable breast lesions over the current wire placement method. MRgFUS can be used to create lesions which are fully registered with the MRI, circumscribing the tumor, thus, providing a visible and palpable lesion that the surgeon can use as a guide for excision during breast conservation surgery. The potential for a visible and palpable lesion is to provide reduced and more accurate tumor-free margins over wire localization techniques.

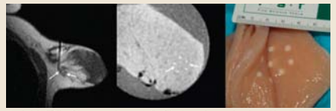

Axial MRI of human breast (left) showing wire localization of tumor volume (white arrows). Coronal MRI of the tissue phantom (middle) and photograph of excision (right) showing MRgFUS localization spots surrounding an agar tumor (white arrows).

The initial phase of this study used ex-vivo chicken breast as a tissue phantom model. A non-palpable artificial tumor was injected using an aqueous agar gel. The HIFU localization was performed in a GE 3T scanner using the InSightec ExAblate 2000 system. In this study 5 small sonications (60 W) lasting 16 seconds each, were made around the perimeter of the artificial tumor. Sonication temperatures were monitored using MR thermometry, and the tissue was imaged subsequent to the localization (Figure 1). From outside the tissue, the cigar shaped ablations were not visible, but were easily palpable. The current efforts of this study include aims to characterize the stiffness and palpability of MRgFUS lesions in human tissue from excised female cadaver breasts.

References/Funding Source

NIH/NCI: CA-09695-19

PRF Shift in Frozen Tissue at 3T

Elena Kaye[1,2], Aiming Lu[3], Marcus Alley[1] , Bruce Daniel[1], Kim Butts Pauly[1]
Depts of [1]Radiology and,[2]Electrical Engineering, Stanford University,CA ; [3]Center for MR Research, University of Illinois at Chicago, IL

MRI-guided cryoablation is a minimally invasive treatment for prostate cancer. To investigate the potential of MRI-based thermometry in cryoablation, we study the sensitivity of the PRF shift to temperature below 0°C. In [1] measurable phase shift was reported during in vivo canine prostate cryoablation. In a 7T spectroscopy study [2], PRF shift was found to change exponentially with temperature at T<0°C. In this work, for the first time, we measure frequency shift in frozen tissue on a clinical 3T MRI scanner with a standard 2DFT pulse sequence.

Two porcine muscle samples were frozen to -15°C and thawed inside an RF coil, and one sample was kept at room temperature as a reference. Fiber optic temperature sensors were placed in the center of each sample. Imaging was performed continuously during tissue thawing on a 3T GE Signa MRI scanner, using a Cartesian 3D SPGR sequence, with TE1/TE2 = 0.8ms/1.4ms. For each TE, phase shift data was fit to a line for T>0°C and to an exponential for T<0°C. Then the frequency shift was calculated.

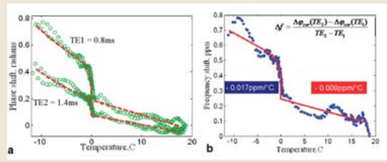

Figure 1 a. Phase Shifts (o) and fits (---). b. PRF shift calculated from phase shift data point by point (dots) and from the fits (line).

The phase shifts and the calculated frequency shift are shown in Figure 1. Between room temperature and T=0°C, PRF linearly decreases with temperature as –0.09ppm/°C. At T=0°C, the proton frequency shift initially grows exponentially rather than linearly, with the greatest gain occurring in [-2°C; 0°C] interval.

Today PRF shift based temperature mapping techniques are successfully being used to monitor thermal therapies, however, so far it has been always limited to the temperatures greater than 0°C. In this study we demonstrated that phase shifts can be measured in frozen tissue on a 3T clinical scanner using a short echo time pulse sequence. In order to study PRF shift in frozen tissue as a potential temperature mapping technique, further experiments will be performed.

References/Funding Source

[1] Lu A. ISMRM07, [2] Kaye E, ISMRM.

FUS Focal Spot Localization with Single Shot Flyback EPI

Elena Kaye[1,2], Jean Chen[1,2] , Oleg Prus[3], Yoav Medan[3], Kim Butts Pauly[1]
Depts of [1]Radiology and [2]Electrical Engineering, Stanford University,CA; [3]InSightec Ltd., Tirat Carmel, Israel

MRI is often used during the targeting stage of HIFU treatments for visualization of the FUS focal spot, which relies on “test spots” of a small temperature rise. In [1,2] it was proposed to use FUS in the mechanical mode and to use MR-ARFI to image the displacement of tissue in the focal spot instead of temperature rise. To obtain displacement maps we developed a rapid imaging sequence that combines reduced FOV single-shot DW-EPI and MR-ARFI methods based on displacement encoding with motion sensitizing gradients.

In addition to focal spot localization, the displacement maps provide information about tissue stiffness, which can be used for assessment of the treatment. Such assessments can be done by rastering the ultrasound focal spot through the tissue of interest. To increase efficiency of treatment evaluation, we focused the ultrasound beam to a line to increase the focal spot area.

The MRI pulse sequence triggered the HIFU system to emit ultrasound pulses during the encoding gradients. The imaging sequence was tested in gel phantom and porcine tissue on a 3T GE MRI scanner equipped with an InSightec ExAblate 2000 HIFU system. To map displacement pair of MR images were obtained with identical imaging and sonication parameters, but with opposite polarity of the gradients. From these images a phase difference image was calculated and converted to displacement.

References/Funding Source

[1] N.McDannold et al, 2008;
[2] J.Chen et al. 2008.

In both samples our pulse sequence detected a measurable displacement in the focal spot (Fig 1), with maximum displacement greater in porcine tissue than in gel phantom. Line focus displacement (Fig 2) showed that more work is needed to make the focal line more contiguous. In conclusion, reduced FOV EPI MR-ARFI sequence allows rapid visualization of the FUS focal spot and can be potentially useful during the targeting and the assessment stages of a HIFU treatment.

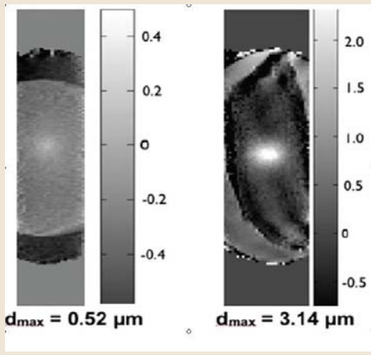

Figure 1 MR-ARFI measurements in the gel phantom (left) and porcine muscle (right) demonstrate six times the displacement in the porcine muscle for the same acoustic power of 40W.
Figure 2 MR-ARFI images of porcine muscle tissue in water, obtained with a “line” focus.

Real Time MR Thermometry for Monitoring HIFU Ablations of the Liver

A.B. Holbrook[1,2], J.M. Santos[3], E. Kaye[1,3], V. Rieke[1], and K. Butts Pauly[1]
Depts of [1]Radiology, [2]Bioengineering, [3]Electrical Engineering, Stanford University, CA

A high resolution and high speed pulse sequence is presented for monitoring high intensity focused ultrasound (HIFU) ablations in the liver in the presence of motion. The sequence utilizes polynomial-order phase saturation bands to perform outer volume suppression, followed by spatial-spectral excitation and three readout segmented EPI interleaves. Images are processed with referenceless thermometry to create temperature rise images every frame. The sequence and reconstruction were implemented in RTHawk and used to image stationary and moving sonications in a polyacrylamide gel phantom (62.4 acoustic W, 50 sec, 550 kHz). Temperature rise images were compared between moving and stationary experiments. Heating spots and corresponding temperature rise plots matched very well. The stationary sonication had a temperature standard deviation of 0.15◦ C, compared to values of 0.28◦C and 0.43◦ C measured for two manually-moved sonications at different velocities. Moving the phantom (while not heating) with respect to the transducer did not cause false temperature rises, despite susceptibility changes. The system was tested on non-heated livers of 5 normal volunteers. The mean temperature rise was −0.05◦ C with a standard deviation of 1.48◦C. This standard deviation is acceptable for monitoring HIFU ablations, suggesting real time imaging of moving HIFU sonications can be clinically possible.

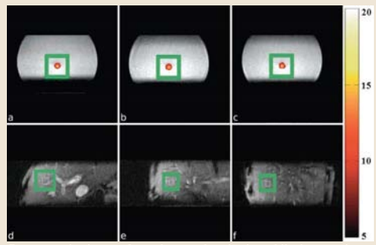

Representative images from ultrasound sonication while the setup is stationary (a), rocking automatically via the scanner (b), and moving manually (c) are shown along the top row. Axial (d), coronal (e), and sagittal (f) images of the abdomen are shown along the bottom row. Color temperature rise overlays from 5-10°C were displayed. The polynomial curve fit was performed from the green frame ROI for each timepoint. The calculated baseline phase was subtracted from the all pixels within the outer boundary of the green frame ROI. The gray box in the in-vivo images was the region used to determine the appropriate multicoil phase combination phase offsets.

References/Funding Source

Holbrook AB, Santos JM, Kaye E, Rieke V and K Butts Pauly. “Real Time MR Thermometry for Monitoring Focused Ultrasound in the Liver.” ISMRM 17th Scientific Meeting & Exhibition. Honolulu, HI. April 20, 2009.
R01 CA092061, P41 RR009784

REAL-TIME MR IMAGING FOR ADAPTIVE RADIOTHERAPY

A. Sawant[1], M. Alley[2], S. Vasanawala[2], K. Butts Pauly[2] and P. Keall[1]
Depts of [1]Radiation Oncology, [2]Radiology, Stanford University, CA

Purpose: A critical and outstanding problem in radiation therapy of moving tumors (e.g.,tumors in the lung, liver or pancreas) is that there is no non-invasive modality that can provide the position of the tumor target in real-time. An exciting approach to address this issue is the development of integrated MRI+linac systems, which can potentially yield complete spatio-temporal knowledge of the irradiated anatomy during treatment - representing the ideal guidance strategy for 4D radiotherapy delivery. We report on rapid imaging strategies for such devices to enable real-time, MR-guided, motion-adaptive radiation delivery.

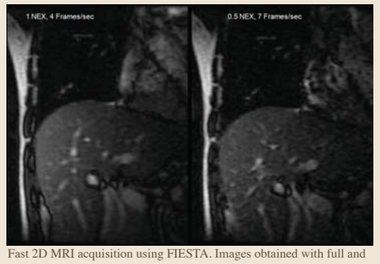

Fast 2D MRI acquisition using FIESTA. Images obtained with full and half Fourier acquisition from a healthy, free breathing volunteer. Image specifications: 5 mm thick slice, 1.6 x 3.33 mm2 pixels.

Method and Materials: (1) Balanced SSFP (FIESTA) and SPGR sequences were employed to acquire 2D and 3D time series from five, free-breathing, healthy human subjects on a stand-alone 1.5T scanner (GE Signa), using a 4-channel cardiac coil. We investigated the trade-offs between SNR and the acquisition speed, both of which impact the spatio-temporal accuracy of real-time guidance. (2) We also examined strategies to further speed up image acquisition using three different methods of sub-sampling K-space (i) half-Fourier acquisition (ii) parallel imaging and (iii) compressed sensing.

Results: 2D images acquired using FIESTA and SPGR were obtained at ~4 frames/second (full Fourier) and ~7 frames/second (half Fourier). While the SPGR acquisition showed poor image SNR, the images acquired with FIESTA exhibited adequate SNR so as to visualize the boundary of the diaphraghm against the background of the lung - considered adequate for radiotherapy guidance. (The diaphragm presents contrast levels comparable to a lung tumor against the signal-poor lung parenchyma.) Furthermore, the motion and deformation of vessels in the liver could be clearly delineated. The acquisition speed for 3D images using parallel imaging and compressed sensing (both with acceleration of 4) was on the order of 1 second/volume (8 slices, 25 x 25 cm2). The half Fourier sequence yielded a slightly slower acqusition time (~1.3 seconds/ volume). The volumetric images exhibited significant motion blur compared to the 2D images - likely due to the slower acquisition speed.

Conclusion: These initial studies indicate the feasibility of real-time MR imaging for monitoring and adaptive motion management during radiotherapy. Ongoing work involves the investigation of strategies and pulse sequences to further increase the acquisition speed of 3D images while retaining adequate SNR.

REFERENCES/FUNDING SOURCE

Real-time MR Imaging for Adaptive Radiotherapy, Amit Sawant, Marcus Alley, Shreyas Vasanawala, Kim Butts Pauly and Paul Keall, Lucas Center Report, July 2009
American Association of Physicists in Medicine (AAPM) 2008 Research Seed Funding Grant

MR-GUIDED BLOOD BRAIN BARRIER DISRUPTION WITH ULTRASOUND

K. Townsend[2], R. King[2], and K. Butts Pauly[1]
Depts of [1]Radiology, [2]Bioengineering, Stanford University, CA

Introduction: Drug delivery into the brain is difficult due to the neuroprotective blood-brain barrier, which prevents the entry of large molecules into the brain. Previous studies have shown the ability of focused ultrasound with microbubbles to temporarily disrupt focal areas of the barrier. The purpose of this work was to investigate the MR appearance of the whole brain after disruption of the entire blood-brain barrier in a rat model.

Materials and Methods: In three rats, gadolinium-based MR contrast agent (Gd; Bayer Healthcare, Magnevist, 0.5ml/kg)) was administered prior to sonication, and axial T1-weighted (TE/TR- 10/500 ms, FOV 12cm, 4 NEX, 2mm slice thickness, 4 ETL) FSE images were acquired as a baseline. Next, ultrasound microbubble contrast agent was administered (GE Healthcare, Optison, 0.5ml/kg) and allowed to circulate for 10 seconds before sonication. A 753 kHz planar PZT transducer, about 70% efficient, diameter 1.8cm, sonicated the rat brain for 10 seconds, with electrical power 500mVpp, and imaging protocol was repeated. One control animal was given microbubbles and Gd, but not sonicated.

Discussion and Conclusion: In the control experiment, contrast-enhanced MR imaging showed brightening of surrounding structures, but not of the brain itself. After giving Gd, the control whole brain signal change averaged across slices was 0.2%±5%, indicating Gd is not entering the brain tissue without sonication. After sonication in the three experimental studies, the brain displayed an increase in signal. On average, the whole brain signal increase over baseline was 18.5%, with range -7% to 87% between slices. Averaged across three animals, anterior slices showed less signal increase (2.4%) than posterior (23%). In conclusion, disruption of the blood-brain barrier was achieved using ultrasound, but inter-slice and intra-slice regional variation require further investigation.

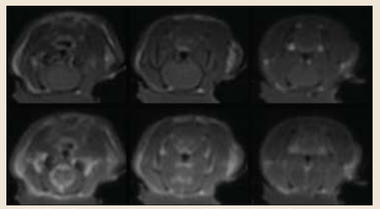
Axial slices from posterior to anterior (left to right), before (top) and after (bottom) sonication.

REFERENCELESS MR THERMOMETRY USING REWEIGHTED-L[1] REGRESSION

W.A. Grissom[1,2], M. Lustig[2], V. Rieke[1], A.B. Holbrook[1,3], J.M. Pauly[2], K. Butts-Pauly[1]
Depts of [1]Radiology, [2]Electrical Engineering, [3]Bioengineering, Stanford University, CA

Proton resonance frequency (PRF)-shift MR thermometry is a promising tool for monitoring thermal therapies. In PRF-shift thermometry, temperature change maps are estimated by subtracting image phase in a pretreatment (baseline) state from image phase in a heated state. Baseline phase can be obtained from a pretreatment image, however, this approach is sensitive to motion. Referenceless thermometry avoids this problem by estimating pretreatment phase using the treatment image only, via least-squares (L^2) polynomial regression. To avoid temperature and thermal dose underestimation, the hot spot be masked out of the regression, and therefore the user must know the location of the hot spot a priori. We have developed a new referenceless method that is robust to the hot spot, obviating the need to mask it out.

Referenceless thermometry methods assume that in the absence of therapy-induced phase changes, image phase varies smoothly over space and can be accurately represented as a superposition of polynomial basis functions, the coefficients of which are estimated via regression. In this context, the phases at spatial locations within the hot spot are regarded as outliers whose influence on the coefficients is to be avoided. Instead of masking them out of the regression, we avoid their influence using an iteratively reweighted L^1 regression algorithm that is robust to outliers [1-3].

The figure shows experimental results from a phantom HIFU heating experiment, in which the phantom was moved during heating and imaging. The figure shows that if hot spot masking is not used (which may occur if the spot is not accurately tracked), the conventional method significantly underestimates the true temperature. However, temperature estimates using the new method match those produced by conventional L^2 thermometry, without requiring accurate placement of a hot spot mask. The method therefore requires less human interaction to obtain accurate temperature maps.

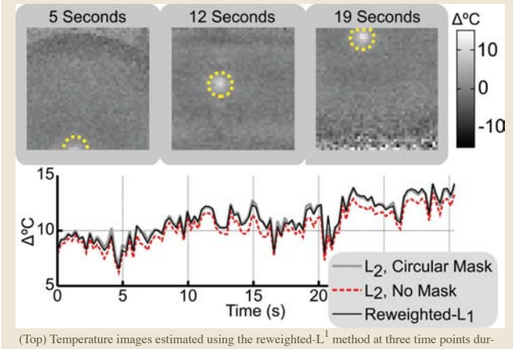

(Top) Temperature images estimated using the reweighted-L^1 method at three time points during a phantom heating experiment, during which the phantom was moved. The dashed yellow circles indicate the boundary of the circular mask whose accurate placement is necessary for successful temperature estimation using the conventional L^2 method. (Bottom) The plot of temperature vs time shows that in the hot spot center, the reweighted-L^1 and the masked L^2 temperature estimates coincide, while the unmasked L^2 method underestimates the temperature rise due to bias.

REFERENCES/FUNDING SOURCE

[1] W. A. Grissom, M. Lustig, V. Rieke, A. B. Holbrook, J. M. Pauly, and K. Butts Pauly. Referenceless MR thermometry using iteratively-reweighted l1 regression. 17th ISMRM, p. 444, 2009.
[2] W. A. Grissom, K. B. Pauly, M. Lustig, V. Rieke, J. M. Pauly, and N. McDannold. Regularized referenceless temperature estimation in PRF-shift MR thermometry. 6th IEEE ISBI, p. 1235–8, 2009.
[3] W. A. Grissom, V. Rieke, J. M. Pauly, N. McDannold, and K. Butts Pauly. Regularized multicoil MR thermometry. 17th ISMRM, p. 2516, 2009.
NIH RO1 CA121163

PRACTICAL THOUGHTS ON USING REPEATED BIPOLAR GRADIENTS FOR MR-ARFI

Jing Chen[1,2], Kim Butts Pauly[2]
[1]Inst. of Biophysics, Chinese Academy of Sciences, China; [2]Dept of Radiology, RSL, Stanford University, CA

MR acoustic radiation force imaging (MR-ARFI) is a promising monitoring method for monitoring high intensity focused ultrasound (HIFU) treatments. MR-ARFI uses motion sensitizing gradients to detect the displacement introduced by the acoustic radiation force. Therefore, it could potentially be used for targeting of HIFU thermal ablation, and monitoring HIFU mechanical treatments. Our previous work has shown that using repeated bipolar gradients as the displacement encoding gradient can significantly improve the accuracy and precision of the displacement measurement. In this work, we provide some practical thoughts on using the repeated bipolar gradients for MR-ARFI.

Imaging was performed with a line scan on a 3T GE Signa MR scanner. The first consideration is the bulk motion sensitivity of the bipolar encoding gradient vs. the conventional unipolar gradient. The vibration of the scanner introduced constant and linear phase terms, as seen on phase difference images. The linear phase terms are an order of magnitude smaller with the repeated gradients than with the unipolar gradients. This robustness against random bulk motion comes without any lost of the sensitivity towards radiation force induced displacement.

The second consideration is the optimized encoding width δ. The signal-to-noise ratio (SNR) of the displacement map is a function of δ. A simulation was performed for four tissue types with different T2 and apparent diffusion coefficient (ADC) to look for the optimized δ, as shown in the Figure for the white matter. Compared to the results obtained with the unipolar gradients, SNR is significant enhanced by the repeated bipolar gradients, with a maximized SNR at the encoding width of 19 ms. The calculated optimized δ is shown in the table for kidney, liver, and prostate.

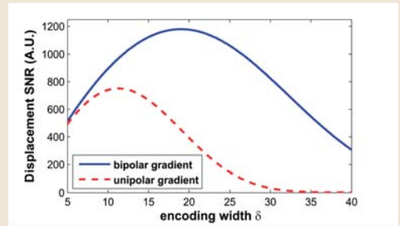

Tissue Type	T2 (ms)	ADC (10^{-3} mm^2/s)	Optimized δ (ms)
White matter	92	1.5 (parallel dir)	19
Kidney	58	1.63	16.6
Liver	43	0.69	17.2
Prostate	74	1.64	17.8

SNR simulation of the white matter. For the repeated bipolar gradient, the encoding width should be set to 19 ms for maximized SNR.

REFERENCES/FUNDING SOURCE

J. Chen, K. Butts Pauly. Practical Thoughts on Using Repeated Bipolar Gradients for MR-ARFI, 17th ISMRM, Honolulu, 2009
NIH RO1 CA111981, RO1 CA121163 and P41 RR009784

The Effect of the Rat Skull on the Ultrasound Beam Profile in the Brain

R. King[1,2], K. Butts Pauly[1], and V. Rieke[1]
Depts of [1]Radiology, [2]Bioengineering, Stanford University, CA

Objectives: MR-guided therapeutic ultrasound is being investigated for a range of brain treatments including localized tumor ablation, pain alleviation, and localized drug delivery. In the development of an appropriate animal model, the influence of the skull on the acoustic field needs evaluation. Wave propagation simulations through the intact skull of the mouse have shown to cause minimal beam distortion, and thermal deposition. While this may be true in the mouse, it may not hold true for the rat. The purpose of this work was to measure the effect of the skull on ultrasound propagation through the rat skull.

Methods: Experiments were performed both ex-vivo and in-vivo with the InSightec Exablate System in a 3T GE MRI scanner, using a 2D PZT array comprised of 1024 elements at 0.55MHz. Three sets of experiments were performed: a) in two gel phantoms, two grid patterns of 41 sonications total were performed, b) in ex-vivo rat skulls, sonications were performed in a grid pattern encompassing the entire skull, 48 locations total across three different skulls, and c) in 1 in-vivo experiment, sonications were performed in 4 locations. In all experiments, the beam was assessed by quantitation of the temperature profile using PRF thermometry 2-3 mm from the inner surface of the skull.

Results: When sonicating into a phantom with no skull, 39/41 sonications created single temperature spots, which were, on average within 0.5mm from the expected location. Ex-vivo, 11/48 sonications created small single spots showing a temperature rise in the phantom material. In all other sonications the heat was diffuse with multiple foci. In-vivo, only 1/4 sonications created a single thermal spot.

Conclusion: Unexpectedly, the effect of the rat skull needs to be considered and possibly compensated for, when using it as a model to perform therapeutic ultrasound in the brain.

MRI-guided Focused Ultrasound Ablation of the Rat Liver

R. King[1,2], K. Butts Pauly[1], and V. Rieke[1]
Depts of [1]Radiology, [2]Bioengineering, Stanford University, CA

Introduction To study the treatment of hepatocellular carcinoma using high intensity focused ultrasound, an appropriate animal model must be established. Rodent models are preferred because of the cost associated with survival studies, convenience of experimental setup, and available tumor cell lines. In previous HIFU studies the rat liver has been exteriorized to allow access to the tissue. However, to be a useful model, the effects of the ribcage, on the ultrasound beam must be able to be ignored without exteriorizing the liver. In the following study we show that it is possible to sonicate through the ribcage of the rat thermal lesions localized to the liver.

Methods The animals used in this study were Sprague-Dewey rats placed head first in prone position on the therapy table inside the MRI using a standard GE 3-inch surface coil attached under the rat so that the abdomen is suspended through the coil into a water bath In vivo rats (n=15) were anesthetized while their heart rate and oxygen saturation were monitored. Sonications were performed using 1.35 MHz and energy levels of 716-797 Joules.

Results and Discussion In this in vivo study, we found it was possible to create thermal lesions localized to the liver of rats by sonicating directly through the ribcage. Respiratory and bowel motion, as well as flow artifact from the cardiovascular system of the rat were minimized in several ways No thermal burns were observed by visual inspection on the skin. Lesions size was determined using T1 contrast enhanced images. HIFU lesion sized correlated very well between MR images and necropsy measurements with a resulting R2 value of 0.97.

Conclusions It is possible to ignore the effect of the ribs and the sternum in rats and create in vivo thermal lesions localized to the liver of the rat, while obtaining MR temperature maps and accumulated thermal dose. Such models are needed for the advancement of patient procedures.

Real Time High Intensity Ultrasound for Treatment of the Prostate

A.B. Holbrook[1,2], T. Juang[3], P. Prakash[3], C. Planey[2], J.M. Santos[4], C. Diederich[3], F.G. Sommer[2], and K. Butts Pauly[2]
Depts of [1]Bioengineering, [2]Radiology, [3]Radiation Oncology, [4]Electrical Engineering, Stanford University, CA

High intensity ultrasound is a potential treatment for conditions of the prostate, particularly BPH and prostate cancer. We have demonstrated the potential for this treatment in past studies at 0.5T. Our current work involves moving this project to 3T, while also implementing transducer feedback for automated control.

In this work, real time MRI using RTHawk has been integrated with catheter based interstitial sectored ultrasound applicators. RTHawk allows real time slice positioning and sequence modifications or switching without needing to stop the scanner. This was utilized to acquire temperature images of slices through the transducer. Mean temperatures in user defined ROIs set near the transducer boundary and another further away were processed by LabVIEW, which modulated the power of the amplifier controlling the transducer element. We successfully tested this in a phantom (see figure), heating a section in a single slice.

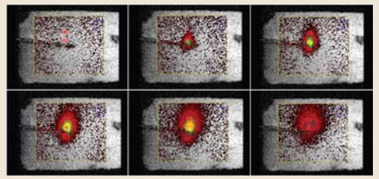

Images during phantom ablation. The top left image shows the two ROIs used to control the power of the transducer. The remaining images from left to right, top to bottom show the phantom temperature rise over time.

Our next steps involve integration of multiple slices and multiple transducers in RTHawk. This includes a semi-automated drawing process for determining the ROI locations, which will allow LabVIEW to control multiple amplifiers at once. Additionally, tracking coils will be added to the catheters, allowing for real time transducer positioning and monitoring inside the prostate. Switching between tracking and temperature imaging will be seamless in RTHawk, minimizing procedure down time. Altogether, this will lead to a rapid whole volume prostate protocol with automated transducer control.

References/Funding Source

P41 RR009784, CA111981

Multiple gradient- and spin-echo EPI with z-shimming to compensate for susceptibility-induced off-resonances

H. Schmiedeskamp[1], M. Straka[1], R. D. Newbould[2], S. Skare[1], K. P. Pruessmann[3], and R. Bammer[1]
Dept of [1]Radiology, Stanford University, CA; [2]GSK Clinical Imaging Centre, London, United Kingdom; [3]Institute for Biomedical Engineering, University and ETH Zurich, Switzerland

MRI images obtained with gradient-echo echo planar imaging (GRE-EPI) suffer from magnetic field variations within the brain, such as in regions adjacent to air-tissue interfaces. Conventional GRE-EPI pulse sequences used for perfusion-weighted imaging or functional MRI usually confine image analysis to homogeneous brain regions. Compensation mechanisms based on z-shimming [1] apply additional field gradients prior to repeated signal readouts, with the drawbacks of prolonging scan time ([2],[3]) or increasing image distortions ([4],[5]). Extending PERMEATE [6], a multi-echo EPI pulse sequence developed for perfusion quantification, z-shimming gradients were added prior to the first and second echo train, to restore T2*-related signal dropouts in the first echo train, while maintaining regular contrast for the following echo trains [7]. In this study, we added z-shimming to a combined gradient-echo/spin-echo (GRE-/SE-) EPI sequence [8], in which each EPI train is preceded by z-shim gradients in order to restore susceptibility-induced signal dropouts and facilitate full-brain coverage (see Fig. 1). Square-root-sum-of-squares images were produced from the gradient-echo EPI trains (Fig. 2a-b) as well as from combined gradient-echo/spin-echo EPI trains (Fig. 2c-d). Fig. 2e shows the spin-echo image acquired at TESE. Signal dropouts caused by susceptibility effects could be compensated for in the square-root-sum-of-squares images (Fig. 2f-g) in areas close to the ear canals as well as above the nasal cavities, therefore approaching the spin-echo image in terms of signal dropouts. The presented technique allows the simultaneous acquisition of a GRE-signal, a combined GRE-/SE-signal, as well as a SE-signal, all of them with minimal signal dropouts. Multi-echo simultaneous GRE- and SE-EPI acquisitions with z-shimming benefit from reduced signal contributions from large vessels in order to increase signal specificity through SE-EPI readout, while increased sensitivity in typical signal dropout regions can be achieved in the GRE-EPI readouts, rendering this technique particularly suitable for perfusion-weighted imaging and functional MRI.

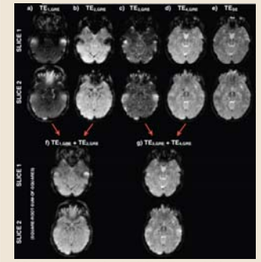

Multi-echo combined GRE-/SE-acquisition with signal dropout compensation through z-shimming gradients.

References/Funding Source

[1] Frahm et al, MRM 6:474-480, 1988; [2] Song et al, MRM 46:407-411, 2001; [3] Gu et al, NeuroImage 17:1358-1364, 2002; [4] Posse et al, NeuroImage 18:390-400, 2003; [5] Yang et al, MRM 52:1418-1423, 2004; [6] Newbould et al, MRM 58:70-81, 2007; [7] Schmiedeskamp et al, Proc. ISMRM 2008, p3561, [8] Newbould et al, Proc. ISMRM 2007, p1451
NIH (2R01EB002711, 1R21EB006860, 1R01EB008706, P41RR09784), Lucas Foundation, Oak Foundation.

b-Matrix Correction Applied to High Resolution DTI

M. Aksoy[1], S. Holdsworth[1], S. Skare[1], R. Bammer[1]
Dept of [1]Radiology, Stanford University, CA

High resolution Diffusion Tensor Imaging has been an active area of research due to challenges resulting from the random phase effects that change between successive shots and pixel-by-pixel misregistration caused by patient motion. Short Axis readout PROPELLER-EPI (SAP-EPI) has been very effective in reducing distortion and motion artifacts in high resolution DTI. One shortcoming of SAP-EPI is that it cannot correct for the alterations in the diffusion encoding direction (i.e., the b-matrix) due to gross subject motion. In this study, we combined SAP-EPI [1] with the single-step non-linear diffusion tensor estimation to perform b-matrix correction for SAP-EPI and achieve high-resolution motion corrected DTI.

Experiments were conducted on a healthy volunteer with a 1.5T whole-body MRI unit and an eight-channel head coil. DTI datasets were acquired with a twice refocused diffusion preparation scheme to avoid blurring due to eddy currents. Two b=0 and 15 diffusion directions were acquired with b = 1000 s/mm^2. The following parameters were used for the SAP-EPI sequence: 9 blades with a blade width of 64, a target in-plane resolution of 288 x 288, a GRAPPA-acceleration factor R = 3, Partial Fourier encoding with 18 overscans, a slice thickness of 5 mm, TR = 3 s, a FOV = 26 cm. The volunteer was asked to perform varying degrees of motion during each experiment.

The SAP-EPI acquisition used in this study significantly reduced geometric distortions due to the high bandwidth in the phase-encode direction and had self-navigated phase and motion correction capabilities. Furthermore, the non-linear conjugate gradient based single-step tensor estimation scheme circumvented the issue of changing diffusion encoding direction between successive interleaves due to motion and increased the accuracy of the data even further. It is possible to further eliminate the geometric distortions for SAP-EPI using an extended gradient polarity method.

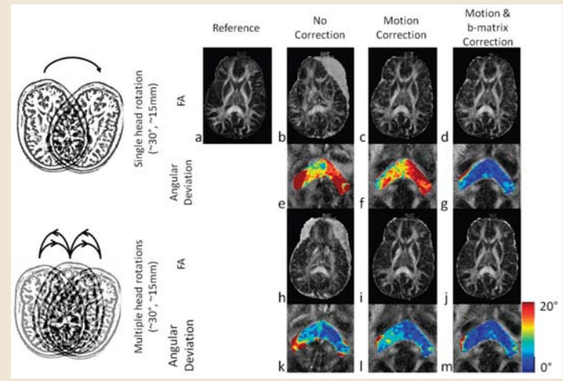

Images without and with b-matrix correction are shown. For both motion schemes (shown on the left), the major eigenvector orientations obtained with motion & b-matrix correction are closest to the reference orientations.

References/Funding Source

M Aksoy, S Holdsworth, S Skare, R Bammer, "b-Matrix Correction Applied to High Resolution DTI", Proceedings of the 17th Annual Meeting of ISMRM, Honolulu, Hawaii, 2009
This work was supported in part by the NIH (2R01EB002711, 1R01EB008706,1R21EB006860), the Center of Advanced MR Technology at Stanford (P41RR09784), Lucas Foundation and Oak Foundation.

3D SAP-EPI FOR MOTION-CORRECTED FAST SUSCEPTIBILITY WEIGHTED IMAGING

S. J. Holdsworth[1], S. Skare[1], K. Marty[1], M. Straka[1], and R. Bammer[1]
Dept of [1]Radiology, Lucas MRI/S Center, Stanford University, CA

Introduction: Susceptibility-weighted imaging (SWI) has been utilized as a useful contrast mechanism in MRI that accentuates the paramagnetic properties of blood products (1,2). Typically, a three-dimensional gradient echo (GRE) sequence is used for SWI – however, GRE suffers from a long scan time (~5 mins at 3T), which decreases patient through-put and increases the chances of motion artifacts. Here, a 3D short-axis readout propeller (SAP)-EPI trajectory (3) is suggested as an alternative approach to 3D GRE for motion corrected fast SWI. Here we show motion-corrected SWI SAP-EPI human data from controlled motion experiments.

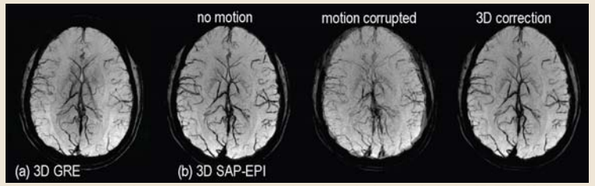

SWI minIP human brain images (14mm thick minimum intensity projection) acquired using 3D GRE (32 slices are acquired in 5mins) and 3D SAP-EPI (64 slices in 1:48mins). Motion corrupted and motion corrected SAP-EPI images are also shown.

Methods: Experiments were conducted on a healthy volunteer using a 3T whole-body GE Excite system and an eight-channel head coil. Both 3D GRE and 3D SAP-EPI images were acquired (SAP-EPI: matrix size = 256 x 256, TR/TE/FA = 55ms/20ms/20, FOV = 24 x 24 x 12.8cm3, 64 z-partitions, slthk = 2 mm, 8 blades of width 64, R = NEX = 4, brick frame rate = 3.5 s, scan time = 1:48 min; GRE: flow compensation, matrix size = 512 x 256, rectangular FOV = 0.75, TR/TE/FA = 37ms/20ms/20, z-partitions = 32, slthk = 2mm, scan time = 5mins). Controlled motion experiments were performed, with a head rotation of up to 10º. Each SAP-EPI brick (or 'stack of blades') were 3D motion corrected in the image domain. SW images were created by generating a phase mask (using a 2D Hanning window), and multiplying this mask 5 times by the magnitude image.

Results: GRE and SAP-EPI images are shown in the figure. While small vessels are more easily depicted in the GRE image, SAP-EPI renders thicker and more prominent larger vessels – probably due to the additional T2*-dephasing that occurs during the EPI readout. Motion corrupted and subsequently corrected SAP-EPI SWI data are also shown.

Conclusion: With SAP-EPI, SW images can be acquired in 1:48min (compared with 5min for GRE) with twice the brain coverage as GRE, and gives us the ability to correct for 3D rigid-body motion. These features make SAP-EPI an attractive alternative for susceptibility-weighted imaging in clinics.

REFERENCES/FUNDING SOURCE

[1] Reichenbach JR et al. Radiology 1997;204:272-77. [2] Hacke EM et al. MRM 2004;52:612-18. [3] Holdsworth SJ et al. ISMRM 2008:1352.
S.J. Holdsworth, S. Skare, K. Marty, M. Straka, R. Bammer, "3D SAP-EPI motion-corrected fast susceptibility weighted imaging". In: 17th Annual Meeting of the ISMRM. Hawaii, #756, 2009
This work was supported in part by the NIH (2R01EB002711, 1R01EB008706, 1R21EB006860), the Center of Advanced MR Technology at Stanford (P41RR09784), Lucas Foundation, Oak Foundation, and the Swedish Research Council (K2007-53P-20322-01-4).

DIFFUSION-WEIGHTED IMAGING OF THE SPINE WITH READOUT-SEGMENTED (RS)-EPI

S. J. Holdsworth[1], S. Skare[1], R. Bammer[1]
Dept of [1]Radiology, Lucas MRI/S Center, Stanford University, CA

Introduction: The development of diffusion-weighted imaging (DWI) of the spine has been hindered by the large off-resonance effects problematic for single-shot EPI. Overcoming these restrictions would open up applications ranging from the diagnosis of spinal cord infarction, vertebral body fractures, lymphoma, trauma, and many other disorders. Navigated interleaved EPI (iEPI) has been shown to overcome this distortion problem both in the brain [1] and in the spine [2], however iEPI may lead to undersampling effects in k-space leading to ghosting [3]. Readout-segmented (RS)-EPI has been shown to be a promising pulse sequence for high-resolution DWI of the human brain, with significantly reduced distortions and reduced ghosting [4-6]. Here we produce RS-EPI DW images with significantly reduced distortions compared with EPI.

Methods: DW images were acquired on two volunteers on a 3T whole-body GE Excite system using a four-channel spine coil. Single-shot (ss)-EPI and ss-RS-EPI DW images were acquired of cervical and thoracic spine.

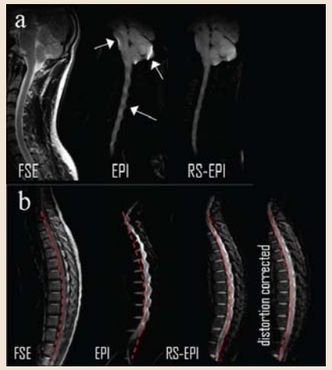

Distortion reduction at 3T with DW-RS-EPI in (a) the cervical spine, and (b) thoracic spine. The red line in (b) shows the improvement in distortion using RS-EPI and distortion corrected RS-EPI. Both methods used a matrix size of 192x192, TE = minimum (RS-EPI: 61 ms, EPI: 84ms), 32 overscans, slthck = 4 mm, TR = 3s. RS-EPI used 7 blinds of size 32x192 (freq. phase), and EPI used 7 NEX to keep the scan time equivalent. Cervical spine images (a) were acquired with a FOV = 30 x 15cm, scan time = 2:27mins, seven b = 500 s/mm^2 diffusion directions. Thoracic spine images (b) were acquired with a FOV = 40 x 20cm, scan time = 6:18mins, three b = 0 s/mm^2 and 15 isotropically distributed DW directions with b = 500 s/mm^2.

For RS-EPI, an additional b = 0 s/mm2 image was acquired with a negative phase encoding gradient, and – with the use of a b = 0 s/mm2 image from the positive phase encoding gradient – this data was used to perform distortion correction [7]. FSE images were also acquired for geometric comparison.

Results: The accompanying figure compares EPI and RS-EPI images of the cervical spine (isotropic b = 500 s/mm2, top row), and thoracic spine (b = 0 s/mm2, bottom row). The RS-EPI trajectory significantly reduces the 'zig-zag' appearance of the spinal cord compared with EPI (cf. FSE image, left panel), with a theoretical reduction in distortion of 57%. The bottom row also shows that further reduction in distortion for RS-EPI (as indicated by the red line) can be achieved with additional post-processing.

Conclusion: This work shows that RS-EPI can be useful for imaging the spine, with considerably reduced geometric distortions in a clinically reasonable scan time. If further reduction in distortion is warranted, one may perform distortion correction with the use of an image acquired with a negative phase-encoding gradient.

REFERENCES/FUNDING SOURCE

[1] Butts K. MRM 1996;35:763-770. [2] Bammer R. JMRI 2002;15:364-373. [3] Atkinson MRM 2000;44:101-109. [4] Porter D. ISMRM 2004;442. [5] Porter D. ISMRM 2008;3262. [6] Holdsworth SJ. ISMRM 2008;757. [7] Andersson JL. Neuroimage 2003;20(2):870-888.
S.J. Holdsworth, R. Bammer, S. Skare, "Diffusion-weighted imaging of the spine with readout-segmented (RS)-EPI". In: 17th Annual Meeting of the ISMRM. Hawaii, #634, 2009
This work was supported in part by the NIH (2R01EB002711, 1R01EB008706, 1R21EB006860), the Center of Advanced MR Technology at Stanford (P41RR09784), Lucas Foundation, Oak Foundation, and the Swedish Research Council (K2007-53P-20322-01-4).

STEADY-STATE FREE PRECESSION (SSFP) DIFFUSION IMAGING USING 3D ROTATING SPIRALS (3DRS)

A. Zhang[12], C. Liu[3], and M. Moseley[2]
Depts of [1]Electrical Engineering, [2]Radiology, Stanford University, CA; [3]Brain Imaging and Analysis Center, Duke University, NC

3D diffusion imaging provides good properties such as isotropic resolution, higher SNR efficiency, and less inflow effect. However, it also suffers from long scan time and consequently more severe motion artifacts. By combining SSFP-DWI and 3D Rotating Spiral (3DRS) readouts in this approach, high quality diffusion weighted volumes can be rapidly acquired with very high SNR efficiency and low sensitivity to motion artifacts. Interleaved variable density (VD) spiral trajectories are used here to sample the 3D k-space [1], which yields a couple of advantages over 3D EPI and radial imaging. First, every echo is acquired at k-space center and samples near k-space origin can be utilized for phase correction. Next, dense sampling of k-space center provides high SNR efficiency. Finally, this oversampling also improves image quality by reducing its sensitivity to subject motions. Fig 1 shows the SSFP-3DRS pulse sequence. In vivo DTI scans were performed on a healthy volunteer at a 3T GE-DV750 scanner with an 8-channel head coil. The following parameters were used: TE/TR = 23ms/35ms, FA = 50, FOV = 24cm, matrix size = 128x128x128, BW = 125kHz. The voxel size was 1.8mmx1.8mmx1.8mm isotropic. Each single DWI volume was acquired with a scan time of 1.5 minutes. DTI experiments were implemented with beff=600. Six plus one diffusion gradient directions were applied to acquire diffusion tensor volumes [6]. For each interleaf, samples near k-space center were used to estimate the 0-th order phase error and this error was subtracted out before combining all interleaves. Fig 2 shows the calculated ADC and FA maps for selected slices. Compared with other techniques, our approach can achieve much higher SNR with desired diffusion weighting and limited imaging time. And this benefit could lead to either higher spatial resolution or more tensor acquisitions in future work.

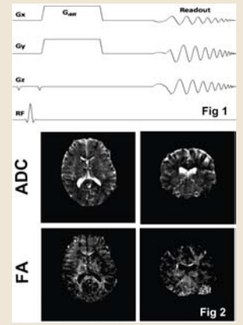

Figure 1: SSFP-3DRS pulse sequence: rotating spiral-in trajectories are interleaved to acquire the M- signal.
Figure 2: Trace of ADC and FA maps of axial and coronal slices.

REFERENCES/FUNDING SOURCE

1. Zhang J et al., ISMRM 2007, p9; 2. Buxton R., Magn Reson Med, 29, 235-243, 1993; 3. Mille K., et al., Magn Reson Med, 50, 343-353, 2003; 4. Bosak E., et al., J Magn Reson 12, 167-176, 2001; 5. Zur Y., et al., Magn Reson Med, 6, 175-193, 1988; 6. Skare S., et al., J Magn Reson 147, 340-352, 2000.
Lucas Foundation, NCRR P41 RR09784, 5K99EB007182-02.

DECONVOLVING HAEMODYNAMIC RESPONSE FUNCTION IN FMRI UNDER HIGH NOISE BY COMPRESSIVE SAMPLING

C. Law[1,2], G. Glover[1]
Depts of [1]Radiology, RSL, [2]Electrical Engineering, Stanford University, CA

Introduction. A simple technique to deconvolve haemodynamic response function (HRF) from fMRI data using 1-norm minimization is introduced. The true HRF is typically sparse after wavelet transform, but we find the proposed technique to be robust w.r.t relative sparsity. Higher activation volume can be detected using subject's deconvolved HRF as reference than from using canonical HRF plus derivatives [1].

Theory. The true HRF is assumed sparse under Coiflet 4 wavelet transform. The proposed technique finds HRF by solving the following optimization problem:

$$\underset{h}{\text{minimize}} \ \|Wh\|_1 + \lambda \|y - Dh\|_2 \quad \text{where } h \in \mathbf{R}^n \text{ is the unknown HRF,}$$

$$\text{subject to } h(1) = h(n) = 0 \qquad Wh \in \mathbf{R}^n \text{ is the discrete wavelet transform of } h,$$

$$\|\nabla^3 h\|_1 \le \varepsilon \qquad y \in \mathbf{R}^m \text{ is fMRI data, } D \in \mathbf{R}^{m \times n} \text{ is a convolution matrix.}$$

Methods. in vivo experiments consist of two visual stimulus scans:

(1) HRF calibration experiment: measured HRF directly by applying event-related (ER) design with fixed inter-stimulus-interval (ISI): 1s on, 29s off, 20 cycles.

(2) jittered ER experiment: 1s on, average ISI = 11.8s, total scan time = 512s.

Eight oblique slices were collected with single-shot spiral-out trajectory at a 1.5T GE Signa scanner. Scanning parameters were: TR/TE/FA/matrix size/FOV = 1s/40ms/70°/64×64/20cm.

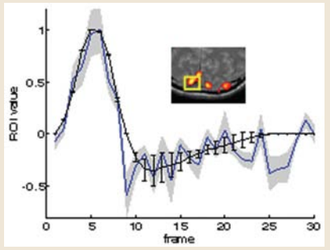

Figure 1 Pixelwise-median reference-HRF (blue) and standard deviation (gray bounds) with deconvolved HRF (black) from a visual stimulus.

Data from the HRF calibration was synchronously averaged over all stimulus-cycles to generate reference HRF, while data from the second experiment was used to deconvolve HRF using the proposed technique.

Results. Figure 1 show the pixelwise median HRF from calibration experiment and its standard deviation (gray bounds) for the highlighted ROI from one subject. Time-series from actual jittered ER fMRI experiment were extracted to deconvolve HRF by the proposed technique (shown in black). Figure 2 shows activation maps from one volunteer using (a) HRF proposed deconvolution method, (b) canonical HRF, (c) canonical HRF + derivative as reference.

Discussion. Experiments show that our technique can estimate HRF from actual scan-data just as well as it can by performing an fixed ISI HRF measurement; in other words, we can dispense separate measurement of HRF and recover additional signal from the subject's own HRF as shown in Fig 2.

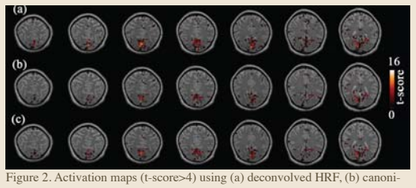

Figure 2. Activation maps (t-score>4) using (a) deconvolved HRF, (b) canonical HRF, and (c) canonical HRF + derivative as reference.

REFERENCES/FUNDING SOURCE

[1] Hopfinger J.B.; Büchel C.; Holmes A.P.; Friston K.J. A Study of Analysis Parameters That Influence the Sensitivity of Event-Related fMRI Analyses. NeuroImage 2000; 11(4) , 326-333.
P41 RR009784, Lucas Foundation, GEMS.

IN-VIVO APPLICATIONS OF OPTICAL REAL-TIME MOTION CORRECTION USING A MONOVISION SYSTEM

M. Aksoy[1], M. Straka[1], S. Skare[1], R. Newbould[2], S. Holdsworth[1], J. Santos[3], R. Bammer[1]
Depts of [1]Radiology, [3]Electrical Engineering, Stanford University, CA; [2]GlaxoSmithKline, London, UK

Correction of motion artifacts is one of the unsolved but highly relevant topics in MRI. Due to the limitations of imaging-based methods that require additional navigator readouts, real-time optical motion correction systems have been proposed to perform rigid head motion correction. Recently, an in-bore optical motion correction system has been proposed that uses a single camera and a planar marker to detect and correct for rigid head motion in real time. In this study, we demonstrate the in-vivo applications of this system.

A single camera was used for real-time motion correction, which was attached to an 8 channel head coil. This camera took the images of a planar marker which was attached to the patient's head and sent these images to a laptop where they were processed. The estimated marker pose was sent to the scanner in real time using the real-time scanner control protocol rtHAWK. According to the new geometry information coming from the laptop, the gradients and RF frequency were updated so that the scan plane followed the patient motion.

Two healthy volunteers were scanned on a 1.5T GE Signa scanner using an 8 channel head coil. Two sequences were used: 1) GRE with cartesian line-by-line readout, TR/TE=200/7ms, flip angle=20°, 256x256 resolution, FOV=24cm, slice thickness=5mm, 5 slices. 2) Spin echo with spiral readout, TR/TE=2500/90ms, 256x256 resolution, FOV=24cm, 24 interleaves, slice thickness=5mm, 7 slices. For both sequences, the volunteer was asked to perform two types of voluntary motion: 1) Head rotation around SI axis 2) Nodding motion around RL axis. For each case, the volunteer performed a single motion in the middle of the scan and continuous motion throughout the whole scan. Experiments were carried out with the motion correction system turned on and off.

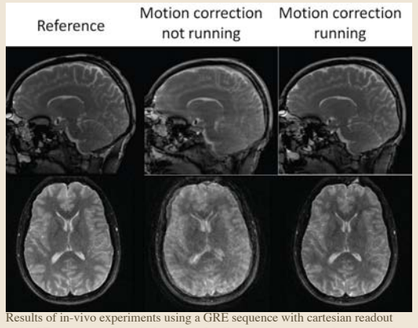

Results of in-vivo experiments using a GRE sequence with cartesian readout and a SE sequence with spiral readout. In all cases, the structure loss caused by patient motion is recovered if the real-time optical motion correction system is turned on. The main advantage of this system is that it can correct for through-plane motion which occurs for nodding motion

REFERENCES/FUNDING SOURCE

M Aksoy, M Straka, S Skare, R Newbould, S Holdsworth, J Santos, R Bammer, "In-vivo Applications of Optical Real-time Motion Correction Using a Monovision System", Proceedings of the 17th Annual Meeting of ISMRM, Honolulu, Hawaii, 2009
This work was supported in part by the NIH (2R01EB002711, 1R21EB006860), the Center of Advanced MR Technology at Stanford (P41RR0978 4), Lucas Foundation and Oak Foundation.

LST-BAESED OPTIMIZATION OF PATIENT SPECIFIC CONTRAST MEDIA ADMINISTRATION FOR CE-MRA

D. Kopeinigg[1,2], D. Fleischmann[1], R. Bammer[1], and R. Stollberger[2]
Dept of [1]Radiology, Stanford University, CA; [2]University of Technology Graz, Austria

Introduction: Synchronizing the k-space acquisition with the intravascular enhancement after contrast media bolus administration is very crucial in contrast enhanced MRA(CE-MRA). So far, high temporal resolution, fluoroscopic triggering and test bolus injection have been proposed to achieve optimal vessel opacification, since the pharmacokinetic relationship between the intravenously injected contrast media and the resulting concentration time curve varies between each individual. Therefore, a forward approach -- as introduced last year -- uses a test bolus of contrast media to extract patient-specific physiological properties with the objective to compute an injection profile that results in a desired intravascular enhancement profile. The test bolus is followed by a saline flush, which turned out to be a very decisive component of the injection profile and especially important for the low contrast dosages used in MRI. In this study, 1) the implemented forward approach facilitated by a graphical user interface (GUI) was validated via phantom and volunteer studies, and 2) the influence of saline chaser on modulated injection profile was demonstrated.

Materials and Methods: We validated our model by phantom experiments and volunteer studies on a 1.5T unit (GE Healthcare) using a power injector. To measure exact concentration values without inflow effects, a dynamic single-slice SR sequence was prescribed. The image acquisition was synchronized with the beginning of the injection and the images were then pushed from the scanner to a Laptop where the 'forward' approach was used to design and predict the target enhancement. Results & Conclusion: The LST-based approach to optimize patient-specific contrast injections for individualized vascular enhancement profiles was validated on phantoms and volunteers. The measured time courses were in excellent agreement with the predicted waveforms and demonstrated the practical feasibility of this approach. Furthermore, the small Gd injection volumes used in CE-MRA it could be shown how a wrong choice of parameters for the saline flush can impair the desired vascular enhancement.

REFERENCES/FUNDING SOURCE

[1]D.Kopeinigg, et al. ISMRM 2008; [2]Stollberger R, et al. ISMRM 2006; [3]J.P. van Osch M, et al., MRM 49:1067-76, 2003;[4]Gerhard Laub, AngioClub 2008; [5]Fleischmann D, Hittmair K, JCAT 23:474-84, 1999. Acknowledgements: The project is supported by NIH (1R01EB002771+S1, 1R21EB006860, P41RR09784), Lucas Foundation. The authors are grateful to Bracco Diagnostic for providing the contrast

IS REDUCED CBV A RELIABLE SURROGATE MARKER FOR INFARCT CORE AND CAN IT BE USED TO IDENTIFY MISMATCH?

M. Straka[1], M. G. Lansberg[2], S. Christensen[3], M. Mlynash[2], D. A. De Silva[4], J.-M Olivot[2], B. C. Campbell[5], G. A. Donnan[6], S. M. Davis[4], G. W.Albers[2], R. Bammer[1]
Dept of [1]Radiology, [2]Stroke Center, Stanford University, CA; Depts of [3]Radiology, [5]Neurology, Royal Melbourne Hospital, University of Melbourne, Australia; [4]Natl Neuroscience Inst, Singapore General Hospital campus, Singapore;[6]Florey Neuroscience Institutes, Australia

A limitation of perfusion CT imaging for evaluation of acute stroke is the lack of a clear marker for identification the ischemic core. Previous studies have suggested that CBV_{CT} correlates well with DWI, however these were limited by restricted spatial coverage with CBV_{CT} and time differences between the CT and MRI. These limitations can be alleviated if CBV_{MR} is compared to DWI. To assess whether CBV is an accurate surrogate for the ischemic core, we studied the relationship between CBV_{MR} and DWI lesion volumes and the agreement between $Tmax/CBV_{MR}$ with Tmax/DWI for classification of mismatch. 133 cases with sufficient quality baseline DWI and PWI data from the DEFUSE-EPITHET pooled database were analyzed. The stroke core was identified by automated software using a combined relative DWI and absolute ADC threshold. The CBV lesions were manually outlined on relative CBV_{MR} maps guided by regions that were hyperintense on DWI. Critically hypoperfused tissue was defined as the PWI lesion with a Tmax > 6s. Ischemic core was defined by the DWI or CBV_{MR} volume. Mismatch was defined as PWI (Tmax > 6s)/core ≥1.2 and an absolute mismatch volume ≥10ml. Correlation between CBV_{MR} and DWI lesion volumes among all cases was excellent (r2=0.89). However, in the subgroup of patients with small lesions (DWI <= 10ml) the correlation was poor (r2=0.20). All correlations were statistically significant ($p < 0.001$).

Using the PWI/DWI mismatch pattern as reference, the sensitivity of the $Tmax/CBV_{MR}$ approach was 0.98 and specificity was 0.76. The $Tmax/CBV_{MR}$ mismatch resulted in 90 true positive, 31 true negative, 10 false positive and 2 false negative results. The study represents an optimized scenario as MR imaging artifacts were excluded; under these circumstances the DWI and CBV lesion volumes correlate strongly for large but not for small lesions. The findings imply that DWI is superior to CBV_{MR} for detecting the early ischemic core.

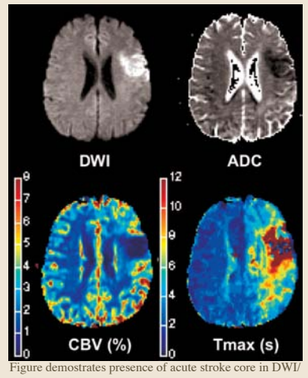

Figure demostrates presence of acute stroke core in DWI/ADC and CBV_{MR} maps. The Tmax map shows critically underperfused tissue that might be possible to salvage.

REFERENCES/FUNDING SOURCE

Submitted to International Stroke Conference 2010, San Antonio, TX, USA, Feb 23-26, 2010
Funding: Anonymous philantropist

BOLUS PERFUSION-WEIGHTED IMAGING MEASUREMENT OF QUANTITATIVE CEREBRAL BLOOD FLOW CAN BE IMPROVED USING AN ARTERIAL SPIN LABEL DERIVED SCALING FACTOR: A COMPARATIVE XENON CT STUDY

G. Zaharchuk[1], M. Straka[1], A. Shankaranarayan[2], D. C. Alsop[3], M. E. Marks[1], M. E. Moseley[1], and R. Bammer[1]
Depts of [1]Radiology, [2]Neurology, Stanford University, Stanford, CA; [3]Appled Sciences Laboratory-West, GE Healthcare, Menlo Park, CA; [4]Department of Radiology, Beth Israel Deaconess Hospital, Boston, MA

Bolus dynamic susceptibility contrast (DSC) perfusion-weighted imaging (PWI) and arterial spin labeling (ASL) are two methods of measuring cerebral blood flow (CBF) using MRI. Each has different strengths and weaknesses. ASL CBF levels are reliable in high flow regions, but suffer from errors and low SNR in regions with long arterial arrival times. PWI, particularly when using delay-invariant deconvolution, is in theory unaffected by long arrival times. However, absolute quantitation is challenging, due to uncertainties in AIF & VOF partial volume and the nonlinear relationship between transverse relaxivity and contrast concentration. This study describes a method that uses ASL CBF measurements in regions with short transit delays (as measured by Tmax) to scale PWI CBF measurements. Stable xenon CT was used as a gold standard for CBF. Practically, a single global scaling factor will never improve correlation within an individual patient. Also, the upper limit of the improvement in between-patients correlation is set by the accuracy of ASL. However, specifically in regions with long Tmax, we found improved CBF correlation for corrected bolus PWI compared to either uncorrected PWI or ASL CBF. While we used a 6 min high resolution ASL sequence as this is part of our standard imaging, in principle, much lower resolution ASL CBF maps with shorter acquisition times could be obtained, since the scaling factor is determined from a relatively large volume of tissue.

We conclude that the combined ASL-PWI method is superior to either method alone for measuring quantitative CBF with MRI.

REFERENCES/FUNDING SOURCE

G. Zaharchuk, M. Straka, A. Shankaranarayan, D. C. Alsop, M. E. Marks, M. E. Moseley, and R. Bammer. Bolus Perfusion-Weighted Imaging Measurement Of Quantitative Cerebral Blood Flow Can Be Improved Using An Arterial Spin Label Derived Scaling Factor: A Comparative Xenon CT Study. Proceedings of the ISMRM, 2009, Honolulu Hawaii.
NIH (2R01EB002711, 1R21EB006860, P41RR09784, PERFUSE), the Lucas foundation, and the Oak foundation.

STEADY-STATE FREE PRECESSION (SSFP) DIFFUSION IMAGING USING 3D ROTATING SPIRALS (3DRS)

J. Zhang[1,2], C. Liu[1], and M. E. Moseley[1]
Depts of [1]Radiology, [2]Electrical Engineering, Stanford University, CA

Although signal in SSFP-DWI is composed of both spin echo and multiple stimulated echoes, experiments have shown that motion induced artifacts in SSFP-DWI can still be reduced by correcting navigated phase errors or averaging multiple DWI scans. In this work, we will present a SSFP 3D rotating spiral (3DRS) method for fast DWI and diffusion tensor imaging (DTI) acquisition, which is based on our previously reported 3D-SNAILS technique [1]. By combining SSFP-DWI and 3DRS readouts in this approach, high quality diffusion weighted volumes can be rapidly acquired with very high SNR efficiency and low sensitivity to motion artifacts. One key result of the proposed auto-calibrated kSPA algorithm is that the reconstruction kernel can be computed using calibration data acquired at any location. To accomplish that we only need to translate the surrounding sampling points to center at a set of grid points in the middle of the calibration region. We then repeat the reconstruction for each coil to form the final image similar to the GRAPPA algorithm.

In this work, we have demonstrated the acquisition of diffusion-weighted whole brain volumes using a SSFP-3DRS sequence. Compared with other diffusion techniques, our approach can achieve much higher SNR with desired diffusion weighting and limited imaging time. The 3DRS sampling strategy also benefits from reduced sensitivity of subject motion. However, since only the 0th order phase error term can be extracted and corrected, images may still be contaminated by residual motion artifacts, especially for high b-values. A proper 3D navigator should help further improve the image quality, which is still under investigation. Furthermore, with its high SNR efficiency, SSFP-3DRS can be feasibly applied to acquire DTI volumes under even higher resolution, which is usually desirable for tractography.

REFERENCES/FUNDING SOURCE

Zhang J, Liu C, Moseley ME. Steady-State Free Precession (SSFP) Diffusion Imaging Using 3D Rotating Spirals (3DRS). Proceedings of the ISMRM, 2009, Honolulu Hawaii.
NIH-1K99NS057943, Lucas Foundation, and NCRR P41RR09784

HIGH-RESOLUTION, FAT-SUPPRESSED, DIFFUSION-WEIGHTED MRI OF THE BREAST USING A SELF-NAVIGATED MULTI-SHOT TECHNIQUE

W. B. Veldhuis[1], C. Liu[1], R. Bammer[1], B. L. Daniel[1], and M. E. Moseley[1]
[1]Department of Radiology, Stanford University, CA

For breast MRI, with increasing resolution the readout time for conventional single-shot MR lengthens to the point that blurring and geometric distortions impair image acquisition. The strong gradients needed for diffusion-weighting (DW) worsen this problem. Parallel imaging can partially reduce these distortions, which was recently shown for breast MRI, using ASSET. Another approach is to use a multishot technique, such as SNAILS: a fat-saturated twice-refocused spin echo sequence with an analytically designed interleaved variable-density spiral readout trajectory, which has been applied successfully to high-resolution DWI in the brain. We assess its technical feasibility in the body, for breast MRI, and compare it to ASSET-DW-EPI in healthy volunteers to show ASSET-EPI and SNAILS diffusion-weighted images.

Even with ASSET, DW-EPI was not possible at a 256x256 matrix size. SNAILS allowed distortion free acquisition of 256x256 resolution images. In addition, the high resolution and relative insensitivity to motion of SNAILS, allowed for high quality multiplanar reformats with the 'PET-like' contrast-reversal now popular in DWI screening studies.

For SNAILS there was no significiant difference in ADC values measured at 256x256 or at 128x128 matrix size. For DW-EPI ADC values could not be reliably determined at 256x256 matrix size; The values obtained with DW-EPI at 128x128 resolution fall within the range of values reported in the literature, which vary mainly with varying b-value. The results suggest that with identical prescribed b-values, difference in sequence design can cause within-subject variation of ADC values. We conclude that free-breathing, high-resolution DWI of the breast using SNAILS, is feasible at clinically available gradient-strengths, within reasonable acquisition times.

REFERENCES/FUNDING SOURCE

B. Veldhuis, C. Liu, R. Bammer, B. L. Daniel, and M. E. Moseley. High-Resolution, Fat-Suppressed, Diffusion-Weighted MRI Of The Breast Using A Self-Navigated Multi-Shot Technique. Proceedings of the ISMRM, 2009, Honolulu Hawaii.
Lucas Foundation, NCRR P41RR09784, KWF - Dutch Cancer Society, and NIH-5K99EB007182-02

DIAGNOSTIC ACCURACY OF HIGH-RESOLUTION MULTI-SHOT DIFFUSION-WEIGHTED MRI FOR THE DETECTION OF BREAST CANCER

W. B. Veldhuis[1], C. Liu[1], Y. Do[1], M. E. Moseley[1], and B. L. Daniel[1]
Dept of [1]Radiology, Stanford University, CA

Diffusion-weighted imaging (DWI) may provide information - physically unrelated to microvascular changes detected by contrast-enhanced MRI - that can improve the specificity of MRI for breast cancer diagnosis. Attempts thus far to benefit from the information content that DWI may offer have been limited by the use of single-shot techniques, with inherent sensitivity to geometric distortions and limitations in detected lesion size. The aim of this HIPAA-compliant, IRB-approved study was to compare the sensitivity and specificity of high-resolution DWI of the breast to 'conventional' dynamic-contrast enhanced MRI, and to pathology. We performed a retrospective analysis of diffusion-weighted data sets acquired in 103 consecutive women (mean age 50.3 years, range: 15-81) undergoing 1.5T MRI for the evaluation of breast cancer. Pathological confirmation was obtained for all but one of the lesions marked as 'suspicious' on ftADC. As expected, the sensitivity of DCE-MRI was very high, with a lower specificity. The specificity of blind DWI- and especially of the blind ftADC-analysis, was much higher. The present data suggest that a contrast-free MRI-protocol, that includes DW imaging, may have a clinically acceptable diagnostic performance. This is relevant in light of recent issues with gadolinium-induced nephrogenic systemic fibrosis, and may also be relevant to discussions on breast cancer screening with MRI. Lastly, we are aware that the conventional breast imaging protocol will include contrast-enhanced-sequences for some time to come. However, even with such a protocol, patients may still benefit from a diagnosis-modifying effect – in terms of up- or down-staging – of adding ftADC-maps to the analysis. For the current data set, retrospective addition of ftADC-mapping resulted in the correct downstaging of 22 of 65 pathology-verified lesions (data not shown). Large, multi-center validation will have to precede actual clinical implementation of this technique.

REFERENCES/FUNDING SOURCE

W. B. Veldhuis, C. Liu, Y. Do, M. E. Moseley, and B. L. Daniel. Diagnostic Accuracy Of High-Resolution Multi-Shot Diffusion-Weighted MRI For The Detection Of Breast Cancer. Proceedings of the ISMRM, 2009, Honolulu Hawaii.
Lucas Foundation, NCRR P41RR09784, KWF - Dutch Cancer Society, and NIH-5K99EB007182-02

BENIGN-MALIGNANT LESION DIFFERENTIATION USING FUNCTIONAL ADC-THRESHOLDING – ALLOWING EXPERT RADIOLOGIST INTERPRETATION – VERSUS CONVENTIONAL THRESHOLDING BASED ON ADC CUT-OFF VALUES

W. B. Veldhuis[1], C. Liu[1], Y. Do[1], T. J. Brosnan[1], M. E. Moseley[1], and B. L. Daniel[1]
Dept of [1]Radiology, Stanford University, CA

Diffusion-weighted imaging (DWI) may aid in the discrimination of benign from malignant (breast) lesions. Approaches to benefit from the information contained in the DWI dataset have mostly been based on trying to define a cut-off value for the lesion ADC. This may be limiting because of the relatively low SNR, the relatively high variability of lesion ADC - even within one hospital or patient population - and the limited potential of the results to be extrapolated to different field strengths, pulse-sequences or b-values. We used an approach in which the high CNR of DWI and the quantitative information of the ADC are presented to the radiologist in a "functionally-thresholded ADC (ftADC) map" that increases the conspicuity of lesions of interest, much like phase-images are used to increase vascular conspicuity in susceptibility-weighted imaging. Radiologists can "window-level" ftADC-maps at their discretion and diagnose a lesion as "ftADC-bright" without having to choose an ADC-threshold value; Similar to, for example, a cystic lesion being interpreted as "T2-bright" without using T2-cut-off values. We performed a retrospective, HIPAA-compliant, IRB-approved analysis of DW data sets of 103 consecutive women who underwent 1.5T MRI for the evaluation of breast cancer. Conventional ADC-thresholding was compared to ftADC-mapping and to dynamic contrast-enhanced (DCE) MRI, for all pathology-verified lesions.

The results confirm that lower ADCs are correlated with a higher chance of a malignant diagnosis, but that the discriminatory power of setting an ADC cut-off value – evaluated using ROC curves – is low. In addition, attempts to reduce variability by within-patient normalization of lesion ADC to muscle ADC are shown to be unsuccessful. ftADC-mapping may improve lesion discrimination in (breast) MRI. In theory, after large-scale validation of the results, a significant number of patients could be downstaged from BIRADS-3 and possibly even from BIRADS-4, to a benign diagnosis, and thus be spared a biopsy.

REFERENCES/FUNDING SOURCE

W. B. Veldhuis1, C. Liu1, Y. Do1, T. J. Brosnan1, M. E. Moseley1, and B. L. Daniel1. Benign-Malignant Lesion Differentiation Using Functional ADC-Thresholding – Allowing Expert Radiologist Interpretation – Versus Conventional Thresholding Based On ADC Cut-Off Values. Proceedings of the ISMRM, 2009, Honolulu Hawaii.
Lucas Foundation, NCRR P41RR09784, KWF - Dutch Cancer Society, and NIH-5K99EB007182-02

ESTIMATION OF CBF VALUES USING MULTI-ECHO DSC-MRI: A COMPARISON WITH A XENON CT

M. Straka[1], G. Zaharchuk[1], RD. Newbould[2], GW. Albers[3], ME. Moseley[1], and R. Bammer[1]
Depts of [1]Radiology, [2]Electrical Engineering, [3]Stanford Stroke Center, Stanford University, CA

Spatial distortions in EPI sequences and clipping of vascular signals during bolus passage peak a scanning sequence for perfusion with multiple echoes and temporal enhancement (PERMEATE) was developed, in which the confounding artifacts should be reduced. Data acquired with first (short) echo should be used to properly recover the vascular signals, whereas the later echoes are used to determine signals in the tissue manifesting better signal-to-noise ratio therein. Such state-of-the-art perfusion acquisition is complemented by a PWI post-processing pipeline, including correction for partialvolume effect (PVE) in vascular signals and susceptibility effect of the paramagnetic tracer in large vessels. The purpose of this study was to evaluate the benefits of such advanced acquisition scheme with the PVE and bulk-blood corrections and to quantify the improvement of values in the computed quantitative perfusion maps.In this work, we have demonstrated the acquisition of diffusion-weighted whole brain volumes using a SSFP-3DRS sequence. Compared with other diffusion techniques, our approach can achieve much higher SNR with desired diffusion weighting and limited imaging time. The 3DRS sampling strategy also benefits from reduced sensitivity of subject motion. However, since only the 0th order phase error term can be extracted and corrected, images may still be contaminated by residual motion artifacts, especially for high b-values. A proper 3D navigator should help further improve the image quality, which is still under investigation. Furthermore, with its high SNR efficiency, SSFP-3DRS can be feasibly applied to acquire DTI volumes under even higher resolution, which is usually desirable for tractography.

REFERENCES/FUNDING SOURCE

M. Straka, G. Zaharchuk, RD Newbould, GW Albers, ME Moseley, and R Bammer. Estimation of CBF Values Using Multi-Echo DSC-MRI: a Comparison with a Xenon CT. Proceedings of the ISMRM, 2009, Honolulu Hawaii.

ARTERIAL SPIN LABEL CBF MAPS CAN SHOW ABNORMALITIES IN CLINICAL PATIENTS WITH NORMAL BOLUS PERFUSION-WEIGHTED IMAGING: IDENTIFICATION OF THE "WATERSHED SIGN"

G. Zaharchuk[1], A. Shankaranarayan[2], R. Bammer[1], M. Straka[1], D. C. Alsop[3], N. J. Fischbein[1], S. W. Atlas[1], and M. E. Moseley[1]
Dept of [1]Radiology, Stanford University, CA; [2]Appled Sciences Laboratory-West, GE Healthcare, Menlo Park, CA; [3]Dept of Radiology, Beth Israel Deaconess Hospital, Boston, MA

Bolus perfusion-weighted imaging (PWI) and arterial spin labeling (ASL) are two popular methods to evaluate hemodynamic abnormalities in a wide range of cerebrovascular diseases. ASL is very sensitive to prolonged arterial arrival times, since the label decays with blood T1. This increased sensitivity may differentiate between truly normal hemodynamics and mild/bilateral abnormalities of CBF and arrival time. This study examines whether additional findings are seen on ASL images in patients with normal PWI.

3D FSE background-suppressed pcASL [5] has reasonable SNR, reduced motion sensitivity, and improved performance in high susceptibility regions compared with EPI readout methods, making it a promising ASL method at 1.5 T. This study shows that additional information relating to perfusion can be identified using ASL in patients with normal bolus PWI. We believe that the watershed sign is a reflection of either (a) longer than normal arrival times, (b) lower CBF, or (c) a combination of both. In theory, bolus PWI parameters such as Tmax should be sensitive to arterial arrival delays, though only those greater than or equal to the repetition time of the EPI sequence, which in our study ranged between 1.225 and 2 s; by definition, this was not observed in our patients who had normal PWI. Based on our findings, we recommend the supplemental use of ASL imaging in all cases of suspected or known cerebrovascular disease.

REFERENCES/FUNDING SOURCE

G. Zaharchuk, A. Shankaranarayan, R. Bammer, M. Straka, D. C. Alsop, N. J. Fischbein, S. W. Atlas, and M. E. Moseley. Arterial Spin Label Cbf Maps Can Show Abnormalities In Clinical Patients With Normal Bolus Perfusion-Weighted Imaging: Identification Of The "Watershed Sign". Proceedings of the ISMRM, 2009, Honolulu Hawaii.
NIH (2R01EB002711, 1R21EB006860, P41RR09784, PERFUSE), the Lucas foundation, and the Oak foundation.

TOWARD 0-NORM RECONSTRUCTION BY CONVEX ITERATION

C. Law[1,2], G. Glover[1]
Depts of [1]Radiology, RSL, [2]Electrical Engineering, Stanford University, CA

Introduction. We repeat Candès' image reconstruction experiment [1] which led to discovery of sparse sampling theorems. But we achieve perfect reconstruction with an algorithm based on vanishing gradient of the compressed sensing problem's Lagrangian; empirically computes faster than contemporary methods because

1. we formulate the problem as contraction which is solved efficiently by conjugate gradient method,
2. matrix multiplications are replaced by FFT, and
3. the number of constraints is cut in half by sampling symmetrically.

Theory. Denoting an unknown image $u \in R^{n \times n}$, total variation operator $\Psi \in R^{4n^2 \times n^2}$, inverse Fourier transform of incomplete k-space sample operator P, and aliased image f. The optimization problem to recover an unknown image by cardinality minimization is

$$\underset{u}{\text{minimize}} \ \|\Psi \operatorname{vec} u\|_0 \quad \text{subject to} \quad P \operatorname{vec} u = f \quad (1)$$

Problem (1) is hard to solve. The common approach is to replace 0-norm by 1-norm. When enough samples are taken, 1-norm yields results identical to a 0-norm formulation. [2] Instead of 1-norm, we introduce a direction vector y as part of a convex iteration method [3] [4] that requires fewer samples than 1-norm while optimal solution more closely approaches a 0-norm result: i.e., there exists a vector , such that (1) is equivalent to a Lagrangian form

$$\underset{u}{\text{minimize}} \ \left|\left\langle \Psi \operatorname{vec} u, y^* \right\rangle\right| + \frac{1}{2}\lambda \|P \operatorname{vec} u - f\|_2^2 \quad (2)$$

Direction vector y is initialized to $\mathbf{1}$ until the fixed point is found; i.e. the first sequence of contractions calculates solution .

Vector y is updated according to cardinality estimate c :

$$\sum_{i=c+1}^{4n^2} \pi\left(\left|\Psi \operatorname{vec} u^*\right|\right)_i = \underset{y \in R^{4n^2}}{\text{minimize}} \ \left\langle \left|\Psi \operatorname{vec} u^*\right|, y \right\rangle \quad \text{subject to} \quad 0 \prec y \prec 1, \quad y^T 1 = 4n^2 - c \quad (3)$$

where sorting operator π provides sum of the $4n^2-c$ smallest entries of the objective. Problems (2) and (3) are iterated until convergence.

Results. Figure 1 shows aliasing of phantom resulting from 4.1% (10 lines) k-space subsampling (Fig.2).

Reconstruction (Fig.3) with error = -104dB and run-time = 96s.

Discussion. Perfect reconstruction of the Shepp-Logan phantom is quickly achieved with 4.1% subsample data. Because reconstruction approaches optimal solution to a 0-norm problem, minimum number of Fourier-domain samples is bounded below by cardinality of the image-gradient at 1.9%.

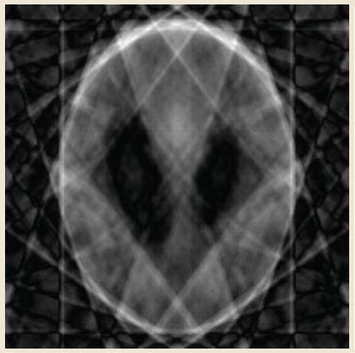

Figure 1. Aliasing of Shepp-Logan phantom.

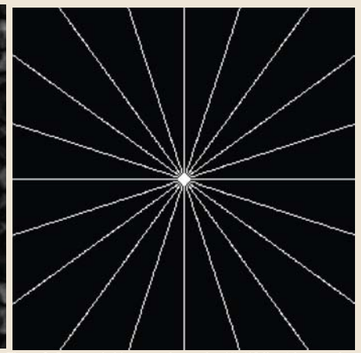

Figure 2. Symmetric binary mask samples 4% (10 lines) k-space data.

Figure 3. Reconstructed image, error = -104dB.

REFERENCES/FUNDING SOURCE

[1] Candès et al. IEEE Trans. Info Theory, 52(2):489, 2006.
[2] Donoho. IEEE Trans. Info Theory, 52(4):1289,2006.
[3] Dattorro. Convex Optimization & Euclidean Distance Geometry. Meboo, 2005.
[4] Chretien. An alternating l1 approach to the compressed sensing problem, arxiv.org/PS cache/arxiv/pdf/0809/0809.0660v1.pdf
P41 RR009784, Lucas Foundation, GEMS.

RELATIONSHIP BETWEEN RESPIRATION, END-TIDAL CO2, AND BOLD SIGNALS IN RESTING-STATE FMRI

C. Chang[1,2] and G. Glover [1,2]
Depts of [1]Electrical Engineering and [2]Radiology

A significant component of BOLD fMRI physiological noise is caused by variations in the depth and rate of respiration. It has previously been demonstrated that a breath-to-breath metric of respiratory variation (respiratory volume per time; RVT), computed from pneumatic belt measurements of chest expansion, has a strong linear relationship with resting-state BOLD signals across the brain. RVT is believed to capture breathing-induced changes in arterial CO_2, which is a cerebral vasodilator; indeed, separate studies have found that spontaneous fluctuations in end-tidal CO_2 ($PETCO_2$) are correlated with BOLD signal time series. The present study quantifies the degree to which RVT and $PETCO_2$ measurements relate to one another and explain common aspects of the resting-state BOLD signal. It is found that RVT (particularly when convolved with a particular impulse response, the "respiration response function") is highly correlated with $PETCO_2$, and that both explain remarkably similar spatial and temporal BOLD signal variance across the brain. In addition, end-tidal O_2 is shown to be largely redundant with $PETCO_2$. Finally, the latency at which $PETCO_2$ and respiration belt measures are correlated with the time series of individual voxels is found to vary across the brain and may reveal properties of intrinsic vascular response delays.

REFERENCES/FUNDING SOURCE

Chang, C. and Glover, GH. Relationship between respiration, end-tidal CO2, and BOLD signals in resting-state fMRI. NeuroImage 47:1381-93 (2009).
NIH F31-AG032168 to CC and P41-RR09784 to GHG.

PATTERN SEPARATION AND GENERALIZATION IN THE HUMAN HIPPOCAMPUS

V A Carr[1], R K Olsen[1], and A D Wagner[1]
Dept of [1]Psychology, Stanford University, CA

The hippocampus is thought to engage in processes which amplify differences in cortical input patterns, facilitating the rapid formation of unique memory representations. However, the hippocampus is composed of several subfields which may contribute differently to such pattern separation processes. Extant animal research suggests that activity patterns in the dentate gyrus and CA3 readily differentiate between similar contexts, whereas activity patterns in CA1 generalize across similar contexts. Using high-resolution fMRI of the hippocampus, we examined whether these findings translated to the healthy human brain. While being scanned, participants viewed a series of objects as follows: three repetitions of the same object followed by either a fourth repetition of that object, an object with high similarity to the original object, an object with moderate similarity, or an unrelated object. Given previous evidence of repetition suppression in the hippocampus, we hypothesized that trials in which the same stimulus was repeated four times would lead to attenuated BOLD signal relative to trials ending with presentation of an unrelated object. Of specific interest were differences in activity patterns among hippocampal subfields for trials ending with presentation of an object with high to moderate similarity to the original object. Based on the above-mentioned animal findings, we hypothesized that repetition suppression would not be observed for such trials in the dentate gyrus and CA3 due to coding of the new, similar object as different from the original object. Conversely, in area CA1 we expected to see graded repetition suppression with respect to high and moderate levels of stimulus similarity, such that this region would generalize the new stimulus as being the same as the original stimulus. Data collection and analyses are ongoing at this time, but preliminary findings support functional heterogeneity among hippocampal subfields in supporting pattern separation vs. generalization.

REFERENCES/FUNDING SOURCE

NARSAD PTA: 1097313-100-UAWAC

EFFECTS OF MODEL-BASED PHYSIOLOGICAL NOISE CORRECTION ON DEFAULT MODE NETWORK ANTI-CORRELATIONS

C Chang[1,2] and G Glover[1,2]
Depts of [1]Electrical Engineering and [2]Radiology

Previous studies have reported that the spontaneous, resting-state time course of the default-mode network is negatively correlated with that of the "task-positive network", a collection of regions commonly recruited in demanding cognitive tasks. However, all previous studies have employed some form of normalization or regression of the whole-brain average signal ("global signal"); these processing steps alter the time series of voxels in an uninterpretable manner as well as introduce spurious negative correlations. Thus, the extent of negative correlations with the default mode network without global signal removal has not been well characterized, and it is has recently been hypothesized that the apparent negative correlations in many of the task-positive regions could be artifactually induced by global signal pre-processing. The present study aimed to examine negative and positive correlations with the default-mode network when model-based corrections for respiratory and cardiac noise are applied in lieu of global signal removal. Physiological noise correction consisted of (1) removal of time-locked cardiac and respiratory artifacts using RETROICOR (Glover et al., 2000), and (2) removal of low-frequency respiratory and heart rate variations by convolving these waveforms with predetermined transfer functions (Birn et al., 2008; Chang et al., 2009) and projecting the resulting two signals out of the data. It is demonstrated that negative correlations between the default-mode network and regions of the task-positive network are present in the majority of individual subjects both with and without physiological noise correction. Physiological noise correction increased the spatial extent and magnitude of negative correlations, yielding negative correlations within task-positive regions at the group level. Furthermore, physiological noise correction caused region-specific decreases in positive correlations within the default-mode network, reducing apparent false positives.

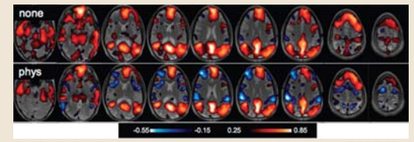

Positive (red) and negative (blue) correlations with the precuneus/PCC ROI, thresholded at |r|>0.15. Maps depict correlation coefficients for one subject (A) before correction ("none"), and (B) after physiological noise correction ("phys").

REFERENCES/FUNDING SOURCE

Chang, C. and Glover, GH. Effects of model-based physiological noise correction on default mode network anti-correlations and correlations. NeuroImage 47:1448-59 (2009)
NIH F31-AG032168 to CC and P41-RR09784 to GHG

Mechanisms of Analgesic Response during IV lidocaine Infusions in Neuropathic Pain Patients

N Chatterjee[1], S Mackey[1], W Peterson[1], R Moulton[1], M Tieu[1], I Carroll[1]
Dept of [1]Anesthesia, Stanford Systems Neuroscience and Pain Lab, Stanford University, CA

Introduction: For millions of Americans with neuropathic pain even a light touch hurts. This symptom is called mechanical allodynia. Our understanding of the neurophysiology underlying mechanical allodynia, and how sodium channel blockers relieve it, remains incomplete. With this case study of a single subject with neuropathic pain, we aim to elucidate the brain systems mediating mechanical allodynia, and the analgesic changes induced by the sodium channel blocker lidocaine.

Methods: One subject with mechanical allodynia in the right foot was recruited. An FSPGR sequence was used for anatomical reference. fMRI scans of the patients were conducted while receiving brush stimulation for 40 sec on and 30 sec off in a seven minute block design. The subject was first brushed in an area not affected by mechanical allodynia. For the remaining three scans, the subject was brushed in the area affected by allodynia, first while receiving no infusion, again while receiving a saline placebo, and finally while given intravenous lidocaine.

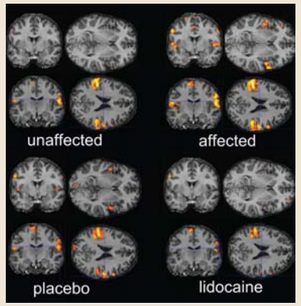

Figure 1

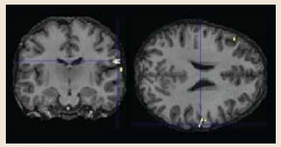
Figure 2

An anesthesiologist was present for the entire session. The resulting data was analyzed using SPM5.

Results: Each condition showed activation in the contralateral sensory cortex (SI), and brushing of the affected area showed additional activation on the ipsilateral side ($p<.05$ FWE corrected) (Fig 1). After administering placebo, activation was decreased in multiple areas including the sensory cortex. Administering intravenous lidocaine lead to further activation decreases in these areas and also decreased activity in the secondary sensory cortex (SII) (Fig2).

Conclusions: We have demonstrated in a single subject that cortical activation during mechanical stimulation of allodynia greatly reduced by the administration of intravenous lidocaine. In addition to further deactivating systems associated with the placebo response, lidocaine also elicited deactivation of SII. This suggests that SII activity plays an important role in the analgesic effects of lidocaine.

References/Funding Source

Presented at the 2009 Organization for Human Brain Mapping conference
This study was supported by a Mentored Research Training grant from the Foundation for Anesthesia Education and Research (FAER)

Using DTI-Based Fiber Tracking to Characterize Diffuse Perinatal White Matter Injury

J Yeatman[1], M Ben-Shachar[2,3], R Bammer[4], and H Feldman[1]
Depts of [1]Pediatrics, [3]Psychology, [4]Radiology, Stanford University, CA; Dept of [2]Linguistics and Gonda Brain Research Center, Bar-Ilan University, Israel

Prematurity is associated with white matter injury. Diffusion Tensor Imaging (DTI), a new magnetic resonance imaging technique, identifies white matter fiber tracts and quantifies structural properties. We used DTI-based fiber tracking to compare white matter characteristics in a 12-year-old born prematurely and full-term control. We divided fibers passing through the corpus callosum into seven segments based on cortical projection zones and analyzed them for fractional anisotropy, axial diffusivity, and radial diffusivity. We also compared corticospinal and somatosensory tracts in the subject and control. The subject had decreased factional anisotropy in every callosal segment, particularly in superior and posterior parietal projections. Fractional anisotropy of the corticospinal and somatosensory tracts was not lower in the subject than control. DTI-based fiber tracking allowed precise localization and visualization of white matter injuries of the corpus callosum associated with prematurity. Quantitative DTI measures suggested myelin deficiencies across the corpus callosum, particularly in parietal projections.

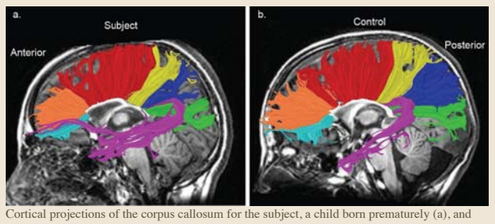

Cortical projections of the corpus callosum for the subject, a child born prematurely (a), and a control (b), based on procedures from Dougherty et al 11. Segement (color code): occipital (green), posterior parietal (blue), superior parietal (yellow), superior frontal (red), anterior frontal (orange), orbital (cyan), and temporal (purple).

References/Funding Source

Yeatman JD, Ben-Shachar M, Bammer R, Feldman HM. Using diffusion tensor imaging and fiber tracking to characterize diffuse perinatal white matter injury: a case report. J Child Neurol. 2009;24:795-800.
National Institutes of Health, Eunice Kennedy Shriver National Institute of Child Health and Human Development, RO1 HD046500

White Matter Alterations of the Fusiform Gyrus in Williams Syndrome: A Diffusion Tensor Tractography Study

B W Haas[1], F Hoeft[1], U Bellug[2], A L Reiss[1]
Dept of [1]Psychiatry & Behavioral Sciences, Stanford University, CA; [2]Laboratory for Cognitive Neuroscience, Salk Institute for Biological Studies, San Diego, CA

Williams syndrome (WS) is a genetic disorder caused by a hemizygous microdeletion on chromosome 7q11.23. WS is associated with a compelling symptom profile characterized by relative deficits in visiospatial function and relative strengths in face and language processing. Recently, functional brain imaging research in WS has demonstrated that regions such as fusiform gyrus exhibit abnormal levels of activation during face processing compared to typically developing (TD) controls. It is unknown however, if white matter projecting from the fusiform gyrus may also be aberrant in WS. Based on behavioral research demonstrating that WS is associated with atypical face processing and functional brain imaging research demonstrating abnormal activation in the fusiform gyrus, we predicted that white matter projections from the fusiform gyrus would be altered in WS. In this study, twenty individuals underwent magnetic resonance imaging. Each participant was imaged using a high resolution spoiled gradient-recalled (SPGR) sequence as well as a diffusion weighted sequence with a total of 13 directions. The left and right fusiform gyrus was delineated for on each participant's SPGR image using a standardized protocol. Results indicated that the WS group exhibited smaller total volumes of left and right fusiform gyrus compared to the TD group. However, the WS group exhibited higher FA of fibers projecting from the left and right fusiform gyrus compared to the TD group. Additionally, the WS group exhibited a greater amount of total white matter reconstructed fibers projecting from the left and right fusiform gyrus. The differences between the WS and TD groups in FA and the number of reconstructed fibers remained significant after controlling for the total volume of each seed ROI. Combined, these results provide a white matter structural correlate to heightened or preserved face processing in WS.

References/Funding Source

Haas, B.W., Hoeft, F., Bellugi U., Reiss, A.L. White Matter Alterations of the Fusiform Gyrus in Williams Syndrome: A Diffusion Tensor Tractography Study. Human Brain Mapping Abstracts, 15, San Francisco, CA.
NICHD Grant P01 HD033113-12Genentech 403-C03 (M4354S)

Heightened Fusiform Gyrus and Amygdala Functional Connectivity during emotional face processing in Williams Syndrome

B W Haas[1], F Hoeft[1], U Bellug[2], A L Reiss[1]
Dept of [1]Psychiatry and Behavioral Sciences, Stanford University, CA; [2]Laboratory for Cognitive Neuroscience, Salk Institute for Biological Studies, CA

Williams syndrome (WS) is a genetic disorder caused by a hemizygous microdeletion on chromosome 7q11.23. WS is associated with a compelling symptom profile characterized by relative deficits in visiospatial function and relative strengths in face and language processing. Interestingly, WS is also characterized as being associated with a heightened drive towards social engagement. Recent brain imaging studies have demonstrated atypical fusiform gyrus and amygdala response to emotional stimuli in WS. However, emotional processing is extremely complex and involves a large neural network including the functional connections between the fusiform gyrus, amygdala and other brain structures. Based on the established social/emotional phenotype of WS, we predicted that the functional connectivity within this network would be aberrant in WS during emotional face processing. We used fMRI to study a sample of WS and typically developing (TD) participants who performed a gender discrimination task of emotional facial expressions (happy, fearful and neutral). The WS sample exhibited greater functional connectivity between the fusiform gyrus and medial prefrontal cortex compared to the TD sample during emotional face processing (both happy and fearful). The WS sample also exhibited greater functional connectivity between the amygdala and prefrontal cortex during happy face processing compared to the TD sample. These findings provide evidence that abnormal social/emotional processing in WS is in part due to atypical functional connectivity between a network of brain structures.

References/Funding Source

Haas, B.W., Hoeft, F., Bellugi, U., Reiss, A.L. (2009). Heightened Fusiform Gyrus and Amygdala Functional Connectivity during emotional face processing in Williams syndrome. Cognitive Neuroscience Annual Meeting. San Francisco, CA
NICHD Grant P01 HD033113-12Genentech 403-C03 (M4354S)

Investigating source memory decisions via reinstated mnemonic evidence: An fMRI pattern analysis study

A M Gordon,[1], J Rissman[1], and A D Wagner[1,2]
Dept of [1]Psychology and [2]Neurosciences Program, Stanford University, CA

Source memory decisions, like perceptual decisions, require the weighing of evidence in relation to decision criteria. At present, the neural mechanisms subserving memory-based evidence accumulation en route to source decisions remain underspecified. Here, we used multivoxel pattern analysis of fMRI data to examine how reinstated patterns of encoding activation (i.e., mnemonic evidence) relate to source memory decisions. During each source encoding trial, subjects encountered an adjective and generated either a face or scene described by that adjective, thus giving rise to patterns of neural activity associated with word-face or word-scene processing. During each retrieval trial, subjects were re-presented with the words encountered in the encoding phase and were asked to recollect which of the two sources (face or scene) they had associated with each word. Using the encoding fMRI data, a multivoxel pattern classifier was trained to distinguish patterns of distributed BOLD activity associated with the two encoding tasks. The encoding-trained classifier was then presented with the BOLD data from the retrieval task, enabling not only a test of classifier accuracy but also a quantitative measure of the degree to which evidence for the face and scene encoding patterns were present during each retrieval trial. Initial analyses (N=4) revealed (a) above-chance classification accuracy of the retrieval data using an encoding-data trained classifier, indicating that source memory decision making involves reinstatement of source-specific encoding patterns, and (b) activation in frontal and parietal cortical regions that was sensitive to the degree of absolute reinstated mnemonic evidence during decision-making.

References/Funding Source

Gordon, A. M., Rissman, J., & Wagner, A.D. (2009) Investigating source memory decisions via reinstated mnemonic evidence: An fMRI pattern analysis study. Society for Neuroscience
National Institute of Mental Health (R01 MH080309)

Bound Pool Fractions Complement Diffusion Measurements in Characterizing White Matter Pathways

N Stikov[2], L Perry[2], J Pauly[1], R Dougherty[2], and Wandel1[2]
Depts of [1]Electrical Engineering and [2]Psychology, Stanford University, CA

We explore combining two quantitative MR contrast mechanisms in order to better understand the structure of white matter in the brain. Diffusion tensor imaging (DTI) can identify white matter fascicles and measure their diffusivity. The bound pool fraction (BPF) estimates the proportion of protons bound to macromolecules, such as myelin. We combine these two in order to obtain concurrent information about the direction, diffusivity, and myelin content of white matter tracts

The modest correlation between BPF and FA shows that these are relatively independent quantities that should be combined to provide a more complete insight into tissue microstructure. We compute the mean fractional anisotropy (FA) and mean bound pool fraction (BPF) along fiber tracts obtained using DTI tractography, and isolate the fibers with highest FA and BPF scores. We conclude that fiber tracts with high anisotropy do not necessarily have a high BPF. Hence, these tracts need not be heavily myelinated.

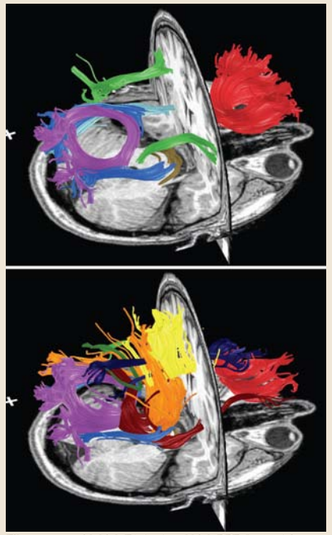

Fiber groups with high FA (top) and high BPF (bottom) in one subject. Most high-FA fibers pass through the corpus callosum. The high-BPF fibers also include several callosal fiber groups (anterior frontal, temporal and occipital), but high BPF also identifies several major fiber groups that do not have high FA, including the superior and inferior longitudinal fasciculi and the optic radiations.

References/Funding Source

Proceedings of the 15th Annual Meeting, Organization of Human Brain Mapping, San Francisco, June 2009
NIH Grant EY015000

Visual field coverage of human V4

J Winawer[1], R Sayres[1], H Horiguchi[1,2], K Amano[3], B A Wandell[1]
Dept of [1]Psychology, Stanford University, CA; Dept of [2]Ophthalmology, Jikei University, Tokyo, Japan; Dept. of [3]Complexity Sciences and Engineering, Univ. of Tokyo, Japan

Purpose: To resolve two claims about the fourth human visual field map, hV4. One claim is that hV4 covers a contiguous region of ventral cortex adjacent to ventral V3 (V3v), representing the entire contralateral visual hemifield (Wade et al, 2002). Others claim that hV4 is split, with the ventral portion excluding coverage of the lower vertical meridian, and a second portion adjacent to dorsal V3 representing the remaining lower field (Hansen et al, 2007).

Methods: We measured hV4 using model-based receptive field mapping (Dumoulin & Wandell, 2008). FMRI images were acquired while subjects viewed drifting checkerboards through a moving bar aperture. A 2D-Gaussian population receptive field was fit to each voxel that best predicted the time series.

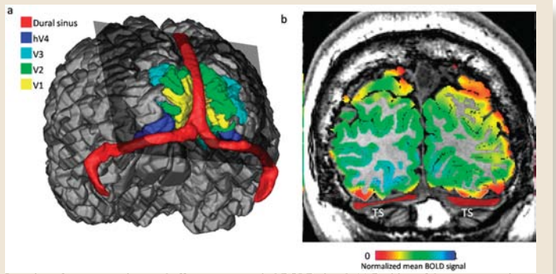

Location of transverse sinus and effect on mean spiral BOLD signal. (a) Position of the transverse sinus with respect to the cortical surface and several visual field maps. (b) Cross-sectional view as indicated on the mesh: The spiral mean-field map is significantly lower in the neighborhood of the TS (black outline, red shading) compared to other locations. The mean map intensity color scale is normalized to the minimum and maximum signal across all voxels. Regions affected by the TS tend to have unreliable time series and hence cannot be mapped confidently.

Results: We discovered a significant problem associated with measurements in ventral occipital cortex, particularly near hV4. In most hemispheres the hV4 BOLD data are contaminated by artifacts from the transverse sinus (TS); this large artifact is evident from inspection of the raw image data. In many cases, the TS artifact masks responses in the region of cortex that distinguishes the hV4 models. Whether hV4 covered the lower vertical meridian depended on the location of the TS artifact: When the TS was displaced from the lateral edge of hV4, the visual field coverage extended to the lower meridian, or nearly so, consistent with the hemifield model. In hemispheres in which the TS was further from hV4, the coverage was reduced, consistent with the split V4 model.

Discussion: BOLD imaging of the ventral surface is limited by TS artifacts. Subjects in which the TS effects are most remote from hV4 yield the most reliable measurements. In these subjects, hV4 represents all or most of the contralateral hemifield. The missing lower field representation in many subjects is likely due to limitations caused by this TS artifact.

References/Funding Source

Winawer, J, Sayres, R., Amano, K, Wandell, BA. Visual field coverage of human V4. Vision Sciences Society Annual Meeting (2009).
National Eye Institute Grant EY03164 (B.W.)

Evidence for development of face-selective cortex during adolescence

G Golarai[1], A Liberman[1], S Hong[1], J M D Yoon[1], K Grill-Spector[1,2]
Dept of [1]Psychology, [2]Neuroscience Institute, Stanford University, CA

Functional magnetic resonance imaging (fMRI) studies on adults have delineated a number of regions in the occipitotemporal cortex that preferentially respond to specific visual categories. Regions responding more to faces than objects are found in the fusiform gyrus (fusiform face area, FFA), the inferior lateral occipital cortex (IOG), and in the posterior superior temporal sulcus (pSTS). Regions responding more to places than objects are found in the collateral sulcus and parahippocampal gyrus, (parahippocamal place area, PPA). We recently found evidence for development of the FFA and PPA after age seven, manifesting as a substantial spatial expansion of these regions. However, it is not known if this development (i) continues into adolescence (ii) is specific to the FFA and PPA or occurs also in other regions (iii) depends on specific face or place stimuli. Adolescents (ages 12 – 16, n = 14) and adults (n = 11) underwent fMRI in a 3T scanner (3x3x3 mm) and viewed faces of men, boys, objects, scenes and scrambled images presented in pseudo-random ordered blocks. Using standard general linear methods (GLM), in each subject we defined several face-selective regions (*boys > objects*, p< 0.001, voxel level) in the fusiform gyrus (FFA), inferior occipital gyrus (IOG) and posterior superior temporal sulcus (STS). We also defined a place-selective region (PPA) in the parahippocampal gyrus *(scenes > objects, p< 0.001, voxel level)*. We found that the right FFA and IOG volume were significantly smaller in adolescents compared to adults. In contrast w e found no between group differences in the pSTS or PPA size. Furthermore, this development was independent of the age of face stimuli. These findings indicate the prolonged development of the FFA and IOG during adolescence, after the pSTS and PPA reach their adult-like size.

References/Funding Source

Golarai G, Liberman A, Yoon JMD and Grill-Spector K (2009). Evidence for development of face-selective and place-selective cortex during adolescence. Human Brain Mapping Annual Meeting, San Francisco.
NSF: BCS-0617688, NIH 1R21EY017741, Klingenstein Fellowship in Neuroscience

Structural and functional neuroanatomy of rapid naming, phonology and word identification

J M Black[1], M Nagamine[1], A L Reiss[1], F Hoeft[1]
[1]Center for Interdisciplinary Brain Sciences Research, Stanford University, CA

The double-deficit hypothesis (DD) posits that naming speed is an independent core deficit in addition to the phonological processing deficits seen in individuals with developmental dyslexia. According to this theory, individuals with a 'double-deficit' have more severe deficits in reading than those with single deficits or without any deficits. It is not yet clear, however, how these deficits are related to each other and to reading. Examination of the neural substrates of these processes may have substantial implications not only in understanding the DD, but also for the identification and treatment of reading disabilities. We therefore examined the relationship between morphometric and functional neuroanatomy and these skills. Participants were 62 children (age 13.5 + 2.6) representing a wide range of reading skills from severely impaired (meeting the criteria for dyslexia) to superior. A standard battery of neuropsychological assessment was given including rapid naming of letter and number (RAN) and real word identification (ID). In addition, we collected high-resolution MRI data to examine regional gray matter volume and functional magnetic resonance imaging (fMRI) data during a real word rhyme judgment task to examine phonological processing. Voxel-based morphometry (VBM) analyses identified overlapping regions that showed significant positive correlations with regional volume and RAN as well as ID in the left supramarginal, posterior superior temporal, precentral and inferior frontal gyri. Regions involving the cerebellum showed negative correlation. These regions also showed significant associations with fMRI activation during phonological processing. These findings suggest that these regions maybe critical in the DD.

References/Funding Source

Black, J.M., Nagamine, M., Reiss, A.L., Gabrieli, J.D.E., and Hoeft, F. Morphometric and Functional Neuroanatomy of Rapid Naming, Phonological processing and word identification in children with a wide range of reading ability: Implications for the double-deficit hypothesis of developmental dyslexia. Proceeding of the Cognitive Neuroscience Society Annual Meeting. March 2009; San Francisco, CA, USA
This work was supported by grants from the Lucile Packard Foundation for Children's Health (PRF-CHRP) and the National Institute of Child Health and Human Development (NICHD 5K23HD054720).

fMRI of Emotional Reactivity, Cognitive Regulation, and CBT for Social Phobia

J Gross[1], P Goldin[1]
Dept of [1]Psychology, Stanford University, CA

The overall goal of this study is to elucidate the neural bases of emotional reactivity and cognitive regulation in social phobia (SP) and to identify the neural mechanisms underlying therapeutic change associated with cognitive-behavioral therapy (CBT) for SP. In this randomized clinical trial study, patients with social anxiety disorder are randomly assigned to CBT or waitlist, and are administered a battery of assessments in order to examine therapeutic change and change in brain systems related to emotion reactivity and regulation.

To date, 93 adults have entered the study, including 30 non-psychiatric healthy controls, and 63 adults diagnosed with generalized social anxiety disorder (who have been randomized to either immediate CBT or waitlist followed by CBT). 2 Group (CBT, Waitlist) x 2 Time (Pre Time 1, Post Time 2) repeated-measures ANOVAs have demonstrated a significant interaction of group by time showing that, compared to waitlist participants, CBT completers have lower social anxiety symptom severity (Liebowitz Social Anxiety Scale; F=5.24, p<.05, eta2=.42) and fear of negative evaluation (BFNE; F=5.90, p<.05, eta2=.38).

fMRI sessions include experiments that directly assess emotional reactivity and regulation across three different types of emotional probe stimuli. Based on data from the first 58 patients with social anxiety disorder who have completed assessments, from Time 1 (Baseline) to Time 2 (either CBT or waitlist), we are observing (a) a reduction in negative emotion reactivity to negative social self-beliefs for the CBT but not for the WL group, and (b) increased effectiveness of cognitive reappraisal of negative social self-beliefs for the CBT, but not the WL group. Brain analysis is showing increased recruitment of cognitive regulation related PFC areas and decreased activity in emotion related limbic region.

References/Funding Source

R01 MH076074-01A1 Awarded to James Gross

Is fragile X syndrome an appropriate neuroanatomical model for autism?

E Walter[1], F Hoeft[1], J Piven[2], A Reiss[1]
[1]Center for Interdisciplinary Brain Sciences Research (CIBSR), Stanford University, CA; [2]Neurodevelopmental Disorders Research Center, University of North Carolina, Chapel Hill, NC

Fragile X syndrome (FXS) is the most common known genetic cause of autism. However not all individuals with FXS are diagnosed with autism (AUT) and it is not presently clear whether FXS provides a helpful neuroanatomical model for AUT. If FXS is a good model for AUT, then both disorders should show similar anatomical differences from the brains of control participants from an early age. In order to explore this possibility, we performed voxel-based morphometry to compare the neuroanatomy of boys between the ages of 1.5 and 4 years old who were diagnosed with FXS or AUT (with no diagnosis of FXS), with a control sample comprised of typically developing (TD) and developmentally delayed (DD) boys (FXS: n=52; AUT: n=63; TD: n=31; DD: n=19). We found that FXS and control participants were maximally different in a region comprising bilateral basal ganglia, cingulate cortex and insula. In contrast, differences between AUD and controls were seen primarily in the cerebellum and ventral temporal lobe as well as bilateral inferior frontal gyrus.

In addition, support-vector machine (SVM) analyses designed to maximally differentiate groups were best able to discriminate FXS brains from AUT, and FXS from control participants. The SVM was not very accurate at discriminating AUT from controls. This analysis provides further evidence that neuroanatomical development in FXS follows a trajectory that differs from boys with autism, as well as from control participants. In short, FXS may not provide a helpful anatomical model of autism, at least at this young age.

References/Funding Source

Walter, E., Hoeft, F., Piven, J. and Reiss, A.L. (2009, March). Is fragile X syndrome an appropriate neuroanatomical model for autism? Poster presented at the 16th Annual Meeting of the Cognitive Neuroscience Society, San Francisco, CA.
This study was funded by MH64708-05 (A.L.R., J.P.), MH61696 (J.P.) HD03110-36 (J.P.), NIH T32-MH19908 (E.W.), 1K23HD054720-01 (F.H.), and a Child Health Research Program (CHRP) from Stanford University School of Medicine (F.H.).

Characteristics of Language and Reading in a Child with a Missing Arcuate Fasciculus on DTI

J Yeatman[1], B Laura[1], and H Feldman[1]
Dept of [1]Pediatrics, Stanford University, CA

The superior longitudinal fasciculus (SLF), and particularly the arcuate fasciculus (AF) is considered to be important for the development of proficient language and reading skills. Consistent with this view, a recent case study described a 15-year-old adolescent with severe dyslexia in the presence of relatively preserved language skills; the profound dyslexia was attributed to severe, bilateral AF damage subsequent to radiation treatment at age 5 years (Rauschecker, et al., 2009). To further explore the functional specificity of the AF in language and reading development, we studied a 12-year-old patient ("WL") whose premature birth was notable for periventricular leukomalacia (PVL), which severely damaged her SLF/AF compared to other tracts around the time of birth. We used DTI to characterize the neural sequelae of her injuries, and a battery of standardized measures to evaluate her language, reading, and general intelligence abilities. Using the same DTI-based fiber-tracking methods as Rauschecker, et al., we were able to identify all of WL's main association and projection tracts, with the exception of her SLF/AF, which appeared to be missing bilaterally. Despite the neural damage, WL's standard scores (where M=100, SD=15) were within the normal range on all behavioral measures: (a) Weschler Abbreviated Scales of Intelligence - Verbal (106), Performance (92), and Full Scales (99); (b) Clinical Evaluation of Language Fundamentals - Receptive (99), and Expressive (99) subscales; (c) the Woodcock-Johnson-III – Decoding (89) and Passage Comprehension (110) subscales; and (d) Peabody Picture Vocabulary Test (107). However, the standard scores did not reflect WL's long and often tangential speech when producing verbal responses. These findings suggest that in the context of severe injury to the AF, alternative connections can support the development of language and reading skills. The integrity of long-range fiber tracts may be important for rapid and precise execution of these skills (Just & Varma, 2007).

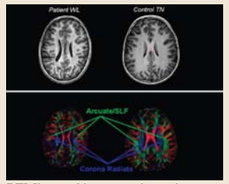

DTI fiber-tracking comparing patient (WL) and control (TN): Patient lacks longitudinal fibers (arcuate fasciculus).

References/Funding Source

Yeatman, J., Barde, L.H.F., & Feldman, H.M. (2009, October). Characteristics of Language and Reading in a Child with a Missing Arcuate Fasciculus on Diffusion Tensor Imaging. Poster session presented at the annual meeting of the Society for Neuroscience, Session 673, Chicago, Illinois.
National Institutes of Health, Eunice Kennedy Shriver National Institute of Child Health and Human Development, RO1 HD046500

Hippocampal and Amygdala Volume in Psychotic and Nonpsychotic Unipolar Depression

J Keller[1], L Shen[1], R Gomez[1], A Garrett[1], H B Solvason[1], A Reiss[1], A F Schatzberg[1]
Dept of [1]Psychiatry & Behavioral Sciences, Stanford University, CA

Objective: The limbic system is thought to underlie dysfunctional affective and cognitive processes in depression. Neuroanatomical studies in depression often investigate hippocampal and amygdala structure since they are two key structures in this system. Research has often, but not always, found reduced hippocampal volume in major depression. The present study investigated hippocampal and amygdala volume differences in depression subtypes compared to healthy controls.

Method: Patients with major depression with psychosis (PMD) and without psychosis (NPMD) and healthy controls were studied. All participants underwent a structural magnetic resonance imaging (MRI) to examine hippocampal and amygdala volume. We further examined the effects of clinical and chronicity data on these brain structures.

Results: After controlling for age, gender, and total brain volume, psychotic depressed patients had a significantly smaller mean amygdala volume than did nonpsychotic depressed or healthy control subjects. Nonpsychotic depressed and healthy controls did not differ from one another. Correlational analyses suggest that age of depression onset was strongly associated with amygdala volume. No group differences in hippocampal volumes were found.

Conclusions: There were no differences between depressed patients and healthy controls in hippocampal volume. However, psychotic but not nonpsychotic depression was associated with reduced amygdala volume. Reduced amygdala volume was not associated with severity of depression or psychosis but was associated with age of onset of depression. Smaller amygdala volume may be a risk factor for the later development of psychotic depression. Chronicity of depression and depression subtype may be two important factors in the variable literature on hippocampal and amygdala volume in depression.

References/Funding Source

Keller, J., Shen, L., Gomez, R.G., Garrett, A., Solvason, H.B., Reiss, A.L. & Schatzberg, A.F. (2008). Hippocampal and amygdalar volumes in psychotic and nonpsychotic unipolar depression. American Journal of Psychiatry, Jul;165(7):872-80.
NIMH RO1-50604 and the Pritzker Foundation

Neurofunctional Correlates of Cognitive Control in Adolescent Eating Disorders

J D Lock [2], A Garrett[1,2], S Forsberg[2], J Beenhakker[2], A L Reiss[1,2]
[1]Center for Interdisciplinary Brain Sciences Research and Dept of [2]Psychiatry and Behavioral Sciences, Stanford University, CA

Background: Behavior and personality characteristics differ among patients with Eating Disorders depending on whether they have a restrictive eating style (RE), such as in anorexia nervosa, or an impulsive eating style (ImpE), such as in anorexia binge/purge subtype, or bulimia nervosa. RE patients are typically anxious, inhibited, and obsessive, while ImpE are often emotionally labile and behaviourally disinhibited. Neural differences in executive functioning related to cognitive control may be associated with these characteristics. This study investigates brain activation during a response inhibition task in adolescent females with eating disorders and healthy controls (HC). Participants: 10 RE, 13 ImpE, and 12 HC. Procedure: All subjects played an event-related go-nogo task in which they responded to all letters except for the infrequent letter X. FMRI data were analyzed in SPM5 to locate activation related to correctly inhibited trials. Results: Adolescents with the ImpE diagnosis were significantly older than the RE or HC groups. However, because all subjects fell within a mid-adolescent range (14-17 years old), and the sample size was very small, age was not covaried. There were no group differences in task accuracy or response time. Between group comparisons showed that the RE subjects had lesser activation in the left orbitofrontal cortex (OFC) and gyrus rectus compared to HC, but greater activation in the DLPFC. Compared to ImpE patients, RE patients had lesser activation in the right OFC and greater activation in the right inferior frontal gyrus. Conclusions: These results illustrate significant differences in brain function in adolescents with Eating Disorders compared to HC. Further, the subgroup having RE shows evidence of greater cognitive control compared to both HC and ImpE groups. However, decreased OFC activation in RE compared to ImpE could be related to the cognitive and emotional inflexibility of this subtype.

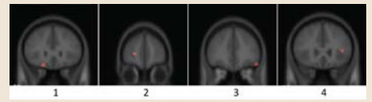

Sites of Group Differences: (1) RE subjects have lower levels of left OFC activation compared to HC; (2) RE subjects have greater left DLPFC activation compared to HC; (3) ImpE have greater right OFC activation than RE subjects; (4) RE have greater right IFG activation than ImpE subjects.

References/Funding Source

To be presented as a poster at the American Academy of Child and Adolescent Psychiatry, Annual Meeting, October, 2009.
NIH K24 MH074457 and the Lucile Packard Children's Hospital Research Fund

FMRI during a verbal working memory task in Psychotic Major Depression (PMD)

A Garrett[1,2], R Kelley[1,2], R Gomez[2], J Keller[2], A Reiss[1,2], and A Schatzberg[1]
[1]Center for Interdisciplinary Brain Sciences Research and Dept of [2]Psychiatry and Behavioral Sciences, Stanford University, CA

Background: PMD is associated with neuropsychological deficits in several areas including working memory. To better understand the neural circuitry associated with these deficits, this study examined brain function during a working memory task in PMD patients. Subjects included 16 with PMD, 15 with nonpsychotic major depression (NPMD), and 19 healthy controls (HC). Method: FMRI data were collected while subjects performed an N-back task in which they responded to letter stimuli if they were repeated in the previous trial (1-back blocks) or in the second-to-previous trial (2-back blocks). Neuroimaging data were processed using SPM5 using ANOVA. Clusters of activation showing a significant effect of group were examined further in SPSS. Results: Group differences in gender distribution were covaried in all analyses. Behaviorally, the NPMD group had a significantly slower response time than the HC group during the 2back trials. Examination of the ANOVA group effect showed that the PMD group had significantly greater activation in the right parahippocampal cortex compared to HC group during the 1-back and 2-back tasks, while the NPMD group showed greater right parahippocampal activation during the 2-back task only. The PMD group had greater activation than the NPMD and HC group in the right temporo-parietal junction during the 2-back task. The NPMD group showed decreased activation in the right dorsolateral prefrontal cortex compared to the HC group. Conclusion: While both the PMD and the NPMD groups show aberrant right parahippocampal compensatory activation, the PMD group shows this abnormality at a lower level of task demands. Unlike DLPFC abnormalities in the NPMD group, the PMD group shows abnormalities in right hemisphere regions associated with reorienting to behaviorally relevant stimuli, suggesting hyperactivity in the "circuit-breaker" network.

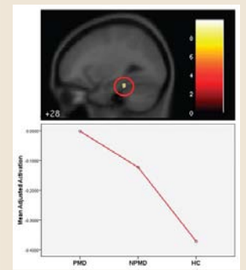

Greater activation in the PMD group compared to the HC group during the 1-Back Task. The parahippocampal cluster is circled in red on the brain image. Mean activation is plotted for the PMD, NPMD, and HC group respectively

References/Funding Source

NIMH R01 MH50604 Schatzberg (PI)

POPULATION RECEPTIVE FIELD MEASUREMENTS IN HUMAN VENTRAL CATEGORY-SELECTIVE CORTEX

R Sayres[1], K Weiner[1], J Winawer[1], B Wandell[1,2], and KGrill-Spector[1,2]
Dept of [1]Psychology and [2]Neuroscience Institute, Stanford University, CA

Introduction: Category-selective regions in extrastriate cortex are conventionally defined by comparing responses to images from different categories (e.g., faces vs. houses). What is the representation of the visual field in these regions?

Methods: We scanned seven subjects on separate experiments to localize category-selective regions, and measure visual field maps (GE 3T scanner). For retinotopic experiments, subjects viewed moving bar stimuli containing different stimuli, including slowly drifting checkerboards and frontal face images. The bars extended out to around 14° eccentricity from the fovea, and had a width of ~2.6°. We employed a recently-developed method for estimating population receptive fields (pRFs) using fMRI (Dumoulin and Wandell, *Neuroimage*, 2008), which estimates pRF center and size for each cortical location.

Results: Face-containing bars produced substantially larger responses than checkerboards along the fusiform gyrus, improving our ability to measure visual field maps in these regions. Eccentricity maps revealed two foveal representations, which may correspond to visual field map clusters previously identified as VO and VT (Wandell et al., *Neuro-opth*. Jpn., 2006). These foveas are within or adjacent to two fusiform face-selective regions, and are separated by smoothly-varying extrafoveal maps.

For several subjects, pRF sizes systematically increased with eccentricity in face-selective regions. The distribution of pRF sizes were substantially larger than in earlier visual cortex, but comparable to recent measurements made in lateral occipital cortex.

Conclusion: We find two spatially separate face-selective regions along the fusiform gyrus, with comparable visual field coverage, separated by a representation of intermediate eccentricities. This indicates these two regions are likely to fall within different visual field maps. Current work addresses possible effects of low-level visual features (e.g. spatial frequency) and stimulus visibility in driving the observed face-selective retinotopic responses.

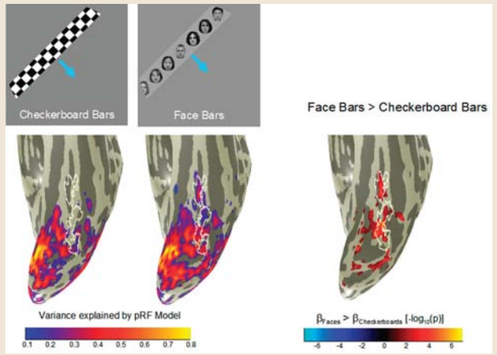

Mapping population receptive fields (pRFs) with face-containing stimuli elicits retinotopically-sensitive responses in ventral regions which do not respond to conventional stimuli. Left: Goodness-of-fit measure of a population receptive field (pRF) model across the ventral stream of a representative subject, for checkerboard and face-containing mapping stimuli. Shown is a representation of the gray matter surface viewed from below; the surface has been computationally inflated to show sulci (dark gray) and gyri (light gray). The overlay indicates the proportion of each voxel's time series variability explained by a population receptive field model, thresholded at 10%. Above are examples of the mapping stimuli: bars which swept slowly across the visual field from multiple directions, containing either drifting checkerboards (left) or sliding faces (center). Right: Regions showing significantly greater BOLD modulation to face than checkerboard mapping stimuli ($p < 0.01$, T test). White outline indicates face-selective regions identified with a separate localizer.

REFERENCES/FUNDING SOURCE

Sayres R, Weiner K, Dumoulin S, Wandell B, and Grill-Spector K. Population receptive field measurements in human ventral category-selective cortex Vision Sciences Society 2009 meeting, Sarasoata, FL.
NEI EY 03164 to BW; NSF: BCS-0617688 & NIH: 1R21EY017741 and NSF BCS 0920865 to KGS.

PREDICTION ERROR AND ASSOCIATIVE NOVELTY IN HUMAN HIPPOCAMPUS AND MEDIAL TEMPORAL CORTEX: A HIGH-RESOLUTION FMRI STUDY

J Chen[1] and A Wagner[1]
Dept of [1]Psychology, Stanford University, CA

The hippocampus is hypothesized to support the detection of associative novelty when retrieved knowledge—a form of prediction—deviates from current sensory reality. The mismatch between associatively cued prediction and sensory input constitutes a form of prediction error that may foster novelty encoding. From this perspective, the CA1 subfield of hippocampus is posited to act as a comparator, detecting the presence of mismatch between retrieved patterns and current sensory input. A central question is whether the magnitude of this putative prediction error signal varies with associative prediction strength. In this experiment, high-resolution fMRI assessed hippocampal subfield responses to different magnitudes of expectation violation, using an incidental processing 1-back paradigm. Participants were scanned at 3T while viewing sequences of objects. Each sequence consisted of four objects (quartets) centrally presented for 1-s each, followed by a 1.6-s fixation and then a second quartet that was either an exact repetition of the first (Rep1) or a rearranged version of the original sequence (Rea1) in which the third and fourth objects were temporally reversed. The Rea1 condition was designed to trigger the retrieval of the initial pattern via repetition of the first two objects, effectively eliciting a prediction about the order of upcoming items that was then violated. To manipulate prediction strength, all Rep1 double-quartets were presented again in the immediately following block, with half appearing in the same order (Rep2) and half in rearranged order (Rea2). As the sequences in the Rep2 and Rea2 conditions were previously repeated double-quartets, prediction strength was higher than on Rep1 and Rea1 trials. Anatomically based fMRI analyses revealed "prediction error" (mismatch) activity in CA1 and perirhinal cortex for second presentations (Rep2>Rea2) but not for first presentations, suggesting that these regions are differentially sensitive to associative novelty under conditions of high compared to low prediction strength. Conversely, parahippocampal cortex displayed less activation during second than first presentations, suggesting a repetition suppression effect that was insensitive to sequence rearrangement. These results support the hypothesis that the magnitude of the prediction error signal in human MTL varies with the predictive strength of the input pattern.

REFERENCES/FUNDING SOURCE

Chen, J. and Wagner, A.D. (2009). Prediction error and associative novelty in human hippocampus and medial temporal cortex: A high-resolution fMRI study. Society for Neuroscience Abstracts.
National Institute of Mental Health (R01 MH076932)

CONTROLLING VARIABILITY REVEALS STRONGER RESPONSES IN FACE-SELECTIVE REGIONS TO FACES NEAR THE MEAN

N Davidenko[1], K Grill-Spector[1,2]
Dept of [1]Psychology and [2]Neuroscience Institute, Stanford University, CA

Extensive research has identified cortical regions that respond selectively to faces. However, it is unknown how these regions represent different faces. Current theories diverge over whether faces are represented with respect to the average, or mean face (norm-based model) or with respect to stored exemplar faces (exemplar-based model). Norm-based models predict stronger neural responses to faces that deviate more from the mean face, whereas exemplar-based models predict stronger responses near the mean face where face exemplars are most densely distributed. To distinguish between these models, we constructed blocks of parameterized face silhouettes and matched either the "angular variability" in face space (MAV condition) or the "physical variability" in face space (MPV condition) across blocks (Figure 1A,B). Using HR-fMRI (1.5mm isotropic voxels), we scanned 12 subjects (MAV: 10; MPV: 9; 7 overlapping) and measured responses in face-selective (Fus-faces and IOG-faces) and object-selective (LO) ventral occipital regions as subjects performed a 1-back task on the blocks of face silhouettes. In the MAV condition, responses in both face- and object-selective regions increased with distance from the mean face (Figure 1C-E, gray). However, in the MPV condition, face-selective responses decreased with distance from the mean face, while object-selective responses were constant (Figure 1C-E, blck). A multiple regression analysis revealed that distance from the mean face had an overall negative weight on responses in face-selective regions only, while physical variability had a positive weight on responses across face- and object-selective regions. Our results support the exemplar-based model and suggest that more neural resources in face-selective regions are allocated to represent the dense region of face space near the mean face. Furthermore, these data highlight the importance of controlling the physical variability of face stimuli when investigating the neural mechanisms of face representation.

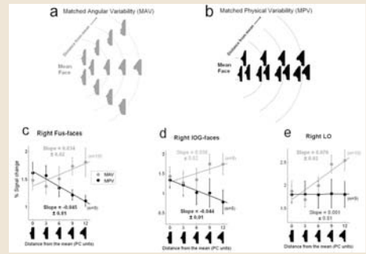

(A-B) Design of experimental conditions. (A): angular variability is matched across blocks but physical variability increases with distance from the mean; (B) physical variability is matched across blocks but angular variability decreases with distance from the mean (C-E) Responses in face- (C-D) and object- (E) selective regions to blocks of face silhouettes that differ from the mean in the MAV (gray) and MPV (black) conditions.

REFERENCES/FUNDING SOURCE

Davidenko N and Grill-Spector K (2009) Face-selective cortex prefers typical over distinctive faces. Association for Psychological Science (APS) Annual meeting, San Francisco.
This research was funded by NIH NRSA fellowship EY18279-01A1 to N.D. and Whitehall grant 2005-05-111-RES and NSF BCS 0920865 to K.G.S.

CUE-INVARIANT RESPONSES IN POSTERIOR OCCIPIOTEMPORAL SULCUS TO VISUAL WORD FORMS

A M Rauschecker[1,2], R F Dougherty[2], L M Perry[2], M Ben-Shachar[2,3], B A Wandell[2]
[1]Neurosciences Program & Medical Scientist Training Program and Dept of [2]Psychology, Stanford University, CA; [3]English Department and The Gonda Brain Research Center, Bar Ilan University, Israel

Introduction: When we read, do we decode word forms in the same cortical region regardless of the defining stimulus feature? The posterior occipitotemporal sulcus (pOTS) appears to be a key site for conventional, contour-defined word form processing (Cohen et al., 2003). We are testing the hypothesis that word form information is invariably communicated to left pOTS, even if the word form is defined by other stimulus features such as motion.

Methods: We presented 4-letter words (2s) defined by black and white dots on a gray background (Fig 1B). Words were defined by one of four different cues: 1) *Luminance Form*: white static dots inside the word form, gray uniform field outside; 2) *Motion Form*: rightward moving white dots inside the word form, leftward moving white dots outside; 3) *Combination Form*, rightward moving white dots in the word form, gray uniform field outside; or 4) *Motion Control*, rightward moving white dots in the image, with no word form. We compared the BOLD signal for these stimuli in pOTS, defined functionally (Fig 1A) in an independent localizer (contour-defined words vs. their unreadable phase scrambled versions). Stimuli were presented in blocks, 12 seconds per block, with 8 blocks interleaved with a uniform gray fixation in the experimental scan, and 6 blocks interleaved with fixation in the localizer. Data were collected on a GE 3T at 1.6-2mm isotropic voxel resolution.

Results: Word forms defined by any stimulus feature elicited a significantly greater left pOTS activation than the Motion Control or Fixation conditions. Not only did left pOTS respond strongly to word form stimuli defined by motion cues alone (Motion Form), but further, in three of four subjects Motion Form elicited the greatest activity of any condition in left pOTS. In the fourth subject the Motion Form activation was equivalent to the other word form conditions (Fig 1C). Interestingly, Combination Form stimuli produced a similar activation profile to the Luminance Form condition, despite containing both luminance and motion cues. Responses in V1 and hMT+ were predominantly driven by motion rather than word-form.

Conclusions: The pOTS responds to visual word stimuli defined by both contour and motion cues. Such cue invariance suggests that the existence of letter strings, not only in the overlearned luminance defined form, is a sufficient condition for engaging pOTS. These results support the hypothesis that pOTS receives signals about visual word forms irrespective of their defining features. We note that pOTS also responds to simple line drawings (Ben-Shachar et al., 2007), and thus the present results may extend to other motion-defined stimuli. Just as the lateral occipital complex as a whole may have a special role in processing visual objects (Grill-Spector et al., 1998), pOTS may be part of the interface between perception and language by processing letter strings of any kind.

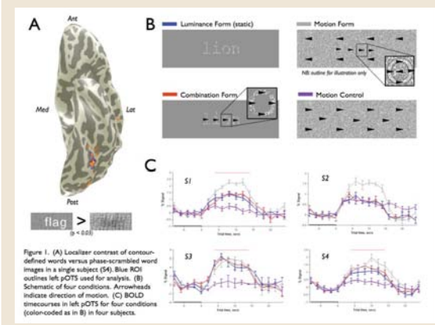

Figure 1. (A) Localizer contrast of contour-defined words versus phase-scrambled word images in a single subject (S4). Blue ROI outlines left pOTS used for analysis. (B) Schematic of four conditions. Arrowheads indicate direction of motion. (C) BOLD timecourses in left pOTS for four conditions (color-coded as in B) in four subjects.

REFERENCES/FUNDING SOURCE

Rauschecker AM, Dougherty RF, Perry LM, Ben-Shachar M, Wandell BA. (2009). Cue-invariant responses in posterior occipitotemporal sulcus to visual word forms. Human Brain Mapping Meeting
AMR was funded by the Medical Scientist Training Program and the Bio-X Graduate Student Fellowship Program at Stanford. This study was supported by NIH Grant EY015000.

DISSOCIABLE NEURAL REPRESENTATIONS OF ANTICIPATED REWARD MAGNITUDE AND DELAY ACCOUNT FOR INDIVIDUAL DIFFERENCES IN TEMPORAL DISCOUNTING.

K Ballard[1], B Knutson[1]
Dept of [1]Psychology, Stanford University, CA

In "temporal discounting," individuals often prefer smaller, immediate rewards to larger, delayed rewards, implying that they trade off reward magnitude against delay. Individuals with substance abuse disorders tend to show more temporal discounting than healthy individuals [1]. Thus, an understanding the neural bases of temporal discounting may illuminate processes relevant to addiction [2]. Prior functional magnetic resonance imaging (fMRI) studies of temporal discounting studies, however, have generated conflicting findings [3,4]. We sought to reconcile these accounts by identifying dissociable neural responses to the magnitude and delay of future rewards. We also correlated these neural responses with individual differences in temporal discounting behavior.

Methods: 16 subjects (8 female) were scanned with FMRI (GE 1.5 T scanner, voxel size = 4 mm cubic, TR = 2000 ms, spiral in/out pulse sequence) as they engaged in a temporal-discounting task. A novel task design separated presentation of information related to an immediate option, magnitude of the future reward, delay of the future reward, and choice.

Results: Results indicated that while ventral striatal (including the nucleus accumbens, NAcc) and mesial prefrontal cortical (MPFC) activation positively correlated the magnitude of future rewards, dorsolateral prefrontal cortex (DLPFC) and posterior parietal cortex (PPC) activation negatively correlated with the delay of future rewards. Further, individuals with higher temporal discounting rates showed decreased NAcc sensitivity to the magnitude of future rewards and increased MPFC, DLPFC, and PPC sensitivity to the delay of future rewards.

Discussion: These findings indicate that while mesolimbic dopamine projection regions show greater sensitivity to future reward magnitude, lateral cortical regions show greater sensitivity to future reward delay, potentially reconciling different accounts of the neural basis of temporal discounting. Additionally, the degree of mesolimbic sensitivity to future reward magnitude and lateral cortical sensitivity to future reward delay can account for individual differences in temporal discounting.

REFERENCES/FUNDING SOURCE

Funding for this project was provided by NIH Grant AG024957-03

DECREASED HIPPOCAMPUS VOLUME IN HEALTHY GIRLS AT RISK FOR DEPRESSION

M C Chen[1], J P Hamilton[1], and I H Gotlib[1]
Dept of [1]Psychology, Stanford University, CA

Researchers have documented that the hippocampus is smaller in depressed than in nondepressed individuals. The temporal or causal association of this reduction in hippocampal volume in depression, however, is not known. To test the hypothesis that reduced hippocampal volume precedes and, therefore, may be implicated in the onset of, depression, we used magnetic resonance imaging to examine brain structure volume in individuals at high and low familial risk for depression. 55 girls between the ages 9 and 15 were scanned: 23 daughters of mothers with recurrent episodes of depression in the daughter's lifetime (high-risk) and 32 age-matched daughters of mothers with no history of psychopathology (low-risk). None of the girls had any past or current Axis-1 psychopathology. Voxel-based morphometry analyses indicated that individuals at high risk for depression had significantly less gray matter density in clusters in bilateral hippocampus (p<0.001) than did low-risk participants. Manual tracing yielded a volumetric reduction in the left hippocampus in the high-risk participants (p<0.05). Compared with individuals at low familial risk for the development of depression, high-risk individuals have reduced hippocampal volume, indicating that neuroanatomical anomalies associated with depression may precede the onset of a depressive episode and influence the development and course of this disorder.

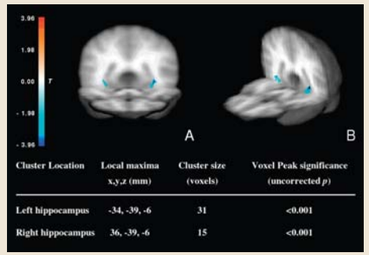

Figure 1. Visualization of voxel-based morphometry analysis showing clusters of gray matter volume difference between high-risk and low-risk girls on a normalized smoothed brain, with positive T values representing clusters of increased matter in high-risk and negative values representing reduced matter in high-risk individuals.

REFERENCES/FUNDING SOURCE

This research was supported by a Distinguished Scientist Award from the National Alliance for Research on Schizophrenia and Affective Disorders and National Institute of Mental Health Grant MH074849 to Ian H. Gotlib and a National Science Foundation Graduate Research Fellowship to Michael C. Chen.

FUNCTIONAL MAGNETIC RESONANCE IMAGING AND COGNITIVE FUNCTION IN OBSTRUCTIVE SLEEP APNEA

O Prilipko[1], N Huynh[1], C Kushida[1], S Schwartz[2], C Guilleminault[1]
Dept of [1]Psychiatry, Stanford Sleep Clinic and Center for Human Sleep Research, Stanford University, CA; [2]Medical Center of University of Geneva, Switzerland

Purpose : Advances in neuroimaging techniques have enabled the exploration of neuronal correlates of the behavioral cognitive performance of patients suffering from obstructive sleep apnea (OSA). There is a growing body of evidence that indicates that OSA is associated with cerebral alterations that may explain the observed cognitive changes in OSA patients. Functional Magnetic Resonance Imaging (fMRI) is a powerful technique that has a unique temporal and spatial resolution that enables the investigation of cerebral function in correlation with behavioral performance as well as cerebro-vascular function.

Methods : We review and compare the existing fMRI studies of cognitive function of OSA patients focusing on working memory and verbal memory aspects as well as findings from the study we are currently conducting at the Stanford Sleep Clinic.

Result : Distinct, but not necessarily conflicting results emerge from the existing literature. Discrepancies in findings can be explained by various factors such as the type of cognitive task, the sensitivity of a given aspect of cognitive function to OSA, the severity of OSA of studied subjects as well as behavioral performance levels and the presence of vascular co-morbidities.

Conclusion : FMRI technique yields a unique way of investigation of cerebral correlate of cognitive performance and further studies are needed in order to gain comprehensive insight into the brain function and cognitive deficits and their dynamics in OSA patients. Moreover, we draw attention to potential confounds specific to this technique such as differences in basal cerebral flow and vascular reactivity.

REFERENCES/FUNDING SOURCE

Oral symposia at 9th World Congress on Sleep Apnea, Seoul, Korea. This study was supported by research grants from Swiss National Foundation for Scientific Research and FSBMB, as well as Respironics, Resmed, and Covidien.

BDNF GENOTYPE MODULATES RESTING FUNCTIONAL CONNECTIVITY IN CHILDREN

M E Thomason[1], D J Yoo[1], G H Glover[2], and I H Gotlib[1]
Depts of [1]Psychology and [2]Radiology, Stanford University, CA

A specific polymorphism of the brain-derived neurotrophic factor (BDNF) gene is associated with alterations in brain anatomy and memory; its relevance to functional connectivity of brain networks, however, is unclear. Given the altered hippocampal function and structure that has been found in adults who carry the methionine (met) allele of the BDNF gene, and the molecular studies elucidating the role of BDNF in neurogenesis and synapse formation, we examined in the association between BDNF gene variants and neural resting connectivity in children. We observed a reduction in hippocampal and parahippocampal to cortical connectivity at rest in carriers of the met allele within each of the three resting networks examined: the default-mode, executive, and paralimbic networks. This study demonstrates that the BDNF gene, known to regulate synaptic plasticity and connectivity in the brain, affects functional connectivity at rest in major neural networks. This report also provides the first images demonstrating that the spatial topography of multiple high-level resting state networks in children and adolescents is similar to that observed in adults.

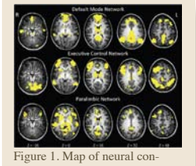

Figure 1. Map of neural connectivity for the 3 major resting-state networks across all subjects (n = 38). p < .0001

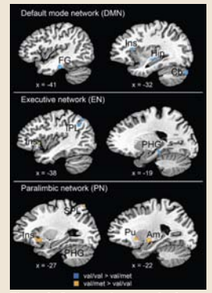

Figure 2. One-sample t-tests for 3 major resting-state networks. BDNF gene group differences (val/val > val/met: blue; val/met > val/val: orange) across 3 resting networks. FG = fusiform gyrus, Ins = insula, Hip = hippocampus, IPL = inferior parietal lobule, PHG = parahippocampal gyrus, SPL = superiorparietal lobe, Pu = putamen, Am = amygdala; p < .01, uncorrected.

Figure 3. BDNF gene group differences (val/val > val/met: blue; val/met > val/val: yellow) for each of the 3 resting networks within hippocampal ROIs.

REFERENCES/FUNDING SOURCE

This project was supported by awards from the National Institute of Mental Health [MH081583 to MET; MH074849 to IHG], and by a NARSAD Young Investigator Award to MET

EPISODIC RETRIEVAL AND PARIETAL CORTEX: RELATING MEMORY TO ATTENTION

J BHutchinson[1], M R Uncapher[1], D W Bressler[3], M A Silver[4], A D Wagner[1,2]
[1]Dept. of Psychology & [2]Neurosciences Program, Stanford University, CA; [3]Vision Science Graduate Program, and [4]Helen Wills Neuroscience Institute and School of Optometry, University of California, Berkeley, CA

Episodic retrieval is a multi-process act that has been known to depend on the medial temporal lobe and prefrontal cortex. More recently, a large body of neuroimaging evidence indicates that lateral posterior parietal cortex (PPC)—including the intraparietal sulcus and inferior parietal lobule—is engaged during event remembering. Given the rich literature demonstrating PPC involvement in visuo-spatial attention, a debate has emerged over the degree to which PPC activations during episodic retrieval can be understood as reflecting the engagement of parietal attentional processes during remembering. Resolution of this debate may partially come from within-subject analysis of the overlap between parietal correlates of episodic retrieval and (a) topographically organized maps of spatial attention within the intraparietal sulcus (IPS1-IPS4) and (b) ventral parietal structures implicated in bottom-up (reflexive) attentional orienting. To this end, the present functional MRI study examined the relationship between recognition memory and visuo-spatial attention effects in parietal cortex at the single-subject level. During the memory task, subjects encoded visually presented words, and were scanned during a subsequent recognition memory test that probed item recognition and source recollection. In a separate session, subjects performed (a) a covert visuo-spatial attention task that mapped topographically organized regions along IPS that subserve goal-directed visuo-spatial attention, and (b) a reflexive (Posner cuing) attentional orienting task that engaged ventral parietal cortex. While the fMRI episodic retrieval data revealed mnemonic effects in IPS and IPL, initial analyses suggest that the localization of these IPS effects were predominantly non-overlapping with the IPS regions demonstrating topographically organized spatial attention maps. Additionally, ventral parietal regions recruited during the memory task were largely distinct from regions elicited by target detection during the Posner task. Taken together, these findings suggest a possible anatomical and functional distinction between mechanisms associated with episodic retrieval and processes of top-down and bottom-up spatial attention.

REFERENCES/FUNDING SOURCE

Hutchinson, JB et al. Episodic Retrieval and Parietal Cortex: Relating Memory to Topographic Maps of Visuo-Spatial Attention and Reflexive Orienting. Society for Neuroscience Annual Meeting, 2008
NIMH (5R01–MH080309 and 5R01–MH076932), Alfred P. Sloan Foundation, and Fight for Sight Foundation

An fMRI study of the effect of CPAP treatment on verbal memory encoding in Obstructive Sleep Apnea patients.

N Huynh[1], O Prilipko[1], V Tantrakul[1], D Nichols[1], E Leary[1], C Kushida[1], C Guilleminault[1]
Dept of [1]Psychiatry, Stanford Sleep Clinic and Center for Human Sleep Research, Stanford University, CA

Introduction: This study used a double blind randomized design to investigate cerebral correlates of verbal memory (VM) encoding in patients with untreated OSA by the means of functional magnetic resonance imaging (fMRI) before and after 2 months of either active or sham CPAP treatment.

Methods: Forty patients with untreated moderate or severe OSA have been randomized to either an active or sham CPAP group and scanned before and after 2 months of treatment. Brain activation during word encoding was measured using a block-design fMRI task. Task blocks alternated between semantic and lettercase decision blocks. A delayed recall task was administered after the scan.

Results: As expected, semantic decision condition yielded a higher level of subsequent recollection as compared to the lettercase condition. However, there were no differences in accuracy between groups for both conditions and scans. Left frontal, bilateral occipital and thalamic regions showed significantly higher BOLD activations at the individual level analysis (whole brain, p=0.05, FWE corrected for multiple comparisons). Group analysis performed using random effects modeling has not shown any significant group-scan interaction changes in brain activation.

Conclusions: OSA patients show a similar pattern of brain activation on a VM encoding task as healthy subjects as reported in previous studies. However, no significant differences in the pattern of cerebral activation during VM encoding have been seen between the active and the sham CPAP group. This can be due to that fact that VM encoding is less severely impaired in OSA and/or is less sensitive to CPAP therapy.

References/Funding Source

Oral presentation at 9th World Congress on Sleep Apnea, Seoul, Korea.
This study was supported by research grants from Swiss National Foundation for Scientific Research and FSBMB, as well as Respironics, Resmed, and Covidien.

Cholinergic Dysfunction and Intervention in Fragile X Syndrome

S R Kesler[1], A A Lightbody[1], and A L Reiss[1]
Dept of [1]Psychiatry and Behavioral Sciences, Stanford University, CA

Males with fragile X syndrome (FRAX) are at risk for significant executive function and memory deficits. Disruption of the cholinergic system secondary to fragile X mental retardation protein deficiency may contribute to these impairments. We measured choline (Cho) in the dorsolateral prefrontal cortex of 9 males with FRAX and 9 age-matched typically developing controls using 1H magnetic resonance spectroscopy (MRS). Right choline/creatine (Cho/Cre) was significantly reduced in the FRAX group compared to controls. In controls, both left and right Cho was significantly positively correlated with intelligence and age was significantly negatively correlated with left Cho. There were no correlations in the FRAX group. A separate group of males with FRAX participating in an open-label trial of donepezil, an acetylcholinesterase inhibitor, showed significantly improved cognitive-behavioral function as measured by the Continuous Naming Test, Achenbach Checklist and Aberrant Behavior Scales. Our findings suggest that the use of neuroimaging techniques can help identify biologic targets for syndrome-specific pharmacologic intervention.

References/Funding Source

Kesler, SR, Lightbody, AA, & Reiss, AL (2009). Cholinergic dysfunction in fragile X syndrome and potential intervention: a preliminary 1H MRS study. Am J Med Genet A, 149A(3), 403-407.
NIH grants MH50047 (PI: Allan Reiss) and a gift from the Canel family to support fragile X syndrome research.

Reward Modulation of Hippocampal Subregions during Motivated Associative Encoding

S M Wolosin[1], J C Liang[1,3], D Zeithamova[1,3], N T Schmandt[1], & A R Preston [1,2,3]
[1]Center for Learning and Memory, Dept of [2]Psychology, and [3]Institute for Neuroscience, The University of Texas at Austin, Austin, TX

Emerging data suggest that hippocampal memory processing is modulated by midbrain regions under conditions of reward resulting in enhanced encoding of episodic information—long-term memory for events. Current theories further suggest that hippocampal subregions may have distinct roles in episodic memory formation, and may be differentially influenced by dopaminergic midbrain inputs. Using high-resolution functional magnetic resonance imaging (fMRI), the present study investigated hippocampal subregional function as well as activation in surrounding medial temporal lobe (MTL) cortex during associative encoding under varying conditions of reward. A high-value or low-value monetary cue preceded a pair of objects indicating potential reward for successful retrieval of the association. At test, participants performed cued recall followed by match (correct association) or mismatch (incorrect association) probe decisions and received feedback on their performance. Behaviorally, cued recall performance was superior for pairs preceded by high reward cues at encoding relative to pairs preceded by low reward cues. fMRI analysis revealed activation associated with successful memory formation in CA3 and subiculum as well as parahippocampal cortex for high reward trials but not low reward trials, with greater activation for high correct relative to high incorrect trials. We further interrogated encoding related midbrain activation in the ventral tegmental area (VTA) where activation was modulated by reward but not successful memory formation. Reward-related individual differences in encoding activation within hippocampus, but not VTA, were correlated with the degree of behavioral reward modulation. Moreover, functional connectivity between VTA and hippocampus tracked individual differences in performance. These findings suggest that motivation during learning affects hippocampal processing specifically in CA3 and subiculum, and that individual differences in performance are reflected not by activation of VTA but rather the interaction of VTA with hippocampal subregions.

References/Funding Source

Presented at Society for Neuroscience 2009

Neural basis of phonological processing in kindergarten children at risk for dyslexia

N Masanori[1], J M Black[1], P Mazaika[1], H Tanaka[1], L Stanley[1], J Heitzmann[1], N Zakerani[1], S Red[1], N Digby[1], M Saleh[1], G H Glover[2], A L Reiss[1], F Hoeft[1]
[1]Center for Interdisciplinary Brain Sciences Research and Dept of [2]Radiology, Stanford University, CA

The goal of this study was to examine whether kindergarten children with a family history of dyslexia (FH+) compared to those without (FH-) show differences in brain activation patterns during phonological processing. Methods: A total of 18 native English speakers (FH+: N=9, Age 5.9±6; FH-: N=9, Age 5.7±3) were scanned. There was no significant difference between FH+ and FH- groups for age, IQ, single letter/word reading and decoding measures. We collected fMRI data during a picture-rhyme judgment task, where children saw two pictures and determined whether the two pictures started with the same sounds. All data were preprocessed with a custom method to reduce the effects of head motion, and one subject was excluded for too much motion. Statistical analysis was performed with SPM5 (http://www.fil.ion.ucl.ac.uk/spm/software/spm5/). Individual subject analysis was performed using a fixed effects model contrasting Rhyme vs. Rest conditions. Group analyses were performed using one-sample t-tests for FH+ and FH- groups separately, and a two-sample t test to compare between group differences (P = 0.001, extent threshold = 20). Results: Task performance was not significantly different between groups. One sample t-test showed similar brain activation in bilateral occipito-temporal, parieto-temporal, inferior frontal and occipital visual regions for both groups. Direct comparison between groups showed that FH+ compared to FH- had significantly greater activation in the left parahippocampal gyrus. On the other hand, FH- compared to FH+ exhibited significantly greater activation in the right inferior frontal to insula region, anterior cingulate cortex and left claustrum. Conclusion: We show preliminary evidence of abnormal activation patterns in kindergarten children with a family history of dyslexia. Studies such as ours may shed light on who is at greater need and what type of interventions is needed for these at-risk children.

References/Funding Source

Nagamine, M., Black, J. M., Mazaika, P.K., Tanaka, H., Stanley, L. M., Heitzmann, J., Zakerani, N., Red, S., Digby, N. P., Saleh, M., Glover, G. H., Reiss, A. L., and Hoeft, F. Neural basis of phonological processing in kindergarten children at risk for dyslexia. Proceeding of the Organization for Human Brain Mapping Annual Meeting, June 2009; San Francisco, CA, USA
This work was supported by grants from the Lucile Packard Foundation for Children's Health (PRF-CHRP) and the National Institute of Child Health and Human Development (NICHD 5K23HD054720).

Neural correlates of phonological processing in reading disabled children with typical and low aptitudes

H Tanaka[1], J M Black[1], A L Reiss[1], F Hoeft[1]
[1]Center for Interdisciplinary Brain Sciences Research, Stanford University, CA

This is the first neuroimaging study to examine whether there are neurobiological differences between reading disabled children with or without low aptitude. Methods: Neural correlates of phonological processing in a total of 102 good and poor readers in the 3rd and 5th grades were examined by fMRI. Based on the performance of two neuropsychological tests, single-word reading skills (word identification, WID) and verbal IQ-equivalent (VIQ), the samples were assigned to one of the three groups: (1) Low achievement – low aptitude (LALA): low WID and low VIQ (N=15, 9 girls, age =10.89+1.12); (2) Low achievement – high aptitude (LAHA): low WID and high VIQ (N=16, 7 girls, age =10.69+0.95); or, (3) Typical Readers (High achievement – high aptitude, HAHA): and high WID and high VIQ (N=26, 18 girls, age =9.99+1.02). Statistical analysis was performed using SPM2 (http://www.fil.ion.ucl.ac.uk/spm/software/spm2/). Individual subjects were analyzed using a fixed effects model contrasting rhyme versus rest conditions. Group differences were analyzed using analysis of covariance (ANCOVA) with individual task performances as a nuisance variable, and regions that showed significant main effect of group were further analyzed using two-sample t-tests (P = 0.001, extent threshold = 20). Results: Task performance was not significantly different between LALA and LAHA groups, but there was a significant difference between poor readers (LALA or LAHA) and typical readers (HAHA). There was a main effect of group in brain activation of bilateral inferior parietal lobules, left inferior frontal region, right dorsolateral prefrontal cortex, and right middle temporal region. Further analyses showed that these regions showed significantly reduced activation for LALA compared to HAHA and LAHA compared to HAHA. There were, however, no significant differences in brain activation between LALA and LAHA. Conclusion: The results of our study indicate the validity of dyslexia identification using the low achievement (LA) model and challenge identification based on the aptitude-achievement discrepancy (AAD) model.

References/Funding Source

Tanaka, H., Black, J. M., Reiss, A. L., and Hoeft, F. Neural correlates of phonological processing in children with low achievement, aptitude-achievement discrepancy and no reading impairment. Proceeding of the Association for Psychological Science Annual Meeting, June 2009; San Francisco, CA, USA
This work was supported by grants from the Lucile Packard Foundation for Children's Health (PRF-CHRP) and the National Institute of Child Health and Human Development (NICHD 5K23HD054720).

Real-time fMRI intervention to improve executive function and sociability in girls with Fragile X

S Bray[1], K Sheau[1], F Hoeft[1], and A Reiss[1]
Dept of [1]Psychiatry, Stanford University, CA

Fragile-X patients present with cognitive deficits in the areas of sociability and executive function. Previous studies have correlated these dysfunctions with abnormal patterns of neural activity, compared to healthy controls. More specifically, Fragile-X patients show elevated activity in the anterior insula when looking at forward gazing faces, relative to controls. This increased activity is presumed to be due to increased anxiety. We propose to use a real-time fMRI neurofeedback paradigm to train subjects to suppress this activation. We will present subjects with feedback of the BOLD response in their anterior insula while they look at faces, and ask them to attempt to decrease signal levels. Our hope is that by training subjects to suppress anxiety-related brain activity, they may overcome some of their aversion to looking at faces. In a second study, we are aiming to ameliorate performance on response inhibition tasks. Fragile-X patients are often impaired at inhibiting inappropriate responses. In healthy controls, successful response inhibition is characterized by fronto-striatal activations, frequently in the right inferior frontal gyrus (IFG). Notably, even on tasks where Fragile-X patients perform similarly to controls, they do not show this pattern of activation. We aim to assist Fragile-X patients in bringing the appropriate network online during response inhibition, by providing real-time feedback of the BOLD signal in right IFG while they perform a task involving response inhibition. We will instruct subjects to attempt to increase the regional BOLD signal while performing the task. Our overarching goal is to improve behavioral performance on these tasks.

Neural correlates of different models in classifying poor reading children

F Hoeft[1], J M Black[1], H Tanaka[1], A L Reiss[1]
[1]Center for Interdisciplinary Brain Sciences Research, Stanford University, CA

Purpose – To perform fMRI analyses with implications for understanding the neural correlates of three major classification models for reading disability: Low Achievement (LA), Aptitude-Achievement Discrepency (AAD) and Response To Intervention (RTI). Method – Functional MRI (fMRI) data during phonological processing were examined in a total of 60 3rd and 5th grade poor readers initially identified by school teachers and confirmed by neuropsychological testing. Among these, 39 children underwent remedial programs focused on word-level instructions. Regression analyses were performed between brain activation and decoding scores, between brain activation and difference in verbal IQ-equivalent and decoding scores, and between brain activation and change in decoding scores before and after intervention in order to examine the LA, AAD and RTI models, respectively. Results – Lower achieving children showed less activation mainly in the left pre-central, inferior frontal, parieto-temporal and occipito-temporal regions and greater right parieto-temporal and occipito-temporal regions. Children with greater discrepancy scores showed less left occipito-temporal activation and greater left prefrontal activation. Children with less change in reading skills in response to interventions showed less right occipito-temporal and greater left inferior frontal activation. Conclusions – This is the first neuroimaging study to examine the neural correlates of different classification models in poor reading children. The results indicate that there are large differences based on the model and that the neurobiological interpretation of reading disability may change depending on the classification used. Future fMRI analyses comparing typical and poor readers defined by different classification models, as well as detailed examination of the relationship between various neuropsychological measures will be of interest.

References/Funding Source

Hoeft, F., Black, J. M., Hulme, C., Tanaka, H., and Reiss, A.L.. Neural correlates of low achievement (LA), aptitude-achievement discrepancy (AAD) and response to intervention (RTI) models in poor reading children. Proceeding of the Society for the Scientific Study of Reading Annual Meeting, June 2009; Boston, MA, USA
This work was supported by grants from the Lucile Packard Foundation for Children's Health (PRF-CHRP) and the National Institute of Child Health and Human Development (NICHD 5K23HD054720).

Structural Differences Associated With Chronic Lower Back Pain

N Chatterjee[1], A Crowell[1], U Maeda[1], R Moulton[1], S Mackey[1]
Dept of [1]Anesthesia, Stanford Systems Neuroscience and Pain Lab, Stanford University, CA

Introduction: Chronic lower back pain (CLBP) affects millions of people, and by some estimates costs over $100 billion per year in the United States alone and constitute one quarter of all disabling occupational injuries. Investigators have implicated central changes as playing a role in amplifying and maintaining CLBP. For example, recent evidence by Apkarian et al suggests that chronic back pain may cause structural changes in the brain's grey matter (GM), but these findings are confounded by the medications of the subject population. This study used voxel based morphometry (VBM) to investigate GM changes in an opioid-free chronic axial back pain population. We hypothesized that CLBP would be associated with GM changes in regions implicated in the processing and perception of pain.

Methods: 21 subjects with chronic lower back pain (male, age 39.1 ±12.7)) and 18 healthy age-matched controls (male, age 37.1 ± 13.5) were recruited for this study. Subjects were excluded on pain relieving medication other than intermittent acetaminophen, with radicular symptoms, or with a history of a major psychiatric disorder. Anatomical images were acquired using an FSPGR pulse sequence (TR = 8.18s, TE =1.71ms, 124 slices , 1.5 mm thickness). Using SPM5 software, all images were segmented, normalized using DARTEL, modulated by the Jacobian determinants from normalization, and smoothed by 8mm. A two-sample t-test was applied to the modulated GM images from both groups with total gray matter added as a covariate.

Results: Subjects suffering from chronic back pain showed more gray matter than controls in the bilateral premotor cortex, hippocampus, and VMPFC and less gray matter in the DMPFC. Whether these GM increases make individuals more likely to develop chronic pain or whether they are structural changes brought upon by the pain condition remains a target for further investigation.

References/Funding Source

Presented at the 2009 Organization for Human Brain Mapping conference
This study was supported by Eli Lilly and the Chris Redlich Pain Research Fund.

Interpretable Classifiers for fMRI Improve Prediction of Purchases

L Grosenick[1], S Greer[1], and B Knutson[1]
Dept of [1]Psychology, Stanford University, CA

Objective: Despite growing interest in applying machine learning to neuroimaging analyses, few studies have gone beyond classifying sensory input to directly predicting behavioural output. With spatial resolution on the order of seconds, functional magnetic resonance imaging (FMRI) is a promising technology for such applications. However, FMRI data's low signal-to-noise ratio, high dimensionality, and extensive spatiotemporal correlations present formidable analytic challenges. Here, we apply different machine-learning algorithms to previously acquired data to examine the ability of fMRI activation in three regions—the nucleus accumbens (NAcc), medial prefrontal cortex (MPFC), and insula—to predict purchasing. Our goal was to improve spatiotemporal interpretability as well as classification accuracy.

Methods: Sparse Penalized Discriminant Analysis (SPDA) was applied to volume of interest data from a previously acquired dataset in which 25 individuals decided whether or not to buy 80 products (Knutson et al., 2007; Neuron), along with several other machine learning algorithms for purposes of comparison.

Results: SPDA enabled automatic selection of correlated variables, yielding interpretable models that generalized well to new data. Relative to logistic regression, linear discriminant analysis, and linear support vector machines, SPDA not only increased interpretability but also improved classification accuracy.

Conclusions: SPDA promises to allow more precise inferences about when specific brain regions contribute to purchasing decisions.

More broadly, this approach provides a general framework for using neuroimaging data to build interpretable models, including those that predict choice.

References/Funding Source

This work was supported in part by a FINRA Investor Education Grant and in part by the National Institute of Aging under Grant R21 030778.

NIRS-fMRI comparison in Fragile X Syndrome in a cognitive inhibition task

X Cui[1], E Walter[1], S Bray[1], A Reiss[1]
Dept of [1]Psychiatry and Behavioral Sciences, Stanford University, CA

Throughout last year, patients with fragile X syndrome, the most common known genetic cause of autism, have participated in our research study. Each of these participants has undergone functional magnetic resonance imaging (fMRI) while they performed a cognitive inhibition task (Stop Signal Reaction Time, SSRT). In this task, while participants usually had to press a button as quickly as possible following a visual cue on the screen, they had to inhibit their response in ¼ of the trials. Some patients also repeated the SSRT experiment while their brain activity was measured by Near Infrared Spectroscopy (NIRS) imaging technology (Hitachi, ETG4000). Our goal is to compare the pattern of brain activation measured with fMRI and NIRS. We have found that even though the activation patterns from the two technologies are not identical, they are very similar. In the contrast nogo-go, both technologies show the lateral frontal cortex is activated (see attached figure); in the go-nogo contrast, both show the motor cortex is activated. These data suggest NIRS is a promising imaging technology to study brain functions, especially for populations that can't tolerate the high demanding environment of fMRI, or for experiments where a natural environment is required.

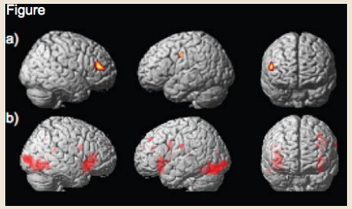

fMRI and NIRS show similar pattern of brain activation during a inhibition task

Reward Processing in Adolescent Girls with Mood Disorders

M Singh[1], N Adleman[2], B Haas[1], R Kelley[1], M Howe[1], K Chang[1], A Reiss[1]
Dept of [1]Psychiatry and Behavioral Sciences, Stanford University, CA; [2]National Institutes of Mental Health, Mood and Anxiety Disorders Program, Bethesda, MD

Objective: To evaluate performance and neural activation during a monetary incentive delay (MID) task in adolescents with bipolar and major depressive disorders (MOOD), hypothesizing that the MOOD group will exhibit greater activation than will healthy controls (HC) in the nucleus accumbens and amygdala in anticipation of reward, and greater activation in the anterior cingulate cortex, insula, and caudate in response to anticipation of loss.

Methods: Unmedicated adolescent girls (ages 13-18 years) with either unipolar (N=11) or bipolar depression (N=8) were recruited along with age comparable HC adolescents (N=11) without any psychiatric diagnosis. Functional images were acquired with a 3T GE Signa scanner using a standard whole-head coil (General Electric, Milwaukee) with a high-resolution, T1-weighted, spoiled GRASS sequence. Activation foci were superimposed on high-resolution T1-weighted images, with locations determined by known neuroanatomical landmarks. Regions that survived the threshold (p=0.001 uncorrected, cluster size, k >40) were reported.

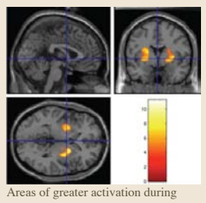
Areas of greater activation during the MID task during anticipation of increasing gains in healthy controls compared with adolescent girls with either unipolar or bipolar depression.

Results: Both HC and MOOD groups exhibited increased activation of the ventral striatum while anticipating increasing gains. In increasing anticipation of loss cues, HC showed greater activation in the parietal cortex relative to subjects with a mood disorder. Between group comparisons did not yield any significant differences in neural activation across conditions. When correlating activation to depressive symptom severity, neither depressed nor HC adolescents showed any correlation between neural activation and CDRS ratings.

Discussion: Unmedicated adolescent girls with mood disorders show neural activations in response to increasing reward stimuli similar to demographically similar HC, but the latter appear to show increased activation in higher cortical regions during the anticipation of loss. Depression severity ratings do not appear to be correlated with significant activation patterns within the MOOD group. Further longitudinal studies characterizing motivational factors in adolescents with mood disorders are warranted to clarify the role of reward processing in the neurophysiology of pediatric mood disorders.

References/Funding Source

Presented at the 54th Annual Meeting of the American College of Neuropsychopharmacology, Scottsdale, AZ, December 7-11, 2008.
The authors gratefully acknowledge the Rocky Family, the National Alliance for Research on Schizophrenia and Depression (NARSAD), and the Klingenstein Third Generation Foundation.

ALTERED TIMING OF AMYGDALA ACTIVATION AS A FUNCTION OF 5-HTTLPR GENOTYPE

D J Furman[1], J P Hamilton[1], J Joormann[2], and I H Gotlib[1]
Dept of [1]Psychology, Stanford University, CA; Dept of [2]Psychology, University of Miami, FL

A functional variant of the serotonin transporter gene (5-HTTLPR) has been associated with increased risk for major depression in the context of stress. In attempting to elucidate the mechanisms mediating this relation, researchers have documented the effects of the 5-HTTLPR polymorphism on the magnitude of amygdala activation to emotional stimuli; little is known, however, about how elevated reactivity relates to the timing of neural events or about whether such chronometric features may themselves represent a risk phenotype for MDD. In this study we examined the hypothesis that girls at genetic risk for depression would activate the amygdala more quickly than would low-risk girls as they increase the intensity of sad mood. Comparing rise time to peak amygdala activation in 5-HTTLPR short-allele carriers and long-allele homozygotes, we found that participants with at least one copy of the short allele showed both stronger and earlier activation in left amygdala as they increased a sad mood state. These results suggest that individuals at genetic risk for depression exhibit a neural "readiness" to engage and enhance negative affect.

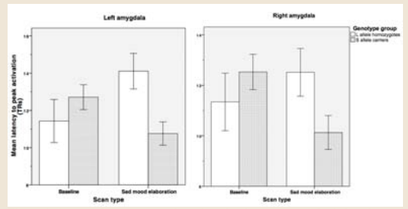

Figure 1. Average latency to reach peak activation (± s.e.m.) for left and right amygdala regions of interest (ROIs) during baseline and sad mood elaboration.

REFERENCES/FUNDING SOURCE

This research was supported by grants from the National Alliance for Research in Schizophrenia and Affective Disorders to JJ and IHG and the National Institute of Mental Health (MH74849) to IHG.

NEURAL BASIS OF CONGENITAL PROSOPAGNOSIA

N Witthoft[1], S Poltorski[1], A Carney[1] and K Grill-Spector[1,2]
Dept of [1]Psychology, and [2]Neuroscience Institute, Stanford University, CA

Congenital prosopagnosia (CP) is a condition in which individuals are unable to recognize faces despite having otherwise normal visual and cognitive function. Unlike acquired prosopagnosia, this deficit is not the result of brain injury, but rather is a condition experienced throughout the subject's lifetime. Our study investigates the neural basis of CP by examining well studied visual category selective responses in congenital prosopagnosics and comparing these to controls of various age groups. In particular, we are interested in whether regions known to show selective responses for faces such as the fusiform face area (FFA) differ in size or selectivity relative to controls. Previous work in our lab has shown that the size of the FFA inceases during development, and one possibility is that the face selective responses of CP subjects will be most comparable to that of children. Results from 5 subjects show that the FFAs in our CP group appear to be much smaller, while other category selective regions such as the PPA (parahippocampal place area) are of normal size, suggesting that this decrease is category specific. Our studies also include a number of behavioral tasks measuring various aspects of face processing such as idenitity recognition, memory, emotion recognition, and judgments of similarity, which help us both to identify persons with CP and divide them into subgroups. Results from these studies suggest that there are at least two distinct types of CP, with one group showing disordered emotion perception in addition to poor face recognition. Along with our data, we also collect DTI scans from each of our prosopagnosic subjects, as there is a strong possibility that at least some forms of CP may result from failures of connectivity between regions supporting face perception and those parts of the brain important for memory.

REAL-TIME FMRI INTERVENTION TO IMPROVE VISUOSPATIAL FUNCTION IN GIRLS WITH TURNER'S SYNDROME

S Bray[1], K Sheau[1], A Reiss[1]
Dept of [1]Psychiatry, Stanford University, CA

Patients with Turner's syndrome show deficits in visuospatial tasks, such as mental rotation. These deficits have been correlated with reduced neural activity in parietal regions, relative to healthy controls. In the present study we aim to use a real-time fMRI neurofeedback paradigm to train subjects to engage parietal brain regions while performing mental rotation tasks. Candidate regions for real-time feedback will first be established in each subject using a mental rotation task, in which subjects must mentally rotate letters of the alphabet in order to compare two exemplars. We will choose a region of interest in the right superior parietal region, based on each individual subjects' activation patterns. During feedback training, subjects will be presented with cues to 'increase' or 'decrease' activity, followed by a line graph of ongoing neural activity. This line graph will be updated as each new 3D scan is acquired (~1.6s). Subjects will use a strategy of imagining letters of the alphabet and rotating them, and attempt to improve at increasing signal levels over four, six minute, feedback sessions. Following the feedback sessions, subjects will again attempt the mental rotation task. Our goal is to demonstrate that the feedback training increases parietal activation during mental rotation, and this increase is associated with improved performance.

ALTERED NEURAL AND BEHAVIORAL RESPONSE IN CHILDREN WITH THE SHORT-ALLELE OF THE SEROTONIN TRANSPORTER GENE

M E Thomason[1], M L Henry[1], J P Hamilton[1], J Joormann[2], H M Louro[1], and I H Gotlib[1]
Dept of [1]Psychology, Stanford University, CA; Dept of [2]Psychology, University of Miami, FL.

Recent research in adults indicates that a genetic polymorphism in the promoter region (5-HTTLPR) of the serotonin transporter (5-HTT) gene (SLC6A4) is related to anomalies in the structure and function of neural areas that have been implicated in emotion regulation and stress reactivity (dosolateral and ventrolateral prefrontal cortex (VLPFC; BA 47), bilateral amygdala, striatal regions, and cingulate cortex). Little is known, however, about neural aspects of this gene-brain association in children and adolescents. In this study we examined the association of 5HTT allelic variation and behavioral and neural responses to rapid processing of emotional faces presented both subliminally and supraliminally. We found that carriers of the short (s) allele of the 5-HTTLPR gene demonstrate significantly greater attentional bias to emotional fear faces than did long (l)-allele homozygotes. Furthermore, s-allele carriers showed widespread increased neural activation measured using blood oxygen level dependent fMRI to emotion faces, compared to l-allele homozygotes in regions of the brain shown to have altered response in adult carriers of the s allele (i.e., VLPFC/BA 47, striatal regions, cingulate cortex). These results suggest that altered neural processing is evident in early life, distinguishing s-allele carriers from l-allele homozygotes at a younger age than has previously been examined.

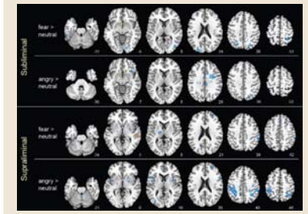

Figure 1. Between-groups whole brain t tests ($p < .01$ uncorrected) show that, overall, carriers of the short (s) allele demonstrate greater neural response to emotion faces across conditions than long (l)-allele homozygotes. Regions in which neural response was greater in s-allele carriers are shown in blue; regions in which neural response was greater in l-allele homozygotes are shown in orange.

REFERENCES/FUNDING SOURCE

This project was supported by awards from the National Institute of Mental Health [MH081583 to MET; MH074849 to IHG], and by a NARSAD Young Investigator Award to MET

FMRI DURING A VERBAL WORKING MEMORY TASK IN PSYCHOTIC MAJOR DEPRESSION (PMD)

A Garrett[1,2], R Kelley[1,2], R Gomez[2], J Keller[2], A Reiss[1,2], and A Schatzberg[1]
[1]Center for Interdisciplinary Brain Sciences Research and Dept of [2]Psychiatry and Behavioral Sciences, Stanford University, CA

Background: PMD is associated with neuropsychological deficits in several areas including working memory. To better understand the neural circuitry associated with these deficits, this study examined brain function during a working memory task in PMD patients. Subjects included 16 with PMD, 15 with nonpsychotic major depression (NPMD), and 19 healthy controls (HC). Method: FMRI data were collected while subjects performed an N-back task in which they responded to letter stimuli if they were repeated in the previous trial (1-back blocks) or in the second-to-previous trial (2-back blocks). Neuroimaging data were processed using SPM5 using ANOVA. Clusters of activation showing a significant effect of group were examined further in SPSS. Results: Group differences in gender distribution were covaried in all analyses. Behaviorally, the NPMD group had a significantly slower response time than the HC group during the 2back trials. Examination of the ANOVA group effect showed that the PMD group had significantly greater activation in the right parahippocampal cortex compared to HC group during the 1-back and 2-back tasks, while the NPMD group showed greater right parahippocampal activation during the 2-back task only. The PMD group had greater activation than the NPMD and HC group in the right temporo-parietal junction during the 2-back task. The NPMD group showed decreased activation in the right dorsolateral prefrontal cortex compared to the HC group. Conclusion: While both the PMD and the NPMD groups show aberrant right parahippocampal compensatory activation, the PMD group shows this abnormality at a lower level of task demands. Unlike DLPFC abnormalities in the NPMD group, the PMD group shows abnormalities in right hemisphere regions associated with reorienting to behaviorally relevant stimuli, suggesting hyperactivity in the "circuit-breaker" network.

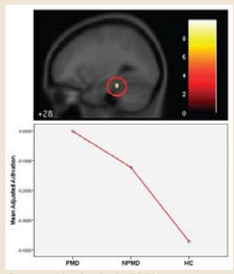

Greater activation in the PMD group compared to the HC group during the 1-Back Task. The parahippocampal cluster is circled in red on the brain image. Mean activation is plotted for the PMD, NPMD, and HC group respectively

REFERENCES/FUNDING SOURCE

NIMH R01 MH50604 Schatzberg (PI)

Changes in Cerebral Activation on Working Memory Task in Obstructive Sleep Apnea patients after CPAP or sham CPAP treatment

O Prilipko[1], N Huynh[1], V Tantrakul[1], C Kushida[1], E Leary[1], D Nichols[1], C Guilleminault[1]
Dept of [1]Psychiatry, Stanford Sleep Clinic and Center for Human Sleep Research, Stanford University, CA

Introduction: Functional magnetic resonance imaging (fMRI) studies enable investigation of neural correlates underlying behavioral performance. In the present study we used a double blind randomized design to investigate the visuo-spatial working memory (WM) function of patients with untreated obstructive sleep apnea (OSA) as compared to healthy controls before and after 2 months of CPAP or sham CPAP treatment.

Methods: A parametric fMRI experiment with four levels of a spatial N-back task was used to investigate the pattern of cortical activations across the various degrees of load in 25 patients with moderate or severe OSA and 11 age and gender-matched healthy controls. Patients were randomized to either an active or a sham CPAP group in a double-blind fashion and an fMRI session was performed before and after 2 months of active or sham treatment.

Results: As expected, we found activations in a similar cortical network in patients and healthy subjects, involving bilateral the supplementary motor area, dorsolateral prefrontal cortex (DLPFC), precentral and parietal regions. The activity in these regions increased linearly with increasing load.

Whole brain group analysis using random effect modeling of the two groups (patients and controls) demonstrated a significantly ($p<0.001$, uncorrected) higher BOLD activation in right frontal regions (BA 32, BA 6) in healthy controls at maximum WM loads. There were no brain regions displaying higher BOLD activation in patients' group as compared to healthy volunteers.

Conclusion: Our results indicate that at maximal WM loads (3-back) healthy controls display higher brain activation in several right frontal regions as compared to OSA patients.

References/Funding Source

poster at SLEEP 2009 23rd Annual Meeting of the Associated Professional Sleep Societies in Seattle, Washington
This study was supported by research grants from Swiss National Foundation for Scientific Research and FSBMB, as well as Respironics, Resmed, and Covidien.

Default Mode Network Connectivity Tracks Clinical Progression in Alzheimer's Disease

J S Damoiseaux[1], K E Keller[2], V Menon[2], M D Greicius[1,2]
Functional Imaging in Neuropsychiatric Disorders (FIND) Lab, Depts of [1]Neurology and Neurological Sciences, [2]Psychiatry & Behavioral Sciences and Program in Neuroscience, Stanford University, CA

Introduction: It has been shown that functional connectivity within a specific resting-state network, known as the default mode network (DMN), is decreased in patients with Alzheimer's disease (AD) compared to healthy controls (1). However it remains unknown whether connectivity within this network decreases as the disease progresses. Here we examine longitudinal functional connectivity changes in the DMN in AD and healthy aging.

Methods: 10 AD patients and 10 healthy controls who participated in our resting-state fMRI study over the last 4 years recently returned for a follow-up session. Subjects were scanned at 'rest', lying awake with eyes closed. At each session two scans consisting of 180 whole brain spiral T2*-images were acquired at 3T. The difference in DMN connectivity was assessed using an independent component analysis (ICA), which was used to de-compose individual data in the spatial and temporal domain. A spatial template-matching algorithm was used to select the DMN and a control network in which we did not expect to see AD-related differences (the sensorimotor network). For each network, the best-fit components of the two runs were averaged for both the baseline and follow-up sessions. The mean images were consequently compared between sessions (within groups) using paired t-tests.

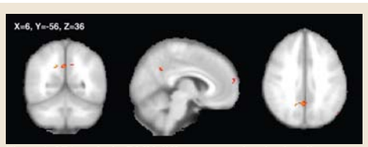

Figure 1: ICA analysis. DMN difference map showing baseline > follow-up in AD patients

Results: The results showed decreased connectivity in AD at follow-up compared to baseline within the DMN (PCC, precuneus and frontal pole, Brodmann areas (BA) 31/7/10; uncorrected $p=0.01$, 15 voxel minimum, see figure 1). The inverse contrast did not show significant changes. As expected, no altered connectivity was observed in the sensorimotor network in AD. Controls did not show any significant changes in DMN or sensorimotor functional connectivity when comparing baseline with follow-up.

Conclusions: Functional connectivity within the DMN of AD patients deteriorates over time as the disease progresses, affecting different regions than in healthy controls. These findings suggest that connectivity strength in the DMN is a potential surrogate marker of clinical status in AD and, therefore, a candidate for an early objective marker of treatment efficacy in clinical trials.

References/Funding Source

Damoiseaux J.S., Keller K.E., Menon V., Greicius M.D., "Default Mode Network Connectivity Tracks Clinical Progression in Alzheimer's Disease". Fifteenth Annual Meeting, Human Brain Mapping 2009.
Greicius MD, Srivastava G, Reiss AL, Menon V. (2004), 'Default-mode network activity distinguishes Alzheimer's disease from healthy aging: evidence from functional MRI', Proc Natl Acad Sci U S A. Mar 30;101(13):4637-42.
NIH: NS048302

Neural processing of dynamic social stimuli in fragile X syndrome

E Walter[1], ALightbody[1], S Hall[1], F Hoeft[1], AReiss[1]
Dept of [1]Psychiatry, Stanford University, CA

Individuals with fragile X syndrome (FXS) often exhibit high levels of anxiety during social interactions. In order to understand the neural pathways underlying this difficulty, we created a stimulus set comprising two second video clips of a live actor who performed either a social gesture (e.g. waving, handshake) or a non-social gesture that was matched for amount and direction of movement (e.g. reaching for mug, wiping counter). In half of the clips, the actor was facing the participant (i.e. facing the camera), and in the other half of the clips the actor was turned at an angle (i.e. as if they were addressing an unseen individual just off camera). With this 2 (Social vs Nonsocial) x 2 (Towards vs Away) design we hoped to tease apart the influence of social interaction directed towards the participant, from social interactions directed towards other individuals, as well as from nonsocial gestures that have similar visual characteristics.

We conducted a whole-brain functional MRI (3T) study, with adolescents diagnosed with fragile X syndrome, as well as with matched control individuals (who had developmental delay of unknown origin). We found that control participants activated left inferior temporal (BA 20) regions more strongly during Social actions versus Nonsocial actions, than did the FXS participants ($p < 0.001$). No regions were more active in the FXS participants than in controls, when viewing Social versus Nonsocial actions. During the SocialTowards condition compared to the NonsocialTowards condition, FXS individuals activated right insula (BA 13) as well as a right-lateralized network of frontal regions (including inferior and middle frontal gyrus, BA 47/11), while control participants activated a left lateralized frontal network (including inferior and middle frontal gyrus, BA 47/8). During the SocialTowards versus the SocialAway condition, FXS participants activated right superior temporal gyrus (BA 38) more strongly than control participants. This suggests aberrant processing of social stimuli in FXS and greater activity of insular cortical regions associated with autonomic overarousal and anxiety.

References/Funding Source

Walter, E., Lightbody, A., Hall, S.S., Hoeft, F. and Reiss, A.L. (June, 2009). Neural processing of dynamic social stimuli in fragile X syndrome. Poster presented at the 15th Annual Meeting of the Organization for Human Brain Mapping, San Francisco, CA.
We gratefully acknowledge the support of grant NIH5R01-MH50047 (ALR).

Interaction between top-down cognitive control and bottom-up mnemonic evidence in decision-making

E A Race[1], G Lawson[1], and A D Wagner[1]
Dept of [1]Psychology, Stanford University, CA

Multiple levels of learning from past experience can have dissociable neural and behavioral consequences during subsequent decision-making. Specifically, recent fMRI data (Race et al., 2008) indicate that stimulus processing is facilitated by learning at three distinct representational levels, with dissociable patterns of BOLD repetition suppression obtained for conceptual learning, stimulus-decision associative learning, and stimulus-response associative learning. While these data demonstrate that different levels of learning yield neural 'benefits' during subsequent decision-making, mnemonic information may also produce behavioral and neural 'costs' when goals change. Indeed, Race et al. reported that neural processing demands increased when a previously learned response was no longer goal-appropriate. However, this neural 'cost' was not accompanied by behavioral (RT) evidence for response-switch costs, raising the possibility that response-switch costs may be offset by stimulus-level facilitation. To investigate this possibility, the current study manipulated top-down preparatory control (cue-to-stimulus interval, CSI), providing a means of temporally separating the influences of learning at distinct levels of representation. Behavioral priming (RT facilitation) due to stimulus-decision learning was observed at both short (300ms) and long (1100ms) CSIs, as was priming due to stimulus-response learning when current responses were congruent with the previously learned response. By contrast, incongruent responses produced an RT cost after short CSI, whereas there was no evidence for stimulus-level facilitation nor response conflict after long CSI. Collectively, these results suggest that retrieval of learned stimulus-response associations occurs rapidly, but that increased top-down preparatory control can reduce the influence of stimulus-response mnemonic conflict to enable faster, task-appropriate responding.

References/Funding Source

NIMH (5R01–MH080309) and Alfred P. Sloan Foundation

Methods and Software for fMRI Analysis for Clinical Subjects

P K Mazaika[1], F Hoeft[1], G H Glover[2], and A L Reiss[1]
Depts of [1]Psychiatry and [2]Radiology, Stanford University, CA

A key issue to improve mental health is to better understand the abnormal cognitive processing in mentally impaired populations. Thousands of fMRI data sets have been collected for many types of patients, often at large cost, but the data is difficult to analyze because clinical subjects often move during a scan session. Furthermore, the most commonly used quality control method for group experiments is to discard subjects based only on a rule-of-thumb for amount of total motion. Based on fMRI experiments performed at Lucas Center, we developed new data analysis algorithms to automatically correct for large motions and repair artifacts in the data. New subject selection methods were developed to more accurately detect outlier subjects within group studies. New signal processing methods were developed to improve noise reduction in case of imaging artifacts. All methods and algorithms have been implemented for use by other neuroscience researchers as a plug-in toolbox for the widely available SPM software. Software and documentation have been downloaded by more than 900 users from our website, and we answer questions from users via the SPM email list. All downloads are validated by user name to maintain an accurate count of software demand. Within CIBSR, the methods have been applied to over 500 Lucas Center data sets from pediatric and clinical subjects with conditions including FraX syndrome, Turner syndrome, Williams syndrome, bipolar disorder, ADHD, cancer survivors, post-traumatic stress disorder, preterm birth, and dyslexia in order to help understand the neural correlates of these conditions.

References/Funding Source

Full publication or presentation citation: Mazaika, P.K., Hoeft, F., Glover, G.H., and Reiss, A.L. Methods and Software for fMRI Analysis for Clinical Subjects, Presented at annual meeting for Organization for Human Brain Mapping, San Francisco, June 19, 2009.
Supported by the National Institute of Mental Health Grant K25MH077309-03.

Disrupted amygdalar subregion functional connectivity and evidence for a compensatory network in generalized anxiety disorder

A Etkin[1], K E Prater[1], A F Schatzberg[1], V Menon[1,2], M D Greicius[1,2,3]
Depts of [1]Psychiatry and Behavioral Sciences, [2]Program in Neuroscience, [3]Neurology and Neurological Sciences, Stanford University, CA

Context: Little is known about the neurobiology of generalized anxiety disorder (GAD). Studies in other anxiety disorders have implicated the amygdala, but work in GAD has yielded conflicting results. The amygdala is composed of distinct subregions that interact with dissociable brain networks, which have been studied only in experimental animals. A functional connectivity approach at the subregional level may therefore yield novel insights into GAD.

Objective: To determine whether distinct connectivity patterns can be reliably identified for the basolateral and centromedial subregions of the human amygdala, and to examine subregional connectivity patterns in GAD, as well as potential compensatory amygdalar connectivity.

Design: cross-sectional study. Setting: Academic medical center. Participants: Two cohorts of healthy subjects (N=17, N=31) and patients with GAD (N=16).

Main Outcome Measures: Functional connectivity with cytoarchitectonically-determined basolateral and centromedial regions of interest, measured during functional magnetic resonance imaging performed while subjects were resting quietly in the scanner. Amygdalar gray matter volume was also investigated with voxel-based morphometry.

Results: Reproducible subregional differences in large-scale connectivity were identified in two cohorts of healthy subjects. The basolateral amygdala was differentially connected with primary and higher order sensory and medial prefrontal cortices. The centromedial amygdala was connected with the midbrain, thalamus and cerebellum. In patients with GAD, basolateral and centromedial amygdalar connectivity patterns were significantly less distinct and increased gray matter volume was noted primarily in the centromedial amygdala. Across subregions, patients had increased connectivity with a previously characterized fronto-parietal "executive control" network and decreased connectivity with an insula and cingulate-based "salience" network.

Conclusion: Our findings provide new insights into the functional neuroanatomy of the human amygdala and converge with connectivity studies in experimental animals. In GAD, we find evidence for both an intra-amygdalar abnormality, as well as engagement of a compensatory fronto-parietal executive control network, consistent with cognitive theories of GAD.

Socioeconomic status and brain activation are differentially associated for dyslexic versus typically-reading adolescents

J M Black[1], A L Reiss[1], F Hoeft[1]
[1]Center for Interdisciplinary Brain Sciences Research, Stanford University, CA

Purpose: Findings from functional neuroimaging studies suggest that individuals with dyslexia show hypoactivation in the left parieto-temporal and occipito-temporal regions, and hyperactivation in right homologous regions. Socioeconomic status (SES) is a robust predictor of reading ability; higher SES is related to greater reading proficiency. SES may reflect underlying differences in opportunities related to schooling, access to supplementary academic support, and reading experiences. Bridging these two lines of research, our goal was to elucidate the neural correlates between SES and reading independently in adolescents with and without dyslexia. Method: Twenty-nine adolescents (age 12.87 + 2.5) completed a standard battery of neuropsychological assessments; 16 participants met our criteria for dyslexia. A composite SES score (parental education, occupation, family income) was calculated for each participant. Functional magnetic resonance imaging (fMRI) data were collected during a sentence comprehension task. Regression analyses between brain activation and SES controlling for IQ were conducted. Results: Brain activation during sentence comprehension that covary with SES differed by group. Among typical readers, positive correlation with SES emerged in bilateral parieto-temporal and left temporal regions. Among the dyslexic group, negative correlation was evident in right temporal, lateral prefrontal regions and bilateral occipito-temporal regions. Conclusion: The primarily negative association for adolescents with dyslexia suggests that lower SES dyslexic readers may display compensatory mechanisms primarily in right hemisphere regions, unlike the negative correlation in typical readers showing dominance in the left hemisphere. These findings may be critical to understanding the differential role SES may have on typical versus impaired readers' brain activation.

References/Funding Source

Black, J. M., Digby, N. P., Reiss, A. L., and Hoeft, F. Socioeconomic status and brain activation are differentially associated for dyslexic versus typically-reading adolescents. Proceeding of the Society for the Scientific Study of Reading Annual Meeting, June 2009; Boston, MA, USA
This work was supported by grants from the Lucile Packard Foundation for Children's Health (PRF-CHRP) and the National Institute of Child Health and Human Development (NICHD 5K23HD054720).

Reward Modulation of Medial Temporal Lobe Subregions during Associative Encoding and Cued Recall

S M Wolosin[1,2,] DZeithamova[1,2], N T Schmandt[1,2], & A R Preston [1 2]
Dept of [1]Psychology, and [2]Center for Learning and Memory, The University of Texas at Austin, Austin, TX

The medial temporal lobe (MTL) is critical for episodic memory—memory for individual events. Emerging data suggest that MTL processing is modulated by midbrain regions under conditions of reward resulting in enhanced episodic encoding. Current theories further suggest that MTL subregional function may be differentially influenced by midbrain inputs that signal reward. Using high-resolution fMRI, the present study characterized MTL subregion function during associative encoding under reward as well as reward-related effects on later cued recall performance. During associative encoding, high- and low-value monetary cues preceded paired associates indicating potential reward for successful retrieval. At test, participants performed cued recall followed by match (correct association) or mismatch (incorrect association) probe decisions and received feedback on their performance. Behaviorally, cued recall performance was superior for pairs preceded by high reward cues at encoding relative to pairs preceded by low reward cues. Initial analyses revealed successful memory formation associated with activation in hippocampus, perirhinal cortex, and midbrain regions that was modulated by reward with greater subsequent memory effects observed for high relative to low reward pairs. Successful memory retrieval during cued recall was further modulated by reward status where correct relative to incorrect retrieval was greater for high relative to low reward pairs in hippocampal and perirhinal regions. Moreover, hippocampal and midbrain activation differentiating associative novelty at probe (mismatch vs. match) was greater for high relative to low reward pairs. These findings suggest that motivation during learning affects MTL-based memory formation as well as later retrieval processes through interactions with midbrain regions.

References/Funding Source

Presented at Cognitive Neuroscience Society 2009

fMRI during a verbal working memory task in Psychotic Major Depression (PMD)

A Garrett[1,2], R Kelley[1,2], R Gomez[2], J Keller[2], A Reiss[1,2], and A Schatzberg[1]
[1]Center for Interdisciplinary Brain Sciences Research and Dept of [2]Psychiatry and Behavioral Sciences, Stanford University, CA

Background: PMD is associated with neuropsychological deficits in several areas including working memory. To better understand the neural circuitry associated with these deficits, this study examined brain function during a working memory task in PMD patients. Subjects included 16 with PMD, 15 with nonpsychotic major depression (NPMD), and 19 healthy controls (HC). Method: FMRI data were collected while subjects performed an N-back task in which they responded to letter stimuli if they were repeated in the previous trial (1-back blocks) or in the second-to-previous trial (2-back blocks). Neuroimaging data were processed using SPM5 using ANOVA. Clusters of activation showing a significant effect of group were examined further in SPSS. Results: Group differences in gender distribution were covaried in all analyses. Behaviorally, the NPMD group had a significantly slower response time than the HC group during the 2back trials. Examination of the ANOVA group effect showed that the PMD group had significantly greater activation in the right parahippocampal cortex compared to HC group during the 1-back and 2-back tasks, while the NPMD group showed greater right parahippocampal activation during the 2-back task only. The PMD group had greater activation than the NPMD and HC group in the right temporo-parietal junction during the 2-back task. The NPMD group showed decreased activation in the right dorsolateral prefrontal cortex compared to the HC group. Conclusion: While both the PMD and the NPMD groups show aberrant right parahippocampal compensatory activation, the PMD group shows this abnormality at a lower level of task demands. Unlike the prefrontal abnormalities in NPMD, the PMD group shows abnormalities in right hemisphere attention regions associated with detecting infrequent, task-relevant targets. This suggests that the working memory circuits in PMD are compromised at the basic level of detecting a task-relevant stimulus from among other more frequent stimuli.

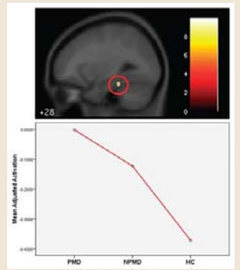

Greater activation in the PMD group compared to the HC group during the 1-Back Task. The parahippocampal cluster is circled in red on the brain image. Mean activation is plotted for the PMD, NPMD, and HC group respectively

References/Funding Source

NIMH R01 MH50604 Schatzberg (PI)

Neural Mechanisms Underlying MBSR in Healthy and Socially Phobic Individuals

J Gross[1], P Goldin[1]
Dept of [1]Psychology, Stanford University, CA

The overall goal is to identify the neural mechanisms associated with Mindfulness-Based Stress Reduction (MBSR). Clinical research has shown that MBSR reduces psychological distress and increases well-being, but the mechanisms underlying these changes in not well described. Basic research has examined the neural bases of emotion and emotion regulation, but this research has not examined changes following MBSR. We employ a translational framework that characterizes the impact of MBSR on emotion regulation in terms of interactions between ventral emotion-generative brain regions and dorsal emotion-regulatory brain regions. We propose to compare the effects of MBSR and an active control condition (ACC) in participants with generalized social phobia (SP). SP will be randomly assigned to MBSR or ACC and assessed using self-report inventories and functional magnetic resonance imaging (fMRI) before and after MBSR and the ACC. Aim 1 investigates the effects of MBSR on anxiety and well-being. For the MBSR participants, we expect significant (a) decreases in anxiety, and (b) increases in well-being at immediately post-intervention and at the 3-month follow-up compared to pre-intervention. For the ACC participants, we expect no change in anxiety or well-being from pre- to post-intervention. Aim 2 investigates the effects of MBSR on attentional and cognitive emotion regulation. We expect MBSR participants to show improvements in attentional regulation, but no change in cognitive regulation from pre- to post-intervention, as indicated by (a) greater reductions in negative emotion ratings, (b) greater reductions in ventral emotion-generative brain regions, as well as (c) greater increases in attention-related dorsal emotion-regulatory brain regions. We do not expect ACC participants to show changes in either form of regulation from pre- to post-ACC. Aim 3 investigates whether MBSR-related changes in attentional emotion regulation mediate MBSR treatment response (decreases in anxiety and increases in well-being) at post-treatment and at the 3-month follow-up.

References/Funding Source

R21 AT003644 Awarded to James Gross

DON'T STOP THINKING ABOUT TOMORROW: NEURAL MEASURES OF FUTURE SELF-CONTINUITY PREDICT TEMPORAL DISCOUNTING

H Ersner-Hershfield[1], G E Wimmer[2] Brian Knutson[1,3]
Depts of [1]Psychology and [3]Neuroscience, Stanford University, CA; Dept of [2]Psychology, Columbia University

Objective: We tested the future self-continuity hypothesis that individuals perceive and treat the future self differently from the present self, and so might fail to save for the future. To examine this hypothesis, we used behavioral measures that relied on self-report, as well as neuroimaging measures that did not. Neuroimaging offers a novel means of testing this hypothesis, since previous research indicates that self- versus other-judgments elicit activation in the rostral anterior cingulate (rACC). Using event-related functional magnetic resonance imaging (fMRI), we predicted that there would be individual differences in rACC activation while rating the current versus future self, and that individual differences in current versus future self activation would predict temporal discounting assessed behaviorally a week after scanning.

Methods: In Study 1, 155 community members filled out a novel future self-continuity scale, as well as a comprehensive financial history questionnaire. In Study 2, 18 subjects were scanned with event-related fMRI while making judgments about the extent to which trait adjectives applied to their current self, a future self, a current other, or a future other. A week later, subjects completed a temporal discounting task that yielded an estimate of the degree to which each individual discounted future rewards. Analyses focused on changes in activation in the MPFC and rACC during current vs. future self-ratings.

Results: In Study 1, there was a significant positive correlation between our measure of self-continuity and accrued assets. In Study 2, results indicated that there was a neural difference between thoughts about the current self versus thoughts about the future self: there was greater activation in a portion of the anterior cingulate cortex for current self compared to future self judgments. Importantly, lending further support to the future self-continuity hypothesis, individual differences in the magnitude of this effect predicted the tendency to devalue future rewards. That is, the greater the difference in neural activation between current self and future self judgments, the more a given individual discounted future rewards.

Conclusions: These results suggest that the way one views the future self is an important predictor of saving behavior. Such a relationship was documented using both behavioral and neuroimaging methods. The findings thus may hold implications for understanding and encouraging saving for the future self.

REFERENCES/FUNDING SOURCE

This work was supported by the Center on Advancing Decision Making in Aging Grant AG024957.

STRIATAL CONTRIBUTIONS TO EXPLICIT REMEMBERING: EFFECTS OF MEMORY STRENGTH AND DECISION CONFIDENCE

J Rissman[1] and A D Wagner[1,2]
Dept of [1]Psychology and [2]Neuroscience Program, Stanford University, CA

Functional neuroimaging investigations of episodic retrieval consistently identify a network of prefrontal, parietal, and medial temporal lobe regions that exhibit greater activity when individuals recognize previously encountered stimuli than when they perceive stimuli as novel. Interactions between striatal structures and both prefrontal cortex and the medial temporal lobe raise the possibility that basal ganglia processes contribute to explicit remembering. Here we report converging evidence from two fMRI studies that bilateral regions of the ventral striatum (VS) are highly sensitive to the perceived mnemonic status of items during explicit, but not implicit, retrieval tasks, and that the magnitude of activation varies with memory decision confidence. In the first experiment, participants were scanned while rating their level of recognition memory confidence for face stimuli on a 5-point scale. Areas of VS exhibited enhanced activity to old vs. new stimuli. Importantly, rather than showing a monotonic scaling of activity with mnemonic strength, activity levels scaled with the distance of participants' responses from the old/new decision bound—activity levels were greater for hits and correct rejections that were made with the highest confidence relative to those made with low confidence. By contrast, when participants made male/female judgments on studied and novel faces (i.e., implicit retrieval), the old/new effects in VS were abolished. A second experiment revealed similarly robust old/new effects in overlapping regions of VS while participants made source recollection judgments about studied and novel object stimuli, but not while they made semantic judgments (i.e., implicit retrieval) about these stimuli. Taken together, these two studies demonstrate that regions of VS show a marked sensitivity to the mnemonic status of stimuli during explicit memory tasks. The dependence of these effects on the explicit retrieval demands of the tasks suggests that VS may play a role in goal-directed control processes that facilitate the recovery of memories, evaluate the retrieved information, or select the appropriate behavioral decisions. Alternatively, the activity in VS may track the level of intrinsic reward associated with successful task performance. Functional connectivity analyses promise to further inform how interactions between VS and prefrontal, medial temporal, and midbrain structures contribute to explicit remembering.

REFERENCES/FUNDING SOURCE

Rissman, J. and Wagner, A.D. (2009). Striatal contributions to explicit remembering: Effects of memory strength and decision confidence. To be presented at the Annual Meeting of the Society for Neuroscience, Chicago, IL.
NIMH (R01–MH080309; R01–MH076932); MacArthur Foundation's Law and Neuroscience Project.

COMT GENOTYPE AFFECTS PREFRONTAL WHITE MATTER PATHWAYS IN CHILDREN

M E Thomason[1], R F Dougherty[1], N L Colich[1], L M Perry[1], E I Rykhlevskaia[1,2,3], H M Louro2, J F Hallmaye[3], C E Waugh[1], R Bammer[4], G H Glover[4], and I H Gotlib[1]
Depts of [1]Psychology, [2]Neurology and Neurological Sciences, [3]Psychiatry and Behavioral Sciences, and [4]Radiology, Stanford University, CA

Diffusion tensor imaging is widely used to evaluate the development of white matter. Information about how alterations in major neurotransmitter systems, such as the dopamine (DA) system, influence this development in healthy children, however, is lacking. Catechol-O-metyltransferase (COMT) is the major enzyme responsible for DA degradation in prefrontal brain structures, for which there is a corresponding genetic polymorphism (val158met) that confers either a more or a less efficient version of this enzyme. The result of this common genetic variation is that children may have more or less available synaptic DA in prefrontal brain regions. In the present study we examined the relation between diffusion properties of frontal white matter structures and the COMT val158met polymorphism in 40 children ages 9-15. We found that the COMT val allele was associated with significantly elevated fractional anisotropy values and reduced axial and radial diffusivities. These results indicate that the development of white matter in healthy children is related to COMT genotype and that alterations in white matter may be related to the differential availability of prefrontal DA. This investigation paves the way for further studies of how common functional variants in the genome might influence the development of brain white matter.

REFERENCES/FUNDING SOURCE

This project was supported by awards from the National Institute of Mental Health [MH081583 to MET, RR P41-009874 to GHG, MH074849 to IHG, and NIH EY-15000 to RFD], and by a NARSAD Young Investigator Award to MET

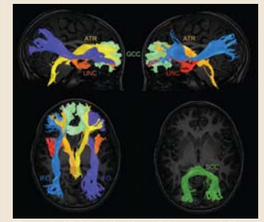

Figure 1. 3D Visualization of the targeted fiber tracts. The top and bottom-left panels show, in a random participant, the major fiber tracts of interest with strong projections to prefrontal cortical regions. ATR = anterior thalamic radiation (left: yellow/orange; right: yellow); GCC = genu of the corpus callosum (light green); IFO = inferior frontal occipital fasciculus (left: blue; right: purple); and UNC = uncinate fasciculus (left: red; right: orange). The bottom-right panel shows the control fiber tract tested to examine the regional specificity of COMT genotype differences: SCC = splenuim of the corpus callosum (dark green).

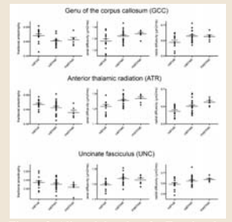

Figure 2. Aligned dot plots for Fractional Anisotropy (FA), Axial Diffusivity (AD), and Radial Diffusivity (RD) by gene group. Larger horizontal bars indicate group means, and smaller horizontal bars above means indicate standard error of the mean. Val-allele homozygotes were significantly different from one or both of the other gene groups (for more detail refer to Table 2) except FA in the GCC, for which the three groups did not differ significantly.

DIFFERENTIAL BRAIN ACTIVATION IN 5- AND 6-YEAR-OLDS WITH AND WITHOUT FAMILY HISTORY OF READING DIFFICULTY

J M Black[1], N Masanori[1], P Mazaika[1], H Tanaka[1], L Stanley[1], J Heitzmann[1], N Zakerani[1], S Red[1], N Digby[1], M Saleh[1], G H Glover[2], A L Reiss[1], F Hoeft[1]
[1]Center for Interdisciplinary Brain Sciences Research and Dept of [2]Radiology, Stanford University, CA

Introduction: The goal of this study was to examine whether kindergarten-aged children with a family history of DD (FH+) compared to those without (FH-) exhibit differential neural activation patterns elicited by phonological working memory. Methods: A total of 18 participants were scanned, yet five participants' data were unusable due to motion artifact. The 13 participants were healthy (6 males, 7 females; 12 right-handed), native English-speakers (FH+: N=7, Age 5.87±68; FH-: N=6, Age 5.75±24). The group mean standard scores (FH+ vs. FH-) did not differ significantly on a battery of standardized tests of reading and IQ. During functional magnetic resonance imaging (fMRI), participants performed a picture-rhyme judgment task by indicating whether the names of the two pictures presented (e.g., an apple and a giraffe) began with the same or a different phoneme. There was a delay between the presentation of the 2 stimuli for the working memory condition (WM+) (vs. WM- condition which was presented simultaneously). Results: In-scanner task performance was not significantly different between groups. Direct comparison between groups showed that FH+ compared to FH- had significantly greater activation in the bilateral occipital visual region and the right posterior cingulate. On the other hand, FH- compared to FH+ exhibited significantly greater activation primarily in the regions known to be associated with language processing and memory, such as the left frontal regions (inferior, middle and superior gryri), bilateral inferior temporal gyrus, the bilateral anterior cingulate, and the right superior and middle temporal regions. Conclusions: Children without a family history show evidence of a more typical recruitment of bilateral regions associated with language and memory during phonological processing. On the other hand, children with a family history show an atypical reliance upon bilateral visual systems alone, perhaps reflecting a compensatory mechanism for an early impairment in the phonological-orthographic loop.

REFERENCES/FUNDING SOURCE

Black, J. M., Nagamine, M., Mazaika, P.K., Tanaka, H., Stanley, L. M., Heitzmann, J., Zakerani□N., Red, S., Digby, N. P., Saleh, M., Glover, G. H., Reiss, A. L., and Hoeft, F. Differential brain activation in 5- and 6-year-olds with and without family history of reading difficulty. Proceeding of the Organization for Human Brain Mapping Annual Meeting, June 2009; San Francisco, CA, USA
This work was supported by grants from the Lucile Packard Foundation for Children's Health (PRF-CHRP) and the National Institute of Child Health and Human Development (NICHD 5K23HD054720).

Individual Differences in Sentence Comprehension in Children: An Event-Related fMRI Investigation

J Yeatman[1], M Ben-Shachar[2,3], G Glover[4], and H Feldman[1]
Depts of [1]Pediatrics, [3]Psychology, [4]Radiology, Stanford University, CA; Dept of [2]Linguistics and Gonda Brain Research Center, Bar-Ilan University, Israel

Functional magnetic resonance imaging studies of healthy adult volunteers show that sentence comprehension tasks activate a dynamic network of cortical areas, which increases in extent and amplitude during the processing of syntactically difficult sentences. We study the cortical network that serves sentence comprehension in children, and examine the relation between individual differences in receptive language skills and changes in the network as a function of syntactic complexity. Fourteen children, 10 to 15 years old, participated in an event-related functional magnetic resonance imaging sentence-picture verification paradigm in which sentences were presented followed by a picture. The participant indicated with a button press if the picture accurately represented the auditory stimulus. The task (compared to fixation) activated large regions of the left and right superior temporal cortex, among other regions. Syntactically difficult sentences led to increased activation in the left temporal-parietal junction and right superior temporal gyrus in comparison to easy sentences, a different pattern than the contrast of long and short sentences. The signal difference between hard and easy sentences in frontal regions was positively correlated with the participant's receptive vocabulary standard score and negatively correlated with reaction time on a receptive grammar test. Thus, individual differences in language skills were associated with the adaptability of the network in response to changing task demands. This framework may be useful in investigating individual differences in language comprehension in clinical populations.

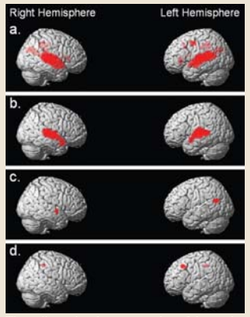

Three dimensional reconstruction of the cortical surface displaying regions of significant activity in red ($p < 0.001$ uncorrected, minimum cluster size > 8 voxels) for: (a) Sentence Comprehension vs. Fixation, (b) Long vs. Short Sentences, (c) Hard vs. Easy Sentences, (d) Positive relationship between reaction time on each trial and BOLD signal.

References/Funding Source

Yeatman, J.D., Ben-Shachar M., Glover G. H., Feldman H.M. (2009). Individual Differences in Sentence Comprehension in Children: An Event-Related Functional Magnetic Resonance Imaging Investigation of Syntactic Processing Demands. Manuscript submitted for publication.
National Institutes of Health, Eunice Kennedy Shriver National Institute of Child Health and Human Development, RO1 HD046500

High-resolution fMRI of medial temporal lobe contributions to rapid integrative encoding and generalization of associative memories

D Zeithamova[1, 2], N T Schmandt[1, 2], & A R Preston [1, 2]
Dept of [1]Psychology, and [2]Center for Learning and Memory, The University of Texas at Austin, Austin, TX

The medial temporal lobe (MTL) is thought to support rapid acquisition of episodic experience and to create memories that are flexible in nature, allowing for generalization from previous experiences to novel events and stimuli. Generalization can be based on integrative processes during encoding of overlapping events as well as inference-based processes at the time of retrieval. The goal of the present study was to investigate MTL subfield contributions to integrative encoding and inferential retrieval using an associative inference paradigm and high-resolution functional MRI. Participants rapidly learned overlapping associations in a single trial and were subsequently probed with novel stimulus combinations that required flexible transfer of learned information. Subsequent memory analyses of encoding data revealed dissociations between hippocampal subregions that predicted successful memory for directly learned pairs and those that predicted successful transfer to novel combinations. Analysis of retrieval data revealed MTL subregions that were associated with correct performance on both directly learned pairs and pairs requiring flexible generalization. In contrast, some hippocampal subregions, such as subiculum and posterior hippocampus, were preferentially associated with correct generalization but not performance related to directly learned associations. Additionally, individual differences in activation during rapid encoding of associative information predicted individual differences in generalization performance in the hippocampal but not MTL cortical subregions. Specifically, encoding activation in CA1 and subiculum tracked generalization performance both within and across participants. Together these findings suggest unique contributions of MTL subregions to integrative encoding and associative retrieval processes that support successful generalization of acquired knowledge.

References/Funding Source

Presented at Society for Neuroscience 2009

Aortic Flow at the Supraceliac and Infrarenal Levels in Patients with Abdominal Aortic Aneurysms

A.S. Les[1], J. J. Yeung[2], G. M. Schultz[2], R.J. Herfkens[3], R.L. Dalman[2], Charles A. Taylor[1]
Depts of [1]Bioengineering, [2]Surgery, and [3]Radiology, Stanford University, CA

Hemodynamic forces are thought to play a critical role in abdominal aortic aneurysm (AAA) growth. Computational hemodynamic simulations can be used to study these forces, but require accurate aortic geometries and boundary conditions. Many AAA simulations use patient-specific geometries derived from readily-available CT and MR studies, but utilize inlet boundary conditions taken from a single, unrelated, healthy young adult. In this study, we imaged 43 AAA patients using a 1.5T MR GE scanner. A 24-frame cardiac-gated 1-component phase-contrast MRI (PC-MRI) sequence was used to measure aortic volumetric flow at the supraceliac (SC) and infrarenal (IR) locations, where flow information is typically needed for simulation. For the first 36 patients, individual waveforms were interpolated to a 12-mode Fourier curve defined at 1000 points, peak-aligned, and averaged. Both the SC and IR averaged waveforms had the biphasic shapes characteristic of older adults, and mean SC and IR flow over the cardiac cycle was 51.2±10.3 ml/s and 17.5±5.44 ml/s, respectively. Allometric scaling equations were derived from log-log plots of mean SC and IR flow versus body mass, height, body surface area (BSA), and fat-free body mass. Linear regression revealed that BSA was most strongly predictive of mean SC and IR flow, with the highest combined R2. We validated our model by comparing predicted and measured mean flows and flow waveforms in the last seven patients (patients 37 through 43); the measured and predicted mean flows and waveforms agreed well. Thus, we present a highly generalizable method to compute more accurate SC and IR mean flows and flow waveforms for AAA simulation.

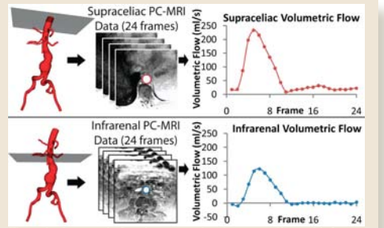

Through-plane aortic flow is measured at the supraceliac and infrarenal locations.

References/Funding Source

A. S. Les, J. J. Yeung, G. M. Schultz, R. J. Herfkens, R. L. Dalman, C. A. Taylor "Supraceliac and Infrarenal Aortic Flow in Patients with Abdominal Aortic Aneurysms: Mean Flows, Waveforms, and Allometric Scaling Relationships" Submitted to American Journal of Physiology-Heart and Circulatory Physiology
This work was supported by the National Institutes of Health (Grants P50 HL083800, and P41 RR09784).

Sparsely-distributed organization of face and limb activations in human ventral temporal cortex

K S Weiner[1] and K Grill-Spector[1,2]
Dept of [1]Psychology and [2]Neuroscience Institute, Stanford University, CA

Functional magnetic resonance imaging (fMRI) studies examining object representation in the human brain support two dichotomous theories. The first is a modular representation where regions in human ventral temporal cortex (VTC) respond preferentially to certain categories, such as faces and bodyparts, relative to other objects. The second is a distributed representation where the activation pattern across VTC discriminates one category from another more so than these isolated regions. An open question remains if there is a consistent fine-scale organization among face and bodypart VTC regions that generates a hybrid organization between these modular and distributed theories. Using high-resolution fMRI (HR-fMRI; inplane resolution 1.5mm), we examined the organization of face and limb activations in VTC across days, tasks, and paradigms. We scanned seven healthy individuals in three experiments across two scanning sessions five months apart.

We report novel findings for a consistent interdigitated organization of face- and limb-selective activations that form complementary and minimally overlapping bands of activity along lateral VTC. These clusters fall in similar anatomical locations both within subjects across sessions, as well as between subjects. While there are highly selective clusters for limbs and for faces forming a fine-grain structure in lateral VTC, medial VTC lacks any face- or limb-selective clusters and contains almost no face- or limb-selective voxels. In spite of this, using multivoxel pattern analyses we find distinct patterns for faces and limbs in medial VTC, showing for the first time that this region is able to discriminate between animate categories. These data support a new model of a sparsely-distributed representation of object categories, whereby sparseness refers to the presence of several face- and limb-selective clusters in VTC with a distinct, non-overlapping organization and distributed refers to the presence of face and limb information in VTC regions that lack clusters selective for these categories.

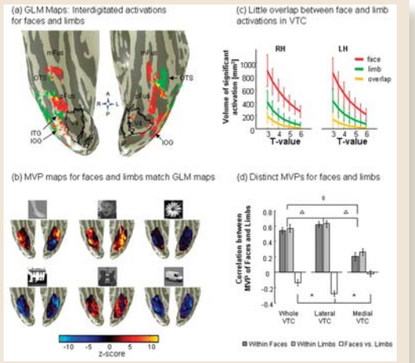

Sparsely-distributed organization of face- and limb-selective activations. (a) GLM contrasts from Exp1, Day1 indicating non-overlapping face vs. objects (cars, houses, flowers and guitars, t >3, voxel level, red), non-overlapping limbs vs. objects (t>3, green), and overlapping (yellow) activations on the inflated cortical surface of a representative subject zoomed on the fusiform gyrus. A=anterior; P=posterior; R=right; L=left. (b) MVP of object categories for the same experiment and subject as in (a). (c) Volume of VTC face- and limb-selective activation and overlap as a function of threshold-value. A value of t=3 is significant at P<0.002, and t=6 is significant at P<10-8. Error bars: SEMs across subjects. (d) Within-category and between-category correlations between face and limb MVPs across Exp1 and Exp2 in Day1. Error bars: SEMs across subjects. Triangles: within-category correlations are significantly

References/Funding Source

Weiner KS and Grill-Spector K (2009) High-resolution fMRI of the human ventral stream: Reproducible sparse-distributed representations of faces and bodyparts. Human Brain Mapping Annual Meeting, San Francisco.
This work was supported by National Eye Institute 1R21EY017741; NSF BCS 0617688 and Whitehall Foundation 2005-05-111-RES grants to KGS.

Molecular Imaging

Molecular imaging is the art of looking inside of a living organism or cell to evaluate biological processes, observe normal cell behavior, identify aberrant behaviors, and develop interventions to halt or rectify such abnormalities. Through molecular and functional imaging we have made huge strides in bridging many other disciplines such as, biology, chemistry, physics, and computer science and ultimately changing and improving how we use imaging in medicine.

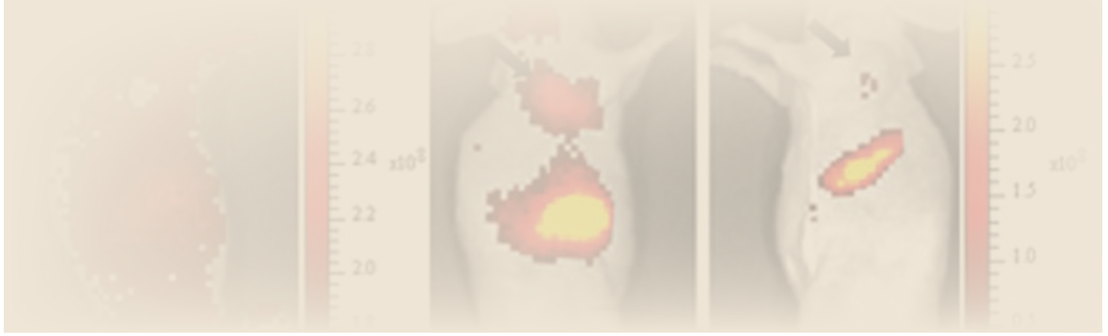

Discovery and In Vivo Evaluation of Two-Helix Small Proteins for HER2 Molecular Imaging

G Re[1] J. Webster[2], R Zhang[2], Z Liu[1], Z Miao[1], S S Gambhir[1], F A Syud[2], Z Cheng[1]
[1]Molecular Imaging Program at Stanford (MIPS), Depts of Radiology, Bioengineering and Bio-X Program, Stanford University, CA; [2]Global Research, General Electric Company

Affibody molecules, nonimmunogenic 3-helix scaffold-based proteins (~7 kDa), have drawn lots of attentions as rapidly developing imaging probes for a variety of molecular targets. We've recently shown that monomeric Affibody constructs substantially perform better *in vivo* relative to their dimeric construct despite the latter's better affinity. In this report, we further develop strategies for discovery smaller Affibody analogs, 2-helix proteins, for *in vivo* cancer molecular imaging.

Methods: The anti-human epidermal growth factor receptor type 2 (HER2) Affibody $Z_{HER2:342}$ was used as a model protein. α-Helix 3, not believed to be in direct contact with the target, was truncated, preserving helices 1 and 2 that contain the binding domain. A number of both sequence mutations and synthetic strategies to optimize the affinity of anti-HER2 2-helix proteins have been developed. A library of 2-helix proteins (> 30) was synthesized. Peptides were then site specifically conjugated with 1,4,7,10-tetraazacyclododecane-1,4,7,10-tetraacetic acid (DOTA) and labeled with PET radionuclide, ^{68}Ga or ^{64}Cu. The resulting radiolabeled peptides were further evaluated for HER2 microPET imaging in SKOV3 tumor mice. Results: Several constrained 2-helix constructs with high HER2 affinity were successfully identified. Conjugation with DOTA still preserved high HER2 binding affinity (DOTA-MUT-DS, K_D = 4.76 nM). Radiolabeled (^{68}Ga or ^{64}Cu) probe displayed high stability in mouse serum and specificity towards HER2 in cell culture. Biodistribution and microPET imaging studies further showed that DOTA-MUT-DS had rapid and high SKOV3 tumor accumulation with lower nonspecific accumulation in normal organs (Figure). The specificity of radiometal labeled MUT-DS for SKOV3 tumors was confirmed by monitoring of modulation of HER2 protein upon treatment of 17-DMAG or unlabeled Affibody *in vivo*.

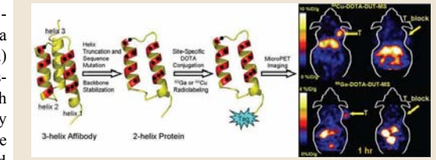

Three-helix Affibody and 2-helix protein scaffold based PET probes for HER2 imaging. Generation, radiolabeling and microPET images of decay corrected coronal images of nude mice bearing SKOV3 tumor on right shoulder at indicated time points after tail vein injection of ^{64}Cu (Top) or ^{68}Ga (Bottom)-DOTA-MUT-DS.

Conclusions: 2-helix proteins with high affinity to biomarkers can be discovered and used for *in vivo* applications. ^{68}Ga or ^{64}Cu-DOTA-MUT-DS is a promising PET probe for imaging HER2 expression *in vivo*.

References/Funding Source

Webster JM ZR, Gambhir SS, Cheng Z, Syud FA. Engineered Two-Helix Small Proteins for Molecular Recognition. ChemBioChem. 2009;In Press.
Ren G, Zhang R, Liu Z, Webster JN, Miao Z, Syud FA, Gambhir SS and Cheng Z. A Novel Two-Helix Small Protein Labeled with 68Ga for PET Imaging of Her2 expression. Journal of Nuclear Medicine, 2009. In Press.
ICMIC, SU Radiology, GE

Molecular Imaging Melanin Targeted Molecular Imaging of Melanoma Metastasis using a ^{18}F-labeled Benzamide Analog

G Ren[1], Z Miao[1], H Liu[1], L Jiang[1], N Limpa-Amara[2], A Mahmood[2], S S Gambhir[1], Z Cheng[1]
[1]Molecular Imaging Program at Stanford (MIPS), Depts of Radiology, Bioengineering and Bio-X Program, Stanford University, CA; [2]Department of Radiology, Division of Nuclear Medicine, Harvard Medical School and Brigham & Women's Hospital

Melanin biosynthesis is an essential metabolic pathway for melanoma cells and melanin has become an attractive target for specific detection of melanoma metastases. Benzamide analogs possess affinities with melanin, suggesting them may be good vehicles to specifically deliver radionuclides and chemotherapeutics for both diagnostic and therapeutic purposes towards malignant melanoma. With the help of state of art positron emission tomography (PET) technologies, we hypothesized ^{18}F labeled benzamide compounds could identify melanotic melanoma metastases *in vivo* with high sensitivity and specificity. Methods: In this research, ^{18}F-N-[2-(diethylamino)ethyl]-4-fluoro-Benzamide (^{18}F-FBZA) was synthesized and by coupling of [N-succinimidyl-4-[^{18}F]fluorobenzoate ([^{18}F]SFB) with the amino group in N,N-Diethylethylenediamine. The radiofluorinated compound was tested for both binding and internalization in B16F10 cells with or without L-tyrosine (2mM) treatment. B16F10 and A375M melanoma bearing mice were used for biodistribution and μPET studies. Non-melanoma tumor, C6, was used as an animal model control, and ^{18}F-FDG-PET imaging of melanoma models was also performed for comparison. Finally, lung metastastic melanoma model was studied using *in vivo* μPET and *ex vivo* radiophosphor imaging. Results: The fast and high uptakes of *18*F-FBZA was observed in B16F10 cells treated with L-tyrosine under 37 °C. *18*F-FBZA based biodistribution and μPET imaging studies showed promising results in terms of differentiation melanotic tumor from amelanotic melanoma *in vivo*. Additionally, in lung melanoma metastases model, higher lung uptake of the probe was detected by μPET compared with that of the normal lung. Ex vivo autoradiography could detect lung micro-metastases as small as 1.0 mm in diameter. Conclusion: ^{18}F-FBZA successfully and specifically target primary and metastastic melanotic melanoma with high uptake *in vivo* in preclinical models.

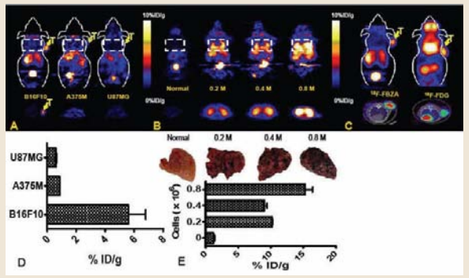

(A) Representative decay-corrected coronal (top) and transaxial (bottom) small-animal μPET images of ^{18}F-FBZA in different subcutaneous tumor models (B16F10 vs. A375M vs. U87MG). About 100 μCi ^{18}F-FBZA were injected through tail vein and images were acquired 1 hr post-injection. Arrows indicate location of tumors. Rectangles indicate lung regions. (B) Representative decay-corrected coronal (top) and transaxial (bottom) small animal PET images of B16F10 melanoma lung metastases model which was established 13 days after tail vein injection of 0.2 (n=3), 0.4 (n=3) or 0.8 × 10^6 (n=2) B16F10 cells. About 100 μCi ^{18}F-FBZA was injected through tail vein and images were acquired 1 h p.i. (C) Representative decay-corrected small animal μPET coronal images (top) and PET/CT fusion transaxial images (bottom) of C57BL/6 mice bearing B16F10 tumors on right shoulders. About 100 μCi ^{18}F-FBZA or ^{18}F-FDG was injected through tail vein and images were acquired 1 h post-injection. (D) Quantification analysis of subcutaneous tumors uptake of ^{18}F-FBZA in different tumor models for comparison. (E) Photographic images of lung metastases biopsy (top) and quantification analysis of melanoma lung metastases uptake of ^{18}F-FBZA (bottom).

References/Funding Source

Ren G, Miao Z, Liu H, Jiang L, Limpa-Amara N, Ashfaq M, Gambhir SS and Cheng Z. Melanin Targeted Pre-clinical PET Imaging of Melanoma Metastasis
Journal of Nuclear Medicine, 2009. In Press.
Melanoma Research Alliance, ICMIC, SU Radiology

^{64}Cu-Labeled Multivalent α-Melanocyte Stimulating Hormone Analogs for MicroPET Imaging of Melanocortin 1 Receptor Expression

H G Liu[1,2], Z Miao[1], G Ren[1], L Jiang[1], R H Kimura , J R Cochran[1], P Z Han[2], Z Cheng[1]
[1]Molecular Imaging Program at Stanford (MIPS), Depts of Radiology and Bio-X Program, Stanford University, CA; [2]Institute of Radiation Medicine, Chinese Academy of Medical Sciences, Peking Union Medical College, China

Multivalent peptides have been explored as a useful strategy to construct molecular imaging probes and drug delivery carriers. It is generally accepted that multivalency has advantages over monovalency for improving binding affinities and even activity. Herein by using multivalent α-melanocyte stimulating hormone (α-MSH) analogs, B16F10 melanoma–bearing mice and microPET imaging technology, we systematically investigated the influence of multivalent effect on α-MSH analogs' binding affinity and in vivo melanoma targeting profiles.

Methods: Three α-MSH analogs named as MSH1, MSH2 and MSH4 were designed and synthesized, which contained one, two or four valency of an α-MSH core sequence, His-d, Phe-Arg-Trp, respectively (Fig. a). α-MSH analog tetramer was constructed using the multiple antigenic peptide (MAP) scaffold. 1,4,7,10-tetraazacyclododecane-1,4,7,10-tetraacetic acid (DOTA) was conjugated to the lysine residue of peptides for radiolabeling with a PET radioisotope, ^{64}Cu. In vitro binding affinity assays were performed with B16F10 melanoma cell line. After radiolabeling with ^{64}Cu, the in vivo performances of the peptides were evaluated in subcutaneous B16F10 melanoma xenografted mice by micro-PET imaging followed by biodistribution studies.

Results: In the receptor competition binding assays, DOTA-MSH4 showed highest binding affinity (IC_{50}= 1.00 nM) which is consistent with its highest ligand density. However, in vivo study demonstrated poor performance of MSH4 as an imaging agent due to its lowest tumor uptake and highest kidney accumulation. In comparison, DOTA-MSH2 displayed medium affinity (IC_{50}=2.06 nM), yet highest tumor uptake and lowest kidney accumulation (Fig. b). Further blocking study of DOTA-MSH2 confirmed its tumor targeting specificity *in vivo*.

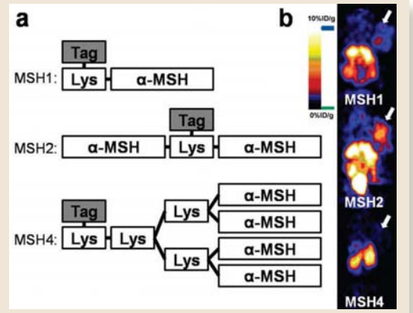

(a) Schematic structures of multivalent alpha-MSH peptides (MSH1, 2 and 4); (b) Decay-corrected coronal micro-PET images of C57 mouse bearing B16F10 tumor at 2 h after tail vein injection of ^{64}Cu-DOTA conjugated α-MSH analogs. Arrows indicate location of tumors.

Conclusion: Multivalency effects have complex impact to peptides' *in vivo* behaviors. Eventhough MSH tetramer shows the higher binding affinities *in vitro*, the better in vivo tumor targeting ability is achieved by MSH dimer. ^{64}Cu labeled dimeric DOTA-MSH2 has been identified as an ideal melanoma PET imaging probe.

References/Funding Source

1. Oral Presentation at the World Molecular Imaging Conference, Montreal, Canada, Sept. 23- 26, 2009.
2. Poster Presentation at the 56th Annual Meeting of the Society of Nuclear Medicine, Toronto, Canada, June 13-17, 2009.
ICMIC, SU Radiology

Near-infrared Fluorescence Imaging of Melanocortin 1 Receptor Expression with A Cy5.5-Labeled α-Melanocyte-Stimulating Hormone Analog

H Liu[1,2], G Ren[1], Z Miao[1], P Han[2], S S Gambhir[1], Z Cheng[1]
[1]Molecular Imaging Program at Stanford (MIPS), Dept of Radiology and Bio-X Program, Stanford University, CA; [2]Institute of Radiation Medicine, Chinese Academy of Medical Sciences, Peking Union Medical College, China

The α-melanocyte-stimulating hormone (α-MSH) receptor (MC1R) is known to be overexpressed in most of murine and human melanoma, making it a promising molecular target for melanoma imaging and therapy. The purpose of this study was to evaluate a near-infrared (NIR) fluorophore, Cy5.5 conjugated α-MSH analog (Cy5.5-MSH, Fig. a), as a contrast agent to visualize tumor MC1R expression in vivo.

Methods: α-MSH analog containing α-MSH core sequences, His-D-Phe-Arg-Trp, was designed and synthesized using Fmoc/HBTU chemistry on a solid-phase peptide synthesizer and conjugated with Cy5.5 through the N-terminal cysteine. The binding affinity of Cy5.5-MSH was determined using a competitive receptor binding assay. Melanoma B16F10, TXM13 and A375M, which has high, medium and low MC1R expression, respectively, were chosen to evaluate the MC1R imaging profiles of Cy5.5-MSH in vitro and in vivo.

Results: Cy5.5-MSH was successfully synthesized and displayed high MC1R binding affinity (0.6nmol/L). In vitro cell fluorescence imaging study revealed that the probe showed high, medium and low cell staining in B16F10, TXM13 and A375M cell lines, respectively, which was in consistence with their receptor expression levels. Co-incubation the probe with a large excess of the α-MSH peptide NDP specifically inhibited the probe uptakes in B16F10 and TXM13 cells. In vivo optical imaging detected little fluorescence in B16F10 tumor (Fig. b), which was mainly caused by the high melanin content in B16F10 tumor that absorbed nearly all excitation and emission NIR lights. To the contrary, melanoma TXM13 with much less melanin content and medium level of MC1R expression could be clearly visualized with Cy5.5-MSH (Fig. c). Finally, amelanotic A375M with the lowest MC1R expression showed poor tumor/normal contrast (Fig. d).

Conclusion: This study suggests that the combination of the specificity of α-MSH peptide with NIR fluorescence detection may be applied to molecular imaging of MC1R expression in melanoma with low melanin content.

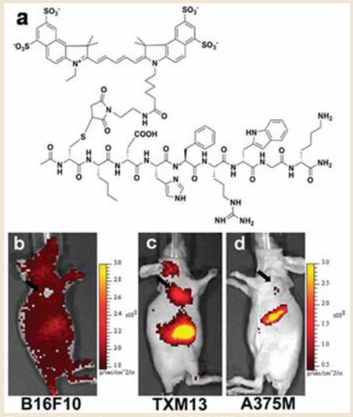

Figure. a. Schematic structure of Cy5.5-MSH. In vivo fluorescence imaging of subcutaneous B16F10 (b), TXM13 (c) and A375M (d) melanoma tumor-bearing nude mice after intravenous injection of 0.5nmol of Cy5.5-MSH. The position of the tumor is indicated by an arrow.

References/Funding Source

Poster Presentation at the World Molecular Imaging Conference, Montreal, Canada, Sept. 23- 26, 2009.
ICMIC, SU Radiology

Affibody Based Molecular Probes for EGFR PET and Optical Imaging

Z Miao [1,2], G Ren [1,2], H Liu [1,2], L Jiang [1,2], Y Wang [1,2], S S Gambhir [1,2], Z Cheng [1,2]
Dept of [1]Radiology (MIPS), MIPS and [2]Bio-X Program, Stanford University, CA

The purpose of this study is to site-specifically label an Affibody protein (Ac-Cys-$Z_{EGFR:1907}$) binding to epidermal growth factor receptor (EGFR) with Cy5.5 and ^{64}Cu-DOTA , investigate its in vitro cell uptake and binding specificity, study Cy5.5-$Z_{EGFR:1907}$ and ^{64}Cu-DOTA-$Z_{EGFR:1907}$ in vivo tumor imaging ability, and evaluate the potential of EGFR PET imaging with ^{64}Cu-DOTA-$Z_{EGFR:1907}$ for clinical translation.

Methods: Molecular probe Cy5.5-$Z_{EGFR:1907}$ and ^{64}Cu-DOTA-$Z_{EGFR:1907}$ were made through solid peptide phase synthesis of Ac-Cys-$Z_{EGFR:1907}$ followed by site-specific conjugation with Cy5.5-mono-maleimide and DOTA-mono-maleimide respectively. DOTA-$Z_{EGFR:1907}$ was then labeled with ^{64}Cu in sodium acetate buffer (pH=5.0) at 40 °C. Cell uptake assay was performed using EGFR expression A431 cell line (epidermoid cancer cell line) with/without pre-incubation of unlabeled Ac-Cys-$Z_{EGFR:1907}$ for blocking. Cy5.5-$Z_{EGFR:1907}$ (500pmol) or ^{64}Cu-DOTA-$Z_{EGFR:1907}$ (40-70 μCi) was injected into A431 tumor bearing nude mice through tail-vein for optical imaging and microPET imaging respectively. Bio-distribution studies were performed at 1, 4 and 24 hours post-injection (p.i.).

Results: In vitro microscopy study showed that majority of Cy5.5-$Z_{EGFR:1907}$ specifically bound to A431 cell surface in 1 h. Optical imaging of Cy5.5-$Z_{EGFR:1907}$ successfully demonstrated EGFR receptor mediated targeting to A431 tumor. For radiolabeled probe, it displayed high (27% at 1 h) and specific in vitro cell uptake. In vivo micro-PET imaging showed high tumor accumulation (> 10 %ID/g at 4 h p.i.) and good contrast of ^{64}Cu-DOTA-$Z_{EGFR:1907}$. Bio-distribution studies demonstrated that ^{64}Cu-DOTA-$Z_{EGFR:1907}$ had high tumor uptakes, and also high blood, liver and kidney uptakes, while kidney and blood uptake dropped significantly 24 h p.i..

Conclusions: Cy5.5 and ^{64}Cu labeled $Z_{EGFR:1907}$ can provide high sensitivity, receptor specific optical and PET imaging of EGFR positive tumors. ^{64}Cu-DOTA-$Z_{EGFR:1907}$ is mainly clearly through kidney-urinary system. Three-helix Affibodies are excellent protein scaffolds for the development of PET probes for clinical translation.

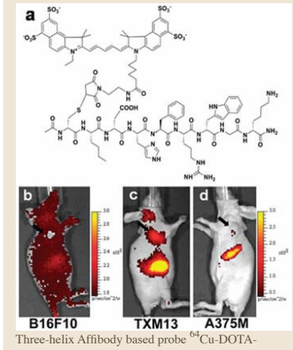

Three-helix Affibody based probe ^{64}Cu-DOTA-$Z_{EGFR:1907}$ and Cy5.5-$Z_{EGFR:1907}$ for EGFR PET and optical imaging. (A) Cartoon of Affibody based probes, the black dots and red regions indicate the amino acid residues responsible for receptor binding. Optical (B) and microPET imaging (C) of a mouse bearing A431 tumor xenograft at 2 h p.i.. Arrows were pointed at tumors. T, tumor; L, liver; K, kidney.

References/Funding Source

Affibody Based Molecular Probes for EGFR PET and Optical Imaging. Z. Miao, G. Ren, H. Liu, L. Jiang, Y. Wang, S. S. Gambhir, Z Cheng. 2009 World Molecular Imaging Congress meeting, Montreal, poster.
This work was supported, in part, by California Breast Cancer Research Program 14IB-0091 (ZC), SNM Pilot Research Grant (ZC) and National Cancer Institute (NCI) Small Animal Imaging Resource Program (SAIRP) grant R24 CA93862.

Agouti-Related Protein: An Excellent Cystine-Knot Peptide Scaffold for Developing Molecular Probes for In Vivo Molecular Imaging

L Jiang,[1,2] R H Kimura,[1] Z Miao,[1] A P Silverman,[1] G Ren,[1] H G Liu[1], P Y Li[2], S S Gambhir,[1] J R Cochran,[1] Z Cheng[1]
[1]Molecular Imaging Program at Stanford, Department of Radiology and Bioengineering, Bio-X Program, Stanford University, CA; Dept of [2]Nuclear Medicine, Ruijin Hospital, Shanghai Jiaotong University, China

Agouti-related protein (AgRP) is a 4-kDa cystine-knot peptide of human origin with four disulfide bonds and four solvent exposed loops that are amenable to directed evolution. An AgRP-based combinatorial library has recently been screened to identify mutants that bind $\alpha_v\beta_3$ integrin with high affinity and specificity. In this study, for the first time we evaluated the feasibility of using AgRP peptides for in vivo cancer molecular imaging. Methods: AgRP peptides were prepared using solid-phase peptide synthesis and an oxidative folding reaction. Receptor competition binding assays were performed to measure their affinity to $\alpha_v\beta_3$ integrin-expressing tumor cells. Mutant 7C-AgRP, which showed high $\alpha_v\beta_3$ integrin binding affinity, was site-specifically conjugated to 1, 4, 7, 10-tetra-azacyclododecane-N, N', N'', N'''-tetraacetic acid (DOTA), and the resulting bioconjugate DOTA-7C-AgRP was then labeled with ^{64}Cu for biodistribution and microPET imaging studies in mice bearing U87MG xenografts. The metabolic stability of ^{64}Cu-DOTA-7C-AgRP was also evaluated in vitro and in vivo. Results: DOTA conjugated 7C-AgRP (IC_{50}=22.6±3.9 nM) was successfully radiolabeled with ^{64}Cu in high radiochemical purity (>99%). Radiolabeled 7C-AgRP showed fast blood clearance, good tumor uptake and retention (2.70±0.93 and 2.37±1.04 %ID/g at 2 and 24 h, respectively) and excellent tumor imaging ability (20.87 and 11.32 at 4 h for tumor-to-blood and tumor-to-muscle, respectively). Integrin $\alpha_v\beta_3$ binding specificity of the probe was confirmed in vitro and in vivo by using large excess of unlabeled c(RGDyK). Metabolite analysis demonstrated that the peptide was very stable in mouse serum. Conclusion: ^{64}Cu-DOTA-7C-AgRP shows great potential as a molecular probe for $\alpha_v\beta_3$ integrin-positive tumor PET imaging. AgRP is an excellent protein scaffold for further development of peptides for tumor imaging and therapy.

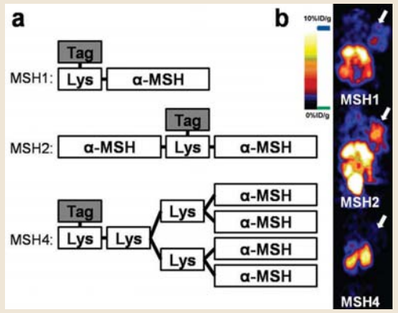

(a) Schematic structures of multivalent alpha-MSH peptides (MSH1, 2 and 4); (b) Decay-corrected coronal micro-PET images of C57 mouse bearing B16F10 tumor at 2 h after tail vein injection of ^{64}Cu-DOTA conjugated α-MSH analogs. Arrows indicate location of tumors.

References/Funding Source

1. Oral Presentation at the World Molecular Imaging Conference, Montreal, Canada, Sept. 23- 26, 2009.
2. Poster Presentation at the 56th Annual Meeting of the Society of Nuclear Medicine, Toronto, Canada, June 13-17, 2009.
ICMIC, SU Radiology

An ^{18}F-Labeled Knottin Peptide for Tumor $\alpha_v\beta_3$ Integrin PET Imaging

Z Miao [1,2], G Ren [1,2], H Liu [1,2], L Jiang [1,2], Y Wang [1,2], R H Kimura[1,2,3], J R Cochran[2,3], S S Gambhir [1,2], Z Cheng [1,2]
Dept of [1]Radiology (MIPS), [2]MIPS and Bio-X Program, [3]Bioengineering, Stanford University, CA

Knottins are small constrained polypeptides that share a common disulfide-bonded framework and a triple-stranded β-sheet fold. Our objectives were to: 1) site-specifically label an integrin $\alpha_v\beta_3$ binding knottin peptide, 2.5D, with $^{18/19}$F, 2) characterize ^{18}F labeled 2.5D (^{18}F-FB-2.5D) in living subjects with microPET imaging methods, and 3) evaluate the translational potential of ^{18}F-FB-2.5D.

Methods 2.5D was prepared by solid phase synthesis and followed by oxidation in DMSO. 2.5D was reacted with N-succinimidyl-4-$^{18/19}$F-fluorobenzoate ($^{18/19}$F-SFB) in DMSO at 60°C. Competition binding assays were performed with human glioblastoma U87MG cells using ^{125}I-labeled echistatin. Approximately 100 uCi ^{18}F-FB-2.5D, with and without a molar excess of c(RGDyK), was injected via the tail vein of U87MG tumor bearing mice for microPET imaging performed at 0.5 h, 1 h post-injection (p.i.) In addition, biodistribution studies were conducted at 0.5 h p.i. Finally, dynamic microPET scanning for a 35 min p.i. duration was also performed.

Results and Conclusions ^{19}F-FB-2.5D competed with ^{125}I-echistatin for binding to cell surface integrins with an IC_{50} of 13.2 ± 5.4 nM. Radiofluorinated 2.5D displayed a high specific activity (ca 100 GBq/μmol) throughout the course of our studies. In vivo microPET imaging showed that the radiotracer rapidly accumulated at the tumor (2.7%ID/g, n=3), and also rapidly cleared through the kidneys. These pharmacokinetics leads to promising tumor-to-normal tissue contrast (Figure1). Bio-distribution studies demonstrated that ^{18}F-FB-2.5D had moderate tumor uptakes at 0.5 h p.i. and that co-injection of c(RGDyK) significantly reduced tumor uptake (1.90 ± 1.15 %ID/g vs 0.57 ± 0.14 %ID/g, 70% inhibition, P<0.05). Dynamic scanning showed high kidney uptake at early time points (51.8 %ID/g at 4 min p.i.), followed by rapid clearance within a half an hour (6.2 %ID/g at 35 min p.i.). Finally, the probe displayed relatively low uptake in the liver (1.5 %ID/g at 35min p.i.). Collectively, knottins are excellent peptide scaffolds for development of PET probes for clinical translations.

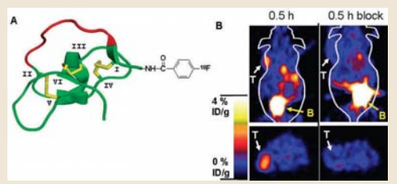

(A) Cartoon representation of a knottin scaffold showing the location of the conjugated radiolabel. The loop that was mutated for integrin binding is indicated in red. (B) The coronal and transaxial microPET images of U87MG tumor-bearing mice at 0.5 h after injection of ^{18}F-FB-2.5D with or without c(RGDyK) co-injection. Tumor(T) and Bladder(B) are indicated by arrows

References/Funding Source

An 18F-Labeled Knottin Peptide for Tumor αvβ3 Integrin PET Imaging
Z. Miao, G. Ren, H. Liu, L. Jiang, R. H. Kimura, J. R. Cochran, S. S. Gambhir, Z. Cheng. 2009 World Molecular Imaging Congress meeting, Montreal, Poster.
This work was supported, in part, by National Cancer Institute (NCI) In Vivo Cellular Molecular Imaging Center (ICMIC) grant P50 CA114747 (SSG), NCI Small Animal Imaging Resource Program (SAIRP) grant R24 CA93862, NCI 5K01 CA104706 (JRC), and the Edward Mallinckrodt Jr. Foundation (JRC).

A PROTEIN SCAFFOLD BASED MOLECULE FOR EGFR PET IMAGING

Z Miao[1,2], G Ren[1,2], H Liu[1,2], L Jiang[1,2], Y Wang[1,2], S S Gambhir[1,2], Z Cheng[1,2]
Dept of [1]Radiology (MIPS), MIPS and [2]Bio-X Program, Stanford University, CA

Site-specifically label a three-helix scaffold based protein ($Z_{EGFR:1907}$) binding to epidermal growth factor receptor (EGFR) with ^{64}Cu, investigate its in vitro cell uptake and binding specificity, study the ^{64}Cu labeled $Z_{EGFR:1907}$ (^{64}Cu-DOTA-$Z_{EGFR:1907}$) in vivo tumor imaging ability, and evaluate its clinical translational potentials.

Methods DOTA-$Z_{EGFR:1907}$ was made through solid phase synthesis of the protein Ac-Cys-$Z_{EGFR:1907}$ followed by the site specific conjugation with a DOTA derivative. The bioconjugate was then labeled with ^{64}Cu in sodium acetate buffer (pH=6.5) at 40°C. Cell uptake test was performed with A431 cell line (epidermoid cancer) and pre-incubation with/without unlabeled DOTA-$Z_{EGFR:1907}$. ^{64}Cu-DOTA-$Z_{EGFR:1907}$ (30-50 μCi) was injected into A431 tumor bearing nude mice through tail-vein for microPET imaging and biodistribution studies at 1, 4, and 24 hours post-injection (p.i.). In vitro analysis of EGFR levels in tumor, liver and blood was studied by western blot analysis using anti-human EGFR antibody.

Results ^{64}Cu-DOTA- $Z_{EGFR:1907}$ displayed a moderate specific activity (30 μCi/μg). In vitro cell uptake of ^{64}Cu-DOTA-$Z_{EGFR:1907}$ was high (~25%) and specific. In vivo microPET imaging showed fast tumor targeting, high tumor accumulation (>10 %ID/g at 4 h p.i.) and good contrast of ^{64}Cu-DOTA-$Z_{EGFR:1907}$. Bio-distribution studies demonstrated that ^{64}Cu-DOTA-$Z_{EGFR:1907}$ had high tumor, blood, liver and kidney uptakes, while blood level was dropped significantly 24 h p.i.. It was also observed high EGFR expression levels in blood, liver and tumor as tested by western blot analysis.

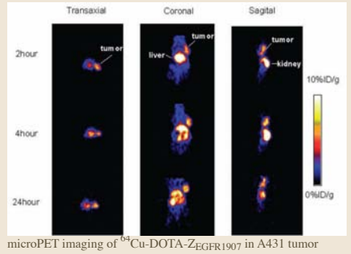

microPET imaging of ^{64}Cu-DOTA-$Z_{EGFR1907}$ in A431 tumor bearing mice. Good contrast imaging was obtained as early as 2hours post-injection and ^{64}Cu-DOTA-$Z_{EGFR1907}$ has good tumor retention up to 24 hours post-injection.

Conclusions ^{64}Cu-DOTA-$Z_{EGFR:1907}$ can provide high contrast, receptor specific PET imaging of EGFR positive tumors. ^{64}Cu-DOTA-$Z_{EGFR:1907}$ was cleared through both liver and kidney. High expression of EGFR in blood doesn't interfere with ^{64}Cu-DOTA-$Z_{EGFR:1907}$ accumulation in tumors.

REFERENCES/FUNDING SOURCE

A protein scaffold based molecule for EGFR PET imaging. Z. Miao, G. Ren, H. Liu, L. Jiang, S. S. Gambhir, Z. Cheng. 2009 SNM annual meeting, Toronto, oral presentation.

This work was supported, in part, by California Breast Cancer Research Program 14IB-0091 (ZC), SNM Pilot Research Grant (ZC) and National Cancer Institute (NCI) Small Animal Imaging Resource Program (SAIRP) grant R24 CA93862.

FACTORS AFFECTING PARTIAL VOLUME CORRECTION OF PET-CT IMAGES BASED ON THE METHOD OF RECOVERY COEFFICIENTS.

D Yerushalmi[1,3], F Habte[2,3], S S Gambhir[2,3]
Depts of [1]Bioengineering, [2]Radiology, and [3]Molecular Imaging Program at Stanford (MIPS), Stanford University, CA

Accurate quantitation of focal tracer uptake in PET-CT images is relevant to a number of applications including treatment monitoring and earlier disease detection. Blurring due to the partial volume effect limits accurate measurement of activity concentration in small tumors. Partial volume correction using recovery coefficients (RC) is an established method for more accurately estimating focal uptake in PET images however its application for quantitation of relatively small lesions has been unreliable. Here we demonstrate the use of phantom studies and computer simulations to investigate the relative effect of different factors contributing to the observed variability including noise, slice thickness, and object placement. A small hollow sphere (radius = 3.95 mm) was filled with a calibrated concentration of activity (~1 μCi/mL). A series of PET-CT scans were performed by varying scan time and object location in order to independently measure the effect of these experimental parameters. In a related study, the Point spread function (PSF) for the PET-CT scanner was measured by imaging a point source positioned about the center of the FOV. The imaging process was then modeled as the convolution of a discretized spherical object with a Gaussian kernel based on prior experimental measurements. Model data was reformatted to account for changing PET slice thickness and object position to better understand the sensitivity of quantitation accuracy as a function of these parameters and for comparison with experimental data. Simulation results suggest that the error due to object offset relative to detector center may be as large as 12±7%. This is much larger than the contribution of noise (~2-3%), and also depends on the accuracy of the PSF measurement at any given position. These results better characterize the factors that limit application of the recovery coefficients and suggest the need for more accurate methods to estimate the scanner PSF.

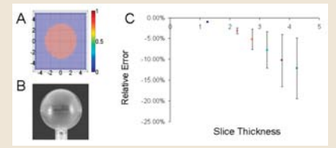

Cross-section through discretized object used for simulation (A), Image of physical phantom used for data acquisition experiments (B), Plot showing predicted Percent Relative Error estimated based on a simulation and showing increasing average error and variability with increasing slice thickness (C)

PRECLINICAL EVALUATION OF RAMAN NANOPARTICLES FOR THEIR POTENTIAL USE IN CLINICAL ENDOSCOPIC IMAGING

C L Zavaleta[1,2], K B Hartman[1,2], Z Miao[1,2], Z Cheng[1,2], S S Gambhir[1,2,3]
[1]Molecular Imaging Program at Stanford, [2]Dept of Radiology and [3]Bio-X Program, Stanford University, CA

Raman spectroscopy continues to prove itself as a powerful non-invasive molecular imaging tool to evaluate nanoparticle delivery in preclinical models. Its pM sensitivity and multiplexing capabilities are unsurpassed. However, its limited depth of light penetration hinders direct clinical translation. Therefore, a more suitable way to harness its attributes in a clinical setting would be to couple Raman spectroscopy with endoscopy. It was recently reported that flat lesions in the colon were five times more likely to contain cancerous tissue than polyps detected by conventional colonoscopy. The use of an accessory Raman endoscope in conjunction with locally administered tumor targeting Raman nanoparticles during a routine colonoscopy could offer a new way to sensitively detect these dysplastic flat lesions. In this study we evaluated the natural biodistribution of gold surface enhanced Raman scattering (SERS) nanoparticles by radiolabeling them with ^{64}Cu and imaging their localization over time using microPET. Mice were injected either intravenously (IV) or intrarectally (IR) with approximately 100 °Ci of ^{64}Cu-SERS nanoparticles and imaged with microPET at various time points: immediately, 30 m, 2, 5, and 24 h post injection. Three mice from each group (IV and IR) were sacrificed at 2, 5 and 24 h and their organs were collected, weighed and counted in a gamma counter to determine % injected dose per gram (%ID/g). Quantitative biodistribution data obtained from each organ correlated well with the corresponding microPET images, revealing that mice injected IV had significantly higher uptake ($p<0.05$) in the liver (5h=18.9% ID/g) (24h=4.8% ID/g), as opposed to mice injected IR (5h=1.27% ID/g) (24h=0.3% ID/g). Mice injected IR showed localized uptake in the large intestine (5h=9% ID/g) (24h=4.3% ID/g) with minimal uptake in other organs. Raman imaging of the excised tissues confirmed the presence of SERS nanoparticles within tissues of interest. These results suggest that topical application of SERS nanoparticles in the colon appears to minimize their systemic distribution, thus avoiding potential toxicity and supporting the clinical translation of Raman spectroscopy as an endoscopic imaging tool.

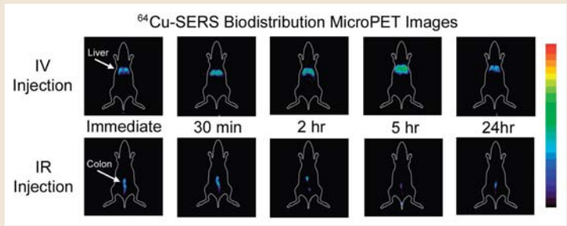

MicroPET imaging in mice after either intravenous (IV) or intrarectal (IR) administration of Cu-64 labeled SERS nanoparticles at various time points post injection. Notice the differences in distribution between the mouse receiving IV injection (top panel) versus the mouse receiving IR injection (bottom panel) of ^{64}Cu-SERS nanoparticles. The SERS nanoparticles appear to localize in the liver immediately after IV injection and remain in the liver over 24 hours whereas the SERS nanoparticles injected IR remain localized in the colon over 24 hours post IR injection. Colored scale bar to the right represents ^{64}Cu-SERS uptake where red represents most uptake and black represents no uptake.

REFERENCES/FUNDING SOURCE

Poster Presentation at World Molecular Imaging Congress 2009

This work was funded in part by NCI CCNE U54 CA119367 (SSG), NIBIB BRP 5-RO1-EBB000312 (SSG), and ICMIC P50 CA114747 (SSG). Special thanks to the Canary Foundation for their generous support. C. Zavaleta received support from NIH Training grant T32 CA09695-15 Advanced Techniques for Cancer Imaging.

AUTOMATED RADIOSYNTHESIS OF [^{18}F]FLUOROURACIL FOR CLINICAL PET STUDIES

F T Chin[1,2], M Subbarayan[1,2], R Berganos[1,2], S S Gambhir[1,2,3], and A Quon[1,2]
[1]Molecular Imaging Program at Stanford, [2]Dept of Radiology and [3]Bio-X Program, Stanford University, CA

Introduction. 5-Fluorouracil (FU) is a known chemotherapeutic agent for treating cancer patients. More recently, other studies have shown that the combination of new drugs with standard chemotherapy can increase response rate and prolong overall survival. Positron emission tomography (PET) with [^{18}F]FU can allow pharmacokinetic study of these drug deliveries and chemotherapy combinations in tumor and normal tissues of patients. A safe, routine, and automated radiosynthesis of [^{18}F]FU had to be developed before PET studies with [^{18}F]FU could begin in our clinic.

Experimental. Optimized radiochemistry was performed in a GE TRACERLab FX_{FE} synthesis module with a Dionex HPLC pump. Uracil (8 mg), acetic acid (2.25 mL), and acetic anhydride (0.75 mL), needed to be sonicated (20 min) and heated (60 °C, 5 min) together before loading into the reactor. [^{18}F]fluorine gas was bubbled at RT into the preloaded reactor and stirred (1 min) before the solution was evaporated with MeOH (2 x 1 mL). The remaining residue was neutralized and reconstituted with 0.15 M NaH2PO4, pH 7.8 (2.2. mL) and injected onto HPLC to give pure [^{18}F]FU which was filtered through a sterile Millex-GS filter (25 mm) into a sterile vial and analyzed for quality control.

Results and Discussion. All radiochemical yields (RCYs) are decay-corrected and reported as means ± SD. The [^{18}F]FU radiosynthesis affords consistent RCYs (20 ± 5%; n = 10) and good specific radioactivity, 450±78 mCi/mmol (12±2 MBq/μmol). High radiochemical and chemical purities exceeded 99% when steps were taken to ensure a homogenous precursor solution. Final dose volumes were halved and more consistent when an adequate HPLC pump was used. The complete automated process (~55 min) will likely also reduce radiation exposure to the radiochemist.

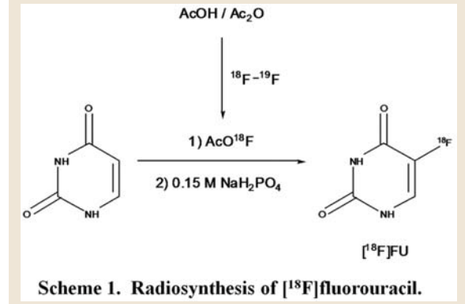

Scheme 1. Radiosynthesis of [^{18}F]fluorouracil.

Conclusion. Radiosynthesis of [^{18}F]FU was implemented in a commercial automated synthesis module to provide [^{18}F]FU routinely and more safely for clinical PET studies.

REFERENCES/FUNDING SOURCE

This research was supported by a Genentech Grant (ID# AVF3679s) and a NCI ICMIC P50 CA114747 Grant.

DYNAMIC MICRORNA EXPRESSION PROGRAMS DURING CARDIAC DIFFERENTIATION OF HUMAN EMBRYONIC STEM CELLS

K D Wilson[1,2,4], S Venkatasubrahmanyam[5], J D Fu[3], F Jia[1,2], RA Li[3], A J Butte[5], J C Wu[1,2,3]
[1]Depts of Radiology, [2]MIPS, [3]Medicine, [4]Bioengineering, [5]Medical Informatics

BACKGROUND: MicroRNAs (miRNAs) are a newly discovered endogenous class of small noncoding RNAs that play important posttranscriptional regulatory roles by targeting mRNAs for cleavage or translational repression. Recent studies have shown that miRNAs help regulate human embryonic stem cell (hESC) self-renewal and differentiation, though little is known about their expression patterns during differentiation to specific lineages such as a cardiac cell. In this study, we define the miRNAs associated with embryonic, cardiomyocyte, and mature heart tissue phenotypes, and identify a number of unique miRNAs that are associated with pluripotency and cardiac differentiation.

METHODS & RESULTS: Cardiomyocytes were differentiated from H7 hESCs based on the protocol published by Laflamme et al. (Nat Biotechnol. 2007). We confirmed successful cardiac differentiation with cardiac marker immunostaining and semi-quantitative RT-PCR. Using Sanger miRBase Version 10.0 miRNA expression microarrays (LC Sciences, Houston, TX) and quantitative PCR, we compared the miRNA profiles of hESCs and cardiomyocytes. As positive and negative controls we also profiled human fetal hearts and fetal fibroblasts (IMR90), respectively. Using a P-value threshold of 0.05, we found a unique group of embryonic miRNAs such as the miR-302 cluster that were highly expressed in hESCs but not in differentiated or mature cells. Several miRNAs, including miR-1, miR-133, and miR-208, that have previously been reported to be important in cardiac development and disease, showed dramatic expression patterns across the four cell types. Lastly, numerous other miRNAs with poorly defined roles in development also showed differential expression across our samples, such as miR-499, an miRNA located in an intronic region of cardiac myosin heavy chain 7B (MYH7B). Lentiviral overexpression of miR-499 in hESCs resulted in increased expression of mesoderm and cardiac-specific genes during differentiation.

CONCLUSION: Our results confirmed the presence of a signature group of miRNAs upregulated in hESCs, and whose expression pattern is altered during differentiation to cardiac tissue. We identified patterns of miRNA expression that suggest an important role for miRNAs in not only pluripotency but also early and late differentiation. Overexpression of some of these miRNAs resulted in altered cardiac and mesoderm gene expression during differentiation. These miRNA profiles will thus provide significant insight into the regulatory networks that govern hESC pluripotency and differentiation, as well as cardiac disease and development.

PRE-CLINICAL EVALUATION OF NOVEL CLINICALLY-TRANSLATABLE KDR-TARGETED MICROBUBBLES FOR MOLECULAR ULTRASOUND IMAGING OF ANGIOGENESIS IN CANCER

M A Pysz[1,2], C M Panje[1,2], S S Gambhir[1,2,3], M Schneider[4], and J K Willmann[1,2]
Depts of [1]Radiology, [2]MIPS, [3]Bioengineering, Stanford University, CA ; [4]Bracco Research, Geneva, Switzerland

The purpose of this study was to develop and test novel human vascular endothelial growth factor receptor type 2 (KDR)-targeted contrast microbubbles (KDR-MBs) using binding chemistry that allows a future use in patients. Previous studies have shown that molecular ultrasound using biotinylated anti-VEGFR2 antibodies conjugated to streptavidin-contrast MBs allows VEGFR2/KDR imaging at the molecular level in murine tumor xenografts. To develop clinically-translatable KDR-MBs, a peptide that binds to KDR with high affinity was isolated with phage display and coupled onto the surface of perfluorobutane-filled, lipid-shelled contrast MBs. First, binding specificity of KDR-MB compared to control MB was shown on KDR-expressing (PAE-KDR) and -negative (PAE) cells under flow stress conditions (100 s^{-1}) in a parallel plate flow chamber ($P<0.05$). In vivo binding specificity of KDR-MB was then tested in human LS174T colon carcinoma tumor xenografts in mice (n=6) using a high-resolution (40 MHz) ultrasound system. In vivo imaging signal was significantly higher ($P<0.001$) with KDR-MB compared with control MB, and significantly ($P<0.007$) dropped by 60% following receptor blocking with an anti-KDR antibody, thus, confirming in vivo binding specificity of KDR-MBs for detection of angiogenic vessels (Figure). To test the use of KDR-MBs for monitoring anti-angiogenic therapy, mice with (n=4) and without (n=4) anti-angiogenic treatment were imaged every 24h for a total of 3 days. In vivo imaging signal was significantly ($P<0.03$) reduced in anti-angiogenic treated tumor-bearing animals compared with non-treated animals. Ex vivo analysis confirmed both reduced microvessel density and KDR expression levels in treated versus non-treated tumors. Our results suggest that human KDR-targeted microbubbles can be developed that allow detection, quantification, and monitoring of KDR expression at the molecular level in vivo. Our study is a further step towards a future clinical translation of molecular ultrasound imaging in cancer patients.

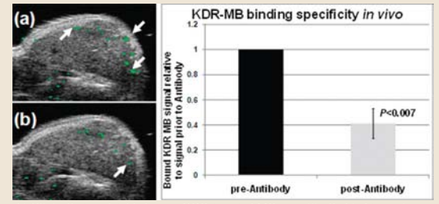

A) Clinically translatable human KDR-targeted MBs specifically bind to angiogenic vessels in tumor-bearing mice (arrows point to green signal from bound microbubbles, overlaid on B-mode ultrasound image). B) Image signal intensity dropped significantly after in vivo blocking of receptors with antibodies. C) Bar chart summarizes in vivo blocking experiments for 3 tumor-bearing mice.

REFERENCES/FUNDING SOURCE

2009 World Molecular Imaging Congress, Montreal, Canada
This work was supported by funding from the Radiological Society of North America (RSNA; grant RSD0809), and the National Institutes of Health/National Cancer Institute (NIH/NCI; grants: CA139279-01A1, CA114747, and CA118681).

MAXIMUM INTENSITY PERSISTENCE ANALYSIS IS A SENSITIVE AND RELIABLE TOOL TO QUANTITATE TUMOR ANGIOGENESIS WITH ULTRASOUND IMAGING

M A Pysz[1,2], C M Panje[1,2], D S Wang[1,2], N S Deshpande[1,2], and J K Willmann[1,2]
Depts of [1]Radiology and [2]MIPS, Stanford University, CA

The purpose of our study was to compare two post-processing techniques, maximum intensity persistence (MIP) technique versus a traditional time-intensity curve analysis (TICA), for quantitation of high-resolution (40 MHz) ultrasound (US) imaging intensities of microbubbles (MBs) in a subcutaneous angiosarcoma tumor xenografts in mice (n=6). Contrast MBs were injected (100 µl) intravenously using an infusion syringe pump, and varied by concentration and infusion rate as follows: $5x10^5$ MBs (injected at 1.2 ml/min), $5x10^6$ (at 1.2 ml/min), $5x10^7$ (at 1.2 ml/min, repeated twice), $5x10^8$ (at 1.2 ml/min), $5x10^7$ (at 0.6 ml/min), and $5x10^7$ MBs (injected at 2.4 ml/min). Regions of interest (ROIs) were drawn over the tumors, and images were processed with MIP persistence, or no persistence (TICA, expressed as upslope, time-to-peak, and peak enhancement). After imaging, tumors were excised, immunostained for CD31 expression (a marker for tumor endothelial cells), and analyzed for microvessel density (MVD). Both MIP and peak enhancement values increased with increasing MB concentrations ($P<0.004$). MIP analysis was more sensitive in detecting tumor angiogenesis at low MB concentrations ($5x10^5$ and $5x10^6$) than all three parameters from the time-intensity analysis (Figure). MIP and peak enhancement were not significantly different for two repeated injections of $5x10^7$ MBs, or by variation of infusion rates (0.6 ml/min, 1.2 ml/min, and 2.4 ml/min); however different flow rates significantly ($P<0.001$) affected both time to peak and the upslope values of the TICA. Ex vivo MVD highly correlated ($R_2>0.9$) with both in vivo MIP and peak enhancement values. Our results suggest that MIP is a straight forward post-processing approach that allows a reliable and accurate assessment of tumor angiogenesis in vivo. Since MIP can be applied during real-time ultrasound imaging, it may be used as a promising bedside tool for tumor angiogenesis quantification in future clinical trials in cancer patients.

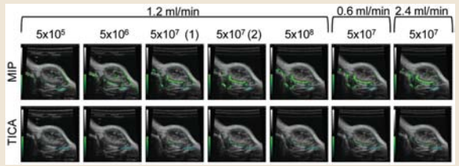

US image intensities (shown by green signal overlay) increase with increasing MB concentration and are not changed by infusion rate when images are processed using MIP persistence or TICA. Notably, MIP-processed signals are more sensitive than TICA-processed signals at lower concentration of contrast agent.

REFERENCES/FUNDING SOURCE

2009 World Molecular Imaging Congress, Montreal, Canada
This work was supported by funding from the Radiological Society of North America (RSNA; grant RSD0809), and the National Institutes of Health/National Cancer Institute (NIH/NCI; grants: CA139279-01A1, CA114747, and CA118681).

DESIGN AND TESTING OF NOVEL ULTRASOUND CONTRAST AGENT FOR MOLECULAR ULTRASOUND IMAGING OF TUMOR ANGIOGENESIS

J K Willmann[1], R H Kimura[1,2], N Deshpande[1], A M Lutz[1], J Rosenberg[1], J R Cochran[2], S S Gambhir[1,2]
[1]Molecular Imaging Program at Stanford and Dept of [2]Bioengineering, Stanford University, CA

Molecular ultrasound imaging is increasingly being recognized as a promising and powerful molecular imaging tool. In this proof-of-principle study we hypothesized that a new class of molecular ultrasound contrast agents could be developed using small (~3 kDa), conformationally constrained integrin-binding peptides that are coupled onto the surface of contrast microbubbles. Directed evolution was used to engineer a small, disulfide-constrained cystine knot peptide (knottin) to bind to $\alpha_v\beta_3$-integrins with nanomolar affinity (knottin$_{Integrin}$). A molecular ultrasound imaging contrast agent was designed by attaching the knottin$_{Integrin}$ onto the shell of perfluorocarbon-filled microbubbles (MB-Knottin$_{integrin}$). A knottin peptide with a scrambled sequence was used to create control microbubbles (MB-Knottin$_{Scrambled}$). Binding of MB-Knottin$_{integrin}$ and MB-Knottin$_{Scrambled}$ to $\alpha_v\beta_3$-integrin-positive cells and control cells was assessed and compared to microbubbles labeled with anti-$\alpha_v\beta_3$-integrin monoclonal antibodies (MB$\alpha_v\beta_3$) and microbubbles labeled with c(RGDfK) (MB-cRGD). In vivo imaging signal of contrast-enhanced ultrasound using the different types of microbubbles was quantified in 49 mice bearing human ovarian adenocarcinoma xenograft tumors. Tumor tissue was stained for $\alpha_v\beta_3$ integrin and CD31, a vascular endothelial cell marker. MB-Knottin$_{Integrin}$ attached significantly more ($P<.0001$) to $\alpha_v\beta_3$-integrin-positive cells (0.47±0.21 microbubbles per cell) than to control cells (0.02±0.02). Control MB-Knottin$_{Scrambled}$ adhered less to $\alpha_v\beta_3$-integrin-positive cells (0.17±0.12) than MB-Knottin$_{Integrin}$. After blocking of integrins, attachment of MB-Knottin$_{Integrin}$ to $\alpha_v\beta_3$-integrin-positive cells significantly decreased ($P<.04$). In vivo ultrasound imaging signal was higher following administration of MB-Knottin$_{Integrin}$ compared to MB$\alpha_v\beta_3$, MBcRGD, and control MB-Knottin$_{Scrambled}$ ($P<.018$). Following in vivo blocking of integrin receptors, the imaging signal after administration of MB-Knottin$_{Integrin}$ significantly ($P<.018$) dropped by 64%. Ex vivo immunofluorescence confirmed integrin expression on tumor endothelial cells of human ovarian adenocarcinoma xenograft tumors. In summary, our study shows that knottin peptides are a promising platform for designing novel contrast agents for molecular ultrasound imaging of tumor angiogenesis. The design of small, evolvable peptide ligands that can be coupled with the surface of microbubbles may facilitate the translation of molecular ultrasound from preclinical animal models to clinical applications in patients in the near future.

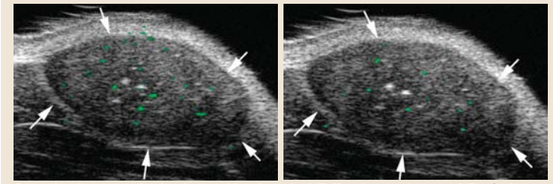

Comparison between molecular ultrasound imaging using MB-Knottin$_{Integrin}$ (a) versus MB$\alpha_v\beta_3$ (b) in a nude mouse with a subcutaneous human ovarian adenocarcinoma xenograft tumor (arrows). Two-dimensional ultrasound imaging was performed in the same session with 30 min between injections to allow clearance of the previously injected microbubbles. The molecular imaging signal from attached microbubbles is color-coded as a green signal overlaid on the gray-scale ultrasound image, and was higher after MB-Knottin$_{Integrin}$ injection compared with MB$\alpha_v\beta_3$ in this tumor. Note, since the subcutaneous human ovarian cancer xenograft tumors are poorly vascularized, only a small but substantial molecular ultrasound imaging signal can be measured.

REFERENCES/FUNDING SOURCE

ICMIC, Developmental Grant, NIH

Molecular Imaging using Nanotubes and a Clinical Optical Breast Imaging System

S M W Y van de Ven[1,3], N Mincu[1,3], J Brunette[1,3], G Ma[1,2], M Khayat[1,2], D M Ikeda[1], S S Gambhir[1,3]
[1]Dept of Radiology and [2]Medicine [3]Molecular Imaging Program,Stanford University, CA

Aim: Optical imaging studies have shown that differences in intrinsic optical absorption often are not pronounced enough to detect breast masses against normal tissue background. A possible solution is to enhance lesions with agents that change light transmission. Single-walled carbon nanotubes (SWNT) could potentially be used as light-absorbing contrast agents for optical breast imaging. We studied phantoms containing varying concentrations of SWNT to determine if SWNT produced detectable optical transmission changes in a clinical optical breast scanner.

Methods: Six concentrations of SWNTs (0.8, 1.6, 2.4, 4, 6.4, 20 nM) were measured in specifically designed phantoms of 3 sizes (200 mm3, 780 mm^3, 1570 mm^3) on a clinical optical breast scanner using 4 wavelengths (684, 732, 781, 827 nm). Each phantom was placed in the system scanner tank where a patient's breast normally would be positioned, and the tank was filled with optical matching medium (OMM), mimicking the average absorption and scattering of a normal breast. We first performed scans using only OMM to acquire the background signal. Then, SWNT absorption scans were done and compared to background absorption. Measurements were repeated on 2 days, 4 weeks apart, to assess reproducibility.

Results: All phantoms of different sizes and SWNT concentrations were detected by our system at all 4 wavelengths, with best results obtained at 684 nm. SWNT absorption was between 10% and 80% higher than background absorption (Fig. 1). Optical absorption signal (y) was dependent on phantom size and SWNT concentration (x), e.g. for 200 mm^3 at 684 nm: y = 0.0003 ln(x) + 0.0038, R2 = 0.93. Reproducibility was excellent with an Intraclass Correlation Coefficient of 0.95 (95% CI 0.92-0.97).

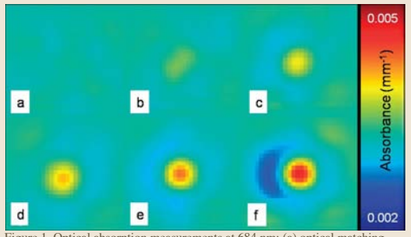

Figure 1. Optical absorption measurements at 684 nm: (a) optical matching medium only; (b-f) 200 mm^3 phantom with different SWNT concentrations, i.e. 0.8 (b), 1.6 (c), 2.4 (d), 6.4 (e), and 20 nM (f).

Conclusion: Nanomolar concentrations of SWNT in phantoms were reproducibly detected. This shows the potential of using highly light-absorbing contrast, with appropriate targeting ligands, as molecular imaging agents for breast disease using a commercially available clinical optical breast scanner.

References/Funding Source

Submitted to 2009 IEEE Medical Imaging Conference, Orlando Florida, October 25-31
NIH grants: R01CA119056, R33 EB003283; Belgian-American Education Foundation (BAEF)

Acceptance Analysis for detector modules used in a breast dedicated PET camera

A Vandenbroucke[1,2], C S Levin[1,2]
Dept of [1]Radiology and [2]Molecular Imaging Program, Stanford University, CA

We are building a dual panel breast dedicated Positron Emission Tomography (PET) camera. The system is built out of 8x8 arrays of 1x1x1 mm3 lutetium oxyorthosilicate (LSO) scintillation crystals converting the 511 keV photons resulting from positron annihilation into optical photons. These scintillation arrays are coupled to position sensitive avalanche photodiodes (PSAPDs), which convert the optical photons to electrical charge.

By reading out the four corners of a resistive sheet coupled to one side of the PSAPD, the position of the interaction is reconstructed. Summing these 4 spatial channels together yields the total charge created by the 511 keV interaction. The PSAPD's other side only has one readout and is referred to as the common.

Each camera panel will measure 16x9.4cm2, and will contain 2304 PSAPDs. In order to determine the performance of all LSO-PSAPD combinations, a dedicated automated analysis chain was implemented. The software uses the ROOT libraries and analyses gain, energy resolution and crystal identification parameters. The software insures that all 64 crystals in the array are performing within specifications.

The attached figure is an example of the software's output. The two leftmost panels of the upper (middle) row show gain (energy resolution) for both the common and the spatial signals for each of the 64 crystals. The gain is expressed in arbitrary ADC units. As expected, the same pattern is observed for the common and spatial signals. The average (RMS) energy resolution is indicated by the red line (yellow box) in the middle row, and is quantified in the lower right of the figure.

The rightmost panel shows the flood histogram. Each of the 64 crystals is clearly identifiable. The lower left and lower center panel show a one-dimensional profile through the flood histogram for the top row and a center row respectively.

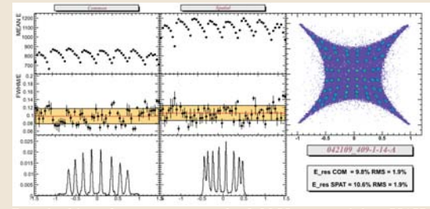

Example of the performance parameters of an 8x8 LSO array coupled to a PSAPD. Gain, % energy resolution (FWHM for 511 keV photopeak) and crystal separation figure of merit measured from crystal flood histogram are shown.

References/Funding Source

Submitted to 2009 IEEE Medical Imaging Conference, Orlando Florida, October 25-31
NIH grants: R01CA119056, R33 EB003283; Belgian-American Education Foundation (BAEF)

Temperature and bias voltage dependence of the detector modules used in a breast dedicated PET camera

A Vandenbroucke[1], J Lee[2], V Spanoudaki[1], F W Y Lau[1,3], C S Levin[1,3]
Depts of [1]Radiology and Molecular Imaging Program, [2]Mechanical Engineering, [3]Electrical Engineering, Stanford University, CA

We are constructing a high resolution, high sensitivity PET detector system with depth of interaction capability. The detectors are built from modules comprising LSO crystal arrays coupled to Position Sensitive Avalanche Photodiodes (PSAPDs). The entire system will have 4,608 densely packed dual LSO-PSAPD modules.

The performance of the large area (1x1 cm2) PSAPDs in our system depends on bias voltage and temperature. Important parameters are energy and time resolution and crystal identification capabilities. These are extremely important in densely packed systems needed for state-of-the art PET.

Coincidence data was obtained by placing a 22Na source between an LSO crystal coupled to a PMT and an LSO-PSAPD module. The bias voltage dependence shows that the energy resolution remains constant around 14.1+/-0.5% FWHM at 511 keV and deteriorates by about 5% at lower bias voltages. Crystal identification capability stays constant over the range of interest. Optimal coincidence time resolution of 2.63+/-0.02ns FWHM was observed around 1740 V. Timing resolution decreases from there by about 10% for a 20 V change. The gain increases by a factor 2 for every 35 volts and can be described by two exponentials. The point where those two exponentials intersect corresponds to the beginning of the avalanche breakdown.

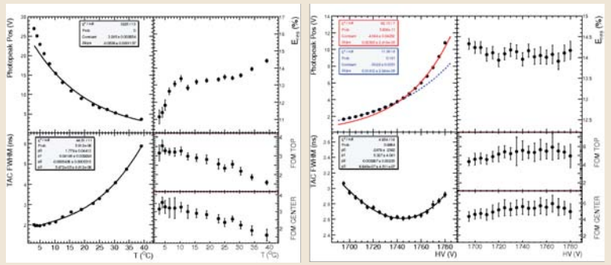

Temperature (left) and bias voltage (right) dependence of gain, energy and time resolution and crystal identification for an LSO-PSAPD module.

The module's temperature was varied using a thermoelectric cooler coupled to a heatsink. In general, decreasing the temperature of a PSAPD improves performance. The coincidence time resolution improved from 5.88+/-0.05ns FWHM at 39 C to 1.96+/-0.03ns at 5 C. 511 keV energy resolution improved from 14.43+/-0.01% at 39 C to 11.82+/-0.01% at 5 C. PSAPD gain increases by 20% every 5 degrees. The rate of gain increase is even larger (10% per degree) at the lowest temperatures. Most of the observed behaviour is attributed to the PSAPD, since the light output of LSO varies only slightly with increasing temperature.

References/Funding Source

Submitted to 2009 IEEE Medical Imaging Conference, Orlando Florida, October 25-31.
NIH grants: R01CA119056, R33 EB003283; Belgian-American Education Foundation (BAEF)

Resolution recovery in PET by online computation of detector response functions.

G Pratx[1,2,3], C Levin[2,3]
Depts of [1]Electrical Engineering, [2]Radiology, and [3]Molecular Imaging Program at Stanford, Stanford University, CA

The response of PET systems is shift-varying. Therefore, the spatial resolution of the system varies throughout the system field-of-view, which can be a confounding factor in quantitative image analysis. The variations in the system response are greater for small-animal than for clinical PET systems, since in clinical systems the detectors are placed further away from the patient. In addition, geometrical aspects of the design can also worsen the resolution variations. When an accurate model of the detector response is used in the reconstruction, the system blurring can be deconvolved. Two issues arise in practice: how to compute and store the system response function? The most accurate description of the response is a non-separable function of seven variables, with no simple analytical expression. In the approach we investigated, we used a graphics card to calculate the shift-varying system response on-the-fly, according to a novel analytical formulation. This formulation relies on several approximations that are valid for small crystals. The resulting reconstructions demonstrate improvements both in terms of the spatial resolution and quantitative accuracy. For a high-resolution CZT-based PET system, the spatial resolution becomes uniform and the contrast recovery / noise trade-off is improved. The approach uses very little data storage since the response model is only calculated when needed. This set-up is ideal for systems in which the geometrical parameters can be adjusted, for example a dual panel PET system with variable panel separation.

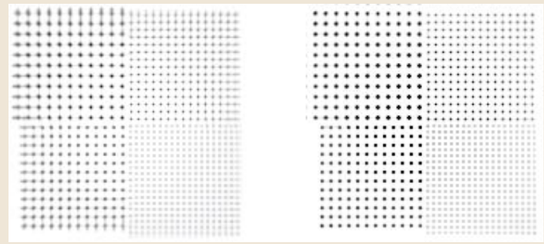

Reconstruction of a sphere phantom (sphere diameters 1, 1.25, 1.5 and 1.75 mm), with list-mode OSEM, using (left) a shift-invariant Gaussian projection kernel and (right) an accurate, shift-varying system response model. The resolution is more uniform for the accurate model thanks to resolution recovery.

References/Funding Source

This work was supported in part by National Institute of Health grant R01 CA120474.

Secretory Gaussia Luciferase in Triple Fusions Enhances its Imaging Applications in Small Animals

R Paulmurugan[1,3,4], A Sathirachinda[1,4], B C Ahn[1,4], H Fan-Minogue[1,4], CChan[1,4], T F Massoud, and S S Gambhir[1,2,3,4]
Depts of [1]Radiology and [2]Bioengineering, the [3]Bio-X Program, [4]Molecular Imaging Program at Stanford (MIPS), Stanford University, CA

Gaussia luciferase, a bioluminescent photoprotein that uses coelenterazine as its substrate, has potential as a reporter gene for different biological applications. In this study we report that the 16-amino acids (1-16) at the N-terminus of this protein are not only important for the secretory nature of this protein, but are also critical for its rapid maturation and proper functionality. We constructed a series of vectors expressing GLUC fusions and N-terminal truncation/substitution (see Figure) to prove the importance of the secretory peptide, and also to improve its intracellular retention for small animal imaging. The 293T, SKBr3 and CHO cells transfected with these constructs were assayed for GLUC-activity immediately after lysis and, at 2, 5, 12, 24, 48, 72 and 120 hrs post-lysis. The results showed significant improvement in the intracellular activity only from the sGLUC fused to mRFP-tTK (10-fold). The cells transfected with tGLUC, tGLUC-GFP and TK-Leader-tGLUC showed minimal intracellular activity when assayed immediately after lysis (<1.0% of sGLUC), the signal increased over time and stabilized at 72 hr. The activity by tGLUC measured at 72 hr was 120±10-fold higher than the initial activity and was ~80% of the sGLUC activity. Tumor xenografts of 293T cells stably expressing tGLUC-GFP, sGLUC-GFP and sGLUC-mRFP-tTK in mice (N=11) were imaged for GLUC, GFP and mRFP signals over time. The imaging results showed no GLUC-signals from the cells transfected with tGLUC-GFP, but showed significant level of fused GFP signal ($p<0.001$). The sGLUC with C-terminal fusions showed a constant intracellular GLUC-signal over time, indicating the importance of the secretory peptide for GLUC-maturation. The enhanced fluorescent signal from GFP and RFP fused to the GLUC, than the corresponding fusions with other bioluminescent reporters, indicates its minimal steric hindrance. In conclusion, we have successfully developed a novel triple fusion that enhances imaging intracellular GLUC protein in small animals.

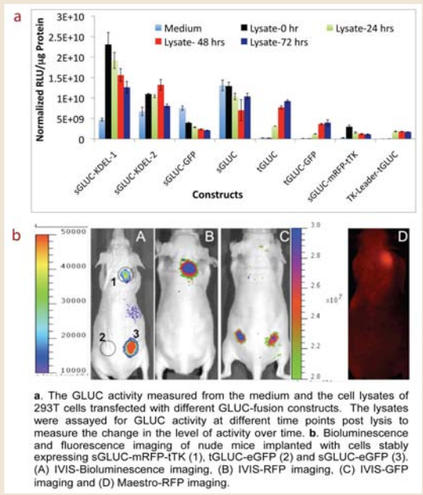

a. The GLUC activity measured from the medium and the cell lysates of 293T cells transfected with different GLUC-fusion constructs. The lysates were assayed for GLUC activity at different time points post lysis to measure the change in the level of activity over time. **b**. Bioluminescence and fluorescence imaging of nude mice implanted with cells stably expressing sGLUC-mRFP-tTK (1), tGLUC-eGFP (2) and sGLUC-eGFP (3). (A) IVIS-Bioluminescence imaging, (B) IVIS-RFP imaging, (C) IVIS-GFP imaging and (D) Maestro-RFP imaging.

Continuous, quantitative, molecular monitoring of a near infrared fluorophore using a novel, microfabricated, implantable biosensor

N Parashurama[1],T O'Sullivan[2], A De La Zerda[1,2], E Munro[3], O Levi[3], J S Harris, Jr[3], and S S Gambhir[1]
[1]Molecular Imaging Program at Stanford, Depts of Radiology and Bioengineering, Bio-X Program, [2]Dept of Electrical Engineering, Stanford University, CA; [3]Institute of Biomaterials and Biomedical Engineering and Deptof Electrical and Computer Engineering, University of Toronto, Canada

Current approaches to detect fluorescence in anesthetized subjects utilize CCD cameras or intravital microscopy and generally take snapshots of a particular molecular process. Alternatively, continuous molecular monitoring in a freely moving subject would be useful in preclinical disease models for monitoring drug delivery, stem cell growth, and metastases. With these objectives in mind, we fabricated a novel cylindrical device (8mm diameter) containing a 1.5mW, 670nm vertical-cavity surface-emitting laser (VCSEL), un-cooled Gallium Arsenide photodiode, an integrated collimation lens, and a commercially available fluorescence emission filter. The field of view was (3x3x3 mm), and for Cy5.5 dye, the in vitro sensitivity was 100nM (R^2= 0.891), with signal saturation at 30µM. The in vivo sensitivity curve was linear (R^2= 0.856) and correlated well with CCD camera data (R^2=0.99), and the in vivo sensitivity was 1µM. We then utilized this device in a glioblastoma (U87 cell line) tumor xenograft model in nude mice in which Cy5.5-RGD specifically binds to integrin receptors on tumor cells. After tail-vein injection of Cy5.5-RGD (50µM in 50µl), the signal was background corrected, and signal to noise ratio was 23.69 ± 2.73 in tumors and 7.59 ± 1.39 in non tumor tissue. This data was statistically significant (P<0.018, N=2 mice). This agreed with the specificity of RGD-Cy5.5 uptake in tumors versus control tissue. Furthermore, we were able to continuously monitor probe uptake, and compare kinetics between mice. We found that the 90% of the max signal occurs at 13.27 ± 4.11 minutes (N=3 mice). Lastly, we demonstrated intraperitoneal (IP) injection of the Cy5.5-RGD (50µM in 50µl) resulted in a delayed 90% of the max signal (approximately 55 minutes) when compared to tail vein injection (approximately 13 minutes). Our future work will be to completely characterize probe kinetics and then transition to cellular sensing. This is the first demonstration of using a VCSEL for the detection of a molecular probe and is a proof-of-principle that should allow expansion of this technology for implanting sensors in freely moving subjects.

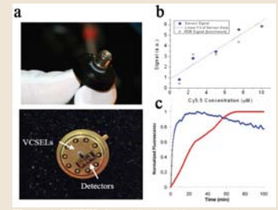

Figure 1. VCSEL-based in vivo biosensor a) VCSEL (671nm excitation) based biosensor, approximately 8mm in diameter, shown with lens and housing in upper panel. The lower panel demonstrates integrated sensor with lens and housing removed, with VCSEL and detector in same plane b) In vivo sensitivity curve of signal (nanoamps) versus Cy5.5 concentration, for both CCD camera (open) and biosensor (closed). Cy5.5 dye was injected subcutaneously in nude mouse. Data demonstrates linearity with change in concentration and high correlation with CCD camera. c) Kinetics of Cy5.5-RGD probe uptake in U87 tumors in nude mice. Data demonstrates a slower entry into the systemic circulation for intraperitoneal injection.

Feeder-Free Derivation of Induced Pluripotent Stem Cells from Adult Human Adipose Stem Cells

N Sun[1,2], N J Panetta[6], D M Gupta[6], K D Wilson[1,2], A Lee[1,2], F Jia[1,2], S Hu[1,2], A M Cherry[3], R C Robbins[4], M T Longaker[6], J C Wu[1,2,5]
Depts of [1]Radiology, [2]MIPS, [3]Pathology, [4]Cardiothoracic Surgery, [5]Medicine and [6]Surgery

BACKGROUND: Ectopic expression of transcription factors can reprogram somatic cells to a pluripotent state. The generation of patient-specific induced pluripotent stem (iPS) cells from adult somatic cells has vast implications for the future of regenerative medicine. However, most of the studies utilized skin fibroblasts as the starting population for reprogramming, which usually take weeks for expansion from a single biopsy. Moreover, reprogramming adult human fibroblasts usually takes prolonged time with very low efficiency (~0.01% to ~0.001). In this study, we show that iPS cells can be generated from adult human adipose stem cells (hASCs) freshly isolated from patients with faster speed and enhanced efficiency.

METHODS & RESULTS: hASCs were isolated from lipoaspirations of four different adult human patients of 45-60 years old. The cells were transduced with lentiviral human Oct4, Sox2, Klf4, and c-MYC. We obtained embryonic stem cell (ESC)-like colonies from hASCs of all four patients after two weeks post transduction in feeder-free culture conditions. Compared to the low efficiency (~0.002%) and prolonged time of reprogramming human IMR90 fibroblasts, ESC-like hASC-derived iPS colonies can be generated from hASCs ~2-fold faster and ~20-fold more efficient with four factors. These hASC-derived iPS cells were successfully expanded in vitro. Immunostaining indicated that hASC-derived iPS cells express strong ESC markers such as Nanog, TRA-1-60, TRA-1-81, SSEA-3, SSEA-4, and alkaline phosphatase. Quantitative-PCR and microarray analysis also indicated that hASC-derived iPS cells expressed a similar gene expression pattern with that of human ESCs. Upon injection into immunodeficient mice, hASC-derived iPS cells formed teratomas containing tissues from the three embryonic germ layers, confirming they are pluripotent cells. We also examined the possible reasons that hASCs are easier to be reprogrammed than fibroblasts. Quantitative-PCR and microarray analysis indicated that hASCs express high level of Klf4 and c-MYC, which are two of the 4 reprogramming factors. FACS analysis and alkaline phosphatase staining indicated some of the hASCs expressed strong alkaline phosphatase activity, which is the most reliable pluripotency marker. Taken together, hASCs represent a better cell source for production of patient-specific iPS cells in the future.

CONCLUSION: Our results indicate that hASCs are an easily obtainable cell source that can be more efficiently reprogrammed into adult, individual-specific iPS cells. Furthermore, iPS cells can be readily derived from adult hASCs in a feeder-free condition, thereby eliminating potential variability caused by using feeder cells. hASCs can be safely and readily isolated from adult humans in large quantities without extended time for expansion, are easy to maintain in culture, and therefore represent an ideal autologous source of cells for generating individual-specific iPS cells. Feeder-free derivation of iPS cells from hASCs thus represents a more clinically applicable method for derivation of iPS cells compared to other cell types, and should enable more efficient and rapid generation of patient-specific and disease-specific iPS cells.

Intravital Molecular Imaging of the Birth of a Tumor from Cancer Stem Cells in a Mouse Model

N Parashurama[1], N Lobo[2], B R Smith[1], M Clarke[2], S S.Gambhir[1]
[1]Molecular Imaging Program, Depts of Radiology & Bioengineering, Bio-X Program, [2]Institute for Stem Cell Biology & Regenerative Medicine, Stanford University

Despite phenotypic enrichment of breast cancer stem cells (CSC), the early detection of breast cancer by targeting CSC remains elusive. We hypothesized that incorporating imaging into CSC assays could provide novel insights into the early mechanisms of tumor initiation from CSC. Furthermore, we reasoned that imaging CSC can be done in the adult, postnatally developing mammary gland, and regenerating mammary gland after transplantation. To image the 4th adult mammary gland, a surgical flap was created and stabilized in an anesthetized, transgenic, virgin, BL6 eGFP (and DsRed) female mouse in which mammary ducts express high levels of fluorescent protein. Mammary ducts and lobules could be visualized with 4, 10, and 20x objectives in both adult (N=10) and developing (age= 3- 4.5 weeks, N= 4) eGFP+ mice. This technique, which utilizes a multichannel intravital microscope, has a spatial resolution of approximately 1 µm, and depth penetration of approximately 150µm. Furthermore, vascular structures, ranging from 1-500µm, were imaged using a fluorescent (750nm) intravascular dye (N=5 mice). To image regenerating mammary ducts, 50,000 cells of an eGFP+, Lin- population, which contains rare mammary stem cells, were transplanted into the cleared fat pads of wild type hosts. Regenerating glands were repetitively imaged at 8 and 12 weeks after transplantation (N=5). Importantly, cellular structures in living subjects could be resolved for the first time in all systems. Furthermore, we imaged 5000 Lineage-, CD44+, human breast CSC that had been lentivirally transduced with reporter gene expressing tomato fluorescent protein, and transplanted into the mammary fat pad of NOD-SCID mice for 10 days. Having established these systems, we will image single CSC, in both mouse and humans, and corresponding changes in microvasculature in tandem. These approaches should markedly change our understanding of breast tumor development in living subjects, and advance the early detection of, or early therapeutic targeting of CSC.

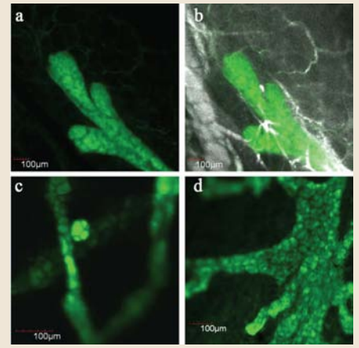

Figure 1. Repetitive, non destuctive intravital imaging of the mammary gland in living mice. All images were captured with a live mouse with surgically exposed mammay gland in eGFP + transgenic mouse, 488nm laser, as part of a depth stack of several images a) Intravital image of a portion of the eGFP + mammary gland in live transgenic mouse 4x objective and zoom =2x. Demonstrates cellular detail in the normal duct. b)Same as (a) except a second channel added, at 750nm, which demonstrates the normal duct surrounded by normal microvasculature (near Infra-red emission), 1 hour ater fluorescent dye injection c) Image of regenerated gland obtained, 8 weeks after transplantation, 10X objective zoom=4x, demonstrating duct and budding area near duct, and cell-like detail in walls of duct d) Image of primary duct and branches of 4.5 week old eGDP + mouse, 4x objective, zoom=3x Demonstrates cellular level detail with numerous subcelluclar features present.

Molecular Imaging of Cell Transplantation in Porcine Myocardium Using Clinical MRI and PET-CT

N Parashurama[1], B Ahn[1], D Yerushalmi[1], J Chung[2] , C Zavaleta[1], J Swanson[3], F Ikeno[2] , T Teramoto[2], J Lyons[2], A Green[2], S Bhaumik[4], S Yagoubhi[1], P Yang[2], P Yock[2], R Robbins[3], S S Gambhir[1]
Dept of [3]Cardiothoracic Surgery, [1]Molecular Imaging Program at Stanford, Departments of Radiology and Bioengineering, Bio-X Program, Division of [2]Cardiovascular Medicine, Stanford University, CA;[4]GE Global Research Center, Niskayuna, NY

Imaging cells after cardiac cellular therapy could be a promising approach to optimizing this new treatment strategy. Marrying the strengths of cardiovascular MRI (high spatial resolution) and PET (high sensitivity) enhances the ability to assess the cell location, viability, survival, and myocardial response to treatment. To build on our previous swine studies with adenovirally transduced cells, Rat Mesenchymal Stem Cells (rMSC) were stably transduced with a second generation, self-inactivating lentivirus carrying a ubiquitin-driven triple fusion (TF) reporter gene (RG), comprised of green fluorescent protein (GFP), firefly luciferase (Fluc) and a mutant truncated herpes simplex virus type 1 thymidine kinase (HSV1-tsr39tk). These TFRG expressing rMSC were loaded overnight with 12 µg/ml Iron bearing SPIO particles (35nm) using a protamine transfection technique. To determine sensitivity, 3 injections of SPIO particles, at varying concentrations, were made into swine hearts, and a T2 weighted sequence, a short axis, Fiesta sequence, was applied to the 3T MRI. Injection of 5mg/ml of SPIO resulted in an SNR (signal to noise ratio) of 0.81, injection of 12µg/ml resulted in an SNR of 4.65, and injection of 4 µg/ml resulted in an SNR of 5.73, where decreasing dose of SPIO leads to an increased signal intensity (N=2 swine). The MRI allowed simple detection of injection site after injection of 150-220 x106 cells. Next, clinical PET-CT was performed dynamically op to five hours after injection of F18-FHBG (14 mCi), and nine hours after injection of the rMSC. Uptake of probe was measured as a SNR ratios 1.34 and 1.16 each injection (N=2 swine). Cell injection sites were localized to areas of heart by MRI T2 weighted images. Future work will aim to use swine TFRG-MSC in survival models of swine infarction. Studies of PET reporter genes in large animals should help translate stem cells to the clinic and establish the role for molecular imaging in monitoring stem cell therapies.

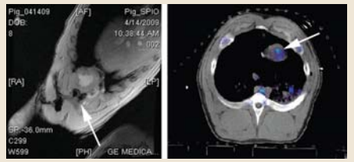

Figure 1. rMSC-TFRG implanted into Porcine swine and imaged with PET-CT and MRI. a) Fast gradient echo sequence sequence short axis view, of the swine heart. 10 x 10^6 rMSC-TFRG cells labeled with 35nm iron bearing SPIO and transplanted into swine hearts. Arrow demonstrates dephasing signal at apex of heart. b) PET-CT coregistered image 9h after injection of rMSC and 5h after injection of F18-FHBG. Transverse section demonstrates coregistered image of CT and PET of apex of heart. Arrow demonstrates signal at bottom of heart, consistent with cell injection and uptake.

References/Funding Source

Work funded by NIH R01CA119056, NIH R33 EB003283

Compact Readout Electronics Module for a High Resolution Breast-Dedicated PET System

P D Reynolds[1,2], A Vandenbroucke[2], F Lau[1,2], C S Levin[1,2]
Depts of [1]Electrical Engineering and [3]Bioengineering, [2]Molecular Imaging Program & Dept of Radiology, Stanford University, CA

We have developed and tested a compact readout electronics module for use in our 1 mm^3 resolution breast-dedicated PET system. The system consists of two 9 cm x 16 cm x 38 cm panels, with each panel requiring 9,216 channels of charge sensing circuitry. To fit this volume, along with front end and auxiliary electronics, the size of the readout electronics needs to be small. The compact readout electronics module can read 64 channels in an 8 cm x 8cm x 0.4 cm volume.

The module is based on the NOVA RENA-3 readout ASIC, which consists of 36 configurable channels of pre-amplifier, Gaussian shaper, trigger and timestamp circuitry. The module incorporates two RENA-3 chips, and due to detector limitations, 32 channels from each chip. A Xilinx XC3S50AN is used for control logic and communication in the module. Each RENA has its own 12-bit analog to digital converter and dedicated transfer link for high speed readout.

A pulser signal of several amplitudes is used to generate charge for testing each channel. The standard deviation of the amplitude for each measurement is typically less than 1.5 ADC counts. This translates into an amplitude resolution of the readout electronics of less than 0.15% in the center of the dynamic range. The timing resolution of pulser data typically measures around 1.23 ns FWHM.

Two position sensitive avalanche photodiodes (PSAPD) with 8x8 arrays of 1x1x1 mm3 LSO crystals were connected to the readouts and data was collected. The global uncompensated energy resolution shows the 511keV photo peak and backscatter peak. Nearly all crystals are visible in position histograms. Additional work will be done to improve the histograms.

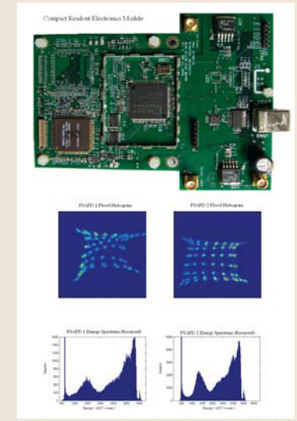

Top, the compact readout electronics module. Middle, individual crystals are visible in the flood histograms of each PSAPD. Bottom, the global energy spectrum for each PSAPD is shown with reversed pulse height scale (highest energy appears furthest to the left). The peak near 1500 is the 511 keV photon photopeak

References/Funding Source

Work funded by NIH R01CA119056, NIH R33 EB003283

Study of a new PET detector design with combined DOI/TOF features.

V Ch Spanoudaki[1,2] and C S Levin[1,2]
Dept of [1]Radiology, [2]MIPS , Stanford University, CA

Objectives: In an effort to enhance image quality and quantification we propose a PET detector design possessing both photon depth of interaction (DoI) and time of flight (ToF) features. In addition, the DoI design enables 3D positioning of individual photon interactions for multi-interaction events. If successful, a PET system built with such detectors enables uniform spatial resolution across the FOV and at the same time enhanced image SNR and contrast resolution.

Methods: High quality ToF information requires sub-nanosecond time resolutions in order to reduce the uncertainty in the photon emission point along a line-of-response. To achieve this goal the design uses stacked layers of thin scintillation detectors, each comprising fast and bright 3 mm width LYSO scintillation crystals coupled one-to-one to novel 4x4 arrays of fast, high-gain silicon photomultiplier (SiPM) photodetectors with 3 mm pixels. DoI (and 3D positioning) information is directly determined by which crystal in a layer within the stack is hit (DoI resolution=crystal height). Optical photon tracking simulations were performed to study and guide the choice of crystal parameters for the DOI scheme. Figures of merit for the simulations are the scintillation light collection efficiency and the photon flight time variations within the crystal volume as a function of crystal length, DoI and crystal surface treatment. First coincidence measurements of detector pairs have been performed.

Results: A minimum time resolution of 250 ps (FWHM) has been measured for a 3x3x5 mm3 LYSO-SiPM detector pair in coincidence. Photon tracking simulations found that for best DOI performance, 3 mm long scintillation crystals (3 mm DoI resolution) with all rough surfaces result in the best trade-off between the light collection efficiency (>64%), the minimum mean photon transit time (~70 ps), and DOI positioning linearity.

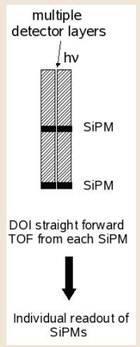

Schematic of the proposed DoI/ToF detector design with individual crystal readout.

References/Funding Source

2009 SNM annual meeting, Toronto, Canada. Journal of Nuclear Medicine 2009, Vol. 50, Suppl.2, pg. 123P
Reference/Funding source: NIH grants R01 CA119056 and R33 EB003283; AXA Research Fund

Pulse Width Modulation: A Novel Readout Scheme For High Energy Photon Detection.

P D Olcott[1,2,3], and C S Levin[1,2]
Depts of [1]Radiology and [3]Bioengineering, [2]Molecular Imaging Program, Stanford University, CA

In standard PET scintillation detection, the energy, timing, and location of the incoming photon are recovered using analog signal processing techniques. The energy and location information are processed using an analog-to-digital (ADC) converter that samples an analog value that is proportional to the integral of the charge created by the scintillation event. We propose to change the paradigm and modulate the width (rather than amplitude) of a digital pulse to be proportional to the integral of the charge created. The analog value of the outgoing digital pulses is recovered by using a time-to-digital converter in the back-end electronics, without the need for an ADC. Note that in this new scenario the same time-to-digital converter used to record the time of the event is used to recover the amplitude.

The main performance parameter that must be optimized is the dynamic range versus the dead-time of the front-end detector. The goal is an 8-bit dynamic range for this pulse-width modulation (PWM) scheme, which is adequate for high resolution PET detectors based on semiconductors such as avalanche photodiode (APD) or cadmium zinc telluride (CZT).

PWM techniques simplify the routing to the back end electronics without degrading the performance of the system. A readout architecture based on PWM processes digital rather than analog pulses, which can be easily multiplexed, enabling one to achieve very high channel density required for ultra-high resolution PET systems.

The PWM circuit has been fabricated and built for high energy photon detection for PET applications. The performance of the circuit is equivalent to standard ADC sampling in terms of dynamic range, linearity and noise without an excessive dead-time

References/Funding Source

P. D. Olcott, C. S. Levin, Pulse Width Modulation: A Novel Readout Scheme For High Energy Photon Detection , 2009 IEEE NSS-MIC Conference Record, pp. 4530-4535, 2008.
GE Sponsored Research Grant, Society of Nuclear Medicine 2008 Pre-doctoral Award.

Novel Electro-Optical Coupling Technique for MR-Compatible PET Detectors

P D Olcott[1,2,3], H Peng[1,2], and C S Levin[1,2,]
Depts of [1]Radiology and [3]Bioengineering, [2]Molecular Imaging Program, Stanford University, CA

A new magnetic resonance (MR)-compatible positron emission tomography (PET) detector design is being developed that uses electro-optical coupling to bring the amplitude and arrival time information of high-speed scintillation pulses out of an MR system. The electro-optical coupling consists of a magnetically insensitive photodetector output signal connected to a non-magnetic vertical cavity surface emitting laser (VCSEL) diode which is coupled to a multi-mode optical fiber. This scheme essentially acts as an optical wire. When compared to signal transmission over standard shielded co-axial cables, this electro-optical coupling will have little influence on an MR system because the optical fibers are not conductive. To test the feasibility of this approach, a single 3 mm x 3 mm x 20 mm lutetium yttrium oxyorthosilicate (LYSO) crystal coupled to a single channel of a silicon photomultiplier (SPM) array was placed in co-incidence with a 4 mm x 4 mm x 4 mm lutetium oxyorthosilicate (LSO) crystal coupled to a fast PMT with both the new non-magnetic VCSEL laser coupling as well as the standard co-axial cable signal transmission scheme. No significant change was measured in photopeak energy resolution and coincidence time resolution for electro-optical (15.6 +/- 0.4\% full-width-at-half-maximum (FWHM) and 1.30 +/- 0.01 ns FWHM, respectively) versus coaxial coupling (15.5 +/- 0.4\% FWHM and 1.32 +/- 0.02 ns FWHM, respectively) schemes. In summary, high-speed analog modulation of a non-magnetic VCSEL laser was successful without degrading signal-to-noise ratio (SNR). This electro-optical coupling technology enables an MR compatible PET block detector that has a significantly reduced electronic footprint compared to the current MR compatible PET detector signal transmission schemes. This advance facilitates the goal of developing a large axial field of view (FOV) whole body clinical PET insert containing hundreds to thousands of detector modules without influencing the performance of a whole body clinical MR system.

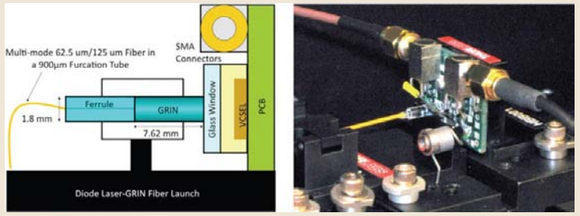

Block diagram (left) of a VCSEL (vertical cavity surface emitting laser) coupling scintillation signals over multi-mode fiber. The VCSEL laser (right) has been tested and shown to not significantly degrade any PET parameters when coupling scintillation signals over fiber.

References/Funding Source

Olcott PD, Peng H, Levin CS., Novel electro-optical coupling technique for magnetic resonance-compatible positron emission tomography detectors., Mol Imaging. 2009 Mar-Apr;8(2):74-86.
GE Sponsored Research Grant, Society of Nuclear Medicine 2008 Pre-doctoral Award

Impact of Multiple-Interaction Photon Events in a High-resolution Small Animal PET System

Y Gu[1,2], C S Levin[1,2]
Depts of [1]Electrical Engineering, [3]Radiology, and [2]Molecular Imaging Program, Stanford University, CA

We are developing a 1 mm resolution small animal PET system using cadmium zinc telluride (CZT) photon detectors. The detectors are 40×40×5 mm^3 monolithic CZT crystals patterned with a cross-strip electrode design creating 1×5.4×1 mm^3 voxels, and are capable of positioning the 3-D coordinates of individual photon interactions. Detectors are arranged to create an 8×8×8 cm^3 box-shaped field of view. Challenges exist in achieving accurate event line of response (LOR) positioning, arrival time, and coincident photon pairing for high event rates due to CZT's relatively low effective Z (high probability of Compton scattering), its finite charge drift velocity, and effects of the electrode electric field configuration on charge collection. This work studies the effect of multiple-interaction photon events on the system's LOR positioning capability and photon sensitivity, in order to guide the design of algorithms for accurate estimation of position and arrival time for these types of events.

Monte Carlo simulation was performed using a realistic mouse phantom (300 µCi uniformly distributed) centered on the system axis for a simulated acquisition time of 1 second, during which 1013104 (100%) photons interacted at least once with the detector volume (71.6% had summed energy within 511keV±3%). Results yielded a mode inter-scatter distance of 1.8 mm, causing 17.4% of photons to have indistinguishable multiple interactions within the same 1×5.4×5 mm^3 detector voxel. Approximately 37.3% of photons interacted more than once in at least one of the detectors they traversed, giving rise to challenges in positioning with cross-strip readout. However, 29.7% out of the 37.3% involve just 2 interactions; an algorithm is currently being developed to accurately position photons and identify coincidence pairs to achieve 93.4% photon retention rate by resolving positioning ambiguity associated with these two-interaction photons.

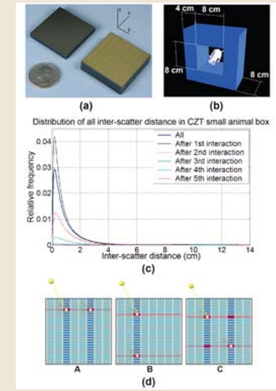

The CZT detector, small animal PET system design, and simulation results. (a) Anode and cathode sides of the 40×40×5 mm^3 cross-strip CZT detector, (b) 3-D high-resolution small animal PET system under development using CZT detectors, (c) Distribution of photon inter-scatter distance in CZT, (d) Three classes of positioning ambiguities in cross-strip detectors (blue: cathode strip; red: anode strip).

References/Funding Source

Submitted to 2009 IEEE Medical Imaging Conference, Orlando Florida, October 25-31.
This work was supported in part by National Institute of Health (NCI) grant R01 CA120474.

Preclinical and clinical PET detector design considerations using silicon photomultipliers (SPM)

H Peng[1,2], P D Olcott[1,2,3], C S Levin[1,2]
Depts of [1]Radiology and [3]Bioengineering, [2]Molecular Imaging Program, Stanford University, CA

We are developing a new high-resolution PET block detector using the silicon photomultiplier (SPM) for both clinical (~3 mm resolution) and preclinical (~1 mm resolution) PET/MRI applications. As a new type of photon detection device, each SPM comprises thousands of microscopic avalanche photodiodes operated in Geiger mode; This detector exhibits the advantages of compact size, high gain and the ability to operate in a strong magnetic field. We investigated coupling arrays of 3 mm and 1 mm scintillation crystals to a 4x4 array of 3x3 mm SPM pixels.

For the 3.2 mm crystal pitch array, 2x2 crystals were coupled one-to-one to a 2x2 portion of the 4x4 SPM array. The 511 keV photopeak energy resolution (the average for four SPM pixels) is 15.3+/-0.2% FWHM. The individual crystals in the array can be clearly resolved with average peak-to-valley ratio of 23.1+/-0.8.

For the case of a 6x6 array of 1 mm crystals directly coupled to 2x2 pixels of the SPM array with only optical multiplexing (i.e. using a thin light guide made of acrylic to spread out the light from scintillation crystals), individual 1 mm crystals were not well resolved as the size of the SPM (3 mm) is too coarse to resolve the crystals of finer size (1 mm). When we coupled an 8x8 array of 1 mm crystals through a 1.5 mm thick light diffuser to a 3x3 portion of the 4x4 SPM array, an electrical multiplexing was implemented along with the optical multiplexing to further reduce 9 readout channels down to 4. All 64 crystals are resolved with an average peak-to-valley ratio of 4.48+/-2.06. The 511 keV photopeak energy resolution of the global energy spectrum (after the normalization per 1 mm crystal) was 21.2+/-0.4% FWHM.

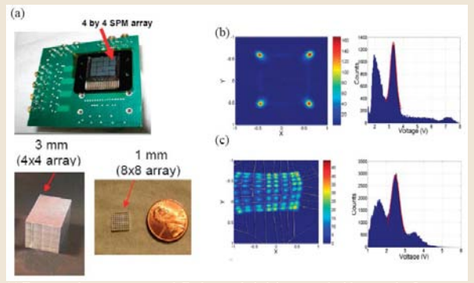

(a) Two crystal arrays were tested. Each crystal pitch is wrapped with spectral reflectors. The crystal size is 3.2x3.2x20 mm3 and 1.0x1.0x1.0 mm3 respectively. (b) The crystal flood histogram and the global energy spectrum for the 3.2 mm pitch arrays. (c) The crystal flood histogram and the global energy spectrum for the 1.0 mm pitch array.

References/Funding Source

Submitted to the 2009 IEEE Medical Imaging Conference, Orlando FL, October 25-31, 2009.
GE Sponsored Research Grant

Photon Interaction Rate Studies for a CZT-Based High-Resolution Small Animal PET System

Y Gu[1, 2], C S Levin[1,2]
Dept of [1]Electrical Engineering and [2]Molecular Imaging Program & Dept. of Radiology, Stanford University, CA

We are developing a 1 mm resolution 3-D positioning small animal PET system using cadmium zinc telluride (CZT) photon detectors. The detectors are 40×40×5 mm^3 monolithic CZT crystals patterned with a cross-strip electrode design with 1 mm anode strip pitch, 5.5 mm cathode strip pitch, and are capable of positioning the 3-D coordinates of individual photon interactions. The system has an 8×8×8 cm^3 box-shaped field of view formed by 16 layers of axially stacked square-shaped detector rings. For signal readout, detectors are arranged into modules each comprising a stacked pair of CZT detectors. Module signals are read out using a commercially-available application specific integrated circuit (ASIC).

Flux and spatial distribution of photon interactions within the system's detector volume were quantified, specifically how they translate to data acquisition bandwidth specifications that are compatible with the readout ASIC capabilities.

Monte Carlo simulation was performed using a realistic mouse phantom (300 µCi uniformly distributed within) at the system center over a simulated acquisition time of 1 second (11181701 counts above a 15keV energy threshold). The flux of photon interactions was discretized according to anode and cathode detection volumes to enable calculation of expected hit rates on individual anode and cathode strips. Simulation results showed maximum per anode and cathode strip hit rates of 5694/s and 59190/s respectively. The hit rate was seen to reduce by up to an order of magnitude for electrode strips near the corners and away from the system center. Based on this data and the ASICs estimated maximum of 138.14k triggers/s throughput, each ASIC is expected to be capable of reading 30 anodes with an average hit rate of ~4500 independent triggers per second. Careful load balancing across the ASIC for cathode readout will allow 6 ASICs to provide adequate readout bandwidth for every detector module throughout the system.

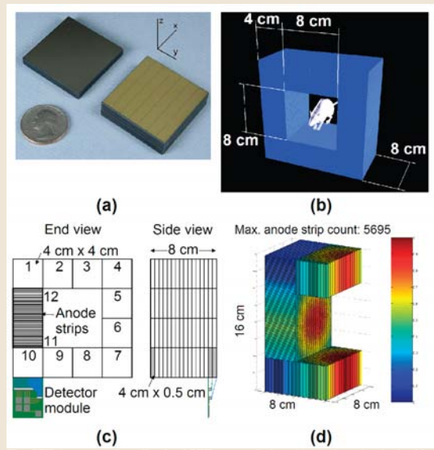

The CZT detector and small animal PET system design. (a) Anode and cathode sides of the 40×40×5 mm^3 cross-strip CZT detector, (b) 3-D high-resolution small animal PET system under development using CZT detectors, (c) Data readout of the 3-D high-resolution small animal PET system, (d) Cutaway view of the photon interaction rate discretized by anode detection volumes.

References/Funding Source

Submitted to 2009 IEEE Medical Imaging Conference, Orlando Florida, October 25-31.
This work was supported in part by National Institute of Health grant R01 CA120474

DETECTOR AND FRONT-END ELECTRONICS FOR 1MM^3 RESOLUTION BREAST-DEDICATED PET SYSTEM

F W Y Lau[1,2,4], A Vandenbroucke[2,4], P D Reynolds[1,2,4], P D Olcott[1,3,4], M A Horowitz[1], C S Levin[1,2,3,4]
Depts of [1]Electrical Engineering, [2]Radiology, [3]Bioengineering, [4]Molecular Imaging Program at Stanford, Stanford University, CA

We are developing a 1mm^3 resolution PET system with a geometry dedicated to breast imaging. We aim to increase the roles of PET in early stage cancer detection, diagnosis, staging, monitoring and advance the limits of clinical PET spatial resolution.

The detector comprises stacked layers of 8x8 arrays of 1x1x1 mm^3 LSO scintillation crystals coupled to thin Position Sensitive Avalanche Photodiodes (PSAPDs) mounted on flex circuits. Photons hit the detector modules "edge-on", providing 1mm directly measured photon depth of interaction positioning.

Custom circuitry was added to adapt the front-end readout ASIC (RENA-3 from NOVA R&D) for use with PSAPDs.

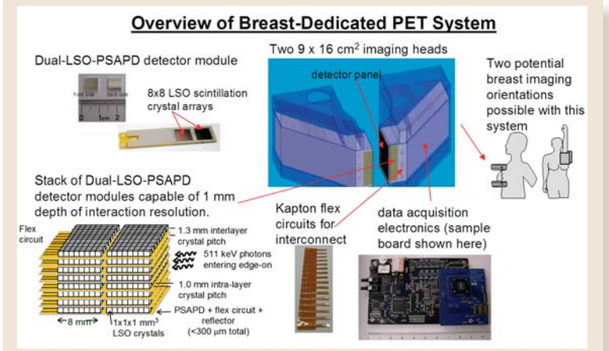

Overview of breast-dedicated PET system, showing how the detector modules and data acquisition electronics will be assembled to form the imaging head.

The system contains 4608 PSAPDs, resulting in 18,432 channels emerging from our 9 x 16 cm^2 detector panel. To achieve the required high density interconnection between the PSAPDs and the front-end RENA-3 ASICs, we use flex circuits with Kapton substrates for signal and bias routing. Kapton is flexible and has sufficient dielectic breakdown strength to route the 1750V bias signals for the PSAPDs.

Characterization of the detector using the RENA-3 ASIC showed that the energy resolution is 14.4% +/- 0.8% at FWHM for the 511 keV photo-peak and the paired coincidence photon time resolution is 6.9 +/- 0.2 ns FWHM. An 8x8 array of 1 mm^3 LSO crystals can be resolved with >14:1 peak-valley ratio.

Functionality of the electronic read-out chain was verified and good performance metrics were obtained. Work on scaling up the design to a full system with thousands of channels is underway.

We are developing a 1mm^3 resolution PET system with a geometry dedicated to breast imaging. We aim to increase the roles of PET in early stage cancer detection, diagnosis, staging, monitoring and advance the limits of clinical PET spatial resolution.

The detector comprises stacked layers of 8x8 arrays of 1x1x1 mm^3 LSO scintillation crystals coupled to thin Position Sensitive Avalanche Photodiodes (PSAPDs) mounted on flex circuits. Photons hit the detector modules "edge-on", providing 1mm directly measured photon depth of interaction positioning.

Custom circuitry was added to adapt the front-end readout ASIC (RENA-3 from NOVA R&D) for use with PSAPDs.

The system contains 4608 PSAPDs, resulting in 18,432 channels emerging from our 9 x 16 cm2 detector panel. To achieve the required high density interconnection between the PSAPDs and the front-end RENA-3 ASICs, we use flex circuits with Kapton substrates for signal and bias routing. Kapton is flexible and has sufficient dielectic breakdown strength to route the 1750V bias signals for the PSAPDs.

Characterization of the detector using the RENA-3 ASIC showed that the energy resolution is 14.4% +/- 0.8% at FWHM for the 511 keV photo-peak and the paired coincidence photon time resolution is 6.9 +/- 0.2 ns FWHM. An 8x8 array of 1 mm3 LSO crystals can be resolved with >14:1 peak-valley ratio.

Functionality of the electronic read-out chain was verified and good performance metrics were obtained. Work on scaling up the design to a full system with thousands of channels is underway.

REFERENCES/FUNDING SOURCE

: F. W. Y. Lau, A. Vandenbroucke, P. D. Reynolds, P. D. Olcott, M. A. Horowitz, C. S. Levin, "Detector and Front-End Electronics for 1mm3 Resolution Breast-Dedicated PET System," Journal of Nuclear Medicine, Supplement 2, vol 50, p307, May 2009.
NIH grants R01 CA119056, R33 EB003283; Stanford Bio-X Graduate Fellowship

AUTOMATED RADIOSYNTHESIS OF [18F]EF-5 FOR IMAGING HYPOXIA IN HUMAN

F T Chin[1], M Subbarayan[1], J Sorger[2], S S Gambhir[1], and E E Graves[3]
Depts of [1]Radiology, [3]Radiation Oncology, Stanford University; [2]Varian Medical Systems, Palo Alto, CA

Objectives. Hypoxia is a common phenomenon in human tumors, with most tumors possessing lower oxygenation than their corresponding tissue of origin. 2-(2-Nitro-1[H]-imidazol-1-yl)-N-(2,2,3,3,3-pentafluoropropyl)-acetamide (EF-5) is known to measure tumor hypoxia in animals and humans via immunohistochemical methods. More recently, EF-5 has been labeled with fluorine-18 and preliminary imaging results obtained with [18F]EF-5 in rats and humans suggest that it has more homogeneous biodistribution and bioavailability as well as improved stability relative to other hypoxia PET probes. Since the current radiosynthetic procedure is not optimal for providing [18F]EF-5 for the clinic, a safe and automated radiosynthesis for preparing [18F]EF-5 routinely needed to be developed for future PET studies imaging hypoxia in humans.

Methods. Optimized radiochemistry was performed in a commercial synthesis module with a quaternary HPLC pump. The cyclotron target and delivery lines were preconditioned three times with neon and fluorine gas. 2-(2-Nitro-1H-imidazol-1-yl)-N-(2,3,3-trifluoroallyl)acetamide (22 mg) and trifluoroacetic acid (7 mL) was loaded into the reactor prior delivery of radioactivity. [18F]fluorine gas was bubbled at RT into the preloaded reactor and stirred (1 min) before the solution was evaporated with MeOH (2 x 1 mL). The remaining residue was neutralized and reconstituted with 60:40 ethanol/0.02 N NaOH (4.0 mL) and injected onto HPLC to afford pure [18F]EF-5 which was processed by C-18 solid-phase extraction, filtered through a sterile Millex-GS filter (25 mm) into a sterile vial, and analyzed for quality control. Formulated [18F]EF-5 (~150 μCi) was injected into mouse to evaluate tracer biodistribution with microPET.

Results. All radiochemical yields (RCYs) are decay-corrected and reported as means ± SD. Recent validation runs for preparing [18F]EF-5 gave consistent RCYs (6.1 ± 1.4%; n = 4) and good specific radioactivity, 1004±130 mCi/mmol (37±5 MBq/μmol). High radiochemical and chemical purities exceeded 99% and the formulated batch passed the normal battery of quality control tests. Since the entire synthesis is completed with a module and without rotoevaporation, the overall automated process took a total of 80 minutes and reduced radiation exposure to the radiochemist. Tracer uptake (%ID/g) was observed primarily in the gall bladder (12.7 ± 8.1) and intestine (12.0 ± 3.9) but also in liver (3.6 ± 0.8), tumor (2.8 ± 1.5), and muscle (1.1 ± 0.3) with a tumor to muscle ratio of 2.43.

Conclusion. We have developed a method to safely provide clinical-grade [18F]EF-5 with a commercial automated synthesis module for future PET studies imaging hypoxia

REFERENCES/FUNDING SOURCE

This research was supported by a Varian Biosynergy Grant (and a NCI ICMIC P50 CA114747 Grant.

A MAXIMUM NEC PHOTON DIRECTION WINDOW FOR 3-D PET DETECTORS

G Chinn[1,2] and C S Levin[1,2]
Dept of [1]Radiology and [2]MIPS

In this work, we develop a new method to reject random coincidences and identify true coincidences from multiple photon coincidences using 3-D photon positioning PET detectors. In conventional PET, coincident photon pairs are used to produce lines of response (LOR) for tomographic image reconstruction. However, unrelated annihilation events can also produce "random" coincidences and using these LORs reduces reconstructed image contrast. When three or more photons are in coincidence, the photons are discarded reducing the photon sensitivity. We are developing scintillation and cadmium zinc telluride (CZT) detectors with the ability to position the 3-D coordinates of every detector interaction with 1 mm intrinsic spatial and <2.5% FWHM energy resolution at 511 keV. For multiple interactions, the position of the first two interactions and the energy of the first interaction are used to electronically collimate single photons by the kinematics of Compton scatter. We use this directional information to differentiate true lines of response from random lines of response. Using a hypothesis testing framework, we derive a threshold for directional agreement between the LOR and Compton collimation that maximizes the noise equivalent counts (NEC) of the system. NEC is a measure that approximates the signal-to-noise ratio of the system. This new method is compared against conventional coincidence processing for a dual-panel breast CZT PET system under development in our laboratory. For a simplified approximation of our maximum NEC derivation, we show that the addition of a direction window reduced random coincidences by 55-60%. At high activities, the ability to recover trues from multiple coincidences increased the true coincidence rate of the system by as much as 11%.

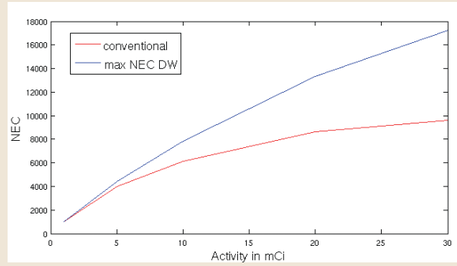

Shown is a plot of NEC vs. activity for conventional PET and 3-D PET detectors using the maximum NEC direction window.

REFERENCES/FUNDING SOURCE

G. Chinn and C.S. Levin, "A method to reject random coincidences and extract true from multiple coincidences in PET using 3-D detectors," 2008 IEEE Nuclear Science and Medical Imaging Symposium Conference Record, pp. 5249-5254.
This work was supported in part by the NIH (grants R01 CA119056, NIH R33 EB003283, and NIH R01 CA120474).

Ultra High Sensitivity Targeted Photoacoustic Imaging Agents for Cancer Early Detection in Living Mice

A de la Zerda[1,5], Z Liu[2], S Bodapati[4,5], R Teed[5], C Zavaleta[4,5], S Vaithilingam[1], X Chen[4,5], B T Khuri-Yakub[1], H Dai[2], S S Gambhir[3,4,5]
Depts of [1]Electrical Engineering, [2]Chemistry, [3]Bioengineering, [4]Radiology, and [5]Molecular Imaging Program at Stanford, Stanford University, CA

Photoacoustic molecular imaging of living subjects offers high spatial resolution at increased tissue depths compared to optical imaging strategies. We have recently demonstrated single walled carbon nanotubes (SWNTs) conjugated to Indocyanine Green (SWNT-ICG) as targeted photoacoustic imaging agents in-vitro.

In the current work, we created a significantly improved SWNT-ICG particle with over 1000-times better sensitivity than plain SWNT and demonstrated their ability to target tumors when injected intravenously to a living mouse.

The targeted SWNT-ICG particles were synthesized by coupling of ICG molecules to the surface of SWNT-RGD particles through pi-pi stacking interactions. Control SWNT-ICG particles were created using the untargeted SWNT-RAD instead.

We verified the particles are stable in serum and target αvβ3 integrin through cell uptake studies with U87 cells. We found the photoacoustic signal produced by the particles to be highly linear to their concentration both in phantom studies (R2 = 0.99) as well as in living mice injected with the particles subcutaneously (R2 = 0.971). We further measured the detection sensitivity of SWNT-ICG in living mice (n = 3 mice) and found it to be 30 pM. This represents more than 3 orders of magnitude improvement compared to plain SWNTs sensitivity in living mice ($p < 0.05$). Furthermore, xenograft-bearing mice were tail-vein injected with RGD-targeted SWNT-ICG. At 2 hours post-injection, mice injected with the RGD-targeted particles showed 2.1-times higher photoacoustic signal in the tumor compared to mice injected with control particles ($p < 0.05$, n = 4 mice). Finally, we demonstrated the superiority of the SWNT-ICG-RGD particles by incubating them with U87 cells and detecting in living mice 1000-times such cells than if the cells were incubated with plain SWNT-RGD.

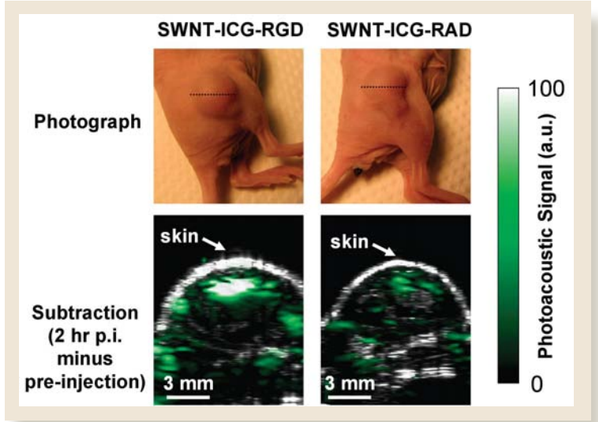

This is the first photoacoustic imaging agent tested and targeted in living animals that we know of that can reach such a high sensitivity of 30 pM.

Photoacoustic Imaging of the Eye for Improved Disease Detection

A de la Zerda[1,2], Y M Paulus[3], D M Moshfeghi[3], S S Gambhir[1,4]
Depts of [1]Electrical Engineering, [2]Radiology, [3]Ophthalmology and [4]Bioengineering, Stanford University, CA

Ophthalmologists lack good functional and molecular imaging tools for the evaluation of angiogenesis in patients. Solving this need would allow earlier detection and improved intervention to multiple ophthalmic diseases including diabetic retinopathy, macular degeneration and ocular malignancies.

We report on the first demonstration of photoacoustic retinal imaging in living animals. The photoacoustic device can not only be used with photoacoustic contrast agents for molecular imaging but can be used without contrast agents, in which case the eye blood vessels are visualized. The device has high spatial resolution (250 µm) and high depth of penetration allowing it to visualize the retina, choroid, sclera and optic nerve. This is particularly important as most eye diseases originate deep in the eye where they cannot be visualized with existing imaging tools.

The device illuminates the eye with a wide laser beam at a safe power (800 nm wavelength at 0.5 mJ/cm2). The light is absorbed by hemoglobin producing ultrasound waves that emerge from the eye and detected by an ultrasound transducer. The transducer scans the eye from multiple locations creating a three-dimensional map of blood distribution in the eye.

We scanned living rats and rabbits eyes (n = 3 of each animal) and enucleated pigs eyes (n = 3). Along with the photoacoustic scan, we acquired an ultrasound scan to visualize the eye's anatomy. The field of view included most of the eyeball (~2 cm in diameter) and time of acquisition was 20 minutes using a 25 MHz transducer (Fig. 1).

This is the first demonstration of photoacoustic ocular imaging in living animals. Such system has uses not only in clinical diagnosis but also in the drug development process where ophthalmic diseased animal models can be scanned for the first time with high depth of penetration.

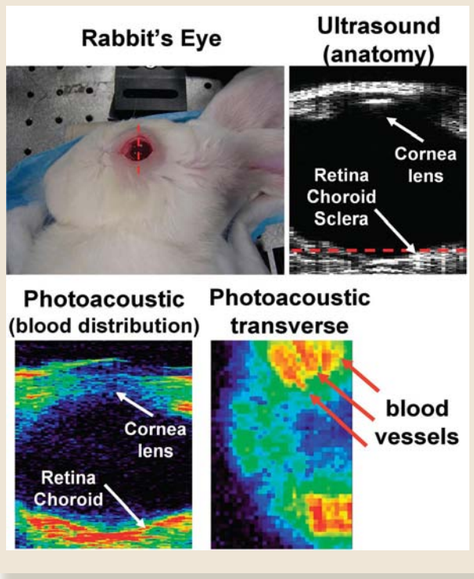

Synthesis of a New PET Radiotracer Targeting Carbonic Anhydrase IX

S D Apte[1], F T Chin[2] and E E Graves[1]
Depts of [1]Radiation Oncology and [2]Radiology, Stanford University, CA

Objectives: Hypoxia is a key modulator of tumor aggressiveness and therapeutic sensitivity. Lack of oxygen induces a host of molecular responses including stabilization of the transcription factor HIF-1 and expression of downstream genes. Carbonic anhydrase IX (CAIX) is a transmembrane protein that is regulated by HIF-1 and overexpressed under hypoxic conditions, and its expression has been shown to strongly correlate with clinical outcome. We sought to develop a radiotracer for positron emission tomography (PET) using a sulfonamide group that has been shown previously to bind specifically to CAIX. Such an imaging agent allows noninvasive monitoring of tumor CAIX status. We chose to synthesize 6-fluoro-N-(3-sulfamoylphenyl)hexanamide (FSPH) as it can be produced from a tosylated precursor via a fluorine exchange reaction, resulting in a product with high specific activity as is needed in this application.

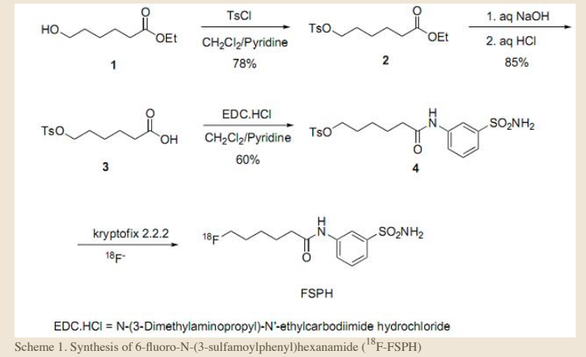

Scheme 1. Synthesis of 6-fluoro-N-(3-sulfamoylphenyl)hexanamide (^{18}F-FSPH)

Methods: Commercially available ethyl 6-hydroxyhexanoate (1) was converted to its tosylate (2). Base hydrolysis of the ester gave the tosylated carboxylic acid (3). The acid was coupled to 3-aminobenzenesulfonamide to obtain the amide (4), which is the precursor for the labeling reaction to produce FSPH. Radiochemical labeling was performed in commercial GE TracerLab FXFN synthesis module. ^{18}F-fluoride containing ^{18}O-water was passed through a SepPak QMA cartridge. The fluoride was eluted from the cartridge with Kryptofix-222 and K_2CO_3 in acetonitrile. The eluate was dried under vacuum with heating. The solution of precursor (4) in dimethyl sulfoxide (DMSO) was added to the dry ^{18}F-fluoride and heated at 110°C for 15 minutes. The resulting mixture was separated on HPLC using Gemini 5 µ C6-phenyl column (110A°, 250 X 10.0 mm) with water-ethanol (9:1) as eluant. The retention time was 35 minutes with the flow rate of 5 mL/min. To obtain cold ^{19}F-FSPH, the precursor (4) was heated at 120°C with excess KF in DMF for 1 h. The product was purified by preparative TLC using 100% ethyl acetate.

Results: The ^{1}H- and ^{13}C-NMR spectra of the ^{19}F–FSPH indicate the formation of the desired product. The coinjection of the ^{18}F-FSPH reaction mixture along with the authentic ^{19}F-FSPH indicates that the radiolabeled product is chemically identical as FSPH. Radiochemical yield was approximately 10% at the end of synthesis.

Conclusions: The proposed synthetic pathway has been shown to produce FSPH with acceptable radiochemical yield. Previous work in our group has focused on labelling CAIX imaging probes with ^{18}F-^{19}F substitution reactions, resulting in products with low specific activities that cannot be effectively quantitated due to inherent competition for CAIX targets between hot and cold probe molecules within the formulated dose. FSPH has the potential to overcome this limitation and offer a clinically-viable strategy for detecting and quantifying CAIX expression in vivo. This agent is currently undergoing in vitro and in vivo testing to evaluate its specificity for CAIX as well as its biodistribution and pharmacokinetics.

References/Funding Source

Apte S. D.; Chin F. T.; Graves E. E. In: 18th International Symposium on Radiopharmaceutical Sciences, Edmonton, Canada, 2009.
1. Fyles, A. W. et al. Radiother. Oncol. 1998;48:149-56.
2. Stadler, P et al. Int J. Radiat. Oncol. Biol. Phys. 1999; 44:749-54.
3. Semenza, G. L. Crit. Rev. Biochem. Mol. Biol. 2000; 35:71-103.
4. (a) Raleigh, J. A. et al Semin. Radiat. Oncol. 1996; 6: 37-45.
(b) Chapman, J. D. et al Radiothe. Oncol. 1998; 46: 229-237.
(c) Rajendran, J. G et al Radiol. Clin. North. Am. 2005; 43:169-87.
5. Opavsky, R. et al Genomics 1996; 33: 480-487.
6. (a) Supuran, C. T. et al Bioorg. Med. Chem. Lett. 2004; 14: 2351-2356.
(b) Masereel, B. et al J. Med. Chem. 2006; 49: 2743-2749.
(c) Supuran, C. T. et al J. Med. Chem. 2003; 46: 2197-2204.
(d) Supuran, C. T. et al Med. Res. Rev. 2002; 23: 146-189.
7. Graves E. E. et al In: Annual Conference of Academy of Molecular Imaging, Orlando, FL, 2006.
Stanford Cancer Center seed project

Publications and Presentations

Peer-Reviewed Presentations at Scientific Meetings

ISMRM 2009 (April 18-24, Honolulu, Hawaii)

Aksoy D, Bammer R, Venkatasubramanian C, Gupta SN, Mlynash M, Wijman CA.	Assesment of Blood-Brain Barrier Injury Following Acute Intracerebral Hemorrhage by DCE MRI.
Aksoy M, Holdsworth S, Skare S, Bammer R.	b-Matrix Correction Applied to High Resolution DTI.
Aksoy M, Straka M, Skare S, Newbould R, Holdsworth S, Santos J, Bammer R.	Real-time Optical Motion Correction for Diffusion Tensor Imaging.
Aksoy M, Straka M, Skare S, Newbould R, Holdsworth S, Santos J, Bammer R.	In-vivo Applications of Optical Real-time Motion Correction Using a Monovision System.
Cebral JR, Putman CM, Alley MT, Bammer R, Calamante F.	Studying the hemodynamics in cerebral arteries using image-based computational fluid dynamics and 4D phase-contrast magnetic resonance.
Draper C, Besier T, Santos J, Fredericson M, Beaupre G, Delp S, Gold G.	Differences Between Weight-Bearing Patellofemoral Joint Kinematics and Static Joint Alignment. International Society for Magnetic Resonance in Medicine (ISMRM) Workshop on Advances in Musculoskeletal Magnetic Resonance Imaging; February 14-17, 2009; San Francisco, CA.
Holdsworth SJ, Bammer R, Skare S.	Diffusion-weighted imaging of the spine with readout-segmented (RS)-EPI.
Holdsworth SJ, Bammer R, Skare S.	Reducing distortion in EPI using partial Fourier encoding in the kx-direction.
Holdsworth SJ, Skare S, Bammer R.	On the application of phase correction and use of k-space entropy in partial Fourier diffusion-weighted EPI.
Holdsworth SJ, Skare S, Marty M, Straka M, Bammer R.	3D SAP-EPI motion-corrected fast susceptibility weighted imaging.
Holdsworth SJ, Skare S, Yeom K, Bammer R.	T1-weighted 3D SAP-EPI for use in pediatric imaging without general anesthesia.
Keenan K, Han E. Beaupre G, Gold G.	T1p Sequences as Predictors of Proteoglycan Content in Articular Cartilage. International Society for Magnetic Resonance in Medicine (ISMRM) Workshop on Advances in Musculoskeletal Magnetic Resonance Imaging; February 14-17, 2009; San Francisco, CA.
Koo S, Clark D, Kwon A, Gold G, Andriacchi T.	T1 and T2 Relaxation Times in Musculoskeletal Tissues at 7T. International Society for Magnetic Resonance in Medicine (ISMRM) Workshop on Advances in Musculoskeletal Magnetic Resonance Imaging; February 14-17, 2009; San Francisco, CA.
Kopeinigg D, Fleischmann D, Stollberger R, Bammer R.	LST-Based Optimization of Patient Specific Contrast Media Administration for CE-MRA: Validation Studies in Phantoms and Volunteers.
Sareen PK, Kwong A, Ikeda DM, Klifa C.	Mammographic and MR Density in Dense Breasts: Is There a Correlation?
Schmiedeskamp H, Aksoy M, Glover GH, Bammer R.	Motion-compensated interleaved spiral acquisition for fMRI.
Schmiedeskamp H, Straka M, Newbould RD, Skare S, Pruessmann KP, Bammer R.	Multiple gradient-and spin-echo EPI acquisition technique with z-shimming to compensate for susceptibility-induced offresonance effects.
Skare S, Holdsworth S, Newbould RD, Bammer R.	On the battle between Rician noise and phase-interferences in DWI.
Skare S, Holdsworth S, YeomK, Bammer R.	GRAPPA-accelerated high-resolution diffusion tensor imaging of infants without the need for general anesthesia.
Spielman DM	Hyperpolarized 13C Spectroscopy.
Straka M, Lansberg MG, Albers GW, Bammer R.	Software Solution For Automated Assessment of DWI/PWI Mismatch In Acute Stroke Patients: the RAPID MISMATCH.

ISMRM 2009 (April 18-24, Honolulu, Hawaii)

Straka M, Mlynash M, Zaharchuk G, Albers GW, Bammer R.	Can a Human Operator Be Replaced By a Computer For Processing of Bolus-Tracking Perfusion Data?
Straka M, Zaharchuk G, Newbould R, Albers GW, Moseley ME, Bammer R.	Estimation of CBF Values Using Multi-Echo DSC-MRI: a Comparison with a Xenon CT.
Veldhuis WB, Liu C, Bammer R, Daniel BL, Moseley ME.	High-resolution, fat-suppressed, diffusion-diffusion weighted MRI of the breast using a self-navigated multi-shot technique.
Zaharchuk G, Shankaranarayan A, Bammer R, Straka M, Alsop DC, Fischbein NJ, Atlas SW, Moseley ME.	Arterial Spin Label CBF Maps Can Show Abnormalities in Clinical Patients with Normal Bolus Perfusion-weighted Imaging: Identification of the “Watershed Sign.”
Zaharchuk G, Straka M, Shankaranarayan A, Alsop DC, Marks MP, Moseley ME, Bammer R.	Bolus Perfusion-weighted Imaging Measurement of Quantitative Cerebral Blood Flow can be Improved using an Arterial Spin Label Derived Scaling Factor: A Comparative Xenon CT Study.

RSNA 2008 (Nov 30-Dec 5, Chicago, Illinois)

Aggarwal A, Rubin G.	Lung Nodule CAD False Positive Reduction Using a Novel Non-parametric Shape Analysis Approach in Chest CT.
Atlas S.	Health Issues in Asia: Health Care Access in Rural Asia, and Medical Tourism. GE Healthcare Asian Pacific American Forum.
Arvin D, Erickson B, Chang P, Rubin GD.	Image Overload: Dealing with It.
Barnes P.	Update on Brain Imaging in Nonaccidental Trauma.
Barth RA.	MR Imaging of the Fetal Neck and Chest: Review of the Clinical Indications, Normal Anatomy, and Correlation with Postnatal Outcome.
Barth RA.	Fetal MRI. Hospital Timone Enfants; October 31,2008; Marseille, France.
Basu P, Dalsem V.	Creating a Patient-centered Radiology Facility: Logistics, Barriers, and Recommendations in Implementing an Outpatient Imaging Center Where Radiologists Consult Directly with Their Patients.
Blankenberg FG.	Refresher Course, Molecular Imaging Advances in Oncology: Apoptosis Imaging.
Brinton T, Rosenberg J, Stein W.	Non-Invasive Imaging of Gene Expression in Implanted Human Mesenchymal Stem Cells in the Porcine Heart: A Further Step Towards Clinical Translation.
Chan F.	Pediatric Cardiac-gated CT Imaging.
Chang C, Quon A, Olson M, Wakelee H, Weerasuriya D.	Mid-Radiation PET is a Prognostic Factor for Disease Progression in Non-Small Cell Lung Cancer.
Chang J, Rao J.	Functional Detection of Glucose Oxidase Activity by Electron Transfer to Quantum Dots.
Chen C, Kijowski R, Reeder S, Block W, Busse R, Gold G.	Comparison of IDEAL-SPGR, 3D-FSE, and VIPR for Rapid Evaluation of Cartilage Morphology.
Desser TS, Ahlqvist J, Johansson M et al.	Technical Development of a Virtual Reality Simulator for GI Fluoroscopy.
Desser TS, Ahlqvist J, Johansson M et al.	Virtual Reality Simulator for Training Technologists in Cervical Spine Radiography: Development, Implementation and Evaluation.
Do H.	Intracranial Dural Arteriovenous Fistulas: Evaluation with CT Angiography.

Eslamy H, Quon A.	F18-FDG PET/CT in Pediatric Malignancies.
Fahey B.	Virtual Palpation of the Liver Using Sonographic Elastography: How Does this New Commercially Available Technique Work and What Added Information Can It Give Me?
Faruque J, Oralkan O, Jeffrey Jr. RB, Khuri-Yakub BT, Napel S.	Automated Detection of Carotid Peak Blood Velocity (PBV) Using a Novel Transducer Array and Intelligent Software: Feasibility Study.
Fleischmann D.	The ABCs of Aortic Dissection.
Gambhir SS, Paulmurugan R, Tamrazi A.	Bioluminescence Imaging as Novel Approaches for Studying Mechanism of Estrogen Receptor Action.
Gianella D.	Intracranial Dural Arteriovenous Fistulas: Evaluation with CT Angiography.
Glazer G.	Creating a Patient Centered Radiology Facility: Logistics, Barriers and Recommendations in Implementing an Outpatient Imaging Center where Radiologists Consult Directly with Their Patients.
Gold G.	High Field Imaging of Cartilage.
Guccione S, Kode K, Paik D.	An Informatics Perspective on the Experience of Developing and Populating a Database of Cancer-related Nanotechnology.
Guccione S, Mayer D, O'Connell-Rodwell C.	In Vivo Imaging of Luciferase Activity Under the Control of an hsp70 Promoter Combined with MRI Imaging Under Antiangiogenic Therapy in a M21 Tumor Model.
Hallett R.	Postprocessing, Work Flow, and Interpretation.
Herfkens R, Young P.	The Coronary Arteries: A Primer for Radiologists.
Hovsepian D	Fallopian Tube Recanalization (Refresher Course)
Hsu J, Busse RF, Zaharchuk G.	Feasibility of 3D XETA Fast Spin Echo Sequence for T1-based Quantitative Cerebrospinal Fluid Oxygenation Measurements.
Ikeda DM.	RC215: How to Set Up a high-Quality Breast MR Imaging Program: Breast MR Imaging Interpretation, including BI-RADS.
Kamaya S, Behera D, Lee S, Yeomans D, Gold G, Biswal S.	Manganese-enhanced MRI (MEMRI) Functionally Highlights Peripheral Nerves in Neuropathic Pain.
Kijowski R, Davis K, Woods M, DeSmet A, Gold G, Busse R.	Comprehensive Knee Joint Assessment at 3T Using an Isotropic Resolution Three-dimensional Fast Spin-Echo Sequence (FSE-Cube).
Kleper V, Mongkolwat P, Supekar K, Kogan A, Rubin DL, Channin DS.	ANIVATR: caBIG in Vivo Imaging Workspace's Annotation and Image Markup (AIM) Open Source Tool for Validation and Transcoding between AIM XML, DICOM SR and HL7 CDA.
Kothary N.	Optimizing Targeted Treatment of Liver Cancers.
Le Q-T, Loo B, Maxim P, McMillan A.	Mid-Radiation FDG-PET Is a Prognostic Factor for Disease Progression in Patients with Non-Small Cell Lung Cancer
Lee SH, Cha JH, Park K, Lee S-W, Biswal S, Kim K et al.	Assessment of near-infrared fluorescence imaging in collagen-induced arthritis using Cy5.5. conjugated with hydrophobically modified glycol chitosan nanoparticle: Correlation between 18F-FDG PET.
Levy MA, Rubin DL.	Is Current Radiology Reporting Sufficient for Evaluating the Clinical Response to Treatment? An Analysis of Information Content in Radiology Images and Reports.
Liu YI, Kamaya A, Desser TS, Rubin DL.	A Bayesian Approach to Decision Support for Evaluating Thyroid Nodules Based on Multi-Variate Features.
Lu W, Gold G, Butts RK, Pauly J, Hargreaves B.	Distortion-free Magnetic Resonance Imaging Near Metallic Implants.

Lubner MG, Madison WI, Desser TS et al.	The Complicated Fibroid: A Pictorial Review.
McLoud T, Rubin GD, Vlahos I, White C, Gruden JF.	New Thoracic Imaging Technologies: 64-Slice Multidetector CT, Postprocessing, CAD, Lung Nodule Volumetry, and MR Applications.
McNutt L, Mittra ES, Iagaru A, Quon A.	Does a Dedicated Head/Neck PET/CT Acquisition Provide Significant Benefit over Whole Body PET/CT for Evaluating Head and Neck Cancer?
Middleton WD, Anderson L, Desser TS et al.	Analysis of Sonographic Features and Recommendations for Management of Thyroid Nodules in Patients with a Family History of Thyroid Cancer.
Paik DS, Aggarwal A, Olsen D, Roos J, Rubin GD, Napel S.	Lung Nodule CAD False Positive Reduction Using a Novel Non-parametric Shape Analysis Approach in Chest CT.
Paik DS, Choudhury KR, Yi CA, Napel S, Roos J, Rubin G.	Assessing Operating Characteristics of CAD Algorithms in the Absence of a Gold Standard.
Raman B, Raman R, Desser TS.	Paperless Radiology Residency Conference Attendance Tracking Using Radiofrequency Identification (RFID) Technology.
Roos R.	Contrast Medium.
Rose S.	Optimizing Targeted Treatment of Liver Cancers.
Rubin DL.	Natural Language Processing and its Role in Radiology.
Rubin DL.	Utility of Terminologies for Image Annotation and Information Retrieval.
Rubin DL, Dodd L, Gorniak RJ, Friedman DP, Freymann J, Madhavan S, Flanders A.	Defining Imaging Biomarkers Predicting Clinical Outcomes: A Terminology and Reporting System for Assessing Brain Tumors.
Rubin DL, Mongkolwat P, Kleper V, Supekar K, Channin DS.	Saying It in Pictures: Annotation and Image Markup in Radiology.
Rubin GD.	Imaging Endografts: What Is Important?
Rubin GD.	Coronary Artery Disease I: Native Vessel Disease in Cardiac CT Mentored Case Review: Part II.
Rubin GD.	Image Overload: Dealing with It.
Rubin GD.	Challenging CT Angiography and MR Angiography Cases: Interactive Interpretation with the Experts (An Interactive Session).
Rubin G.	Unique Charateristics of Dual-Source CT for Cardiac Imaging.
Schmitzberger F, Roos J, Napel S, Rubin GD, Paik DS.	A Thin Client 2D+3D Architecture for Coordinating Multicenter CAD Trials.
Sedati P, Nguyen E, Fleischmann D, Rubin GD.	ECG-gated Computed Tomography Angiography of the Ascending Aorta Following Surgical Repair: Normal Anatomy and Pitfalls.
Shin LK, Kamaya A, Brant-Zawadzki G, Jeffrey RB.	Intraoperative Ultrasound of the Pancreas. CME Educational Exhibit.
van den Bosch A.	Computer-Aided Detection (CAD) for Breast MRI: Evaluation of Efficacy at 3.0T.
Wang A, Pelc NJ, Wang A.	Optimal multi-energy binning in photon counting detectors with energy discrimination capabilities.
Willmann JK, Lutz AM, Paumurugan R, Patel MR, Rosenberg J, Gambhir SS.	Dual-targeted contrast agent for ultrasonic assessment of tumor angiogenesis in vivo.

RSNA 2008 (Nov 30-Dec 5, Chicago, Illinois)

Willmann JK, Paulmurugan R, Stein W, Brinto TJ, Rosenberg J, Gambhir SS.	Non-invasive imaging of gene expression in implanted human mesenchymal stem cells in the porcine heart: a further step towards clinical translation.
Won JH, Rubin G, Wong H, Roos J, Rosenberg J, Napel S.	Towards a Single Uncluttered View of the Abdominal Aortic Vessel Tree from CTA or MRA: Method and Preliminary Results.
Zaharchuk G, Shankaranarayan A, Alsop DC.	Noncontrast Arterial Spin Labeling Perfusion Imaging of Cerebrovascular Disease.
Zaharchuk G, Shankaranarayan A, Alsop DC.	Removing Large Vessel Contamination from Arterial Spin Label MR Perfusion Images using Signal Preparation.

SNM 2009 (June 13-17, Toronto, Canada)

Blankenberg F, Levashova Z, Backer M, Backer J.	Fluorescent tomographic imaging subacute and chronic sterile abscesses using scVEGF/Cy5.5.
Blankenberg F, Levashova Z, Tait J.	Selective localization of annexin V within depolarized skeletal muscle.
Cao Q, Liu S, Niu G, Yan Y, Liu Z, Chen X.	Phage display peptide probes for imaging early response to antiangiogenic treatment.
Cao Q, Yan Y, Liu S, Niu G, Wang H, Chen X.	[18F]FPRGD2 imaging of abraxane therapy response.
Gambhir SS, Barai S, Madhusudhanan P, Ora M.	Renal reserve – Its relation with various stages of chronic renal dysfunction.
Iagaru A, Mittra E, Goris M.	131I-Tositumomab (Bexxar) vs. 90Y-Ibritumomab (Zevalin) Therapy of Low Grade Refractory/Relapsed Non-Hodgkin Lymphoma.
Iagaru A, Mittra E, Quon A, Goris M, Gambhir SS.	A novel strategy for a cocktail 18F fluoride and 18F FDG PET/CT scan for evaluation of malignancy: Results of the pilot phase study.
Iagaru A, Sze D, Gambhir SS.	CT and FDG PET/CT evaluation of response to NV1020 for liver colorectal metastases.
Jia B, Yu Z, Liu Z, Shi J, Zhao H, Chen X, Wang F.	Targeted radiotherapy of integrin vβ3-positive tumors with 90Y-labeled RGD tetramer.
Lau F, Vandenbroucke A, Reynolds P, Olcott P, Horowitz M, Levin C.	Detector and front-end electronics for 1mm3 resolution breast-dedicated PET system.
Levashova Z, Blankenberg F, Backer M, Backer J.	Tc99m-scVEGF SPECT imaging of anti-angiogenic therapy with Sutent.
Lin M, Liu Z, McGuire M, Li S, Chen X, Brown K, Sun X.	A Ga-68 labeled peptide for imaging of vβ6 positive tumor
Liu H, Miao Z, Ren G, Jiang L, Kimura R, Cochran J, Han P, Cheng Z.	In vivo evaluation of melanoma targeted multivalent -melanocyte-stimulating hormone analogs using microPET studies.
Liu Y, Jia B, Liu Z, Zhao H, Chen X, Wang F.	Radioimmunotherapy of EGFR-positive tumors with 90Y-labeled panitumumab.

SNM 2009 (June 13-17, Toronto, Canada)

Liu Z, Liu S, Wang F, Liu S, Chen X.	Non-invasive imaging of tumor integrin expression using 18F-labeled RGD dimer peptide with PEG4 linkers.
Liu Z, Wang F, Chen X.	MicroPET imaging of breast cancer with 68Ga-labeled RGD-Bombesin heterodimer.
Miao Z, Ren G, Liu H, Jiang L, Cheng Z, Gambhir SS.	A protein scaffold based molecule for EGFR PET imaging.
Mittra E, Iagaru A, Kunz P, Quon A, Gambhir SS.	Value of FDG PET/CT for the restaging of colorectal cancer after treatment with Erbitux.
Niu G, Li Z, Chen X.	Non-invasive PET imaging of downregulation of HER-2 in 17-DMAG treated ovarian cancers.
Niu G, Li Z, Xie J, Le QT, Chen X.	PET imaging of EGFR antibody distribution in head-neck squamous cell carcinoma models.
Olcott P, Peng H, Levin C.	Solid state photomultiplier (SSPM)-based PET detector with capacitively multiplexed readout and electro-optical coupling for PET/MR.
Olcott P, Pratx G, Johnson D, Mansouri M, Mittra E, Levin C.	Clinical feasibility of a high sensitivity intra-operative hand-held gamma camera (IHGC) for sentinel lymph node biopsy (SLNB).
Pratx G, Surtri S, Levin C.	GPU-accelerated list-mode reconstruction for 3-D time-of-flight (TOF) PET.
Ren G, Liu Z, Miao Z, Liu H, Jiang L, Subbarayan M, Chin F, Zhang L, Gambhir SS, and Cheng Z.	Molecular imaging of malignant melanoma using a 18F-labeled metallopeptide.
Ren G, Miao Z, Liu H, Jian L, Limpa-Amara N, Mahmood A, Gambhir SS, Cheng Z.	Melanin targeted molecular imaging of melanoma metastasis using a 18F-labeled benzamide analog.
Spanoudaki V, Levin C.	Study of a new PET detector design with combined DOI/TOF features.
Win S, Goris M.	FDG PET-CT and I-123 MIBG in the evaluation of neuroblastoma.
Xie J, Chen K, Chen X.	RGD-human serum albumin conjugates as efficient tumor targeting probes.
Xie J, Chen K, Xu H, Biswal S, Wang A, Chen X.	Renal clearing iron oxide nanoparticles for tumor integrin targeting.

World Molecular Imaging Congress 2009 (Sept 10-13, Nice, France)

Chan C, Reeves R, Yaghoubi Y, Solow-Cordero D, Paulmurugan R, Gambhir SS.	A Unified System for Discovery and Validation of Isoform-Selective Heat Shock Protein 90 (Hsp90) Inhibitors by High-Throughput Screening (HTS), Coupled with Multimodality Molecular Imaging of Hsp90/Co-Chaperone P23 Interactions in Living Subjects. World Molecular Imaging Congress; September 10-13, 2008; Nice, France.
Chang P, Prescher J, Foss C, Ray P, Gambhir SS, Pomper M, Bertozzi C.	A Strategy for the Noninvasive Imaging of Cancer-Associated Glycans In Vivo. World Molecular Imaging Congress; September 10-13, 2008; Nice, France.
Chen I, Paulmurugan R, Nielsen C, Willmann J, Robbins R, Gambhir SS.	A Titratable Two-Step Transcriptional Amplification Strategy for Cardiac Gene Therapy Based on Ligand-Induced Intramolecular Folding of a Mutant Estrogen Receptor. World Molecular Imaging Congress; September 10-13, 2008; Nice, France.
Chen I, Gheysens O, Wang Q, Li Z, Rasooly J, Paulmurugan R, Rodriguez-Porcel M, Willmann J, Swijnenburg R, Robbins R, Wu J, Contag C, Gambhir SS.	Molecular Imaging of Transcriptionally Targeted and Enhanced Hypoxia-Inducible Factor-1 Alpha Gene Therapy for Myocardial Ischemia. World Molecular Imaging Congress; September 10-13, 2008; Nice, France.

Chin F, Subbarayan M, Berganos R, Gambhir SS, Quon A.	Automated Radiosynthesis of 5-[18F] Fluorouracil for Clinical PET Studies. World Molecular Imaging Congress; September 10-13, 2008; Nice, France.
De A, Namavari M, Zhang R, Gowrishankar G, Padilla De Jesus O, Patel M, Ray P, Cheng Z, Wang S, Lee B, Kovacs E, Webster J, Grade H, Faisal S, Gambhir SS.	Tunable Model of Tumor Surface Biomarker Expression for Verification of Micropet Imaging Sensitivity Using HER2 Targeted [18F]-Labeled Affibody Molecules. World Molecular Imaging Congress; September 10-13, 2008; Nice, France.
De A, Ray P, Loening A, Gambhir SS.	A Red-Shifted Bioluminescence Resonance Energy Transfer (BRET) Based Integrated Platform for Imaging Protein-Protein Interactions from Single Live Cell and Living Animals. World Molecular Imaging Congress; September 10-13, 2008; Nice, France.
de la Zerda A, Liu Z, Zavaleta C, Bodapati S, Vaithilingam S, Chen X, Cheng Z, Khuri-Yakub B, Dai H, Gambhir SS.	High Sensitivity Multiplexing of Targeted Photoacoustic Molecular Imaging Agents in Living Mice. World Molecular Imaging Congress; September 10-13, 2008; Nice, France.
de la Zerda A, Zavaleta C, Keren S, Vaithilingam S, Bodapati S, Liu Z, Levi J, Smith B, Ma T, Oralkan O, Cheng Z, Chen X, Dai H, Khuri-Yakub B, Gambhir SS.	Photoacoustic Molecular Imaging Using Single Walled Carbon Nanotubes in Living Mice. World Molecular Imaging Congress; September 10-13, 2008; Nice, France.
D'Souza A, Tseng J, Butts-Pauly K, Guccione S, Rosenberg J, Gambhir SS, Glazer G.	Use of Ultrasound to Amplify and Localize the Detection of Cancer Biomarkers. World Molecular Imaging Congress; September 10-13, 2008; Nice, France.
Fan-Minogue H, Paulmurugan R, Chan C, Gambhir SS.	A Novel Phosphorylation Sensor for Imaging Insulin Signaling in Living Animals. World Molecular Imaging Congress; September 10-13, 2008; Nice, France.
Kimura R, Cheng Z, Gambhir SS, Cochran J.	Cystine-Knot Scaffolds for Molecular Imaging of the Tumors in Mice. World Molecular Imaging Congress; September 10-13, 2008; Nice, France.
Lutz A, Paulmurugan R, Patel M, Chu P, Rosenberg J, Gambhir SS.	Dual-Targeted Contrast Agent for Ultrasonic Assessment of Tumor Angiogenesis In Vivo. World Molecular Imaging Congress; September 10-13, 2008; Nice, France.
Lutz A, Willmann J, Ray P, Cochran F, Gambhir SS.	Mathematical Models for Minimal Tumor Size Detection Based on Blood Biomarker Levels. World Molecular Imaging Congress; September 10-13, 2008; Nice, France.
Namavari M, De A, Yaghoubi S, Gambhir SS.	Synthesis and Biodistribution of an [18F]-Lapatinib Derivative for Imaging Dual Erbb-1/Erbb-2 Tyrosine Kinases with Positron Emission Tomography. World Molecular Imaging Congress; September 10-13, 2008; Nice, France.
Patel M, Hardy J, Chen I, Bachmann B, Chang Y, Contag C, Gambhir SS.	In Vivo Imaging of Cytotoxic T-Cell Activation in Response to Bacterial Infection. World Molecular Imaging Congress; September 10-13, 2008; Nice, France.
Paulmurugan R, Ahn B, Gambhir SS.	Novel Transgenic Mouse Model Expressing an Estrogen Receptor (ER) Intramolecular Folding Sensor for Imaging ER-Ligand Interactions. World Molecular Imaging Congress; September 10-13, 2008; Nice, France.
Paulmurugan R, Ahn B, Willmann J, Gambhir SS.	Estrogen Regulated Transcriptional Activation System to Simultaneously Monitor the Expression of Reporter (Firefly Luciferase) and a Therapeutic Gene (P53) in Living Animals. World Molecular Imaging Congress; September 10-13, 2008; Nice, France.
Ray P, Junutula A, Patel M, Gambhir SS.	Development of Third Generation Multimodality Fusion Reporters for Non-Invasive Imaging in Live Cells and in Living Subjects. World Molecular Imaging Congress; September 10-13, 2008; Nice, France.
Smith B, Liu Z, De A, Zavaleta C, Shawn X, Dai H, Gambhir SS.	Imaging the Microscale Delivery of Targeted Carbon Nanotubes to Individual Tumor Cells in Living Subjects. World Molecular Imaging Congress; September 10-13, 2008; Nice, France.
Tong R, Ray P, Gambhir SS.	The Universal Donor Mouse: a Mouse Expressing a Tri-Fusion Reporter Gene in all Tissues. World Molecular Imaging Congress; September 10-13, 2008; Nice, France.

Vandenbrouke A, Lau F, Olcott P, Reynolds P, Foudray A, Levin C.	An Advanced PET System Dedicated to Breast Cancer Imaging. World Molecular Imaging Congress; September 10-13, 2008; Nice, France.
Willmann J, Cheng Z, Davis C, Lutz A, Schipper M, Nielsen C, Gambhir SS.	Targeted Microbubbles for Imaging Tumor Angiogenesis: Assessment of Whole-Body Biodistribution with Dynamic Micropet Imaging in Mice. World Molecular Imaging Congress; September 10-13, 2008; Nice, France.
Willmann J, Paulmurugan R, Stein W, Brinton T, Connolly A, Nielsen C, Lutz A, Chen I, Rodriguez-Porcel M, Yock P, Robbins R, Gambhir SS.	Non-Invasive Imaging of Gene Expression in Implanted Human Mesenchymal Stem Cells in the Porcine Heart: a Further Step Toward Clinical Translation. World Molecular Imaging Congress; September 10-13, 2008; Nice, France.
Yen YF, LeRoux P, Mayer D, Spielman DM, Tropp J, Pfefferbaum A, Hurd RE.	Tissue-specific T2 of Hyperpolarized 13C Metabolites. World Molecular Imaging Congress; September 10-13, 2008; Nice, France.
Yerushalmi D,	Small Lesion Activity Quantification using PET-CT Images. World Molecular Imaging Congress; September 10-13, 2008; Nice, France.
Zavaleta C, Walton I, Doering B, Dais B, Shojaei B, Gambhir SS.	Multiplexed Imaging in Living Mice Using Non-Invasive Raman Spectroscopy in Conjunction with 10 Spectrally Unique Raman Particles. World Molecular Imaging Congress; September 10-13, 2008; Nice, France.
Ahn B, Paulmurugan R, Gambhir SS.	Molecular Imaging of Cellular De-Differentiation. World Molecular Imaging Congress; September 10-13, 2008; Nice, France.
Benoit MR, Mayer D, Barak Y, Chen IY, Cheng Z, Hu W, Wilson RJ, Wang SX, Spielman DM, Gambhir SS, Matin AC.	Use of Magnetotactic Bacteria for Enhancing MRI Contrast in Tumors. World Molecular Imaging Congress; September 10-13, 2008; Nice, France.
Willmann JK, Paulmurugan R, Stein W, Brinton TJ, Connolly AJ, Nielsen CH, Lutz AM, Chen IY, Rodriguez-Porcel M, Yock P, Robbins RC, Gambhir SS.	Molecular imaging of gene expression in human mesenchymal stem cell: from small to large animals.

Other Scientific Meeting Presentations

Other Presentations 2009

Olcott P, Levin C.	Pulse Width Modulation: A Novel Readout Scheme For High Energy Photon Detection. IEEE Nuclear Science Symposium and Medical Imaging Conference; October 25-28, 2008; Dresden, Germany.
Chinn G, Levin C.	A Novel Method to Use Multiple-Interaction Information in 3-D Photon Positioning Detectors to Reject Random Coincidences and Retain Multiple Coincidences for PET. IEEE Nuclear Science Symposium and Medical Imaging Conference; October 25-28, 2008; Dresden, Germany.
Gu Y, Levin CS.	Effects of Photon Multiple Interactions in a High Resolution PET System that Uses 3-D Positioning Detectors. IEEE Nuclear Science Symposium and Medical Imaging Conference; October 25-28, 2008; Dresden, Germany.
Gu Y, Matteson J, Skelton RT, Deal AA, Stephan EA, Duttweiler F, Gasaway TM, Levin CS.	Study of a High Resolution, 3-D Positioning Cross-Strip Cadmium Zinc Telluride Detector for PET. IEEE Nuclear Science Symposium and Medical Imaging Conference; October 25-28, 2008; Dresden, Germany.
Lau F, Vandenbroucke A, Reynolds P, Olcott P, Horowitz M, Levin C.	Front-end Electronics for a 1mm3 Resolution LSO-PSAPD-based PET System with Multiplexing. IEEE Nuclear Science Symposium and Medical Imaging Conference; October 25-28, 2008; Dresden, Germany.

Matteson J, Skelton R, Deal A, Stephan E, Duttweiler F, Gasaway T, Gu Y, Levin C.	Detector performance of CZT-based high resolution PET imagers. IEEE Nuclear Science Symposium and Medical Imaging Conference; October 25-28, 2008; Dresden, Germany.
Olcott P, Peng H, Levin C.	Novel Electro-Optically Coupled MR Compatible PET Detectors. IEEE Nuclear Science Symposium and Medical Imaging Conference; October 25-28, 2008; Dresden, Germany.
Peng H, Olcott P, Levin C.	Can large-area avalanche photodiodes be used for a clinical PET/MRI block detector? IEEE Nuclear Science Symposium and Medical Imaging Conference; October 25-28, 2008; Dresden, Germany.
Pratx G, Chinn G, Olcott P, Levin C.	Fast, Accurate and Shift-Varying Line Projections for Iterative Reconstruction Using the GPU. IEEE Nuclear Science Symposium and Medical Imaging Conference; October 25-28, 2008; Dresden, Germany.
Pratx G, Reader A, Levin C.	Faster Maximum-Likelihood Reconstruction via Explicit Conjugation of Search Directions. IEEE Nuclear Science Symposium and Medical Imaging Conference; October 25-28, 2008; Dresden, Germany.
Reynolds P, Olcott P, Lau F, Levin. C	Convex Optimization of PET Coincidence Time Resolution Using List Mode Data. IEEE Nuclear Science Symposium and Medical Imaging Conference; October 25-28, 2008; Dresden, Germany.
Vandenbrouke A, Foudray A, Lau F, Olcott P, Reynolds P, Levin C.	Performance characterization of a new ultra-high resolution, 3-D positioning PET scintillation detector. IEEE Nuclear Science Symposium and Medical Imaging Conference; October 25-28, 2008; Dresden, Germany.
Vandenbrouke A, Levin C.	Study of Scintillation Crystal Array Parameters for an Advanced PET Scanner Dedicated to Breast Cancer Imaging. IEEE Nuclear Science Symposium and Medical Imaging Conference; October 25-28, 2008; Dresden, Germany.
Zhuang X, Lin D, Faruque J, Oralkan O, Napel S, Jeffrey RB, Khuri-Yakub BT.	A 5-Plane CMUT Array for Operator-Independent Carotid Artery Screening: Initial Results. IEEE International Ultrasonics Symposium; November 2-5, 2008; Beijing, China.
Baek J, Pelc NJ.	Analytical construction of 3D NPS for a cone beam CT system. Society of Photographic Instrumentation Engineers (SPIE) Medical Imaging Conference; February 17-21, 2008; San Diego, CA.
Baek J, Pelc NJ.	SNR efficient 3D reconstruction algorithm for multi-source inverse geometry CT system. Society of Photographic Instrumentation Engineers (SPIE) Medical Imaging Conference; February 17-21, 2008; San Diego, CA.
Baek J, Pelc NJ.	A new reconstruction method to improve SNR for an inverse geometry CT system. Society of Photographic Instrumentation Engineers (SPIE) Medical Imaging Conference; February 17-21, 2008; San Diego, CA.
DeMan B, Pelc NJ, Bernstein T.	Propagation of quantum noise in multiplexed x-ray imaging. Society of Photographic Instrumentation Engineers (SPIE) Medical Imaging Conference; February 17-21, 2008; San Diego, CA.
Ganguly A, Pelc NJ.	On the angular dependence of Bremsstrahlung x-ray emission. Society of Photographic Instrumentation Engineers (SPIE) Medical Imaging Conference; February 17-21, 2008; San Diego, CA.
Mazin S, Pelc NJ.	A Fourier rebinning algorithm for conebeam CT. Society of Photographic Instrumentation Engineers (SPIE) Medical Imaging Conference; February 17-21, 2008; San Diego, CA.
Wang AS, Xie Y, Pelc NJ.	Effect of the frequency content and spatial location of raw data errors on CT images. Society of Photographic Instrumentation Engineers (SPIE) Medical Imaging Conference; February 17-21, 2008; San Diego, CA.
Wang AS, Pelc NJ.	Optimal energy thresholds and weights for separating materials using photon counting x-ray detectors with energy discriminating capabilities. Society of Photographic Instrumentation Engineers (SPIE) Medical Imaging Conference; February 17-21, 2008; San Diego, CA.
Xie Y, Wang AS, Pelc NJ.	Lossy raw data compression in computed tomography with noise shaping to control image effects. Society of Photographic Instrumentation Engineers (SPIE) Medical Imaging Conference; February 17-21, 2008; San Diego, CA.
Gold G, Lu W, Chen W, Brau A, Pauly K, Giori N, Caragee E, Goodman S, Hargreaves B.	Visualization and enhancement patterns of radiofrequency ablation lesions with iodine contrast-enhanced cardiac C-arm CT. Society of Photographic Instrumentation Engineers (SPIE); February 9-12, 2009; Lake Buena Vista, FL.

Yoon S, Gang JG, Tward DJ, Siewerdsen JH, Fahrig R.	Analysis of lung nodule detectability and anatomical clutter in tomosynthesis imaging of the chest. Society of Photographic Instrumentation Engineers (SPIE); February 9-12, 2009; Lake Buena Vista, FL.
Zhu L, Gao H, Bennett NR, Xing L, Fahrig R.	Scatter correction for X-ray conebeam CT using one-dimensional primary modulation. Society of Photographic Instrumentation Engineers (SPIE) - The International Society for Optical Engineering; February 9-12, 2009; Lake Buena Vista, FL.
Baek J, Pelc NJ.	Analytical derivation of the noise power spectrum for a fan-beam CT system. American Association of Physicists in Medicine (AAPM); July 27-31, 2008; Houston, TX.
Fahrig R.	Design and Performance Evaluation of Cone Beam CT Systems: Cone Beam Angio CT. American Association of Physicists in Medicine (AAPM) annual meeting; July 27-31, 2008; Houston, TX.
Fahrig R.	Image Guidance during Minimally Invasive Cardiac Interventions: Beyond Fluoroscopy. Imaging Symposium: Advances in Cardiovascular Imaging. American Association of Physicists in Medicine (AAPM) annual meeting; July 27-31, 2008; Houston, TX.
Bammer R.	Parallel Acquisition Methods for Neuroimaging – Seeing the Invisible: Recent Advances in MRI. Annual Meeting of the American Association of Medical Physicists; August, 2008; Houston, TX.
Kumar MA, Campbell DM, Olivot JM, Vangala H, Eyngorn I, Belgude A, Lansberg M, Wijman C, Tong DC, Mylnash M, Moseley M, Albers GW.	MRI-Based Diagnostic Evaluation has Substantial Impact on Final Stroke Diagnosis. American Heart Association; November 8-12, 2008; New Orleans, LA.
Rubin DL, Channin DS, Guccione S, Kahn C.	Imaging Informatics: Opportunities and Research Challenges from Molecules to Man. American Medical Informatics Association Annual Meeting; November 8-12, 2008; Washington, D.C.
Rubin DL, Talos IF, Halle M, Musen MA, Kikinis R.	Toward Computational Neuroanatomy: A Functional Representation of Neural Components and Connectivity. Summit on Translational Bioinformatics, American Medical Informatics Association; March 10-12, 2008; San Francisco, CA.
Levy MA, Rubin DL.	Tool Support to Enable Evaluation of the Clinical Response to Treatment. American Medical Informatics Association Annual Meeting; November 8-12, 2008; Washington, D.C.
Liu Y, Kamaya A, Desser T, Rubin DL.	A Bayesian Classifier for Differentiating Benign versus Malignant Thyroid Nodules using Sonographic Features. American Medical Informatics Association Annual Meeting; November 8-12, 2008; Washington, D.C.
Mejino J, Rubin DL, Brinkley J.	FMA-RadLex: An Application Ontology of Radiological Anatomy derived from the Foundational Model of Anatomy Reference Ontology. American Medical Informatics Association Annual Meeting; November 8-12, 2008; Washington, D.C.
Musen MA, Shah N, Noy N, Dai B, Dorf M, Griffith N, Buntrock J, Jonquet C, Montegut M, Rubin DL.	BioPortal: Ontologies and Data Resources with the Click of a Mouse. American Medical Informatics Association Annual Meeting; November 8-12, 2008; Washington, D.C.
Rubin DL, Channin DS.	Translational Imaging Informatics: Research Challenges and Real World Opportunities. Summit on Translational Bioinformatics, American Medical Informatics Association; March 10-12, 2008; San Francisco, CA.
Tulipano P, Paynes P, Rubin DL, Butte A, Starren J.	Challenges and Opportunities for Multidisciplinary Approaches to Personalized Medicine Research and Delivery. American Medical Informatics Association Annual Meeting; November 8-12, 2008; Washington, D.C.
Chari R, Gambhir SS, Geevarghese S, Geller DA, Iagaru A, Meschder A, Nemunaitis J, Reid TR, Sze DY, Tanabe K.	Efficacy of an Oncolytic Herpes Simplex Virus (NV1020) in Patients with Colorectal Cancer Metastatic to Liver. American Society of Clinical Oncology (ASCO) Annual Meeting; May 31-June 3, 2008; Chicago, IL.
Levy M, Rubin DL, Edwards K, Burtness B, Guardino A.	Radiologist-Oncologist Workflow Analysis in Application of RECIST. 44th Annual Meeting of the American Society of Clinical Oncology; May 30-June 12, 2008; Chicago, Il.

Sze DY, Gambhir SS, Chari R, Geller DA, Iagaru A, Mescheder A, Nemunaitis J, Reid TR, Tanabe K.	Imaging Characteristics and Response after Intraarterial Administration of the Oncolytic Herpes Virus NV1020 to Treat Hepatic Colorectal Metastases. American Society of Clinical Oncology (ASCO) Annual Meeting; May 31-June 3, 2008; Chicago, IL.
Hargreaves BA, Han M, Cunningham CH, Pauly JM, Daniel BL.	Dynamic Contrast-Enhanced Spiral Bilateral Breast MRI. ISMRM Workshop on Data Sampling and Image Reconstruction; January 25-29, 2009; Sedona, AZ.
Fahrig R.	The Scatter Environment in MDCT. Stanford multidetector computed tomography (MDCT) course; May 13, 2008; San Francisco, CA.
Fahrig R.	Cardiac Imaging in the Interventional Suite. Stanford multidetector computed tomography (MDCT) course; May 13, 2008; San Francisco, CA.
Gold G, Staroswiecki E, Bangerter N, Koo S, Watkins R, Hargreaves B.	Early Detection of Osteoarthritis in Patients with ACL Injury Using Sodium MRI. Cum Laude Award Winner; Society of Computed Body Tomography and Magnetic Resonance (SCBT-MR); March 1-6, 2009; Miami, FL.
Vasanawala S, Alley M, Pauly J, Gold G, Herfkens R, Lustig M.	Faster Pediatric MRI with Compressed Sensing. SCBT-MR, Miami, March 2009. Lauterbur Award Winner, Best MRI Paper; Society of Computed Body Tomography and Magnetic Resonance (SCBT-MR); March 1-6, 2009; Miami, FL.
Njuguna N, Flanders AE, Rubin DL, Siddiqui KM, Kim W, Siegel EL.	What are Radiologists Looking for? The Demographics and Usage Statistics for a Novel Radiology-Centric Websearch Engine. Society for Imaging Informatics in Medicine Annual Scientific Meeting; May 15-18, 2008; Seattle, WA.
Rubin DL, Flanders AE, Kim W, Kahn CE, Siddiqui KM.	Ontology-Assisted Analysis of Web Queries to Determine the Knowledge Radiologists Seek. Society for Imaging Informatics in Medicine Annual Scientific Meeting; May 15-18, 2008; Seattle, WA.
Chan KT, Sze DY, Kuo WT, Kothary N, Louie JD, Hovsepian DM, Hwang GL, Hofmann LV.	Common Iliac Vein Stenosis and Risk of Pulmonary Embolism: A Negative Correlation. Society of Interventional Radiology; March 7-12, 2009; San Diego, CA.
Chan KT, Sze DY, Kuo WT, Kothary N, Louie JD, Hovsepian DM, Hwang GL, Hofmann LV.	Iliac Vein Stenosis and Thrombus Volume: A Positive Correlation in Lower Extremity Deep Venous Thrombosis. Society of Interventional Radiology, March 7-12, 2009; San Diego, CA.
Kothary N, Dua R, Louie JD, Hwang G, Kuo WT, Hovsepian D, Leung A, Hofmann LV, Sze DY.	CT Guided Percutaneous Needle Biopsy of the Indeterminate Pulmonary Nodule: Efficacy of Obtaining a Diagnostic Sample. Society of Interventional Radiology, March 7-12, 2009; San Diego, CA.
Kothary N, Tognolini A, Louie JD, Hwang G, Kuo WT, Hovsepian DM, Hofmann L, Sze DY.	Impact of C-Arm CT on Treatment Planning in Patients Undergoing Chemembolization for Tumors Located in Segments with Watershed Arterial Supply. Society of Interventional Radiology, March 7-12, 2009; San Diego, CA.
Kothary N, Tognolini A, Louie JD, Hwang G, Kuo WT, Hovsepian DM, Hofmann L, Sze DY.	Impact of C-Arm CT in Patients with Hepatocellular Carcinoma Undergoing Transhepatic Arterial Chemoembolization. Society of Interventional Radiology, March 7-12, 2009; San Diego, CA.
Kuo WT, Tong RT, Hwang GL, Louie JD, Sze DY, Morshedi MM, Lebowitz EA, Hofmann LV.	High-Risk Retrieval of Adherent and Chronically Implanted IVC Filters: Techniques for Removal and Management of Procedural Thrombotic Complications. Society of Interventional Radiology, March 7-12, 2009; San Diego, CA.
Butts Pauly K	Ultrasound for small animal workshop. November, 2008; Stanford University.
Fahrig R.	X-ray Computed Tomography Physics and Instrumentation: Brief Overview. Small Animal Imaging Workshop; November 5, 2008; Stanford, CA.
Levin C.	Introduction to the Small Animal Imaging Workshop at Stanford. Small Animal Imaging Workshop; November 5-8, 2008; Stanford, CA.
Levin C.	Radionuclide Imaging Physics and Instrumentation: Brief Overview. Small Animal Imaging Workshop; November 5-8, 2008; Stanford, CA.

Spielman DM.	Real-Time Metabolic Imaging of the Rat using Hyperpolarized 13C-Labeled Pyruvate. Small Animal Imaging Workshop; November 5, 2008; Stanford University.
Barth RA, Newman B, Rubesova E, Hintz S, Vasanawala SS.	Congenital lobar overinflation (CLO)/congenital lobar emphsysema (CLE) - not an uncommon cause for a fetal chest mass. Society for Pediatric Radiology; April 21-25, 2009; Carlsbad, CA.
Eslamy HK, Barth RA, Rubesova E.	MRI in pregnancy for assessment of congenital anomalies of the chest, abdomen and pelvis (Poster). Society for Pediatric Radiology; April 21-25, 2009; Carlsbad, CA.
Eslamy HK, Yeom K, Rubesova E, Hahn J, Barnes P, Barth RA, et al.	Correlation of fetal and postnatal brain MRI (Poster). Society for Pediatric Radiology; April 21-25, 2009; Carlsbad, CA.
Rubesova E, Barth RA, Rosenberg J, Brau JC, Vasanawala SS.	3D T1-weighted fetal MRI. Society for Pediatric Radiology; April 21-25, 2009; Carlsbad, CA.
Rubesova E, Vasanawala SS, Rosenberg J, Barth RA.	Single shot SSFSE versus balanced steady state imaging: which sequence to choose to image fetal body. Society for Pediatric Radiology; April 21-25, 2009; Carlsbad, CA.
Yeom, K.	Correlation of Fetal and Post-natal Brain MRI. Society for Pediatric Radiology; April 22-25, 2009; Carlsbad, CA.
Kuo WT.	Catheter-Directed Therapy for Massive Pulmonary Embolism: Systematic Review and Meta-Analysis of the Modern Technique; United States Food and Drug Administration Center for Devices and Radiological Health; April, 2008; Rockville, MD.
Rubin DL.	"Devising Current and Future Bioinformatics Strategies: Creating the Required Interoperability." National Cancer Institute's workshop: The Role of Biomedical Informatics in Overcoming Barriers in Cancer Research; May, 2008; Columbus OH.
Bammer R.	Parallel Receive and Transmit for Neuroimaging. Workshop on Modern Optics in Biomedical Research. May, 2008; International Max Planck Research School for Optics and Imaging; University of Erlangen-Nuremberg, Germany.
Girard-Hughes E, Al-Ahmad A, Mehdizadeh A, Boese J, Lauritsch G, Wang P, Hsia H, Zei P, Rosenberg J, Fahrig R.	The Impact of Atrial Fibrillation on the Accuracy of Three-Dimensional Imaging of the Left Atrium: A Study Using ECG Gated Multisweep C-arm CT. Poster, 29th Annual Scientific Sessions of the Heart Rhythm Society; May 14-17, 2008; San Francisco, CA.
Gold G, Koo S, Starosweicki E, Watkins R, Bangerter N, Hargreaves B.	The Impact of Atrial Fibrillation on the Accuracy of Three-Dimensional Imaging of the Left Atrium: A Study Using ECG Gated Multisweep C-arm CT. Poster, 29th Annual Scientific Sessions of the Heart Rhythm Society; May 14-17, 2008; San Francisco, CA.
Ikeda DM.	Digital Mammography. Radiology International Postgraduate Course; May 18-25, 2008; Prague, Czech Republic; Vienna, Austria.
Ikeda DM.	Breast MRI. Radiology International Postgraduate Course; May 18-25, 2008; Prague, Czech Republic; Vienna, Austria.
Ikeda DM.	MRI-guided Needle localization. Radiology International Postgraduate Course; May 18-25, 2008; Prague, Czech Republic; Vienna, Austria.
Bammer R.	High-Resolution Diffusion Imaging: Advanced Acquisition and Reconstruction Methods. June, 2008; Neuroradiology Section, Mayo Clinic; Rochester, MN.
Yoon S.	Simultaneous Segmentation and Reconstruction: A Level Set Method Approach for Limited View Computed Tomography. Stanford Bio Engineering 393 Forum; June, 2008.
Levin C.	Integrating Positron Emission Tomography and Magnetic Resonance Imaging; June 4, 2008; GE Executives of the Global Climate and Energy Project (GCEP); Stanford, CA.
Levin C.	PET Instrumentation that can be Operated Within an MRI System; June 7, 2008; Palo Alto Veterans Administration Health Care, Palo Alto, CA.

Levin C.	New imaging system technologies to enhance the molecular sensitivity of positron emission tomography; June 17, 2008; Department of Engineering Physics, Tsinghua University, Beijing, China.
Levin C.	PET Instrumentation that can Operate Within a Magnetic Resonance Imaging (MRI) System; June 18, 2008; Department of Engineering Physics, Tsinghua University, Beijing, China.
Levin C.	Organ-Specific Radionuclide Cameras for More Sensitive Cancer Imaging; June 18, 2008; Department of Engineering Physics, Tsinghua University, Beijing, China.
Rieke V, Chen J, Holbrook A, Bouley D, Diederich C, Sommer G, Butts Pauly K.	High Intensity Ultrasound Ablation of the Canine Prostate: Monitoring and Post -Procedural Assessment with Magnetic Resonance Imaging. World Conference on Interventional Oncology; June 22-25, 2008; Los Angeles, CA.
Iagaru A, Mittra ES, Quon A, Jacobs C, Marina N, Gambhir SS.	Repeatability of in vivo sodium MRI of Cartilage in Early Osteoarthritis. Annual Workshop on Imaging-based Measures of Osteoarthritis; June-27-28, 2008; Boston, MA.
Koo S, Hargreaves B, Andriacchi T, Gold G.	Toward Automatic Segmentation of Knee Articular Cartilage in Osteoarthritis. Annual Workshop on Imaging-based Measures of Osteoarthritis; June-27-28, 2008; Boston, MA.
Kuo WT.	Endovascular Therapy for Massive PE. Western Angiographic and Interventional Society 38th Annual Meeting; August, 2008; Maui, HI.
Levin C.	Radionuclide physics in cancer imaging; July 2, 2008; Department of Physics Summer Research Program; Stanford, CA.
Fahrig R.	Reconstruction and Correction Issues in C-arm CT. Erlangen Graduate School in Advanced Optical Technologies (SAOT) Seminar Series. Friedrich-Alexander-Universitat; July 8, 2008; Erlangen-Nurnberg, Germany.
Kaye E, Butts Pauly K.	MR Parameters of Frozen Tissue: Proton Resonant Frequency and R2. 45th Annual Meeting of the Society for Cryobiology; July 20 – 23, 2008; Charlotte, NC.
Fahrig R.	CT Surgery Suite of the Future; Japanese Technologist Summer Training Program; July 22, 2008
Spielman DM.	Hyper Polarized MR at High Field. JSTOR Summer Symposium on State of the Art Imaging; July 24, 2008; Stanford University.
Koo S, Clark D, Kwon A, Gold G, Andriacchi T.	Walking exercise affects bone metabolic activity as seen with 18F-PET. American Society of Biomechanics; August 5-9, 2008; Ann Arbor, MI.
Levin C.	Advanced positron emission tomography (PET) camera dedicated to breast cancer imaging; August 19, 2008; Department of Electrical Engineering. Research Experience for Undergraduates (REU) Program; Stanford, CA.
Chen J, Watkins R, Butts Pauly K.	Optimization of Encoding Gradients for Magnetic Resonance Acoustic Radiation Force Imaging. 8th International Symposium on Therapeutic Ultrasound (ISTU); September 10-13, 2008; Minneapolis, MN.
Fischbein N.	Nasopharynx and Skull Base: Normal Anatomy. 42nd Annual Meeting of the American Society of Head and Neck Radiology; September 10-14, 2008; Toronto, Ontario, Canada.
Holbrook A, Santos J, Rieke V, Kaye E, Butts Pauly K.	Fast Referenceless PRF Thermometry Using Spatially Saturated, Spatial-spectrally Excited Flyback EPI. 8th International Symposium on Therapeutic Ultrasound (ISTU); September 10-13, 2008; Minneapolis, MN.
King RL, Rieke V, Butts Pauly K.	Liver Ablation through the Ribcage and Cartilage in a Rodent Model. 8th International Symposium on Therapeutic Ultrasound (ISTU); September 10-13, 2008; Minneapolis, MN.
Butts Pauly K	MRI of the Cryolesion. 7th Interventional MRI Symposium; September 12-13, 2008; Baltimore, Maryland.
Moseley M.	Current Concepts of Magnetic Resonance. RSL Radiology Post-Graduate Course; October, 2008; Monterey, CA.
Moseley M.	High-Field MR for Neuroscience; Department of Neurosciences Retreat; October, 2008.

Butts Pauly K	MR-Guided High Intensity Ultrasound of the Prostate. Focused Ultrasound Symposium; October 6-7, 2008; Washington, D.C.
Fischbein N.	Radiologic Evaluation of the Sinuses. Western States Rhinology Course; October 16-18, 2008; Sonoma, CA.
Levin C.	Clinical whole body PET/MRI development at Stanford; October 17, 2008; 1st Imaging Symposium, University Hospital; Tübingen, Germany.
Lau F, Fang C, Reynolds P, Vandenbroucke A, Olcott P, Olutade F, Pratx G, Horowitz M, Levin C.	1mm3 Resolution Breast-Dedicated PET System. 4th International Workshop on the Molecular Radiology of Breast Cancer (MRBC); October 20-21, 2008; Dresden, Germany.
Spanoudaki V, Vandenbroucke A, Lau F, Fang C, Gu Y, Olcott P, Levin C.	Effects of Thermal Regulation Structures on the Photon Sensitivity and Spatial Resolution of a 1 mm3 Resolution Breast-Dedicated PET System. 4th Annual Workshop on the Molecular Radiology of Breast Cancer; October 20-21, 2008; Dresden, Germany.
Levin C, Olcott P.	High Performance PET Detectors for Whole Body Clinical PET/MR that do not Use Shielded Cables. Workshop on MR-PET: A Hybrid Imaging System; October 27-28, 2008; Forschungszentrum, Jülich, Germany.
Singh MK, Spielman DM, Chang K.	Glutamatergic Pathways in Children with and at Risk for Developing Mania. 55th Annual Meeting of the American Academy of Child and Adolescent Psychiatry; October 28 - November 2, 2008; Chicago, IL.
Bammer R.	Advances in MRI. November, 2008; Technical University of Erlangen; Erlangen, Germany.
Fischbein N.	Imaging of Sensorineural Hearing Loss and Vertigo. Stanford Otology and Neurotology Update 2008; November 6-8, 2008; San Francisco, CA.
Spielman DM.	Spectroscopic Imaging of Neurotransmitters. International Society of Magnetic Resonance in Medicine Workshop on MR Spectroscopy and Neurotransmitter Function in Neuropsychiatric Disorders; November 7, 2008; Quebec City, Quebec, Canada.
Iagaru A.	131I-Tositumomab (Bexxar®) Therapy of Refractory/Relapsed Non-Hodgkin Lymphoma: Clinical Experience. European Association of Nuclear Medicine Annual Congress; October 11-15, 2008; Munich, Germany.
Iagaru A.	18F FDG PET/CT Evaluation of Osseous and Soft Tissue Sarcomas: Differences between Adult and Pediatric Patients. European Association of Nuclear Medicine Annual Congress; October 11-15, 2008; Munich, Germany.
Iagaru A.	18F Sodium Fluorine: An Unfinished Business. Invited lecture, MIPS Seminar; November 17, 2008; Stanford, CA.
Iagaru A.	Old Tracers, New Ideas: Clinical Research in Nuclear Medicine. Invited Lecture, Nuclear Medicine Grand Rounds; November 18, 2008; Stanford, CA.
Chang K, DelBello M, Howe M, Mills M, Bryan H, Adler C, Rana M, Welge J, Spielman DM, Strakowski S.	Neurochemical correlates of response to quetiapine in youth with bipolar depresson. 55th Annual Meeting of the American Academy of Child and Adolescent Psychiatry; October 28 - November 2, 2008; Chicago, IL.
Levin C.	Organ-specific positron emission tomography camera to enhance cancer sensitivity; December 15, 2008; UCLA Crump Institute/Johnson Comprehensive Cancer Center Molecular Imaging Program Monthly Seminar Series; Los Angeles, CA.
Moseley M.	Speaker, Lab Animal Technician Appreciation Week; January, 2009; Stanford, CA.
Moseley M.	Lectures “MR Basic Concepts,” “MR Advanced Topics.” American Society of Neuroimaging; January 22-25, 2009; Orlando, FL.
Levin C.	New Technology to facilitate high performance, artifact-free PET/MR; January 30, 2009; Community of Bay Area Radionuclide Imagers, UC Davis Center for Genomic and Molecular Imaging; Davis, CA.
Levin C.	Progress towards a 1 mm resolution clinical PET system for cancer imaging; February 3, 2009; Nuclear Medicine/ Molecular Imaging grand rounds lecture series; Stanford, CA.

Girard-Hughes E, Al-Ahmad A, Moore T, Lauritsch G, Boese J, Fahrig R.	Visualization and enhancement patterns of radiofrequency ablation lesions with iodine contrast-enhanced cardiac C-arm CT. Medical Imaging 2009: Biomedical Applications in Molecular, Structural, and Functional Imaging; February 9-12, 2009; Lake Buena Vista, FL.
Iagaru A.	The Physiology of 18F FDG and Principles of PET Scanning. Invited lecture, Stanford PET/CT Symposium; February 12, 2009; Las Vegas, NV.
Iagaru A.	Vascular Tracer Activity: Disease or Not? Invited lecture, Stanford PET/CT Symposium; February 12, 2009; Las Vegas, NV.
Iagaru A.	PET/CT as an Adjunctive Test for Infectious or Inflammatory Disease? Invited lecture, Stanford PET/CT Symposium; February 12, 2009; Las Vegas, NV.
Stikov N, Keenan K, Gold G, Pauly J.	Cartilage Bound Pool Fraction Maps In Vivo. International Society for Magnetic Resonance in Medicine (ISMRM) Workshop on Advances in Musculoskeletal Magnetic Resonance Imaging; February 14-17, 2009; San Francisco, CA.
Fischbein N.	Anterior and Central Skull Base. 9th Annual MR Advances in Neuroradiology and Sports Medicine Imaging; February 19-21, 2009; Lake Tahoe, CA.*
Fischbein N.	White Matter Disease. 9th Annual MR Advances in Neuroradiology and Sports Medicine Imaging; February 19-21, 2009; Lake Tahoe, CA.*
Fischbein N.	CNS Infection. 9th Annual MR Advances in Neuroradiology and Sports Medicine Imaging; February 19-21, 2009; Lake Tahoe, CA.
Giordano G, Lindsey D, Gold G, Zaffagnini S, Safran M.	Strains Within the Intact Acetabular Labrum During Passive Range of Motion. Annual Meeting, Orthopaedic Research Society; February 22-25, 2009; Las Vegas, NV.
Gold G, Staroswiecki E, Bangerter N, Jordan N, Koo S, Watkins R, Hargreaves B.	Improved MRI around Metal Implants using SEMAC and auto-calibrated parallel imaging. Annual Meeting, Orthopaedic Research Society; February 22-25, 2009; Las Vegas, NV.
Iagaru A, Knox SJ, Goris ML.	In Vivo Whole Knee Sodium MRI at 3.0T in ACL Injured Patients. Annual Meeting, Orthopaedic Research Society; February 22-25, 2009; Las Vegas, NV.
Safran M, Giordano G, Lindsey D, Gold G, Zaffagnini S.	Effect of Acetabular Labrum Tears and Resection on Labral Strain. Annual Meeting, Orthopaedic Research Society; February 22-25, 2009; Las Vegas, NV.
Safran M, Zaffagnini S, Lopomo N, Vaughn Z, Lindsey D, Gold G, Bignozzi S, Marcacci M.	The Influence of Soft Tissues on Hip Joint Kinematics: An In Vitro Computer Assisted Analysis. Annual Meeting, Orthopaedic Research Society; February 22-25, 2009; Las Vegas, NV.
Desser TS.	Women in Radiology. Michelle R. Clayman Institute on Gender; February 26, 2009; Stanford University.
Moseley M.	Advances in Neuroimaging. 61st Annual Meeting, San Francisco Neurological Society; February 27-March 1, 2009; Monterey, CA.
Desser TS.	Understanding THIDs and THADs. 2009 Abdominal Radiology Course; March 15-20, 2009; Maui, HI.
Koo S, Sung K, Han M, Hargreaves B, Gold G.	Bexxar® and Zevalin® Radioimmunotherapy in Non-Hodgkin Lymphomas. Invited lecture, Stanford's Stampede (Nuclear Medicine Technologist Meeting); March 21, 2009; Stanford, CA.
Fischbein N.	Imaging of Acute Stroke. 17th Annual Diagnostic Imaging Update on Maui; March 23-27, 2009; Maui, HI.
Fischbein N.	Imaging of Non-Traumatic Myelopathy. 17th Annual Diagnostic Imaging Update on Maui; March 23-27, 2009; Maui, HI.
Rubin DL.	Informatics-Enabled Research in Radiology: Data Warehousing and Data Mining. Association of University Radiologists; March 25-29; Seattle, WA.

Yen YF, Le Roux P, Mayer D, Takahashi A, Tropp J, Spielman DM, Pfefferbaum A, Hurd R.	Multi-excitation non-CPMG with low flip angles (MENLO): Preliminary tests toward hyperpolarized 13C applications. 50th Experimental Nuclear Magnetic Resonance Conference (ENC); March 29 - April 3, 2009; Pacific Grove, CA.
Mayer D, Yen YF, Takahash A, Tropp J, Hurd R, Pfefferbau A, Spielman DM.	Single-shot metabolic imaging in the rat after injection of hyperpolarized 13C1-pyruvate using a high-performance gradient insert. 50th Experimental Nuclear Magnetic Resonance Conference (ENC); March 29 - April 3, 2009; Pacific Grove, CA.
Moseley M.	Diffusion MRI in Neuroimaging. American Academy of Neurology (AAN); April 25-May 2, 2009; Seattle, WA.
Kuo WT.	Embolotherapy for Lower Gastrointestinal Hemorrhage. IR Fellows Conference, Pathway to Excellence; May, 2009; San Francisco, CA.
Yeom, K.	2. Serial Perfusion and Diffusion MRI in Pediatric Diffuse Intrinsic Brainstem Glioma. American Society of Neuroradiology; May 16-21, 2009; Vancouver, B.C., Canada.
Bammer R.	Novel Acquisition Methods for Improved Spatial Localization, Capillary Sensitivity, and Distortion Reduction in FMRI and Perfusion MRI. Neurosciences Seminar Series, University of Hawaii.
Bammer R.	Diffusion MRI Beyond the Tensor. Neurosciences Seminar Series, University of Hawaii.
Bammer R.	Advances in Diffusion MRI. November, 2008; University of Freiburg, Germany, Department of Radiology.
Kothary N, Dua R, Louie JD, Hwang G, Kuo WT, Hovsepian D, Leung A, Hofmann LV.	Guided Percutaneous Needle Biopsy of the Indeterminate Pulmonary Nodule: Efficacy of Obtaining a Diagnostic Sample. Society of Interventional Radiology; March 7-12, 2009; San Diego, CA.
Levin C.	Organ-Specific Positron Emission Tomography Camera for More Sensitive Cancer Imaging; April 11, 2008; University of Connecticut Department of Electrical and Computer Engineering.
Kothary N, Louie JD, Kuo WT, Hovsepian DM, Sze DY, Hofmann LV.	Safety and Efficacy of Percutaneous Fiducial Marker Implantation for Image-guided Radiotherapy. Society of Interventional Radiology; March 7-12, 2009; San Diego, CA.

Published Papers

Ai L, Rouhanizadeh M, Wu JC, Takabe W, Yu H, Alavi M, Li R, Chu Y, Miller J, Heistad DD, Hsiai TK.	Shear stress influences spatial variations in vascular Mn-SOD expression: implication for LDL nitration. Am J Physiol Cell Physiol. 2008 Jun;294(6):C1576-85.
Aksoy M, Liu C, Moseley ME, Bammer R.	Single-step nonlinear diffusion tensor estimation in the presence of microscopic and macroscopic motion. Magn Reson Med. 2008 May;59(5):1138-50.
Al-Ahmad A, Wigström L, Sandner-Porkristl D, Wang PJ, Zei PC, Boese J, Lauritsch G, Moore T, Chan F, Fahrig R.	Time-resolved three-dimensional imaging of the left atrium and pulmonary veins in the interventional suite--a comparison between multisweep gated rotational three-dimensional reconstructed fluoroscopy and multislice computed tomography. Heart Rhythm. 2008 Apr;5(4):513-9.
Andersson I, Ikeda DM, Zackrisson S, Ruschin M, Svahn T, Timberg P, Tingberg A.	Breast tomosynthesis and digital mammography: a comparison of breast cancer visibility and BI-RADS classification in a population of cancers with subtle mammographic findings. Eur Radiol. 2008 Dec;18(12):2817-25.
Arakawa H, Marks MP, Do HM, Bouley DM, Strobel N, Moore T, Fahrig R.	AJNR Am J Neuroradiol. 2008 Apr;29(4):766-72. Experimental study of intracranial hematoma detection with flat panel detector C-arm CT.
Arnow BA, Millheiser L, Garrett A, Lake Polan M, Glover GH, Hill KR, Lightbody A, Watson C, Banner L, Smart T, Buchanan T, Desmond JE.	Women with hypoactive sexual desire disorder compared to normal females: a functional magnetic resonance imaging study. Neuroscience. 2009 Jan 23;158(2):484-502. Epub 2008 Oct 2.

Arakawa H, Marks MP, Do HM, Bouley DM, Strobel N, Moore T, Fahrig R. Experimental study of intracranial hematoma detection with flat panel detector C-arm CT. AJNR Am J Neuroradiol. 2008 Apr;29(4):766-72.

Assimes TL, Knowles JW, Basu A, Iribarren C, Southwick A, Tang H, Absher D, Li J, Fair JM, Rubin GD, Sidney S, Fortmann SP, Go AS, Hlatky MA, Myers RM, Risch N, Quertermous T. Susceptibility locus for clinical and subclinical coronary artery disease at chromosome 9p21 in the multi-ethnic ADVANCE study. Hum Mol Genet. 2008 Aug 1;17(15):2320-8.

Augustine E, Spielman D, Barnes P, Sutcliffe T, Dermon J, Mirmiran M,Clayton D, Ariagno R. Can magnetic resonance spectroscopy predict neurodevelopmental outcome in very low birth weight preterm infants? J Perinatol. 2008 Sep;28(9):611-8.

Backer MV, Levashova Z, Levenson R, Blankenberg FG, Backer JM. Cysteine-containing fusion tag for site-specific conjugation of therapeutic and imaging agents to targeting proteins. Methods Mol Biol. 2008;494:275-94.

Baek J, Pelc NJ. Direct two-dimensional reconstruction algorithm for an inverse-geometry CT system. Med Phys. 2009 Feb;36(2):394-401.

Baker LC, Atlas SW, Afendulis CC. Expanded use of imaging technology and the challenge of measuring value. Health Affairs 2008 Nov-Dec;27(6):1467-78.

Balchandani P, Pauly J, Spielman DM. Interleaved narrow-band PRESS sequence with adiabatic spatial-spectral refocusing pulses for 1H MRSI at 7T. Magn Reson Med. 2008 May;59(5):973-9.

Balchandani P, Pauly J, Spielman DM. Slice-selective tunable-flip adiabatic low peak-power excitation pulse. Magn Reson Med. 2008 May;59(5):1072-8.

Balchandani P, Spielman DM. Fat suppression for 1H MRSI at 7T using spectrally selective adiabatic inversion recovery. Magn Reson Med. 2008 May;59(5):980-8.

Bammer R, Holdsworth SJ, Veldhuis WB, Skare ST. New methods in diffusion-weighted and diffusion tensor imaging. Magn Reson Imaging Clin N Am. 2009 May;17(2):175-204.

Barnes P, Krasnokutsky M, Monson K, Ophoven J. Traumatic spinal cord injury: accidental versus nonaccidental injury. Semin Pediatr Neurol. 2008 Dec;15(4):178-84.

Benedetti N, Desser TS, Jeffrey RB. Imaging of Hepatic Infections. Ultrasound Quarterly 2008 Dec;24(4):267-78.

Besier TF, Gold GE, Delp SL, Fredericson M, Beaupre GS. The influence of femoral internal and external rotation on cartilage stresses within the patellofemoral joint. J Orthop Res. 2008 Dec;26(12):1627-35.

Blankenberg FG. Imaging the molecular signatures of apoptosis and injury with radiolabeled annexin V. Proc Am Thorac Soc. 2009 Aug 15;6(5):469-76.

Blankenberg FG. In vivo detection of apoptosis. J Nucl Med. 2008 Jun;49 Suppl 2:81S-95S.

Blankenberg FG. In vivo imaging of apoptosis. Cancer Biol Ther. 2008 Oct;7(10):1525-32.

Blankenberg FG. Monitoring of treatment-induced apoptosis in oncology with PET and SPECT. Curr Pharm Des. 2008;14(28):2974-82.

Bracken JA, DeCrescenzo G, Komljenovic P, Lillaney PV, Fahrig R, Rowlands JA. Closed bore XMR (CBXMR) systems for aortic valve replacement: active magnetic shielding of x-ray tubes. Med Phys. 2009 May;36(5):1717-26.

Bracken JA, Komljenovic P, Lillaney PV, Fahrig R, Rowlands JA. Closed-bore XMR (CBXMR) systems for aortic valve replacement: x-ray tube imaging performance. Med Phys. 2009 Apr;36(4):1086-97.

Bracken JA, Lillaney PV, Fahrig R, Rowlands JA. Closed bore XMR (CBXMR) systems for aortic valve replacement: investigation of rotating-anode x-ray tube heat loadability. Med Phys. 2008 Sep;35(9):4049-62.

Brau AC, Beatty PJ, Skare S, Bammer R. Comparison of reconstruction accuracy and efficiency among autocalibrating data-driven parallel imaging methods. Magn Reson Med. 2008 Feb;59(2):382-95.

Brown GG, McCarthy G, Bischoff-Grethe A, Ozyurt B, Greve D, Potkin SG, Turner JA, Notestine R, Calhoun VD, Ford JM, Mathalon D, Manoach DS, Gadde S, Glover GH, Wible CG, Belger A, Gollub RL, Lauriello J, O'Leary D, Lim KO. Brain-performance correlates of working memory retrieval in schizophrenia: a cognitive modeling approach. Schizophr Bull. 2009 Jan;35(1):32-46.

Bug WJ, Astahkov V, Boline J, Fennema-Notestine C, Grethe J, Gupta A, Kennedy DN, Rubin DL, Sanders B, Turner J, Martone M. Data Federation in the biomedical informatics research network: tools for semantic annotation and query of distributed multiscale brain data. AMIA Annu Symp Proc. 2008 Nov 6:1220.

Burt JR, Iribarren C, Fair JM, Norton LC, Mahbouba M, Rubin GD, Hlatky MA, Go AS, Fortmann SP. Incidental findings on cardiac multidetector row computed tomography among healthy older adults: prevalence and clinical correlates. Arch Intern Med. 2008 Apr 14;168(7):756-61.

Cai W, Guzman R, Hsu AR, Wang H, Chen K, Sun G, Gera A, Choi R, Bliss T, He L, Li ZB, Maag AL, Hori N, Zhao H, Moseley M, Steinberg GK, Chen X. Positron emission tomography imaging of poststroke angiogenesis. Stroke 2009 Jan;40(1):270-7.

Cao F, Li Z, Lee A, Liu Z, Chen K, Wang H, Cai W, Chen X, Wu JC. Noninvasive de novo imaging of human embryonic stem cell-derived teratoma formation. Cancer Res. 2009 Apr 1;69(7):2709-13.

Cao F, Wagner RA, Wilson KD, Xie X, Fu JD, Drukker M, Lee A, Li RA, Gambhir SS, Weissman IL, Robbins RC, Wu JC. Transcriptional and functional profiling of human embryonic stem cell-derived cardiomyocytes. PLoS One. 2008;3(10):e3474.

Chang C, Cunningham JP, Glover GH. Influence of heart rate on the BOLD signal: the cardiac response function. Neuroimage. 2009 Feb 1;44(3):857-69. Epub 2008 Oct 7.

Chang C, Thomason ME, Glover GH. Mapping and correction of vascular hemodynamic latency in the BOLD signal. Neuroimage. 2008 Oct 15;43(1):90-102. Epub 2008 Jul 4.

Chang DT, Schellenberg D, Shen J, Kim J, Goodman KA, Fisher GA, Ford JM, Desser TS, Quon A, Koong AC. Stereotactic radiotherapy for unresectable adenocarcinoma of the pancreas. Cancer 2009 Feb;115(3):665-72.

Channin DS, Mongkolwat P, Kleper V, Sepukar K, Rubin DL. The caBIG Annotation and Image Markup Project. J Digit Imaging 2009 Mar 18.

Chen CA, Lu W, John CT, Hargreaves BA, Reeder SB, Delp SL, Siston RA, Gold GE. Multiecho IDEAL Gradient-Echo Water-Fat Separation for Rapid Assessment of Cartilage Volume at 1.5 T: Initial Experience. Radiology. 2009 Jun 15.

Chen IY, Greve JM, Gheysens O, Willmann JK, Rodriguez-Porcel M, Chu P, Sheikh AY, Faranesh AZ, Paulmurugan R, Yang PC, Wu JC, Gambhir SS. Comparison of optical bioluminescence reporter gene and superparamagnetic iron oxide MR contrast agent as cell markers for noninvasive imaging of cardiac cell transplantation. Mol Imaging Biol. 2009 May-Jun;11(3):178-87.

Chen J, Daniel BL, Diederich CJ, Bouley DM, van den Bosch MA, Kinsey AM, Sommer G, Butts Pauly K. Monitoring prostate thermal therapy with diffusion-weighted MRI. Magn Reson Med. 2008 Jun;59(6):1365-72.

Chen MQ, Xie X, Hollis Whittington R, Kovacs GT, Wu JC, Giovangrandi L. Cardiac differentiation of embryonic stem cells with point-source electrical stimulation. Conf Proc IEEE Eng Med Biol Soc. 2008;2008:1729-32.

Chun HJ, Narula J, Hofstra L, Wu JC. Intracellular and extracellular targets of molecular imaging in the myocardium. Nat Clin Pract Cardiovasc Med. 2008 Aug;5 Suppl 2:S33-41.

Cukur T, Lee JH, Bangerter NK, Hargreaves BA, Nishimura DG. Non-contrast-enhanced flow-independent peripheral MR angiography with balanced SSFP. Magn Reson Med. 2009 Jun;61(6):1533-9.

Cunningham CH, Chen AP, Lustig M, Hargreaves BA, Lupo J, Xu D, Kurhanewicz J, Hurd RE, Pauly JM, Nelson SJ, Vigneron DB. Pulse sequence for dynamic volumetric imaging of hyperpolarized metabolic products. J Magn Reson. 2008 Jul;193(1):139-46.

Daadi MM, Li Z, Arac A, Grueter BA, Sofilos M, Malenka RC, Wu JC, Steinberg GK. Molecular and magnetic resonance imaging of human embryonic stem cell-derived neural stem cell grafts in ischemic rat brain. Mol Ther. 2009 Jul;17(7):1282-91.

Desser TS, Gross M. Multidetector CT of small bowel obstruction. Seminars in Ultrasound, CT, and MRI 2008 Oct;29(5):308-21.

Douglas PS, Cerqueria M, Rubin GD, Chin AS. Extracardiac findings: what is a cardiologist to do? JACC Cardiovasc Imaging. 2008 Sep;1(5):682-7.

Dragulescu-Andrasi A, Liang G, Rao J. In Vivo Bioluminescence Imaging of Furin Activity in Breast Cancer Cells Using Bioluminogenic Substrates. Bioconjug Chem. 2009 Jul 31.

Draper CE, Santos JM, Kourtis LC, Besier TF, Fredericson M, Beaupre GS, Gold GE, Delp SL. Feasibility of using real-time MRI to measure joint kinematics in 1.5T and open-bore 0.5T systems. J Magn Reson Imaging 2008 Jul; 28:158-166.

Eslamy HK, Newman B. Imaging of the pediatric airway. Paediatr Anaesth. 2009 Jul;19 Suppl 1:9-23.

Eslamy HK, Quon A. PET/CT imaging of gastrointestinal stromal tumor with calcified peritoneal implants after imatinib therapy. Clin Nucl Med. 2008 Dec;33(12):864-5.

Ford JM, Roach BJ, Jorgensen KW, Turner JA, Brown GG, Notestine R, Bischoff-Grethe A, Greve D, Wible C, Lauriello J, Belger A, Mueller BA, Calhoun V, Preda A, Keator D, O'Leary DS, Lim KO, Glover G, Potkin SG; FBIRN, Mathalon DH. Tuning in to the voices: a multisite FMRI study of auditory hallucinations. Schizophr Bull. 2009 Jan;35(1):58-66. Epub 2008 Nov 5.

Franklin JD, Mejino JL, Detwiler LT, Rubin DL, Brinkley JF. Web service access to semantic web ontologies for data annotation. AMIA Annu Symp Proc. 2008 Nov 6:946.

Friedman L, Stern H, Brown GG, Mathalon DH, Turner J, Glover GH, Gollub RL, Lauriello J, Lim KO, Cannon T, Greve DN, Bockholt HJ, Belger A, Mueller B, Doty MJ, He J, Wells W, Smyth P, Pieper S, Kim S, Kubicki M, Vangel M, Potkin SG. Test-retest and between-site reliability in a multicenter fMRI study. Hum Brain Mapp. 2008 Aug;29(8):958-72.

Fueger BJ, Yeom K, Czernin J, Sayre JW, Phelps ME, Allen-Auerbach MS. Comparison of CT, PET, and PET/CT for staging of patients with indolent non-Hodgkin's lymphoma. Mol Imaging Biol. 2009 Jul-Aug;11(4):269-74.

Gaab N, Gabrieli JD, Glover GH. Resting in peace or noise: scanner background noise suppresses default-mode network.Hum Brain Mapp. 2008 Jul;29(7):858-67.

Ganzel BL, Kim P, Glover GH, Temple E. Resilience after 9/11: Multimodal neuroimaging evidence for stress-related change in the healthy adult brain. Neuroimage. 2008 Apr 1;40(2):788-955.

Garrett A, Penniman L, Epstein JN, Casey BJ, Hinshaw SP, Glover G, Tonev S, Vitolo A, Davidson M, Spicer J, Greenhill LL, Reiss AL. Neuroanatomical abnormalities in adolescents with attention-deficit/hyperactivity disorder. J Am Acad Child Adolesc Psychiatry. 2008 Nov;47(11):1321-8.

Geraghty PR, van den Bosch MA, Spielman DM, Hunjan S, Birdwell RL, Fong KJ, Stables LA, Zakhour M, Herfkens RJ, Ikeda DM. MRI and (1)H MRS of the breast: presence of a choline peak as malignancy marker is related to K21 value of the tumor in patients with invasive ductal carcinoma. Breast J. 2008 Nov-Dec;14(6):574-80.

Glaser N, Marcin J, Wootton-Gorges S, Buonocore M, Rewers A, Strain J, Dicarlo J, Neely E, Barnes P, Kupperman N. Correlation of clinical and biochemical findings with diabetic ketoacidosis-related cerebral edema in children using magnetic resonance diffusion-weighted imaging. J Pediatr. 2008 Oct;153(4):541-6.

Gilbertson-Dahdal DL, Dutta S, Varich LJ, Barth RA. Neonatal malrotation with midgut volvulus mimicking duodenal atresia. AJR Am J Roentgenol. 2009 May;192(5):1269-71.

Gonella MC, Fischbein NJ, So YT. Disorders of the trigeminal system. Semin Neurol. 2009 Feb;29(1):36-44.

Gu M, Kim DH, Mayer D, Sullivan EV, Pfefferbaum A, Spielman DM. Reproducibility study of whole-brain 1H spectroscopic imaging with automated quantification. Magn Reson Med. 2008 Sep;60(3):542-7.

Gu M, Liu C, Spielman DM. Parallel spectroscopic imaging reconstruction with arbitrary trajectories using k-space sparse matrices. Magn Reson Med. 2009 Feb;61(2):267-72.

Gu M, Spielman DM. B1 and T1 insensitive water and lipid suppression using optimized multiple frequency-selective preparation pulses for whole-brain 1H spectroscopic imaging at 3T. Magn Reson Med. 2009 Feb;61(2):462-6.

Guzman R, Lee M, Achrol A, Bell-Stephens T, Kelly M, Do HM, Marks MP, Steinberg GK. Clinical outcome after 450 revascularization procedures for moyamoya disease. J Neurosurg. 2009 May 22.

Han M, Daniel BL, Hargreaves BA. Accelerated bilateral dynamic contrast-enhanced 3D spiral breast MRI using TSENSE. J Magn Reson Imaging 2008 Dec;28(6):1425-34.

Hare TA, Tottenham N, Galvan A, Voss HU, Glover GH, Casey BJ. Biological substrates of emotional reactivity and regulation in adolescence during an emotional go-nogo task. Biol Psychiatry. 2008 May 15;63(10):927-34.

Heilmaier C, Sutter R, Lutz AM, Seifert B, Willmann JK. Dynamic MRI of the liver with parallel acquisition technique: characterization of focal liver lesions and analysis of the hepatic vasculature in a single MRI session. Rofo. 2008 May;180(5):440-8.

Hendry SL 2nd, van der Bogt KE, Sheikh AY, Arai T, Dylla SJ, Drukker M, McConnell MV, Kutschka I, Hoyt G, Cao F, Weissman IL, Connolly AJ, Pelletier MP, Wu JC, Robbins RC, Yang PC. Multimodal evaluation of in vivo magnetic resonance imaging of myocardial restoration by mouse embryonic stem cells. J Thorac Cardiovasc Surg. 2008 Oct;136(4):1028-1037.

Hiona A, Wu JC. Noninvasive radionuclide imaging of cardiac gene therapy: progress and potential. Nat Clin Pract Cardiovasc Med. 2008 Aug;5 Suppl 2:S87-95.

Hoeft F, Wu DA, Hernandez A, Glover GH, Shimojo S. Electronically switchable sham transcranial magnetic stimulation (TMS) system. PLoS One. 2008 Apr 9;3(4):e1923.

Holdsworth SJ, Bammer R. Magnetic resonance imaging techniques: fMRI, DWI, and PWI. Semin Neurol. 2008 Sep;28(4):395-406.

Holman HY, Bjornstad KA, Martin MC, McKinney WR, Blakely EA, Blankenberg FG. Mid-infrared reflectivity of experimental atheromas. J Biomed Opt. 2008 May-Jun;13(3):030503.

Horoschak M, Tran PT, Bachireddy P, West RB, Mohler D, Beaulieu CF, Kapp DS, Donaldson SS. External Beam Radiation Therapy Enhances Local Control in Pigmented Villonodular Synovitis. Int J Radiat Oncol Biol Phys. 2009 Feb 9.

Hsiai TK, Wu JC. Hemodynamic forces regulate embryonic stem cell commitment to vascular progenitors. Current Cardiology Reviews 2008;4:269□74.

Hsu CS, Hellinger JC, Rubin GD, Chang J. CT angiography in pediatric extremity trauma: preoperative evaluation prior to reconstructive surgery. Hand. 2008 Jun;3(2):139-45.

Hsu JJ, Zaharchuk G, Glover GH. Rapid methods for concurrent measurement of the RF-pulse flip angle and the longitudinal relaxation time. Magn Reson Med. 2009 Jun;61(6):1319-25.

Hu Y, Glover GH. Increasing spatial coverage for high-resolution functional MRI. Magn Reson Med. 2009 Mar;61(3):716-22.

Huang M, Chan DA, Jia F, Xie X, Li Z, Hoyt G, Robbins RC, Chen X, Giaccia AJ, Wu JC. Short hairpin RNA interference therapy for ischemic heart disease. Circulation. 2008 Sep 30;118(14 Suppl):S226-33.

Iagaru A, Goris ML. Rhabdomyosarcoma diffusely metastatic to the bone marrow: suspicious findings on 99mTc-MDP bone scintigraphy confirmed by 18F FDG PET/CT and bone marrow biopsy. Eur J Nucl Med Mol Imaging 2008 Sep;35(9):1746.

Iagaru A, Gambhir SS, Goris ML. 90Y-Ibritumomab (Zevalin®) Therapy in Refractory Non-Hodgkin's Lymphoma: Observations from 111In-Ibritumomab Pre-Treatment Imaging. J Nucl Med. 2008 Nov;49(11):1809-1812.

Iagaru A, Mittra ES, McDougall IR, Quon A, Gambhir SS. 18F FDG PET/CT Evaluation of Patients with Ovarian Carcinoma. Nucl Med Commun. 2008 Dec;29(12):1046-51.

Iagaru A, Wang, Y, Mari C, Quon A, Goris ML, Horning S, Gambhir SS. 18F FDG PET/CT Evaluation of Response to Therapy in Lymphoma: When is the Optimal Time for the First Re-evaluation Scan? Hell J Nucl Med. 2008 Sep-Dec;11(3):153-6.

Iagaru AH, Mittra ES, McDougall IR, Quon A, Gambhir SS. Nucl Med Commun. 2008 Dec;29(12):1046-51.

Iagaru A, Mittra ES, Yaghoubi S, Dick DW, Quon A, Goris ML, Gambhir SS. 18F-FDG PET/CT evaluation of patients with ovarian carcinoma. A Novel Strategy for a Cocktail 18F Fluoride and 18F FDG PET/CT Scan for Evaluation of Malignancy: Results of the Pilot Phase Study. J Nucl Med. 2009 Apr;50(4):501-505.

Iagaru A, Wang Y, Mari C, Quon A, Goris ML, Horning S, Gambhir SS. (18)F-FDG-PET/CT evaluation of response to treatment in lymphoma: when is the optimal time for the first re-evaluation scan? Hell J Nucl Med. 2008 Sep-Dec;11(3):153-6.

Iagaru A, Kundu R, Jadvar H, Nagle D. Evaluation by 18F FDG PET of patients with anal squamous cell carcinoma. Hell J Nucl Med. 2009 Jan-Apr;12(1):26-8.

Iribarren C, Hlatky MA, Chandra M, Fair JM, Rubin GD, Go AS, Burt JR, Fortmann SP. Incidental pulmonary nodules on cardiac computed tomography: prognosis and use. Am J Med. 2008 Nov;121(11):989-96.

Jack CR Jr, Bernstein MA, Fox NC, Thompson P, Alexander G, Harvey D, Borowski B, Britson PJ, L Whitwell J, Ward C, Dale AM, Felmlee JP, Gunter JL, Hill DL, Killiany R, Schuff N, Fox-Bosetti S, Lin C, Studholme C, DeCarli CS, Krueger G, Ward HA, Metzger GJ, Scott KT, Mallozzi R, Blezek D, Levy J, Debbins JP, Fleisher AS, Albert M, Green R, Bartzokis G, Glover G, Mugler J, Weiner MW. The Alzheimer's Disease Neuroimaging Initiative (ADNI): MRI methods. J Magn Reson Imaging. 2008 Apr;27(4):685-91.

Jiang T, Xing B, Rao J. Recent developments of biological reporter technology for detecting gene expression. Biotechnology and Genetic Engineering Reviews 2008; 25: 41-76

Josan S, Kaye E, Pauly JM, Daniel BL, Butts Pauly K. Improved half RF slice selectivity in the presence of eddy currents with out-of-slice saturation. Magn Reson Med. 2009 May;61(5):1090-5.

Josan S, Pauly JM, Daniel BL, Butts Pauly K. Double half RF pulses for reduced sensitivity to eddy currents in UTE imaging. Magn Reson Med. 2009 May;61(5):1083-9.

Josephs SC, Rowley HA, Rubin GD; American Heart Association Writing Group 3. Atherosclerotic Peripheral Vascular Disease Symposium II: vascular magnetic resonance and computed tomographic imaging. Circulation. 2008 Dec 16;118(25):2837-44.

Jung WS, Kang CY, Paik DS, Vasiljev PE, Kim JD, Yoon SJ. Dynamic properties of an omni-directional piezoelectric motor for precision position control.

Kahn CE Jr, Rubin DL. Automated semantic indexing of figure captions to improve radiology image retrieval. J Am Med Inform Assoc. 2009 May-Jun;16(3):380-6.

Kakuda W, Lansberg MG, Thijs VN, Kemp SM, Bammer R, Wechsler LR, Moseley ME, Marks MP, Albers GW. Optimal definition for PWI/DWI mismatch in acute ischemic stroke patients. J Stroke Cerebrovasc Dis. 2008 Jul-Aug;17(4):235-40.

Kamaya A, Shin L, Chen B, Desser TS. Emergency gynecologic imaging. Seminars in Ultrasound, CT, and MR 2008 Oct;29(5):353-68.

Kaneoya K, Ueda T, Suito H, Nanazawa Y, Tamaru J, Isobe K, Naya Y, Tobe T, Motoori K, Yamamoto S, Rubin GD, Minami M, Ito H. Functional computed tomography imaging of tumor-induced angiogenesis: preliminary results of new tracer kinetic modeling using a computer discretization approach. Radiat Med. 2008 May;26(4):213-21.

Katz M, Liu C, Schaer M, Parker KJ, Ottet MC, Epps A, Buckmaster CL, Bammer R, Moseley ME, Schatzberg AF, Eliez S, Lyons DM. Prefrontal plasticity and stress inoculation-induced resilience. Dev Neurosci. 2009;31(4):293-9.

Keller KA, Barnes P. Rickets vs. Abuse, A National & International Epidemic. Pediatric Radiology 2008 Nov;38:1210-1216.

Kelly ME, Guzman R, Sinclair J, Bell-Stephens TE, Bower R, Hamilton S, Marks MP, Do HM, Chang SD, Adler JR, Levy RP, Steinberg GK. Multimodality treatment of posterior fossa arteriovenous malformations. J Neurosurg. 2008 Jun;108(6):1152-61.

Kim DH, Gu M, Cunningham C, Chen A, Baumer F, Glenn OA, Vigneron DB, Spielman DM, Barkovich AJ. Fast 3D (1)H MRSI of the corticospinal tract in pediatric brain. J Magn Reson Imaging. 2009 Jan;29(1):1-6.

Kim DH, Gu M, Spielman DM. Gradient moment compensated magnetic resonance spectroscopic imaging. Magn Reson Med. 2009 Feb;61(2):457-61.

Kinsey AM, Diederich CJ, Rieke V, Nau WH, Pauly KB, Bouley D, Sommer G. Transurethral ultrasound applicators with dynamic multi-sector control for prostate thermal therapy: in vivo evaluation under MR guidance. Med Phys. 2008 May;35(5):2081-93.

Kobayashi C, Glover GH, Temple E. Switching language switches mind: linguistic effects on developmental neural bases of 'Theory of Mind'. Soc Cogn Affect Neurosci. 2008 Mar;3(1):62-70.

Kothary N, Dieterich S, Louie JD, Chang DT, Hofmann LV, Sze DY. Percutaneous implantation of fiducial markers for imaging-guided radiation therapy. AJR Am J Roentgenol. 2009 Apr;192(4):1090-6.

Kothary N, Dieterich S, Louie JD, Chang DT, Hofmann LV, Sze DY. Techniques for Percutaneous Implantation of Fiducial Markers for Image Guided Radiotherapy. AJR Am J Roentgenol. 2009 Apr;192(4):1090-6.

Kothary N, Dieterich S, Louie JD, Koong AC, Hofmann LV, Sze DY. A primer on image-guided radiation therapy for the interventional radiologist. J Vasc Interv Radiol. 2009 Jul;20(7):859-62.

Kothary N, Heit JJ, Louie JD, Kuo WT, Loo BW Jr, Koong A, Chang DT, Hovsepian D, Sze DY, Hofmann LV. Safety and efficacy of percutaneous fiducial marker implantation for image-guided radiation therapy. J Vasc Interv Radiol. 2009 Feb;20(2):235-9.

Kuo WT, van den Bosch MA, Hofmann LV, Louie JD, Kothary N, Sze DY. Catheter-directed embolectomy, fragmentation, and thrombolysis for the treatment of massive pulmonary embolism after failure of systemic thrombolysis. Chest. 2008 Aug;134(2):250-4.

Kutschka I, Sheikh AY, Sista R, Hendry SL, Chun HJ, Hoyt G, Kutschka W, Pelletier MP, Quertermous T, Wu JC, Robbins RC. A novel platform device for rodent echocardiography. ILAR J 2008;49:E1□7.

Kwong A, Hancock SL, Bloom JR, Pal S, Birdwell RL, Mariscal C, Ikeda DM. Mammographic screening in women at increased risk of breast cancer after treatment of Hodgkin's disease. Breast J. 2008 Jan-Feb;14(1):39-48.

La TH, Filion EJ, Turnbull BB, Chu JN, Lee P, Nguyen K, Maxim P, Quon A, Graves EE, Loo BW Jr, Le QT. Metabolic tumor volume predicts for recurrence and death in head-and-neck cancer. Int J Radiat Oncol Biol Phys. 2009 Aug 1;74(5):1335-41.

Lansberg MG, Thijs VN, Bammer R, Olivot JM, Marks MP, Wechsler LR, Kemp S, Albers GW. The MRA-DWI mismatch identifies patients with stroke who are likely to benefit from reperfusion. Stroke 2008 Sep;39(9):2491-6.

Law CS, Glover GH. Interleaved spiral-in/out with application to functional MRI (fMRI). Magn Reson Med. 2009 May 15.

Law CS, Liu C, Glover GH. Sliding-window sensitivity encoding (SENSE) calibration for reducing noise in functional MRI (fMRI). Magn Reson Med. 2008 Nov;60(5):1090-103.

Le QT, Koong A, Lieskovsky YY, Narasimhan B, Graves E, Pinto H, Brown JM, Spielman D. In vivo 1H magnetic resonance spectroscopy of lactate in patients with stage IV head and neck squamous cell carcinoma. Int J Radiat Oncol Biol Phys. 2008 Jul 15;71(4):1151-7.

Lee JH, Dumoulin SO, Saritas EU, Glover GH, Wandell BA, Nishimura DG, Pauly JM. Full-brain coverage and high-resolution imaging capabilities of passband b-SSFP fMRI at 3T. Magn Reson Med. 2008 May;59(5):1099-110.

Lee SW, Greve JM, Leaffer D, Lollini L, Bailey P, Gold GE, Biswal S. Early findings of small-animal MRI and small-animal computed tomography correlate with histological changes in a rat model of rheumatoid arthritis. NMR Biomed. 2008 Jun;21:527-536.

Lee SW, Padmanabhan P, Ray P, Gambhir SS, Doyle T, Contag C, Goodman SB, Biswal S. Stem cell-mediated accelerated bone healing observed with in vivo molecular and small animal imaging technologies in a model of skeletal injury. J Orthop Res. 2009 Mar;27(3):295-302.

Levashova Z, Backer M, Backer JM, Blankenberg FG. Direct site-specific labeling of the Cys-tag moiety in scVEGF with technetium 99m. Bioconjug Chem. 2008 May;19(5):1049-54.

Levashova Z, Backer MV, Horng G, Felsher D, Backer JM, Blankenberg FG. SPECT and PET imaging of EGF receptors with site-specifically labeled EGF and dimeric EGF. Bioconjug Chem. 2009 Apr;20(4):742-9.

Levita L, Hare TA, Voss HU, Glover G, Ballon DJ, Casey BJ. The bivalent side of the nucleus accumbens. Neuroimage. 2009 Feb 1;44(3):1178-87.

Levy MA, Rubin DL. Tool support to enable evaluation of the clinical response to treatment. AMIA Annu Symp Proc. 2008 Nov 6:399-403.

Li SH, Lai TY, Sun Z, Han M, Moriyama E, Wilson B, Fazel S, Weisel RD, Yau T, Wu JC, Li RK. Tracking cardiac engraftment and distribution of implanted bone marrow cells: Comparing intra-aortic, intravenous, and intramyocardial delivery. J Thorac Cardiovasc Surg. 2009 May;137(5):1225-33.

Li Z, Lee A, Huang M, Chun H, Chung J, Chu P, Hoyt G, Yang P, Rosenberg J, Robbins RC, Wu JC. Imaging survival and function of transplanted cardiac resident stem cells. J Am Coll Cardiol. 2009 Apr 7;53(14):1229-40.

Lindquist MA, Zhang CH, Glover G, Shepp L. The acquisition and statistical analysis of rapid 3D fMRI data. Statistica Sinica 18:1395-1419 (2008).

Liu YI, Kamaya A, Desser TS, Rubin DL. A Bayesian classifier for differentiating benign versus malignant thyroid nodules using sonographic features. AMIA Annu Symp Proc. 2008 Nov;6: 419-23.

Liu YI, Shin LK, Kamaya A, Jeffrey RB. An unusual imaging and clinical presentation of papillary thyroid carcinoma. J Ultrasound Med. 2008 Aug;27(8):1241-4.

Lorberboym M, Feldbrin Z, Hendel D, Blankenberg FG, Schachter P. The use of 99mTc-recombinant human annexin V imaging for differential diagnosis of aseptic loosening and low-grade infection in hip and knee prostheses. J Nucl Med. 2009 Apr;50(4):534-7.

Louie JD, Kothary N, Kuo WT, Hofmann LV, Goris ML, Iagaru A, Sze DY. Treatment Planning for Yttrium Radioembolization Incorporating use of Cone-Beam CT. J Vasc Interv Radiol. 2009 May;20(5):606-13.

Louie JD, Kothary N, Kuo WT, Hwang GL, Hofmann LV, Goris ML, Iagaru A, Sze DY. Incorporating Cone-beam CT into the Treatment Planning for Yttrium-90 Radioembolization. J Vasc Interv Radiol. 2009 May;20(5):606-13.

Lu A, Daniel BL, Pauly JM, Butts Pauly K. Improved slice selection for R2* mapping during cryoablation with eddy current compensation. J Magn Reson Imaging. 2008 Jul;28(1):190-8.

Lu W, Butts Pauly K, Gold GE, Pauly JM, Hargreaves BA. SEMAC: Slice Encoding for Metal Artifact Correction in MRI. Magn Reson Med. 2009 Jul;62(1):66-76.

Lu W, Hargreaves BA. Multiresolution field map estimation using golden section search for water-fat separation. Magn Reson Med. 2008 Jul;60(1):236-44.

Lu W, Yu H, Shimakawa A, Alley M, Reeder SB, Hargreaves BA. Water-fat separation with bipolar multiecho sequences. Magn Reson Med. 2008 Jul;60(1):198-209.

Lutz AM, Willmann JK, Cochran FV, Ray P, Gambhir SS. Cancer screening: a mathematical model relating secreted blood biomarker levels to tumor sizes. PLoS Med. 2008 Aug 19;5(8):e170.

Marks MP, Olivot JM, Kemp S, Lansberg MG, Bammer R, Wechsler LR, Albers GW, Thijs V. Patients with acute stroke treated with intravenous tPA 3-6 hours after stroke onset: correlations between MR angiography findings and perfusion- and diffusion-weighted imaging in the DEFUSE study. Radiology 2008 Nov;249(2):614-23.

Mayer D, Kim DH, Spielman DM, Bammer R. Fast parallel spiral chemical shift imaging at 3T using iterative SENSE reconstruction. Magn Reson Med. 2008 Apr;59(4):891-7.

Mazin SR, Pelc NJ. A Fourier Rebinning Algorithm for Cone Beam CT. Med Phys. 2008 35:4857-62.

McAdams TR, Biswal S, Stevens KJ, Beaulieu CF, Mandelbaum BR. Tibial aperture bone disruption after retrograde versus antegrade tibial tunnel drilling: a cadaveric study. Knee Surg Sports Traumatol Arthrosc. 2008 Sep;16(9):818-22.

Melvin JS, Mackenzie JD, Nacke E, Sennett BJ, Wells L. MRI of HAGL lesions: four arthroscopically confirmed cases of false-positive diagnosis.AJR Am J Roentgenol. 2008 Sep;191(3):730-4.

Mittra E, Quon A. Positron emission tomography/computed tomography: the current technology and applications. Radiol Clin North Am. 2009 Jan;47(1):147-60.

Mlynash M, Olivot JM, Tong DC, Lansberg MG, Eyngorn I, Kemp S, Moseley ME, Albers GW. Yield of combined perfusion and diffusion MR imaging in hemispheric TIA. Neurology 2009 Mar 31;72(13):1127-33.

Mogensen M, Lin A, Chang K, Berry G, Barnes P, Fischbein N. Salivary gland anlage tumor in a neonate presenting with respiratory distress radiographic and pathologic correlation. AJNR Am J Neuroradiol. 2009 May;30(5):1022-3.

Mogensen M, Lin AC, Chang KW, Berry GJ, Barnes PD, Fischbein NJ. Salivary Gland Anlage Tumor in a Neonate Presenting with Respiratory Distress: Radiographic and Pathologic Correlation. AJNR Am J Neuroradiol. 2008 Dec;26. [Epub ahead of print]

Moseley ME. Molecular imaging and stroke. Stroke 2009 Mar;40(3 Suppl):S30-3.

Moseley ME, Liu C, Rodriguez S, Brosnan T. Advances in magnetic resonance neuroimaging. Neurol Clin. 2009 Feb;27(1):1-19.

Müller MA, Mayer D, Seifert B, Marincek B, Willmann JK. Recurrent lower-limb varicose veins: effect of direct contrast-enhanced three-dimensional MR venographic findings on diagnostic thinking and therapeutic decisions. Radiology. 2008 Jun;247(3):887-95.

Nahrendorf M, Sosnovik DE, French BA, Swirski FK, Bengel F, Sadeghi MM, Lindner JR, Wu JC, Kraitchman DL, Fayad ZA, Sinusas AJ. Multimodality cardiovascular molecular imaging, Part II. Circulation: Cardiovascular Imaging 2009;2:56–70.2009;2:56–70.

Newman B, Grosse-Wortmann L, Charron M, Yoo SJ. A pitfall of radioisotope quantification of the ratio of pulmonary blood flow to systemic blood flow (Qp/Qs) in a patient with severe postoperative pulmonary venous obstruction. Clin Nucl Med. 2008 Aug;33(8):521-4.

Nguyen JT, Peterson JS, Biswal S, Beaulieu CF, Fredericson M. Stress-related injuries around the lesser trochanter in long-distance runners.

Noël P, Bammer R, Reinhold C, Haider MA. Parallel imaging artifacts in body magnetic resonance imaging. Can Assoc Radiol J. 2009 Apr;60(2):91-8.

Ochsner KN, Zaki J, Hanelin J, Ludlow DH, Knierim K, Ramachandran T, Glover GH, Mackey SC. — Your pain or mine? Common and distinct neural systems supporting the perception of pain in self and other. Soc Cogn Affect Neurosci. 2008 Jun;3(2):144-60.

Olcott PD, Peng H, Levin CS. — Novel electro-optical coupling technique for magnetic resonance-compatible positron emission tomography detectors. Mol Imaging. 2009 Mar-Apr;8(2):74-86.

Olivot JM, Mlynash M, Thijs VN, Kemp S, Lansberg MG, Wechsler L, Schlaug G, Bammer R, Marks MP, Albers GW. — Relationships between infarct growth, clinical outcome, and early recanalization in diffusion and perfusion imaging for understanding stroke evolution (DEFUSE). Stroke 2008 Aug;39(8):2257-63.

Olivot JM, Mlynash M, Thijs VN, Purushotham A, Kemp S, Lansberg MG, Wechsler L, Bammer R, Marks MP, Albers GW. — Relationships between cerebral perfusion and reversibility of acute diffusion lesions in DEFUSE: insights from RADAR. Stroke 2009 May;40(5):1692-7.

Olivot JM, Mlynash M, Zaharchuk G, Straka M, Bammer R, Schwartz N, Lansberg MG, Moseley ME, Albers GW. — Perfusion MRI (Tmax and MTT) correlation with xenon CT cerebral blood flow in stroke patients. Neurology 2009 Mar 31;72(13):1140-5.

Pear J, Wu JC. — Pear J, Wu JC. Seeing is believing: tracking cells to determine the effects of cell transplantation. Seminar Cardiothoracic Surgery. 20008;20(2):102–9.

Potkin SG, Turner JA, Brown GG, McCarthy G, Greve DN, Glover GH, Manoach DS, Belger A, Diaz M, Wible CG, Ford JM, Mathalon DH, Gollub R, Lauriello J, O'Leary D, van Erp TG, Toga AW, Preda A, Lim KO; FBIRN. — Working memory and DLPFC inefficiency in schizophrenia: the FBIRN study. Schizophr Bull. 2009 Jan;35(1):19-31.

Pratx G, Chinn G, Olcott PD, Levin CS. — Fast, accurate and shift-varying line projections for iterative reconstruction using the GPU. IEEE Trans Med Imaging. 2009 Mar;28(3):435-45.

Preston AR, Bornstein AM, Hutchinson JB, Gaare ME, Glover GH, Wagner AD. — High-resolution fMRI of Content-sensitive Subsequent Memory Responses in Human Medial Temporal Lobe. J Cogn Neurosci. 2009 Jan 13.

Pu J, Roos J, Yi CA, Napel S, Rubin GD, Paik DS. — Adaptive border marching algorithm: automatic lung segmentation on chest CT images. Comput Med Imaging Graph. 2008 Sep;32(6):452-62.

Qiu P, Gentles AJ, Plevritis SK. — Fast calculation of pairwise mutual information for gene regulatory network reconstruction. Comput Methods Programs Biomed. 2009 May;94(2):177-80.

Qiu P, Plevritis SK. — Simultaneous class discovery and classification of microarray data using spectral analysis. J Comput Biol. 2009 Jul;16(7):935-44.

Rakow-Penner R, Gold G, Daniel B, Stevens K, Rosenberg J, Mazin S, Pauly J, Glover GH. — Reduction of truncation artifacts in rapid 3D articular cartilage imaging. J Magn Reson Imaging 2008 Apr;27:860-865.

Rakow-Penner R, Hargreaves B, Glover GH, Daniel BL. — Breast MRI at 3T. Applied Radiology 2009;38(3):

Rakshe T, Fleischmann D, Rosenberg J, Roos JE, Straka M, Napel S. — An improved algorithm for femoropopliteal artery centerline restoration using prior knowledge of shapes and image space data. Med Phys. 2008 Jul;35(7):3372-82.

Raman R, Raman B, Napel S, Rubin GD. — Semiautomated quantification of the mass and distribution of vascular calcification with multidetector CT: method and evaluation. Radiology. 2008 Apr;247(1):241-50.

Raman R, Raman B, Napel S, Rubin GD. — Improved speed of bone removal in computed tomographic angiography using automated targeted morphological separation: method and evaluation in computed tomographic angiography of lower extremity occlusive disease. J Comput Assist Tomogr. 2008 May-Jun;32(3):485-91.

Rao J. — Shedding light on tumors using nanoparticles. ACS Nano. 2008 Oct 28;2(10):1984-6.

Ren PG, Lee SW, Biswal S, Goodman SB. — Systemic trafficking of macrophages induced by bone cement particles in nude mice. Biomaterials. 2008 Dec;29(36):4760-5.

Rodriguez-Porcel M, Brinton TJ, Chen IY, Gheysens O, Lyons J, Ikeno F, Willmann JK, Wu L, Wu JC, Yeung AC, Yock P, Gambhir SS. — Reporter gene imaging following percutaneous delivery in swine moving toward clinical applications. J Am Coll Cardiol. 2008 Feb 5;51(5):595-7.

Rodriguez-Porcel M, Cai W, Gheysens O, Willmann JK, Chen K, Wang H, Chen IY, He L, Wu JC, Li ZB, Mohamedali KA, Kim S, Rosenblum MG, Chen X, Gambhir SS. — Imaging of VEGF receptor in a rat myocardial infarction model using PET. J Nucl Med. 2008 Apr;49(4):667-73.

Roos JE, Rakshe T, Tran DN, Rosenberg J, Straka M, El-Helw T, Sofilos MC, Napel S, Fleischmann D. — Lower extremity CT angiography (CTA): initial evaluation of a knowledge-based centerline estimation algorithm for femoro-popliteal artery (FPA) occlusions. Acad Radiol. 2009 Jun;16(6):646-53.

Rose J, Butler EE, Lamont LE, Barnes PD, Atlas SW, Stevenson DK. — Neonatal brain structure on MRI and diffusion tensor imaging, sex, and neurodevelopment in very-low-birthweight preterm children. Dev Med Child Neurol. 2009 Jul;51(7):526-35.

Rubin DL, Rodriguez C, Shah P, Beaulieu C. — iPad: Semantic Annotation and Markup of Radiological Images. AMIA Annu Symp Proc. 2008 Nov 6:626-30.

Sahoo D, Dill DL, Gentles AJ, Tibshirani R, Plevritis SK. — Boolean implication networks derived from large scale, whole genome microarray datasets. Genome Biol. 2008 Oct 30;9(10):R157.

Schipper ML, Iyer G, Koh AL, Cheng Z, Ebenstein Y, Aharoni A, Keren S, Bentolila LA, Li J, Rao J, Chen X, Banin U, Wu AM, Sinclair R, Weiss S, Gambhir SS. — Particle size, surface coating, and PEGylation influence the biodistribution of quantum dots in living mice. Small. 2009 Jan;5(1):126-34.

Schmitzberger FF, Roos J, Napel S, Rubin G, Paik DS. — Thin Client Architecture in Support of Remote Radiology Learning. Proceedings of the 24th Annual ACM Symposium on Applied Computing, 842-46, 2009.

Shachaf CM, Gentles AJ, Elchuri S, Sahoo D, Soen Y, Sharpe O, Perez OD, Chang M, Mitchel D, Robinson WH, Dill D, Nolan GP, Plevritis SK, Felsher DW. — Genomic and proteomic analysis reveals a threshold level of MYC required for tumor maintenance. Cancer Res. 2008 Jul 1;68(13):5132-42.

Shahbaba B, Gentles A, Beyene J, Plevritis SK, Greenwood CMT. — A Bayesian nonparametric method for model evaluation: Application to gene-disease studies. Journal of Nonparametric Statistics 2009 21(3):379-396.

Sherbondy AJ, Dougherty RF, Ben-Shachar M, Napel S, Wandell BA. — ConTrack: finding the most likely pathways between brain regions using diffusion tractography. J Vis. 2008 Jul 29;8(9):15.1-16.

Sherbondy AJ, Dougherty RF, Napel S, Wandell BA. — Identifying the human optic radiation using diffusion imaging and fiber tractography. J Vis. 2008 Dec 17;8(10):12.1-11.

Shin LK, Brant-Zawadzki G, Kamaya A, Jeffrey RB. — Intraoperative ultrasound of the pancreas. Ultrasound Quarterly 2009 Mar;25(1):39-48.

Singer OC, Berkefeld J, Lorenz MW, Fiehler J, Albers GW, Lansberg MG, Kastrup A, Rovira A, Liebeskind DS, Gass A, Rosso C, Derex L, Kim JS, Neumann-Haefelin T — Risk of symptomatic intracerebral hemorrhage in patients treated with intra-arterial thrombolysis. Cerebrovasc Dis. 2009;27(4):368-74.

Sinusas AJ, Bengel F, Nahrendorf M, Epstein FH, Wu JC, Villanueva FS, Fayad ZA, Gropler RJ. — Multimodality cardiovascular molecular imaging, Part I. Circulation: Cardiovascular Imaging 2008;1:244□256.

Siston RA, Cromie MJ, Gold GE, Goodman SB, Delp SL, Maloney WJ, Giori NJ. Averaging different alignment axes improves femoral rotational alignment in computer-navigated total knee arthroplasty. J Bone Joint Surg Am. 2008 Oct;90(10):2098-104.

Skare S, Newbould RD, Nordell A, Holdsworth SJ, Bammer R. An auto-calibrated, angularly continuous, two-dimensional GRAPPA kernel for propeller trajectories. Magn Reson Med. 2008 Dec;60(6):1457-65.

Smith CA, Stebbins GT, Bartt RE, Kessler HA, Adeyemi OM, Martin E, Bammer R, Moseley ME. White matter anisotropy and depression symptoms in patients with HIV. J Neuropsychiatry Clin Neurosci. 2008 Fall;20(4):458-65.

Spielman DM, Mayer D, Yen YF, Tropp J, Hurd RE, Pfefferbaum A. In vivo measurement of ethanol metabolism in the rat liver using magnetic resonance spectroscopy of hyperpolarized [1-(13)C]pyruvate. Magn Reson Med. 2009 Jun 12.

Stebbins GT, Nyenhuis DL, Wang C, Cox JL, Freels S, Bangen K, deToledo-Morrell L, Sripathirathan K, Moseley M, Turner DA, Gabrieli JD, Gorelick PB. Gray matter atrophy in patients with ischemic stroke with cognitive impairment. Stroke. 2008 Mar;39(3):785-93.

Stevens KJ, Busse RF, Han E, Brau AC, Beatty PJ, Beaulieu CF, Gold GE. Ankle: isotropic MR imaging with 3D-FSE-cube--initial experience in healthy volunteers. Radiology 2008 Dec;249(3):1026-33.

Stillman AE, Rubin GD, Teague SD, White RD, Woodard PK, Larson PA. Structured reporting: coronary CT angiography: a white paper from the American College of Radiology and the North American Society for Cardiovascular Imaging. J Am Coll Radiol. 2008 Jul;5(7):796-800.

Sundaram P, Zomorodian A, Beaulieu C, Napel S. Colon polyp detection using smoothed shape operators: preliminary results. Med Image Anal. 2008 Apr;12(2):99-119.

Sutter R, Heilmaier C, Lutz AM, Weishaupt D, Seifert B, Willmann JK. MR angiography with parallel acquisition for assessment of the visceral arteries: comparison with conventional MR angiography and 64-detector-row computed tomography. Eur Radiol. 2009 Jun 13.

Swijnenburg RJ, Schrepfer S, Cao F, Pearl JI, Xie X, Connolly AJ, Robbins RC, Wu JC. In vivo imaging of embryonic stem cells reveals patterns of survival and immune rejection following transplantation. Stem Cells Dev. 2008 Dec;17(6):1023-9.

Swijnenburg RJ, Schrepfer S, Govaert JA, Cao F, Ransohoff K, Sheikh AY, Haddad M, Connolly AJ, Davis MM, Robbins RC, Wu JC. Immunosuppressive therapy mitigates immunological rejection of human embryonic stem cell xenografts. Proc Natl Acad Sci U S A. 2008 Sep 2;105(35):12991-6.

Sze DY, Lee DP, Hofmann LV, Petersen B. Biopsy of cardiac masses using a stabilized intracardiac echocardiography-guided system. J Vasc Interv Radiol. 2008 Nov;19(11):1662-7.

Sze DY, van den Bosch MAAJ, Dake MD, Miller DC, Hofmann LV, Varghese R, Malaisrie SC, van der Starre PJA, Rosenberg J, Mitchell RS. Factors portending endoleak formation after thoracic aortic stent-graft repair of aortic dissection. Circ Cardiovasc Intervent. 2009 (2):105-112.

Tedesco MM, Terashima M, Blankenberg FG, Levashova Z, Spin JM, Backer MV, Backer JM, Sho M, Sho E, McConnell MV, Dalman RL. Analysis of In Situ and Ex Vivo Vascular Endothelial Growth Factor Receptor Expression During Experimental Aortic Aneurysm Progression. Arterioscler Thromb Vasc Biol. 2009 Jul 2.

Thomason ME, Chang CE, Glover GH, Gabrieli JD, Greicius MD, Gotlib IH. Default-mode function and task-induced deactivation have overlapping brain substrates in children. Neuroimage. 2008 Jul 15;41(4):1493-503.

Thomason ME, Race E, Burrows B, Whitfield-Gabrieli S, Glover GH, Gabrieli JD. Development of spatial and verbal working memory capacity in the human brain. J Cogn Neurosci. 2009 Feb;21(2):316-32.

Thomason ME, Waugh CE, Glover GH, Gotlib IH. COMT genotype and resting brain perfusion in children. Neuroimage. 2009 Oct 15;48(1):217-22.

Thorne SH, Barak Y, Liang W, Bachmann MH, Rao J, Contag CH, Matin A. CNOB/ChrR6, a new prodrug enzyme cancer chemotherapy. Mol Cancer Ther. 2009 Feb;8(2):333-41.

Tran DN, Straka M, Roos JE, Napel S, Fleischmann D. Dual-energy CT discrimination of iodine and calcium: experimental results and implications for lower extremity CT angiography. Acad Radiol. 2009 Feb;16(2):160-71.

Troy SB, Blackburn BG, Yeom K, Caulfield AK, Bhangoo MS, Montoya JG. Severe encephalomyelitis in an immunocompetent adult with chromosomally integrated human herpesvirus 6 and clinical response to treatment with foscarnet plus ganciclovir. Clin Infect Dis. 2008 Dec 15;47(12):e93-6.

Turken A, Whitfield-Gabrieli S, Bammer R, Baldo JV, Dronkers NF, Gabrieli JD. Cognitive processing speed and the structure of white matter pathways: convergent evidence from normal variation and lesion studies. Neuroimage 2008 Aug 15;42(2):1032-44.

van den Bosch MA, Josan S, Bouley DM, Chen J, Gill H, Rieke V, Butt -Pauly K, Daniel BL. MR imaging-guided percutaneous cryoablation of the prostate in an animal model: in vivo imaging of cryoablation-induced tissue necrosis with immediate histopathologic correlation. J Vasc Interv Radiol. 2009 Feb;20(2):252-8.

van der Bogt KE, Schrepfer S, Yu J, Sheikh AY, Hoyt G, Govaert JA, Velotta JB, Contag CH, Robbins RC, Wu JC. Comparison of transplantation of adipose tissue- and bone marrow-derived mesenchymal stem cells in the infarcted heart. Transplantation 2009 Mar 15;87(5):642-52.

van der Bogt KE, Sheikh AY, Schrepfer S, Hoyt G, Cao F, Ransohoff KJ, Swijnenburg RJ, Pearl J, Lee A, Fischbein M, Contag CH, Robbins RC, Wu JC. Comparison of different adult stem cell types for treatment of myocardial ischemia. Circulation 2008 Sep 30;118(14 Suppl):S121-9.

Vandevenne JE, Vanhoenacker F, Beaulieu CF, Bergman AG, Butts Pauly K, Dillingham MF, Lang PK. All-in-one magnetic resonance arthrography of the shoulder in a vertically open magnetic resonance unit. Acta Radiol. 2008 Oct;49(8):918-27.

Vasanawala SS, Kennedy WA, Ganguly A, Fahrig R, Rieke V, Daniel B, Barth RA. MR voiding cystography for evaluation of vesicoureteral reflux. AJR Am J Roentgenol. 2009 May;192(5):W206-11.

Vertinsky AT, Schwartz NE, Fischbein NJ, Rosenberg J, Albers GW, Zaharchuk G. Comparison of multidetector CT angiography and MR imaging of cervical artery dissection. AJNR Am J Neuroradiol. 2008 Oct;29(9):1753-60.

Wang Y, Ikeda DM, Narasimhan B, Longacre TA, Bleicher RJ, Pal S, Jackman RJ, Jeffrey SS. Estrogen receptor-negative invasive breast cancer: imaging features of tumors with and without human epidermal growth factor receptor type 2 overexpression. Radiology. 2008 Feb;246(2):367-75.

Wang ZJ, Joe BN, Coakley FV, Zaharchuk G, Busse R, Yeh BM. Urinary oxygen tension measurement in humans using magnetic resonance imaging. Acad Radiol. 2008 Nov;15(11):1467-73.

Wen Z, Fahrig R, Williams ST, Pelc NJ. Shimming with permanent magnets for the x-ray detector in a hybrid x-ray/ MR system. Med Phys. 2008 Sep;35(9):3895-902.

Wen Z, Reeder SB, Pineda AR, Pelc NJ. Noise considerations of three-point water-fat separation imaging methods. Med Phys. 2008 Aug;35(8):3597-606.

Wijman CAC, Mlynash M, Finley Caulfield A, Hsia AW, Eyngorn I, Bammer R, Fischbein N, Albers GW, Moseley M. Prognostic Value of Brain Diffusion Weighted Imaging After Cardiac Arrest. Ann Neurol. 2009 Apr;65(4):394-402.

Willmann JK, Chen K, Wang H, Paulmurugan R, Rollins M, Cai W, Wang DS, Chen IY, Gheysens O, Rodriguez-Porcel M, Chen X, Gambhir SS. Monitoring of the biological response to murine hindlimb ischemia with 64Cu-labeled vascular endothelial growth factor-121 positron emission tomography. Circulation. 2008 Feb 19;117(7):915-22.

Willmann JK, Cheng Z, Davis C, Lutz AM, Schipper ML, Nielsen CH, Gambhir SS. Targeted microbubbles for imaging tumor angiogenesis: assessment of whole-body biodistribution with dynamic micro-PET in mice. Radiology. 2008 Oct;249(1):212-9.

Willmann JK, Lutz AM, Paulmurugan R, Patel MR, Chu P, Rosenberg J, Gambhir SS. Dual-targeted contrast agent for US assessment of tumor angiogenesis in vivo. Radiology. 2008 Sep;248(3):936-44.

Willmann JK, Paulmurugan R, Chen K, Gheysens O, Rodriguez-Porcel M, Lutz AM, Chen IY, Chen X, Gambhir SS. US imaging of tumor angiogenesis with microbubbles targeted to vascular endothelial growth factor receptor type 2 in mice. Radiology 2008 Feb;246(2):508-18.

Willmann JK, Paulmurugan R, Rodriguez-Porcel M, Stein W, Brinton TJ, Connolly AJ, Nielsen CH, Lutz AM, Lyons J, Ikeno F, Suzuki Y, Rosenberg J, Chen IY, Wu JC, Yeung AC, Yock P, Robbins RC, Gambhir SS. Imaging gene expression in human mesenchymal stem cells: from small to large animals. Radiology 2009 Jul;252(1):117-27.

Wilson KD, Li Z, Wagner R, Yue P, Tsao P, Nestorova G, Huang M, Hirschberg DL, Yock PG, Quertermous T, Wu JC. Transcriptome alteration in the diabetic heart by rosiglitazone: implications for cardiovascular mortality. PLoS One. 2008 Jul 9;3(7):e2609.

Wilson KD, Venkatasubrahmanyam S, Jia F, Sun N, Butte AJ, Wu JC. MicroRNA profiling of human-induced pluripotent stem cells. Stem Cells Dev. 2009 Jun;18(5):749-58.

Wilson K, Yu J, Lee A, Wu JC. In vitro and in vivo bioluminescence reporter gene imaging of human embryonic stem cells. Journal Vizualized Experiments 2008 May 2;(14). pii: 740.

Wintermark M, Albers GW, Alexandrov AV, Alger JR, Bammer R, Baron JC, Davis S, Demaerschalk BM, Derdeyn CP, Donnan GA, Eastwood JD, Fiebach JB, Fisher M, Furie KL, Goldmakher GV, Hacke W, Kidwell CS, Kloska SP, Köhrmann M, Koroshetz W, Lee TY, Lees KR, Lev MH, Liebeskind DS, Ostergaard L, Powers WJ, Provenzale J, Schellinger P, Silbergleit R, Sorensen AG, Wardlaw J, Wu O, Warach S. Acute stroke imaging research roadmap. Stroke 2008 May;39(5):1621-8.

Wong SH, Kupnik M, Zhuang X, Lin DS, Butts Pauly K, Khuri-Yakub BT. Evaluation of wafer bonded CMUTs with rectangular membranes featuring high fill factor. IEEE Trans Ultrason Ferroelectr Freq Control. 2008 Sep;55(9):2053-65.

Wong SH, Watkins RD, Kupnik M, Pauly KB, Khuri-Yakub BT. Feasibility of MR-temperature mapping of ultrasonic heating from a CMUT. IEEE Trans Ultrason Ferroelectr Freq Control. 2008 Apr;55(4):811-8.

Wu JC. Can radionuclide imaging predict future response to stem cell therapy? J Nucl Cardiol. 2008 May-Jun;15(3):308-10.

Wu JC. Molecular imaging: antidote to cardiac stem cell controversy. J Am Coll Cardiol. 2008 Nov 11;52(20):1652-60.

Xia Z, Rao J. Biosensing and imaging based on bioluminescence resonance energy transfer. Curr Opin Biotechnol. 2009 Feb;20(1):37-44.

Xia Z, Xing Y, So MK, Koh AL, Sinclair R, Rao J. Multiplex detection of protease activity with quantum dot nanosensors prepared by intein-mediated specific bioconjugation. Anal Chem. 2008 Nov 15;80(22):8649-55.

Xie X, Chan KS, Cao F, Huang M, Li Z, Lee A, Weissman IL, Wu JC. Imaging of STAT3 signaling pathway during mouse embryonic stem cell differentiation. Stem Cells Dev. 2009 Mar;18(2):205-14.

Xing Y, Rao J. Quantum dot bioconjugates for in vitro diagnostics & in vivo imaging. Cancer Biomark. 2008;4(6):307-19.

Xing Y, Xia Z, Rao J. Semiconductor quantum dots for biosensing and in vivo imaging. IEEE Trans Nanobioscience. 2009 Mar;8(1):4-12.

Yaghoubi SS, Jensen MC, Satyamurthy N, Budhiraja S, Paik DS, Czernin J, Gambhir SS Noninvasive Detection of Therapeutic Cytolytic T Cells with 18F-FHBG PET in a Patient with Glioma. Nature Clinical Practice Oncology 2009; 6(1):53-8.

Yeatman JD, Ben-Shachar M, Bammer R, Feldman HM. Using Diffusion Tensor Imaging and Fiber Tracking to Characterize Diffuse Perinatal White Matter Injury: A Case Report. J Child Neurol. 2009 May 11.

Yerushalmi D, Mullick R, Quon A, Fahrig R, Pelc NJ, Fann JI, Gambhir SS. Simulations of virtual PET/CT 3-D bronchoscopy imaging using a physical porcine lung-heart phantom. Mol Imaging Biol. 2009 Jul-Aug;11(4):275-82.

Yoon S, Henry RW, Bouley DM, Bennett NR, Fahrig R. Characterization of a novel anthropomorphic plastinated lung phantom. Med Phys. 2008 Dec;35(12):5934-43.

Zaharchuk G, Martin AJ, Dillon WP. Noninvasive imaging of quantitative cerebral blood flow changes during 100% oxygen inhalation using arterial spin-labeling MR imaging. AJNR Am J Neuroradiol. 2008 Apr;29(4):663-7.

Zhao SH, Logan L, Schraedley P, Rubin GD. Assessment of the anterior spinal artery and the artery of Adamkiewicz using multi-detector CT angiography. Chin Med J (Engl). 2009 Jan 20;122(2):145-9.

Zhao Y, Kuge Y, Zhao S, Strauss HW, Blankenberg FG, Tamaki N. Prolonged high-fat feeding enhances aortic 18F-FDG and 99mTc-annexin A5 uptake in apolipoprotein E-deficient and wild-type C57BL/6J mice. J Nucl Med. 2008 Oct;49(10):1707-14.

Zhu L, Starman J, Fahrig R. An Efficient Estimation Method for Reducing the Axial Intensity Drop in Circular Cone-Beam CT. Int J Biomed Imaging 2008;2008(1):242841.

Zilber S, Lee SW, Smith RL, Biswal S, Goodman SB. Analysis of bone mineral density and bone turnover in the presence of polymethylmethacrylate particles. J Biomed Mater Res B Appl Biomater. 2009 Jul;90(1):362-7.

Books and Book Chapters

Atlas SW, ed. Magnetic Resonance Imaging of the Brain and Spine, 3rd edition; Mandarin Chinese, Spanish, Portuguese. Philadelphia-New York, Lippincott Williams & Wilkins, 2009.

Atlas SW, ed. Magnetic Resonance Imaging of the Brain and Spine, 4th edition. Philadelphia-New York, Lippincott Williams & Wilkins, 2009.

Atlas SW, Do H. Intracranial hemorrhage. In: Atlas SW, ed. Magnetic Resonance Imaging of the Brain and Spine, 4th edition. Philadelphia-New York, Lippincott Williams & Wilkins, 2009.

Atlas SW, Thulborn K. Intracranial vascular malformations and aneurysms. In: Atlas SW, ed. Magnetic Resonance Imaging of the Brain and Spine, 4th edition. Philadelphia-New York, Lippincott Williams & Wilkins, 2009.

Blickman J, Parker B, Barnes P. Pediatric Radiology: The Requisites, 3rd ed. Elsevier: Philadelphia, PA, 2009.

Bammer R, Holdsworth S, Aksoy M, Skare S. Phase error and correction in diffusion MRI. In: Jones D, ed. Diffusion MRI. New York, NY. Oxford University Press (in press).

Barnes P. Neuroimaging in the evaluation of pattern and timing of fetal and neonatal brain abnormalities. In: Stevenson D, Benitz W, Sunshine P, eds. Fetal and Neonatal Brain Injury, 4rd edition, June 2009. New York, NY, Cambridge University Press.

Barnes P. Pediatric brain imaging. In: Blickman J, Parker B, Barnes P. Pediatric Radiology: The Requisites, 3rd ed. Philadelphia PA, Elsevier, July 2009.

Barnes P. Pediatric spine imaging. In: Blickman J, Parker B, Barnes P. Pediatric Radiology: The Requisites, 3rd ed. Philadelphia PA, Elsevier, July 2009.

Barnes P. Pediatric head and neck imaging. In Blickman J, Parker B, Barnes P. Pediatric Radiology: The Requisites, 3rd ed. Philadelphia PA, Elsevier, July 2009.

Books & Book Chapters

Fischbein NJ.	Bilateral basal ganglia. Bilateral thalamus. Midbrain. Pons. Medulla. Multiple foci of GRE/SWI hypointensity. Multiple foci of T2 hypointensity. In: Osborn A, ed. Expert ddx: Brain and Spine. Amirsys Publications: Salt Lake City, UT, 2009.
Fischbein NJ, Lee N.	Radiology of head and neck cancer. In: Leibel S, Phillips T, eds. Textbook of Radiation Oncology, 2nd edition. Philadelphia, PA. Elsevier, 2009.
Gold G.	Technical considerations for clinical MRI of arthritis. In: Gold G, Bruno M, Mosher T. Arthritis in Color. Philadelphia, PA. Elsevier, 2009.
Gold G.	New techniques for imaging OA. In: Gold G, Bruno M, Mosher T. Arthritis in Color. Philadelphia, PA. Elsevier, 2009.
Gold G.	Magnetic resonance imaging. In: Hochberg M et al. Rheumatology. Philadelphia, PA. Elsevier 2010 (submitted).
Hwang G.	Needles, Guidewires, Catheters, and Stents. In: Kandarpa K, Aruny J, eds. Handbook of Interventional Radiologic Procedures. Philadelphia, PA. Lippincott Williams and Wilkins, 2002.
Iagaru A, McDougall IR.	Thyroid imaging: nuclear medicine techniques. In: Wass J, Shalet S, eds. Oxford Textbook of Endocrinology and Diabetes, 2nd Edition. Oxford University Press, Oxford, United Kingdom (in press).
Jack C, Lexa F, Trojanowski J, Braffman B, Atlas SW.	Normal aging, dementia, and neurodegenerative disease. In: Atlas SW, ed. Magnetic Resonance Imaging of the Brain and Spine, 4th edition. Philadelphia-New York, Lippincott Williams & Wilkins, 2009.
Joseph Ph, Atlas SW.	Artifacts. In: Atlas SW, ed. Magnetic Resonance Imaging of the Brain and Spine, 4th edition. Philadelphia-New York, Lippincott Williams & Wilkins, 2009.
Levin C.	Imaging system physics, technology, and methods for visualization and quantification of reporter gene expression in living subjects. In: Gambhir SS, Yaghoubi S, eds. Reporter Gene Imaging. New York, NY. Cambridge University Press (in press).
Skare ST, Bammer R.	EPI-based pulse sequences for diffusion tensor MRI. In: Jones D, ed. Diffusion MRI. New York, NY. Oxford University Press (in press).
Levin C.	Instrumentation and methods to combine small animal PET with other imaging modalities. In: Weissleder R. Molecular Imaging: Principles and Practice. Hamilton, Ontario, Canada. BC Decker Inc.
Torshizy H, Gold G, Chung C.	MR imaging of articular cartilage. In: Pedowitz R, Resnick D, Chung C, eds. Magnetic Resonance Imaging in Orthopedic Sports Medicine. New York, NY. Springer-Verlag, 2008.
Van Tassel P, Mafee M, Atlas SW, Galetta S.	The orbit and visual system. In: Atlas SW, ed. Magnetic Resonance Imaging of the Brain and Spine, 4th edition. Philadelphia-New York, Lippincott Williams & Wilkins, 2009.
Wu JC, Narula J.	Cardiovascular molecular imaging: current progress and future prospects. In: Iskandrian AE, Garcia EV, eds. Nuclear Cardiac Imaging, 4th ed. New York, NY. Oxford University Press.

Papers Submitted or In Press

Aggarwal A, Olsen D, Napel S, Rubin G, Paik D.	Lung nodule CAD false positive reduction using a novel non-parametric shape analysis approach in chest CT. Medical Physics (submitted).
Ahn K, Alley MT, Hargreaves BA, Daniel BL, Horst K, Luxton G, Hristov D.	MRI guidance for accelerated partial breast irradiation in prone position: imaging protocol design and evaluation. Int. Journal of Radiation Oncology, Biology, Physics 2009 (in press).

Papers Submitted or In Press

Baker L, Afendulis C, Atlas S.	The relationship between the use of CT angiography and catheter angiography in the U.S. medicare population, 2001-2005. Stroke (submitted).
Balchandani P, Pauly J, Spielman DM.	Method to design adiabatic RF pulses using the Shinnar Le-Roux algorithm. Magnetic Resonance in Medicine (submitted).
Benoit MR, Mayer D, Barak Y, Chen IY, Hu W, Cheng Z, Wang SX, Spielman DM, Gambhir SS, Matin A.	Visualizing magnetotactic bacteria after colonization of mouse tumors with MRI. Clinical Cancer Research (in press).
Besier TF, Fredericson M, Gold GE, Beaupre GS, Delp SL.	Knee muscle forces during walking and running in patellofemoral pain patients and pain-free controls. J Biomechanics 2009 (in press).
Brittain JH, Shimakawa A, Yu H, Hargreaves BA, Dharmakumar R, Hu B, Wright GA, Reeder SB.	Non-contrast enhanced peripheral angiography using balanced steady-state free precession. Journal of Magnetic Resonance Imaging (submitted).
Chen C, Lu W, Hargreaves B, Johns C, Delp S, Siston R, Gold G.	Multi-echo IDEAL-GRE water-fat separation for rapid assessment of cartilage morphology—initial experience in healthy volunteers. Radiology (in press).
Chen J, Butts Pauly K.	Optimization of encoding gradients for MR-ARFI. Magnetic Resonance in Medicine (in press).
Chinn G, Levin C	A novel method to use multiple-interaction information in 3-D photon positioning detectors to reject random coincidences and retain multiple coincidences for PET. Conference Record of the 2008 IEEE Nuclear Science Symposium and Medical Imaging Conference (submitted).
Cukur T, Shimakawa A, Yu H, Hargreaves BA, Hu BS, Nishimura DG, Brittain JH.	Magnetization-prepared IDEAL bSSFP: A flow-independent technique for noncontrast-enhanced peripheral angiography. Magn Reson Med. (submitted).
Desser T, Ahlqvist J, Johansson M, Cheng R, Youngblood P, Grahn A, Gold G.	Technical development of a simulator for gastrointestinal radiography. AJR (submitted).
Desser TS, Edwards BR, Hunt S, Rosenberg J, Purtill M, Jeffrey RB.	The dangling diaphragm sign: sensitivity and comparison with existing CT signs of blunt traumatic diaphragmatic rupture. Radiology (submitted).
Desser TS, Ahlqvist J; Johansson M; Cheng R; Youngblood, P; Gold GE.	Virtual reality simulators for radiography training: development and assessment. AJR (submitted).
Draper C, Besier, T, Santos J, Jennings F, Fredericson M, Gold G, Beaupre G, Delp S.	Using real-time MRI to quantify altered joint kinematics in subjects with patellofemoral pain and to evaluate the effects of a patellar brace or sleeve on joint motion. Journal of Orthopedic Research 2009 (in press).
Ford J, Elliott T, Adcock A, Bammer R, Roach B, Mathalon D.	The tattered trajectory of the forward model in schizophrenia: EEG and DTI. American Journal of Psychiatry (submitted).
Ganguly A, Simons J, Schneider A, Keck B, Bennett B, Coogan S, Herfkens RJ.	In vivo imaging of superficial femoral artery (SFA) stents for deformation analysis. Journal of Vascular Interventional Radiology (submitted).
Gold G, Chen C, Koo S, Hargreaves B, Bangerter N.	Recent advances in MR imaging of articular cartilage. AJR (submitted).
Grissom W, Kerr A, Holbrook A, Pauly J, Butts Pauly K.	Maximum linear-phase spectral-spatial RF pulses for fat-suppressed PRF-shift MR thermometry. Magnetic Resonance in Medicine (in press).
Gu Y, Levin C.	Effects of photon multiple interactions in a high resolution PET system that uses 3-D positioning detectors. Conference Record of the 2008 IEEE Nuclear Science Symposium and Medical Imaging Conference (submitted).
Gu Y, Matteson J, Skelton R, Deal A, Stephan E, Duttweiler F, Gasaway T, Levin C.	Study of a high resolution, 3-D positioning cross-strip cadmium zinc telluride detector for PET. Conference Record of the 2008 IEEE Nuclear Science Symposium and Medical Imaging Conference (submitted).

Haeberlin M, Skare S, Pruessmann K, Bammer R.	Matrix formulation and regularization of the HYPR algorithm. Magnetic Resonance in Medicine (submitted).
Han M, Beatty PJ, Daniel BL, Hargreaves BA.	Independent slab-phase modulation combined with parallel imaging in bilateral breast MRI. Magn Reson Med. (submitted).
Holdsworth S, Skare S, Newbould R, Bammer R.	Practical Implementation of GRAPPA-accelerated readout-segmented EPI for diffusion imaging. Magn Reson Med. (in press).
Holzbaur K, Lateva Z, Gold G, McGill K, Murray W.	In vivo multi-scale characterization of a series-fibered human muscle. Muscle and Nerve (submitted).
Iagaru A, Mittra ES, Quon A, Gambhir SS.	18F-FDG PET/CT in cancers of the head and neck: What is the definition of whole-body scanning? Clin Nucl Med. 2009 (submitted).
Iagaru A, Mittra ES, Ganjoo K, Knox SJ, Goris ML.	131I-Tositumomab (Bexxar®) vs. 90Y-Ibritumomab (Zevalin®) therapy of refractory/relapsed non-Hodgkin Lymphoma. Mol Imag Biol. 2009 (in press).
Josan S, Bouley D, van den Bosch M, Daniel B, Butts Pauly K.	MRI-guided cryoablation - in vivo assessment of focal canine prostate cryolesions. JMRI (in press).
Kahn CE, Langlotz C, Burnside E, Carrino J, Channin D, Hovsepian D, Rubin DL.	Towards best practices in radiology reporting. Radiology 2009 (in press).
Keenan K, Kourtis L, Besier T, Lindsey D, Gold G, Delp S, Beaupre G.	New resources for the computation of cartilage biphasic material properties with the interpolant response surface method. Computer Methods in Biomechanics and Biomedical Engineering (in press).
Keller KA, Barnes PD.	Rickets vs. Abuse – evidence & ideology: reply to editorial commentaries. Pediatr Radiol. (In press).
Kijowski R, Davis K, Woods M, Lindstrom M, Gold G, Busse R.	Comprehensive knee joint assessment using a three-dimensional, isotropic resolution fast spin-echo sequence (FSE-Cube): diagnostic performance compared to conventional MR imaging. Radiology 2009 (in press).
Koo S, Giori N, Gold G, Dyrby C, Andriacchi T.	Accuracy of cartilage thickness measurement in MRI changes with cartilage thickness: laser scanner based validation of in vivo osteoarthritic cartilage. Journal of Biomechanical Engineering (in press).
Kuo WT, Tong RT, Hwang GL, Louie JD, Lebowitz EA, Sze DY, Hofmann LV.	High-risk retrieval of adherent and chronically implanted IVC filters: techniques for removal and management of procedural thrombotic complications. J Vasc Interv Radiol (in press).
Kothary N, Tognolini A, Louie JD, Hwang GL, Hofmann LV, Sze DY.	Impact of Cone-Beam CT on Treatment Planning in Patients with Hepatocellular Carcinoma Undergoing Transarterial Hepatic Chemoembolization. J Vasc Interv Radiol (in press).
Lau F, Fang C, Reynolds P, Vandenbroucke A, Olcott P, Olutade F, Pratx G, Horowitz M, Levin C.	1mm3 sesolution breast-dedicated PET system. Conference Record of the 2008 IEEE Nuclear Science Symposium and Medical Imaging Conference (submitted).
Lau F, Vandenbroucke A, Reynolds P, Olcott P, Horowitz M, Levin C.	Front-end electronics for a 1mm3 Resolution LSO-PSAPD-based PET system with multiplexing. Conference Record of the 2008 IEEE Nuclear Science Symposium and Medical Imaging Conference (submitted).
Levy M, O'Connor M, Rubin DL.	Semantic Reasoning with Image Annotations for Tumor Assessment. AMIA Annu Symp Proc. 2009 (submitted).
Liu C, Zhang J, Moseley M.	Auto-calibrated parallel imaging reconstruction for arbitrary trajectories using k-space sparse matrices (kSPA) (submitted).
Liu YI, Kamaya A, Desser T, Rubin DL.	A controlled cocabulary to represent sonographic features of the thyroid and its application in a Bayesian network to predict thyroid nodule malignancy. AMIA Summit on Translational Bioinformatics 2009 (submitted).
Lu W, Pauly KB, Gold GE, Pauly JM, Hargreaves BA.	SEMAC: Slice encoding for metal artifact correction in MRI. Magn Reson Med. 2009 (in press).

Maloney WJ, Spinnickie A, Lindsey D, Ganguly A, Fahrig R, Kajiyama G, Lane Smith R.	Safety and efficacy of a collagenous-minerallized containment device for enhancement of bone defect healing: an animal study. Journal of Bone and Mineral Research (submitted).
Matteson J, Skelton R, Deal A, Stephan E, Duttweiler F, Gasaway T, Gu Y, Levin C.	Conference Record of the 2008 IEEE Nuclear Science Symposium and Medical Imaging Conference (submitted).
Mayer D, Yen Y-F, Tropp J, Hurd RE, Pfefferbaum A, Spielman DM.	Real-time metabolic imaging in vivo using hyperpolarized 13C1-pyruvate. Magn Reson Med (in press).
Mittra E, El-Maghraby T, Rodriguez CA, Quon A, McDougall IR, Gambhir SS, Iagaru A.	Efficacy of 18F-FDG PET/CT in the evaluation of patients with recurrent cervical carcinoma. Eur J Nucl Med Mol Imaging 2009 (in press).
Mittra ES, Leung A, Iagaru A.	Diagnosis please. Radiology 2009 (in press).
Mlynash M, Campbell JC, Leproust M, Bammer R, Eyngorn I, Hsia A, Moseley ME, Wijman C.	Temporal and spatial profile of brain diffusion-weighted MRI in the first week after cardiac arrest (submitted).
Newbould R, Skare S, Alley M, Clayton D, Markl M, Gold G, Bammer R.	Combined T1, T2, Proton Density, and B1 Mapping with Double-Angle Inversion Recovery (DAIRY) True FISP. Magnetic Resonance in Medicine (submitted).
Newbould R, Skare S, Alley M, Markl M, Gold G, Bammer R.	Three Dimensional T1, T2, and Proton Density Mapping with Inversion Recovery Balanced SSFP. Magnetic Resonance in Medicine (submitted).
Nyenhius D, Stebbins G, Williamson J, Cox J, Freels S, Moseley M, Bammer R, Gorelick P.	White matter classification probability, fractional anisotropy and cognition in ischemic stroke (in press).
Olcott P, Levin C.	Pulse width modulation: a novel readout scheme for high energy photon detection. Conference Record of the 2008 IEEE Nuclear Science Symposium and Medical Imaging Conference (submitted).
Olivot J, Minynash M, Thijs V, Purushotham A, Kemp S, Lansberg M, Wechsler L, Gold G, Bammer R, Marks M, Albers G.	Geography, structure and evolution of the diffusion and perfusion lesion in DEFUSE. Stroke (submitted).
Peng H, Olcott P, Levin C.	Can large-area avalanche photodiodes be used for a clinical PET/MRI block detector? Conference Record of the 2008 IEEE Nuclear Science Symposium and Medical Imaging Conference (submitted).
Prakash S, Dumoulin S, Fischbein N, Wandell BA, Liao YJ.	Congenital achiasma and infantile see-saw nystagmus in a patient with VACTERL. J Neuro-Ophthalmology (in press).
Pratx G, Levin C.	Robust Bayesian reconstruction of photon interaction sequences for high-resolution PET detectors. Physics in Medicine and Biology (submitted).
Pratx G, Reader A, Levin C.	Faster maximum-likelihood reconstruction via explicit conjugation of search directions. Conference Record of the 2008 IEEE Nuclear Science Symposium and Medical Imaging Conference (submitted).
Prümmer M, Hornegger J, Lauritsch G, Wigström L, Girard-Hughes E, Fahrig R.	Cardiac C-arm CT: A unified framework for motion estimation and dynamic CT. IEEE TMI (submitted).
Raman B, Raman R, Napel S, Rubin G.	Automated quantification of aortoaortic and aortoiliac angulation for CT angiography (CTA) of abdominal aortic aneurysms (AAA) prior to endovascular repair. Radiology (accepted).
Reynolds P, Olcott P, Lau F, Levin C.	Convex optimization of PET coincidence time resolution using list mode data. Conference Record of the 2008 IEEE Nuclear Science Symposium and Medical Imaging Conference (submitted).
Rogalski EJ, Murphy CM, deToledo-Morrell L, Shah RC, Moseley ME, Bammer R, Stebbins GT.	Changes in parahippocampal white matter integrity in amnestic mild cognitive impairment: a diffusion tensor imaging study (submitted).

Roos J, Olsen D, Paik D, Napel S, Liu E, Rubin G.	The nature of radiologists performance in the detection of lung nodules using computer-aided detection (CAD) in CT scans. Academic Radiology (submitted).
Roos JE, Paik DS, Olsen D, Liu EG, Chow LC, Leung AN, Mindelzun R, Naidich DP, Napel S, Rubin GD.	Computer-aided detection (CAD) of lung nodules on CT: Radiologist performance and reading time with incremental CAD assistance. European Radiology (in press).
Rubin DL, Mongkolwat P, Channin DS.	A semantic image annotation model to enable integrative translationalrResearch. AMIA Summit on Translational Bioinformatics, San Francisco, CA, 2009 (in press).
Rubin DL, Mongkolwat P, Kleper V, Supekar K, Channin D.	Annotation and image markup: accessing and interoperating with the semantic content in medical imaging. IEEE Intelligent Systems 2009 (in press).
Schmiedeskamp H, Newbould R, Bammer R.	Comparitive evaluation of a multi-echo fMRI acquisition technique using parallel imaging. Magnetic Resonance in Medicine (submitted).
Schmitz A, Rieke V, van den Bosch M, Butts Pauly K, Dirbas F, Daniel B.	3.0T MR-guided focused ultrasound for pre-operative localization of non-palpable breast tumors: an initial experimental study. JMRI (in press).
Schwartz N, Skare S, Newbould R, Lansberg M, Wijmann C, Albers G, Bammer R.	High-resolution DWI increases clinical yield in stroke. Neurology (submitted).
Singh MK, Spielman DM, Adleman N, Alegria D, Howe M, Reiss AL, Chang KD.	Brain glutamatergic characteristics of pediatric offspring of parents with bipolar disorder. Psychiatric Research - Neuroimaging (submitted).
Smith C, Martin E, Kessler H, Bartt R, Bammer R, Moseley M, Adeyemi A, Stebbins G.	Gender effects on HIV-associated white matter alterations: A voxel-wise DTI study (in press).
Staroswiecki E, Bangerter N, Gurney P, Grafendorfer T, Daniel B, Gold G, Hargreaves B.	In vivo sodium imaging with a 3D cones trajectory at 3T and 7T. Magn Reson Med. (submitted).
Stebbins G, Smith C, Bartt R, Kessler H, Adeyemi O, Martin E, Cox J, Bammer R, Moseley M.	White matter classification probability, fractional anisotropy and cognition in ischemic stroke. Neuroimage (submitted).
Stevens K, Akizuki K, Crain J, Beaulieu CF.	Internal oblique strains in baseball pitchers. Am J Sports Med. (submitted).
Tu S, Peleg M, Carini S, Bobak M, Rubin DL, Sim I.	A Practical Method for Transforming Free-Text Eligibility Criteria into Computable Criteria. AMIA Annu Symp Proc. 2009 (submitted).
Vandenbroucke A, Foudray A, Lau F, Olcott P, Reynolds P, Levin C.	Performance characterization of a new ultra-high resolution, 3-D positioning PET scintillation detector. Conference Record of the 2008 IEEE Nuclear Science Symposium and Medical Imaging Conference (submitted).
Vandenbroucke A, Levin C.	Study of scintillation crystal array parameters for an advanced PET scanner dedicated to breast cancer imaging. Conference Record of the 2008 IEEE Nuclear Science Symposium and Medical Imaging Conference (submitted).
Veldhuis W, Liu C, Do Y, Moseley M, Daniel B.	High-resolution multi-shot diffusion-weighted MRI of the breast with functional ADC mapping (submitted).
Vertinsky T, Rubesova E, Krasnokutsky M, Bammer S, Rosenberg J, Barnes P, Bammer R.	Performance of PROPELLER FSE T2-weighted imaging relative to standard FSE-T2 in pediatric brain magnetic resonance imaging. Pediatric Radiology (in press).
Wang B, Luo G, Sommer GH, Spielman DM, Dairiki-Shortliffe LM.	Evaluation of MRI in detecting renal scarring in a rat injury model. Journal of Magnetic Resonance Imaging (submitted)

Wang C, Stebbins G, Medina D, Shah R, Stroub T, Bammer R, Moseley M, de Toledo-Morrell L.	Hippocampal disconnection in mild Alzheimer's Disease: atrophy and dysfunction of parahippocampal white matter projections. Journal of Neurosurgery (submitted).
Won JH, Rosenberg J, Rubin GD, Napel S.	Uncluttered single-image visualization of the abdominal aortic vessel tree: method and evaluation. Medical Physics (accepte).
Yen Y-F, Le Roux P, Mayer D, King R, Spielman DM, Tropp J, Butts-Pauly K, Pfefferbaum A, Vasanawala S, Hurd RE.	T2 Relaxation times of 13C metabolites in a rat hepatocellular carcinoma model measured in vivo using 13C-MRS of hyperpolarized [1-13C]Pyruvate. NMR in Biomedicine (submitted).
Zaharchuk G, Bammer R, Atlas S, Albers G, Moseley M.	Arterial spin label imaging in patients with normal bolus perfusion-weighted magnetic resonance imaging: identification of the watershed signal. Radiology (in press).
Zaharchuk G, Bammer R, Straka M, Newbould R, Rosenberg J, Olivot J, Mlynash M, Lansberg M, Schawartz N, Albers G, Moseley M.	Improving dynamic susceptibility contrast MRI measurement of quantitative cerebral blood flow using corrections for partial volume and nonlinear contrast relaxivity: a xenon CT comparative study (submitted).
Zaharchuk G, Newbould R, Lansberg M, Wijmann C, Albers G, Moseley M, Bammer R.	Quantitative Dynamic Multi-Echo DSC PWI: A Comparative Evaluation with Xe-CT. Stroke (in press).

Funded Research Projects

NIH Supported Research

PI	Type	Title
Roland Bammer, PhD	R01	Improving SENSE MRI for Spiral and Echo-Planar Imaging
Roland Bammer, PhD	R01	*†Short Axis EPI for Diffusion Tensor MRI at Hi Field
Roland Bammer, PhD	R01	*†Novel Acquistion Methods for Diffusion MRI
Roland Bammer, PhD	R21	Real-Time MRI Motion Correction System
Francis Blankenberg, MD	R01	*†scVEGF Targeted Radiotherapy of Mammary and Colonic Cancer
Kim Butts Pauly, PhD	R01	MR-Image Guided Focused Ultrasound for Treatment of Liver and Renal Cancer
Catie Chang, MS	F32	Temporal Characteristics of Intrinsic Brain Networks
Xiaoyuan Chen, PhD	R01 (MPI)	Carbon Nanotubes as Multifunctional Spectroscopic Markers & Delivery Agents for Cancer Therapy
Xiaoyuan Chen, PhD	R01	*†VEGFR-2 Targeted Imaging
Zhen Cheng, PhD	R01	Radiolabeled RGD Peptides for Breast Cancer Imaging and Therapy
Zhen Cheng, PhD	R21	Quantum Dots for NIR Fluorescence Imaging of Tumor Angiogenesis
Bruce Daniel, MD	R01	Techniques for MRI-Guided Cryosurgery of Prostate Cancer
Rebecca Fahrig, PhD	R01	*†C-Arm CT for Guidance of Cardiac Interventions
Rebecca Fahrig, PhD	R01	†#MR Compatible X-Ray Tube
Rebecca Fahrig, PhD	R21	Efficient Scatter Correction
Sam Gambhir, MD, PhD	P50	In Vivo Cellular and Molecular Imaging Center at Stanford (ICMIC)
Sam Gambhir, MD, PhD	R01	*Imaging Cytolytic T Cells in Cancer Patients Using Reporter Gener/Reporter Probes
Sam Gambhir, MD, PhD	R25	Stanford Molecular Imaging Scholars (SMIS)
Sam Gambhir, MD, PhD	U54	#Center of Cancer Nanotechnology Excellence Focused on Therapy (CCNE)
Sam Gambhir, MD, PhD	R01	**Molecular Imaging of Intracellular Networks
Arun Ganguly, PhD	K99	*High Performance CMOS Based X-Ray Detector for C-Arm CT Imaging
Gary M. Glazer, MD	T32	Advanced Techniques for Cancer Imaging
Gary Glover, PhD	P41	Center for Advanced Magnetic Resonance Technology at Stanford (CAMRT)
Garry Gold, MD	R01	Real-Time MRI and 3D Modeling: Development and Application to Patellofemoral Pain
Brian Hargreaves, PhD	R01	*†High-Resolution Whole-Breast MRI at 3.0T
Brian Hargreaves, PhD	R21	*MR Imaging near Metallic Implants
Craig Levin, PhD	R01	Advanced PET System Dedicated to Breast Cancer Imaging
Craig Levin, PhD	R01	Enhancing Molecular Cancer Imaging with Cadmium Zinc Telluride PET
Craig Levin, PhD	R13	Workshop on the Nuclear Radiology of Breast Cancer

* New for 2009
† ARRA funds used to fund this new project
** Longstanding R01 renewed for another 4-5 years
# ARRA funds used to supplement an existing project

For additional awards, see Awards and Honors pages 26-27, and Trainee Awards pages 30-31.

PI	Type	Title
Craig Levin, PhD	R33	New Scintillation Light Detection Concepts for PET
Michael Moseley, PhD	R01	**Microvascular Measures of Perfusion in Stroke Recanalization
Norbert Pelc, ScD	R01	Inverse Geometry CT for Dose-efficient Volumetric Imaging
Sylvia Plevritis, PhD	U01	Breast Cancer Trend Analysis Using Stochastic Simulation
Sylvia Plevritis, PhD	U56	Computational Modeling of Cancer Biology
Jianghong Rao, PhD	R01	*QD-BRET nanosensors for protease detection and imaging
Jianghong Rao, PhD	R01 (MPI)	Actively Controlled and Targeted Single-Molecule Probes for Cellular Imaging
Geoffrey Rubin, MD	R01	Improving Radiologist Detection of Lung Nodules with CAD
Graham Sommer, MD	R01	Precise MRI-Directed Sonic Ablation of Prostate Cancer
Graham Sommer, MD	R21	*MRI-guided Ultrasonic Ablation of Pancreatic Cancer
Daniel Spielman, PhD	R01	IH MRSI of the Human Brain at 7T
Juergen Willmann, MD	R21	*Early Detection of Pancreatic Cancer with Targeted Contrast-enhanced Ultrasound
Joseph Wu, MD, Phd	DP2	*09: Inducing Pluripotency with MiRNAs: New Paradigm Shif in Cell Reprogramming
Joseph Wu, MD, Phd	K08	Molecular Imaging of Cardiac Cell Transplantation
Joseph Wu, MD, Phd	R01	*Molecular Imaging of Targeted Cardiac Gene Therapy
Joseph Wu, MD, Phd	R21	Nanostructuring and Molecular Imaging of Engineered Cardiovascular Tissues
Joseph Wu, MD, Phd	R21	*†Biological Insights into Dynamics of Stem Cell Differentiation and Misbehavior
Greg Zaharchuk	R01	*Quantifying Collateral CBF with ASL

* New for 2009
† ARRA funds used to fund this new project
** Longstanding R01 renewed for another 4-5 years
# ARRA funds used to supplement an existing project

NIH Collaborations (Sub-Contracts)

PI	Type	Title
Francis Blankenberg, MD	Sub (SibTech)	Radiotherapy of Murine Collagen Induced Arthritis with scVEGF
Xiaoyuan Chen, PhD	Sub (Purdue)	99mPTc-Labeled Cyclic RGD Peptide Tetramers for Breast Cancer Imaging
Xiaoyuan Chen, PhD	Sub (USC)	Integrin - Targeted Drug Design, Delivery, and Imaging
Sam Gambhir, MD, PhD	Sub (UCLA)	Multimodel Qdot Probes for Bioimaging of Cells & Tumors in Small Animals
Gary Glover, PhD	Sub (UCI)	Functional Imaging Research in Schizophrenia Testbed

* New for 2009
† ARRA funds used to fund this new project
** Longstanding R01 renewed for another 4-5 years
# ARRA funds used to supplement an existing project

For additional awards, see Awards and Honors pages 26-27, and Trainee Awards pages 30-31.

NIH Collaborations (Sub-Contracts)

PI	Type	Title
Garry Gold, MD	Sub (UCSF)	Data Coordinating Center for Osetoarthritis Initiative
Lawrence Hofmann, MD	Sub (WashU)	Pharmacomechanical Catheter-Directed Thrombolysis for Acute DVT-Attract Trial
Debra Ikeda, MD	Sub (Spectros)	Survey of Optical Measures of Breast Tissue in the Clinic
Dirk Mayer, PhD	Sub (Scripps)	*INIA: Effects of Acute Alcohol Exposure on Rat Brain Metabolites Detected by MRS
David Paik, PhD	Sub (BAH)	New caBIG Integrated Cancer Research (ICR) Nanotechnology Working Group
Daniel Rubin, MD	Sub (BAH)	*task 4: (IMG WG DR)
Daniel Rubin, MD	Sub (Brigham)	Neuroimaging Analysis Center
Daniel Rubin, MD	Sub (RSNA)	*Enriching the RadLex Ontology to Enable Biomedical Imaging Research in Neuroimaging
Daniel Rubin, MD	Sub (U Pitt)	*A Web-Based of Inventoried Resources Enabling Clinical and Trasnlational Research across the CTSA and Beyond
Daniel Rubin, MD	Sub (BAH)	caBIG Imaging Workspace Participant
Daniel Rubin, MD	Sub (BAH)	New caBIG Integrative Cancer Reserach Wrokspace Task Group Participant - Task 3
Daniel Rubin, MD	Sub (BAH)	caBIG Master Agreement - Subcontract # 95077NBS23
Daniel Rubin, MD	Sub (BAH)	Imaging Workspace in EY2
Daniel Spielman, PhD	Sub (SRI)	*Dynamic Metabolic Imaging of Hyperpolarized Substrates
Daniel Spielman, PhD	Sub (SRI)	In Vivo Diffusion and Spectroscopic Brain Imaging in Alcoholism
Daniel Spielman, PhD	Sub (U Miami)	Partnership for MR Spectroscopic Imaging Data

* New for 2009
† ARRA funds used to fund this new project
** Longstanding R01 renewed for another 4-5 years
# ARRA funds used to supplement an existing project

Stanford Supported Research

PI	Type	Title
Sandip Biswal, MD	OTHER Stanford	*Development of a Saxitoxin-Based Image-Guided Approach for the Management of Chronic Pain
Terry Desser, MD	Wallenberg	Learning Radiology in Simulated Environments
Garry Gold, MD	Wallenberg	Learning Radiology in Simulated Environments
Shreyas Vasanawala, MD, PhD	Morgridge Foundation	*Anesthesia-Free in Pediatric MRI

* New for 2009
† ARRA funds used to fund this new project
** Longstanding R01 renewed for another 4-5 years
# ARRA funds used to supplement an existing project

For additional awards, see Awards and Honors pages 26-27, and Trainee Awards pages 30-31.

Professional Society & Foundation Supported Research

PI	Type	Title
Zhen Cheng, PhD	Melanoma Research Fd	*18F Labeled Benzamides for Pre-Clinical PET Imaging of Melonoma Metastases
Zhen Cheng, PhD	SNM	Engineered Small Proteins for HER2 Imaging
Sam Gambhir, MD, PhD	Doris Duke	Molecular Imaging of Cancer with a Voltage Sensor
David Wang, MD	RSNA	Ultrasound - Mediated Suicide gene Therapy with Molecularly Targeted microbubbles in a murine model for tumor angiogenesis
Mei Huang, PhD	AHA	Molecular Imaging of Non-Viral Cardiac Gene therapy
Mei Huang, PhD	AHA	*Novel Non-viral Gene Therapy for Heart Disease
Li, Zongjin , MD, PhD	SNM	Molecular Imaging of Stem Cell Differentiation and Function
Amelie Lutz, MD	Marsha Rivkin	*Early Detection of Ovarian Cancer using Targeted Microbubbles-Ehances Ultrasound
MacKenzie/Vasanawala	SPR	Evaluation of Pediatric Diseases with Hyperpolarized Carbon-13 MRI
Peter Olcott, MS	SNM	Optically coupled pulse width modulation PET detectors for combined whole body clinical PET/MR systems
Andrew Quon, MD	NCCN	Evaluating Sunitinib Therapy in Renal Cell Carcinoma
Jianghong Rao, PhD	BWF	Career Award at the Scientific Interface
Jianghong Rao, PhD	HFSP	Imaging mRNA in Synaptic Plasticity
Jianghong Rao, PhD	Texas A&M/ Gates Fd	Development of Fluorogenic Probes for In Vivo Imaging of TB
Daniel Rubin, MD	ACR	American College of Radiology Imaging Network (ACRIN) Committee Agreement Rubin
Lewis Shin, MD	RSNA	*RSNA Research Seed Grant
Shreyas Vasanawala, MD, PhD	ISMRM	Non-Contrast-Enhanced Renal MRA Using Multiple Inversion Recovery
Juergen Willmann, MD	National Pancreatic Fd	*Development of a Novel Translatable Molecular Imaging Approach for Early Detection of Pancreatic Cancer
Juergen Willmann, MD	RSNA	Pancreatic Cancer and Microbubbles
Juergen Willmann, MD	SGR	*Anti-Angiogenic Treatment in Abdominal and Pelvic Cancer Molecular Ultrasound: First Step Towards Clinical Translation
Joseph Wu, MD, PhD	AHA	In Vivo Tracking of Stem Cells in the Ischemic Myocardium
Joseph Wu, MD, PhD	BWF	Molecular and cellular mechanisms of cardiac regeneration
Joseph Wu, MD, PhD	Edward Mallinckrodt Jr.	*Innovative Approach for Regrpgramming Stem cells for Regenerative Medicine
Joseph Wu, MD, PhD	ACCF	Multi-Modality Imaging of Cardiac Stem Cell
Joseph Wu, MD, PhD	AHA	Safety and Efficacy of Novel iPSC Derived Cardiomyocytes

* New for 2009
† ARRA funds used to fund this new project
** Longstanding R01 renewed for another 4-5 years
# ARRA funds used to supplement an existing project

For additional awards, see Awards and Honors pages 26-27, and Trainee Awards pages 30-31.

Professional Society & Foundation Supported Research

PI	Type	Title
Greg Zaharchuk, MD, PhD	NERF	Optimizing Arterial Spin Label MRI for the Visualization of Collateral Flow in Moyamoya Disease
Michael Zieneh, MD, PhD	RSNA	*Ultra-High Resolution Clinical Imaging of the Human Medial Temporal Lobe with 7T MRI
Keren Ziv, PhD	Life Science Rsch Fd	Non-Invasive and Real-Time Monitoring of Stem Cells Using Photoacoustic Molecular Imaging in Living Mice

* New for 2009
† ARRA funds used to fund this new project
** Longstanding R01 renewed for another 4-5 years
# ARRA funds used to supplement an existing project

Other Government Supported Research

PI	Type	Title
Qizhen Cao, PhD	CA-TRDRP	alpha 7-nAChR Targeted Imaging and Therapy of Lung Cancer
Zhen Cheng, PhD	CA-CBCRP	Novel Small Proteins for PET Imaging of Breast Cancer
Xiaoyuan Chen, PhD	DOD	Molecular Imaging of Ovarian Carcinoma Angiogenesis
Zhen Cheng, PhD	DOD	Mesenchymal Stem Cell as Targeted-delivery Vehicle in Breast Cancer
Adam de la Zerda, PhD	DOD	*Early Assesment of Breast Cancer Therapy Response Using Photoacoustic Molecular Imaging
Misung Han, PhD	Dept of Defense	Improving Breast Cancer MRI
Brian Hargreaves, PhD	CA-CBCRP	Multinuclear MRI of Breast Tumors
Brian Hargreaves, PhD	VA	Cartilage Compression Study for VA
Gang Niu, PhD	DOD	*Imaging Heat Shock Protein 90 (Hsp90) Activity in Hormone-Refractory Prostate Cancer
Rebecca Rakow-Penner, PhD	CA-CBCRP	Functional Breast MRI with BOLD Contrast
Jianghong Rao, PhD	Dept of Defense	*Enzyme-triggered Polymerization: a new platform for breast cancer imaging
Jianghong Rao, PhD	Dept of Army	Ribozyme-Mediated Imaging of p53 Expression in Breast Tumor Cells
Joseph Wu, MD, PhD	CA-CIRM	In Vivo Imaging of Human Embryonic Stem Cell Derivatives and Tumorigenicity
Joseph Wu, MD, PhD	CA-UCOP	Imaging of Novel Stem Cell Therapy Targeting Breast Cancer

* New for 2009
† ARRA funds used to fund this new project
** Longstanding R01 renewed for another 4-5 years
# ARRA funds used to supplement an existing project

For additional awards, see Awards and Honors pages 26-27, and Trainee Awards pages 30-31.

Industry Supported Research

PI	Type	Title
Sandip Biswal, MD	Kai Pharma	*Evaluation of the Efficacy of KAI-1678 with Manganese-Enhanced Magnetic Resonance Imaging (MEMRI)
Francis Blankenberg, MD	Genentech	*Choline MRS Correlated with Markers of Apoptosis (TUNEL) biotinylated annexin V & Autophagy (Type II cell death)
Francis Blankenberg, MD	Glaxo Sm Kl	*Using Targeted VEGF receptor (VEGFR) imaging to monitor treatment with pazopanib in a mouse tumor model.
Francis Blankenberg, MD	SibTech-R44	Development of Cu-64 Labeled EGF for In Vivo Imaging of EGFR Expression
Terry Desser, MD	Berlex Labs	Simulation-based Medical Training Exercise in Management of Contrast Media Adverse Reactions for Residents
Rebecca Fahrig, PhD	Siemen's Medical Solutions	Gated 3D DynaCT for Cardiac Applications
Rebecca Fahrig, PhD	Siemen's Medical Solutions	Perfusion Imaging using C-arm CG: Brain and Liver
Rebecca Fahrig, PhD	Siemen's Medical Solutions	Cardiac Imaging using C-arm CT: EP registration and perfusion
Sam Gambhir, MD, PhD	GE	Multimodality Molecular Pre-Clinical Imaging
Sam Gambhir, MD, PhD	Genentech	PET Imaging of Lymphoma Patients using Radiolabeled Rituximab
Sam Gambhir, MD, PhD	General Electric Company	Developing Tools for Cell Therapy - specifically cell tracking and quality assurance
Sam Gambhir, MD, PhD	Schering Plough Institute	*MicroPET Imaging studies for anti-HGF pgm in U87 glioblastoma model OR SCH-XXX in Orthotopic U87 Glioblastoma Model
Sam Gambhir, MD, PhD	Bayer Schering	Collaborative Research Agreement: Project 1: Tumor Lymphangiogenesis Imaging
Gary M. Glazer, MD	GE	GE PACS System
Garry Gold, MD/Gary Glover, PhD	GE	MR/Advanced MR Imaging - TIGER TEAM
Lawrence Hofmann, MD	OmniSonics Medical Technologies, Inc.	Study of the OmniWave Endovascular System in Subjects with Lower and Upper Extremity Deep Vein Thrombosis: Sonic I Study
Lawrence Hofmann, MD	Pfizer	*A safety and efficacy trial evaluating the use of apixaban in the treatment of symtomatic deep vein thrombosis and pulmonary embolism
Lawrence Hofmann, MD	Pfizer	*CV185056- A safety and efficacy trial evaluating the use of apixaban in the treatment of symtomatic deep vein thrombosis and pulmonary embolism
Debra Ikeda, MD	Advanced Research Technologies Inc.	SSC-311 Adjunctive Efficacy Study of the SoftScan Optical Breast Imaging System

* New for 2009
† ARRA funds used to fund this new project
** Longstanding R01 renewed for another 4-5 years
# ARRA funds used to supplement an existing project

For additional awards, see Awards and Honors pages 26-27, and Trainee Awards pages 30-31.

Industry Supported Research

PI	Type	Title
Nishita Kothary, MD	Siemens Corporate Research	Clinical Feasibility and Evaluation of RoRo (Rotational Mapping); Optimal imaging protocol of HCC undergoing TACE utilizing DynaCT; & Needle Guided Procedures Utilizing DynaCT, Laser Guidance, and 2D3D Registration
Craig Levin, PhD	GE	Combined PET MR System
Norbert Pelc, ScD	GE	Advanced Computed Tomography (CT) Systems Including Inverse Geometry CT (IGCT)
Andrew Quon, MD	Genentech, Inc.	Avastin/[18F]-5-fluorouracil PET/CT Imaging Feasibility Project
Geoffrey Rubin, MD	Biosense, Inc.	Core Lab for NaviStar ThermCool Catheter for the Radiofrequency Ablation of Paroxysmal Atrial Fibrillation
Geoffrey Rubin, MD	Cook Med Institute, Inc.	Zenith TX2 Thoracic TAA Endovascular Graft
Virginia Spanoudaki, PhD	Axa Group	*1mm Resolution Position Emission Tomography for Enhanced Molecular Breast Cancer Imaging
Daniel Sze, MD	Cook Incorporated	Zenith TX2 Thoracic TAA Ebdovascular Graft
Daniel Sze, MD	Cook Incorporated	The Zilver PTX Drug Eluding Vascular Stent in the Above the Knee Femoralpopliteal Artery
Daniel Sze, MD, PhD	Angiotech Pharma	A Prospective Randomized Multi-centered Safety and Efficacy Evaluation of the Bio-seal Biopsy Track Plug for Reducing Pneumothorax Rates Post Lung Biopsy Procedures
Daniel Sze, MD, PhD	W.L. Gore & Associates	A Clinical Study Evaluating the Use of the Thoracic EXCLUDER Endoprostheis in the Treatment of Descending Thoracic Aortic Diseases
Daniel Sze, MD, PhD	W.L. Gore & Associates	Treatment IDE for Use of the GORE TAG Thoracic Endoprosthesis in Subjects with Descending Thoracic Aortic Aneurysms Requiring Surgical Repair
Daniel Sze, MD, PhD	W.L. Gore & Associates	Evaluation of the GORE TAG Thoracic Endoprosthesis-45 mm for the Primary Treatment of Aneurysm of the Descending Thoracic Aorta

* New for 2009
† ARRA funds used to fund this new project
** Longstanding R01 renewed for another 4-5 years
# ARRA funds used to supplement an existing project

Projects made possible in part by industry seed funding grants

PI	Type	Title
Kim Butts Pauly, PhD	GE Healthcare	Neuromodulation with Focused Ultrasound
John MacKenzie, MD	GE Healthcare	Evaluation of [1–13C]–Methionine as a Novel Hyperpolarized Carbon–13 Compound for MR Molecular Imaging of Inflammatory Arthritis
Garry Gold, MD	GE Healthcare	Optimization of 3D Fast Spin Echo Imaging for Musculoskeletal Applications
Lewis Shin, MD	GE Healthcare	The Utility of Cine MRI for evaluation of Small and Large Bowel Dysmotility
Brian Rutt, PhD, Ron Watkins	GE Healthcare	Proton Lower Torso Transmit Receive Coil for 2 Channel Parallel Transmit
Juergen Willmann, MD	GE Healthcare	Inflammatory Bowel Disease: Prediction of Remission by a Novel Dynamic Contrast-enhanced Magnetic Resonance Imaging Approach in a Rat Colitis Model

* New for 2009
† ARRA funds used to fund this new project
** Longstanding R01 renewed for another 4-5 years
# ARRA funds used to supplement an existing project

For additional awards, see Awards and Honors pages 26-27, and Trainee Awards pages 30-31.

Collaborators Outside of Stanford

We also enjoy many collaborations with foundations, agencies, institutions, and industry for whose support we are indeed thankful. We look forward to continued success in these collaborative endeavors as well.

Advanced Research Technologies, Inc.
Alza Corporation
American College of Cardiology
American College of Radiology
American Heart Foundation
Angiotech
Axa Group
Berlex
Biosense
Booz-Allen & Hamilton, Inc
California Insitute for Regenerative Medicine
Canary Foundation
Cedars Sinai, Los Angeles
Chiron Corporation
Colorado State University—Boulder
Concentric Medical, Inc.
Cook Incorporated
Cook Medical Institute, Inc.
Department of Defense
Diversified Diagnostic Products, Inc.
Doris Duke Foundation
Edward Mallinckrodt Jr. Foundation
FeRx, Inc.
Fred Hutchinson Cancer Research Center
GE Healthcare
Genentech
Geron
Glaxo Smith Kline
Intronn Inc.
Kai Pharmaceuticals
Kaufmann Foundation
Life Science Research Foundation
Lucile Packard Foundation
Marsha Rivkin Center for Ovarian Cancer
Medimmune Inc.
Melanoma Research Foundation
Micrus Corporation
National Institutes of Health
Nova R&D Inc.
OmniSonics Medical Technologies, Inc
Palo Alto Veterans Administration
Pfizer
Prostate Cancer Foundation
Purdue University
Radiological Society of North America
Richard M. Lucas Cancer Foundation
Riken, Saitama, Japan
Schering AG
Scripps Research Institute
SibTech, Inc
Sidney E. Frank Foundation
Siemen's Medical Solutions
Siemens Corporate Research
Sir Peter & Lady Michael Foundation
Society for Pediatric Radiology
Society of Nuclear Medicine
Spectros Corporation
SRI International
Texas A&M
University of California, Berkeley
University of California, Davis
University of California, Irvine
University of California, Los Angeles
University of California, San Diego
University of California, San Francisco
University of Chicago
University of Miami
University of Pittsburgh
University of Southern California
University of Texas, A & M
University of Texas, Austin
University of Washington
U-Systems
Varian Associates
W.L. Gore and Associates
Wallenberg
Weston Havens Foundation

Collaborating Stanford Departments

We work with almost three hundred faculty, postdoctoral fellows, students, and research staff from across the University. We wish to thank you all for the friendly, productive collaborations that we enjoy all year long. Stanford departments with whom we have long-standing research projects include the following:

Aeronautics and Astronautics
Anesthesia
Applied Physics
Biochemistry
Bioengineering
Bio-X
Cancer Biology
Cancer Center
Cardiothoracic Surgery
Chemistry
Comparative Medicine
Computer Sciences
Developmental Biology
Electrical Engineering
Electrical Engineering
ENT
Freeman Spogli Institute
Functional Restoration
Genetics
Health Research and Policy
Hematology
Infectious Diseases
Lucile Packard Children's Hospital
Materials Science and Engineering
Mechanical Engineering
Medical Informatics
Medicine
Microbiology and Immunology
Molecular and Cellular Physiology
Neurobiology
Neurology and Neurological Sciences
Neurosurgery
Obstetrics & Gynecology
Oncology
Orthopedics/Orthopedic Surgery
Otolaryngology
Palo Alto VA
Pathology
Pediatrics
Pediatrics/Neonatology
Psychiatry and Behavioral Sciences
Psychology
Radiation Oncology
Stanford Center for Biomedical Ethics
Stroke Center
Surgery

Welcome New Research Faculty

Ramasamy Paulmurugan, PhD

Assistant Professor of Radiology
Molecular Imaging Program at Stanford (MIPS)

Ramasamy Paulmurugan, PhD, Assistant Professor of Radiology in the Molecular Imaging Program at Stanford (MIPS), trained in molecular imaging at UCLA and joined the MIPS program in 2003 as research scientist. The reporter protein-fragment assisted complementation strategy developed by Dr. Paulmurugan has made it possible to image protein-protein interactions, the heart of signal transductions, and important therapeutic targets in cells at different pathological conditions, for the first time in living animals. His research mainly focuses on the use of complementation strategies for studying the biology of breast cancer including tamoxifen resistance in estrogen receptor (ER) positive breast cancer, tissue specific action of ER in response to different ER-ligands and the collaborative role of ER-sub types (a/b) in regulating the ER-pathway. He will also focus on developing high affinity ER-ligands for the early diagnosis of ER-positive breast cancers.

Welcome Senior Scientists

Amelie Lutz, MD

Clinical Instructor/Research Scientist in Radiology
Molecular Imaging Program at Stanford (MIPS)

Amelie M. Lutz, MD, PD, Clinical Instructor and Research Scientist, Department of Radiology recently joined our department following a research fellowship in molecular imaging. After completing medical school and internship in Internal Medicine/Endocrinology at the Albert-Ludwigs-University in Freiburg, Germany, Dr. Lutz did her residency in Diagnostic Radiology at the University Hospital in Zurich, Switzerland and a fellowship in Body Imaging/Musculoskeletal Imaging at the Kantonal Hospital in Frauenfeld, Switzerland. In 2008 she received the venia legendi (member of the academic faculty, PD) in Diagnostic Radiology at the University of Zurich. Her research interests include the development of novel diagnostic strategies for early detection of cancer, especially of ovarian cancer. She is currently working on preclinical and translational studies including multimodality strategies using blood biomarker tests and imaging for ovarian cancer early detection as well as the development of novel PET probes for cancer staging.

Arutselvan Natarajan, PhD

Instructor of Radiology
Molecular Imaging Program at Stanford (MIPS)

Arutselvan Natarajan, PhD, recently joined the Molecular Imaging Program at Stanford (MIPS) as an Instructor in the Department of Radiology. Dr. Natarajan completed his PhD in biological/industrial chemistry at the Alagappa University Karaikudi, India. After completion of his PhD he became a Research Associate in a CSIR lab, in India. Subsequently, he joined the University of California Davis as an advanced postdoctoral fellow in the Radiodiagnosis and Therapy section in the School of Medicine. In 2005, he was promoted to Assistant Research Professor in UC Davis Medical Center. At UC Davis, his research focus was the development of GMP grade radiopharmaceutical doses for the NCI sponsored clinical trials for human cancer patients, using antibody, antibody fragments, small molecules, peptides, and selective high affinity ligands for multi modality cancer imaging and therapy. His current research focus at Stanford is the development of antibody based imaging agents, clinical translational science for human patient studies, and early diagnosis of cancer using protein biomarkers, miRNA, and nanotechnology.

Welcome Senior Scientists

Mark Stolowitz, PhD

Science and Engineering Associate
Director of the Proteomics Core Facility
Canary Center for Cancer Early Detection

Mark L. Stolowitz, PhD, is the Director of the Proteomics Core Facility in the Canary Center for Cancer Early Detection at Stanford. A seasoned technical professional with over 25 years experience involving conceptualization and development of life sciences research tools, his efforts are recently focused on the development of an immunoaffinity mass spectrometry platform for biomarker verification. This technology will be exploited by the Canary Center at Stanford to develop a high throughput biomarker verification platform. A prolific innovator, Dr. Stolowitz has been issued 43 United States Patents related to bioconjugation, SPR biosensors, protein biochips, protein and nucleic acid immobilization, protein chromatography, and protein sequencing.

Welcome Scientific Staff

Sanjiv Bhandari, MS - Programmer and Web Page Designer for Radiological Sciences Lab, Lucas Center, Radiology

Edwin Chang, PhD - Research Associate, Molecular Imaging Program at Stanford

Samantha Holdsworth, PhD - Research Associate, Radiological Sciences Lab, Lucas Center, Radiology

Richard Kimura, PhD - Research Associate, Molecular Imaging Program at Stanford

Jelena Levi, PhD - Research Associate, Molecular Imaging Program at Stanford

George Montoya - Research Assistant, Molecular Imaging Program at Stanford

Rafael O'Halloran, PhD - Research Associate, Molecular Imaging Program at Stanford

New Administrative Support Staff

Patricia Riley joined the Department in May of 2009 and works with Zhen Cheng, PhD and Fred Chin, PhD. Pat's office is located in the Lucas Center Expansion building.

Jean Stevens joined the Radiology Department in March, 2009 and has been involved in the start up of the Canary Center for Cancer Early Detection at Stanford. Her office is located at the California Avenue site.